

**SYNTHESIS OF NEW BIS-N-HETEROCYCLIC CARBENE
COMPLEXES AND THEIR APPLICATIONS AS
POTENTIOMETRIC SENSOR FOR Ag(I) AND Hg(II) IONS**

NUR RAHIMAH SAID

**FACULTY OF SCIENCE
UNIVERSITY OF MALAYA
KUALA LUMPUR**

2016

**SYNTHESIS OF NEW BIS-N-HETEROCYCLIC
CARBENE COMPLEXES AND THEIR APPLICATIONS
AS POTENTIOMETRIC SENSOR FOR
Ag(I) AND Hg(II) IONS**

NUR RAHIMAH SAID

**THESIS SUBMITTED IN FULFILMENT OF THE
REQUIREMENTS FOR THE DEGREE OF DOCTOR OF
PHILOSOPHY**

**FACULTY OF SCIENCE
UNIVERSITY OF MALAYA
KUALA LUMPUR**

2016

UNIVERSITI MALAYA

ORIGINAL LITERARY WORK DECLARATION

Name of Candidate: **NUR RAHIMAH BINTI SAID**

Registration/Matric No: **SHC110082**

Name of Degree: **DOCTOR OF PHILOSOPHY (EXCEPT MATHEMATICS & SCIENCE PHILOSOPHY)**

Title of Project Paper/Research Report/Dissertation/Thesis ("this Work"):

SYNTHESIS OF NEW BIS-N-HETEROCYCLIC CARBENE COMPLEXES AND THEIR APPLICATIONS AS POTENTIOMETRIC SENSOR FOR Ag(I) AND Hg(II) IONS

Field of Study: **INORGANIC CHEMISTRY**

I do solemnly and sincerely declare that:

- (1) I am the sole author/writer of this Work;
- (2) This Work is original;
- (3) Any use of any work in which copyright exists was done by way of fair dealing and for permitted purposes and any excerpt or extract from, or reference to or reproduction of any copyright work has been disclosed expressly and sufficiently and the title of the work and its authorship have been acknowledged in this Work;
- (4) I do not have any actual knowledge nor do I ought reasonably to know that the making of this Work constitutes an infringement of any copyright work;
- (5) I hereby assign all and every rights in the copyright to this Work to the University of Malaya ("UM"), who henceforth shall be owner of the copyright in this Work and that any reproduction or use in any form or by any means whatsoever is prohibited without the written consent of UM having been first had and obtained;
- (6) I am fully aware that if in the course of making this Work I have infringed any copyright whether intentionally or otherwise, I may be subject to legal action or any other action as may be determined by UM.

Candidate's Signature

Date

Subscribed and solemnly declared before,

Witness's Signature

Date

Name:

Designation:

Witness's Signature

Date

Name:

Designation:

ABSTRACT

A new series of bis-benzimidazolium salts namely, L₁.Br, L₂.Br, L₃.Br, L₁.PF₆, L₂.PF₆ and L₃.PF₆ have been successfully synthesized and characterized by using fourier transform infrared (FT-IR), ¹H and ¹³C nuclear magnetic resonance (NMR), and CHNS elemental analysis. The crystal structure of L₁.Br and L₁.PF₆ were confirmed, by single crystal X-ray diffraction analysis. The selective complexation of synthesized bis-benzimidazolium salts were found by using conductometric method. L₁.Br has been used to study the complexation process with Ni²⁺, Zn²⁺, Pd²⁺, Hg²⁺ and Ag⁺ metal ions in MeOH:H₂O binary phases at different temperatures. The stoichiometric of the complexation reactions for Ni²⁺, Zn²⁺, and Pd²⁺ are 1:1 [M:L₁.Br]. While, for Hg²⁺ and Ag⁺, two stoichiometries were obtained (2:1 [M:L₁.Br] and 1:1 [M:L₁.Br]). The stability constants ($\log K_f$) obtained from GENPLOT software show that the values for Hg²⁺ and Ag⁺ ions are higher than the other metal ions. The thermodynamic parameters (ΔG_C^o , ΔH_C^o , ΔS_C^o) revealed that the complexations of L₁.Br in all cases were found to be enthalpy destabilized but entropy stabilized. The negative value of calculated ΔG_C^o is an evidence to prove the ability of the ligand to form stable complexes with metal cations and the process trends to proceed spontaneously. The experimental data was tested by using artificial neural network (ANN) program and was in a good agreement with the estimated data. The calculations based on density functional theory (DFT) were used to predict the metal binding capability of complexes. The combination of all the results revealed that the selective complexation of L₁.Br is in the sequence of Ni²⁺<Pd²⁺<Zn²⁺<Hg²⁺<Ag⁺. Subsequently, new potentiometric self-plasticizing polypyrrole sensors based on L₁.Br as ionophore were fabricated for determination of Hg²⁺ and Ag⁺ cation. The optimum membrane composition was obtained by using 89.4 wt.% monomer (pyrrole), 4.8 wt.% photoinitiator (DMPP), 0.2 wt.% lipophilic salt (NaTFB), and 5.6 wt.% ionophore (L₁.Br). These sensors demonstrated good Nernstian responses of 28.10±0.29 mV/decade and 58.61±1.12 mV/decade with working ranges of 1.0×10⁻⁶-1.0×10⁻² M and 2.5×10⁻⁶-1.0×10⁻¹ M for Hg²⁺ and Ag⁺ cations, respectively. Both electrodes performed satisfactory over wide pH range and showed fast response time which was about 20 s with a good repeatability and reproducibility. The proposed electrodes can be used over a period of 30 (Hg-ISE) and 50 (Ag-ISE) days without showing any significant drift in working concentration range, slope and response time. It also had no significant interference in the performance of the fabricated Hg-ISE and Ag-ISE for determining Hg²⁺ and Ag⁺ cations. The proposed electrode was successfully used to determine various concentrations of Hg²⁺ and Ag⁺ cation in water and standard solution samples with satisfactory results. All data proved that the proposed Hg-ISE and Ag-ISE can be applied in determination of Hg²⁺ and Ag⁺ cations present in solution, respectively. The corresponding complexes of mercury(II) and silver(I) for all synthesized bis-benzimidazolium salts were prepared in order to understand the coordination of complexes formation. The bis-benzimidazolium salts were coordinated with Hg²⁺ and Ag⁺ metal cations through the carbene carbon, respectively which were proved by FT-IR and NMR data. The single crystal X-ray diffraction analysis data for L₁.AgBr and L₃.HgBr revealed that the coordination geometry of complexes is tetrahedral.

ABSTRAK

Siri baru garam bis-benzimidazolium iaitu $L_1\text{Br}$, $L_2\text{Br}$, $L_3\text{Br}$, $L_1\text{PF}_6$, $L_2\text{PF}_6$ dan $L_3\text{PF}_6$ telah berjaya disintesis dan dicirikan dengan menggunakan spectroskopi transformasi fourier inframerah (FT-IR), ^1H dan ^{13}C resonan magnet nukleus (NMR), analisis unsur CHNS, dan struktur kristal $L_1\text{Br}$ dan $L_1\text{PF}_6$ telah disahkan oleh analisis pembelauan sinar-X kristal tunggal. Kompleks selektif garam bis-benzimidazolium telah didapati dengan menggunakan kaedah konduktometrik. $L_1\text{Br}$ telah digunakan untuk mengkaji proses kompleksnya dengan kation logam Ni^{2+} , Zn^{2+} , Pd^{2+} , Hg^{2+} dan Ag^+ dalam fasa binari $\text{MeOH}: \text{H}_2\text{O}$ pada suhu yang berbeza. Ini memberikan stoikiometri tindak balas kompleks untuk Ni^{2+} , Zn^{2+} , dan Pd^{2+} adalah 1: 1 [M: $L_1\text{Br}$]. Manakala, untuk Hg^{2+} dan Ag^+ , dua stoichiometri diperolehi (2: 1 [M: $L_1\text{Br}$] dan 1: 1 [M: $L_1\text{Br}$]). Pemalar kestabilan ($\log K_f$) yang diperolehi daripada GENPLOT menunjukkan bahawa nilainya untuk kation logam Hg^{2+} dan Ag^+ adalah lebih tinggi berbanding kation logam lain. Parameter termodynamik (ΔG_c° , ΔH_c° , ΔS_c°) menunjukkan bahawa proses kompleks $L_1\text{Br}$ dalam semua kes didapati bukan kestabilan entalpi, tetapi kestabilan entropi. Nilai kiraan ΔG_c° yang negatif membuktii bahawa keupayaan $L_1\text{Br}$ untuk membentuk kompleks yang stabil dengan kation logam serta prosesnya adalah secara spontan. Data eksperimen telah diuji dengan menggunakan program rangkaian neural tiruan (ANN) dan menunjukkan persamaan dengan data yang dianggarkan. Pengiraan berdasarkan teori fungsi ketumpatan (DFT) digunakan untuk meramalkan keupayaan mengikat logam kompleks. Gabungan daripada kesemua data yang diperolehi, mendapati bahawa keupayaan $L_1\text{Br}$ membentuk kompleks dengan kation logam adalah dalam turutan $\text{Ni}^{2+} < \text{Pd}^{2+} < \text{Zn}^{2+} < \text{Hg}^{2+} < \text{Ag}^+$. Seterusnya, penderia potentiometrik *self-plasticizing* polipirol baru telah dihasilkan berdasarkan $L_1\text{Br}$ sebagai *ionophore* untuk mengesan kation Hg^{2+} dan Ag^+ . Komposisi membran optimum bagi elektrod telah didapati dengan menggunakan 89.4 wt.% monomer (pirol), 4.8 wt.% *photoinitiator* (DMPP), 0.2 wt.% garam *lipophilic* (NaTFB), and 5.6 wt.% *ionophore* ($L_1\text{Br}$). Penderia ini masing-masing telah menunjukkan kecerunan Nernstian yang baik iaitu $28.10 \pm 0.29 \text{ mV/dekad}$ dan $58.61 \pm 1.12 \text{ mV/dekad}$ dengan julat kerja $1.0 \times 10^{-6} - 1.0 \times 10^{-2} \text{ M}$ dan $1.0 \times 10^{-5} - 1.0 \times 10^{-1} \text{ M}$ untuk kation Hg^{2+} dan Ag^+ . Kedua-dua elektrod menunjukkan pencapaian yang memuaskan dalam julat pH yang luas dan masa tindak balas yang singkat iaitu kira-kira 20 s dengan kebolehulangan yang baik. Elektrod yang dicadangkan boleh digunakan dalam tempoh masa 30 (Hg-ISE) dan 50 (Ag-ISE) hari tanpa menunjukkan sebarang perubahan ketara dalam julat kerja kepekatan, kecerunan dan masa tindak balas. Ia juga tidak menujukkan sebarang gangguan yang signifikan dalam keupayaan Hg-ISE dan Ag-ISE yang dicadangkan untuk menentukan kepekatan kation Hg^{2+} dan Ag^+ . Elektrod yang dicadangkan telah berjaya digunakan untuk menentukan pelbagai kepekatan kation Hg^{2+} dan Ag^+ dalam sampel air dan larutan piawai dengan keputusan yang memuaskan. Semua data yang diperolehi membuktikan bahawa Hg-ISE dan Ag-ISE yang dicadangkan dapat digunakan dalam mengesan kation Hg^{2+} dan Ag^+ yang berada di dalam larutan masing-masing. Kompleks merkuri(II) dan perak(I) untuk kesemua garam bis-benzimidazolium yang disintesis telah disediakan untuk memahami koordinasi pembentukan kompleksnya. Koordinasi kompleks garam bis-benzimidazolium dengan kation logam Hg^{2+} dan Ag^+ telah berlaku pada posisi karbene karbonnya dan telah dibuktikan dengan menggunakan data FT-IR dan NMR. Data analisis pembelauan sinar-X kristal tunggal bagi $L_1\text{AgBr}$ dan $L_3\text{HgBr}$ telah membuktikan bahawa geometri koordinasi kompleks adalah tetrahedral.

ACKNOWLEDGEMENTS

All praised to Allah, the Almighty God with His mercy has given me the strength, patience, blessing and the time to complete this study.

Immeasurable appreciation and deepest gratitude for the help and support are extended to the following persons who have contributed in the making this study possible. First, to my supervisors Prof. Dr. Yatimah Alias and Dr. Ninie Suhana Abdul Manan for their patience, supervision, encouragement and thoughtful guidance towards the completion of this thesis. To Dr. Majid Rezayi and Dr. Leila Narimani for their assistance and supplying relevant literature and information. To all group members which have provided kindly help, and support.

I am also indebted to the Universiti Teknologi Mara (UiTM), and Ministry of Education Malaysia for a scholarship to pursue postgraduate study. Thank to University of Malaya Centre for ionic Liquid (UMCiL) and University of Malaya for funding this research and providing instrument facilities.

Last but not least, to my family members especially my mother, Umi Kalthum Jarkasi, my father, Said Portu and my husband, Irwanshah Amanshah for the precious love and support till the end.

TABLE OF CONTENTS

ORIGINAL LITERARY WORK DECLARATION.....	ii
ABSTRACT.....	iii
ABSTRAK	iv
ACKNOWLEDGEMENTS	v
TABLE OF CONTENTS	vi
LIST OF FIGURES	x
LIST OF SCHEMES	xiv
LIST OF TABLES	xv
LIST OF APPENDICES	xvii
LIST OF SYMBOLS AND ABBREVIATIONS	xxii
CHAPTER 1	1
INTRODUCTION	1
1.1 General introduction	1
1.2 Objectives of the research.....	4
1.3 Scope of the research	4
1.4 Thesis outline	5
CHAPTER 2	7
LITERATURE REVIEW.....	7
2.1 N-Heterocyclic carbene (NHC) ligand	7
2.1.1 Bis-N-Heterocyclic carbene (bis-NHC) precursor.....	12
2.2 Different approaches to complexation	14
2.2.1 Complexation study in solution	14
2.2.2 Complexation study by theoretical calculation.....	15
2.2.3 Synthesis of N-heterocyclic carbene (NHC) metal complex	17
2.2.3.1 Complexation of bis-N-heterocyclic carbenes.....	18

2.2.3.2 Coordination of bis-N-heterocyclic carbene mercury(II) and silver(I) complexes.....	19
2.3 Applications of N-heterocyclic carbene (NHC).....	25
2.4 Ion selective electrode (ISE)	32
2.4.1 Sensor fabrication	34
2.4.1.1 Membrane composition	34
2.4.1.2 Fabrication of electrode membrane.....	36
2.4.2 Analyte of interest.....	39
CHAPTER 3.....	44
METHODOLOGY	44
3.1 Chemicals and instruments	44
3.2 Synthesis of bis-NHC precursor	45
3.2.1 Synthesis of <i>N</i> -[(4-methylbenzenesulfonyl)-bis((4-methylbenzenesulfonyl-(oxy))ethyl]amine; (tri-sulfonamide)	47
3.2.2 Synthesis of <i>N,N'</i> -Bis[(benzimidazol-1-yl)ethyl]-4-methylbenzenesulfonamide; (bis-benzimidazole).....	48
3.2.3 Synthesis of bis-benzimidazolium salts	49
3.3 Conductometric study of L ₁ .Br	53
3.4 Fabrication of ion selective electrode (ISE) based on L ₁ .Br ionophore.....	55
3.4.1 Sensor fabrication and optimization	55
3.4.2 Sensor evaluation	55
3.4.3 Effect of pH on electrode performance.....	57
3.4.4 Response time of proposed electrode	57
3.4.5 Repeatability, reproducibility and stability of proposed electrode	58
3.4.6 Determination of selectivity coefficients	58
3.4.7 Analytical application of fabricated ISEs	59

3.4.7.1	Potentiometric titration	59
3.4.7.2	Real sample applications.....	59
3.5	Synthesis of metal complexes	60
3.5.1	Synthesis of bis-NHC mercury(II) complexes.....	60
3.5.2	Synthesis of bis-NHC silver(I) complexes.....	65
CHAPTER 4	70
RESULTS AND DISCUSSIONS		70
4.1	Characterizations of bis-benzimidazolium salts	70
4.1.1	Fourier Transfer Infrared (FT-IR) spectroscopy.....	75
4.1.2	Nuclear Magnetic Resonance (NMR) spectroscopy	78
4.1.2.1	^1H -NMR of synthesized compounds	78
4.1.2.2	^{13}C -NMR of synthesis compound.....	81
4.1.3	Single crystal X-ray diffraction.....	82
4.2	Conductometric study of L ₁ .Br	85
4.2.1	Stoichiometry of complex formation	85
4.2.2	Stability constant of complex formation.....	87
4.2.3	Thermodynamic parameter of complexes.....	91
4.2.4	Effect of ionic radius in complex formation	95
4.2.5	Artificial neural network modeling study	96
4.2.6	Theoretical study.....	100
4.3	Fabrication of ion selective electrode (ISE) based on L ₁ .Br ionophore....	102
4.3.1	Optimization of fabricated membranes.....	102
4.3.1.1	Optimization of fabricated membranes in determination of Hg ²⁺	103
4.3.1.2	Optimization of fabricated membranes in determination of Ag ⁺	108
4.3.2	Potentiometric response towards fabricated ISEs.....	110
4.3.3	Characterization of fabricated selective PPy membranes	112

4.3.3.1 Uv-Vis spectroscopy	112
4.3.3.2 Fourier Transfer Infrared (FT-IR) spectroscopy	113
4.3.3.3 Field Emission Scanning Electron Microscopy (FESEM) - Energy-dispersive X-ray (EDX)	115
4.3.3.4 X-ray diffraction (XRD)	118
4.3.4 Optimization of fabricated PPy selective electrodes	119
4.3.4.1 Effect of pH.....	119
4.3.4.2 Response time of proposed electrodes	121
4.3.4.3 Repeatability, reproducibility and stability of proposed electrodes	
.....	123
4.3.5 Sensing mechanism of fabricated ISE	126
4.3.6 Determination of selectivity coefficients	127
4.3.7 Analytical application of fabricated ISEs	129
4.3.7.1 Potentiometric titration	129
4.3.7.2 Real sample application	131
4.3.8 Comparative studies of Hg-ISE and Ag-ISE	133
4.4 Complexation of synthesized bis-benzimidazolium salts	136
CHAPTER 5	150
CONCLUSION AND RECOMMENDATIONS	150
5.1 Conclusion	150
5.2 Recommendations	153
REFERENCES.....	154
SUPPLEMENTARY.....	170
LIST OF PUBLICATIONS.....	170
LIST OF PAPERS PRESENTED	171
APPENDIX.....	172

LIST OF FIGURES

Figure 1.1: Different types of carbenes based on electronic structure.....	1
Figure 1.2: General structure of difference types NHCs ligands.....	2
Figure 2.1: (a-c) the examples of bis-NHC precursor with a different bridging linker (Ashley et al., 2012; Cao et al., 2010; Yagyu et al., 2014)	13
Figure 2.2: Optimal conformation structure obtained from GAUSSIAN 09 program (Gümüş et al., 2014).....	16
Figure 2.3: General structure of formation bis-NHC metal complexes; NHC= N-heterocyclic carbene, M= metal (Liu et al., 2013)	19
Figure 2.4: Examples of crystal structure bis-NHC silver(I) complexes, a to d (Liu Q.-X. et al., 2011a; Liu et al., 2013)	21
Figure 2.5: Examples of crystal structure bis-NHC mercury(II) complexes, e to h (Budagumpi et al., 2012b; Haque et al., 2011; Liu Q.-X. et al., 2011b; Liu et al., 2012)	24
Figure 2.6: Bis-NHC precursor applied in human colon cancer as anti-cancer agents (Haque et al., 2012b).....	27
Figure 2.7: Bis-NHCs silver(I) complexes applied in human colon cancer as anti-cancer agent (Haque et al., 2013; Haque et al., 2012b)	28
Figure 2.8: Structure of synthesized NHCs gold(I) (a and c), and gold(III) (b and d) which used as anti-cancer agent (Sivaram et al., 2012; Sivaram et al., 2013).....	29
Figure 2.9: The structure of anion receptor compound (a, b, c) and the interaction of receptor (a) with chloride anion (d) (Sato et al., 1999).....	30
Figure 2.10: The interaction of bis-NHC complexes with (a) NO_3^- and (b) Ag^+ ions (Liu et al., 2015a; Liu et al., 2015b)	31
Figure 2.11: (a) Fluorescence spectra of bis-NHC metal complex (1×10^{-5} mol/L) upon the addition of the tetrabutyl ammonium salts of F^- , Cl^- , Br^- , I^- , H_2PO_4^- , HSO_4^- , OAc^-	

and NO_3^- (10.0 mol equiv.) in acetonitrile at 25 °C. (b) Fluorescence spectra of bis-NHC metal complex (1×10^{-5} mol/L) upon the addition of salts (30 mol equiv.) of Li^+ , Na^+ , NH_4^+ , Ag^+ , Ca^{2+} , Co^{2+} , Ni^{2+} , Cu^{2+} , Zn^{2+} , Cd^{2+} , Cr^{3+} , Al^{3+} , Pb^{2+} and Hg^{2+} in MeOH at 25 °C (Liu et al., 2015a; Liu et al., 2015b)	32
Figure 2.12: Self-plasticizing acrylic membrane	38
Figure 2.13: The structure of ionophore (a) shift base lariat ether, (b) oxime (Gupta et al., 2009; Sardahan-Koseoglu et al., 2015).....	43
Figure 3.1: The experimental setup for conductometric study	54
Figure 3.2: Diagram of the fabrication electrode membrane	57
Figure 4.1: Molecular structure of N -[(4-methylbenzenesulfonyl)-bis((4-methylbenzenesulfonyl-(oxy))ethyl)amine; (tri-sulfonamide)	70
Figure 4.2: Molecular structure of N,N' -Bis[(benzimidazol-1-yl)ethyl]-4-methylbenzenesulfonamide; (bis-benzimidazole).....	72
Figure 4.3: Molecular structures of synthesized bis-benzimidazolium salts	73
Figure 4.4: Ortep diagram of the molecule structure of benzimidazolium salt (L_1Br).84	
Figure 4.5: Ortep diagram of the molecule structure of benzimidazolium salt (L_1PF_6)	84
Figure 4.6: Plot of molar conductance, Λ_m versus mole ration, $[\text{L}_1\text{Br}]_t/[\text{M}^{n+}]_t$ for the binding of Ag^+ , Hg^{2+} , Ni^{2+} , Pd^{2+} and Zn^{2+} with L_1Br in pure MeOH at 25 °C	87
Figure 4.7: Stability constant ($\log K_f$) of complexes in MeOH-H ₂ O binary system (mol% MeOH; 0.00, 9.99, 22.66, 39.73, 63.72 and 100.00%) at different temperature (♦ = 15 °C, ■= 25 °C, ▲ =35 °C, ●= 45 °C) for Ag^+ cation	91
Figure 4.8: Van't Hoff plot for $\text{L}_1\text{Br}-\text{M}^{n+}$ complex for Ag^+ in MeOH-H ₂ O binary system at different temperatures	92
Figure 4.9: Plot of ΔH_C^o (kJ/mol) versus $T\Delta S_C^o$ (kJ/mol) for $\text{L}_1\text{Br}-\text{M}^{n+}$ ($\text{M}=\text{Ni}^{2+}$, Pd^{2+} , Zn^{2+} , Hg^{2+} and Ag^+) in different MeOH-H ₂ O binary systems ($R^2=0.9537$).....	95

Figure 4.10: Changes of stability constant ($\log K_f$) of $L_1\cdot Br$ with all metal cation in MeOH-H ₂ O binary at 25 °C	96
Figure 4.11: Structure of neural network adopted in this study.....	97
Figure 4.12: Comersion of estimated $\log K_f$ with experimental data (A) training data set and (B) test data set	98
Figure 4.13: Surface and contour plots of the stability constant ($\log K_f$) as a function of the mol% of water and ionic radius of cations (Ni^{2+} , Pd^{2+} , Zn^{2+} , Hg^{2+} and Ag^+).....	99
Figure 4.14: Optimal conformation structures obtained from GAUSSIAN 09 program for (a) $L_1\cdot Br$ ligand, (b) $L_1\cdot Br-Zn^{2+}$ and (c) $L_1\cdot Br-Ag^+$ complexes.....	101
Figure 4.15: Nyquist and phase plots of the impedance spectra recorded for fresh electrode membranes (a) without, E6 (b) with NaTFB additive, E3 and (c) without $L_1\cdot Br$ ionophore, E5, (Z_{im} = impedance imagine; Z_{re} =impedance real; f= frequency; R_s = resistance; R_{ct} = charge transfer resistance; Q= quality factor)	106
Figure 4.16: Calibration plot of the optimized Hg^{2+} ion-selective sensor	107
Figure 4.17: Calibration plot of the optimized Ag^+ ion-selective sensor	110
Figure 4.18: The potential responses of (A) Hg-ISE and (B) Ag-ISE membrane electrodes based on $L_1\cdot Br$ ionophore towards various metal cations.....	111
Figure 4.19: UV-Vis absorption spectra of (A) $HgCl_2$ solution 1.0×10^{-4} M (Hg^{2+}), ionophore solution 1.0×10^{-4} M ($L_1\cdot Br$) and 1:1 (V/V) mixture of ionophore and Hg^{2+} solution ($L_1\cdot Br-Hg$), and (B) $AgNO_3$ solution 1.0×10^{-4} M (Ag^+), ionophore solution 1.0×10^{-4} M ($L_1\cdot Br$) and 1:1 (V/V) mixture of ionophore and Ag^+ solution ($L_1\cdot Br-Ag$)	113
Figure 4.20: FT-IR spectra for $L_1\cdot Br$ ionophore, optimized PPy membrane after use (Hg-ISE), and optimized PPy membrane after use (Ag-ISE)	114
Figure 4.21: FESEM micrographs of optimized membrane: (A) HEMA-inner layer, (B) Hg-ISE fresh optimized PPy membrane before, (B1) after used and (C) Ag-ISE fresh optimized PPy membrane before, (C1) after used	116

Figure 4.22: EDX spectrum of optimized membrane electrode for (A) fresh and after conditioning in (B) Hg^{2+} and (C) Ag^+ solutions.....	117
Figure 4.23: X-Ray diffraction pattern of proposed membrane sensor for (A) Hg-ISE and (B) Ag-ISE before and after used.....	118
Figure 4.24: Effect of pH test solutions on the response of the proposed (A) Hg-ISE and (B) Ag-ISE in different concentrations	120
Figure 4.25: Dynamic response time of the (A) Hg-ISE and (B) Ag-ISE for the step changes in metal cations test solution from low to high concentration	122
Figure 4.26: Stability response of (A) Hg-ISE and (B) Ag-ISE	125
Figure 4.27: (a) Ionophore in neutral, deprotonated and complex form; (b and c) schematic diagram of the composition of membrane with an ionophore and cationic sites in contact with sample solution at different pH values. The boxes= membrane phases; $\text{M}^{\text{n}+}$ = targated metal cation; H^+ = hydrogen ion; R^+ = lipophilic ionic salts; L_1Br : and L_1Br = ionophore in deprotonated and neutral form, respectively; $\text{L}_1\text{Br}\text{-M}^{\text{n}+}$ =the complexes of primary ion with respective ionophore	127
Figure 4.28: Potentiometric titration curve of (A) 25 ml 1.0×10^{-4} M, Hg^{2+} solution with 1.0×10^{-3} M EDTA and (B) 20.0 ml 5.0×10^{-2} M, Ag^+ solution with NaCl (1.0×10^{-1} M) by using the proposed sensor as an indicator electrode	131
Figure 4.29: Structure of bis-NHC mercury(II) complexes.....	138
Figure 4.30: Structure of bis-NHC silver(I) complexes.....	139
Figure 4.31: Absorbance spectra of (A) bis-benzimidazolium salts, (B) bis-NHC mercury(II) metal complexes and (C) bis-NHC silver(I) metal complexes.....	145
Figure 4.32: Ortep diagram of the molecule structure of L_1AgBr complex	148
Figure 4.33: Ortep diagram of the molecule structure of L_3HgBr complex	148

LIST OF SCHEMES

Scheme 2.1: The formation of free carbene for different types of ring; (a) 4-membered, (b) 6-membered, and (c) 7-membered (Alder et al., 1999; Despagnet-Ayoub et al., 2004; Iglesias et al., 2007)	10
Scheme 2.2: Synthesis routes in the preparation of imidazolium salts; (a) alkylation reaction, (b-e) ring closing reaction (Arduengo, 1992; Jazza et al., 2006; Kuhn et al., 2008)	11
Scheme 2.3: Synthesis of 2,6-bis[(3-benzylbenzimidazolium-1-yl)methyl]pyridine dibromide (Budagumpi et al., 2012b)	12
Scheme 2.4: The general synthesis routes for NHCs metal complexes	18
Scheme 2.5: Examples of catalytic reaction which use bis-NHC metal complexes as catalyst, (a) Mirozuki-Heck, (b) Hydrovinylation, and (c) Suzuki-Miyaura reactions (Liu et al., 2012; Saito et al., 2011; Serra et al., 2011)	26
Scheme 3.1: Synthesis routes in the preparation of bis-benzimidazolium salts.....	46
Scheme 3.2: Synthesis route in the preparation of bis-NHC mercury(II) complexes....	61
Scheme 3.3: Synthesis route in the preparation of bis-NHC silver(I) complexes.....	66
Scheme 4.1: The proposed mechanism of complex reaction between bis-benzimidazolium salts and mercury(II)	137

LIST OF TABLES

Table 2.1: Summary of bond distances and bond angles of bis-NHC silver(I) complexes	22
Table 2.2: Summary of bond distances and bond angles of bis-NHC mercury(II) complexes	25
Table 2.3: The applications of potentiometric ISE in determination of various analytes	34
Table 2.4: The comparative evaluation of selective electrode, responsive with mercury(II) and silver(I)	41
Table 3.1: The different composition of ISE membrane based on L ₁ .Br ionophore for the potentiometric detection of metal cations	56
Table 4.1: General characteristic of bis-benzimidazolium salts (bis-NHC precursor) ..	74
Table 4.2: The significant of FT-IR absorption bands (cm ⁻¹) for synthesized compounds, (types of absorption bands; w= weak, m= medium, s= strong)	77
Table 4.3: Crystal data and structures refinement for L ₁ .Br and L ₁ .PF ₆	83
Table 4.4: The log K _f values of L ₁ .Br-M ⁿ⁺ in MeOH-H ₂ O binary mixtures at different temperatures for studied metal cations.....	89
Table 4.5: Summary of thermodynamic parameters values of the L ₁ .Br-M ⁿ⁺ complexes in MeOH-H ₂ O binary mixture solvent.....	93
Table 4.6: The calculated binding energies ΔE, in the formation of L ₁ .Br-M ⁿ⁺ by DFT method, where E _{L₁.Br} is -1969.8454 (Hartree)	102
Table 4.7: The compositions of ISE membrane used based on L ₁ .Br ionophore for the potentiometric detection of Hg ²⁺	104
Table 4.8: Impedance parameters for electrodes E3, E6 and E5 as determinate using the equivalent circuit presented in Figure 4.15	107

Table 4.9: The compositions of ISE membrane used based on L ₁ .Br ionophore for the potentiometric detection of Ag ⁺	109
Table 4.10: Different concentrations of NaNO ₃ added in the Ag ⁺ test solution	110
Table 4.11: The repeatability and reproducibility studies of optimize composition membrane electrodes.....	123
Table 4.12: Selectivity coefficient values of various cations for the proposed Hg-ISE	128
Table 4.13: Selectivity coefficient of various ions for the proposed Ag-ISE	129
Table 4.14: Potentiometric determination of Hg ²⁺ in different samples by using proposed electrode	132
Table 4.15: Potentiometric determination of Ag ⁺ in different samples by using proposed electrode	133
Table 4.16: Comparison of fabricated electrode based on PVC membrane by using different type of ionophore	135
Table 4.17: General characteristic of bis-NHC metal complexes.....	140
Table 4.18: The significant of FT-IR absorption bands (cm ⁻¹) for synthesized bis-NHC mercury(II) complexes, (types of absorption bands; w= weak, m= medium, s= strong)	142
Table 4.19: The significant of FT-IR absorption bands (cm ⁻¹) for synthesized bis-NHC silver(I) complexes, (types of absorption bands; w= weak, m= medium, s= strong) ...	143
Table 4.20: Crystal data and structures refinement for L ₁ .AgBr and L ₃ .HgBr complexes	147

LIST OF APPENDICES

APPENDIX A1: FT-IR spectrum of <i>N</i> -[(4-methylbenzenesulfonyl)-bis-((4methylbenzenesulfonyl)-(oxy))ethyl]amine; (tri-sulfonamide)	172
APPENDIX A2: FT-IR spectrum of <i>N,N'</i> -Bis[(benzimidazo-1-yl)ethyl]-4-methylbenzenesulfonamide; (bis-benzimidazole).....	173
APPENDIX A3: FT-IR spectrum of <i>N,N'</i> -Bis[1-benzyl-benzimidazolium-ethyl]-4-methylbenzenesulfonamide dibromide (L ₁ .Br).....	173
APPENDIX A4: FT-IR spectrum of <i>N,N'</i> -Bis[4-nitro-1-benzyl-benzimidazolium-ethyl]-4-methylbenzenesulfonamide dibromide (L ₂ .Br).....	174
APPENDIX A5: FT-IR spectrum of <i>N,N'</i> -Bis[4-chloro-1-benzyl-benzimidazolium-ethyl]-4-methylbenzenesulfonamide dibromide (L ₃ .Br).....	174
APPENDIX A6: FT-IR spectrum of <i>N,N'</i> -Bis[1-benzyl-benzimidazolium-ethyl]-4-methylbenzenesulfonamide dihexafluorophosphate (L ₁ .PF ₆).....	175
APPENDIX A7: FT-IR spectrum of <i>N,N'</i> -Bis[4-nitro-1-benzyl-benzimidazolium-ethyl]-4-methylbenzenesulfonamide dihexafluorophosphate (L ₂ .PF ₆).....	175
APPENDIX A8: FT-IR spectrum of <i>N,N'</i> -Bis[4-chloro-1-benzyl-benzimidazolium-ethyl]-4-methylbenzenesulfonamide dihexafluorophosphate (L ₃ .PF ₆).....	176
APPENDIX B1: ¹ H-NMR spectrum of <i>N</i> -[(4-methylbenzenesulfonyl)-bis-((4methylbenzenesulfonyl)-(oxy))ethyl]amine; (tri-sulfonamide)	177
APPENDIX B2: ¹ H-NMR spectrum of <i>N,N'</i> -Bis[(benzimidazo-1-yl)ethyl]-4-methylbenzenesulfonamide; (bis-benzimidazole).....	178
APPENDIX B3: ¹ H-NMR spectrum of <i>N,N'</i> -Bis[1-benzyl-benzimidazolium-ethyl]-4-methylbenzenesulfonamide dibromide (L ₁ .Br).....	179
APPENDIX B4: ¹ H-NMR spectrum of <i>N,N'</i> -Bis[4-nitro-1-benzyl-benzimidazolium-ethyl]-4-methylbenzenesulfonamide dibromide (L ₂ .Br).....	180

APPENDIX B5: ^1H -NMR spectrum of <i>N,N'</i> -Bis[4-chloro-1-benzyl-benzimidazolium-ethyl]-4-methylbenzenesulfonamide dibromide (L_3Br).....	181
APPENDIX B6: ^1H -NMR spectrum of <i>N,N'</i> -Bis[1-benzyl-benzimidazolium-ethyl]-4-methylbenzenesulfonamide dihexafluorophosphate (L_1PF_6).....	182
APPENDIX B7: ^1H -NMR spectrum of <i>N,N'</i> -Bis[4-nitro-1-benzyl-benzimidazolium-ethyl]-4-methylbenzenesulfonamide dihexafluorophosphate (L_2PF_6).....	183
APPENDIX B8: ^1H -NMR spectrum of <i>N,N'</i> -Bis[4-chloro-1-benzyl-benzimidazolium-ethyl]-4-methylbenzenesulfonamide dihexafluorophosphate (L_3PF_6).....	184
APPENDIX C1: ^{13}C -NMR spectrum of <i>N</i> -[(4-methylbenzensulfonyl)-bis((4methylbenzenesulfonyl)-(oxy))ethyl]amine; (tri-sulfonamide)	185
APPENDIX C2: ^{13}C -NMR spectrum of <i>N,N'</i> -Bis[(benzimidazo-1-yl)ethyl]-4-methylbenzenesulfonamide; (bis-benzimidazole).....	186
APPENDIX C3: ^{13}C -NMR spectrum of <i>N,N'</i> -Bis[1-benzyl-benzimidazolium-ethyl]-4-methylbenzenesulfonamide dibromide (L_1Br).....	187
APPENDIX C4: ^{13}C -NMR spectrum of <i>N,N'</i> -Bis[4-nitro-1-benzyl-benzimidazolium-ethyl]-4-methylbenzenesulfonamide dibromide (L_2Br).....	188
APPENDIX C5: ^{13}C -NMR spectrum of <i>N,N'</i> -Bis[4-chloro-1-benzyl-benzimidazolium-ethyl]-4-methylbenzenesulfonamide dibromide (L_3Br).....	189
APPENDIX C6: ^{13}C -NMR spectrum of <i>N,N'</i> -Bis[1-benzyl-benzimidazolium-ethyl]-4-methylbenzenesulfonamide dihexafluorophosphate (L_1PF_6).....	190
APPENDIX C7: ^{13}C -NMR spectrum of <i>N,N'</i> -Bis[4-nitro-1-benzyl-benzimidazolium-ethyl]-4-methylbenzenesulfonamide dihexafluorophosphate (L_2PF_6).....	191
APPENDIX C8: ^{13}C -NMR spectrum of <i>N,N'</i> -Bis[4-chloro-1-benzyl-benzimidazolium-ethyl]-4-methylbenzenesulfonamide dihexafluorophosphate (L_3PF_6).....	192

APPENDIX D1: Crystallographic data for <i>N,N'</i> -Bis[1-benzyl-benzimidazolium-ethyl]-4-methylbenzenesulfonamide dibromide ($L_1\text{.Br}$)	193
APPENDIX D2: Crystallographic data for <i>N,N'</i> -Bis[1-benzyl-benzimidazolium-ethyl]-4-methylbenzenesulfonamide dihexafluorophosphate ($L_1\text{.PF}_6$)	217
APPENDIX E1: Plot of molar conductance, Λ_m versus mole ratio, $[L_1\text{.Br}]_t/[M^{n+}]_t$ for Ag^+	229
APPENDIX E2: Plot of molar conductance, Λ_m versus mole ratio, $[L_1\text{.Br}]_t/[M^{n+}]_t$ for Hg^{2+}	230
APPENDIX E3: Plot of molar conductance, Λ_m versus mole ratio, $[L_1\text{.Br}]_t/[M^{n+}]_t$ for Ni^{2+}	231
APPENDIX E4: Plot of molar conductance, Λ_m versus mole ratio, $[L_1\text{.Br}]_t/[M^{n+}]_t$ for Pd^{2+}	232
APPENDIX E5: Plot of molar conductance, Λ_m versus mole ratio, $[L_1\text{.Br}]_t/[M^{n+}]_t$ for Zn^{2+}	233
APPENDIX F1: Matematical model applied for the curve fitting using GENPLOT software	234
APPENDIX G1: Stability constant ($\log K_f$) of complexes in MeOH-H ₂ O binary solvent system (mol% MeOH; 0.00, 9.99, 22.66, 39.73, 63.72 and 100.00%) at different temperatures ($\blacklozenge = 15^\circ\text{C}$, $\blacksquare = 25^\circ\text{C}$, $\blacktriangle = 35^\circ\text{C}$, $\bullet = 45^\circ\text{C}$) for Hg^{2+} , Ni^{2+} , Pd^{2+} and Zn^{2+}	237
APPENDIX H1: Van't Hoff plot for $L_1\text{.Br}\text{-}M^{n+}$ complex for Hg^{2+} , Ni^{2+} , Pd^{2+} and Zn^{2+} cations in MeOH-H ₂ O binary solvent system (mol% MeOH; $\blacklozenge = 100$, $\blacksquare = 63.72$, $\blacktriangle = 39.73$, $\times = 22.66$, $\divideontimes = 9.90$, $\bullet = 0.00$) at different temperatures.....	238

APPENDIX I1: FT-IR spectrum of L ₁ .HgBr	239
APPENDIX I2: FT-IR spectrum of L ₂ .HgBr	239
APPENDIX I3: FT-IR spectrum of L ₃ .HgBr	240
APPENDIX I4: FT-IR spectrum of L ₁ .HgPF ₆	240
APPENDIX I5: FT-IR spectrum of L ₂ .HgPF ₆	241
APPENDIX I6: FT-IR spectrum of L ₃ .HgPF ₆	241
APPENDIX I7: FT-IR spectrum of L ₁ .AgBr	242
APPENDIX I8: FT-IR spectrum of L ₂ .AgBr	242
APPENDIX I9: FT-IR spectrum of L ₃ .AgBr	243
APPENDIX I10: FT-IR spectrum of L ₁ .AgPF ₆	243
APPENDIX I11: FT-IR spectrum of L ₂ .AgPF ₆	244
APPENDIX I12: FT-IR spectrum of L ₃ .AgPF ₆	244
APPENDIX J1: ¹ H-NMR spectrum of L ₁ .HgBr	245
APPENDIX J2: ¹ H-NMR spectrum of L ₂ .HgBr	246
APPENDIX J3: ¹ H-NMR spectrum of L ₃ .HgBr	247
APPENDIX J4: ¹ H-NMR spectrum of L ₁ .HgPF ₆	248
APPENDIX J5: ¹ H-NMR spectrum of L ₂ .HgPF ₆	249
APPENDIX J6: ¹ H-NMR spectrum of L ₃ .HgPF ₆	250
APPENDIX J7: ¹ H-NMR spectrum of L ₁ .AgBr	251
APPENDIX J8: ¹ H-NMR spectrum of L ₂ .AgBr	252
APPENDIX J9: ¹ H-NMR spectrum of L ₃ .AgBr	253
APPENDIX J10: ¹ H-NMR spectrum of L ₁ .AgPF ₆	254
APPENDIX J11: ¹ H-NMR spectrum of L ₂ .AgPF ₆	255
APPENDIX J12: ¹ H-NMR spectrum of L ₃ .AgPF ₆	256

APPENDIX K1: ^{13}C -NMR spectrum of L ₁ .HgBr	257
APPENDIX K2: ^{13}C -NMR spectrum of L ₂ .HgBr	258
APPENDIX K3: ^{13}C -NMR spectrum of L ₃ .HgBr	259
APPENDIX K4: ^{13}C -NMR spectrum of L ₁ .HgPF ₆	260
APPENDIX K5: ^{13}C -NMR spectrum of L ₂ .HgPF ₆	261
APPENDIX K6: ^{13}C -NMR spectrum of L ₃ .HgPF ₆	262
APPENDIX K7: ^{13}C -NMR spectrum of L ₁ .AgBr	263
APPENDIX K8: ^{13}C -NMR spectrum of L ₂ .AgBr	264
APPENDIX K9: ^{13}C -NMR spectrum of L ₃ .AgBr	265
APPENDIX K10: ^{13}C -NMR spectrum of L ₁ .AgPF ₆	266
APPENDIX K11: ^{13}C -NMR spectrum of L ₂ .AgPF ₆	267
APPENDIX K12: ^{13}C -NMR spectrum of L ₃ .AgPF ₆	268
APPENDIX L1: Crystallographic data for L ₁ .AgBr	269
APPENDIX L2: Crystallographic data for L ₃ .HgBr	285

LIST OF SYMBOLS AND ABBREVIATIONS

ΔG	Gibbs energy
ΔH	Enthalpy
ΔS	Entropy
Λ_m	Molar conductivity
ϵ	Dielectric constant
Aliph	Aliphatic
ANN	Artificial neural network
Ar	Aromatic
BF_4^-	Tetrafluoroborate
CDCl_3	Deuterated chloroform
CH_2Cl_2	Dichloromethane
CHNS	Carbon hydrogen nitrogen sulfur
Cy	Cyclohexyl
DFT	Density functional theory
DMPP	2,2-dimethoxy-2-phenylacetophenone
DMSO	Dimethyl sulfoxide
DMSO- d_6	Deuterated dimethyl sulfoxide
DN	Donor number
EDTA	Ethylenediaminetetraacetic acid
EIS	Electrochemical impedance spectroscopy
Et	Ethyl
Et_3NHCl	Triethylamine hydrochloride
EtOH	Ethanol

FESEM-EDX	Field emission scanning electron microscopy-energy-dispersive X-ray
FT-IR (ATR)	Fourier transform infrared (attenuated total reflectance)
HC(OEt) ₃	Triethyl orthoformate
H ₃ PO ₄	Phosphoric acid
HCl	Hydrochloric acid
<i>i</i> -Pr	Isopropyl
(<i>i</i> -Pr) ₂ NPCl ₂	(Diisopropyl-amino)-dichloro-phosphene
ISE	Ion selective electrode
IUPAC	International union of pure and applied chemistry
KN(SiMe ₃) ₂	Potassium bis-(trimethylsilyl)amide
KOH	Potassium hydroxide
LiSO ₄	Lithium sulphate
LDA	Lithium diiodopropylamide
Log <i>K_f</i>	Stability constant
m.p	Melting point
Mes	Mesityl
MesLi	Mesityl lithium
n-Bu	n-butyl
NaHCO ₃	Sodium bicarbonate
NaN(SiMe ₃) ₂	Sodium bis-(trimethylsilyl)amide
NaTFB	Sodium tetrafluoroborate
NH ₃	Ammonia
NH ₄ BF ₄	Ammonium tetrafluoroborate
NH ₄ Cl	Ammonium chloride
NHC	N-heterocyclic carbene

NMR	Nuclear magnetic resonance
OTF	Trifluoromethanesulfonate
Ome	Methoxy
p-TSCl	<i>p</i> -toluenesulfonyl chloride
pHEMA	Poly(2-hydroxyethyl methylacrylate)
PF ₆	Hexafluorophosphate
PPy	Polypyrrole
PVC	Polyvinylchloride
r.t	Room temperature
RSD	Relative standard deviation
SSM	Separation solution method
THF	Tertrahydrofuran
TMSOTF	Trimethylsilyl-trifluoromethanesulfonate
UV	Ultra violate
XRD	X-ray diffraction

CHAPTER 1

INTRODUCTION

1.1 General introduction

Carbenes are defined as molecules containing a neutral carbon atom with a pair of unshared valence electrons with a general formula of R=C: or R-(C:)-R', where its divalent carbon atom has only six valence electrons. As illustrated in Figure 1.1, different types of carbenes are classified as either singlet or triplet depending on their electronic structure. A singlet carbene is spin-paired and based on valence bond theory; the molecule adopts a sp^2 hybrid structure. While, triplet carbenes have two unpaired electrons which can be either linear or bent (Hahn et al., 2008).

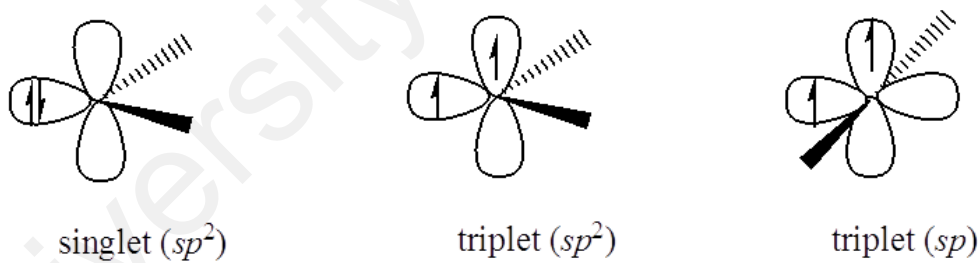


Figure 1.1: Different types of carbenes based on electronic structure

The majority of carbenes are short-lived reactive intermediates. This situation does not account for singlet N-heterocyclic carbenes (NHCs) with the carbene being incorporated in a nitrogen-containing heterocycle molecule (Cazin, 2010). NHCs can be classified as four-membered, five-membered, six-membered, and seven-membered as shown in Figure 1.2. Among of the mentioned types, five-membered NHC ligands are

the most commonly used in complexation with metal ions due to their high stability (Cazin, 2010; Hahn et al., 2008).

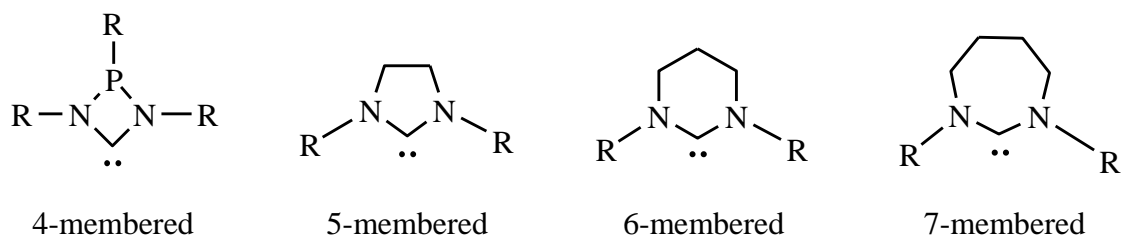


Figure 1.2: General structure of difference types NHCs ligands

Five-membered NHCs have been used widely as a spectator ligands in organometallic chemistry. This type of ligands can be synthesized from imidazole, pyrazole, triazole, and also tetrazole. The NHCs synthesized from imidazole and benzimidazole were found as attractive ligands for complexation due to the structures variety and stability (Haque et al., 2011). Besides, the NHCs are more stable than other types of carbenes, including the Fisher carbenes and Schrock carbenes (Crudden et al., 2004). These ligands can be bonded to either hard or soft transition metal ions or atoms through strong chelation (Budagumpi et al., 2012a). NHCs behave like a typical σ -donor ligands that can substitute classical 2-electrons donor ligands such as amines, ethers and phosphines in metal coordination chemistry. In addition, it is proven that NHCs acts as a better donor compound as compared to the phosphine donor ligand (Díez-González et al., 2007; Herrmann, 2002). Due to such ability, the NHC ligands are emerging as a new class of versatile ancillary ligands in organic chemistry, and use as a replacement for phosphine ligand in numerous applications (Crabtree, 2005).

NHC metal complexes have been applied as catalyst in various organic reactions such as Mirozuki-Heck, Suzuki-Miyaura, Sonongashira, Stille, Kumada and etc. (Liu et al., 2012; Saito et al., 2011; Serra et al., 2011; Valente et al., 2012). The NHCs and their complexes were also demonstrated as anti-cancer agents, representing superior

cytotoxicity effect (Haque Rosenani A et al., 2013; Haque et al., 2012b; Sivaram et al., 2012; Sivaram et al., 2013). In the sensor application, NHCs act as a recognition element which is important factor for the determination of the selectivity of a target ion. Liu and his co-workers developed NHC based chemosensor to determine nitrite anion and silver(I) cation based on fluorescent and UV-Vis spectroscopic titration (Liu et al., 2015a; Liu et al., 2015b). However, the chemosensors has several disadvantages. For example, they require organic solvent for detection, possess complicated synthetic protocol and low sensitivity (Kim et al., 2012; Wang et al., 2014).

Numerous research works have been conducted on the development of NHCs and its metal complexes, but the research works on its application as sensor has yet been well studied, especially as ionophore in ion selective electrode (ISE). The sensor based on potentiometric ISE plays an important role in the sensing application of transition metal cation in various research areas, such as clinical analyses (El-Dien et al., 2012; Mandil et al., 2013), environmental control and industrial processes (Nanda et al., 2007; Radu et al., 2013). The ISE offers advantages like simplicity, good precision, selectivity, sensitivity, low cost and allows direct on-line monitoring of concentration selected species without any pretreatment (Yan et al., 2013).

In the fabrication of ISE electrode, the choice of ionophore as a recognition element is an important factor for determining the selectivity of a particular ion among the other ions in a solution (Abraham et al., 2015; Rezayi et al., 2014). For this reason, the synthesis of novel molecular ionophores which selectively recognizes ionic species brings great attention in the ISE studies. Regarding the ability of NHCs as mentioned earlier, the applications of NHCs as an ionophore in ISE area can be explored. Thus,

this reason encourages us to develop an ISE for the detection of transition metal cations based on bis-N-heterocyclic carbene (bis-NHC).

1.2 Objectives of the research

The main focus of this research is to examine the potential of bis-NHC which is synthesized from benzimidazolium group as a recognition element in potentiometric ISE application. The objectives are as follows:

- i. To develop new class of bis-NHC based on benzimidazolium compounds.
- ii. To conduct a conductometric study of the bis-benzimidazolium salt on targeted transition metal cations.
- iii. To fabricate and optimize a potentiometric ion-selective electrodes (ISEs) sensor.
- iv. To synthesis a metal complexes with bis-NHC compounds.

1.3 Scope of the research

This study involves the synthesis and characterization of six new bis-benzimidazolium salts namely $L_1\text{Br}$, $L_2\text{Br}$, $L_3\text{Br}$, $L_1\text{PF}_6$, $L_2\text{PF}_6$ and $L_3\text{PF}_6$. The characterization of all bis-benzimidazolium salts and its complexes includes the used of CHN elemental analysis, FT-IR, NMR, UV-Vis and single crystal X-ray diffraction analysis.

The conductometric study of $L_1\text{Br}$ with selected transition metal ions has been conducted. The purpose of this study is to investigate the influence of solvent system,

temperature and cationic radius of ligand towards selective complexation of L₁.Br. The ANN program was used as an alternative to obtain a model between independent and dependent variables of the raw thermodynamic data. The computational study of L₁.Br and its complexes with metal cations were carried out by using the GAUSSIAN 09 program.

The synthesis of L₁.Br was used as a novel ionophore in the construction of ISE membrane for detection of targeted Hg²⁺ and Ag⁺ metal cations. The characterization of fabricated selective membrane electrode was done by using UV-Vis, FT-IR, FESEM, EDX, and XRD. While the study of the stability, selectivity, life time, working range, effect of pH, and optimum composition for electrode were conducted in separate experiments.

Finally, in order to understand the coordination of Hg²⁺ and Ag⁺ with synthesized ligand, their corresponding metal complexes were synthesized and characterized using FT-IR, NMR, CHN elemental analysis, UV-Vis and crystal structure X-ray diffraction analysis instrument.

1.4 Thesis outline

This thesis is divided into five chapters which consist of:

Chapter 1 mentions the main purpose of this dissertation which is to synthesis bis-NHC and their applications as ionophores for developing the novel potentimetric ISEs with enhanced the selectivity and sensitivity.

Chapter 2 presents the background of NHC and their metal complexes, followed by applications in various studies. The complexation study, potentiometric ISE function and applications are also listed.

Chapter 3 describes the methodologies used in the design of the experiments, separated into four main sections.

Chapter 4 discusses the successful synthesis of new bis-benzimidazolium salts. It also includes the discussion about significant results such as stoichiometry, stability constant (K_f), and thermodynamic parameter ($\Delta G_C^o, \Delta H_C^o, \Delta S_C^o$) obtained from conductometric study. The fabrication of new potentiometric ISE for detection of Hg^{2+} and Ag^+ cations is also reported. Finally, the successful synthesis of mercury(II) and silver(I) bis-NHC metal complexes is also presented in this chapter.

Chapter 5 summarizes the main conclusions of this thesis and presents an outlook for future work.

CHAPTER 2

LITERATURE REVIEW

2.1 N-Heterocyclic carbene (NHC) ligand

In early 1960s, Wanzlick and Schönherr were pioneer scientists that conveyed NHC complexation to gain general acceptance among researchers (Wanzlick et al., 1968). NHCs are often compared to (tertiary) phosphines because both are strong σ -donor and exhibit poor π -acceptor properties. NHCs are however even stronger σ -donors than tertiary phosphines (Budagumpi et al., 2012b). This accounts for the fact that the metal-carbene bond is stronger and shorter than the bonds encountered in metal-phosphine complexes. This leads to NHC complexes having a higher thermal stability than phosphine complexes. Besides, NHC complexes also exhibit better stability towards oxygen and moisture, as especially trialkyl phosphines tend to be sensitive to oxidation (Clavier et al., 2007).

The NHC ligands are classified to several types based on their rings, such as 4-membered, 5-membered, 6-membered and 7-membered. The synthesis routes of NHCs are illustrated in Scheme 2.1 and Scheme 2.2. Despagnet-Ayoub et al. (2004) first synthesized a stable 4-membered NHC as shown in Scheme 2.1 (a). The iminium salt (a2) was prepared in yield of 66% from the silylamidine (a1) as a white powder by the addition of $(i\text{-Pr})_2\text{NP}\text{Cl}_2$ and TMSOTF in CH_2Cl_2 solvent at room temperature. Followed by the reaction of (a2) under standard condition, carbene (a3) was generated. Alder et al. (1999) reported the first stable 6-membered NHC as showed in Scheme 2.1 (b). Precursor (b1) is conveniently made by refluxing an equimolar mixture of

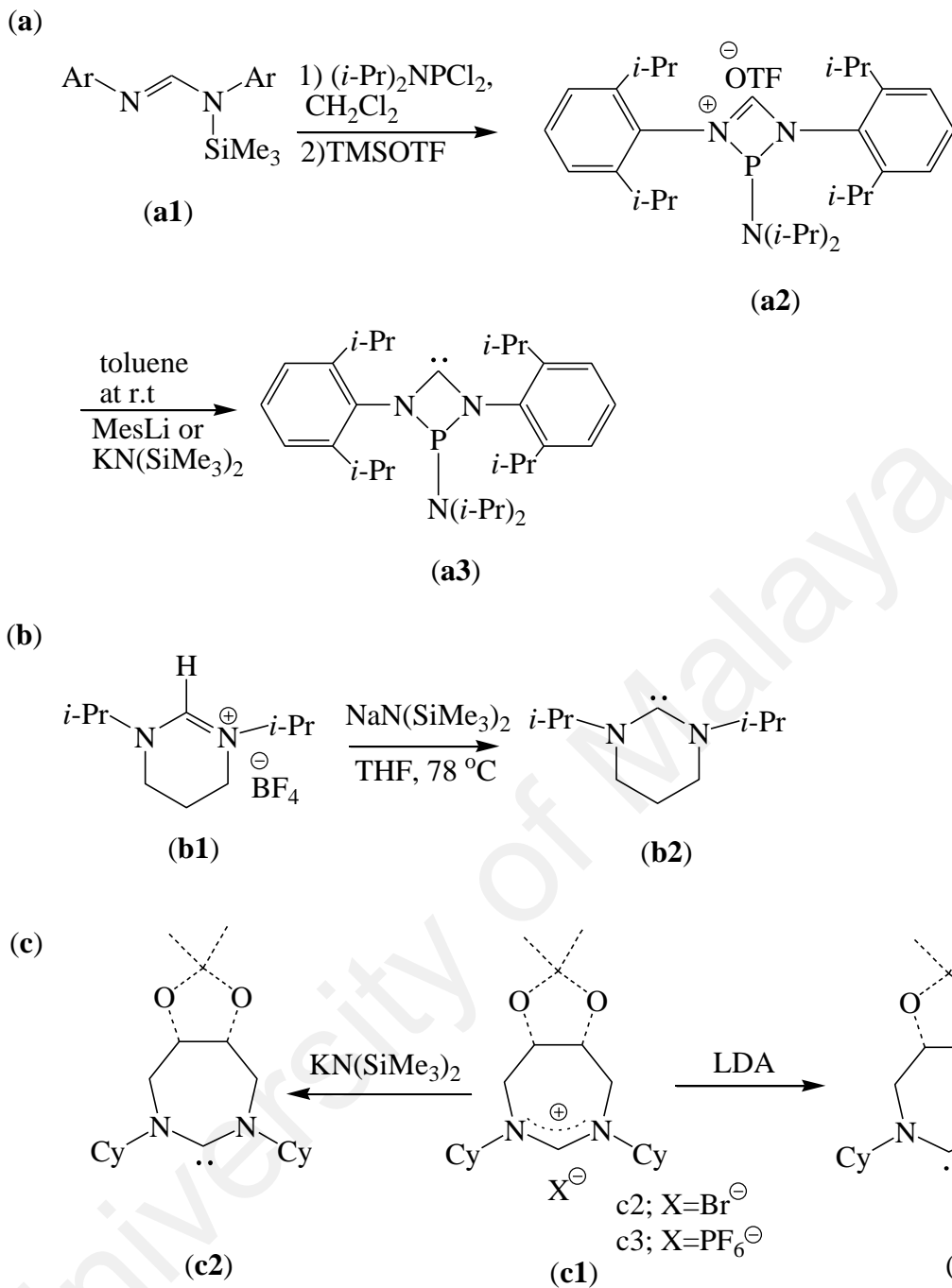
1,3-(diisopropylamino) propane and NH_4BF_4 in HC(OEt)_3 as solvent, with azeotropic removal of EtOH. Deprotonation of (b1) with $\text{NaN}(\text{SiMe}_3)_2$ in THF at 78 °C, gave the desire carbene (b2) in yield of 40%. Iglesia et al. (2007) in their study (Scheme 2.1 (c)) successfully synthesized an amidinium salts (c1) which are the first saturated 7-membered rings reported presenting suitable NHC precursor. Their free carbenes (c2) were generated after the treatment of (c1) with $\text{KN}(\text{SiMe}_3)_2$ in aromatic solvent. While (c3) was formed with the stronger amide base LDA, indicating a higher basicity for (c3) as compared to its unsubstituted (c2) analogue.

The literatures reported that several routes in synthesis of 5-membered ring NHCs ligands and some are illustrated in Scheme 2.2. NHCs may be obtained from the corresponding azonium salts like imidazolium, triazolium, pyrazolium, benzimidazolium, thiazolium, and oxazolium salts by deprotonation and functional groups may be introduced to the imidazole side chain by conventional synthetic method (Peris, 2007).

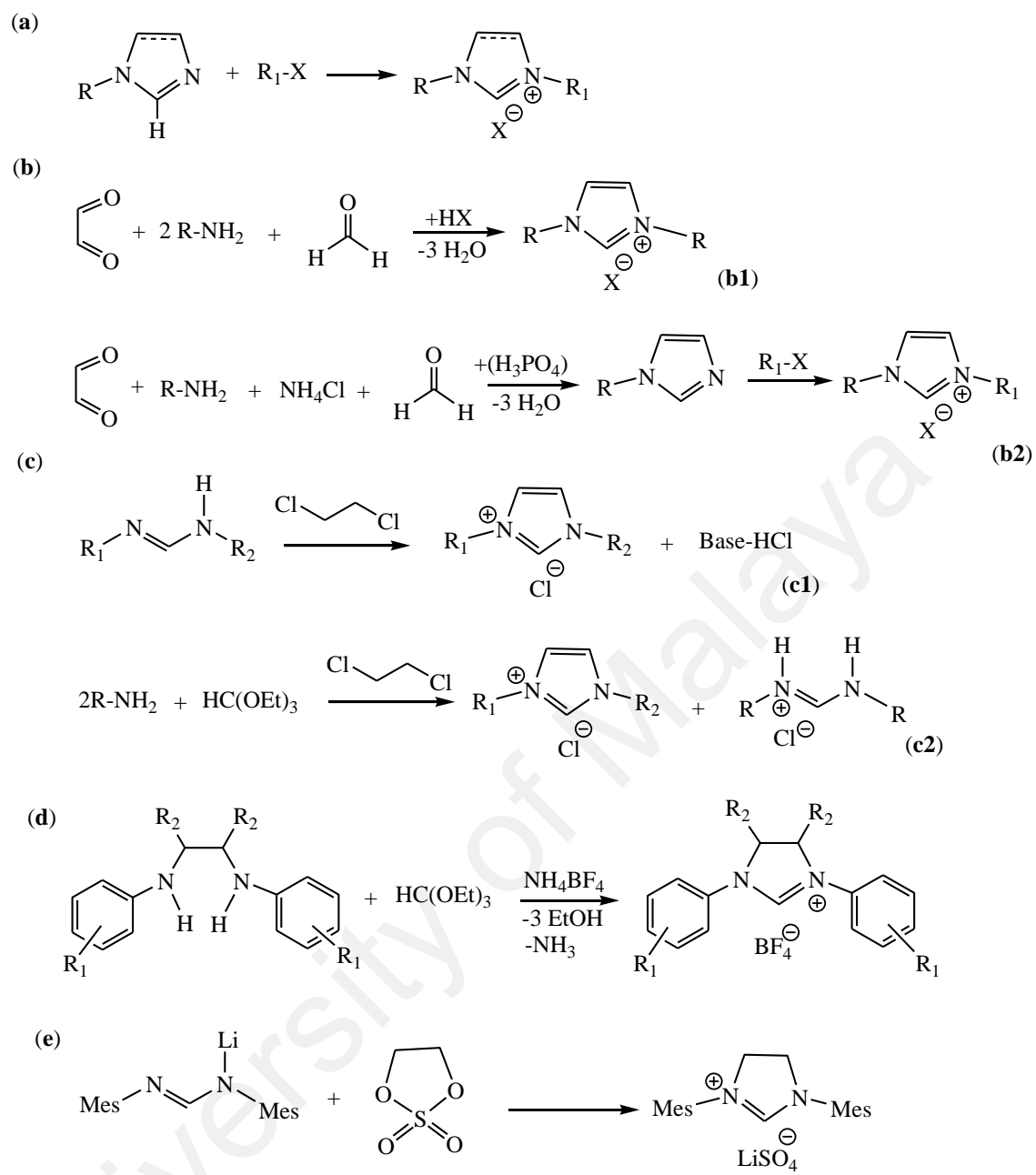
Scheme 2.2 (a) shows the alkylation reaction of substituted imidazole with alkyl or aryl halides ($\text{R}_1\text{-X}$) to give substituted imidazolium salts. In Scheme 2.2 (b) different steps of preparation which are symmetrical and unsymmetrical imidazolium salts are shown. The reactions of primary amine (R-NH_2) with glyoxyl and paraformaldehyde gave symmetrical imidazolium salt (b1), whereas unsymmetrical imidazolium salts (b2) are obtained by the reaction of primary amine (R-NH_2) and NH_4Cl in 1:1 ratio with glyoxal and paraformaldehyde followed by the quaternization of one nitrogen atom with alkyl halide ($\text{R}_1\text{-X}$) (Arduengo, 1992). Another ring-closing reaction was applied in Scheme 2.2 (c) introduced by Grubbs and his co-workers. This methodology involved the reaction of formamidine and 1,2-dichloroethane in the presence of base to form

unsymmetrical imidazolium chloride in excellent yield (c1). On the other hand, symmetrical imidazolium chloride can be prepared directly from substituted aniline by utilizing half of the formamidine intermediate as sacrificial base in moderate yields (c2) (Kuhn et al., 2008). The formation of symmetrical or unsymmetrical imidazolinium salts can be achieved via the ring closure reaction of HC(OEt)_3 in the presence of NH_4BF_4 , under acidic conditions (Scheme 2.2 (d)). Scheme 2.2 (e), which was developed by Jazzar and his co-workers, reported an alternative retrosynthetic disconnection and prepared a range of five-, six-, and seven-membered imidazolinium salts from the addition of bis-electrophiles to lithiated formamidines (Jazzar et al., 2006).

The most widely used of NHCs derived from 5-membered ring were imidazole, benzimidazole, imidazoline, thiazole or triazole (Delaude, 2009). The imidazole moiety found to be important in both chemical and biological contexts. While their fragment in organic molecules have been reported to exert significant influence on the intermolecular and intramolecular interactions such as hydrogen bonding, metal-organic coordination strengths, excited state intramolecular proton-electron transfer (ESIPT) or concerted proton electron transfer (CEPT), 1-, 2-, or 3-dimensional network types in crystal packing, and π - π stacking (Eseola et al., 2012). Therefore, the electronic nature of the 5-membered imidazole ring could be considered to exert notable influence on the physical properties and chemical reactivity tendencies of imidazole-containing material.



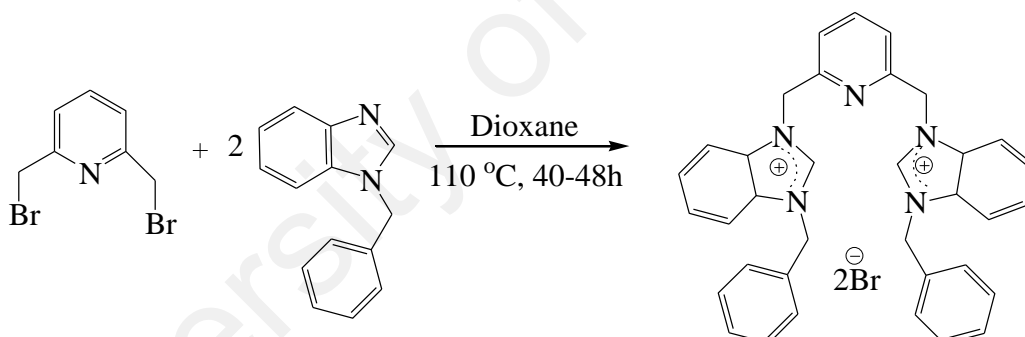
Scheme 2.1: The formation of free carbene for different types of ring; (a) 4-membered, (b) 6-membered, and (c) 7-membered (Alder et al., 1999; Despagnet-Ayoub et al., 2004; Iglesias et al., 2007)



Scheme 2.2: Synthesis routes in the preparation of imidazolium salts; (a) alkylation reaction, (b-e) ring closing reaction (Arduengo, 1992; Jazzar et al., 2006; Kuhn et al., 2008)

2.1.1 Bis-N-Heterocyclic carbene (bis-NHC) precursor

Bis-NHC are linked with various types of bridging linker via the imidazole ring-nitrogen atoms (Schick et al., 2014). Budagumpi and co-workers, reported the preparation of bis-NHC precursor based on benzimidazolium salts via the method reported by Dias and Jin as shown in Scheme 2.3, which afforded moderate to good yield products (Budagumpi et al., 2012b; Dias et al., 1994). The most common types of bridging linker have been reported based on phenylene, pyridyl, ether, and alkyl groups (Kore et al., 2012; Liu et al., 2012; Serra et al., 2011; Yagyu et al., 2014). The evolution in the NHC families is mainly to allow the preparation of new complexes whose stability is entropically improved by chelate effect (Crudden et al., 2004; Peris et al., 2004).



Scheme 2.3: Synthesis of 2,6-bis[(3-benzylbenzimidazolium-1-yl)methyl]pyridine dibromide (Budagumpi et al., 2012b)

Bis-NHC precursor with alkyl group as bridging linker namely 1-methyl-1'-(4''-methoxyphenyl)-3,3'-methylenedimidazolium hexafluorophosphate ($C_6H_3(OMe-4)$) (Figure 2.1(a)) which has been developed by Yagyu and his co-workers. They reported the imidazolium salt of the bidentate ligands implying that the carbene on a methyl-substituted imidazolylidene ring is a stronger donor than one on an aryl-substituted ring. Moreover, the palladium(II) complexes of this ligand shows a good catalytic activity in Heck reaction (Yagyu et al., 2014). While, Ashley et al. prepared series of bis-NHC

precursor with a flexible unsaturated linker as shown in Figure 2.1 (b) (Ashley et al., 2012). Cao and his co-workers synthesized a series of bis-NHC precursor with alkyl bridges, as shown in Figure 2.1 (c) (Cao et al., 2010). Ashley and Cao varied their series by changing the length of linker and observed different catalytic results for different lengths of linker. However, this phenomenon has not been yet explained in literature.

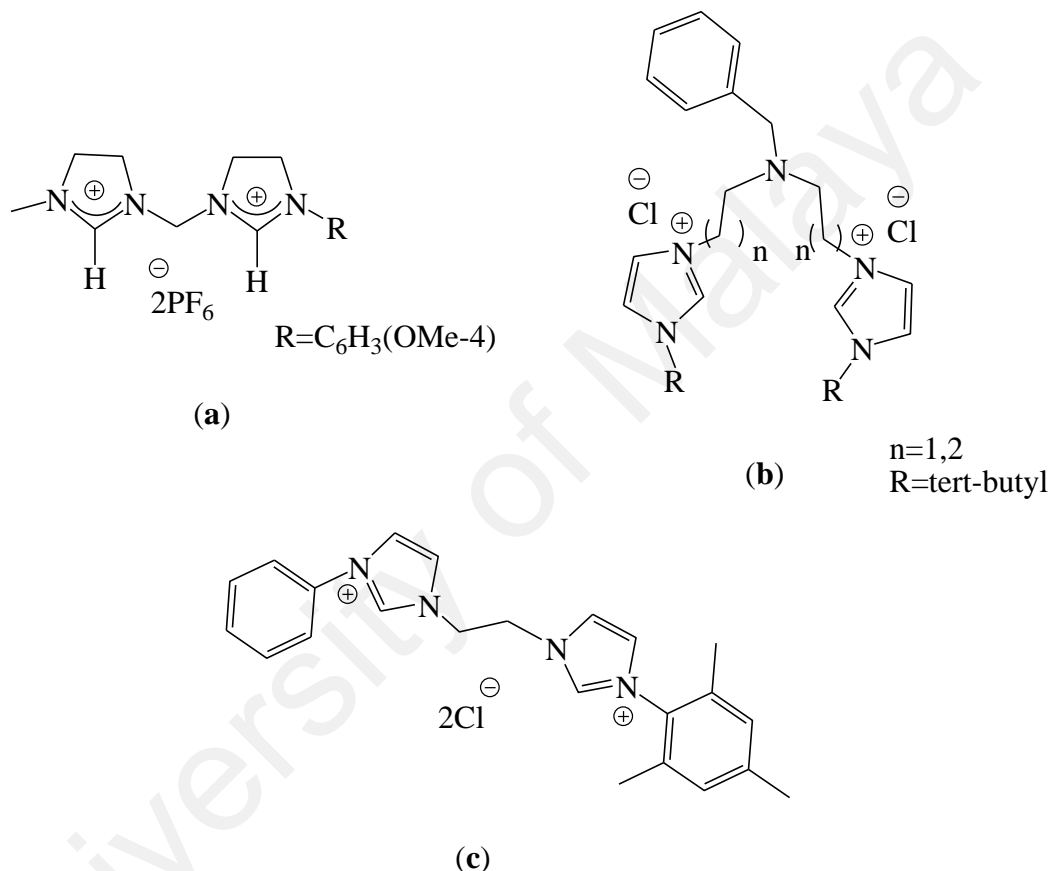


Figure 2.1: (a-c) the examples of bis-NHC precursor with a different bridging linker (Ashley et al., 2012; Cao et al., 2010; Yagyu et al., 2014)

2.2 Different approaches to complexation

2.2.1 Complexation study in solution

Complexation in solution is a simple interaction between a donor (ligand) and an acceptor (substrate). The ligand which has 2 or 3D cavity structure adopts inclusion complexes, in order to host the substrate (Faribod et al., 2008a). In the direction of study of the complex formation, several techniques such as conductometric (Nezhadali et al., 2013; Rezayi et al., 2011), spectrophotometry, calorimetry (Rao et al., 2008), NMR spectroscopy (Jaubert et al., 2014), and potentiometry (Rezayi et al., 2014) were applied.

The complex formation processes in the reported methods are characterized by the thermodynamic stability and selectivity, which depend on the energy amount (K , ΔG , etc.). While the kinetic stability and selectivity depend on the reaction rate. Stability, formation mechanism and formation or dissociation rates are the main parameters in complexation. The complex stoichiometry is another effective factor used to describe a complex. Complexation may happens according to the three routes of distinctive, selective or specific complexation as follows: (i) distinctive complexation- the ligand tends to form complexes with any of the substrates, suggesting that the thermodynamic and kinetic effects between ligand and all substrates are identical and hence all K values are equal, (ii) selective complexation- the ligand prefers one of the substrates to the others and has a higher tendency to form a complex with it and (iii) specific complexation- the ligand forms a complex with only one of the substrates.

Among other techniques, the conductometric has been widely used due to their great sensitivity, low cost as well as simple experimental arrangement. This method provides valuable information such as stability of the cation-ligand complexes and transport phenomena of metal salt-ligand complex in solution (Ghalami-Choobar et al., 2013; Rezayi et al., 2014; Shah et al., 2014)

Moreover, another effect which influences the complexation formation process also can be explored by using this method. Shah and co-workers studied the complexation reaction of group 1 metal with cyclic ligand by using conductometric method and found that the complex formation was influenced by the size of metal cations and cavity size of ligand based on size-fit concept (Shah et al., 2014). El-Sonbati reported the complexation of some transition metal cations such as Mn^{2+} , Co^{2+} , Ni^{2+} , and Cu^{2+} , affected by ligand substituent. The presence of electron donating effect at ligand substituent enhances the electron density by their high positive indicative or isomeric effect, hence increases the stability of complex by strong chelation (El-Sonbati et al., 2001).

2.2.2 Complexation study by theoretical calculation

In order to obtain a clue about the tendency of the ligand to the metal ions in complexation reaction, some ab-initio quantum mechanical calculations can be carried out (Faridbod et al., 2008a; Sakajiri et al., 2012). The pair wise interaction energy, ΔE (A-B), between two molecules (A and B) is estimated as the difference between the energy of the E (A-B) complex and the energies of the isolated partners:

$$\Delta E \text{ (A-B)} = E \text{ (A-B)} - [E \text{ (A)} + E \text{ (B)}] \quad \text{Eq.(2.1)}$$

Abraham et al. (2015) applied this theoretical study by using the GAUSSIAN 09 program based on density functional theory (DFT/B3LYP) to investigate the interaction of several metal cations with their specific ligand. According to the binding energy calculation results Pb^{2+} has shown prominent affinity to their ligand compared to other metals. This method also can provide other supporting information such as spectroscopy data ^1H and ^{13}C in chemical shift, and electronic transition values of the complex in order to confirm the interaction (Gümüş et al., 2014). Figure 2.2, shows the optimal conformation structure of interaction Ag^{2+} with NHC ligand studied by Gümüş et al., (2014) which can predict the values of bond angle and the distance of complexation. In their study, values from theoretical calculation are comparable with X-ray crystallographic data.

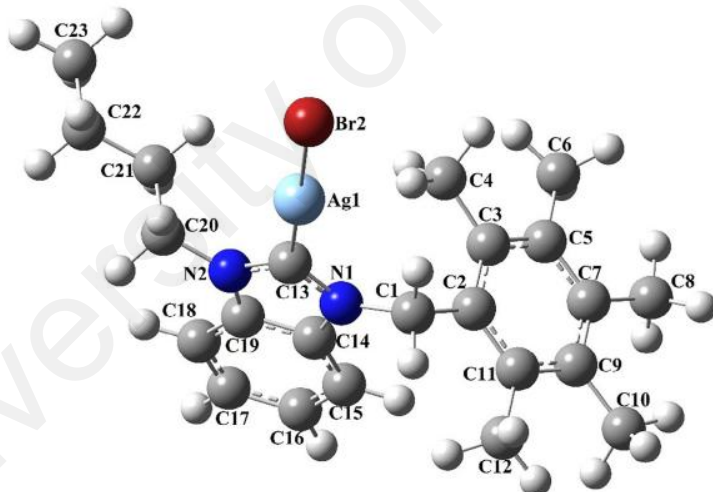


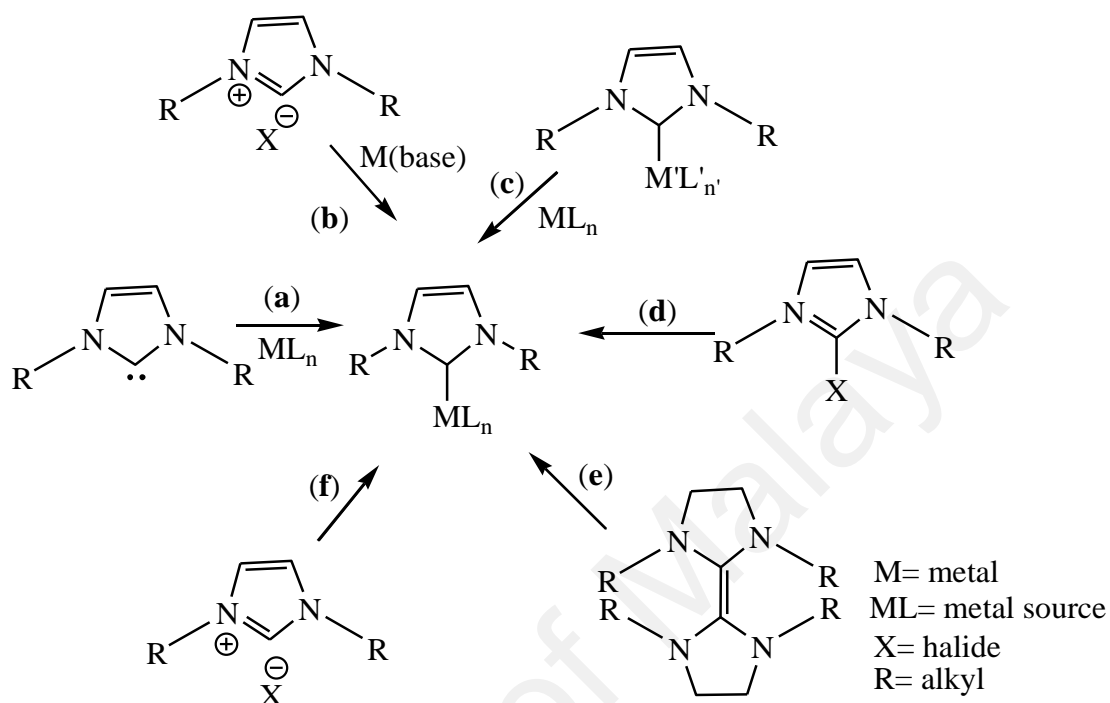
Figure 2.2: Optimal conformation structure obtained from GAUSSIAN 09 program
(Gümüş et al., 2014)

2.2.3 Synthesis of N-heterocyclic carbene (NHC) metal complex

The complexation between ligand and metal cation was achieved by various synthesis routes. In the formation of NHC complexes, the main synthesis routes are depicted in Scheme 2.4. The given methodologies were illustrated by using imidazolidinylidene and imidazolylidene ligands. However, these methods are applicable to other NHCs (Cazin, 2011; Peris, 2007).

The most often method used for the preparation of NHC-metal complexes are shown in Scheme 2.4 (a, b and c). Scheme 2.4 (a) comprises of generating a free carbene by reductive sulfurization, deprotonation of the corresponding salt with strong base, or thermal α -elimination from appropriate NHC precursors, and followed by coordination to a metal center often with concomitant ligand displacement (Peris, 2007). Scheme 2.4 (b) employs metal precursor containing a base as ligand, which is known as *in-situ* deprotonation method by internal base. The base deprotonates the imidazolium salt, leading to the coordination of the NHC with metal cation and of the counter-anion of the salt (Knapp et al., 2010; Liu et al., 2013). Scheme 2.4 (c) is transmetalation from silver-NHC complexes prepared by the direct reaction of imidazolium precursor with Ag_2O to the second metal (Haque et al., 2013; Liu et al., 2013). Scheme 2.4 (d and f) is less frequently encountered; they are consisting of C-X or C-H bond activation via oxidative addition. While Scheme 2.4 (e), involves the cleavage of the C=C bond electron rich of alkene, which leading to the formation of imidazolidinylidene complexes (Özdemir et al., 2010; Peris, 2007). Throughout the methodology, *in-situ* deprotonation by using internal base method is preferable in synthesize of bis-NHC complexes. This offers some advantages such as simplifying

step in the preparation of metal complexes by avoiding the presence of free carbene mostly air and moisture-sensitive (Peris, 2007).



2.2.3.1 Complexation of bis-N-heterocyclic carbenes

Bis-NHC metal complexes with various of type of ligands and metals showed a broad range of coordination modes. Liu et al. illustrated the general structures of bis-NHC coordinated with metal cations as shown in Figure 2.3 (a, b and c) (Liu et al., 2013). Metal complexes coordinated as the monometal monoligand macrocycle (a), the dimetal diligand macrocycle (b) and the open structure are composed of one bidentate dicarbene ligand and two metal atoms (c). The coordination of metal complexes can be influenced by several factors depending on their flexibility and size of bridging linker, the steric hindrance of N-substitutes of imidazole rings, and the structure difference at imidazole ring itself (Liu et al., 2013).

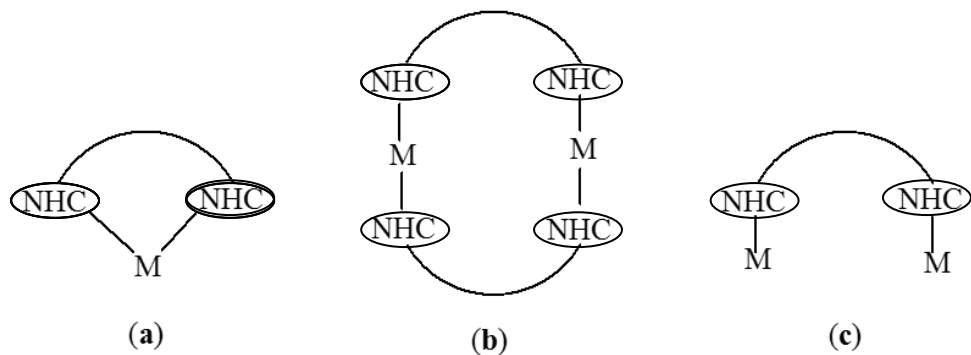


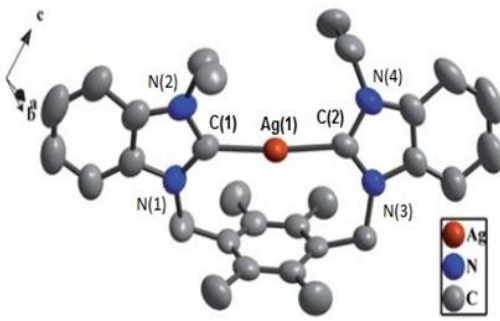
Figure 2.3: General structure of formation bis-NHC metal complexes; NHC= N-heterocyclic carbene, M= metal (Liu et al., 2013)

2.2.3.2 Coordination of bis-N-heterocyclic carbene mercury(II) and silver(I) complexes

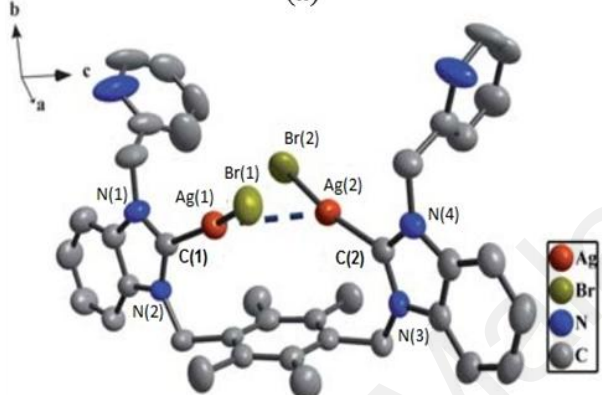
The structural characterization of bis-NHC metal complexes of transition metal cation led to a very complex bonding motif in the solid state, especially in complexes with halide anions. Liu and his co-workers synthesized three silver(I) metal complexes from bis-benzimidazolium salts containing durene linker with a different substituent at -N position of imidazole ring (Rbimi arms) adopting diverse conformation of complexes. The conformation of bis-benzimidazole in the solution can be interchangeably adopted either *cis*-conformation or *trans*-conformation. This condition can be explained by the existence of strong interaction between one anion and two Rbimi arms at the same time in a compound, driving the two arms lie at the same side of durene plane, and mainly adopting *cis*-conformation. While, the compound may adopt *trans*-confirmation when the existence of strong interaction between one anion and only one Rbimi arms, hence the two arms lie in opposite sides of durene plane due to steric hindrance. Figure 2.4 (a to d) shows the different conformation of silver(I) complexes and their structures from X-ray single crystal data (Liu Q.-X. et al., 2011a). The structure of X-ray single crystal data shows that the ligands coordinate with

silver(I) in *cis* (Figure 2.4 (a and b)) and *trans* (Figure 2.4 (c)) conformation. The relevant information about the structure for bis-NHC silver(I) complexes are summarized in Table 2.1.

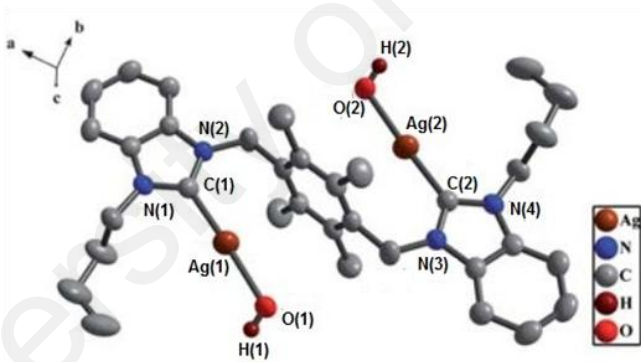
In some cases, the complex formation of silver-halide “staircases” can also take place during the synthesis of bis-NHCs silver(I) complexes (Liu et al., 2013). This silver-halide staircase types form two-dimensional architecture in the solid state on the basis of bridging halides (Garrison et al., 2005). Complex in Figure 2.4 (d) is an example of staircase structure, in which silver(I) NHCs are bridged by bromide to other silver(I) NHCs (Liu et al., 2013). These types of silver(I) complexes form a polymeric structure through a silver-silver interaction (Ag(1)-Ag(2) distance= 2.997(6) Å) to Ag₂Br₄ cluster. All bis-NHCs silver(I) complexes listed in Figure 2.4 have the bond distance of Ag(1)-C(1) in range of 2.081(4) to 2.121(2) Å, which are comparable to known NHC-silver(I) complexes (Baker et al., 2009a). While, the bond distance of Ag···Ag separation of 3.113(7) Å (van der Waals Radii of silver=1.72 Å) in the bis-NHC silver(I) complexes (Figure 2.4 (b)) indicates a weak metal-metal interaction (Rit et al., 2010).



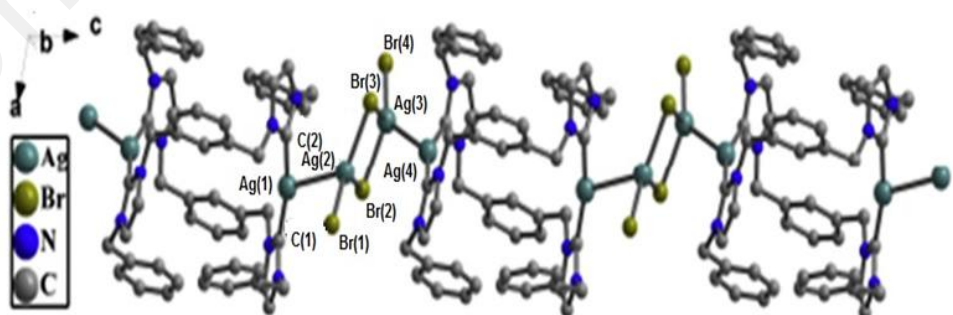
(a)



(b)



(c)



(d)

Figure 2.4: Examples of crystal structure bis-NHC silver(I) complexes, a to d (Liu Q.-X. et al., 2011a; Liu et al., 2013)

Table 2.1: Summary of bond distances and bond angles of bis-NHC silver(I) complexes

Compound	a	b	c	D
Bond distance Å				
Ag(1)-C(1)	2.121(2)	2.081(4)	2.101(3)	2.105(6)
Ag(1)-Br(1)	-	2.492(6)	-	2.548(8)
Ag(1)-O(1)	-	-	2.274(3)	-
Ag(1)-Ag(2)	-	-	-	2.997(6)
Ag(1)···Ag(2)	-	3.113(7)	-	-
Bond angle Å				
C(1)-Ag(1)-C(2)	175.8(6)	-	-	-
C(1)-Ag(1)-Br(1)	-	159.6(1)	-	156.5(2)
C(1)-Ag(1)-O(1)	-	-	177.1(1)	-
Ag(2)-Br(2)-Ag(3)	-	-	-	82.7(3)

Cis-conformation structure is a favorable structure coordination of bis-NHC mercury(II) complex as discussed in literature (Budagumpi et al., 2012b; Haque et al., 2011; Liu Q.-X. et al., 2011b; Liu et al., 2012). Some examples are illustrated in the Figure 2.5 (e to h) and the summary of X-ray data is tabulated in Table 2.2. The listed bis-NHC mercury(II) complexes shows a bond distance from 2.054(3) to 2.108(7) Å. In the Figure 2.5 (e), it was indicated tri-coordinated with two carbene carbons and one bromide atom with linear a bond angle C(1)-Hg(1)-C(2) of 173.7(3) Å (Liu Q.-X. et al., 2011a). Haque et al. (2011) revealed that the complex (Figure 2.5 (f)) with hexafluorophosphate anion adopting linear arrangement bond angle C(1)-Hg(1)-C(2) of 179.5(2) Å with mercury atom is coordinated with two carbene carbons. They also reported that there is a close interaction between Hg centre and one carbon atoms of the aryl linker ring. However, the bond distance of Hg-C(arene) [2.750(5)] is not sufficient to be indicative as a significant bonding interaction. The complex in Figure 2.5 (g) adopts a distorted tetrahedral geometry by coordination of mercury(II) with two carbene carbons, one nitrogen from pyridine ring and one bromide atom. This complex has also approximate linear C(1)-Hg(1)-C(2) bond angles of 173.3(3) Å (Liu et al., 2012). In the structure of complex (Figure 2.5 (h)) interesting features of complex was observed, which indicates two macrometallocycles connected via bridging chlorine atom at two mercury atoms with bond angle Hg(1)-Cl(1)-Hg(2) and I(1)-Hg(1)-Cl(1) are 136.4(6)

and 96.3(1) Å, respectively. This mercury(II) complex adopt tetrahedral geometry with two carbene carbons, chloride and iodide atoms (Liu et al., 2015a).

Nevertheless, a lot of coordination structure reported in the literature. In the coordination of complex study, various factors need to be considered such as different experimental condition, the ratio between ligand and metal source, the solvent used in crystallization, the anion and the structure of ligands itself (Liu et al., 2012). Besides, spectroscopic method such as $^1\text{H-NMR}$ and $^{13}\text{C-NMR}$ also can be used in the characterization of NHC complexes. Simple indicator can be observed in $^1\text{H-NMR}$ spectra of NHC complexes by the absence of chemical shift around δ 8.00-10.00 which refer to proton (-H) at carbene carbon. This is due to deprotonation of -H at carbene carbon indicating that the coordination of metal cation occurred at that position (Baker et al., 2004; Rit et al., 2010). Whereas, in the $^{13}\text{C-NMR}$ spectra a new chemicals shift for carbene carbon coordinating to metal atoms were observed at δ 175-185 for mercury(II) and δ 163.2-213.7 for silver(I), respectively (Baker et al., 2009b; Budagumpi et al., 2012b; Garrison et al., 2005).

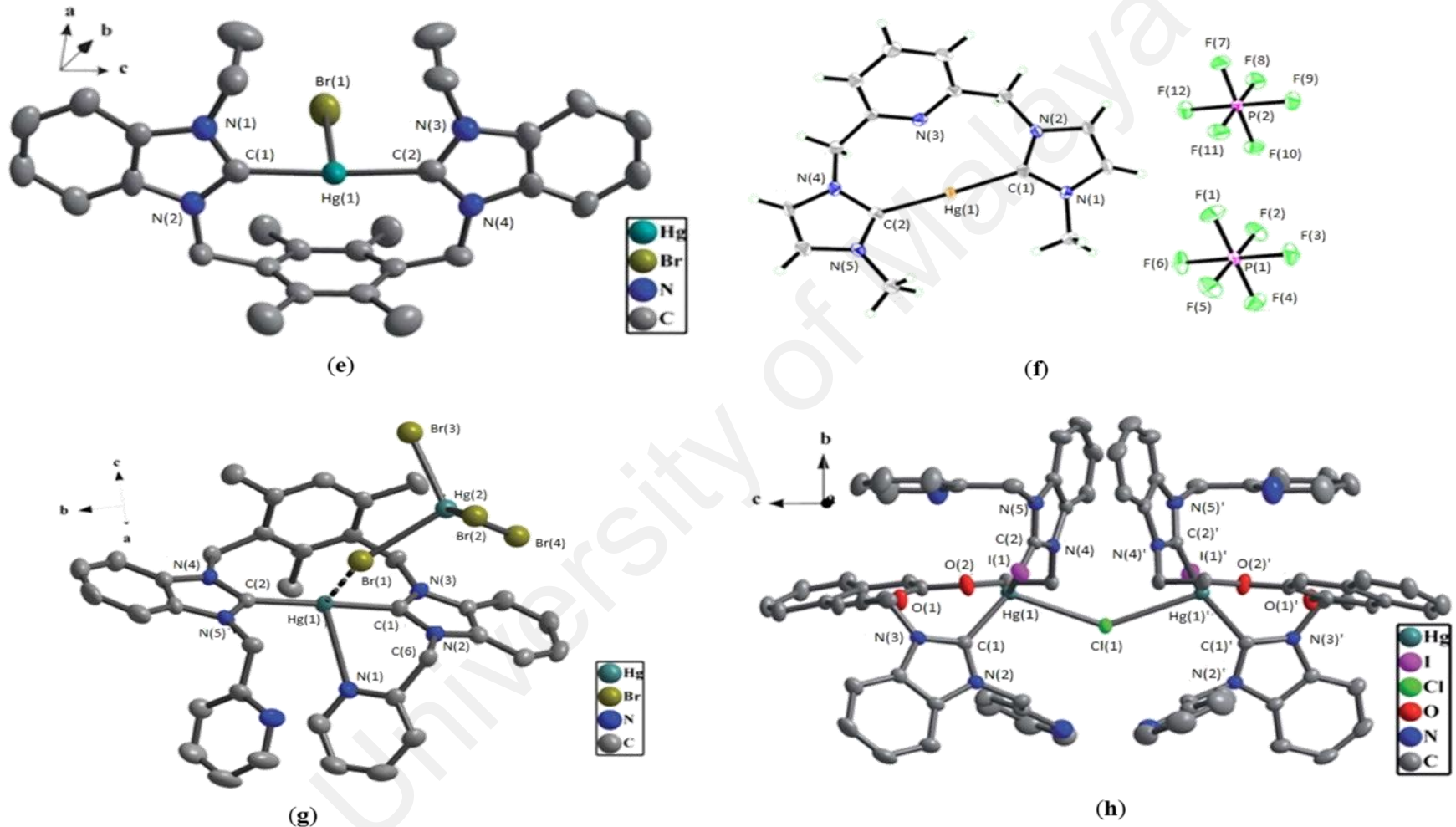


Figure 2.5: Examples of crystal structure bis-NHC mercury(II) complexes, e to h (Budagumpi et al., 2012b; Haque et al., 2011; Liu Q.-X. et al., 2011b; Liu et al., 2012)

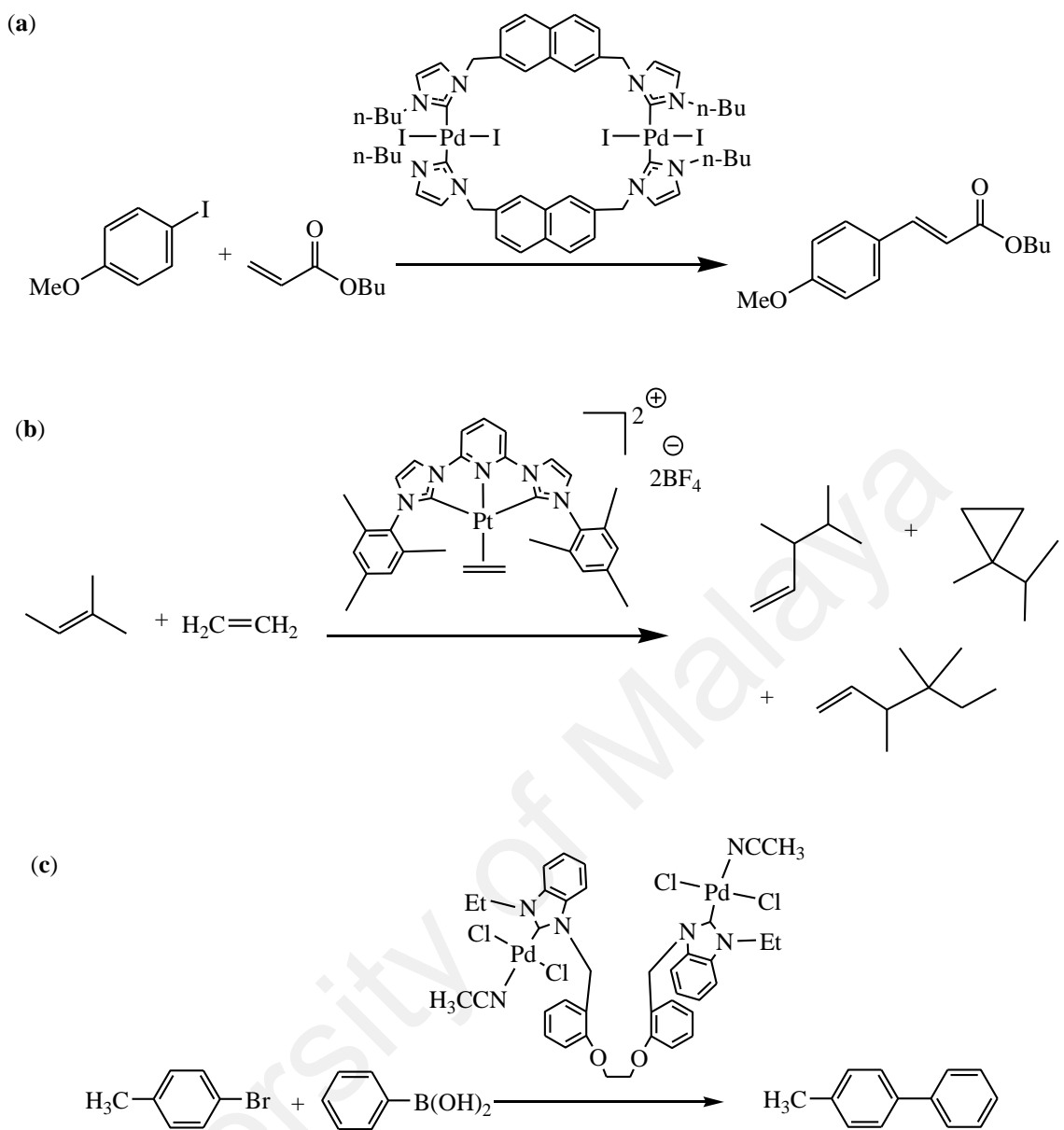
Table 2.2: Summary of bond distances and bond angles of bis-NHC mercury(II) complexes

Compound	e	f	g	h
Bond distance Å				
Hg(1)-C(1)	2.097(6)	2.054(3)	2.108(7)	2.103(4)
Hg(1)-Br(1)	3.076(1)	-	3.001(1)	-
Hg(1)-Cl(1)	-	-	-	3.103(6)
Bond angle Å				
C(1)-Hg(1)-C(2)	173.7(3)	179.5(2)	173.3(3)	160.2(1)
Hg(1)-Cl(1)-Hg(1A)'	-	-	-	136.4(6)

2.3 Applications of N-heterocyclic carbene (NHC)

Catalysis of organic reactions

Numerous researches have reported that the application of NHCs is important in the synthesis of organic compound, in which its metal complexes play the role as catalyst (Cazin, 2011; Glorius et al., 2007). According to the literature, NHC metal complexes have a good catalytic character towards various organic reactions such as in coupling reaction of Mirozuki-Heck, Suzuki-Miyaura, Sonogashira, Stille, and Kumada, Hartwig-Buchwald reaction, α -arylation, hydrogenation, hydrosilylation and many more. This is due to versatile properties of NHCs which have strong σ -donating ability, a strong metal-carbon bond and poor π -accepting ability leading to the formation of many stable metal complexes with various metal ions. As illustrated in Scheme 2.5, (a) Mirozuki-Heck, (b) Hydrovinylation, and (c) Suzuki-Miyaura reactions, showed the catalytic organic synthesis reactions by using bis-NHC metal complexes with a good yield (Liu et al., 2012; Saito et al., 2011; Serra et al., 2011).



Scheme 2.5: Examples of catalytic reaction which use bis-NHC metal complexes as catalyst, (a) Mirozuki-Heck, (b) Hydrovinylation, and (c) Suzuki-Miyaura reactions (Liu et al., 2012; Saito et al., 2011; Serra et al., 2011)

Anti-cancer activity

The applications of the NHC precursor in the biomedical research area are just beginning to unfold and extensively being explored. Researchers found that the bis-NHC can be applied as anti-cancer agent against human colon cancer as previously reported by Haque et al., (2012). In this study, the synthesized benzimidazolium

compounds as illustrated in Figure 2.6 (a to f) were tested against cancer cell (HCT116). The cytotoxicity in the HCT116 cancer cell line is expressed as, IC₅₀ values (μM). The data revealed that from all benzimidazolium compounds the longer alkyl change (e) and aromatic substitution (c) are more efficient in cytotoxic activities. Additionally, it should be noticed that the compound which has bromide anions (a, c, and e) demonstrated appreciable cytotoxic activity with respect to the compound having the hexafluorophosphate anions (b, d, and f).

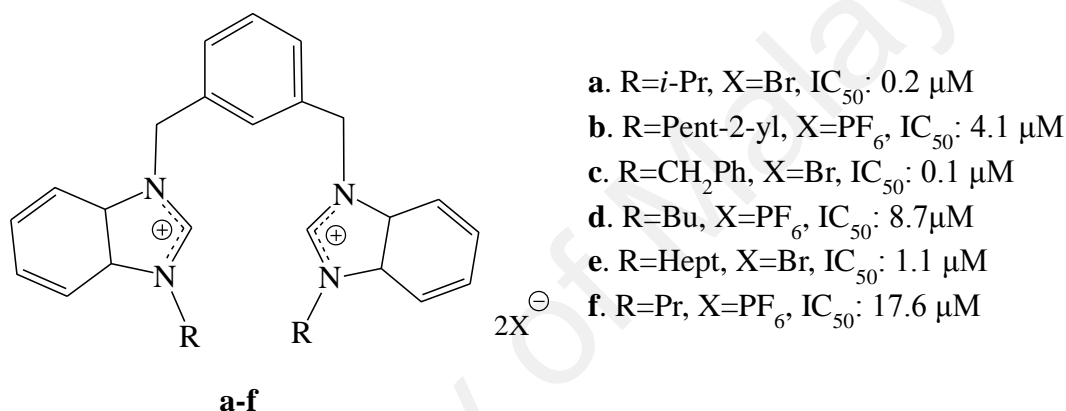


Figure 2.6: Bis-NHC precursor applied in human colon cancer as anti-cancer agents (Haque et al., 2012b)

Moreover, researchers revealed that the NHC metal complexes also can be used in anticancer activity application. For examples, Haque and co-workers used bis-NHC silver(I) complexes against HCT116 cells. The bis-NHC silver(I) complexes of imidazole and benzimidazole which show a significant level of anti-cancer activity against HCT116 cancer cell, were represented in Figure 2.7 (a to d). The results showed the concentration of bis-NHC silver(I) complexes needed was lesser than their corresponding bis-NHCs precursor and some of them displayed no anticancer activity. Therefore, it is possible to conclude that the insertion of silver(I) in bis-NHCs might positively increase the anticancer activity. However, the activity of complexes are

mainly due to the presence of appropriate substitutions on the ligands and the nature of coordinated anions (Haque et al., 2013; Haque et al., 2012b).

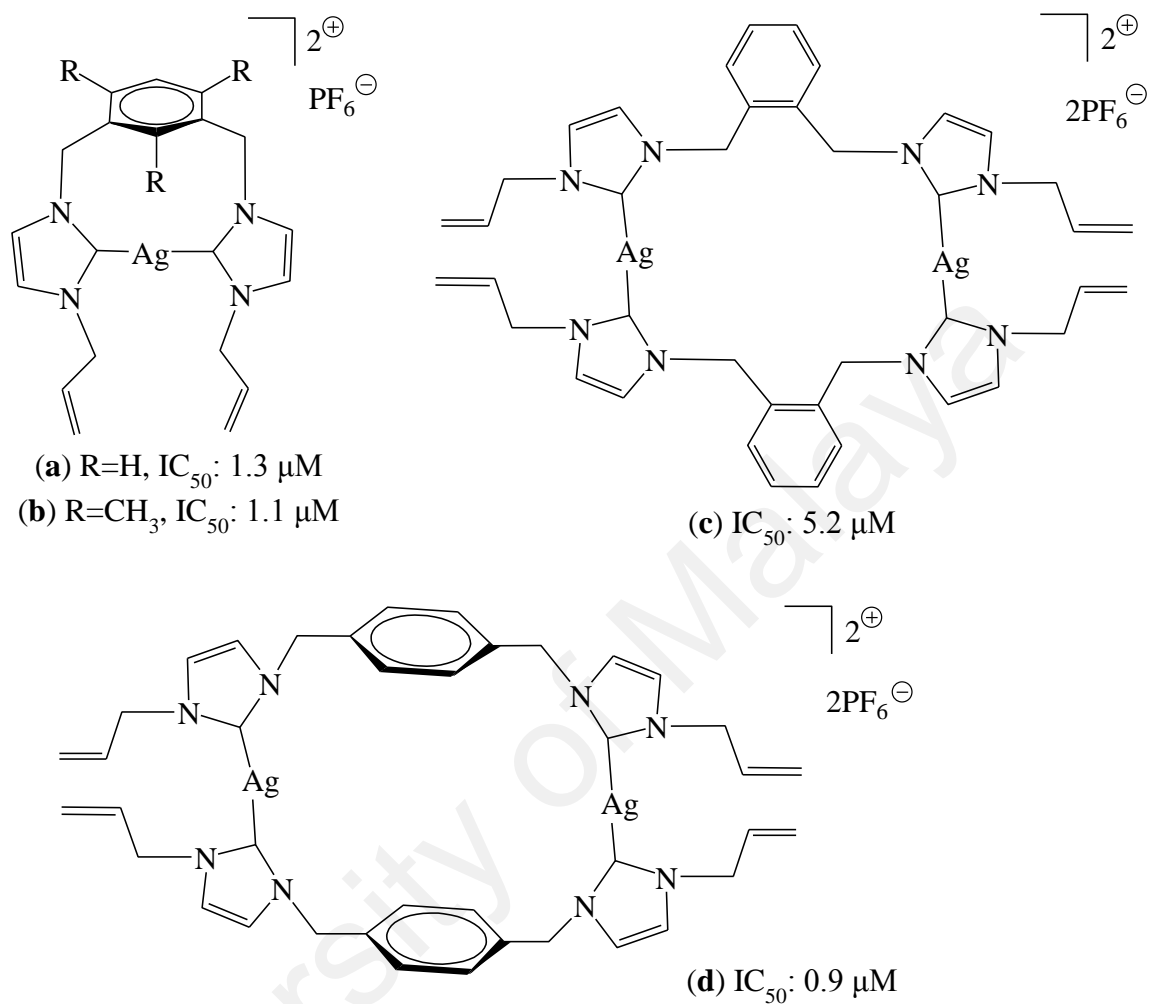


Figure 2.7: Bis-NHCs silver(I) complexes applied in human colon cancer as anti-cancer agent (Haque et al., 2013; Haque et al., 2012b)

In the period of 2012-2013, Sivaram and his co-workers introduced the use of NHCs gold(I) and gold(III) complexes against NCI-H1666 non-small cell lung cancer (Sivaram et al., 2012; Sivaram et al., 2013). This research found that the neutral NHCs gold(I) and gold(III) in Figure 2.8 (a and b) were less toxic than cisplatin which is standard anticancer for NCI-H1666. While, the NHCs gold(I) and gold(III) structure as shown in Figure 2.8 (c and d), represents superior cytotoxicity.

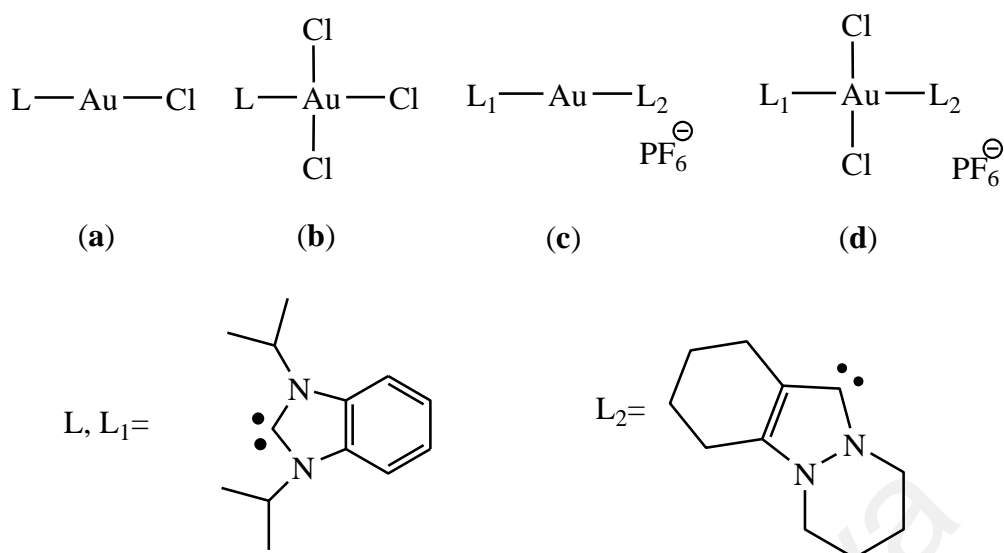


Figure 2.8: Structure of synthesized NHCs gold(I) (a and c), and gold(III) (b and d) which used as anti-cancer agent (Sivaram et al., 2012; Sivaram et al., 2013)

Chemosensor

In 1999, Sato and co-workers synthesized the imidazolium-based tripodal receptor as illustrated in Figure 2.9 (a). This compound has considerable affinity for halide anions in polar solvent through electrostatic interaction and C-H---X⁻ hydrogen bonds, where X refer to Cl⁻, Br⁻ and I⁻ (Sato et al., 1999). Association constant K data revealed that this receptor is highly selective towards Cl⁻ anion with 1:1 stoichiometric. Further titration experiments of other compounds (Figure 2.9 (b and c)) with Cl⁻ anion show the decreasing in association constant values. It was observed that the absence of methyl groups at the ortho positions (Figure 2.9 (b)) and the removal one unit of imidazoliummethyl (Figure 2.9 (c)) influence the complexation reaction with Cl⁻ anion. The interaction of receptor Figure 2.9 (a) with Cl⁻ anions was illustrated in Figure 2.9 (d).

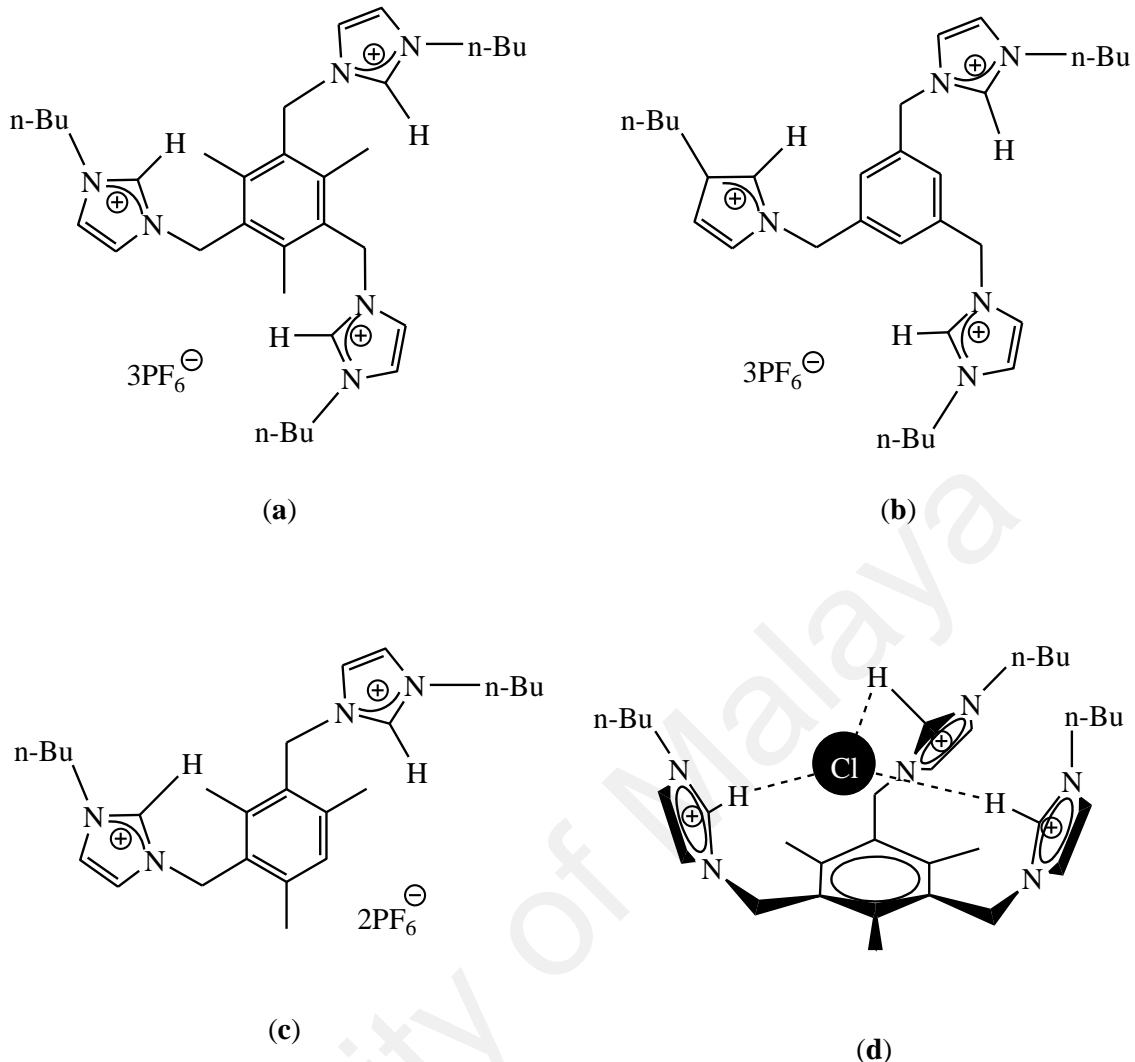


Figure 2.9: The structure of anion receptor compound (a, b, c) and the interaction of receptor (a) with chloride anion (d) (Sato et al., 1999)

Most recently, the application of NHCs metal complexes as chemosensors were discovered by Liu and co-workers. They found that the bis-benzimidazole metal complex may be used as an effective chemosensor for nitrate anion (NO_3^-) and silver(I) cation (Ag^+), respectively (Liu et al., 2015a; Liu et al., 2015b). The study of selective recognition of NO_3^- and Ag^+ were conducted on the basis of fluorescent and UV/Vis spectroscopic titration. Figure 2.10 (a and b) shows, the interaction of bis-NHC metal complex with NO_3^- and Ag^+ ions. Based on the fluorescent spectroscopic titration study, results proved that the proposed bis-NHC metal complexes are more selective towards their targeting ions. As seen in Figure 2.11 (a and b), a great enhancement of emission

intensity occurred upon the addition of NO_3^- and Ag^+ , respectively if compared with others ions.

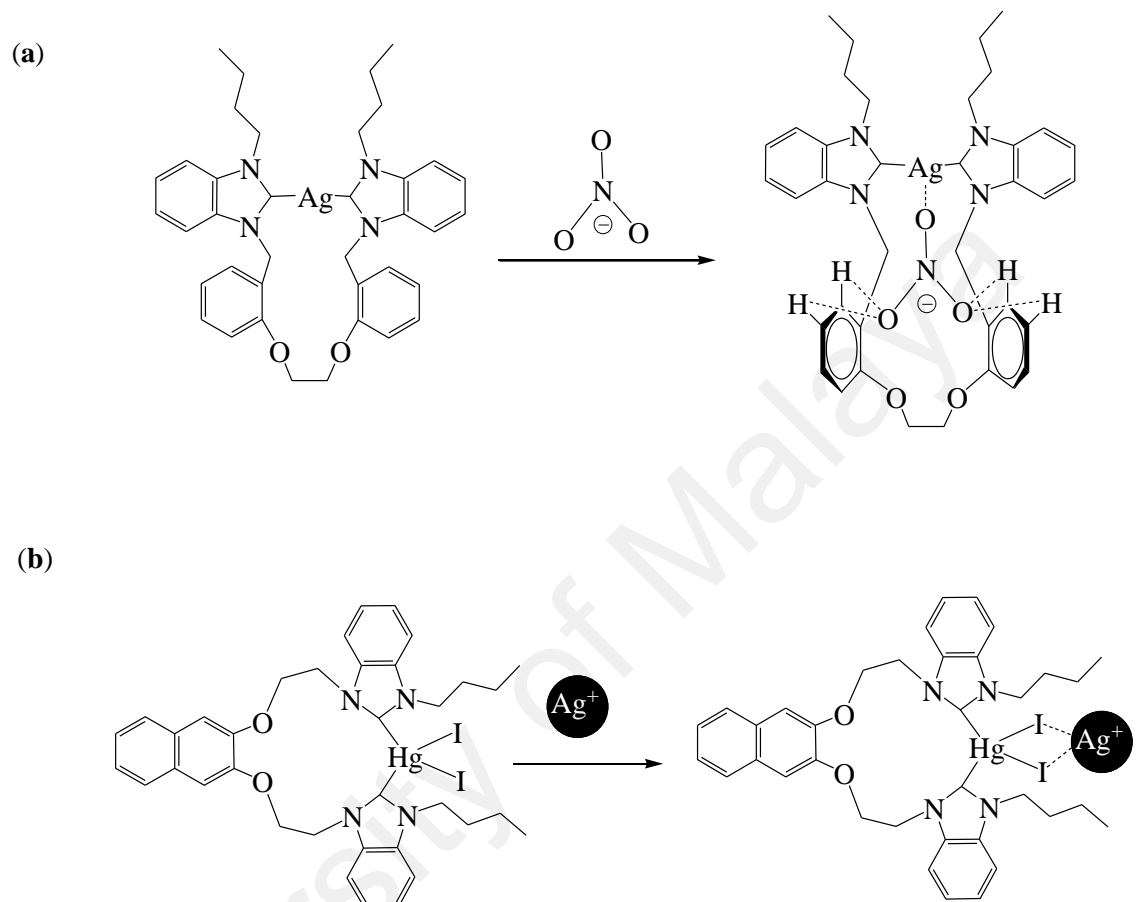


Figure 2.10: The interaction of bis-NHC complexes with (a) NO_3^- and (b) Ag^+ ions (Liu et al., 2015a; Liu et al., 2015b)

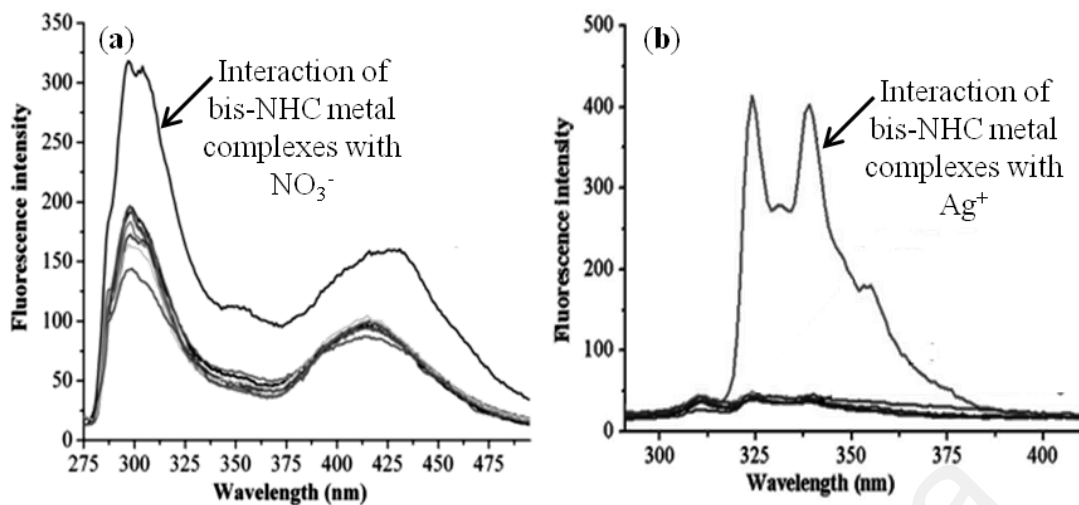


Figure 2.11: (a) Fluorescence spectra of bis-NHC metal complex (1×10^{-5} mol/L) upon the addition of the tetrabutyl ammonium salts of F^- , Cl^- , Br^- , I^- , $H_2PO_4^-$, HSO_4^- , OAc^- and NO_3^- (10.0 mol equiv.) in acetonitrile at 25 °C. (b) Fluorescence spectra of bis-NHC metal complex (1×10^{-5} mol/L) upon the addition of salts (30 mol equiv.) of Li^+ , Na^+ , NH_4^+ , Ag^+ , Ca^{2+} , Co^{2+} , Ni^{2+} , Cu^{2+} , Zn^{2+} , Cd^{2+} , Cr^{3+} , Al^{3+} , Pb^{2+} and Hg^{2+} in MeOH at 25 °C (Liu et al., 2015a; Liu et al., 2015b)

Although the research development of bis-NHC precursor and its metal complexes increase rapidly, their role in sensor still have been relatively well studied, especially as ionophore in potentiometric ion selective electrode (ISE).

2.4 Ion selective electrode (ISE)

Potentiometric measurements are based on monitoring potential values under a zero current flow regime, in order to determine the analytical concentration of the desired components in an analyte (Faridbod et al., 2008b). This method involves the measurement of potential (voltage) generated by a cell under essentially equilibrium condition (Dimeski et al., 2010; Writht et al., 1972). The potentiometric measuring cell consists of two galvanic cells which are ion selective electrode (ISE) and reference electrode (RE) (Lindner et al., 2013). The total potential difference (electromotive force,

EMF) was measured using a schematic galvanic cell as follows: Ag | AgCl | KCl 3M | bridge electrolyte | sample || membrane || inner filling solution | AgCl | Ag.

Ion-selective electrodes (ISEs) are electrochemical transducers that respond selectively, directly and continuously to the activity of the free ions of interest in solution. The measurements are based on the electrical signal generated by a chemical system in electrochemical cell. These types of sensors have some advantages such as low cost, easy fabrication, accuracy and also can be used without previous extraction of samples (Mandil et al., 2013). ISE based on potentiometry have practical utility as a simple analytical technique to measure target analyte in complex samples. Recently, their selectivity and sensitivity were improved and it is possible to do trace analysis in micro and nano molar concentration (Ganjali et al., 2015).

The request for ISEs as potentiometric sensors increases drastically in many areas such as in medicinal (El-Dien et al., 2012; Mandil et al., 2013), environmental monitoring (Nanda et al., 2007; Radu et al., 2013), physiological measurements, agricultural (Heng et al., 2008) and industrial field. Some applications of potentiometric ISE in determination of various analytes are summarized in Table 2.3.

Table 2.3: The applications of potentiometric ISE in determination of various analytes

Application	Ionophore	Analyte	Limit of detection (M)	References
raw milk	1,2-Bis(N'-benzoylthioureido)benzene	Pb ²⁺	2.5×10 ⁻⁸	(Abraham et al., 2015)
erythrocytes	*Valinomycin, ETH 5220, ETH 5234	Mg ²⁺ , Ca ²⁺ Na ⁺ , K ⁺	-	(Malon et al., 2005)
Soy milk	Phytase	Ca ²⁺	-	(Yang et al., 2015)
water	5-chloro-3-[4-(trifluoromethoxy)phenylimino]indolin-2-one	Fe ³⁺	6.3×10 ⁻⁷	(Demir et al., 2015)
environment	thiazole	Co ²⁺	7.9×10 ⁻⁸	(Singhal et al., 2014)
water	N,N'-(4E,4'E)-4,4'-(ethane-1,2-diylbis(azan-1-yl-1-ylidene))bis(2-oxopentan-3-yl-4-ylidene)dibenzamide	Cu ²⁺	2.4×10 ⁻⁹	(Ganjali et al., 2015)
water	*Cu(II)-ionophore	Cu ²⁺	1.1×10 ⁻⁶	(Soleimani et al., 2013)
blood	Shift-base lariat ether	Ag ⁺	4.4×10 ⁻⁸	(Gupta et al., 2009)
environment and biological	2-amino-6-purinethiol	Hg ²⁺	4.4×10 ⁻⁸	(Gupta et al., 2007)
Clinical and environment	Mn(III)-salen complex	CO ₃ ²⁻	2.5×10 ⁻⁵	(Chen et al., 2011)
industrial	Mn(II)[2-formylquinoline thiosemicarbazone]	N ₃ ⁻	8.0×10 ⁻⁶	(Kamel, 2015)
clinical	2-hydroxypropyl-β-cyclodextrin	Cationic drug	3.9×10 ⁻⁶	(Ragab et al., 2015)

*Ionophore was used as purchased

2.4.1 Sensor fabrication

2.4.1.1 Membrane composition

The composition of electrode membrane is a crucial factor that may influence increasing electrode selectivity and sensitivity towards targeted ions. Hence, the construction of electrode membrane for ISE rely on the polymer matrix which contains mixture of active component such as ionophore, ionic additives, and plasticizer (Gupta et al., 2001).

Polymer matrix

The first polymeric ISE membrane was reported based on silicone rubber and PVC by using valinomycin as the ionophore without the addition of lipophilic ionic site. Mostly PVC has been used as polymer matrix in various ISE studies. Instead of PVC, other polymers also can be used, such as the soft polyurethanes, silicone rubber, poly(vinylidene chloride) and polysiloxanes. The main function of polymer matrix is to provide the required physical properties, like elasticity and mechanical stability. Hence, the polymer matrix should be inert and has no chemical interaction towards sensing ions.

Plasticizer

The plasticizer is needed in order to soften membrane by reducing the viscosity, and ensuring a relatively high mobility of the membrane constituents. It also provides homogeneity of the organic phase, to ensure the compatibility of other membrane components. The plasticizer can influence the ion-exchanger characteristic of membrane such as sensitivity, response times and also detection range based on their dielectric constant and polarity (Gupta et al., 2001).

Ionic additives

Ionic additives are ion exchanger, which themselves induce a selective response with or without sufficient ionophore amount. Thus, the addition of lipophilic salt in the electrode membrane without ion-exchanges properties reduces the ohmic resistance of the membrane (Faribod et al., 2007). Additionally, it also improves the membrane

response behavior and selectivity by increasing the ionic strength in the membrane, which helps the neutral-carrier-based ISE membranes work properly (Zhang et al., 2006). Hence, the amount of these species must be adjusted carefully to reach their optimum composition in electrode membrane (Faridbod et al., 2008a).

Ionophore

From all active components inside of the polymer matrix, ionophore plays an important role in the selectivity of the ISE membrane. The ionophore should ideally form relatively strong, selective and reversible complexes only with the target ion, so that no ion-exchange between measuring and interfering ion occurs in the membrane. Additionally, the ionophore should be sufficiently lipophilic in order to make its leaching rate from the membrane to the aqueous testing solution as low as possible (Gupta et al., 2000; Gupta et al., 2001; Gupta et al., 2009).

2.4.1.2 Fabrication of electrode membrane

The potentiometric ISE membranes can be categorized as glass membrane, solid membrane and liquid membrane (Faridbod et al., 2007). However, the development of solid-state membrane electrochemical sensor gains much attention due to low electrical resistance, as well as ease of preparation and handling. The polymeric membranes are fabricated on the solid surface without any internal reference electrolyte solutions; hence offering the advantages of multiple sensors on single chips and mass fabrication for cost reduction (Faridbod et al., 2008b; Piao et al., 2003).

Generally, the construction of ISE based on polyvinyl chloride (PVC) membrane was applied in various industrial, environmental and biochemical samples (Liu et al., 2000; Mahajan et al., 2003). Nevertheless, it gave many problems when used in fabrication of solid-state sensors due to its poor adhesion on solid substances. The PVC membranes can only be prepared from solvent casting procedures and requires a plasticizer, for softening the polymer (Heng et al., 2000; Heng et al., 2008). The addition of plasticizers which is a toxic material to make PVC flexible causes it to leak into the solution during measurements and can be eventually released to the environment. This has become a main cause of toxicity environmental concern nowadays (Zareh, 2012). These problems can be avoided by using a photo-curable and self-plasticizing polymer technique. The idea of a self-plasticizing membrane for ISE was developed, where the acrylic membrane material has been shown to yield functional ion sensors without the incorporation of plasticizers (Heng et al., 2000).

This photocure technique has become increasingly popular due to its ability to provide a quick but simple means of membrane fabrication as compared to other techniques. The main composition of polymer matrix contained ionophore and lipophilic salts, where plasticizer is not required. However, the membrane needs additional component such as initiator and cross-linker to make the fabrication successful (Abramova et al., 2015; Heng et al., 2001). A study by Heng and co-workers found that the initiator such as 2,2-dimethoxy-2-phenylacetophenone (DMPP) was functioning to controlling the photocuring process, while the cross linker can adjust the physical quality of the resulting cross-linked poly(acrylic) matric so that a workable ion-selective membrane without the use of plasticizer could be produced (Heng et al., 2001).

The fabrication of electrode membrane studied by Heng and co-workers was illustrated in Figure 2.12. Electrode membrane was fabricated by depositing the appropriate monomers on Ag/AgCl discs through photocuring. A poly(2-hydroxyethyl methacrylate) (pHEMA) was first deposited to act as the inner conducting layer of the sensor. This layer was photopolymerized under UV radiation for 5 min with continuous purging of nitrogen gas, and followed by conditioning with 0.1 M of targeted analyst solution. The membrane mixture which contained monomer, initiator, cross-linker, lipophilic salt and ionophore were deposited on the surface hydrated pHEMA layer, and was photopolymerized under UV exposure for 8 min. Results from this study show the successful employing of self-plasticizing acrylic matrices as membrane materials for solid-state calcium ion sensors with non-requirement of plasticizer (Heng et al., 2008).

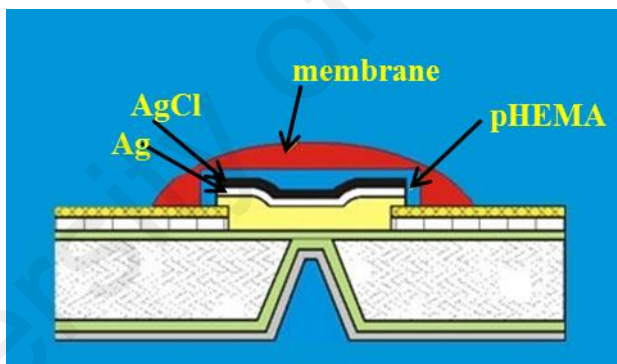


Figure 2.12: Self-plasticizing acrylic membrane

In 2012, Jumal and his co-workers applied this method in the fabrication of potentiometric sensor mercury(II) ISE membrane electrode in the presence of 1,2-bis-(N'-benzoylthioureido)cyclohexane as ionophore. The sensor exhibits linear response in a Nernstian slope of 28.1 mV/decade within concentration working range of 1×10^{-5} to 1×10^{-1} M. The detection limits of this proposed electrode in 2.5×10^{-6} M with a response time within 50-100 second. However, when compared the data with some Hg-ISE in the literature, this electrode shows the lowest electrode performance in

determination of Hg^{2+} cations which gives higher detection limits and longer response time (Jumal et al., 2012). Nevertheless, this self-plasticizing method is a good alternative in preparation of electrode membrane without plasticizer. Therefore, this research study needs more exploration in the searching of suitable and alternative electrode membrane composition in order to increase their sensitivity and selectivity.

2.4.2 Analyte of interest

Mercury possesses high toxicity, mobility and ability to remain longer in the atmosphere (Sears et al., 2012). It can be absorbed by humans and other organisms and can lead to serious health problems to humans. Amyotrophic lateral sclerosis, Alzheimer's, and Parkinson's are the examples of disease caused by mercury. This metal can also cause damages to kidneys and immune system (Holmes et al., 2009; Mutter et al., 2004; Wang et al., 2012). Ahmad and co-workers found out that silver metal effects the liver, lung, brain, vascular system and also reproductive organs (Ahamed et al., 2010). Therefore, there is a strong necessity to develop a new method to determine mercury(II) and silver(I) ions in our surroundings.

The development of new cation selective electrode has drawn a great interest for researchers in recent years. The efforts in introducing new types of carriers achieved significant improvement in the sensitivity and selectivity of ISE. Numerous sensing agents (ionophore) for the PVC membrane electrodes have been reported in the literature with a various targeted analytes and applications. The shift bases (Dadkhah et al., 2014; Hassouna et al., 2010), thiourea (Ghanei-Motlagh et al., 2014), oxime (Sardohan-Koseoglu et al., 2015), crown ether (Gupta et al., 2009) and calixaren

(Yan et al., 2013) are the types of ionophore which have been used in determination of mercury(II) or silver(I) as reported recently and listed in Table 2.4.

These types of ionophore were reported as selective towards their targeted ions. In literature, the effect of various ionophore structures towards the selectivity and sensitivity of electrodes has been discussed. In order to increase the sensitivity of ISE, the chemical structural features of ionophores may turn by incorporating different soft and hard donor atoms in the chelating ring, thereby promoting the stabilization of both low and high oxidation states of the metal centre, as well as forcing metal ions to adopt typical coordination chemistry (Gupta et al., 2007).

Moreover, Gupta and his co-worker studied the selectivity for silver ion due to lariat effect of their sidearms. They synthesized six Schiff-base lariat ether chelates based on 4,13-diaza-18-crown ether as shown in the Figure 2.13. Then, the silver(I) ISE was constructed based on each ionophore, individually. Hence, the performance of electrode were tested and compared as tabulated in Table 2.4. The data listed shows that the performance of electrode with ratio of electrode composition used are similar. As can be observed, the presence of hydroxyl group at the ionophore substituent improved the electrode performance in term of working concentration range, detection limit and also response time (Gupta et al., 2009). Sardohen-Koseoglu et al., also studied the effect of the sidearm of ionophore toward the selectivity of fabricated mercury(II) ISE. They synthesized ionophore based on oxime compound (Figure 2.13) and the sensing results were listed in the Table 2.4 (Sardohen-Koseoglu et al., 2015). It was observed that the presence of electron donating or withdrawing group at the sidearm of structured ligand will effect the complexation with targeted metal ions, thus increase the sensitivity of ionophore in sensing study.

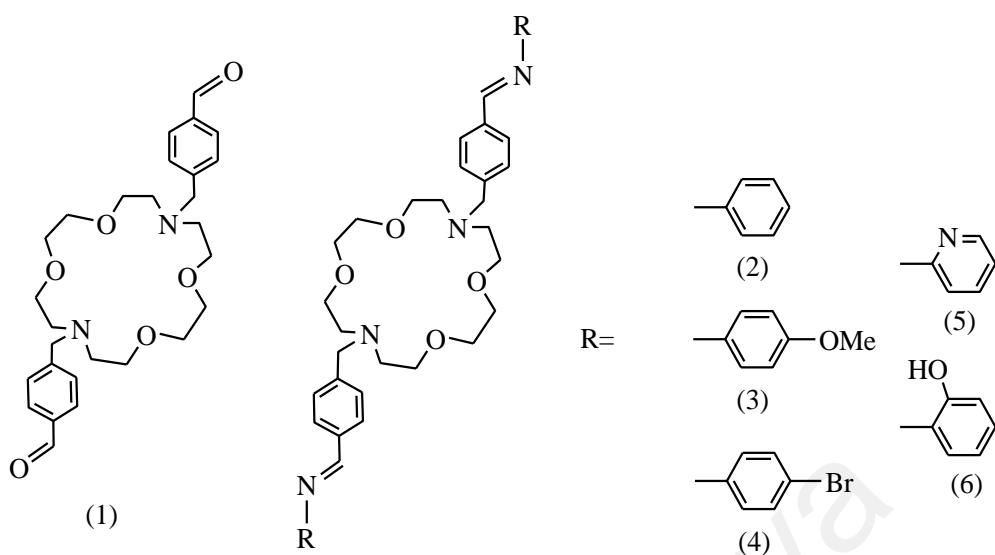
Table 2.4: The comparative evaluation of selective electrode, responsive with mercury(II) and silver(I)

Metal ion	Ionophore	Slope (mV/decade)	Detection limit (M)	Linear range (M)	Response time (s)	Life time (day)	Refs.
Hg^{2+}	Oxime (b), 1	33.4	1.68×10^{-6}	5.6×10^{-6} - 1.0×10^{-2}	10-15	30	(Sardohan-Koseoglu et al., 2015)
	Oxime (b), 2	34.2	1.76×10^{-6}	5.9×10^{-6} - 1.0×10^{-2}	10-15	30	
Hg^{2+}	1,5-diphenylthiocarbazone (dithizone)	29.7	3.0×10^{-6}	5.0×10^{-6} - 1.0×10^{-2}	20	14	(Hassan, 2013)
Hg^{2+}	Thioure	30.3	7.9×10^{-8}	1.0×10^{-7} - 1.0×10^{-2}	15	<100	(Ghanei-Motlagh et al., 2014)
Hg^{2+}	Calix[2]thieno[2]pyrrole	27.8	1.0×10^{-6}	1.0×10^{-6} - 1.0×10^{-1}	20	-	(Abbas, 2012)
Hg^{2+}	1,2-bis-(N'-benzoylthioureido)cyclohexane	28.1	2.5×10^{-6}	1.0×10^{-5} - 1.0×10^{-1}	50-100	-	(Jumal et al., 2012)
Ag^+	N,N'-bis(benophenone imine)formamide	59.5	5.0×10^{-8}	2.2×10^{-7} - 2.2×10^{-2}	<10	>50	(Dadkhah et al., 2014)
Ag^+	p-tert-butylcalix[4]arene	59.8	1.0×10^{-7}	5.0×10^{-7} - 1.0×10^{-3}	<10	>35	(Yan et al., 2013)
Ag^+	N,N'-bis(3-methyl-1-phenyl-4-benzylidene-5-pyrazole)propylenediamine	59.3	9.3×10^{-7}	1.0×10^{-6} - 1.0×10^{-1}	5-30	-	(Hassouna et al., 2010)

Table 2.4, continued.

Metal ion	ionophore	Slope (mV/decade)	Detection limit (M)	Linear range (M)	Response time (s)	Life time (day)	Refs.
Ag ⁺	Isoquinoline-1,3-diones	58.4	5.8×10^{-6}	5.0×10^{-6} - 1.0×10^{-1}	12	<90	(Kamal et al., 2012)
Ag ⁺	Shift-base lariat ethers (a), 6	59.3	4.4×10^{-8}	5.6×10^{-8} - 1.0×10^{-1}	12	-	(Gupta et al., 2009)
	Shift-base lariat ethers (a), 5	58.9	3.1×10^{-7}	5.6×10^{-7} - 1.0×10^{-1}	13	-	
	Shift-base lariat ethers (a), 4	59.4	1.7×10^{-6}	3.1×10^{-6} - 1.0×10^{-1}	13	-	
	Shift-base lariat ethers (a), 3	59.0	4.4×10^{-6}	5.6×10^{-6} - 1.0×10^{-1}	15	-	
	Shift-base lariat ethers (a), 2	59.4	8.9×10^{-6}	1.1×10^{-5} - 1.0×10^{-1}	15	-	
	Shift-base lariat ethers (a), 1	59.3	1.0×10^{-5}	1.4×10^{-5} - 1.0×10^{-1}	16	-	

(a)



(b)

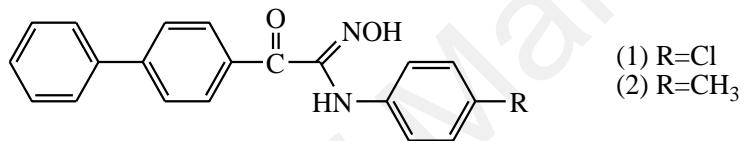


Figure 2.13: The structure of ionophore (a) shift base lariat ether, (b) oxime (Gupta et al., 2009; Sardohan-Koseoglu et al., 2015)

The interaction of M^{n+} -ionophore (ion recognition) with most of the listed carriers relies on the hard-soft acid based (HSAB) concept. According to this concept, in order to find the suitable ionophore, soft base ligands are preferable which has a good affinity to soft acids (Pearson, 1968). NHC is classified as Lewis base 2-electron donors which as relatively soft ligands are not necessarily require backbonding in their complexes. This makes them suitable for coordinating to a range of different centers (Albrecht et al., 2012; Willans, 2010). Due to this character, the potential of bis-NHC as ionophore in ISE application can be explored.

CHAPTER 3

METHODOLOGY

3.1 Chemicals and instruments

All glassware were dried in an oven overnight before use. All chemicals and solvents were purchased from Sigma-Aldrich, MERCK and Fisher, and used as received without further purification. The synthesized products were characterized by Fourier Transfer Infrared (FT-IR) spectroscopy, Nuclear Magnetic Resonance (NMR) spectroscopy, Carbon-Hydrogen-Nitrogen-Sulfur (CHNS) elemental analysis, UV-Vis spectroscopy and single crystal X-ray diffraction analysis.

The melting points of synthesized compounds were measured using a U Met-temp II Laboratory Devices USA. The FT-IR spectra were recorded between 4000-400 cm⁻¹ as attenuated total reflectance (ATR) on Perkin Elmer Spectrum 400 FT-IR spectrometer. ¹H-NMR and ¹³C-NMR were recorded on a Bruker Advance 400 spectrometer at 400 MHz (¹H-NMR) and 100 MHz (¹³C-NMR) using tetramethylsilane (TMS) as an internal standard. The CHNS elemental analysis values were determined using a LECO TruSpec Micro CHNS Elemental Analyzer. The crystal data were collected from a Bruker SMART APEX2 diffractometer and the structures of synthesized compounds were solved using direct methods and were refined by full-matrix least squares using the program SHELXTL-97 Sheldrick. The spectrophotometer type UV/Vis/NIR (UV- 3600 Shimadzu) including the temperature controller TCC-2 was used to obtain the spectra of synthesized compounds, Hg²⁺ and Ag⁺ cations and resulted complex respectively. The Morphologies of membranes were analyzed using a

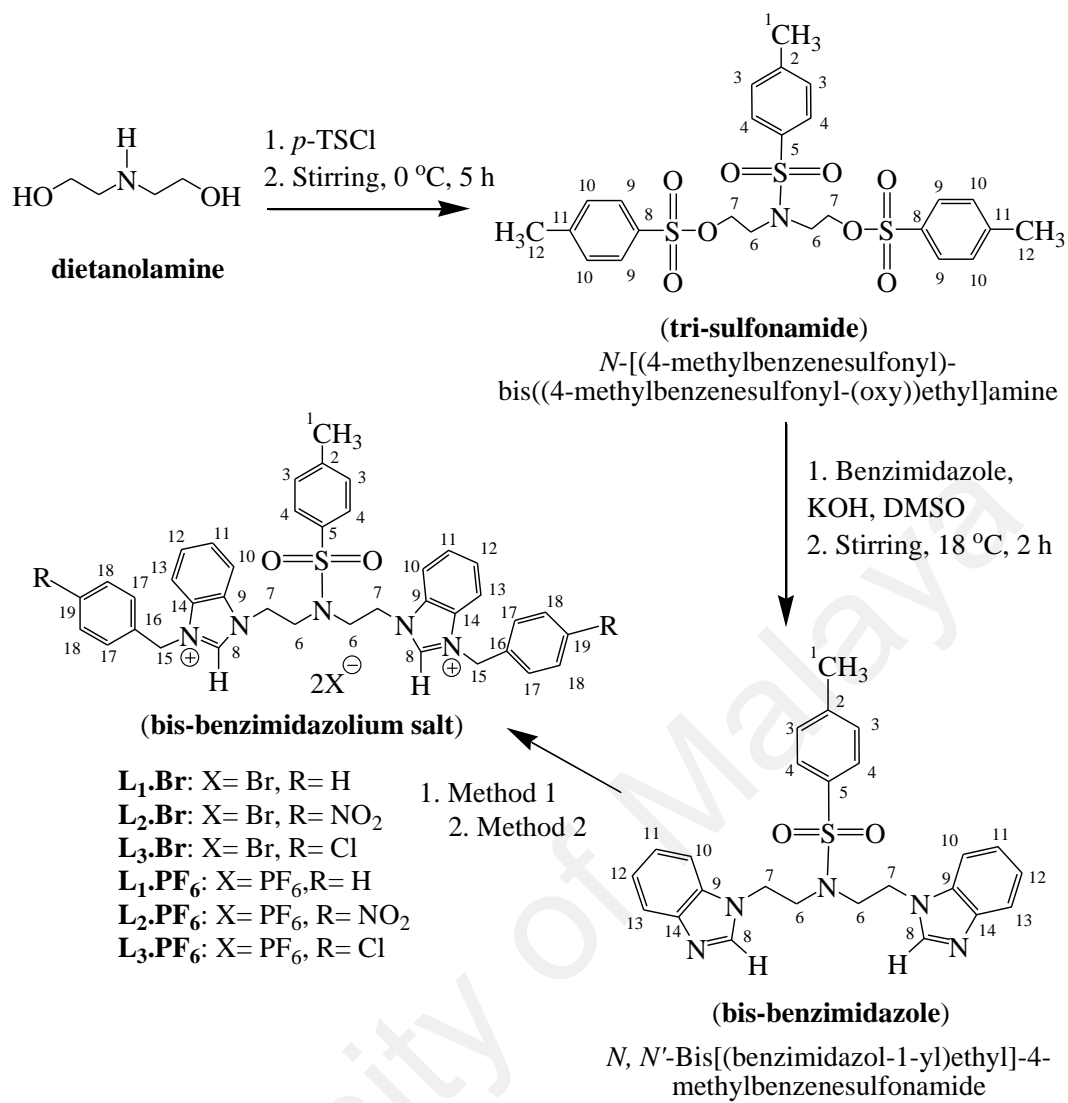
Field Emission Scanning Electron Microscope HITACHI SU8220 equipped with Energy Dispersive facility (FESEM-EDX). The crystallinity structures of membranes were examined using powder X-Ray Diffraction (XRD) PANalytical EMPYREAN at room temperature and scanned from 20 to 80 ° 2θ angles using a step interval of 0.02° with the scan rate of 5° min⁻¹.

The conductometric measurements were carried out using digital Thermo Scientific conductivity device connected to a JULABO F12 thermostated water-bath with a constant temperature maintained within ±0.01 °C. A conductometric electrode model Orion 013005MD with cell constant of 0.99 cm⁻¹ was used in the present studies.

The electromotive force (E/mV) of fabricated sensors were measured relative to Ag-AgCl double-junction reference electrode (Thermo Orion 900200) using a digital pH/ISE meter (Orion Star A214). All measurements were carried out at room temperature.

3.2 Synthesis of bis-NHC precursor

Synthesis routes in the preparation of bis-NHC precursors based on benzimidazolium are shown in Scheme 3.1. The methodologies for each synthesized compound are subsequently mentioned in the upcoming subtopic.



List of synthesized bis-benzimidazolium salts:

- L₁.Br**=*N,N'*-Bis[1-benzyl-benzimidazolium-ethyl]-4-methylbenzenesulfonamide dibromide
- L₂.Br**=*N,N'*-Bis[4-nitro-1-benzyl-benzimidazolium-ethyl]-4-methylbenzenesulfonamide dibromide
- L₃.Br**=*N,N'*-Bis[4-chloro-1-benzyl-benzimidazolium-ethyl]-4-methylbenzenesulfonamide dibromide
- L₁.PF₆**=*N,N'*-Bis[1-benzyl-benzimidazolium-ethyl]-4-methylbenzenesulfonamide dihexafluorophosphate
- L₂.PF₆**=*N,N'*-Bis[4-nitro-1-benzyl-benzimidazolium-ethyl]-4-methylbenzenesulfonamide dihexafluorophosphate
- L₃.PF₆**=*N,N'*-Bis[4-chloro-1-benzyl-benzimidazolium-ethyl]-4-methylbenzenesulfonamide dihexafluorophosphate

Scheme 3.1: Synthesis routes in the preparation of bis-benzimidazolium salts

3.2.1 Synthesis of *N*-(4-methylbenzenesulfonyl)-bis((4-methylbenzenesulfonyloxy)ethyl)amine; (tri-sulfonamide)

Diethanolamine, (4.8 ml, 0.05 mol) was dissolved in dichloromethane (100 ml). The reaction mixture solution was cooled to 0 °C and then triethylamine (27.9 ml, 0.20 mol) was added. At temperature of 0 °C, *p*-toluenesulfonyl chloride (*p*-TSCl) (28.6 g, 0.15 mol) was added gradually, with vigorous stirring over the course of 5 hours to obtain tri-sulfonamide. Then, the reaction mixture was continued being stirred at room temperature overnight and white precipitates of Et₃NHCl were observed. The reaction mixture was filtered to gain colorless filtrate, and washed with 1 M HCl (3 times), distilled water (5×40 ml) and saturated NaHCO₃ solution (5×40 ml). The organic layer was dried over anhydrous magnesium sulfate and the solvent was removed under vacuum to obtain viscous liquid (Al-Mohammed et al., 2013). The product was recrystallized from methanol to form a pure white solid. The solid product obtained was characterized by FT-IR, ¹H-NMR, and ¹³C-NMR. FT-IR, ATR (cm⁻¹), APPENDIX A1: 3065 (C-H)_{Ar}, 2926 (C-H)_{Aliph}, 1495, 1452 (C=C)_{Ar}, 1336, 1156 (O=S=O); ¹H-NMR (DMSO-d₆) δ ppm, APPENDIX B1: 7.74 (d, 4H; H-8), 7.58 (d, 2H; H-4), 7.49 (d, 4H; H-10), 7.37 (d, 2H; H-3), 4.01 (t, 4H; H-7), 3.30 (t, 4H; H-6), 2.44 (s, 6H; H-12), 2.39 (s, 3H; H-1); ¹³C-NMR (DMSO-d₆) δ ppm, APPENDIX C1: 145.65 (2C; C-8), 144.25 (1C; C-5), 135.47 (1C; C-2), 132.42 (2C; C-11), 130.70 (4C; C-9), 130.40 (2C; C-4), 128.06 (4C; C-10), 127.45 (2C; C-3), 68.63 (2C; C-7), 47.77 (2C; C-6), 21.59 (2C; C-12), 21.48 (1C; C-1).

3.2.2 Synthesis of *N,N'*-Bis[(benzimidazol-1-yl)ethyl]-4-methylbenzenesulfonamide; (bis-benzimidazole)

Benzimidazole (2.36 g, 0.02 mol) was completely dissolved in dimethylsulfoxide (DMSO) (20 ml). After that, potassium hydroxide (KOH) (1.68 g, 0.03 mol) was added to the solution and the mixture was stirred for 30 min at 20 °C. Tri-sulfonamide (5.67 g, 0.01 mol) was added portion wise under vigorous stirring in water bath. The stirring continued for another 2 hours (pale yellow viscous reaction mixture was observed), then the distilled water (200 ml) was added to the mixture and extracted with chloroform (6×30 ml). The combined extracts were washed with water and dried over anhydrous magnesium sulfate. The solvent was removed under vacuum and the product was recrystallized from methanol to obtain a white solid of bis-benzimidazole (Al-Mohammed et al., 2013). The solid product obtained was characterized by FT-IR, ¹H-NMR, and ¹³C-NMR spectroscopy. FT-IR, ATR (cm⁻¹), APPENDIX A2: 3051 (C-H)_{Ar}, 2923 (C-H)_{Aliph}, 1594 (C=N), 1499,1460 (C=C)_{Ar}, 1322 and 1155 (O=S=O); ¹H-NMR (DMSO-d₆) δ ppm, APPENDIX B2: 8.10 (s, 1H; H-8), 7.64 (m, 4H; H-13 and H-10), 7.46 (d, 2H; H-4), 7.28 (m, 6H; H-3, H-11, H-12), 4.28 (t, 4H; H-7), 3.51 (t, 4H; H-6), 2.34 (s, 3H; H-1). ¹³C-NMR (DMSO-d₆) δ ppm, APPENDIX C3: 144.45 (1C; C-5), 143.73 (2C; C-9), 135.31 (1C; C-2), 133.99 (2C; C-14), 130.38 (2C; C-8), 130.25 (2C; C-4), 127.41 (2C; C-3), 123.07 (2C; C-10), 122.15 (2C; C-13), 120.06 (2C; C-11), 110.55 (2C; C-12), 48.60 (2C; C-6), 43.65 (2C; C-7), 21.44 (1C; C-1).

3.2.3 Synthesis of bis-benzimidazolium salts

Method 1: Bis-benzimidazole (0.5 mmol) was added to the stirred solution of benzyl bromide, 4-(nitromethyl)benzyl bromide, or 4-(chloromethyl)benzyl bromide (1.0 mmol) in 20 ml of 1,4-dioxane. The mixture was refluxed at 100 °C for 24 hours and the sticky precipitates were obtained (Haque et al., 2011). The product was washed with 1,4-dioxane (2×5 ml) and diethyl ether (2×3 ml), followed by drying in vacuum to give a bis-benzimidazolium bromide salt L₁.Br, L₂.Br and L₃.Br as listed below:

N,N'-Bis[1-benzyl-benzimidazolium-ethyl]-4-methylbenzenesulfonamide dibromide (L₁.Br)

FT-IR, ATR (cm⁻¹), APPENDIX A3: 3120 (C-H)_{Ar}, 3023 (C-H)_{Aliph}, 1559 (C=N), 1494, 1449 (C=C)_{Ar}, 1338, 1156 (O=S=O); ¹H-NMR (DMSO-d₆) δ ppm, APPENDIX B3: 10.24 (s, 2H; H-8), 8.17 (d, 2H; H-13), 8.00 (d, 2H; H-10), 7.73 (m, 4H; H-11, H-12), 7.62 (d, 4H; H-17), 7.44 (m, 8H; H-4, H-18 and H-19), 7.15 (d, 2H; H-3), 5.90 (s, 4H; H-15), 4.94 (t, 4H; H-7), 4.02 (t, 4H; H-6), 2.34 (s, 3H; H-1); ¹³C-NMR (DMSO-d₆) δ ppm, APPENDIX C3: 144.28 (1C; C-5), 135.21 (1C; C-2), 134.33 (2C; C-16), 131.79 (2C; C-9), 131.16 (2C; C-14), 130.09 (2C; C-8), 129.40 to 114.18 (22C; C-4, C-17, C-18, C-19, C-3, C-10, C-13, C-12, C-11), 50.36 (2C; C-15), 46.73 (2C; C-6), 45.44 (2C; C-7), 21.48 (1C; C-1). CHNS elemental analysis (%); calculated: C, 58.43; H, 4.90; N, 8.74; S, 4.00; found: C, 58.40; H, 4.96; N, 8.68; S, 3.72.

N,N'-Bis[4-nitro-1-benzyl-benzimidazolium-ethyl]-4-methylbenzenesulfonamide dibromide (L₂.Br)

FT-IR, ATR (cm⁻¹), APPENDIX A4: 3121 (C-H)_{Ar}, 3026 (C-H)_{Aliph}, 1566 (C=N), 1515 (NO₂), 1488, 1434 (C=C)_{Ar}, 1341, 1157 (O=S=O); ¹H-NMR (DMSO-d₆) δ ppm, APPENDIX B4: 10.24 (s, 2H; H-8), 8.24 (d, 4H; H-18), 8.16 (d, 2H; H-13), 7.92 (d, 2H; H-10), 7.80 (d, 4H; H-17), 7.69 (m, 4H; H-11, H12), 7.44 (d, 2H; H-4), 7.17 (d, 2H; H-3), 6.06 (s, 4H; H-15), 4.93 (t, 4H; H-7), 3.98 (t, 4H; H-6), 2.31 (s, 3H; H-1); ¹³C-NMR (DMSO-d₆) δ ppm, APPENDIX C4: 148.04 (2C; C-19), 144.40 (1C; C-5), 141.74 (2C; C-16), 135.18 (1C; C-2), 131.82 (2C; C-9), 131.14 (2C; C-14), 130.17 (2C; C-8), 129.90 to 114.21 (20C; C-4, C-18, C-17, C-3, C-13, C-10), 49.47 (2C; C-15), 46.97 (2C; C-6), 45.65 (2C; C-7), 21.48 (1C; C-1). CHNS elemental analysis (%); calculated: C, 52.54; H, 4.18; N, 11.00; S, 3.60; found: C, 51.95; H, 4.39; N, 10.48; S, 3.46.

N,N'-Bis[4-chloro-1-benzyl-benzimidazolium-ethyl]-4-methylbenzenesulfonamide dibromide (L₃.Br)

FT-IR, ATR (cm⁻¹), APPENDIX A5: 3121 (C-H)_{Ar}, 3025 (C-H)_{Aliph}, 1561 (C=N), 1492, 1446 (C=C)_{Ar}, 1334, 1155 (O=S=O), 747 (C-Cl); ¹H-NMR (DMSO-d₆) δ ppm, APPENDIX B5: 10.18 (s, 2H; H-8), 8.13 (d, 2H; H-13), 7.95 (d, 2H; H-10), 7.68 (m, 4H; H-11, H-12), 7.61 (d, 4H; H-18), 7.48 (d, 4H; H-17), 7.40 (d, 2H; H-4), 7.13 (d, 2H; H-3), 5.86 (s, 4H; H-15), 4.89 (t, 4H; H-7), 3.96 (t, 4H; H-6), 2.30 (s, 3H; H-1); ¹³C-NMR (DMSO-d₆) δ ppm, APPENDIX C5: 144.32 (1C; C-5), 135.19 (1C; C-2), 133.95 (2C; C-19), 133.30 (2C; C-16), 131.80 (2C; C-9), 131.10 (2C; C-14), 130.81 (2C; C-8), 130.11 to 114.22 (20C; C-4, C18, C-17, C-3, C-10, C-13), 49.57 (2C; C-15), 46.81 (2C; C-6), 45.57 (2C; C-7), 21.47 (1C; C-1). CHNS elemental analysis (%);

calculated: C, 53.81; H, 4.28; N, 8.04; S, 3.68; found: C, 53.57; H, 4.46; N, 7.96; S; 3.40.

Method 2: The resulting bromide salts L₁.Br, L₂.Br, and L₃.Br (1.0 mmol) were directly converted to its hexafluorophosphate (PF₆⁻) counterpart by metathesis reaction using potassium hexafluorophosphate (KPF₆) (1.0 mmol) in 20 ml methanol, respectively (Haque et al., 2011). The mixture was stirred until all solid was dissolved. The mixture solution was then left at room temperature overnight and the precipitates was formed. The filtered product was washed with distilled water giving the bis-benzimidazolium hexafluorophosphate salts L₁.PF₆, L₂.PF₆, and L₃.PF₆ as listed below:

N,N'-Bis[1-benzyl-benzimidazolium-ethyl]-4-methylbenzenesulfonamide dihexafluorophosphate (L₁.PF₆)

FT-IR, ATR (cm⁻¹), APPENDIX A6: 3113 (C-H)_{Ar}, 3019 (C-H)_{Aliph}, 1566 (C=N), 1491, 1451 (C=C)_{Ar}, 1329, 1157 (O=S=O), 834 (PF₆); ¹H-NMR (DMSO-d₆) δ ppm, APPENDIX B6: 10.00 (s, 2H; H-8), 8.07 (d, 2H; H-13), 7.93 (d, 2H; H-10), 7.67 (m, 4H; H-11, H12), 7.54 (d, 4H, H-17), 7.39 (m, 8H, H4, H18, H19), 7.08 (d, 2H, H-3), 5.80 (s, 4H; H-15), 4.83 (t, 4H; H-7), 3.94 (t, 4H; H-6), 2.28 (s, 3H; H-1); ¹³C-NMR (DMSO-d₆) δ ppm, APPENDIX C6: 144.35 (1C; C-5), 135.19 (1C; C-2, 134.22 (2C; C-16), 131.78 (2C; C-9), 131.18 (2C; C-14), 130.09 (2C; C-8), 129.44 to 114.07 (22C; C-4, C-17, C-18, C-19, C-3, C-10, C-13), 50.39 (2C; C-15), 46.62 (2C; C-6), 45.32 (2C; C-7), 21.45 (1C; C-1). CHNS elemental analysis (%); calculated: C, 50.27; H, 4.22; N, 7.52; S, 3.44; found: C, 49.72; H, 4.13; N, 8.03; S, 4.00.

N,N'-Bis[4-nitro-1-benzyl-benzimidazolium-ethyl]-4-methylbenzenesulfonamide dihexafluorophosphate (L₂.PF₆)

FT-IR, ATR (cm⁻¹), APPENDIX A7: 3120 (C-H)_{Ar}, 3031 (C-H)_{Aliph}, 1564 (C=N), 1520 (NO₂), 1491, 1447 (C=C)_{Ar}, 1344, 1157 (O=S=O), 832 (PF₆); ¹H-NMR (DMSO-d₆) δ ppm, APPENDIX B7: 10.10 (s, 2H; H-8), 8.25 (d, 4H; H-18), 8.14 (d, 2H; H-13), 7.92 (d, 2H; H-10), 7.78 (d, 4H; H-17), 7.70 (m, 4H; H-11, H-12), 7.42 (d, 2H; H-4), 7.17 (d, 2H; H-3), 6.02 (s, 4H; H-15), 4.89 (t, 4H; H-7), 3.96 (t, 4H; H-6), 2.31 (s, 3H; H-1); ¹³C-NMR (DMSO-d₆) δ ppm, APPENDIX C7: 148.06 (2C; C-19), 144.42 (1C; C-5), 141.71 (2C; C-16), 135.21 (1C; C-2), 131.82 (2C; C-9), 131.17 (2C; C-14), 130.16 (2C; C-8), 129.84 to 114.21 (20C; C-4, C-17, C-18, C-3, C-10, C-13), 49.49 (2C; C-15), 46.90 (2C; C-6), 45.55 (2C; C-7), 21.47 (1C; C-1). CHNS elemental analysis (%); calculated: C, 45.84; H, 3.65; N, 9.60; S, 3.14; found: C, 46.32; H, 4.02; N, 9.91; S, 3.63.

N,N'-Bis[4-chloro-1-benzyl-benzimidazolium-ethyl]-4-methylbenzenesulfonamide dihexafluorophosphate (L₃.PF₆)

FT-IR, ATR (cm⁻¹), APPENDIX A8: 3161 (C-H)_{Ar}, 3043 (C-H)_{Aliph}, 1565 (C=N), 1494, 1447 (C=C)_{Ar}, 1337, 1157 (O=S=O), 825 (PF₆), 747 (C-Cl); ¹H-NMR (DMSO-d₆) δ ppm, APPENDIX B8: 10.03 (s, 2H; H-8), 8.09 (d, 2H; H-13), 7.94 (d, 2H; H-10), 7.69 (m, 4H; H11, H12), 7.58 (d, 4H; 18), 7.48 (d, 4H; H-17), 7.38 (d, 2H; H-4), 7.12 (d, 2H; H-3), 5.82 (s, 4H; H-15), 4.84 (t, 4H; H-7), 3.93 (t, 4H; H-6), 2.30 (s, 3H; H-1); ¹³C-NMR (DMSO-d₆) δ ppm, APPENDIX C8: 144.34 (1C; C-5), 135.22 (1C; C-2), 133.98 (2C; C-19), 133.25 (2C; C-16), 131.80 (2C; C-9), 131.13 (2C; C-14), 130.76 (2C; C-8), 130.10 to 114.15 (20C; C-4, C-18, C-17, C-3, C-10, C-13), 49.59 (2C; C-15), 46.74 (2C; C-6), 45.40 (2C; C-7), 21.45 (1C; C-1). CHNS elemental analysis (%); calculated: C, 46.81; H, 3.73; N, 7.00; S, 3.20; found: C, 46.66; H, 3.37; N, 7.38; S, 3.28.

3.3 Conductometric study of L₁.Br

The conductometric study of L₁.Br with Ni(NO₃)₂, Zn(NO₃)₂, Pd(NO₃)₂, Hg(NO₃)₂, and AgNO₃ was conducted according to the reported procedures (Ahmadzadeh et al., 2011; Jóźwiak et al., 2014; Rezayi et al., 2011). The experimental setup for conductometric study is shown in Figure 3.1. A solution of Ni²⁺ cation with concentration of 5.0×10^{-5} M was prepared and placed in a water-jacketed cell. This water-jacketed cell is equipped with magnetic stirrer and connected to the thermostat by circulating water line in order to maintain the desired temperature. After that, the solution of L₁.Br with the concentration of 2.5×10^{-3} M is prepared and added by using calibrated micropipette in a stepwise manner. The conductivity of reaction solution mixtures were measured by using conductivity meter and dip-type conductivity cell after each titration. This experiment was conducted in six different binary systems of methanol-water (MeOH-H₂O) (molar percentage of MeOH (mol%); 0.00, 9.99, 22.66, 39.73, 63.72 and 100.00) at varied temperatures (15, 25, 35 and 45 °C), respectively. The procedure was repeated for other metal cations (Zn²⁺, Pd²⁺, Hg²⁺, and Ag⁺). The changes in molar conductivity (Λ_m) of the reaction mixture were observed as a function of molar ratio of the ligand (L₁.Br) and metal cation (Mⁿ⁺), ([L₁.Br]_t/[Mⁿ⁺]_t) of the proposed complexes.

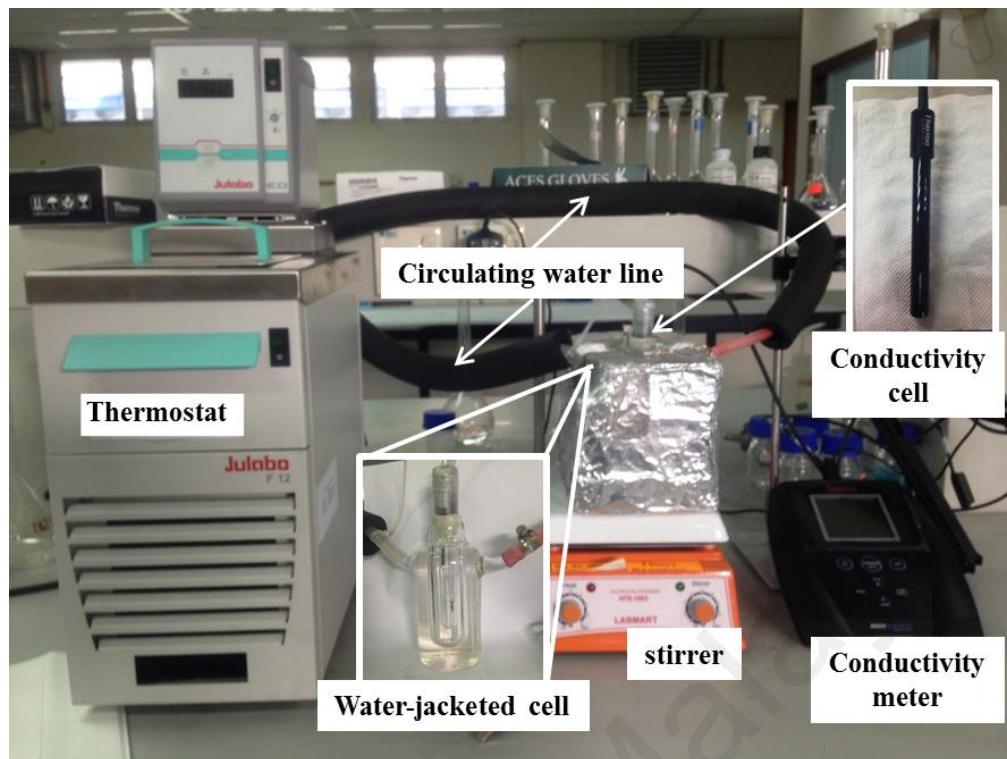


Figure 3.1: The experimental setup for conductometric study

Some results in this section were obtained from computer programs as follows: i) GENPLOT- to determine the stability constant ($\log K_f$) values of complexation reaction between L₁.Br and studied metal cations (Ni²⁺, Zn²⁺, Pd²⁺, Hg²⁺ and Ag⁺) (Genplot, 1989), ii) ANN- to evaluate the accuracy of experimental data (Rezayi et al., 2014), and ii) GAUSSIAN 09- to understand the functional interaction of L₁.Br with Ni²⁺, Zn²⁺, Pd²⁺, Hg²⁺ and Ag⁺ metal cations, respectively (Sakajiri et al., 2012). The details methodologies will be explained in chapter 4.

3.4 Fabrication of ion selective electrode (ISE) based on L₁.Br ionophore

3.4.1 Sensor fabrication and optimization

The sensor membranes were fabricated and photocured according to the modification method reported previously (Jumal et al., 2012). The procedure to prepare ISE membrane was as follows: First, a layer containing a mixture of 96.8 wt% HEMA (monomer) and 3.2 wt% DMPP (photoinitiator) was deposited on the tip of a silver/silver chloride screen printed electrode (SPE). 0.2 μ l of the mixture was photocured under UV radiation (15 w Blacklight F15T8/BL 15 watt; Peak Emission 365 nm) with a constant flow of nitrogen gas for 480 s. The obtained membrane was then conditioning in 0.01 M of metal cations solution for 20 min to form the “inner solution” of the sensor. Finally, 0.5 μ l of the mixture with various compositions as mentioned in Table 3.1 was then deposited on top of the hydrated p(HEMA) inner layer using the photocuring technique as before. The steps for preparation of electrode membrane are illustrated in Figure 3.2.

3.4.2 Sensor evaluation

The responses of the sensors were measured in an electrochemical cell setup. A double-junction Ag/AgCl was used as an external reference electrode with a reference solution (3M KCl) as the inner filling solution (Orion 900002) and 0.1 M lithium acetate (LiOAc) as a gel bridge electrolyte. The ISE membrane was prepared according to the mentioned method in section 3.4.1 and used as a working electrode. Both electrodes were connected to an Orion pH/ISE-meter. The Hg²⁺ and Ag⁺ test solutions were prepared using HgCl₂ and AgNO₃ in deionized water with concentrations ranging from 1×10^{-8} to 1×10^{-1} M, respectively. The potential readings for the metal cations

solution starting from low to high concentrations were recorded when a stable value (mV) was reached after 20-30 seconds. The cell potentials were measured using a schematic galvanic cell as follows:

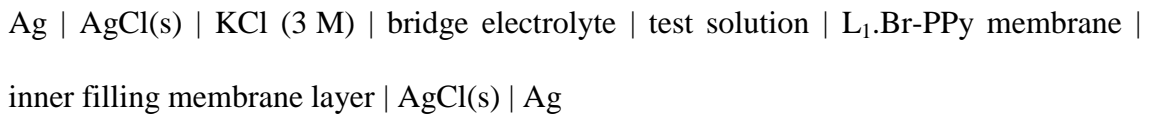


Table 3.1: The different composition of ISE membrane based on L₁.Br ionophore for the potentiometric detection of metal cations

^a Hg-ISE	Composition (w/w%)			
	Pyrrole	DMPP	NaTFB	L ₁ .Br
E1	89.4	4.8	0.8	5.0
E2	88.8	4.8	0.8	5.6
E3	89.4	4.8	0.2	5.6
E4	94.2	0.0	0.2	5.6
E5	95.0	4.8	0.2	0.0
E6	89.6	4.8	0.0	5.6
E7	91.0	4.8	0.2	4.0
E8	89.5	4.8	0.1	5.6
E9	89.0	4.8	0.1	6.1
E10	88.2	5.2	0.1	6.5

^b Ag-ISE	Composition (w/w%)			
	Pyrrole	DMPP	NaTFB	L ₁ .Br
E1	95.0	4.8	0.2	0.0
E2	93.0	3.8	0.2	3.0
E3	91.0	4.8	0.2	4.0
E4	89.4	4.8	0.2	5.6
E5	89.6	4.8	0.0	5.6
E6	88.8	4.8	0.8	5.6
E7	88.2	5.2	0.1	6.5

^amembrane compositions were applied for optimized Hg-ISE membrane, ^bmembrane compositions were applied for optimized Ag-ISE membrane.

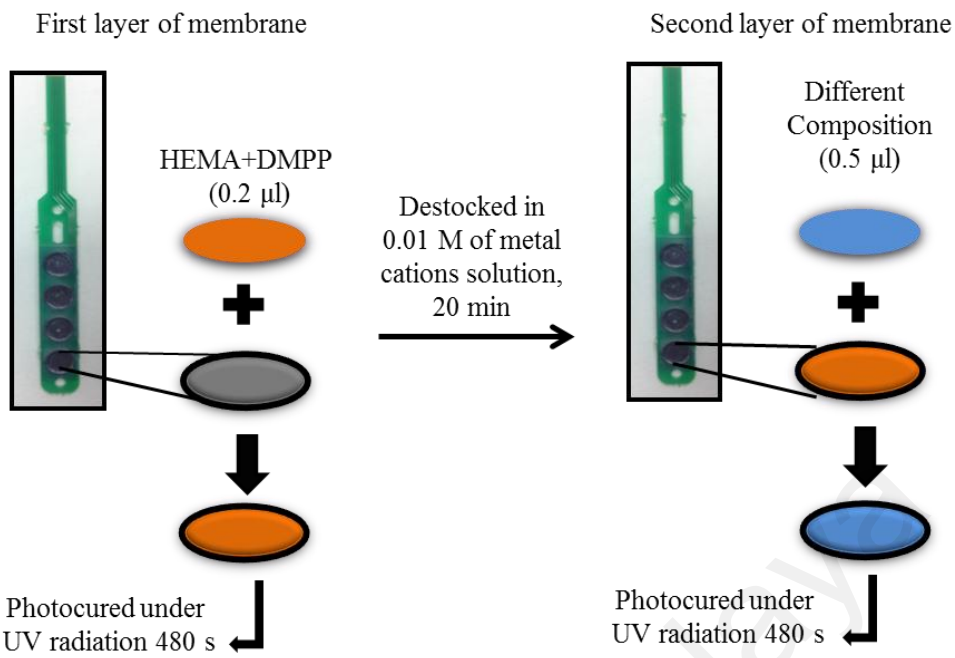


Figure 3.2: Diagram of the fabrication electrode membrane

3.4.3 Effect of pH on electrode performance

The effects of pH on potential responses were evaluated in two different concentrations. They are 1×10^{-5} M and 1×10^{-3} M test solutions at room temperature. The pH of Hg^{2+} and Ag^+ test solutions were adjusted from pH 1.0 to 12.0 and pH 1.0 to 8.0 by addition of HCl and NaOH solutions, respectively (Yan et al., 2007).

3.4.4 Response time of proposed electrode

The response time of a sensor is considered as the required time of potential to reach a steady state within ± 1 mV during the immersion of sensor in a series of respective test solutions. In this study, the dynamic response time of proposed sensor was verified by changing the concentration of test solution from 1.0×10^{-5} to 1.0×10^{-1} M and 1.0×10^{-6} to 1.0×10^{-2} M for Ag^+ and Hg^{2+} metal cations, respectively. The

measurement was conducted from low to high concentration, sequentially (Gupta et al., 2009).

3.4.5 Repeatability, reproducibility and stability of proposed electrode

The parameters such as repeatability, reproducibility and stability of electrode were evaluated in order to validate the performance of proposed ISE. The repeatability of the proposed sensor was tested using three measurements over the working concentration ranges of the optimized electrode membrane within a single day and the reproducibility of ISE was studied using three different optimum composition membrane electrodes. The stability of electrode was determined by using the same electrode within two months (Ghanei-Motlagh et al., 2014; Gupta et al., 2007).

3.4.6 Determination of selectivity coefficients

The potentiometric selectivity coefficients ($K_{X^{y+}, M^{n+}}^{pot}$) were evaluated using the separation solution method (SSM) according to IUPAC recommendations (Umezawa et al., 2000). This method measured potential difference between the reference electrode and the membrane electrode according to the two separate solutions X^{y+} and M^{n+} , where X^{y+} is the target metal cation and M^{n+} is the interfering cations at the same activity ($a_{X^{y+}} = a_{M^{n+}}$). Selectivity coefficients used the following equation:

$$K_{X^{y+}, M^{n+}}^{SSM} = \alpha^{(1-(y/n))} e^{(E_{M^{n+}} - E_{X^{y+}}) yF / (RT)}$$
Eq. (3.1)

Others notations are refer to:

$E_{M^{n+}}$ = potential measured values of interfering cations,

$E_{X^{y+}}$ = potential measured values of target metal cations,

F = Faraday constant (96,485 J),

R = universal gas constant (8.314 J/mol.K), and

T = room temperature at 298 °K

3.4.7 Analytical application of fabricated ISEs

3.4.7.1 Potentiometric titration

A solution of HgCl_2 with the concentration of 1.0×10^{-4} M (25 ml) was prepared and placed in a beaker. After that, the solution of ethylenediaminetetraacetic acid (EDTA) with concentration of 2.5×10^{-3} M was prepared and titrated by using calibrated micropipette in a stepwise manner. The potential of reaction solution mixtures are measured at each titration by using a digital pH/ISE meter and Hg-ISE was used as indicator electrode (Sardohan-Koseoglu et al., 2015). Similar procedure was conducted for Ag-ISE by using 20 ml AgNO_3 (5.0×10^{-2} M) solutions and titrated with a sodium chloride (NaCl) solution (1.0×10^{-1} M) (Dadkhah et al., 2014).

3.4.7.2 Real sample applications

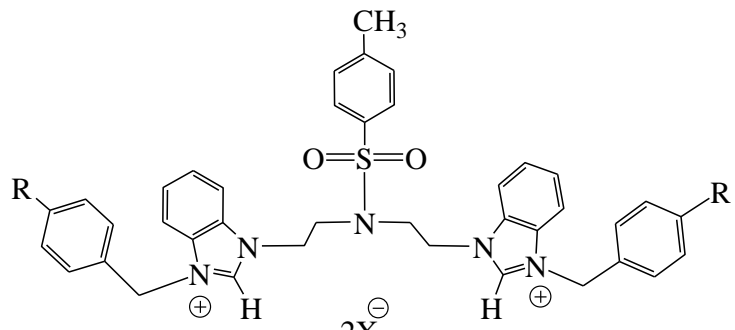
The applicability of the proposed electrode was tested by direct determination of target metal cations in tap water sample and standard sample. The direct determinations of targeted metal cations in tap water were conducted by using spike method (Dadkhah et al., 2014). Three different concentrations of metal cations test solutions were

prepared from HgCl_2 (5.0×10^{-6} M, 5.0×10^{-5} M, and 1.0×10^{-4} M) and AgNO_3 (5.0×10^{-5} M, 1.0×10^{-4} M, and 5.0×10^{-3} M, respectively. While, the determination of Hg^{2+} and Ag^+ in the standard sample solutions, the analysis were conducted by using standard reference material (SRM) 2702 and multi-element calibration standard solution 2A, respectively. The solutions were applied directly without any pretreatment. Each sample was analyzed in triplicate and the analysis was repeated under identical conditions.

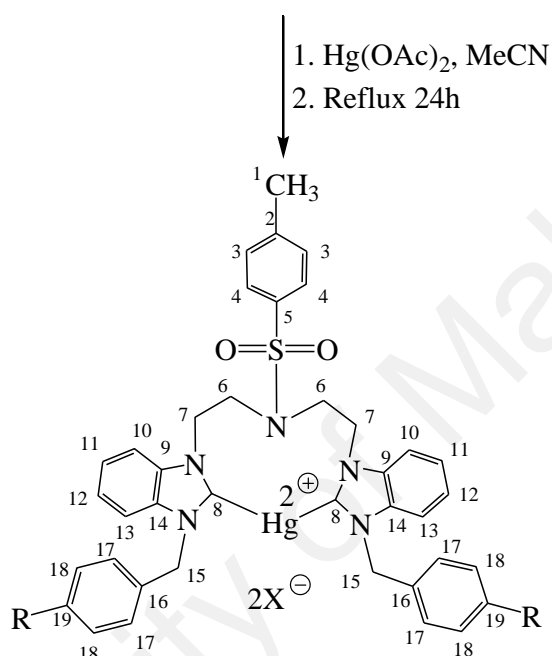
3.5 Synthesis of metal complexes

3.5.1 Synthesis of bis-NHC mercury(II) complexes

Synthesis route in the preparation of bis-NHC mercury(II) complexes were illustrated in Scheme 3.2. Mercury(II) acetate (Hg(OAc)_2) (1 mmol) was added to a solution of bis-benzimidazolium salt (1 mmol) in acetonitrile (40 ml). The mixture was heated at reflux for 24 hours. A clear solution was obtained. The solution was concentrated in vacuo (Haque et al., 2011). The solid residue was washed with water (2×5 ml) and recrystallized from acetonitrile to afford powder compound which is mercury complex. All complexes are listed below:



(bis-benzimidazolium salt)



(bis-NHC mercury(II) complex)

- L₁.HgBr:** X=Br, R=H
- L₂.HgBr:** X=Br, R=NO₂
- L₃.HgBr:** X=Br, R=Cl
- L₁.HgPF₆:** X=PF₆, R=H
- L₂.HgPF₆:** X=PF₆, R=NO₂
- L₃.HgPF₆:** X=PF₆, R=Cl

L₁.HgBr=(k²-C,C')N,N'-Bis[1-benzyl-benzimidazolium-ethyl]-4-methylbenzenesulfonamide mercury(II) dibromide

L₂.HgBr=(k²-C,C')N,N'-Bis[4-nitro-1-benzyl-benzimidazolium-ethyl]-4-methylbenzenesulfonamide mercury(II) dibromide

L₃.HgBr=(k²-C,C')N,N'-Bis[4-chloro-1-benzyl-benzimidazolium-ethyl]-4-methylbenzenesulfonamide mercury(II) dibromide

L₁.HgPF₆=(k²-C,C')N,N'-Bis[1-benzyl-benzimidazolium-ethyl]-4-methylbenzenesulfonamide mercury(II) dihexafluorophosphate

L₂.HgPF₆=(k²-C,C')N,N'-Bis[4-nitro-1-benzyl-benzimidazolium-ethyl]-4-methylbenzenesulfonamide mercury(II) dihexafluorophosphate

L₃.HgPF₆=(k²-C,C')N,N'-Bis[4-chloro-1-benzyl-benzimidazolium-ethyl]-4-methylbenzenesulfonamide mercury(II) dihexafluorophosphate

Scheme 3.2: Synthesis route in the preparation of bis-NHC mercury(II) complexes

(k²-C,C')N,N'-Bis[1-benzyl-benzimidazolium-ethyl]-4-methylbenzenesulfonamide

mercury(II) dibromide (L₁.HgBr)

FT-IR, ATR (cm⁻¹), APPENDIX I1: 3033 (C-H)_{Ar}, 2950 (C-H)_{Aliph}, 1451, 1416 (C=C)_{Ar}, 1336, 1157 (O=S=O); ¹H-NMR (DMSO-d₆) δ ppm, APPENDIX J1: 8.05 (d, 2H; C-13), 7.60-7.42 (m, 6H; H-10, H-11, H-12), 7.39 (d, 4H; H-17), 7.30-7.21 (m, 10H; H-3, H-18, H-19, H-4), 6.20 (s, 4H; H-15), 5.28 (s, 4H; H-7), 3.72 (s, 4H; H-6), 2.32 (s, 3H; H-1); ¹³C-NMR, APT (DMSO-d₆) δ ppm, APPENDIX K1: 185.97 (2C; C-8), 144.48 (1C; C-5), 135.63 (1C; C-2), 134.47 (2C; C-16), 133.68 (2C; C-9), 133.61 (2C; C-14), 130.48 to 112.98 (22C; C-4, C-17, C-18, C-19, C-3, C-10, C-13, C-11, C-12), 52.95 (2C; C-15), 51.21 (2C; C-6), 48.49 (2C; C-7), 21.39 (1C; C-1). CHNS elemental analysis (%); calculated: C, 46.83; H, 3.73; N, 7.00; S, 3.21. found: C, 47.38; H, 3.93; N, 7.10; S, 3.10.

(k²-C,C')N,N'-Bis[4-nitro-1-benzyl-benzimidazolium-ethyl]-4-

methylbenzenesulfonamide mercury(II) dibromide (L₂.HgBr)

FT-IR, ATR (cm⁻¹), APPENDIX I2: 3067 (C-H)_{Ar}, 2936 (C-H)_{Aliph}, 1521 (NO₂), 1450, 1411 (C=C)_{Ar}, 1342, 1157 (O=S=O); ¹H-NMR (DMSO-d₆) δ ppm, APPENDIX J2: 8.06 (d, 2H; H-13), 7.89 (d, 4H; H-18), 7.61-7.43 (m, 10H; H-10, H-11, H-12, H-17), 7.33 (d, 2H; H-4), 7.27 (d, 2H; H-3), 3.74 (s, 4H; H-6), 2.34 (s, 3H; H-1); ¹³C-NMR, APT (DMSO-d₆) δ ppm, APPENDIX K2: 185.09 (2C; C-8), 144.95 (1C; C-5), 142.30 (2C; C-19), 141.42 (2C; C-16), 132.42 (1C; C-2), 131.51 (2C; C-9), 131.48 (2C; C-14), 128.37 to 110.85 (20C; C-4, C-17, C-18, C-3, C-10, C-13, C-11, C-12), 50.76 (2C; C-15), 48.01 (2C; C-6), 46.42 (2C; C-7), 19.27 (1C; C-1). CHNS elemental analysis (%). Calculated: C, 42.97; H, 3.24; N, 8.99; S, 2.94. Found: C, 42.56; H, 3.78; N, 8.96; S, 3.28.

(k²-C,C')N,N'-Bis[4-chloro-1-benzyl-benzimidazolium-ethyl]-4-

methylbenzenesulfonamide mercury(II) dibromide (L₃.HgBr)

FT-IR, ATR (cm⁻¹), APPENDIX I3: 3034 (C-H)_{Ar}, 2947 (C-H)_{Aliph}, 1451, 1410 (C=C)_{Ar}, 1337, 1157 (O=S=O), 739 (C-Cl); ¹H-NMR (DMSO-d₆) δ ppm, APPENDIX J3: 8.08 (d, 2H; H-13), 7.64-7.51 (m, 6H; H-10, H-11, H-12), 7.35-7.22 (m, 12H; H-3, H-17, H-18, H-4), 6.25 (s, 4H; H-15), 5.27 (s, 4H; H-7), 3.73 (s, 4H; H-6), 2.33 (s, 3H; H-1); ¹³C-NMR, APT (DMSO-d₆) δ ppm, APPENDIX K3: 185.74 (2C; C-8), 144.48 (1C; C-5), 134.63 (1C; C-2), 134.63 (2C; C-19), 133.63 (2C; C-16), 133.60 (2C; C-9), 133.05 (2C; C-14), 130.48 to 113.15 (20C; C-4, C-18, C-17, C-3, C-13, C-10, C-11, C-12), 53.00 (2C; C-15), 50.29 (2C; C-6), 48.58 (2C; C-7), 21.40 (1C; C-1). CHNS elemental analysis (%). Calculated: C, 43.81; H, 3.30; N, 6.55; S, 3.00. Found: C, 43.85; H, 3.55; N, 6.91; S, 3.46.

(k²-C,C')N,N'-Bis[1-benzyl-benzimidazolium-ethyl]-4-methylbenzenesulfonamide

mercury(II) dihexafluorophosphate (L₁.HgPF₆)

FT-IR, ATR (cm⁻¹), APPENDIX I4: 3034 (C-H)_{Ar}, 2947 (C-H)_{Aliph}, 1455, 1421(C=C)_{Ar}, 1343, 1159 (O=S=O), 832 (PF₆); ¹H-NMR (DMSO-d₆) δ ppm, APPENDIX J4: 8.12 (d, 2H; H-13), 7.64-7.52 (m, 6H; H-10, H-11, H-12), 7.38-7.24 (m, 14H; H-3, H-4, H-17, H-18, H-19), 6.14 (s, 4H; H-15), 5.21 (s, 4H; H-7), 3.75 (s, 4H; H-6), 2.34 (s, 3H; H-1); ¹³C-NMR, APT (DMSO-d₆) δ ppm, APPENDIX K4: 185.74 (2C; C-8), 144.64 (1C; C-5), 135.57 (1C; C-2), 134.28 (2C; C-16), 133.73 (2C; C-9), 133.50 (2C; C-14), 130.52 to 113.33 (22C; C-4, C17, C-18, C-19, C-3, C-10, C-13, C-11, C-12), 53.14 (2C; C-15), 51.41 (2C; C-6), 48.54 (2C; C-7), 21.40 (1C; C-1). CHNS elemental analysis (%); Calculated: C, 41.44; H, 3.30; N, 6.20; S, 2.84. Found: C, 41.98; H, 3.22; N, 6.01; S, 2.83.

(k²-C,C')N,N'-Bis[4-nitro-1-benzyl-benzimidazolium-ethyl]-4-

methylbenzenesulfonamide mercury(II) dihexafluorophosphate (L₂.HgPF₆)

FT-IR, ATR (cm⁻¹), APPENDIX I5: 3031 (C-H)_{Ar}, 2936 (C-H)_{Aliph}, 1523 (NO₂), 1449, 1416 (C=C)_{Ar}, 1345, 1158 (O=S=O), 827 (PF₆); ¹H-NMR (DMSO-d₆) δ ppm, APPENDIX J5: 8.14 (d, 2H; H-13), 7.94 (d, 4H; H-18), 7.66-7.62 (m, 6H; H-10,H-11, H-12), 7.56 (d, 2H; H-4), 7.43 (d, 4H; H-17), 7.33 (d, 2H; H-3), 6.38 (s, 4H; H-15), 5.24 (s, 4H; H-7), 3.76 (s, 4H; H-6), 2.35 (s, 3H; H-1); ¹³C-NMR, APT (DMSO-d₆) δ ppm, APPENDIX K5: 185.44 (2C; C-8), 147.22 (2C; C-19), 144.64 (1C; C-5), 143.19 (2C; C-16), 134.30 (1C; C-2), 133.62 (2C; C-9), 133.55 (2C; C-14), 130.55 to 113.37 (20C; C-4, C-18, C-17, C-3, C-10, C-13, C-11, C-12), 53.16 (2C; C-15), 50.23 (2C; C-6), 48.68 (2c; C-7), 21.41 (1C; C-1). CHNS elemental analysis (%); Calculated: C, 38.38; H, 2.89; N, 8.03; S, 2.63. Found: C, 37.95; H, 2.90; N, 7.83; S, 2.42.

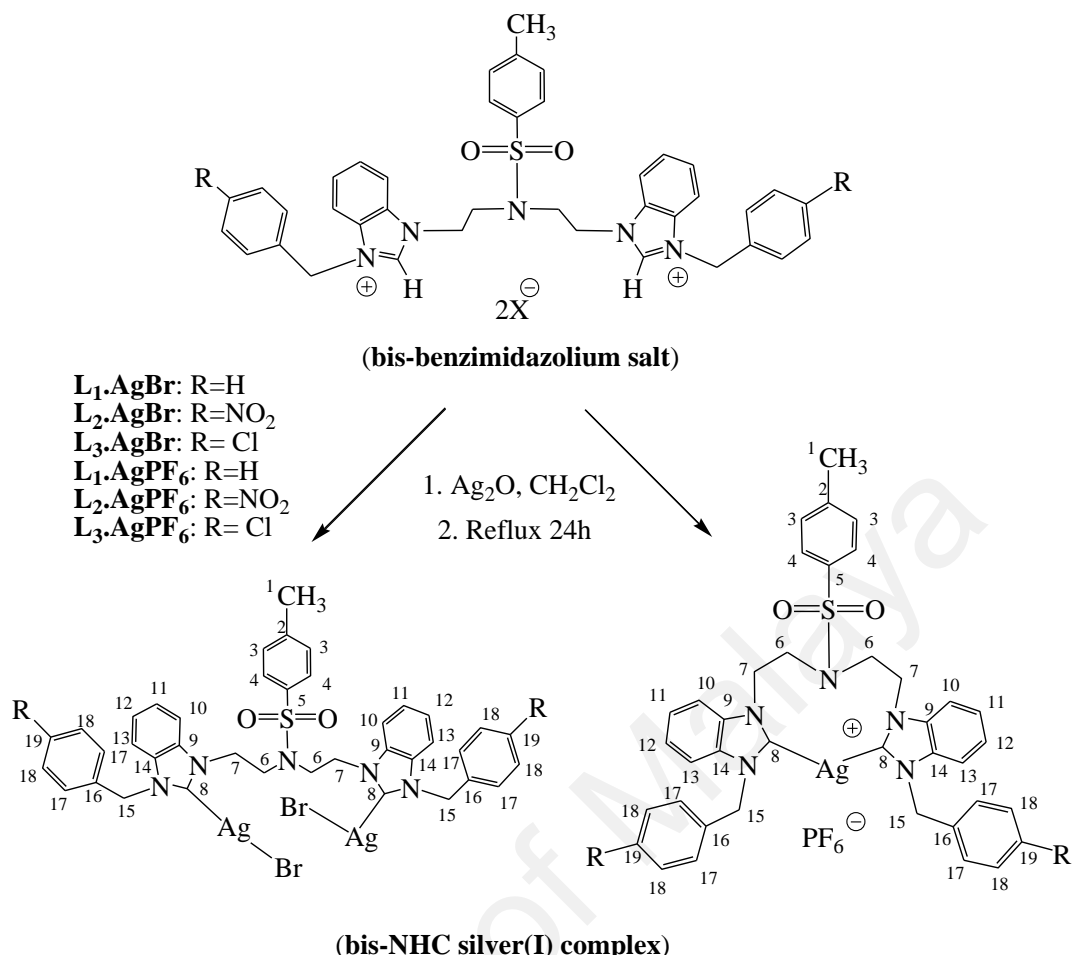
(k²-C,C')N,N'-Bis[4-chloro-1-benzyl-benzimidazolium-ethyl]-4-

methylbenzenesulfonamide mercury(II) dihexafluorophosphate (L₃.HgPF₆)

FT-IR, ATR (cm⁻¹), APPENDIX I6: 3057 (C-H)_{Ar}, 2954 (C-H)_{Aliph}, 1493, 1463 (C=C)_{Ar}, 1329, 1157 (O=S=O), 838 (PF₆), 748 (C-Cl); ¹H-NMR (DMSO-d₆) δ ppm, APPENDIX J6: 8.12 (d, 2H; H-13), 7.67-7.56 (m, 6H; H-10, H-11, H-12), 7.33-7.25 (m, 12H, H-3, H-17, H-18, H-4), 6.19 (s, 4H; H-15), 5.20 (s, 4H, H-7), 3.74 (s, 4H; H-6), 2.34 (s, 3H; H-1); ¹³C-NMR, APT (DMSO-d₆) δ ppm, APPENDIX K6: 185.72 (2C; C-8), 144.61 (1C; C-5), 134.49 (1C; C-2), 134.29 (2C; C-19), 133.62 (2C; C-16), 133.51 (2C; C-9), 133.17 (2C; C-14), 130.52 to 113.36 (20C; C-4, C-18, C-17, C-3, C-13, C-10, C-11, C-12), 53.19 (2C; C-15), 50.43 (2C; C-6), 48.64 (2C; C-7), 21.41 (1C; C-1). CHNS elemental analysis (%). Calculated: C, 39.06; H, 2.94; N, 5.84; S, 2.67. Found: C, 39.44; H, 2.55; N, 5.87; S, 2.54.

3.5.2 Synthesis of bis-NHC silver(I) complexes

The preparation of bis-NHC silver(I) complexes were followed as shown in Scheme 3.3. Silver oxide (Ag_2O) (0.4 mmol) was added to a solution of bis-benzimidazolium salt (0.3 mmol) in dichloromethane (30 ml) and the suspension solution was stirred for 24 hours under refluxing in nitrogen gas protection. The resulting clear solution with black suspension was filtered and concentrated to 5 ml, and Et_2O (5 ml) was added to give a precipitated of complexes (Liu Q.-X. et al., 2011a; Liu et al., 2013). Isolation by filtration gave complexes L_1AgBr , L_2AgBr , L_3AgBr , L_1AgPF_6 , L_2AgPF_6 , and L_3AgPF_6 , respectively. All silver(I) complexes are listed as below:



L₁.AgBr=(C,C')N,N'-Bis[1-benzyl-benzimidazolium-ethyl]-4-methylbenzenesulfonamide disilver(I) dibromide
L₂.AgBr=(C,C')N,N'-Bis[4-nitro-1-benzyl-benzimidazolium-ethyl]-4-methylbenzenesulfonamide disilver(I) dibromide
L₃.AgBr=(C,C')N,N'-Bis[4-chloro-1-benzyl-benzimidazolium-ethyl]-4-methylbenzenesulfonamide disilver(I) dibromide
L₁.AgPF₆=(k²-C,C')N,N'-Bis[1-benzyl-benzimidazolium-ethyl]-4-methylbenzenesulfonamide silver(I) hexafluorophosphate
L₂.AgPF₆=(k²-C,C')N,N'-Bis[4-nitro-1-benzyl-benzimidazolium-ethyl]-4-methylbenzenesulfonamide silver(I) hexafluorophosphate
L₃.AgPF₆=(k²-C,C')N,N'-Bis[4-chloro-1-benzyl-benzimidazolium-ethyl]-4-methylbenzenesulfonamide silver(I) hexafluorophosphate

Scheme 3.3: Synthesis route in the preparation of bis-NHC silver(I) complexes

**(C,C')N,N'-Bis[1-benzyl-benzimidazolium-ethyl]-4-methylbenzenesulfonamide
disilver(I) dibromide (L_1AgBr)**

FT-IR, ATR (cm^{-1}), APPENDIX I7: 3031 (C-H)_{Ar}, 2928 (C-H)_{Aliph}, 1478, 1454 (C=C)_{Ar}, 1336, 1153 (O=S=O); ¹H-NMR (DMSO-d₆) δ ppm, APPENDIX J7: 7.65-7.59 (m, 6H; H-13, H-17), 7.50-7.34 (m, 8H; H-4, H-10, H-11, H-12), 7.29 (d, 2H; H-3), 7.21-7.19 (m, 6H; H-18, H-19), 5.74 (s, 4H; H-15), 4.82 (s, 4H; H-7), 3.76 (s, 4H; H-6), 2.31 (s, 3H; H-1); ¹³C-NMR, APT (DMSO-d₆) δ ppm, APPENDIX K7: 194.05 (2C; C-8), 144.38 (1C; C-5), 136.62 (2C; C-16), 135.55 (1C; C-2), 133.97 (2C; C-9), 133.48 (2C; C-14), 130.54 to 111.61 (22C; C-4, C-3, C-17, C-18, C-19, C-11, C-12), 52.29 (2C; C-15), 49.57 (2C; C-6), 48.09 (2C; C-7), 21.43 (1C; C-1). Calculated: C, 46.13; H, 3.67; N, 6.90; S, 3.16. Found: C, 46.11; H, 3.81; N, 7.26; S, 3.20.

(C,C')N,N'-Bis[4-nitro-1-benzyl-benzimidazolium-ethyl]-4-methylbenzenesulfonamide disilver(I) dibromide (L_2AgBr)

FT-IR, ATR (cm^{-1}), APPENDIX I8: 3029 (C-H)_{Ar}, 2911 (C-H)_{Aliph}, 1517 (NO₂), 1477, 1405 (C=C)_{Ar}, 1340, 1153 (O=S=O); ¹H-NMR (CDCl₃-d) δ ppm, APPENDIX J8: 7.97 (d, 4H; C-13, C-10), 7.64-7.59 (m, 8H; C-17, C-18), 7.34 (t, 2H; H-12), 7.24-7.14 (m, 6H; C-3, C-4, C-11), 5.74 (s, 4H; H-15), 4.94 (t, 4H; H-7), 3.80 (t, 4H; H-6), 2.28 (s, 3H; H-1); ¹³C-NMR, APT (CDCl₃-d) δ ppm, APPENDIX K8: 158.88 (2C; C-8), 147.59 (2C; C-19), 144.22 (1C; C-5), 143.06 (2C; C-16), 136.05 (1C; C-2), 134.18 (2C; C-9), 133.26 (2C; C-14), 130.07 to 111.30 (20C; C-4, C-18, C-17, C-3, C-10, C-13, C-11, C-12), 52.12 (2C; C-15), 49.27 (2C; C-6), 48.40 (2C; C-7), 21.48 (1C; C-1). CHNS elemental analysis (%): Calculated: C, 42.38; H, 3.19; N, 8.87; S, 2.90. Found: C, 41.92; H, 3.22; N, 8.86; S, 3.17.

(C,C')N,N'-Bis[4-chloro-1-benzyl-benzimidazolium-ethyl]-4-

methylbenzenesulfonamide disilver(I) dibromide (L_3AgBr)

FT-IR, ATR (cm^{-1}), APPENDIX I9: 3025 (C-H_{Ar} , 2908 ($\text{C-H}_{\text{Aliph}}$, 1477, 1438 (C=C_{Ar} , 1330, 1153 (O=S=O), 740 (C-Cl); $^1\text{H-NMR}$ (DMSO-d_6) δ ppm, APPENDIX J9: 7.64-7.58 (m, 4H; H-10, H-13), 7.31 (d, 4H; H-18), 7.20-7.07 (m, 12H, H-3, H-4, H-11, H-12, H-17), 5.58 (s, 4H; H-15), 4.96 (s, 4H; H-7), 3.81 (s, 4H; H-6), 2.28 (s, 3H; H-1); $^{13}\text{C-NMR}$, APT ($\text{CDCl}_3\text{-d}$) δ ppm, APPENDIX K9: 153.95 (2C; C-8), 144.05 (1C; C-5), 136.07 (1C; C-2), 134.44 (2C; C-19), 134.30 (2C; C-16), 133.74 (2C; C-9), 133.33 (2C; C-14), 130.05, to 111.13 (20C; C-4, C-18, C-17, C-3, C-10, C-13, C11, C-12), 52.53 (2C; C-15), 49.57 (2C; C-7), 48.41 (2C; C-6), 21.48 (1C; C-1). CHNS elemental analysis (%). Calculated: C, 43.20; H, 3.25; N, 6.46; S, 2.96. Found: C, 43.68; H, 3.46; N, 7.00; S, 2.82.

($k^2\text{-C,C'}$)N,N'-Bis[1-benzyl-benzimidazolium-ethyl]-4-methylbenzenesulfonamide

silver(I) hexafluorophosphate (L_1AgPF_6)

FT-IR, ATR (cm^{-1}), APPENDIX I10: 3045 (C-H_{Ar} , 2961 ($\text{C-H}_{\text{Aliph}}$, 1479, 1452 (C=C_{Ar} , 1336, 1157 (O=S=O), 833 (PF_6); $^1\text{H-NMR}$ (DMSO-d_6) δ ppm: 7.70 (d, 2H; H-13), 7.49-7.33 (m, 20H; H-19, H-18, H-3, H-4, H-12, H-11, H-10, H-17), 5.86 (s, 4H; H-15), 5.02 (s, 4H; H-7), 3.76 (s, 4H; H-6), 2.40 (s, 3H; H-1); $^{13}\text{C-NMR}$, APT (DMSO-d_6) δ ppm: 144.27 (1C; C-5), 136.67 (2C; C-16), 136.57 (1C; C-2), 133.78 (2C; C-9), 133.67 (2C; C-14), 130.39 to 112.11 (22C; C-4, C17, C-18, C-19, C-3, C-10, C-13, C-11, C-12), 60.73 (2C; C-15), 52.29 (2C; C-6), 48.76 (2C; C-7), 21.43 (1C; C-1). CHNS elemental analysis (%). Calculated: C, 52.48; H, 4.18; N, 7.85; S, 3.59. Found: C, 52.75; H, 3.90; N, 7.55; S, 3.72.

(k²-C,C')N,N'-Bis[4-nitro-1-benzyl-benzimidazolium-ethyl]-4-

methylbenzenesulfonamide silver(I) hexafluorophosphate (L₂.AgPF₆)

FT-IR, ATR (cm⁻¹), APPENDIX I11: 3070 (C-H)_{Ar}, 2937 (C-H)_{Aliph}, 1519 (NO₂), 1478, 1448 (C=C)_{Ar}, 1343, 1158 (O=S=O), 834 (PF₆); ¹H-NMR (DMSO-d₆) δ ppm, APPENDIX J11: 8.05 (d, 4H; H-10, H-13), 7.64 (d, 8H; H-17, H-18), 7.51-7.44 (m, 6H; H-4, H-11, H-12), 7.38 (d, 2H; H-3), 6.04 (s, 4H; H-15), 5.03 (s, 4H, H-7), 3.78 (s, 4H; H-6), 2.41 (s, 3H; H-1); ¹³C-NMR, APT (DMSO-d₆) δ ppm, APPENDIX K11: 147.34 (2C; C-19), 144.45 (1C; C-5), 141.75 (2C; C-16), 134.82 (1C, C-2), 133.97 (2C; C-9), 133.59 (2C; C-14), 130.42 to 112.27 (20C; C-4, C-18, C-17, C-3, C-10, C-13, C-11, C-12), 51.25 (2C; C-15), 49.52 (2C; C-7), 49.18 (2C; C-6), 21.39 (1C; C-1). CHNS elemental analysis (%). Calculated: C, 47.56; H, 3.79; N, 9.96; S, 3.26. Found: C, 47.77; H, 3.64; N, 9.56; S, 3.33.

(k²-C,C')N,N'-Bis[4-chloro-1-benzyl-benzimidazolium-ethyl]-4-

methylbenzenesulfonamide silver(I) hexafluorophosphate (L₃.AgPF₆)

FT-IR, ATR (cm⁻¹), APPENDIX I12: 3065 (C-H)_{Ar}, 2932 (C-H)_{Aliph}, 1480, 1449 (C=C)_{Ar}, 1335, 1158 (O=S=O), 836 (PF₆), 741 (C-Cl); ¹H-NMR (DMSO-d₆) δ ppm, APPENDIX J11: 7.91-7.29 (m, 20H; all C-H_{Ar}), 5.83 (s, 4H; H-15), 4.98 (s, 4H; H-7), 3.70 (s, 4H; H-6), 2.33 (s, 3H; H-1); ¹³C-NMR, APT (DMSO-d₆) δ ppm, APPENDIX K12: 144.19 (1C; C-5), 135.82 (1C; C-2), 134.96 (2C; C-19), 134.30 (2C; C-16), 133.55 (2C; C-9), 132.98 (1C; C-14), 130.37 to 112.28 (20C; C-4, C-18, C-17, C-3, C-10, C-13, C-11, C-12), 53.29 (2C; C-15), 121.27 (2C; C-6), 48.88 (2C; C-7), 21.39 (1C; C-1). CHNS elemental analysis (%). Calculated: C, 48.72; H, 3.67; N, 7.28; S, 3.33. Found: C, 49.04; H, 3.22; N, 7.11; S, 3.71.

CHAPTER 4

RESULTS AND DISCUSSIONS

4.1 Characterizations of bis-benzimidazolium salts

The naturally occurring and synthetic available benzimidazole derivatives are non-bridged material. The presence of bridging linker was believed to allow the preparation of new complexes which their stability is entropically improved by chelate effect (Crudden et al., 2004; Peris et al., 2004). In this study, bis-benzimidazolium salts with sulfonamide moieties bridging linker have been synthesized from diethanolamine as starting material. It involves three steps of reactions as discussed in following section.

The first step is to synthesis tri-sulfonamide (Figure 4.1). This compound was produced through the reaction of diethanolamine with *p*-toluenesulfonyl chloride in the presence of triethylamine to give a white solid (90% yield) with a melting point of 98-100 °C.

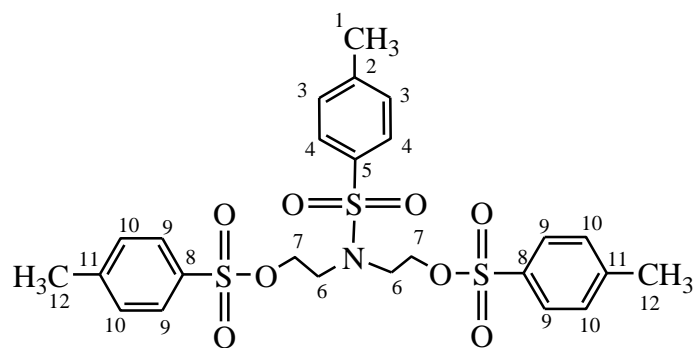


Figure 4.1: Molecular structure of *N*-(4-methylbenzenesulfonyl)-bis((4-methylbenzenesulfonyl)-(oxy))ethyl]amine; (tri-sulfonamide)

In this reaction, *p*-toluenesulfonyl chloride (tosyl unit) was used to convert the alcoholic (–OH) group of diethanolamine into a better leaving group using an organic base, triethylamine, through S_N2 reaction, simultaneously. The lone pair of the alcohol oxygen attacked the sulfur of *p*-toluenesulfonyl chloride and the chloride group was removed to produce the symmetric tosylate product (De Castro et al., 2007; Kumar et al., 2004).

–NH amine position, tosyl group was functioned as a protecting group, which formed sulfonamide with extremely stable structure (Greene et al., 1999). Previous studies have reported that tri-sulfonamide was obtained after 5-7 days to allow its viscous liquid to solidify with 87% yield (Al-Mohammed et al., 2013). In this study, it was found that this step can take shorter, through recrystallization of the viscous liquid of tri-sulfonamide in methanol. Within 1 day, white solid of pure compound was formed with comparable high percentage yield.

The second step is the synthesis of bis-benzimidazole as illustrated in Figure 4.2. This compound was obtained by the reaction of tri-sulfonamide with two moles of benzimidazole in the presence of base to form white solid compound (89% yield) with a melting point of 192-194 °C.

In this synthesis step, potassium hydroxide (KOH) is a strong base functioned as the catalyst. Proton from nitrogen in benzimidazole ring reacted with the base to form benzimidazole anions and it is considered as the key step of the reaction. This negative charge of benzimidazole ring attacked the carbon bearing 4-substituted benzensulfonate in both sides of tri-sulfonamide and produced symmetrical product which was in agreement with literature (Al-Mohammed et al., 2013).

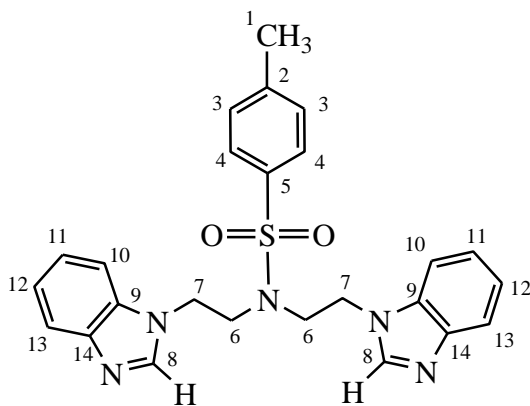
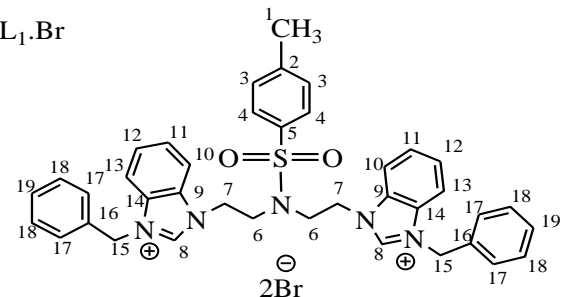


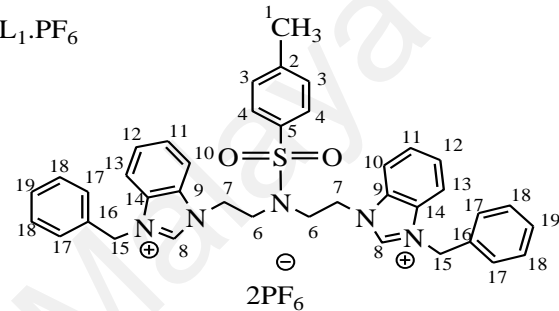
Figure 4.2: Molecular structure of *N,N'*-Bis[(benzimidazol-1-yl)ethyl]-4-methylbenzenesulfonamide; (bis-benzimidazole)

Finally, to produce the bis-benzimidazolium bromide salts, subsequent alkylation method by primary alkyl halide has been used to introduce new substituent at the -N position of the benzimidazole ring (Stringer et al., 2014). In this experiment, the reaction of bis-benzimidazole with two equivalents of benzyl bromide, 4-nitrobenzyl bromide or 4-chlorobenzyl bromide in refluxing dioxane, afforded bis-benzimidazolium bromide salts namely L_1Br , L_2Br and L_3Br , respectively. Then, a part of bromide salts were converted to their corresponding hexafluorophosphate (PF_6^-) counterpart by metathesis reaction using potassium hexafluorophosphate (KPF_6) in methanol at room temperature to give L_1PF_6 , L_2PF_6 , and L_3PF_6 , respectively (Haque et al., 2011). The structures of synthesized bis-benzimidazolium salt are illustrated in Figure 4.3. General characteristic of bis-benzimidazolium salts are summarized in Table 4.1. As can be observed, all synthesized salts were produced with a good percentage yield.

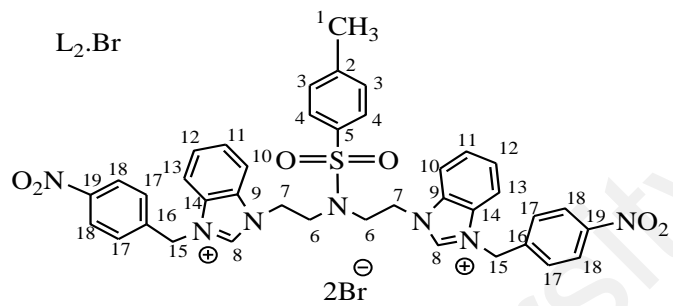
$L_1\cdot Br$



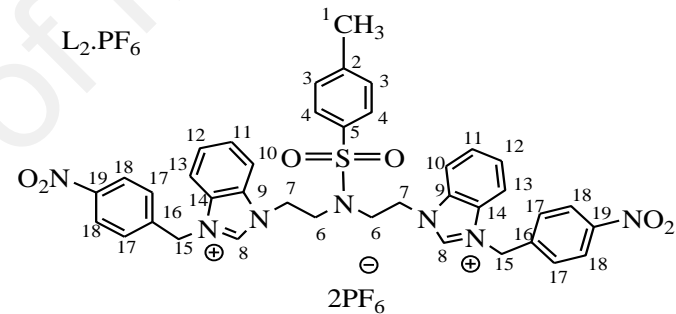
$L_1\cdot PF_6$



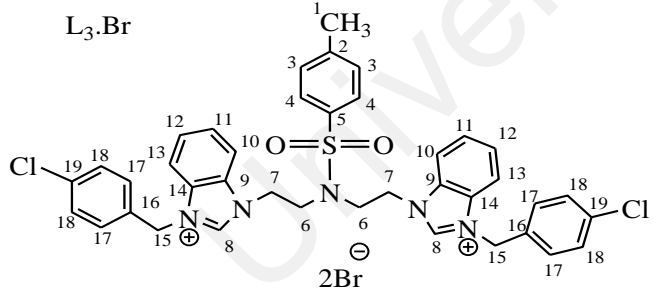
$L_2\cdot Br$



$L_2\cdot PF_6$



$L_3\cdot Br$



$L_3\cdot PF_6$

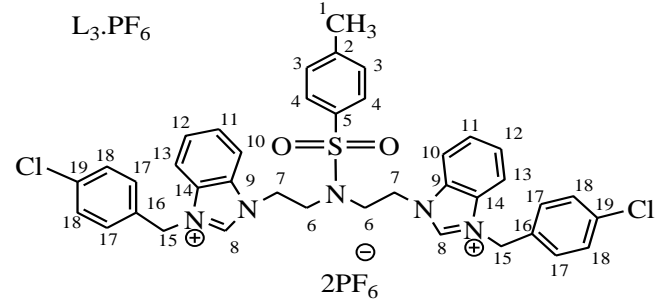


Figure 4.3: Molecular structures of synthesized bis-benzimidazolium salts

The bis-benzimidazolium bromide salts obtained were found to be soluble in polar solvents like methanol and ethanol but remained insoluble in non-polar solvents like diethyl ether. Conversely, regarding the changing counter ions from Br^- to PF_6^- , the solubility of salts is affected. For instance, with PF_6^- as counter anions, the salts become insoluble in methanol and ethanol, but soluble in acetonitrile. However, both types of salts remained soluble in DMSO and DMF, but insoluble in water. Different solubility results of bis-benzimidazolium salts in different types of solvent show the changes of counter anions which may change its polarity. Thus, it has been found that the polarity of bis-benzimidazolium salts increases with the presence of halide as counter anion (Iqbal et al., 2014).

Table 4.1: General characteristic of bis-benzimidazolium salts (bis-NHC precursor)

Bis-NHC precursor	Yield (%)	Color	Melting point (°C)	Molecular formula	Molecular weight (g/mol)
L ₁ .Br	98	Off-white	120-125	C ₃₉ H ₃₉ N ₅ O ₂ SBr ₂	801.6
L ₂ .Br	74	yellow	138-140	C ₃₉ H ₃₇ N ₇ O ₆ SBr ₂	891.6
L ₃ .Br	93	white	80-82	C ₃₉ H ₃₇ N ₅ O ₂ SBr ₂ Cl ₂	870.5
L ₁ .PF ₆	83	white	161-166	C ₃₉ H ₃₉ N ₅ O ₂ SP ₂ F ₁₂	931.8
L ₂ .PF ₆	97	Pale-yellow	168-170	C ₃₉ H ₃₇ N ₇ O ₆ SP ₂ F ₁₂	1021.8
L ₃ .PF ₆	87	white	140-142	C ₃₉ H ₃₇ N ₅ O ₂ SCl ₂ P ₂ F ₁₂	1000.7

4.1.1 Fourier Transfer Infrared (FT-IR) spectroscopy

FT-IR spectra of all synthesized compounds (APPENDIX A) have been determined using the ATR method over the scan range 4000-400 cm^{-1} . The significant FT-IR absorption bands were summarized in Table 4.2. The structure of tri-sulfonamide was confirmed by the presence of O=S=O and C=C aromatic functionalities at 1336, 1156 cm^{-1} , and 1598, 1452 cm^{-1} , respectively (Al-Mohammed et al., 2013). Consequently, a medium and sharp band observed at 1089 cm^{-1} is attributed to the stretching mode vibration of H₂C-N functionality which attached to the *p*-toluenesulfonyl substituent (APPENDIX A1).

The structure of bis-benzimidazole can be distinguished with the appearance of new stretching mode at 1615 cm^{-1} which is assigned to the -HC=N- module of benzimidazole ring. However, this absorption band is weaker when compared to non-aromatic -C=N stretching. This is probably caused by the conjugation of N-HC=N module with the heterocyclic ring system (APPENDIX A2) (Pavia et al., 2008).

As displayed in FT-IR spectra of all bis-benzimidazolium salts (APPENDIX A3-A8), -C=N shifted to lower frequency of 1560 cm^{-1} , due to the resonance effect of -N-C=N module after introducing benzyl substituent to benzimidazole nitrogen atom. The resonance structure introduces single-bond character into -C=N module and thereby lowers the absorption frequency compared to a non-aromatic -C=N (Pavia et al., 2008). This is similar to the FT-IR results reported by Haque et al. (2013), who observed a band of medium intensity in the range of 1560-1590 cm^{-1} , which is assigned to benzimidazole ring $\nu(\text{C}=\text{N})$ vibration. The presence of nitro group in bis-benzimidazolium salts L₂.Br and L₂.PF₆ were observed at 1515 cm^{-1} .

and 1520 cm^{-1} , respectively. Conjugation of a nitro group with an aromatic ring causes the shifts of stretching absorption bands to lower frequencies (Pavia et al., 2008). The changes of anion from Br^- to PF_6^- can be confirmed by the presence of strong and broad absorption frequency in range of $834\text{-}825\text{ cm}^{-1}$. The absorption peaks were clearly seen in FT-IR spectra of bis-benzimidazolium hexafluophosphate salts L_1PF_6 , L_2PF_6 , and L_3PF_6 at 834 cm^{-1} , 832 cm^{-1} and 835 cm^{-1} , respectively. Logacheva and co-workers, reported that this appearance of bands is due to stretching vibration of the PF_6^- anion, which overlaps most of the stretching-bending vibration bands in macromolecule compounds (Logacheva et al., 2009).

Table 4.2: The significant of FT-IR absorption bands (cm^{-1}) for synthesized compounds, (types of absorption bands; w= weak, m= medium, s= strong)

Assignment	Tri-sulfonamide	Bis-benzimidazole	L ₁ .Br	L ₂ .Br	L ₃ .Br	L ₁ .PF ₆	L ₂ .PF ₆	L ₃ .PF ₆
CH _{Ar}	3065 (w)	3051 (w)	3125 (w)	3081 (w)	3121 (w)	3113 (w)	3120 (w)	3161 (w)
CH _{Aliph}	2926 (w)	2923 (w)	3020 (m)	3026 (w)	3025 (w)	3019 (w)	3031 (w)	3043 (w)
H-C≡N	-	1615 (w)	1560 (s)	1566 (s)	1561(s)	1566 (m)	1564 (m)	1565 (m)
C=C	1598, 1452 (m, m)	1594, 1460 (w, m)	1595, 1449 (w, w)	1607, 1434 (m, m)	1597, 1446 (w, w)	1595, 1451 (w, w)	1609, 1447 (w, w)	1596, 1447 (w, w)
O=S=O	1336, 1156 (s, s)	1322, 1155 (m, s)	1338, 1157 (s, s)	1341, 1157 (s, s)	1334, 1155 (s, s)	1329, 1157 (m, m)	1344, 1157 (s, s)	1337, 1157 (m, m)
H ₂ C-N	1089 (m)	1094 (m)	1084 (m)	1087 (w)	1088 (m)	1089 (w)	1089 (w)	1090 (w)
O=N-O	-	-	-	1515 (s)	-	-	1520 (s)	-
PF ₆ ⁻	-	-	-	-	-	834	832	835

4.1.2 Nuclear Magnetic Resonance (NMR) spectroscopy

NMR spectra of all compounds have been analyzed in DMSO-*d*₆ and CDCl₃-*d* over the scan range of 0 to 12 δ (ppm) for ¹H-NMR and 0 to 200 δ (ppm) for ¹³C-NMR studies. The spectra for all synthesized compounds were presented in APPENDIX B (¹H-NMR) and APPENDIX C (¹³C-NMR) and the numbering system used in this discussion is refer to Figure 4.1, Figure 4.2 and Figure 4.3 for each compounds, respectively.

4.1.2.1 ¹H-NMR of synthesized compounds

Regarding to the ¹H-NMR spectrum (APPENDIX B1) of tri-sulfonamide (Figure 4.1), proved that the *p*-toluenesulfonyl group has been successfully reacted to diethanolamine by deprotonation of protons from -NH and -OH functionalities. It can be observed that the presence of methyl protons as a singlet at higher chemical shifts, of δ 2.39 (H-1) and δ 2.44 (H-12) is due to the deshielding effect by the larger anisotropic field generated by the electrons in the rings of π system. In addition, the aromatic protons appeared as doublets and gave four different signals. The doublet centered on δ 7.37 (H-3) and δ 7.49 (H-10) corresponding to the aromatic protons closest to the methyl groups. Whereas, another two doublets centered on δ 7.58 (H-4) and δ 7.74 (H-9) corresponds to the aromatic protons closest to the sulfonyl group. The coupling constant values are 8 Hz for H-3 and H-4. Similar values were also found for H-10 and H-11, respectively. These suggest that the magnetically coupled protons are in ortho position to each other. (Al-Mohammed et al., 2013; Pavia et al., 2008; Wade Jr, 2006).

¹H-NMR spectrum (APPENDIX B2) of bis-benzimidazole (Figure 4.2) showed a singlet at δ 2.34 which is assigned to the methyl group (H-1). Two triplets recorded at δ 3.51 and δ 4.28, are refer to two methylene group protons at H-6 and H-7 position, respectively. The aromatic protons were recorded at the range of δ 7.22-7.66 with three separated chemical shifts multiplet, doublet and doublet. These chemical shifts were assigned to (H-3, H-11, H-12), H-4, and (H-10, H-13) protons, respectively. The most important chemical shift was observed as singlet at δ 8.10, corresponding to carbene proton in benzimidazole ring (H-8). The presence of all chemical shifts in the spectrum proved the successful attachment of benzimidazole groups at both sides of sulfonyl-bridge. These results also show a good agreements with what has been mentioned in literature (Al-Mohammed et al., 2013).

In the synthesis of bis-benzimidazolium bromide salts (Figure 4.3), the attachment of benzyl bromide, 4-nitrobenzyl bromide and 4-chlorobenzyl bromide with bis-benzimidazole, to get the corresponding bis-benzimidazolium bromide salts of L₁.Br, L₂.Br, and L₃.Br, were confirmed by observing the changes in their ¹H-NMR spectra (APPENDIX B3-B5) at specific chemical shifts. For example, in all the three spectra, new significant chemical shifts at δ 5.90, δ 6.06 and δ 5.86 were observed, respectively. This signal was due to the presence of proton -N-CH₂-Ar (H-15), and it was proved that the attachment of corresponding reactant has been occurred. This benzylic hydrogen appeared at higher chemical shifts due to the deshielding by the anisotropic effect of the benzene and benzimidazole rings. In addition, downfield movements have been observed for H-6 (δ 3.51 to 3.95-4.04), H-7 (δ 4.28 to 4.87-4.96) and H-8 (δ 8.10 to 10.18-10.24) in all ¹H-NMR spectra. The results of deshielded carbene proton (C-8) showed a similarity with the work reported by Stringer et al., (2014).

The resonance of the aromatic protons shows a difference in chemical shifts, depending on the type of substituents attached at -N position of benzimidazole ring. In the spectrum of L₁.Br (APPENDIX B3), the aromatic protons were observed in the range of δ 7.14-8.18 as doublet (H-3), multiplet (H-18, H-19, H-4), doublet (H-17), multiplet (H-11, H-12), doublet (H-10) and doublet (H-13). The spectrum of L₂.Br (APPENDIX B4) is differs from L₁.Br, through the absence of chemical shift for H-19 and downfield movement for H-18 and H-17 from δ 7.42-7.48 to 8.24 and from δ 7.62 to 7.80, respectively. This is due to the presence of electron-withdrawing nitro group at C-19, which deshields the attached hydrogens by withdrawing electron density from the ring through resonance interactions. While, in L₃.Br ¹H-NMR spectrum (APPENDIX B5), the absence of H-19 and the downfield movement of H-18 (δ 7.61) was shown due to the presence of halogen -Cl group at C-19 position. The halogen groups also have a deshielding effect due to their electronegativity character (Haque et al., 2012b; Pavia et al., 2008).

After introducing the hexafluorophosphate anion to the bis-benzimidazolium bromide salts, the L₁.PF₆, L₂.PF₆, and L₃.PF₆ were obtained and their ¹H-NMR spectra were also examined (APPENDIX B6-B8). As can be observed, there is a small upfield movement of acidic proton (H-8) in benzimidazole ring in the range of δ 10.18-10.24 for bromide anion to δ 10.00-10.10 for hexafluorophosphate anion (PF₆⁻), showing that the replacement of anion inside the bis-benzimidazolium salts structures were occurred. No significant changes in chemical shifts for other protons were observed as compared to their corresponding bis-benzimidazolium bromide salts. In addition, in all the spectra the signal from acidic proton of benzimidazole ring (H-8) appeared as a singlet in downfield region. Iqbal et al. (2011) stated that, this singlet chemical shift can be seen

in all benzimidazole based salts, due to the presence of an electron withdrawing phenyl group at benzimidazole ring (Iqbal et al., 2011).

4.1.2.2 ^{13}C -NMR of synthesis compound

Similarly, the structures of all compounds were further confirmed by ^{13}C -NMR technique (APPENDIX C). The structure of tri-sulfonamide was confirmed with the presence of tertiary and quaternary carbons of benzyl group in the range of δ 127.45-130.70 and δ 132.43-145.65 (APPENDIX C1). Whereas, in ^{13}C -NMR spectrum of bis-benzimidazole (APPENDIX C2), new chemical shifts were observed at δ 133.99 and δ 143.73, which assigned to the quaternary carbons of C-14 and C-9 in benzimidazolium ring, respectively. Both spectra show a similarity as compared with the compound synthesized in previous literature (Al-Mohammed et al., 2013).

The changes in chemical shifts in ^{13}C -NMR spectra after introducing a new functional group at -N position in benzimidazole ring proved that the bis-benzimidazolium salts were successfully synthesized. The obvious changes in the spectra observed with the appearance of new chemical shift in the range of δ 49.49-50.39, were assigned to secondary methylene carbon of benzyl (C-15), and the presence of quaternary carbon in the range of δ 133.25-141.74 and δ 133.95-148.06 referring to C-16 and C-19, respectively (Liu et al., 2013). However, the ^{13}C -NMR spectra of bis-benzimidazolium bromide salts (L_1Br , L_2Br , and L_3Br) did not show any significant changes to their respective bis-benzimidazolium hexafluorophosphate salts (L_1PF_6 , L_2PF_6 , and L_3PF_6) as can be seen in APPENDIX C3-C8.

Regarding the results obtained from the characterization methods, including CHNS elemental analysis, FT-IR, $^1\text{H-NMR}$ and $^{13}\text{C-NMR}$ the molecular structure of all synthesized compound can be confirmed as illustrated in Figure 4.1, Figure 4.2 and Figure 4.3. This confirmation of molecular structures were supported by the single X-ray crystallographic data obtained for compound L_1Br and L_1PF_6 .

4.1.3 Single crystal X-ray diffraction

The molecular structure of the synthesized bis-benzimidazolium salts were demonstrated using a single crystal X-ray diffraction analysis. Totally, two bis-benzimidazolium salts with Br^- (L_1Br) and PF_6^- (L_1PF_6) counter anions were obtained in crystalline form suitable for X-ray investigation.

The crystalline form of L_1Br and L_1PF_6 were obtained using slow evaporation of a mixture solvent of MeOH/ H_2O at room temperature. Figure 4.4 and Figure 4.5 show the numbering scheme of molecular structures for L_1Br and L_1PF_6 , respectively. The singlw crystal X-ray diffraction data and the structure refinement of these compounds are shown in Table 4.3 (APPENDIX D1 AND APPENDIX D2).

The L_1Br (Figure 4.4) was crystallized as a triclinic lattice containing a pair of bromide anions in asymmetric unit with space group of $P\bar{1}$. In L_1Br structure, there are two molecules per asymmetric unit cell and the whole molecule is not planar, however the benzimidazolium dication is centrosymmetric. The central sulfonyl group makes dihydral angles of $14.4(7)^\circ$, $173.4(6)^\circ$ and $43.6(7)^\circ$, $115.3(6)^\circ$ with the adjacent amine groups. All bond lengths and angles are in normal ranges. The N1-C14, N2-C14, N4-C25 and N5-C25 bond lengths are quite similar (1.32 \AA) indicating a delocalization of electron about the N—C—N bond.

The L₁.PF₆ (Figure 4.5) is also crystallized in a triclinic system with space group *P*[̄]1. In L₁.PF₆ structure, there is one molecule per asymmetric unit cell and the benzimidazolium dication is centrosymmetric. The central sulfonyl group makes dihedral angles of 50.51(17)[°], 118.76[°] and 11.16(17)[°], 179.57(14)[°] with the adjacent amine group. All the bond lengths and angles are in normal ranges. The N1-C8, N2-C8, N4-C26 and N3-C26 bond lengths are quite similar (1.32 Å) indicating a delocalization of electron about the N—C—N bonds.

Table 4.3: Crystal data and structures refinement for L₁.Br and L₁.PF₆

Subject	L ₁ .Br	L ₁ .PF ₆
Empirical formula	C ₃₉ H ₃₉ N ₅ O ₂ SBr ₂	C ₃₉ H ₃₉ N ₅ O ₂ SP ₂ F ₁₂
Formula weight	801.62	931.75
Temperature (K)	100.2 (8)	100 (2)
Crystal system,	Triclinic	Triclinic
Space group	<i>P</i> [̄] 1	<i>P</i> [̄] 1
a(Å), α(°)	14.7495(9), 108.720(5)	9.0853(8), 100.8633(13)
b(Å), β(°)	15.5216(8), 100.073(5)	12.1396(11), 95.1932(13)
c(Å), γ(°)	19.1751(10), 108.177(5)	18.6260(17), 91.7243(13)
Volume (Å ³)	3761.1(3)	2006.9(3)
Z, Calculate density(g/cm ³)	2, 1.4157(2)	2, 1.542
μ/mm ⁻¹	2.251	0.260
F(000)	1638.73	956
Crystal size (mm ³)	0.22 × 0.15 × 0.12	0.28 x 0.19 x 0.10
Goodness-of-fit on F ²	1.072	1.116
Final R indexes [I>=2σ (I)]	R ₁ = 0.0977, wR ₂ = 0.2737	R1 = 0.0428, wR2 = 0.0920
CCDC No.	1051318	89350

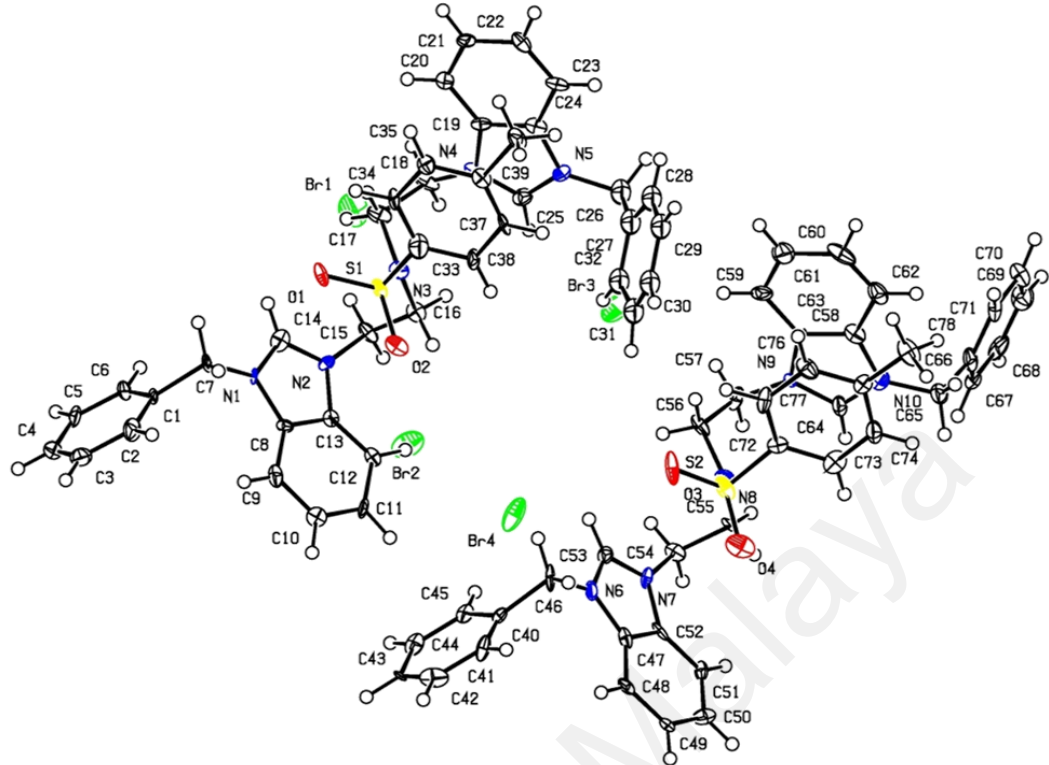


Figure 4.4: Ortep diagram of the molecule structure of benzimidazolium salt (L₁.Br)

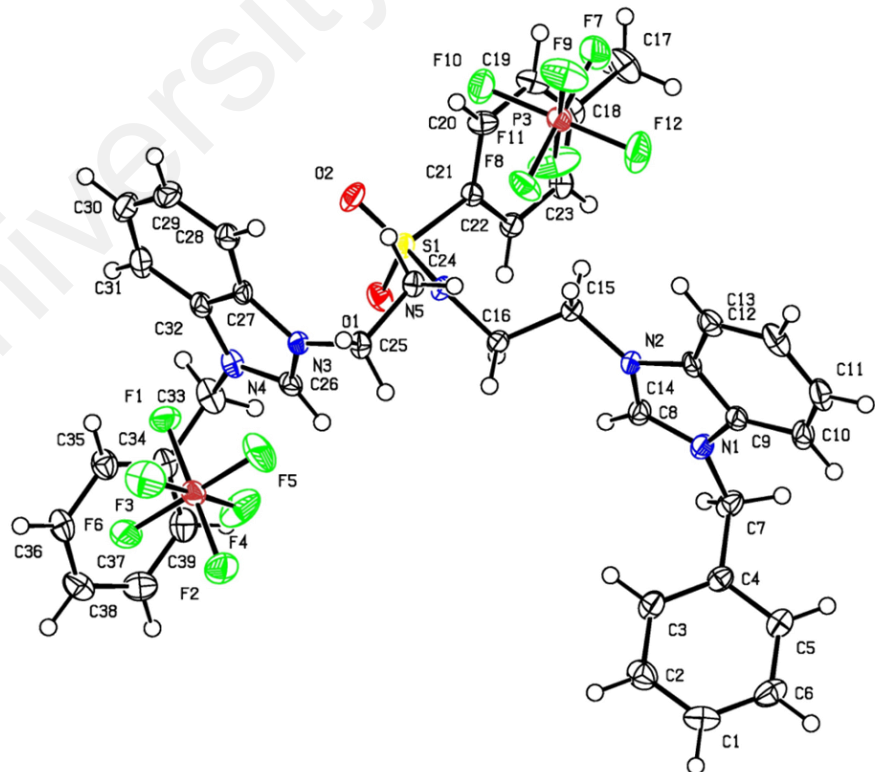


Figure 4.5: Ortep diagram of the molecule structure of benzimidazolium salt (L₁.PF₆)

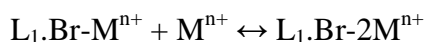
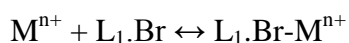
4.2 Conductometric study of L₁.Br

In order to find the selective complexation of bis-benzimidazolium salts with metal cations in liquid phases, conductometric method was applied in methanol-water (MeOH-H₂O) as a solvent system. Due to the high solubility in methanol, L₁.Br has been chosen to understand the complexation process and the stoichiometric of complexes can be recognized. The stability constants ($\log K_f$) of complex formation is determined by fitting the molar conductivity curves using a computer program, GENPLOT and the output shows the $\log K_f$ values for all metal cations. Consequently, thermodynamic parameters ($\Delta G_C^o, \Delta H_C^o, \Delta S_C^o$) are determined conductometrically. The experimental data was validated by using artificial neural network (ANN) program and the capability of metal binding was studied using theoretical DFT calculation.

4.2.1 Stoichiometry of complex formation

The stability constants (K_f) of complex reaction between the L₁.Br and various metal cations (M^{n+}), were carried out using conductometric method. This method was reported as the best method in numerous studies due to its great sensitivity, low cost as well as simple experimental arrangement (Joshaghani et al., 2008; Petković et al., 2013; Rezayi et al., 2011). The complexation reaction of L₁.Br with Ni²⁺, Zn²⁺, Pd²⁺, Hg²⁺, and Ag⁺ cations were investigated. Pure MeOH, pure H₂O and MeOH-H₂O binary mixture system (mol%) have been used as solvent system at different temperatures (15, 25, 35 and 45 °C). The changes in molar conductivity (Λ_m) of the reaction mixture were observed as a function of molar ratio ([L₁.Br]_t/[Mⁿ⁺]_t) of the proposed complexes. The resulting Λ_m versus ([L₁.Br]_t/[Mⁿ⁺]_t) was plotted for all the complexation process as listed in APPENDIX E1-E5.

Figure 4.6, shows the plot of Λ_m versus $([L_1.Br]/[M^{n+}]_t)$ for all studied metal cations in pure MeOH at 25 °C. As observed from the plot of Λ_m versus $([L_1.Br]/[M^{n+}]_t)$ for Ni^{2+} cation, the slope increases in Λ_m parallel to the increase of the ligand concentration. In the study of complexation $L_1.Br$ with Zn^{2+} and Pd^{2+} cation, a similar pattern of slopes were observed. This result is due to the less mobility of free solvated metal ion (M^{n+}), as compared to both of ligand ($L_1.Br$) and complex ($L_1.Br-M^{n+}$). The slopes for Ni^{2+} , Zn^{2+} and Pd^{2+} show that the stoichiometry for these complex reactions were 1:1 [M: $L_1.Br$], with mild breaking point at a $([L_1.Br]/[M^{n+}]_t)$ about 1. While, the Λ_m versus $([L_1.Br]/[M^{n+}]_t)$ plots for Ag^+ cation show the slight decrease in Λ_m with the increasing of ligand concentration, which indicated that ligand mobility ($L_1.Br$) is less than free solvated metal cation (M^{n+}). It also showed an increment after the breaking points at $([L_1.Br]/[M^{n+}]_t)$ about 0.5, indicating that the mobility of the complexes in reaction mixtures is greater than free solvated cations (El-Sonbati et al., 2001; Petković et al., 2013). Whereas, by continuing the addition of ligand to the Ag^+ cation solution a second breaking point of $([L_1.Br]/[M^{n+}]_t)$ at 1 was observed, similar to the previous three cations. The Λ_m versus $([L_1.Br]/[M^{n+}]_t)$ plots for Hg^{2+} cation also gave the same results as Ag^+ cation. It seems that in both complex formations, further addition of ligand to metal cation solution results in formation of 2:1 [M: $L_1.Br$] and 1:1 [M: $L_1.Br$] complexes (Ahmed et al., 2011). Therefore, the general mechanism for all the complexation processes suggested as follows:



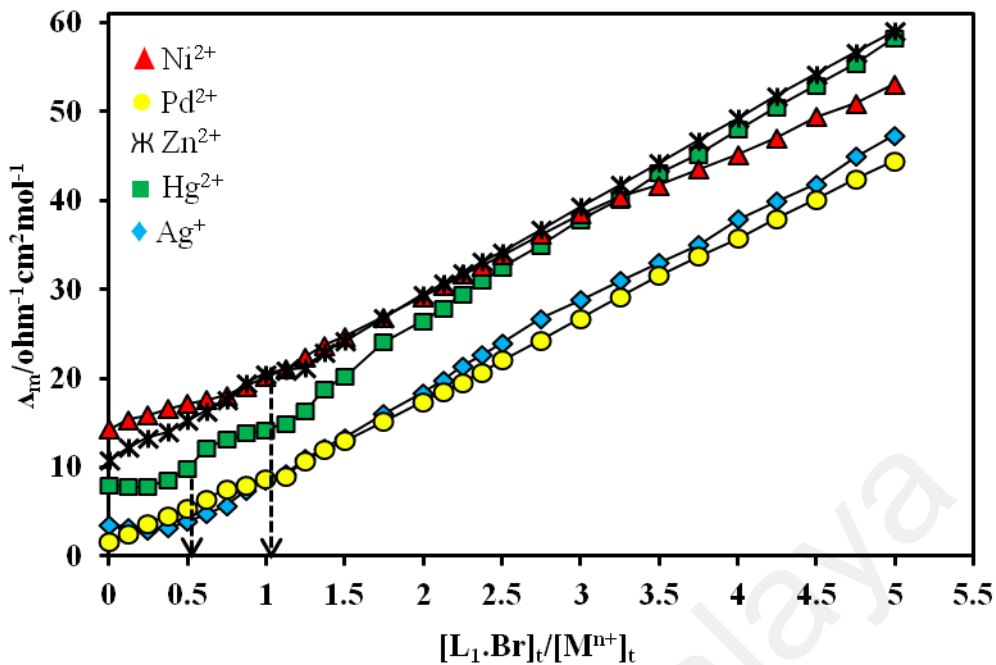


Figure 4.6: Plot of molar conductance, Λ_m versus mole ration, $[L_1\cdot Br]_t/[M^{n+}]_t$ for the binding of Ag^+ , Hg^{2+} , Ni^{2+} , Pd^{2+} and Zn^{2+} with $L_1\cdot Br$ in pure MeOH at 25 °C

4.2.2 Stability constant of complex formation

The stability constant ($\log K_f$) values of complexes for all cations in this study were determined using non-linear least-squares curve fitting program, GENPLOT (APPENDIX F1) from the corresponding Λ_m versus $([L_1\cdot Br]_t/[M^{n+}]_t)$ at different temperatures (Genplot, 1989). The obtaining data are summarized in Table 4.4.

The values of $\log K_f$ for $L_1\cdot Br\text{-}M^{n+}$ complexes increased with the increase of temperature. This is an indication for an endothermic complexation reaction between the ligands and the metal cations in the solutions (Rezayi et al., 2011). However, in some cases the $\log K_f$ reduces when the temperature increased, which can be described by exothermic complexation reaction. It was also observed that in most cases the sequence of the stability constant is $Ni^{2+} < Pd^{2+} < Zn^{2+} < Hg^{2+} < Ag^+$. In majority of reaction

conditions, $\log K_f$ shows that the complexation is more favorable in pure MeOH. This may be due to the high solubility of L₁.Br ligand in pure methanol compared to H₂O. While in the reaction mixture solution, the competition of ligand to excess metal cations which are solvated by solvent molecules to form a complex may increase. Hence, the dissimilarities in the nature of the solvent system may influence the binding properties of L₁.Br, and subsequently, the stability and selectivity of the metal complexes (Mehta et al., 2014; Rezayi et al., 2011).

Table 4.4: The $\log K_f$ values of $L_1\text{-Br-M}^{n+}$ in MeOH-H₂O binary mixtures at different temperatures for studied metal cations

Medium ^a / Ni ²⁺	$\log K_f \pm SD^b$			
	15 °C	25 °C	35 °C	45 °C
Pure MeOH	2.50 ± 0.14	2.43 ± 0.10	2.47 ± 0.07	2.48 ± 0.22
36.27% H ₂ O-63.72% MeOH	2.49 ± 0.31	2.46 ± 0.31	2.56 ± 0.27	2.40 ± 0.36
60.27% H ₂ O-39.73% MeOH	2.42 ± 0.19	2.57 ± 0.07	2.51 ± 0.08	2.46 ± 0.08
77.34% H ₂ O-22.66% MeOH	2.46 ± 0.08	2.55 ± 0.08	2.64 ± 0.07	2.45 ± 0.18
90.10% H ₂ O-9.90% MeOH	2.35 ± 0.31	2.60 ± 0.10	2.45 ± 0.12	2.85 ± 0.10
Pure H ₂ O	2.49 ± 0.08	2.56 ± 0.14	2.77 ± 0.08	2.45 ± 0.09
Medium ^a / Zn ²⁺				
Pure MeOH	2.55 ± 0.08	2.76 ± 0.08	2.76 ± 0.08	2.75 ± 0.08
36.27% H ₂ O-63.72% MeOH	2.43 ± 0.14	2.40 ± 0.15	2.55 ± 0.08	2.56 ± 0.10
60.27% H ₂ O-39.73% MeOH	2.41 ± 0.16	2.43 ± 0.13	2.43 ± 0.15	2.45 ± 0.12
77.34% H ₂ O-22.66% MeOH	2.48 ± 0.11	2.42 ± 0.13	2.55 ± 0.07	2.57 ± 0.07
90.10% H ₂ O-9.90% MeOH	2.55 ± 0.12	2.64 ± 0.06	2.27 ± 0.32	2.86 ± 0.11
Pure H ₂ O	c	c	c	c
Medium ^a / Pd ²⁺				
Pure MeOH	2.46 ± 0.21	2.51 ± 0.39	2.77 ± 0.17	2.58 ± 0.27
36.27% H ₂ O-63.72% MeOH	2.29 ± 0.31	2.45 ± 0.29	2.52 ± 0.17	2.67 ± 0.19
60.27% H ₂ O-39.73% MeOH	2.45 ± 0.21	2.83 ± 0.15	2.82 ± 0.13	2.32 ± 0.25
77.34% H ₂ O-22.66% MeOH	2.86 ± 0.10	2.50 ± 0.10	2.51 ± 0.09	2.45 ± 0.19
90.10% H ₂ O-9.90% MeOH	2.77 ± 0.08	2.41 ± 0.14	2.57 ± 0.08	2.76 ± 0.07
Pure H ₂ O	2.68 ± 0.17	2.54 ± 0.18	2.57 ± 0.19	2.76 ± 0.20
Medium ^a / Hg ²⁺				
Pure MeOH	3.85 ± 0.12	3.86 ± 0.11	3.86 ± 0.12	3.85 ± 0.12
36.27% H ₂ O-63.72% MeOH	3.27 ± 0.35	3.42 ± 0.24	3.41 ± 0.25	3.46 ± 0.22
60.27% H ₂ O-39.73% MeOH	3.45 ± 0.21	3.82 ± 0.26	3.84 ± 0.21	3.84 ± 0.21
77.34% H ₂ O-22.66% MeOH	3.88 ± 0.12	3.45 ± 0.22	3.44 ± 0.30	3.43 ± 0.31
90.10% H ₂ O-9.90% MeOH	c	c	c	c
Pure H ₂ O	c	c	c	c
Medium ^a / Ag ⁺				
Pure MeOH	3.46 ± 0.38	3.86 ± 0.20	3.84 ± 0.20	3.86 ± 0.23
36.27% H ₂ O-63.72% MeOH	3.71 ± 0.19	3.87 ± 0.22	3.78 ± 0.24	3.81 ± 0.23
60.27% H ₂ O-39.73% MeOH	3.51 ± 0.27	3.79 ± 0.22	3.84 ± 0.20	3.86 ± 0.17
77.34% H ₂ O-22.66% MeOH	3.85 ± 0.17	3.46 ± 0.32	3.44 ± 0.34	3.86 ± 0.17
90.10% H ₂ O-9.90% MeOH	3.47 ± 0.40	3.58 ± 0.32	3.86 ± 0.22	3.86 ± 0.22
Pure H ₂ O	3.58 ± 0.29	3.57 ± 0.29	3.57 ± 0.29	3.86 ± 0.22

^aComposition of binary mixtures is expressed in mol% for all mixtures, ^bSD = standard deviation, ^c The data cannot be fitted to the equation in GENPLOT

The stability constant ($\log K_f$) versus mol% MeOH was plotted individually and listed in APPENDIX G1. As can be seen in Figure 4.7, the changes in $\log K_f$ of the complexes versus the composition of the MeOH-H₂O binary systems for Ag⁺ at various temperatures are not linear. The same behaviors also can be seen in other metal cations. This pattern is probably due to solvent-solvent interaction that changed the structure of the solvent mixtures and consequently changed the solvation properties of the metal ions, ligand and the resulting complexes (Joshaghani et al., 2008; Rezayi et al., 2011b). These results can be explained by the Gutmann acceptor-donor number effect. In this study, the binary mixture of MeOH-H₂O has been used. Pure solvent MeOH and H₂O have acceptor number of 41.5 and 54.8 kcal/mol, respectively (Gutmann, 1978). Therefore, the stability constant values of complex in the solvent with lower acceptor ability will increase. This is due to less competition of the ligand with the solvent molecules for the metal cations, which thus increases the formation constant of the complexes. The effect of the Gutmann donor number (DN) of solvents and their mixtures in this study is negligible because of their approximately equal value (DN_{Water}=18 kcal/mol; DN_{MeOH}=19 kcal/mol). By ignoring this parameter, the dielectric constant of solvents, ϵ , plays another important role in the stability constant of complexes. According to the previous studies, the interaction between the oppositely charged ions in the solvent with low dielectric constant (Methanol, $\epsilon=32.6$), as compared to water ($\epsilon=81.7$), increases and causes to form the complexes.

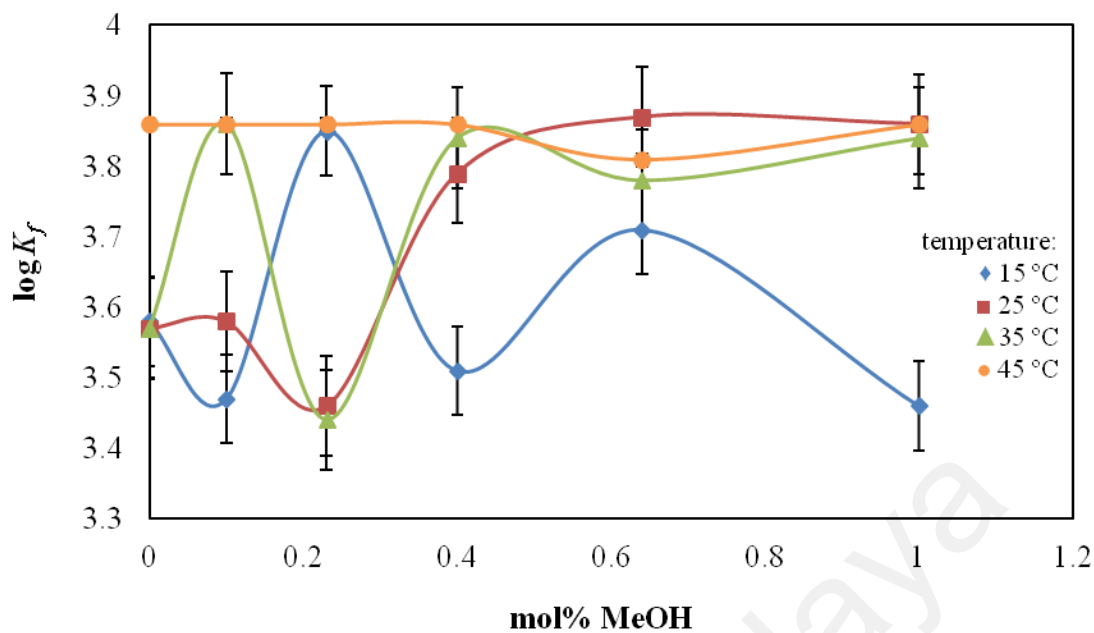


Figure 4.7: Stability constant ($\log K_f$) of complexes in MeOH-H₂O binary system (mol% MeOH; 0.00, 9.99, 22.66, 39.73, 63.72 and 100.00%) at different temperature (◆ = 15 °C, ■ = 25 °C, ▲ = 35 °C, ● = 45 °C) for Ag⁺ cation

4.2.3 Thermodynamic parameter of complexes

The thermodynamic parameter ($\Delta G_c^o, \Delta S_c^o, \Delta H_c^o$) were studied in order to better understand the complexation process. The ΔH_c^o and ΔS_c^o parameters were estimated according to the van't Hoff plots that shows the corresponding $\ln K_f$ versus temperature plots according to the van't Hoff's equation (El-Sonbati et al., 2001). All the van't Hoff plots of $\ln K_f$ versus $1000/T$ for all different metal cations, were constructed individually in APPENDIX H1. Figure 4.8 shows the $\ln K_f$ versus $1000/T$ plot for Ag⁺ metal cation. The data demonstrated that these complexation processes are temperature dependent. The value of standard enthalpy (ΔH_c^o) for the complexation reaction was determined from the slope of the van't Hoff plots based on van't Hoff's Eq. (4.1). Other thermodynamic parameters, the free energy of complex formation (ΔG_c^o) and the value

of the standard entropy (ΔS_C^o) were obtained from thermodynamic relation Eq. (4.2) (Christy et al., 2011). The calculated results are summarized in Table 4.5.

$$\ln K_f = \frac{\Delta_f S_C^o}{R} - \frac{\Delta_f H_C^o}{RT} \quad \text{Eq. (4.1)}$$

$$\Delta G_{C,29815}^o = \Delta H_{C,29815}^o - T\Delta S_C^o \quad \text{Eq. (4.2)}$$

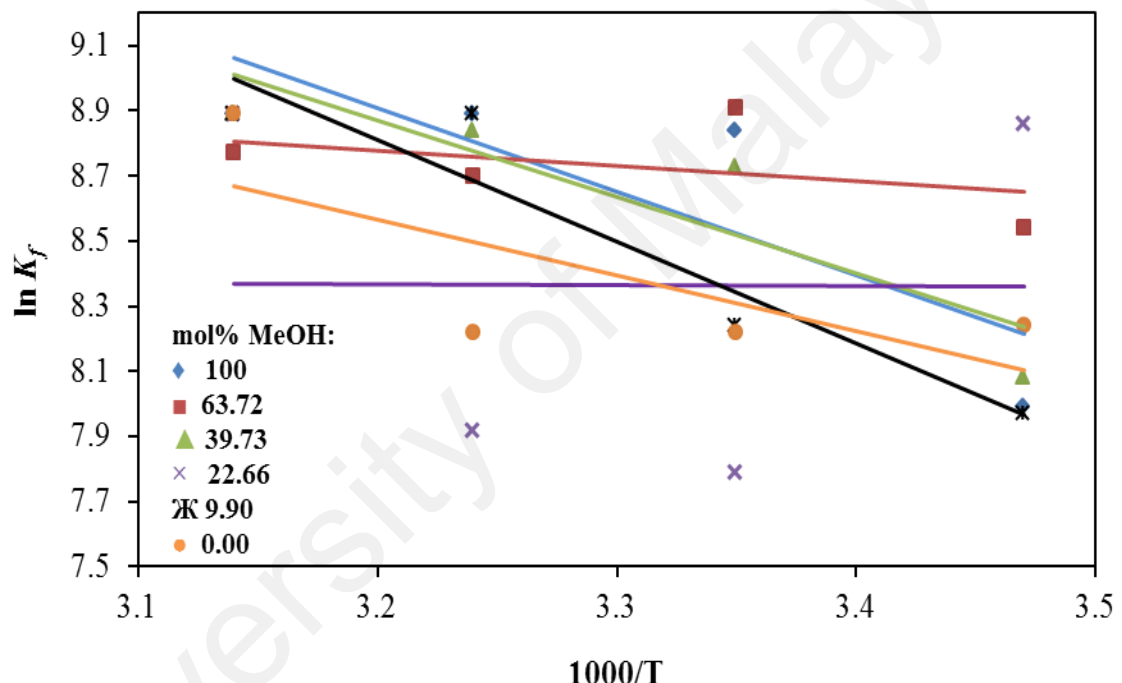


Figure 4.8: Van't Hoff plot for $L_1\cdot Br\cdot M^{n+}$ complex for Ag^+ in MeOH-H₂O binary system at different temperatures

Table 4.5: Summary of thermodynamic parameters values of the L₁.Br-Mⁿ⁺ complexes in MeOH-H₂O binary mixture solvent

Medium ^a /Ni ²⁺	$\Delta G_C^o \pm SD^b$ (kJ/mol)	$\Delta H_C^o \pm SD^b$ (kJ/mol)	$\Delta S_C^o \pm SD^b$ (J/mol)
Pure MeOH	-13.9 ± 0.5	4.6 ± 1.0	62.1 ± 2.8
36.27% H ₂ O-63.72% MeOH	-14.04 ± 1.8	-5.6 ± 0.1	28.2 ± 1.9
60.27% H ₂ O-39.73% MeOH	-14.6 ± 0.4	-9.9 ± 0.3	16.0 ± 1.0
77.34% H ₂ O-22.66% MeOH	-14.5 ± 0.4	14.5 ± 0.4	97.3 ± 0.7
90.10% H ₂ O-9.90% MeOH	-14.8 ± 0.6	28.7 ± 0.3	146.1 ± 4.4
Pure H ₂ O	-14.6 ± 0.8	23.2 ± 7.4	127.0 ± 2.5
Medium ^a /Zn ²⁺			
Pure MeOH	-15.8 ± 0.5	11.0 ± 6.3	89.9 ± 2.0
36.27% H ₂ O-63.72% MeOH	-13.7 ± 0.9	7.3 ± 2.2	70.4 ± 6.9
60.27% H ₂ O-39.73% MeOH	-13.8 ± 0.7	1.1 ± 0.9	50.0 ± 1.6
77.34% H ₂ O-22.66% MeOH	-13.8 ± 0.7	5.5 ± 0.3	64.7 ± 2.2
90.10% H ₂ O-9.90% MeOH	-15.1 ± 0.4	17.9 ± 1.7	110.7 ± 5.6
Pure H ₂ O	c	c	c
Medium ^a /Pd ²⁺			
Pure MeOH	-14.4 ± 2.2	6.9 ± 0.7	71.4 ± 7.0
36.27% H ₂ O-63.72% MeOH	-14.0 ± 1.7	21.0 ± 1.9	117.4 ± 3.3
60.27% H ₂ O-39.73% MeOH	-16.2 ± 0.8	32.3 ± 8.0	162.7 ± 6.3
77.34% H ₂ O-22.66% MeOH	-14.3 ± 0.6	-4.5 ± 4.0	32.9 ± 1.9
90.10% H ₂ O-9.90% MeOH	-13.8 ± 0.8	31.6 ± 2.9	152.3 ± 9.4
Pure H ₂ O	-14.7 ± 1.0	16.5 ± 4.0	104.6 ± 6.9
Medium ^a /Hg ²⁺			
Pure MeOH	-22.0 ± 0.6	1.1 ± 0.5	77.6 ± 2.5
36.27% H ₂ O-63.72% MeOH	-19.5 ± 1.4	11.1 ± 0.9	102.6 ± 3.6
60.27% H ₂ O-39.73% MeOH	-21.8 ± 1.5	24.6 ± 7.6	155.6 ± 5.0
77.34% H ₂ O-22.66% MeOH	-19.7 ± 1.3	-2.3 ± 0.5	58.4 ± 4.0
90.10% H ₂ O-9.90% MeOH	c	c	c
Pure H ₂ O	c	c	c
Medium ^a /Ag ⁺			
Pure MeOH	-21.9 ± 1.1	21.3 ± 9.2	145.0 ± 31.1
36.27% H ₂ O-63.72% MeOH	-22.1 ± 1.8	21.7 ± 8.3	146.9 ± 7.3
60.27% H ₂ O-39.73% MeOH	-21.6 ± 1.3	28.3 ± 9.8	167.4 ± 3.7
77.34% H ₂ O-22.66% MeOH	-19.3 ± 1.9	35.9 ± 3.5	185.1 ± 8.4
90.10% H ₂ O-9.90% MeOH	-20.4 ± 1.3	25.9 ± 6.0	155.4 ± 20.7
Pure H ₂ O	-20.4 ± 1.3	14.2 ± 4.5	116.1 ± 15.7

^aComposition of binary mixtures is expressed in mol% for solvent system, ^bSD = Standard deviation, ^cThe data cannot be fitted to equation

The results reveal that in most cases, the changes in ΔH_C^o for the complexation process is negligible, while the change in ΔS_C^o is significant. Therefore, the formation of complexes between L₁.Br and the studied metal cations in MeOH-H₂O binary mixtures for most cases are endothermic. Consequently, this phenomenon is due to different solvent-solvent interactions which resulted in the change in the flexibility of the ligand during complexation and hence contributed to change in entropy. While the negative value of ΔG_C^o , as evidence that the ability of the ligand to form stable complexes with metal cations as well as the process were spontaneous (Józwiak et al., 2014). The existence of such compensating effect between ΔH_C^o and ΔS_C^o values for the studied binary mixture is shown in Figure 4.9. It is clear that the observed increase or decrease in ΔH_C^o value which depends on the nature of the metal cations will be compensated by an increase (or decrease) in the corresponding ΔS_C^o value. Then the small changes of ΔG_C^o values will be explained due to this compensating effect for ΔH_C^o and ΔS_C^o , independently (Christy et al., 2011; El-Sonbati et al., 2001).

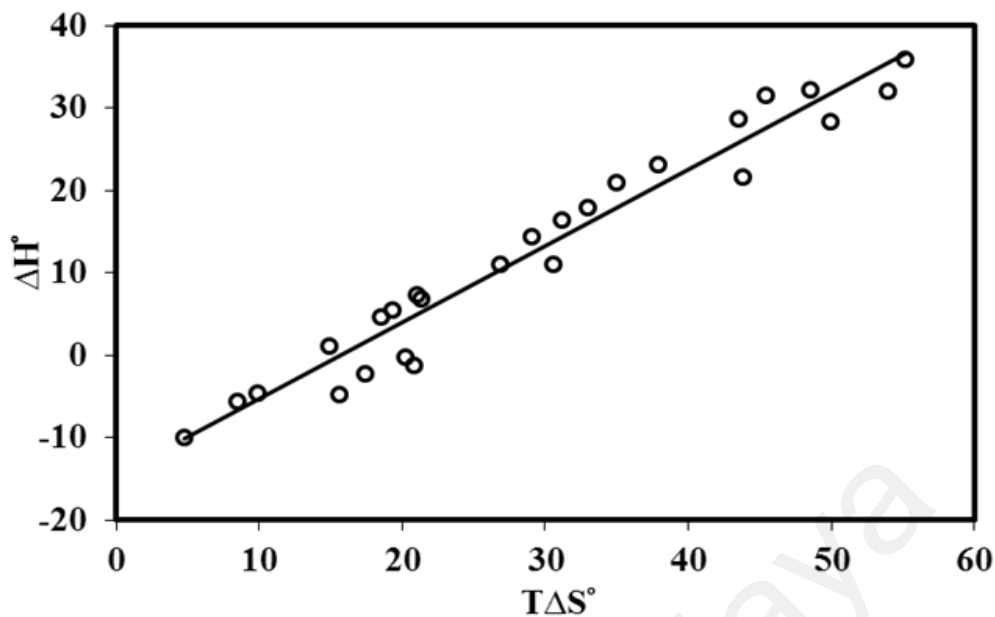


Figure 4.9: Plot of ΔH_c^o (kJ/mol) versus $T\Delta S_c^o$ (kJ/mol) for $L_1\cdot Br\cdot M^{n+}$ ($M = Ni^{2+}, Pd^{2+}, Zn^{2+}, Hg^{2+}$ and Ag^+) in different MeOH-H₂O binary systems ($R^2=0.9537$)

4.2.4 Effect of ionic radius in complex formation

The variation of $\log K_f$ values for the complexation process in contrast with cationic radius in different solvent systems at 25 °C was plotted as illustrated in Figure 4.10. It was clearly observed that the stability constant of complexes increases as the size of a metal cation increases from Ni^{2+} to Ag^+ .

According to Shah et al. (2014), the results can be explained based on fit-size concept, which depends on the size of cation and ligand cavity. They found, the $\log K_f$ values for studied metal cations in sequence of Mg^{2+} (0.74 Å) < Ca^{2+} (1.00 Å) < Sr^{2+} (1.18 Å). This result shows that the formation of stable complex is dependent to the cation size which is closer to the size of ligand cavity (1.34-1.55 Å).

In addition, Christy et al. (2011) found that the complex formation of different ionic radius was influenced by the solvent system effect as well. The small metal cations will be more solvated than the bigger metal cations in the same solvent system and decrease their mobility. Consequently, the competition of ligand with solvent molecules increased and resulted in the decrement of stability constant.

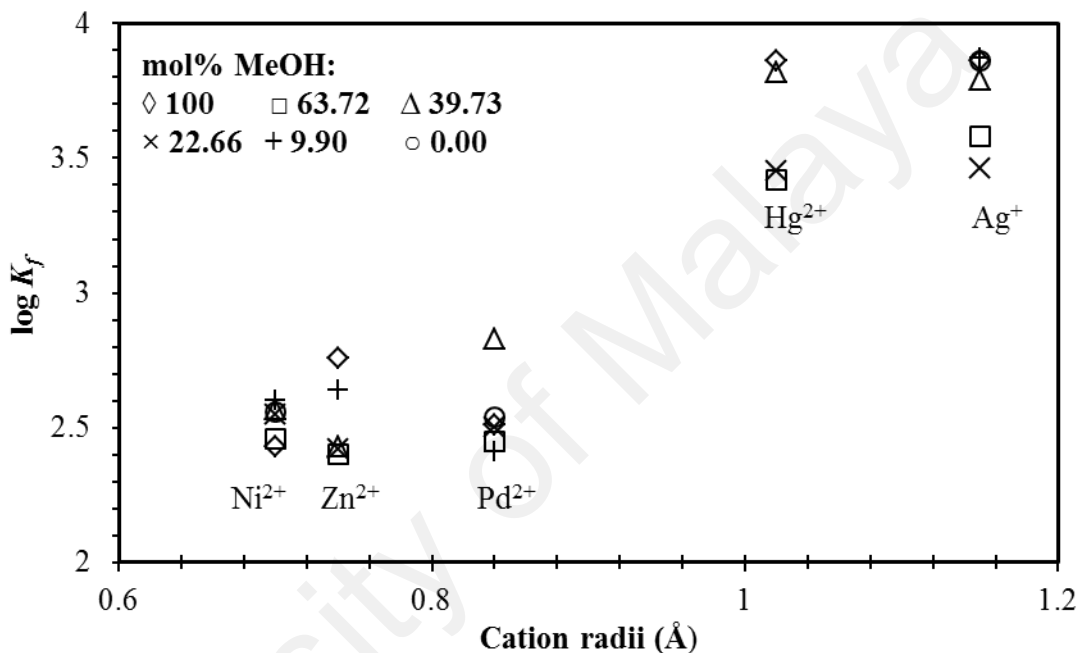


Figure 4.10: Changes of stability constant ($\log K_f$) of L_1Br with all metal cation in $\text{MeOH-H}_2\text{O}$ binary at 25°C

4.2.5 Artificial neural network modeling study

Artificial neural network (ANN) as a mathematical (or computational) model that is inspired by the structure and function of biological neural networks in the brain, is one of the most successful technologies in the last two decades (Abdollahi et al., 2013; Rezayi et al., 2014). In this research work, the ANN was applied for the simulation of property parameters correlation and a good agreement in the experimental and predicted values were obtained. A 4-11-1 (input layer-hidden layer-output layer)

network structure was used as shown in Figure 4.11. The effect of four parameters (cationic radii, temperature, mol% of MeOH in the media and mol% of H₂O in the media) for determining the complex formation (K_f) was the input layer matrix of the network. 59 training examples, 26 testing examples and 20 validating examples (10 times of each node) were prepared for training, testing and validating the network, respectively. The model training based on the quick propagation (QP) learning algorithm was carried out to test data set and determine the minimum value of RMSE as an error function. The regression coefficient of determination (R^2) showed a fairly good correlation between the estimated and experimental data sets for both train (0.959) and test data sets (0.943) (Figure 4.12 (A) and (B)).

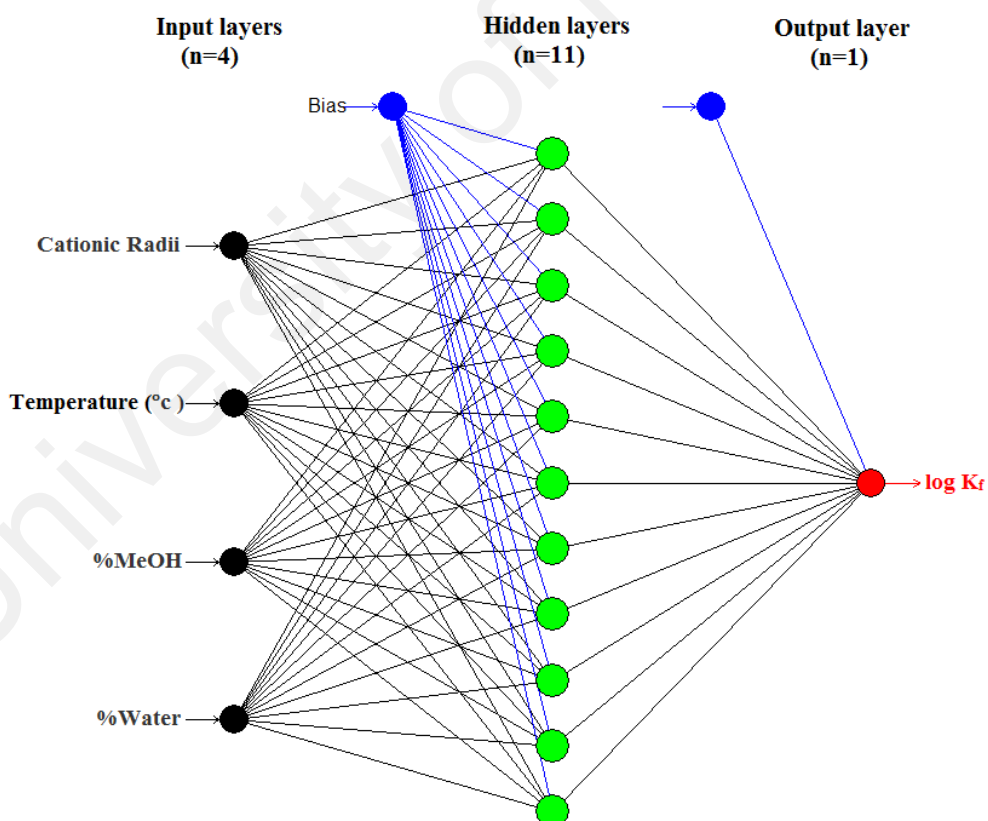


Figure 4.11: Structure of neural network adopted in this study

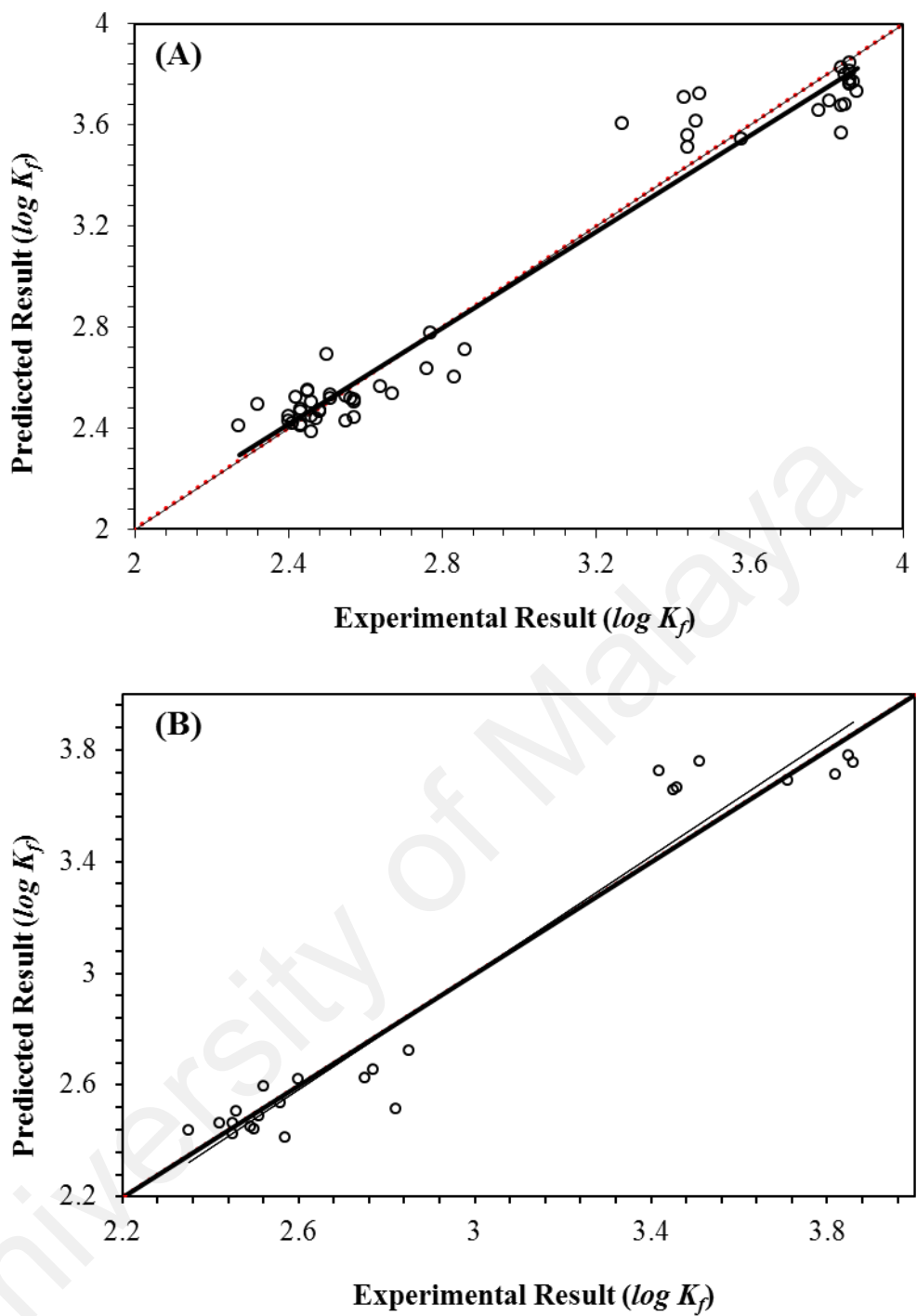


Figure 4.12: Comersion of estimated $\log K_f$ with experimental data (A) training data set and (B) test data set

The obtained formation constants of complex reactions between studied metal cations and $L_1\cdot Br$ using the various mol% of H_2O in MeOH- H_2O media at different temperatures are shown in Figure 4.13 by drawing surface and contour plots of the

stability constant ($\log K_f$) for the complex formation as a function of the mol% of H₂O in the binary mixtures and different studied cationic radius.

As seen in Figure 4.13, increasing the mol% of H₂O and cationic radius causes the changes in constant stability values of complexes ($\log K_f$), respectively. The maximum formation constant of complexes were obtained in zero mol percentage of water (100% of MeOH) and the highest amount of cationic radii was related to Ag⁺ cation (1.15 Å). This result indicated that this model is valid for estimation of stability constant the complexes of Ni²⁺, Pd²⁺, Zn²⁺, Hg²⁺ and Ag⁺ in MeOH-Water binary mixtures at different temperatures. The estimated results based on the ANN program were in a good agreement with the obtained experimental results.

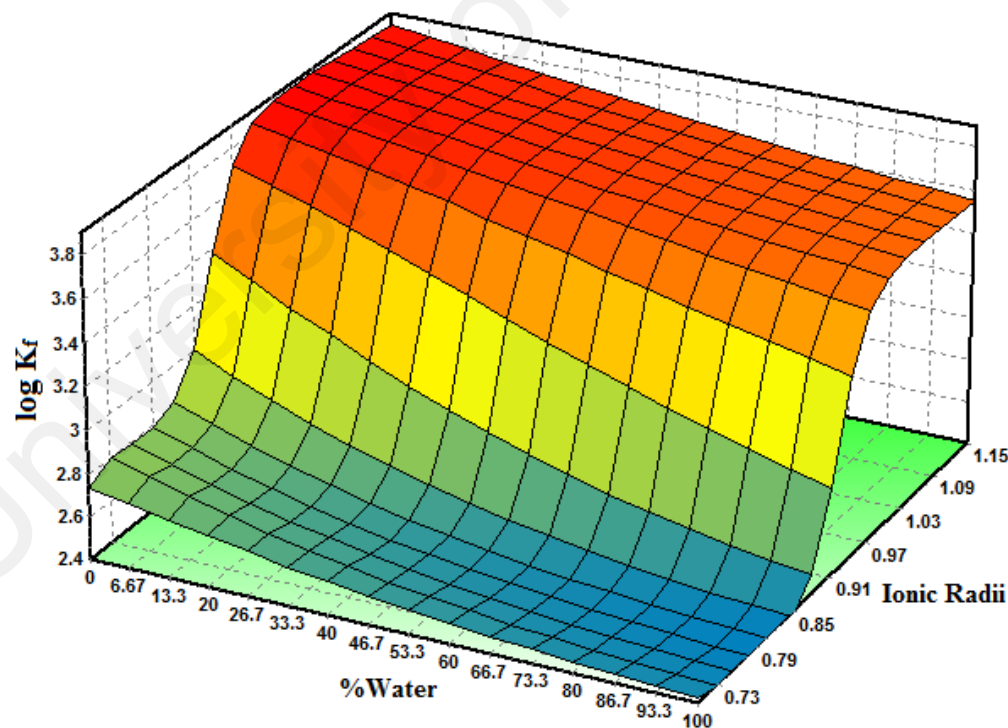


Figure 4.13: Surface and contour plots of the stability constant ($\log K_f$) as a function of the mol% of water and ionic radius of cations (Ni²⁺, Pd²⁺, Zn²⁺, Hg²⁺ and Ag⁺)

4.2.6 Theoretical study

With the purpose of elucidating the obtained experimental results, a density functional theory (DFT) study was conducted. The DFT calculations were carried out with the GAUSSIAN 09 software package and the B3LYP/LANL2DZ basis set. The binding energy ΔE in the complexation between $L_1\cdot Br$ and M^{n+} in MeOH pure solvent is defined by the following equation:

$$\Delta E = E_{L_1\cdot Br-M^{n+}} - (E_{M^{n+}} + E_{L_1\cdot Br}) \quad \text{Eq. (4.3)}$$

Where ΔE , $E_{L_1\cdot Br-M^{n+}}$, $E_{M^{n+}}$ and $E_{L_1\cdot Br}$ are binding energy, $L_1\cdot Br\text{-}M^{n+}$ complex energy, free metal ion energy and $L_1\cdot Br$ energy, respectively (Sakajiri et al., 2012). The optimized structures of free and complexes of $L_1\cdot Br$ with Zn^{2+} and Ag^+ are shown in Figure 4.14 (A, B, C), respectively. While the calculated results of the binding energies for all complexes in MeOH pure solvent are listed in Table 4.6.

It is clear from Table 4.6 shows that the binding energy increases monotonically with increasing the size of the studied cations. Therefore the binding energy of Ag^+ is much larger than other cations, showing prominent affinity to $L_1\cdot Br$ in the MeOH solvent. The obtained data shows a similar agreement with data in the previous sections in which the effect of cationic radius towards complexation process was discussed. Thus, proved that a small cationic radius metals such as Ni^{2+} , Zn^{2+} and Pd^{2+} have high solvation free energy with MeOH that causes them to be more solvated in the solution, and have less interaction with free $L_1\cdot Br$ ligand.

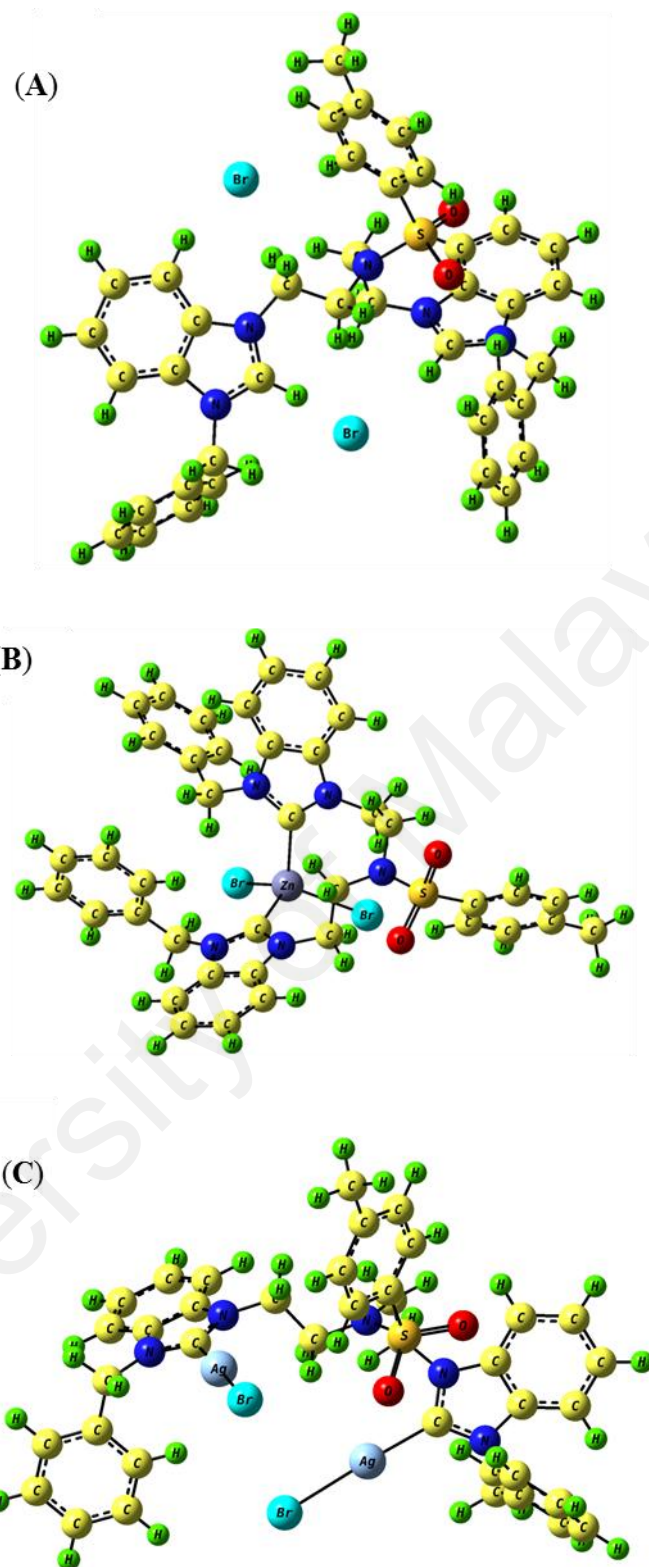


Figure 4.14: Optimal conformation structures obtained from GAUSSIAN 09 program for (a) L_1Br ligand, (b) $\text{L}_1\text{Br-Zn}^{2+}$ and (c) $\text{L}_1\text{Br-Ag}^+$ complexes

Table 4.6: The calculated binding energies ΔE , in the formation of $L_1.Br-M^{n+}$ by DFT method, where $E_{L_1.Br}$ is -1969.8454 (Hartree)

Mⁿ⁺	E_Mⁿ⁺ (Hartree)	E_{L₁.Br} - Mⁿ⁺ (Hartree)	ΔE (Hartree)	ΔE (kJ/mol)
Ni ²⁺	-168.8263978	-2138.0707	0.66742646	1752.327917
Zn ²⁺	-65.30191723	-2034.37409	0.83955559	2204.252883
Pd ²⁺	-126.2368438	-2095.515285	0.63328753	1662.696169
Ag ⁺	-145.6275022	-2114.513658	1.02557279	2692.64097
Hg ²⁺	-42.5030206	-2011.502124	0.91262536	2396.097536

In summary the combination of results obtained from conductometric studies of $L_1.Br$ with Ni²⁺, Pd²⁺, Zn²⁺, Hg²⁺ and Ag⁺, revealed the selective complexation of $L_1.Br$ in sequence Ni²⁺< Pd²⁺<Zn²⁺<Hg²⁺<Ag⁺. This finding confirms that the complexation of $L_1.Br$ is more favorable in Hg²⁺ and Ag⁺ cations in solution.

4.3 Fabrication of ion selective electrode (ISE) based on $L_1.Br$ ionophore

In this part the potential of $L_1.Br$ as an ionophore in ISE sensor towards Hg²⁺ and Ag⁺ cations were investigated. Therefore, a new potentiometric self-plasticizing polypyrrole sensors based on a $L_1.Br$ ionophore for determination of Hg²⁺ and Ag⁺ cations were fabricated.

4.3.1 Optimization of fabricated membranes

The composition of plasticizer-free membranes with the presence of ionophore can affect the potentiometric response and detection limit of sensors. Several studies on the membrane composition of electrodes have reported significant influence on the selectivity and sensitivity of produced ISE (Faribod et al., 2008a; Gupta et al., 2007). In this study, the synthesized $L_1.Br$ was incorporated into the membrane of electrode as an ionophore due to its tendency towards Hg²⁺ and Ag⁺ metal cations. Therefore, in

order to find the optimized membrane composition, different amounts of L₁.Br ionophore, DMPP photoinitiator and NaTFB lipophilic salt have been used for different electrodes. The two electrodes were tested in different concentrations of Hg²⁺ and Ag⁺ metal cations solution in the range of 1×10⁻⁸ to 1×10⁻¹ M.

4.3.1.1 Optimization of fabricated membranes in determination of Hg²⁺

First, the fabricated electrodes E1-E10 have been tested in determination of Hg²⁺ (Hg-ISE) at different concentrations. As seen in Table 4.7, the electrode without ionophore (E5) shows a slightly weak potentiometric response towards Hg²⁺ cation. Addition of various wt.% of ionophore in the construction of electrode E3, E7, E9 and E10 gave different results in Nerstian response. Similar results also can be seen in the electrode E2, E6 and E8 from which the NaTFB wt.% was varied. They exhibited the non-Nernstian potential response with inverted-Nernstian slopes of 22.27 mV/decade, 37.03 mV/decade and 26.58 mV/decade, respectively.

The result indicated that ionophore plays the most important role in the proposed ISE membrane composition for the sensing of Hg²⁺ cation. The observed potentiometric response can also be related to the properties of PPy as the active component of electrochemical sensors toward the target ions and the presence of lipophilic salt, NaTFB in the membrane. The nature and the amount of lipophilic salts, NaTFB in the membrane composition intensely influence the response of sensors in reducing the matrix resistance and enhance its responsive behavior (Peshkova et al., 2008; Tadayon et al., 2014).

Table 4.7: The compositions of ISE membrane used based on L₁.Br ionophore for the potentiometric detection of Hg²⁺

Electrode	Composition (w/w%)				Electrode characteristics			
	Pyrrole	DMPP	NaTFB	L ₁ .Br	Slope (mV/decade)	Linear range (M)	Detection limit (M)	R ²
E1	89.4	4.8	0.8	5.0	38.99	1×10 ⁻⁶ -1×10 ⁻¹	2.0×10 ⁻⁷	0.98
E2	88.8	4.8	0.8	5.6	37.03	1×10 ⁻⁵ -1×10 ⁻¹	2.5×10 ⁻⁶	0.95
*E3	89.4	4.8	0.2	5.6	28.16	1×10 ⁻⁶ -1×10 ⁻²	2.5×10 ⁻⁷	0.99
E4	94.2	0.0	0.2	5.6	26.30	1×10 ⁻⁵ -1×10 ⁻³	6.3×10 ⁻⁶	0.98
E5	95.0	4.8	0.2	0.0	11.80	1×10 ⁻⁴ -1×10 ⁻²	7.9×10 ⁻⁵	0.99
E6	89.6	4.8	0.0	5.6	22.27	1×10 ⁻⁵ -1×10 ⁻²	1.6×10 ⁻⁶	0.97
E7	91.0	4.8	0.2	4.0	23.97	1×10 ⁻⁵ -1×10 ⁻²	3.2×10 ⁻⁶	0.98
E8	89.5	4.8	0.1	5.6	26.58	1×10 ⁻⁵ -1×10 ⁻²	4.0×10 ⁻⁶	0.98
E9	89.0	4.8	0.1	6.1	36.92	1×10 ⁻⁵ -1×10 ⁻²	4.0×10 ⁻⁶	0.99
E10	88.2	5.2	0.1	6.5	39.12	1×10 ⁻⁴ -1×10 ⁻²	8.9×10 ⁻⁵	0.98

*Optimum membrane composition

To investigate the role of NaTFB additive for improving the potential response of the proposed membrane sensor by reducing the ohmic resistance of polymeric membrane electrochemical impedance spectroscopy (EIS) was performed in 1 mM $\text{Fe}[(\text{CN})_6]^{3-4-}$ (1:1) containing 0.1 M KCl solution (Nia et al., 2015a; Nia et al., 2015b). EIS data were recorded at open circuit potential with an AC amplitude of 5 mV and a frequency range from 100 kHz to 0.1 Hz by using the potentiostat/galvanostat with a platinum and SCE as counter and reference electrodes, respectively. The impedance spectra for optimized membrane recorded with (E3) and without (E6) NaTFB additive showed two charge-transfers which were fitted to the equivalent circuit presented at Figure 4.15. The fitting results are summarized in Table 4.8. The first charge-transfer is related to the outer layer polypyrole (PPy layer), while the second charge-transfer is related to the inner layer (pHEMA layer). From Figure 4.15 and from the fitting results summarized in Table 4.8, it is obviously observed that the presence of NaTFB additive causes to reduce in charge transfer resistance (R_{ct}). Moreover, the absence of L₁.Br ionophore (E5) in the membrane composition leads to enhance the charge transfer resistance, and also a tight structure of PPy membrane which shows only a charge-transfer PPy outer layer connected to the electrolyte. This is because of the presence of ionophore increases electrical conductivity and hence the charge transfer resistance decreases. The comparison of the semicircle diameters from the Nyquist plots of the modified electrodes presents the following direction of R_{ct} (Table 4.8): (R_{ctI}): E3>E6>E5.

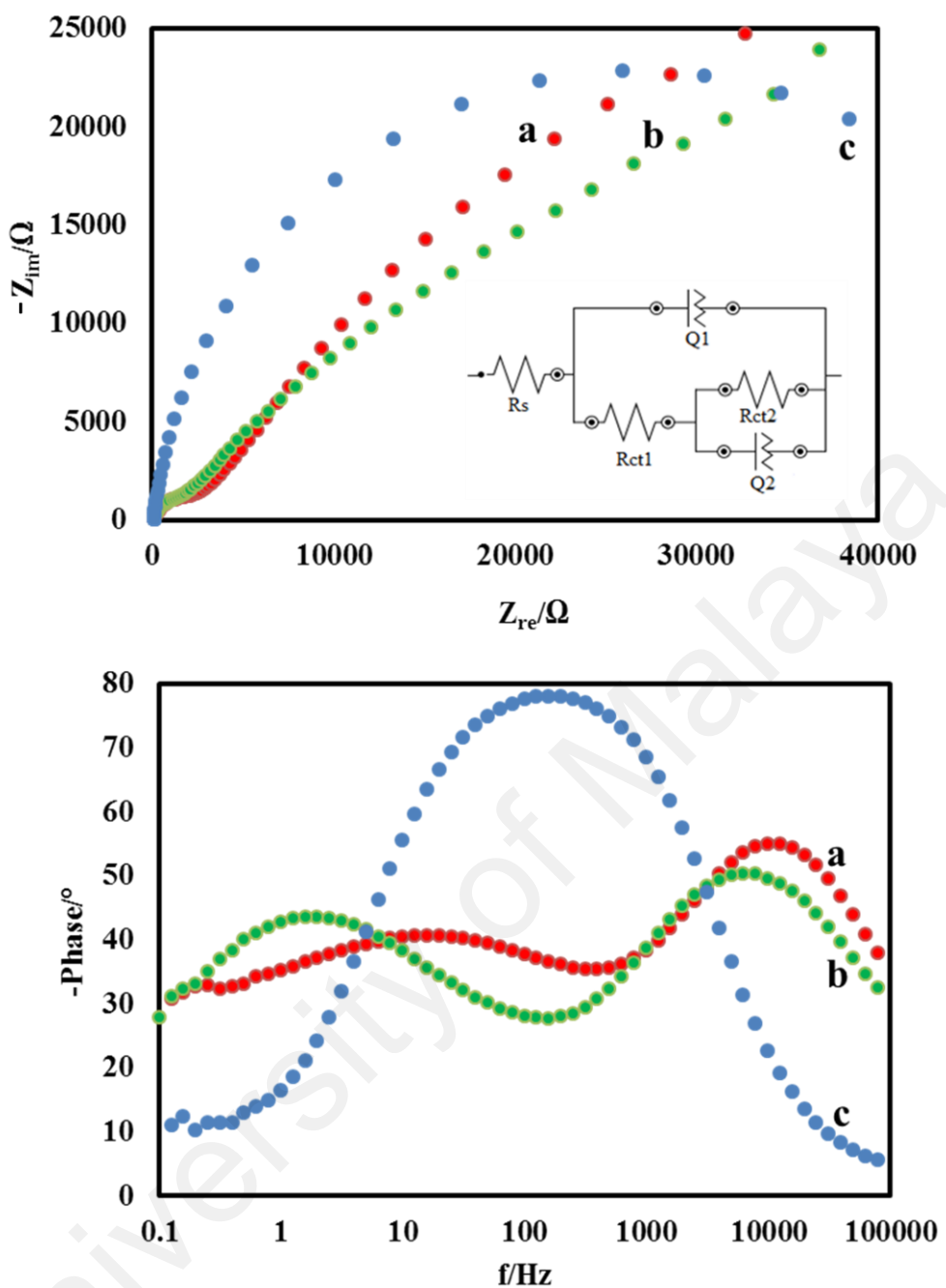


Figure 4.15: Nyquist and phase plots of the impedance spectra recorded for fresh electrode membranes (a) without, E6 (b) with NaTFB additive, E3 and (c) without $L_1.Br$ ionophore, E5, (Z_{im} = impedance imagine; Z_{re} =impedance real; f = frequency; R_s = resistance; R_{ct} = charge transfer resistance; Q = quality factor)

Table 4.8: Impedance parameters for electrodes E3, E6 and E5 as determinate using the equivalent circuit presented in Figure 4.15

Electrode	R_s (Ω)	R_{ct1} ($K\Omega$)	Q_1	n_1	R_{ct2} ($K\Omega$)	Q_2	n_2
E3	97.9	1.57	182	0.82	153	13.7	0.48
E6	101	2.97	646	0.74	111	12.3	0.62
E5	113	50	772	0.91	-	-	-

These results demonstrated the importance of correct amount of ionophore NaTFB in the membrane composition in order to reduce the resistance and maintain the conductivity to optimize the selectivity and sensitivity of the membrane sensor. Thus, it can be concluded that, the optimum membrane composition (E3) was obtained using 89.4 wt.% monomer pyrrole, 4.8 wt.% photoinitiator DMPP, 0.2 wt.% lipophilic salt NaTFB, and 5.6 wt.% ionophore L₁.Br. The membrane electrode with an optimum composition demonstrated a good Nernstian response to Hg²⁺ cations ranging from 1.0×10⁻⁶ to 1.0×10⁻² M with a detection limit of 2.5×10⁻⁷ M and a Nernstian slope of 28.10±0.29 mV/decade. The calibration plot of the optimized Hg²⁺ ion-selective sensor was showed in Figure 4.16.

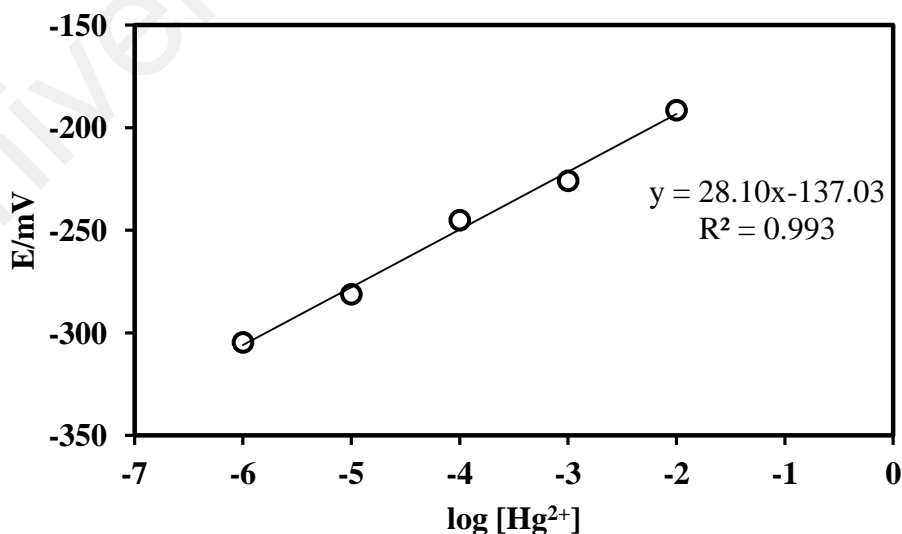


Figure 4.16: Calibration plot of the optimized Hg²⁺ ion-selective sensor

4.3.1.2 Optimization of fabricated membranes in determination of Ag⁺

In the study of optimizing the composition for ISE towards Ag⁺ cations (Ag-ISE), electrode E1-E7 were fabricated. The results are presented in Table 4.9, showing the electrode without ionophore (E1) adopts a non-Nernstian potential response slope toward Ag⁺ cation. After introducing the ionophore in the membrane with a suitable wt.%, the results show a good Nernstian slope of 60.58 mV/decade in the concentration range from 1.0×10^{-5} M to 1.0×10^{-1} M with R² values of about 1. The obtained data revealed that the L₁.Br ionophore are also selective towards Ag⁺ cation in ISE application with the optimum electrode composition; 89.4 wt.% monomer pyrrole, 4.8 wt.% photoinitiator DMPP, 0.2 wt.% lipophilic salt NaTFB, and 5.6 wt.% ionophore L₁.Br. (E4) with detection limit of 5.01×10^{-6} M.

In order to increase the working range and detection limit of the proposed electrode of Ag-ISE, a total ionic strength adjustment buffer (TISAB) was applied by using NaNO₃ solution to overcome this problem. The presence of TISAB will help to stabilize the ionic strength in the test solution by virtually eliminating all of the effect of variation in the ionic composition of the water supply as reported in the literature (Frant et al., 1968; Gholami et al., 2013; Xian-chen et al., 2010). In this work, the optimized membrane composition E4 and four different series of Ag⁺ cation solution containing different concentrations of NaNO₃ solution were tested. The obtained results are summarized in Table 4.10. It was observed that with addition of TISAB (1.0 M) exhibited a good Nernstian response to Ag⁺ cation from the range of 2.5×10^{-6} M to 1.0×10^{-1} M with a low detection limit of 2.0×10^{-6} M and Nernstian slope of 58.48 ± 0.75 mV/decade (Figure 4.17). The detection limit was calculated by extrapolating the linear regions of the calibration graphs to the baseline potentials (Faridbod et al., 2007).

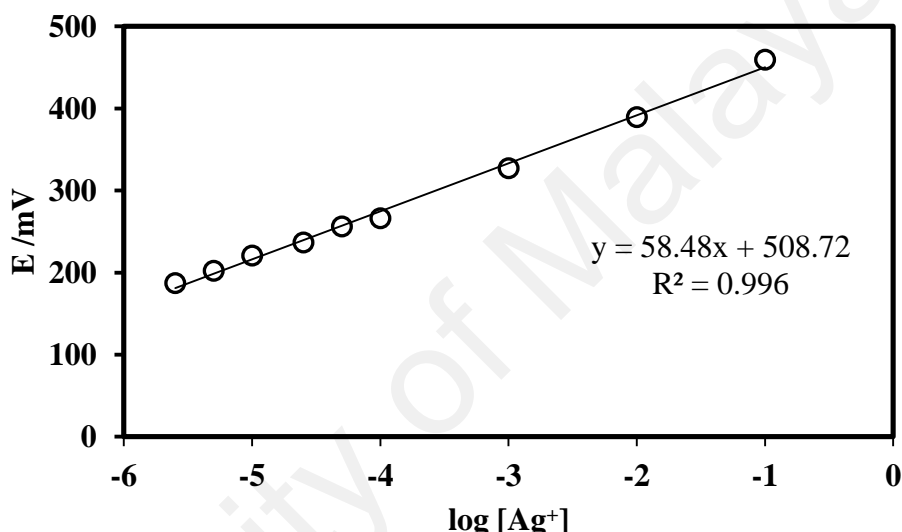
Table 4.9: The compositions of ISE membrane used based on L₁.Br ionophore for the potentiometric detection of Ag⁺

Electrode	Composition (w/w%)				Electrode characteristics			
	Pyrrole	DMPP	NaTFB	L ₁ .Br	Slope (mV/decade)	Linear range (M)	Detection limit (M)	R ²
E1	95.0	4.8	0.2	0.0	42.84±0.37	1×10 ⁻⁵ -1×10 ⁻¹	2.51×10 ⁻⁶	0.96
E2	93.0	3.8	0.2	3.0	49.64±0.43	1×10 ⁻⁵ -1×10 ⁻¹	7.94×10 ⁻⁶	0.99
E3	91.0	4.8	0.2	4.0	49.47±0.40	1×10 ⁻⁵ -1×10 ⁻¹	7.94×10 ⁻⁶	0.99
*E4	89.4	4.8	0.2	5.6	60.58±0.32	1×10 ⁻⁵ -1×10 ⁻¹	5.01×10 ⁻⁶	0.99
E5	89.6	4.8	0.0	5.6	36.96±0.50	1×10 ⁻⁵ -1×10 ⁻¹	6.31×10 ⁻⁶	0.95
E6	88.8	4.8	0.8	5.6	30.19±0.35	1×10 ⁻⁵ -1×10 ⁻¹	3.98×10 ⁻⁶	0.97
E7	88.2	5.2	0.1	6.5	51.47±0.29	1×10 ⁻⁵ -1×10 ⁻¹	3.98×10 ⁻⁶	0.99

*Optimum membrane composition

Table 4.10: Different concentrations of NaNO_3 added in the Ag^+ test solution

NaNO_3 concentration (M)	Slope (mV/decade)	Linear range (M)	Detection limit (M)	R^2
0.10	55.80 ± 0.38	5.00×10^{-6} - 1.00×10^{-1}	2.94×10^{-6}	0.97
0.50	57.22 ± 0.44	2.50×10^{-6} - 1.00×10^{-1}	2.31×10^{-6}	0.98
1.00	58.48 ± 0.75	2.50×10^{-6} - 1.00×10^{-1}	2.00×10^{-6}	0.99
2.00	72.55 ± 0.72	2.50×10^{-6} - 1.00×10^{-1}	2.16×10^{-6}	0.99

**Figure 4.17:** Calibration plot of the optimized Ag^+ ion-selective sensor

4.3.2 Potentiometric response towards fabricated ISEs

The potential responses for the proposed membrane electrodes Hg-ISE and Ag-ISE were studied and compared over other cations, respectively. Optimized membrane sensors were used over a wide concentration range of 1.0×10^{-8} M to 1.0×10^{-1} M for various types of cations. The results are shown in Figure 4.18 (A) and (B), respectively. As can be seen, the Hg^{2+} and Ag^+ cations exhibited a good Nernstian response with the Nernstian slopes of 28.16 mV/decade and 58.48 mV/decade and seem to be suitably determined by the membrane sensor based on L_1Br ionophore, respectively. This can

be justified due to the strong selective complexation behaviors of the ionophore towards Hg^{2+} and Ag^+ as compared to other metal ions as well as the rapid exchange kinetics of the obtained complexes (Faribod et al., 2008a).

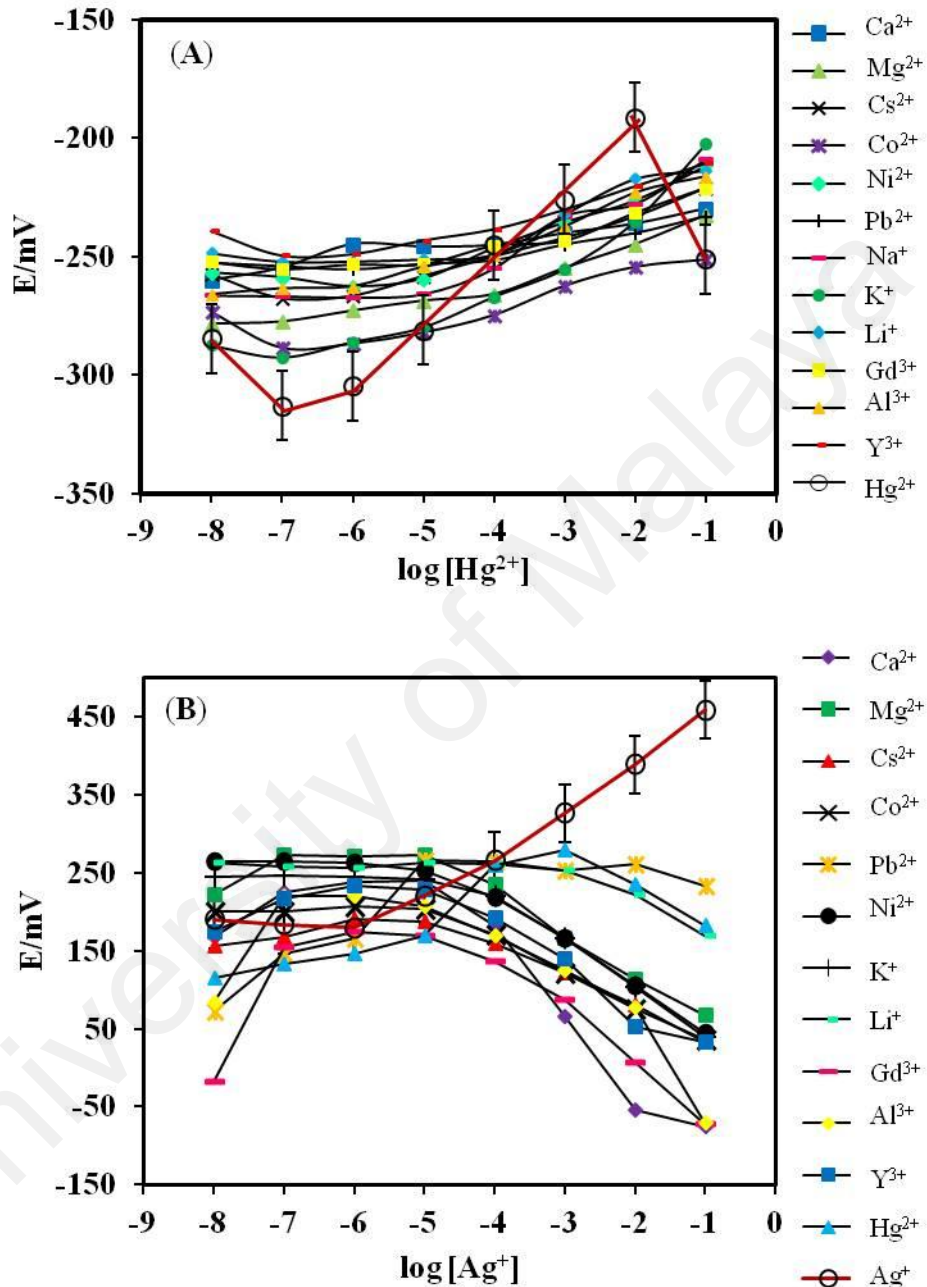


Figure 4.18: The potential responses of (A) Hg-ISE and (B) Ag-ISE membrane electrodes based on L_1Br ionophore towards various metal cations

4.3.3 Characterization of fabricated selective PPy membranes

4.3.3.1 Uv-Vis spectroscopy

The preliminary spectrophotometrically study of the complexation of L₁.Br ionophore with Hg²⁺ and Ag⁺ cations were carried out. Three solutions, L₁.Br inophore in 1.00×10^{-4} M, metal cations solution with a concentration of 1.00×10^{-4} M and their 1:1 mixtures in pure DMSO solvent were prepared. The UV-Vis absorption spectra of complexation study between L₁.Br and both metal cations were illustrated in Figure 4.19 (A) and (B), respectively. The spectra were recorded from 250 to 600 nm. As obvious in Figure 4.19 (A), the spectra of Hg²⁺ solution shows one absorption maxima at 262 nm while the L₁.Br spectrum shows two absorption maxima at 268 nm and 272 nm. With the addition of HgCl₂ to the L₁.Br ionophore, the blue absorption band slightly shifted and its intensity increased. In Figure 4.19 (B), the spectra of Ag⁺ solution shows a maximum absorption peak at 427 nm, whereas L₁.Br spectra shows two maximum absorption peaks at 270 nm and 278 nm. Through the addition of Ag⁺ solution to L₁.Br ligand (1:1, v/v), the characteristic absorption band at 427 nm was disappeared and shifted to 278 nm and 286 nm with the decrease in intensity (Faridbod et al., 2008a; Ngeontae et al., 2008). Thus, the significant changes observed in the spectra indicate the special tendency of L₁.Br ionophore towards Hg²⁺ and Ag⁺ cation, and confirm its selective interaction.

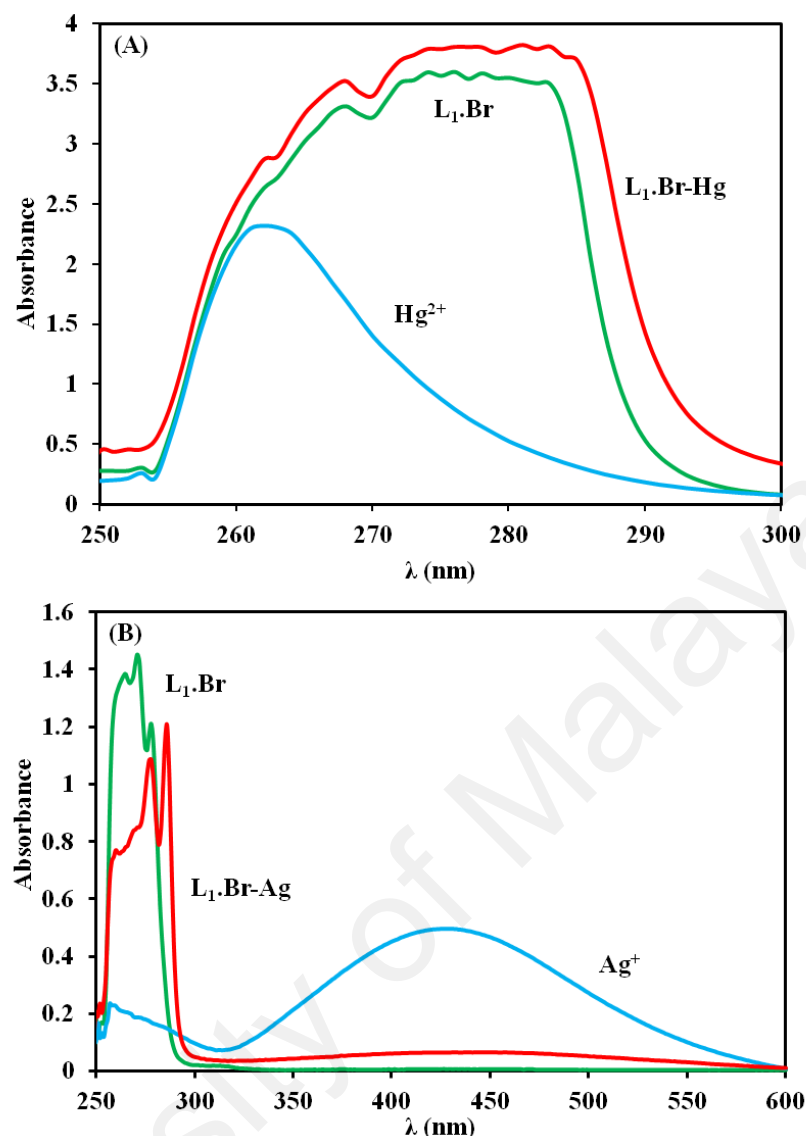


Figure 4.19: UV-Vis absorption spectra of (A) HgCl_2 solution 1.0×10^{-4} M (Hg^{2+}), ionophore solution 1.0×10^{-4} M ($\text{L}_1.\text{Br}$) and 1:1 (V/V) mixture of ionophore and Hg^{2+} solution ($\text{L}_1.\text{Br-Hg}$), and (B) AgNO_3 solution 1.0×10^{-4} M (Ag^+), ionophore solution 1.0×10^{-4} M ($\text{L}_1.\text{Br}$) and 1:1 (V/V) mixture of ionophore and Ag^+ solution ($\text{L}_1.\text{Br-Ag}$)

4.3.3.2 Fourier Transfer Infrared (FT-IR) spectroscopy

The proposed membrane sensor was examined using FT-IR spectroscopy to observe the influence of ionophore in the fabricated selective PPy membranes. Although, this fabricated membrane does not have many functional groups to be distinguished by FT-IR spectroscopic technique, it is possible to compare the spectral features of $\text{L}_1.\text{Br}$ and the complexation occurred in the fabricated membrane. Figure

4.20 represents the characteristic peaks of FT-IR spectra for L₁.Br ionophore, optimized PPy membrane after use (Hg-ISE), and optimized PPy membrane after use (Ag-ISE).

All the FT-IR spectra show the modes of –CH_{aliphatic} stretching vibrational band appeared at 2900-3020 cm⁻¹. However, after complexation the intensity reduced, indicating that the complexation reactions occurred near to the methylene groups (-N-CH₂-). In addition, the stretching vibrations of benzimidazole ring at 1560 cm⁻¹ (-HC=N-) in L₁.Br spectra were disappeared and new peaks were observed at 1400-1500 cm⁻¹ which refers to (-C-N-). These results indicated that the deprotonation of hydrogen at carbene position and the attachment of metal cations were successful (Budagumpi et al., 2012b; Iqbal et al., 2014).

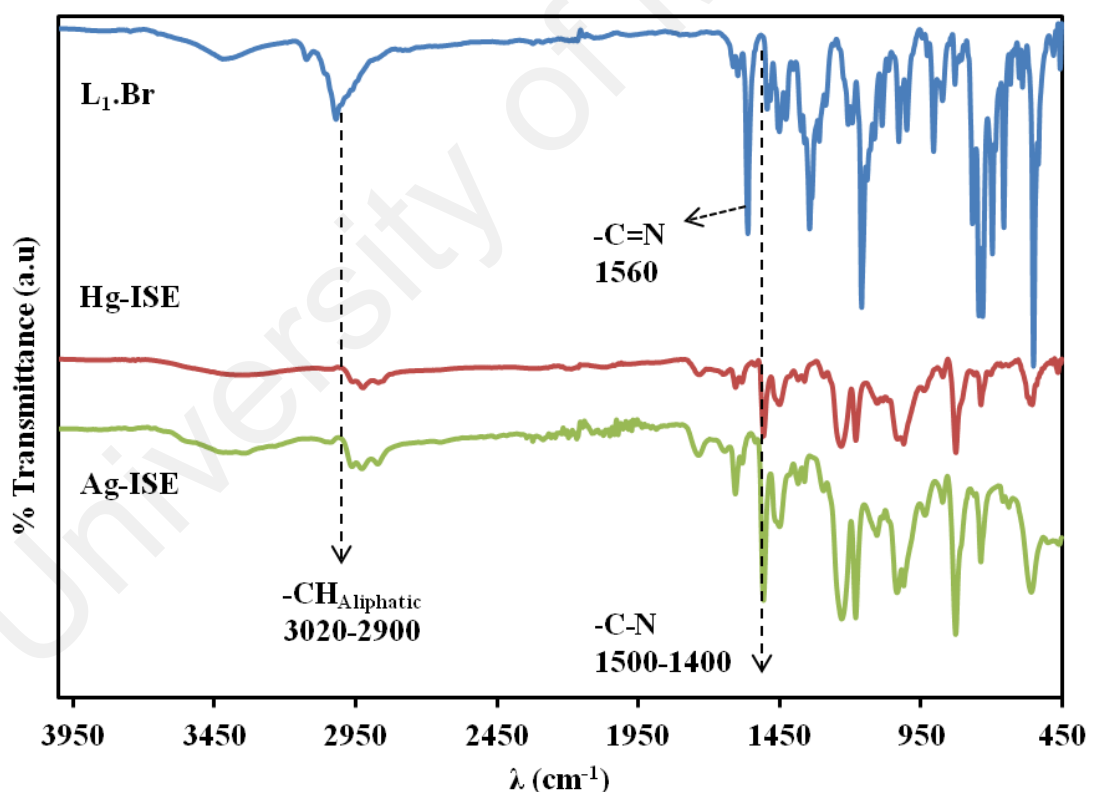


Figure 4.20: FT-IR spectra for L₁.Br ionophore, optimized PPy membrane after use (Hg-ISE), and optimized PPy membrane after use (Ag-ISE)

4.3.3.3 Field Emission Scanning Electron Microscopy (FESEM) - Energy-dispersive X-ray (EDX)

FESEM analysis on the surface morphology of Hg-ISE and Ag-ISE selective membrane was carried out at different magnifications to understand the morphological changes occurring in membrane electrode preparation and after conditioning of fresh membrane in the solutions. The FESEM analysis was employed on the surface of membrane electrode, (A) HEMA inner layer, (B) Hg-ISE fresh optimized PPy membrane before, (B1) after conditioning of fresh membrane into HgCl_2 solution and (C) Ag-ISE fresh optimized PPy membrane before, (C1) after conditioning of it into AgNO_3 solutions. The morphologies of electrode's membranes were presented in Figure 4.21.

A clear change in morphology of HEMA-inner layer (A), after introducing a second layer (B and C) proved that polypyrrole was successfully polymerized on the surface of electrodes. The morphology also changes after conditioning of fresh membrane Hg-ISE in HgCl_2 solutions with the appearance of the spherical shape of mercury atoms (B1). Whereas the changes of Ag-ISE membrane after destocking in AgNO_3 solution was observed with the appearance a cluster of silver atoms (C1). These changes prove the complexation of both metal cations with L_1Br ionophore and its affinity towards the PPy membrane, respectively.

The EDX analysis was carried out on the surface of the optimized membrane electrode for Hg-ISE and Ag-ISE. Spectrums of optimized membrane (A) before and (B and C) after used in HgCl_2 and AgNO_3 solution are shown in Figure 4.22, respectively. The presence of Hg and Ag element in the PPy membrane proves that the Hg^{2+} and Ag^+

cations were successfully complexed to L₁.Br ionophore sites in the PPy matrix of Hg-ISE and Ag-ISE, respectively. Without conditioning in the cations solution no peaks related to the mercury(II) and silver(I) element were observed.

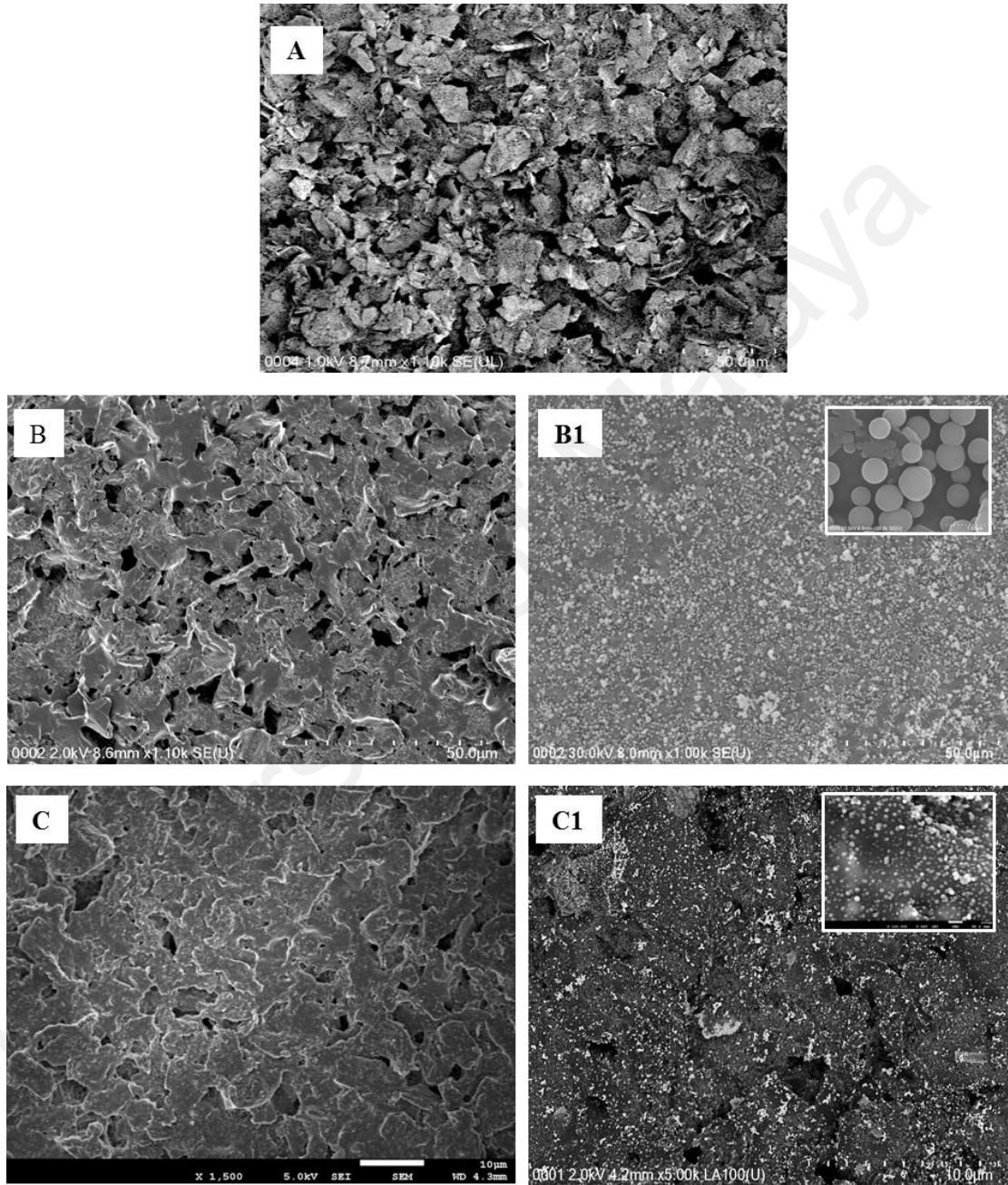


Figure 4.21: FESEM micrographs of optimized membrane: (A) HEMA-inner layer, (B) Hg-ISE fresh optimized PPy membrane before, (B1) after used and (C) Ag-ISE fresh optimized PPy membrane before, (C1) after used

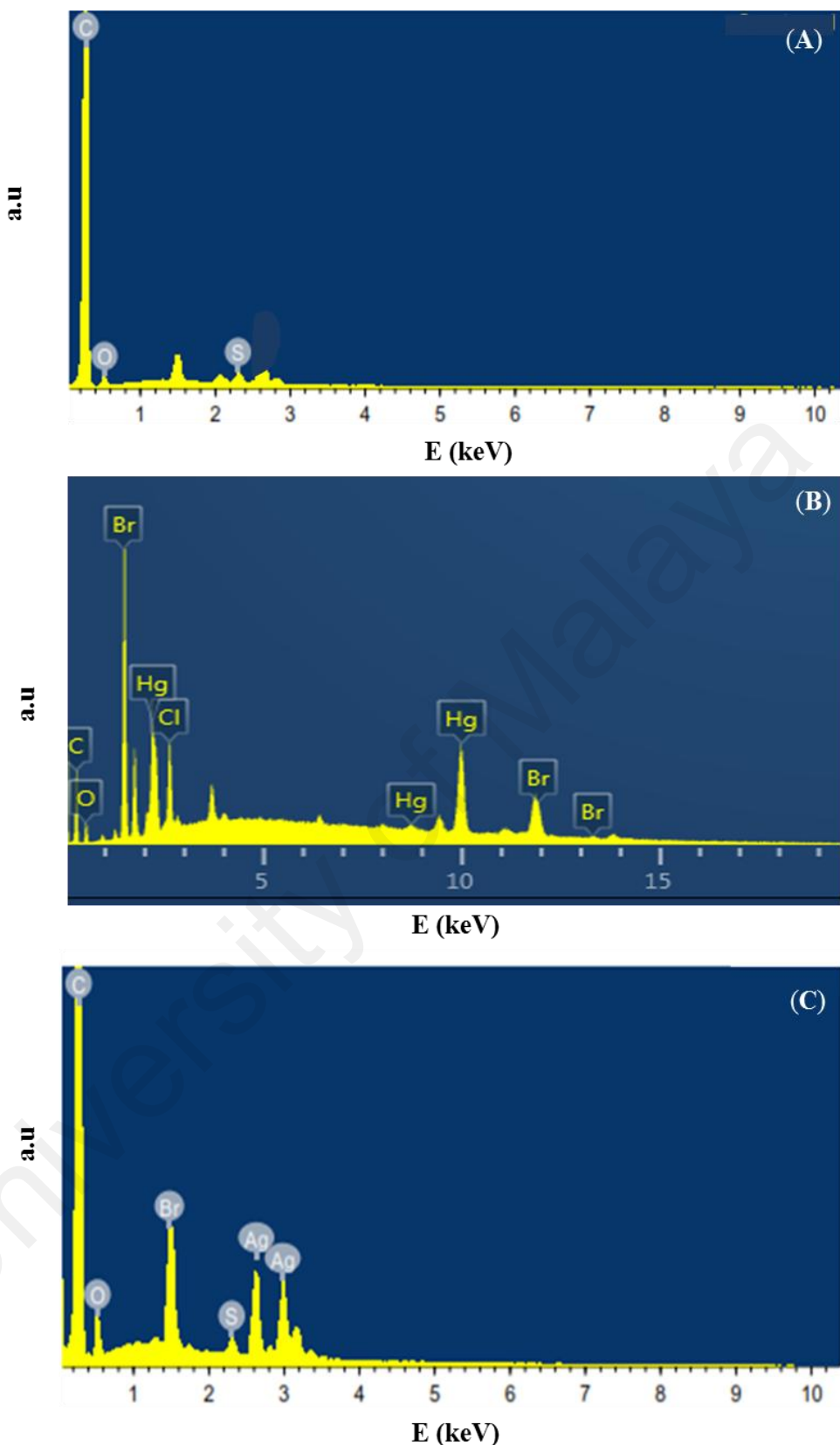


Figure 4.22: EDX spectrum of optimized membrane electrode for (A) fresh and after conditioning in (B) Hg^{2+} and (C) Ag^+ solutions

4.3.3.4 X-ray diffraction (XRD)

XRD pattern in Figure 4.23 shows the optimized PPy membrane for (A) Hg-ISE and (B) Ag-ISE before and after use. It was clearly observed that the electrode membrane exhibited amorphous pattern before being introduced to the metal cations solutions. However, after immersion of the electrode in metal cations solution, the crystal phases were present. This result shows the existence of mercury(II) (library reference number: PDF#00-023-1768) and silver(I) (library reference number: PDF#00-047-2097) in the optimized membrane due to the complexation of L₁.Br ionophore with the Hg²⁺ and Ag⁺ metal cations, respectively.

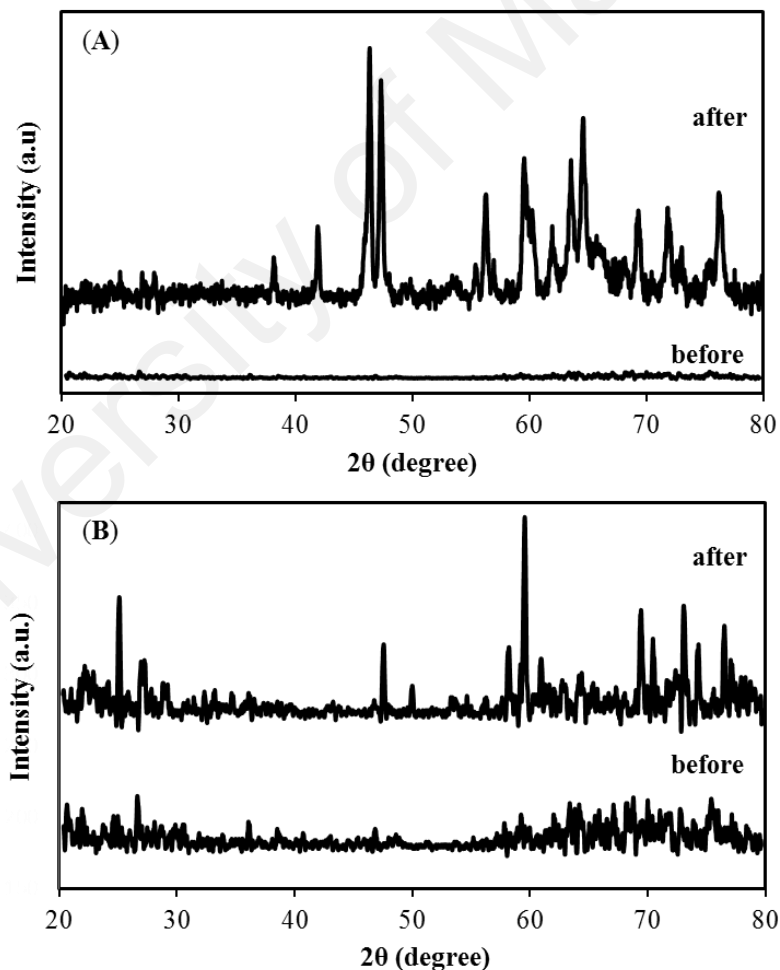


Figure 4.23: X-Ray diffraction pattern of proposed membrane sensor for (A) Hg-ISE and (B) Ag-ISE before and after used

The characterization of the proposed electrode membrane sensor for Hg-ISE and Ag-ISE by using FT-IR, FESEM, EDX and XRD, shows significant changes on the surface of the electrode after being used in the test solution. It was discovered that there is an interaction of ionophore and the studied metal ions on the surface electrode.

4.3.4 Optimization of fabricated PPy selective electrodes

A number of parameters are required for an ISE membrane to be considered as a suitable sensor for quantitative measurement of cations. The linear range, detection limit, selectivity, pH working range, response time, repeatability, reproducibility and lifetime are the most important parameter in order to ascertain the utility of L₁.Br as an ionophore for the preparation of the proposed ISEs.

4.3.4.1 Effect of pH

The pH effects of the test solution on potential response were studied at fixed concentrations and temperatures. The potential values of the test solution in concentrations of 1×10^{-5} M and 1×10^{-3} M were recorded over the pH range of 1.0-8.0, for Hg-ISE and pH range of 1.0-12.0, for Ag-ISE, respectively. HCl and NaOH solutions were used to adjust the pH of the test solutions at the required values.

The results in Figure 4.24 revealed that the electrodes responses were pH independent in the range of 4.5-7.0 and 3.5-9.0 for Hg-ISE and Ag-ISE, respectively. However, it showed a drift in potential values at pH range lower than 4.5 and higher than 7.0 for Hg-ISE. Similar behavior was also observed for Ag-ISE at pH lower than 3.5 and higher than 9.0. This is evidenced that under more acidic solutions, partial

protonation of ionophore happens and causes the loss of tendency to build complex structures with metal cations (Hassan, 2013; Mashhadizadeh et al., 2015). While, in a basic environment, the drift in potential is attributed to the formation of hydroxyl complexes of metal cations in the test solution which is coordinated with the ionophore in the membrane (Ismaiel et al., 2012; Mahajan et al., 2002). However, the effective pH ranges found in this study were wide enough to be used in the samples without critical pH adjustment.

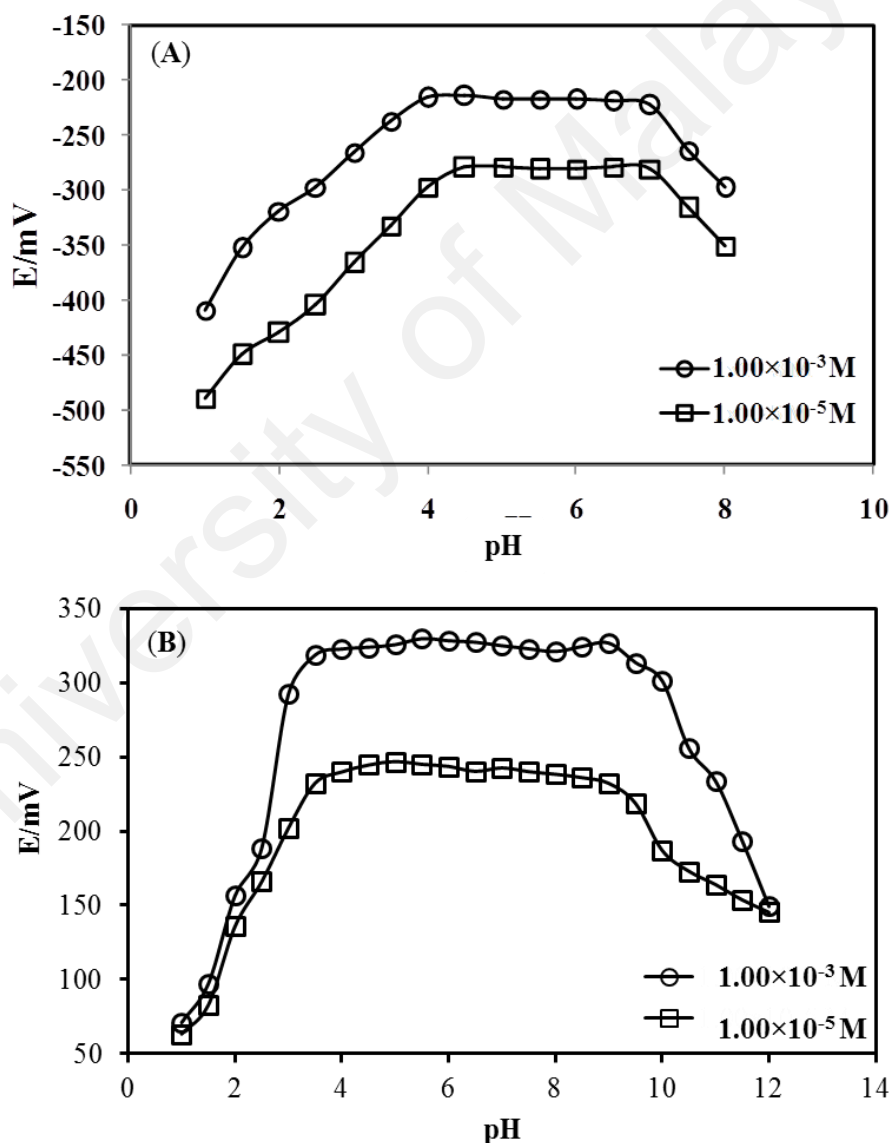


Figure 4.24: Effect of pH test solutions on the response of the proposed (A) Hg-ISE and (B) Ag-ISE in different concentrations

4.3.4.2 Response time of proposed electrodes

The response time of a sensor is considered as the required time of potential to reach a steady state within ± 1 mV during the immersion of sensor in a series of respective test solutions (Kamal et al., 2012). In this study, the dynamic response time of Hg-ISE sensor was obtained by changing the concentration of solution from 1.0×10^{-6} M to 1.0×10^{-2} M (low to high), sequentially. As shown in Figure 4.25 (A), after successive immersions of proposed sensor into the solutions, the time needed to reach a potential within ± 1 mV of final equilibrium value was obtained at about 20 s. Subsequently, the experiment also was conducted for Ag-ISE by changing the concentration of solution from 1.0×10^{-5} M to 1.0×10^{-1} M (low to high). Similar response time was observed as shown in Figure 4.25 (B).

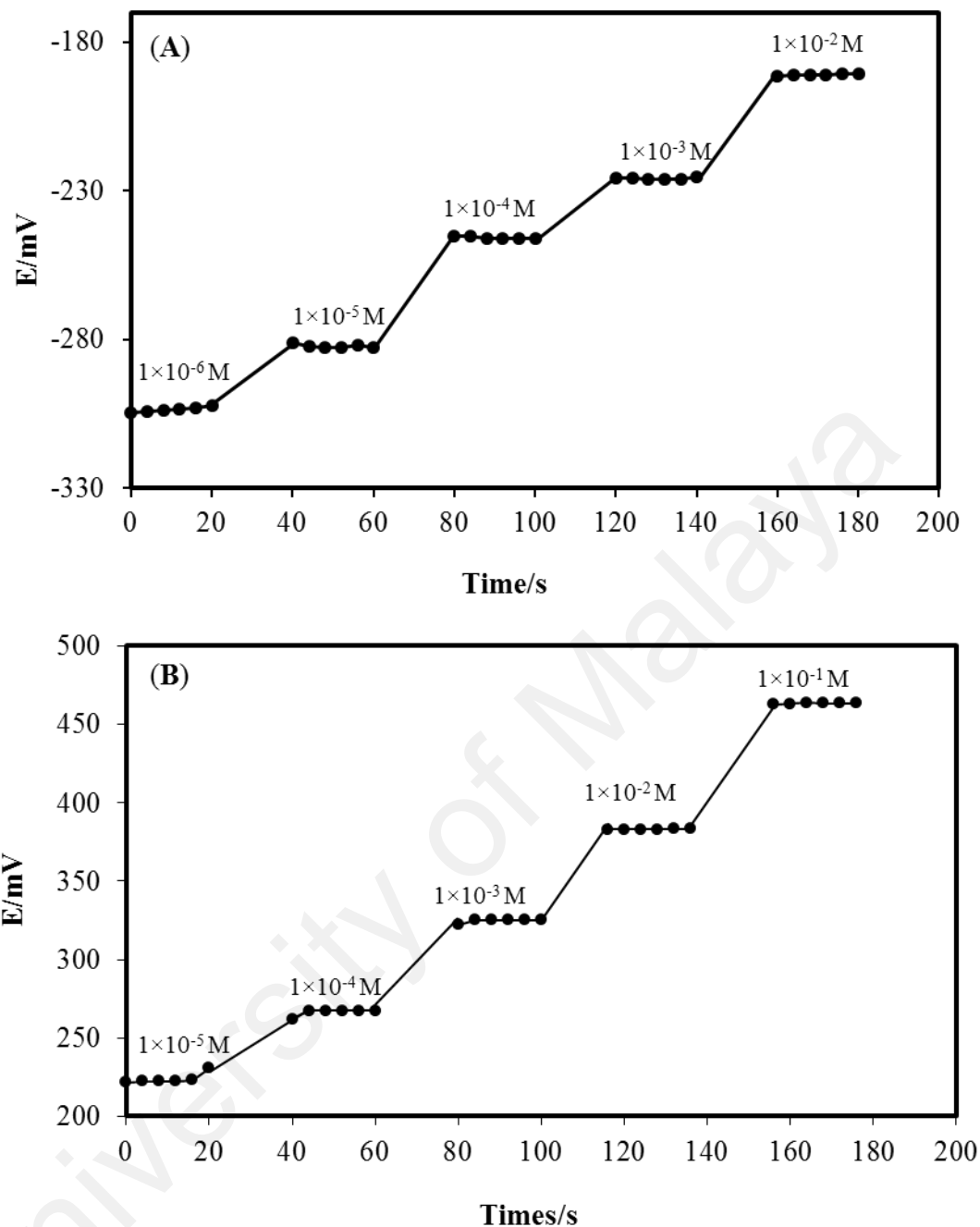


Figure 4.25: Dynamic response time of the (A) Hg-ISE and (B) Ag-ISE for the step changes in metal cations test solution from low to high concentration

4.3.4.3 Repeatability, reproducibility and stability of proposed electrodes

To validate the proposed method, the parameters such as repeatability and reproducibility of electrode were evaluated and the results are summarized in Table 4.11. The repeatability of the Hg-ISE was tested using three measurements over the working concentration ranges of the optimized electrode membrane. Whereas, the reproducibility of Hg-ISE was examined using three different fresh electrodes with optimum composition and each electrode was used only once.

Table 4.11: The repeatability and reproducibility studies of optimize composition membrane electrodes

ISE	Study	Nernstian slope (mV/decade)	Average	Standard deviation	RSD
Hg^{2+}	Repeatability	28.16, 28.30, 27.80	28.10	0.26	0.92
	Reproducibility	28.16, 29.53, 29.62	29.10	0.82	2.82
Ag^+	Repeatability	59.54, 58.48, 59.10	59.04	0.53	0.90
	Reproducibility	58.16, 58.48, 59.49	58.71	0.69	1.18

The repeatability data showed that an average slope is about 28.10 ± 0.26 mV/decade with a relative standard deviation (RSD) of 0.92%. While, for the reproducibility data, the results were obtained by three different electrode measurements and gave the average Nernstian slope of 29.10 ± 0.82 mV/decade. Similar experimental method was repeated for Ag-ISE proposed membrane electrode. The repeatability test shows an average slope of 59.04 ± 0.53 mV/decade with a RSD of 0.90% and the reproducibility study gave the average Nernstian slope of 58.71 ± 0.69 mV/decade with a RSD value of 1.18%.

Both proposed electrodes show RSD values for repeatability study less than one, which indicates a high precision and accuracy of the proposed procedure. However, in the reproducibility study the obtained RSD values were much lower than 5%, which can be considered as an acceptable value for reproducibility studies. The variation of results in this study as compared to the repeatability study could be due to different thickness and morphology of three membranes at different locations, which resulted in fluctuations in the extraction equilibrium of corresponding ions at the vicinity of the interface between the membrane and aqueous layer. Then, different Nernstian slopes from one electrode to another could be vindicated, and consequently, the variation of thicknesses is proved to cause minor changes in the Nernstian slopes of the electrodes (Rezayi et al., 2014).

Long-term stabilities of the proposed Hg-ISE and Ag-ISE were tested by performing periodic calibration with standard solutions and calculating the response and slope over the concentration ranges from 1.0×10^{-6} to 1.0×10^{-2} M and 2.5×10^{-6} to 1.0×10^{-1} M, respectively. The results were illustrated in Figure 4.26. It was found that the life time of Hg-ISE electrode was within 30 days while, for Ag-ISE is more than 50 days without showing any significant drift in the concentration range, slope and response times. The study reported by Yan et al.(2013) and Sardohan-Koseoglu et al. (2015), also observed the lifetime of their propose electrode are around 30 days. These limitation of lifetime in the fabricated proposed sensor could be due to the loss of membrane ingredients in the L₁.Br ionophore and its leaching into the sample solution during the measurement (Faridbod et al., 2007; Gupta et al., 2007).

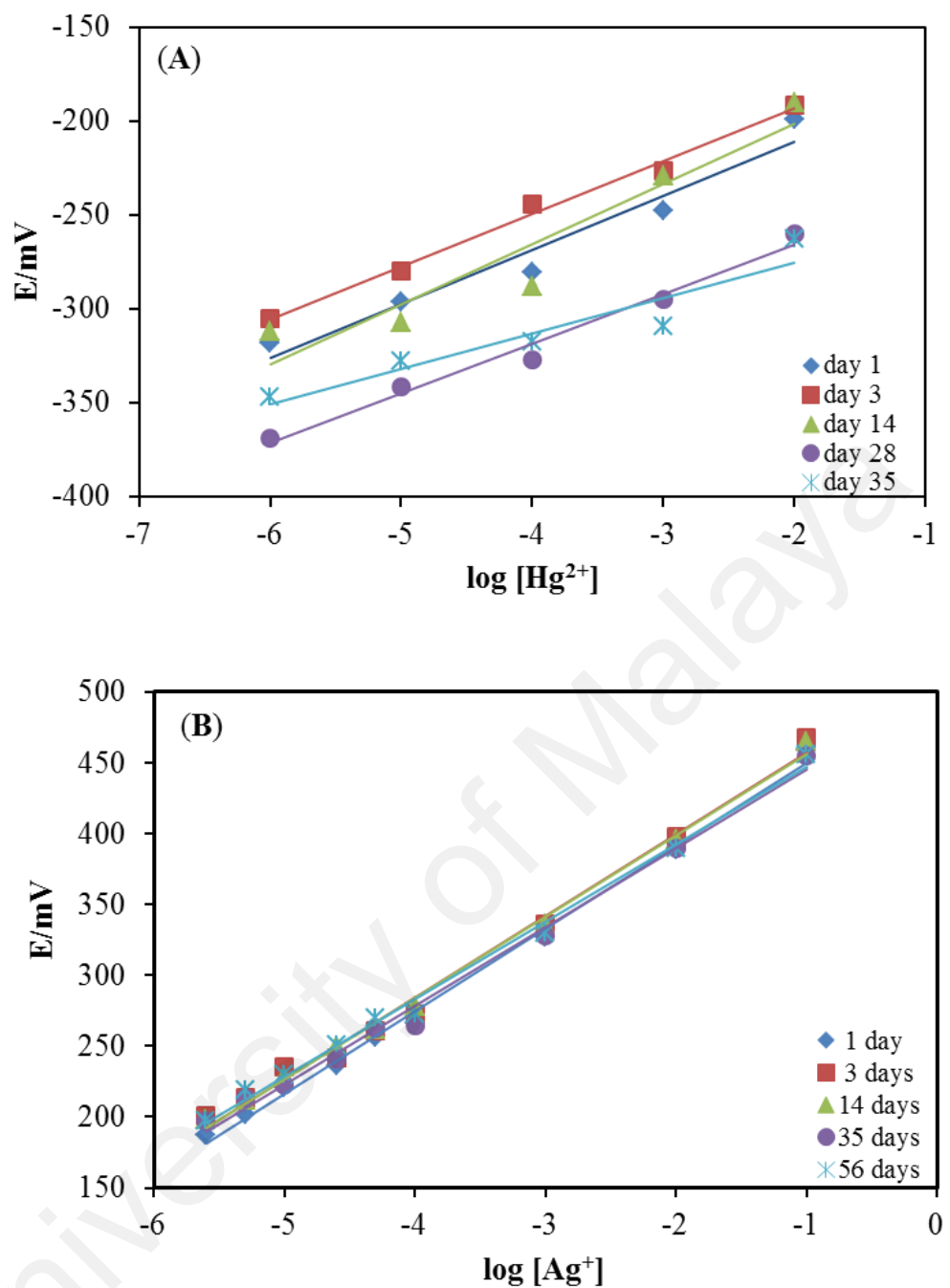


Figure 4.26: Stability response of (A) Hg-ISE and (B) Ag-ISE

4.3.5 Sensing mechanism of fabricated ISE

The L₁.Br ionophore is benzimidazolium salt which contained acidic hydrogen due to resonance of lone pairs on substituted nitrogen atoms in imidazole ring (Figure 4.27 (a)) (Haque et al., 2012b). After conditioning of ISE containing L₁.Br as ionophore with 0.01 M cation solution (HgCl₂ or AgNO₃), the ionophore in membrane maybe present in deprotonated form (L₁.Br:) or neutral form (L₁.Br). Therefore, the carrier mechanism of L₁.Br ionophore, can be explain as partially dissociated ligand and the interaction of ionophore with targeted metal cation (Mⁿ⁺) was confirmed by using UV-Vis, FT-IR and XRD. All the characterization method results suggested that the complexation occurred at C carbene position as illustrated in Figure 4.26 (a).

The selectivity of ionophore was influence by several factors, such as types of ionic sites used in membrane and values of pH during the sensor evaluation. Figure 4.27 (b) shows the effect of cationic site, NaTFB (R⁺) and effect of low acidic condition in the ISE membrane. The cationic site initiate the ionophore working as charge carrier (deprotonated form (L₁.Br:)) in contact with the aqueous sample solution and form a metal complexes (L₁.Br-Mⁿ⁺) with targeted metal cation (Mⁿ⁺) (Schaller et al, 1995). At low acidic condition in the pH range of 4.5-7.0 for Hg-ISE and 3.5-9.0 for Ag-ISE shows that the ionophore present almost as deprotonated species (L₁.Br:), which form complexes (L₁.Br-Mⁿ⁺) with the targeted metal cation (Mⁿ⁺) and expected to give the usual Nernstian responses, respectively. While at high acidic condition, a drift in potential values for both Hg-ISE and Ag-ISE were observed and have been discussed in section 4.3.4.1. This is due to the ionophore present in neutral form (L₁.Br), and prevent the complexation with metal cation (Mⁿ⁺) occurred, as illustrated Figure 4.27 (c) (Amemiya et al., 1998).

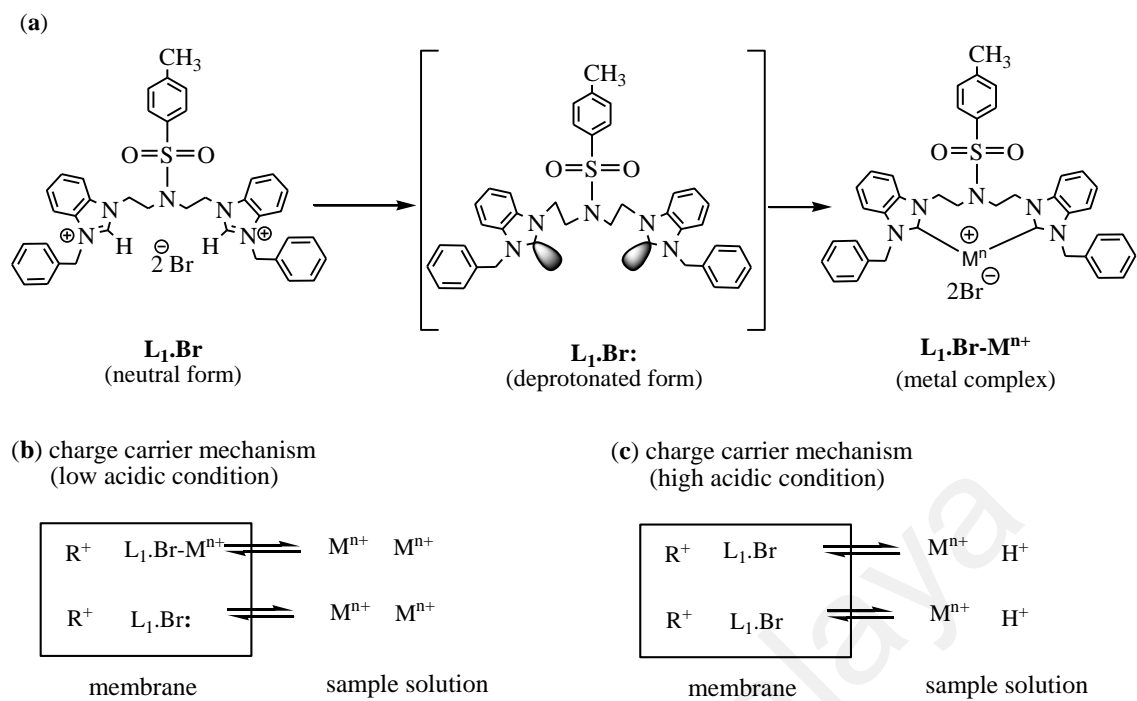


Figure 4.27: (a) Ionophore in neutral, deprotonated and complex form; (b and c) schematic diagram of the composition of membrane with an ionophore and cationic sites in contact with sample solution at different pH values. The boxes= membrane phases; M^{n+} = targated metal cation; H^+ = hydrogen ion; R^+ = lipophilic ionic salts; $L_1.Br$: and $L_1.Br$ = ionophore in deprotonated and neutral form, respectively; $L_1.Br-M^{n+}$ =the complexes of primary ion with respective ionophore

4.3.6 Determination of selectivity coefficients

The selectivity coefficient of the developed ISEs towards their target ions with respect to a wide range of interfering ions were determined by separate solution method (SSM). For selectivity evaluation of the fabricated Hg^{2+} and Ag^+ selective electrodes, the concentration of $1.0 \times 10^{-3} M$ was used for both target ions and interfering ions.

The results from SSM methods are summarized in Table 4.12. It is obvious that the selectivity coefficients of electrodes toward interfering cations are lower than Hg^{2+} cations and most of the selectivity coefficients are very low, indicating no significant interference in the performance of the fabricated electrode for determining Hg^{2+} cations,

except for Pb^{2+} cations. It caused only a slight interference due to the existence of soft donor atoms (carbene) in the ionophore structure where Pb^{2+} and Hg^{2+} act as typical intermediates and the soft acidic ions are more likely to build complex structures with the L_1Br ionophore. However, Pb^{2+} does not cause any interference at low concentrations. All $K_{\text{Hg}^{2+},M}^{\text{pot}}$ values are less than one, showing that the ISE is more selective to primary cations, Hg^{2+} .

Table 4.12: Selectivity coefficient values of various cations for the proposed Hg-ISE

Interfering ion	$(K_{\text{Hg}^{2+},M}^{\text{pot}})$
Ca^{2+}	1.87×10^{-2}
Mg^{2+}	8.94×10^{-2}
Co^{2+}	7.25×10^{-2}
Ni^{2+}	1.99×10^{-2}
Pb^{2+}	1.23×10^{-1}
Cs^+	1.88×10^{-2}
Na^+	4.40×10^{-2}
K^+	2.40×10^{-2}
Li^+	9.32×10^{-1}
Gd^{3+}	7.63×10^{-4}
Al^{3+}	1.83×10^{-3}
Yb^{3+}	5.99×10^{-4}

For selectivity evaluation of the proposed electrode of Ag-ISE, the concentration of 1.0×10^{-3} M was used for both target ion and interfering ions. As seen in Table 4.13, the proposed Ag-ISE electrode demonstrated a relatively high selectivity towards Ag^+ cation over a large number of mono, bi, and tri-valent cations. The results also revealed that the common interfering ions such as K^+ , Cs^+ and Hg^{2+} have no significant interfering effect with the selectivity coefficients in the order of 10^{-3} .

Table 4.13: Selectivity coefficient of various ions for the proposed Ag-ISE

Interfering ion	$K_{Ag^+, M}^{pot}$
Ca^{2+}	1.4×10^{-4}
Mg^{2+}	1.5×10^{-4}
Co^{2+}	1.3×10^{-4}
Ni^{2+}	1.3×10^{-4}
Pb^{2+}	9.0×10^{-4}
Hg^{2+}	2.3×10^{-3}
Cs^+	5.2×10^{-3}
K^+	7.3×10^{-2}
Gd^{3+}	2.4×10^{-5}
Al^{3+}	2.1×10^{-5}
Yb^{3+}	1.9×10^{-5}

4.3.7 Analytical application of fabricated ISEs

In order to validate the applicability of proposed electrode Hg-ISE and Ag-ISE, the analytical application can be conducted, such as potentiometric titration and spike method analysis, respectively. Due to their simplicity and sensitivity, these methods have widely used in the literature as general method used to evaluate the applicability of new fabricated ISE sensor (Dadkhah et al., 2014; Sardohan-Koseoglu et al., 2015).

4.3.7.1 Potentiometric titration

The proposed Hg-ISE was applied as an indicator electrode in titrimetric determination of Hg^{2+} under laboratory conditions. It was successfully proved as an indicator electrode in the potentiometric titration of 25 ml Hg^{2+} solution (1.0×10^{-4} M) with EDTA (1.0×10^{-3} M). As shown in Figure 4.28 (A), the obtained curve has an unsymmetrical shape. The end point of the plot corresponds to 1:1 stoichiometry of EDTA- Hg^{2+} ions complex. The inert Figure 4.28 (A) shows the plot of $\Delta E/\Delta V$ vs. mean volume of value of EDTA added. Before the end point, the potential demonstrated logarithmic changes with the volume of EDTA added, while, it remained constant after

the end point. The obtained potential decreased with the decrease in Hg^{2+} ion concentration due to their complexation with a standard EDTA solution. As a result, it is possible to determine the amount of Hg^{2+} ions in the solution accurately using the fabricated sensor. This method is generally used to evaluate the applicability of the prepared Hg-ISE as mention in Sardohan-Koseoglu et al., (2015).

The potentiometric titration of 20 ml of 5.0×10^{-2} M AgNO_3 solutions was carried out with a 1.0×10^{-1} M solution of NaCl by using the optimized Ag-ISE electrode at laboratory condition. Figure 4.28 (B), shows the amount of silver ions in solution can be accurately determined with the electrode. The end point of titration was obviously observed from the sharp break point corresponding to 1:1 stoichiometric reaction (inert Figure 4.28 (B)). Before the end point, the potential demonstrated usual logarithmic change with the volume of NaCl titration added. However after the end point the potential response remains almost constant. The results show in accordance with previous findings which ascribe the low concentration of free Ag^+ ions in the solution (Dadkhah et al., 2014).

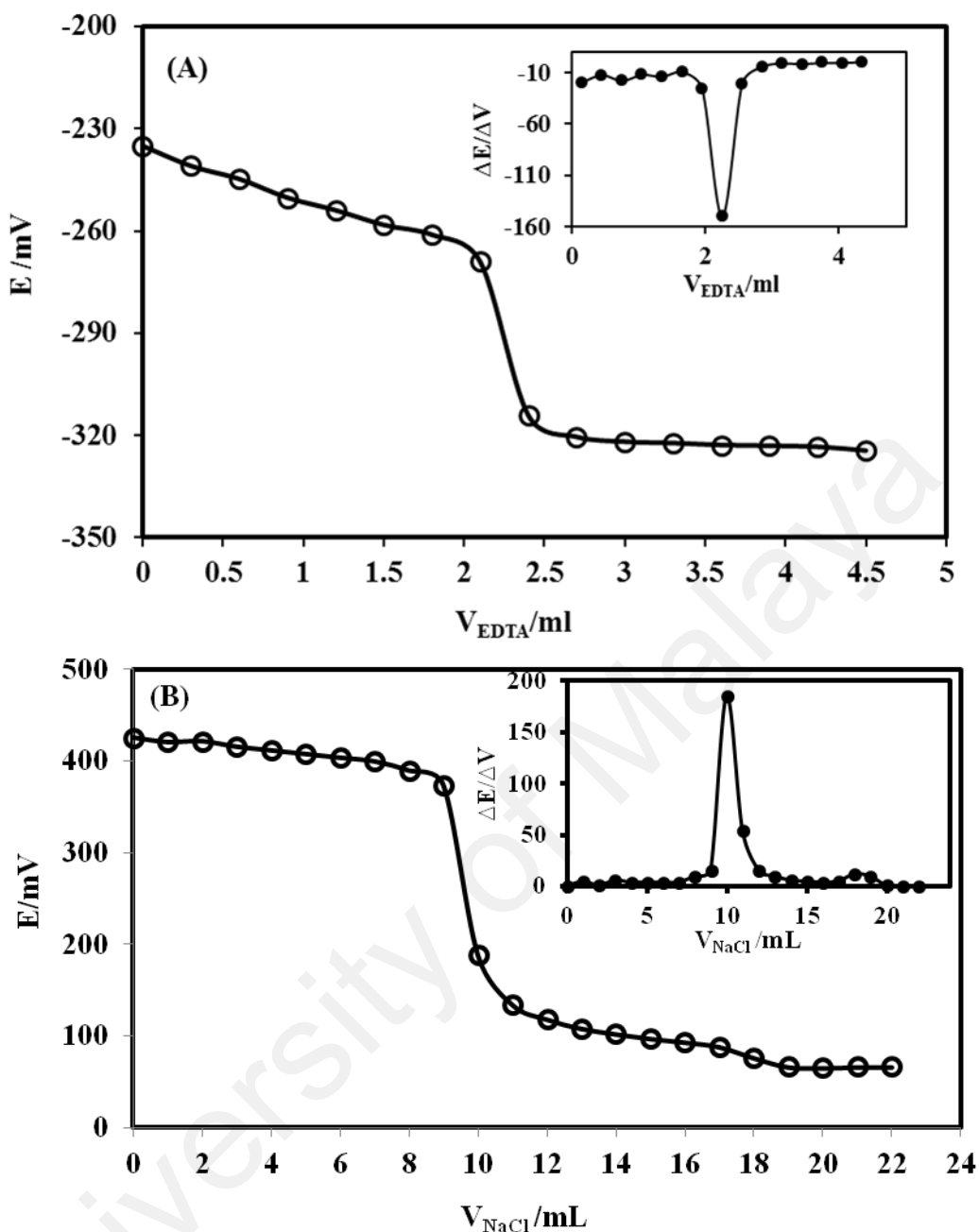


Figure 4.28: Potentiometric titration curve of (A) 25 ml $1.0 \times 10^{-4} \text{ M}$, Hg^{2+} solution with $1.0 \times 10^{-3} \text{ M}$ EDTA and (B) 20.0 ml $5.0 \times 10^{-2} \text{ M}$, Ag^+ solution with NaCl ($1.0 \times 10^{-1} \text{ M}$) by using the proposed sensor as an indicator electrode

4.3.7.2 Real sample application

The applicability of the proposed electrode Hg-ISE was tested through analyzing the direct determination of spiked Hg^{2+} in tap water sample. The results (Table 4.14) approved that the amount of Hg^{2+} obtained by the proposed method agreed well with the

added amount in the recovery range of 110-122%, demonstrating the acceptable performance of the supplied electrode for the recovery of mercury(II) content from water samples with different matrices. Whereas, the relative standard deviation (RSD) values show readings which are lower than 5%, indicating the effectiveness of the proposed electrode. Moreover, the standard reference material (SRM) 2702 as a natural matrix of inorganic compounds was collected from marine sediment with certified concentration values and was used for proposed sensor validation (Sany et al., 2013a; Sany et al., 2013b; Sany et al., 2012). As it can be seen, the results have a good compatibility with known concentration value as mention at bottle container (0.43 ppm or 2.14×10^{-6} M). Therefore, the sensor was verified as applicable device to determine the Hg^{2+} in solution.

Table 4.14: Potentiometric determination of Hg^{2+} in different samples by using proposed electrode

Sample	$\text{Hg}^{2+}, (\text{M})$		^b Recovery, (%)	^c RSD, (%)
	Added	Found		
Tap Water	5.0×10^{-6}	6.1×10^{-6}	122.0	2.8
	5.0×10^{-5}	5.9×10^{-5}	118.0	1.2
	1.0×10^{-4}	1.1×10^{-4}	110.0	4.1
SRM 2702	-	1.8×10^{-6}	-	0.6

^aAverage of three determination, ^bRecovery= (found/added)×100, ^cRSD= (SD/average)×100

Whereas, the practical utility of proposed electrode Ag-ISE was tested by direct determination of spike silver(I) in tap water and multi-element calibration standard solution 2A (Agilent Technologies; Part# 8500-6940). The standard sample was used directly without any pretreatment. Each sample was analyzed in triplicate and the analysis was repeated under identical conditions. It can be observed in Table 4.15 that the determination of concentration standard solution by proposed Ag-ISE has good

compatibility with known concentration value as mention at bottle container (10 ppm or 9.27×10^{-5} M). Other results obtained from the determination of Ag^+ in spike tap water samples show a good agreement with added concentration, hence proved the capability of proposed Ag-ISE in sensing application.

Table 4.15: Potentiometric determination of Ag^+ in different samples by using proposed electrode

Sample	$\text{Ag}^+, (\text{M})$		^b Recovery, (%)	^c RSD, (%)
	Added	Found		
Tap Water	5.0×10^{-5}	5.3×10^{-5}	106.4	0.9
	1.0×10^{-4}	1.1×10^{-4}	105.6	2.4
	5.0×10^{-3}	4.8×10^{-3}	96.4	0.7
Standard 2A	-	10.9×10^{-5}	-	0.3

^aAverage of three determination, ^bRecovery= (found/added)×100, ^cRSD= (SD/average)×100

4.3.8 Comparative studies of Hg-ISE and Ag-ISE

All data proved that the proposed Hg-ISE and Ag-ISE can be applied in determination of Hg^{2+} and Ag^+ cations present in solution, respectively. Consequently, the performance of proposed electrode is compared with the published electrode as shown in Table 4.16. All electrodes listed were PVC-based membrane sensors for determining the Hg^{2+} and Ag^+ cations except for the electrode reported by Jumal in 2012, in which the electrode was based on the self-plasticizing poly(n-butylacrylate) membrane sensor.

The proposed electrode of Hg-ISE gave a better detection limit (2.5×10^{-7} M) and response time (20 s) as compared to the previously suggested Hg-ISE based on the self-

plasticizing method (Jumal et al., 2012). Jumal et al., (2012) has used methyl acrylate as a polymer matrix in their fabrication of free plasticizing membrane electrode with detection limit of 2.5×10^{-6} M and response times of 50-100 s. Due to the poor solubility of L₁.Br in methyl acrylate, pyrrole was introduced in this study. The uses of conducting polymers in the structure of polymeric membrane have been recently reported. Oxidized conducting polymers such as PPy which includes the charge-compensating ions and poly cationic backbones can affect the potentiometric responses as the ionic exchangers, hence increase the selectivity and sensitivity of proposed electrode in these study (Liu Y. et al., 2011; Zanganeh et al., 2007). In contrast, as compared to some Hg-PVC membranes the proposed electrode Hg-ISE exhibited a comparable detection limit, lifetime, working range of electrode and also response time.

The comparative study of Ag-ISE the linear range, detection limit, slope, and response times of the previous researches based on PVC membrane sensors shows that the proposed electrode still suffers from with a low performance. In order to increase the sensitivity of ISE, the chemical structural features of ionophores may generally turn by incorporating different soft and hard donor atoms in the chelating ring which consequently promotes the stabilization of both low and high oxidation states of the metal centre, as well as forcing metal ions to adopt typical coordination chemistry (Gupta et al., 2007). Thus, further studies about the effect on different structure of L₁.Br are strongly needed.

In spite of the deficiencies in this study, all data proved that the proposed Hg-ISE and Ag-ISE can be applied in determination of Hg²⁺ and Ag⁺ cations present in solution, respectively.

Table 4.16: Comparison of fabricated electrode based on PVC membrane by using different type of ionophore

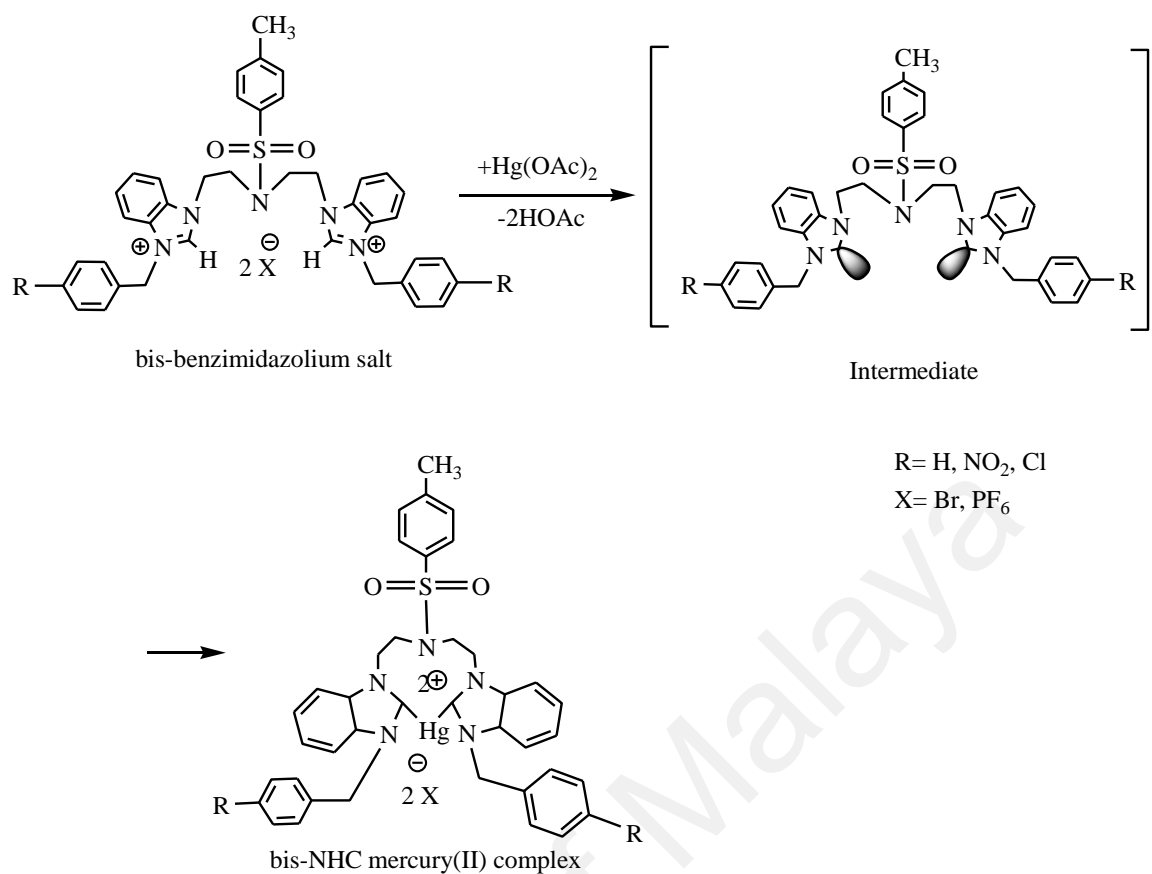
Metal	Ionophore	Slope (mV/decade)	Detection limit (M)	Linear range (M)	Response time (s)	Life time (day)	Refs.
Hg ²⁺	Oxime	33.4	1.68×10 ⁻⁶	5.6×10 ⁻⁶ -1.0×10 ⁻²	10-15	30	(Sardohan-Koseoglu et al., 2015)
Hg ²⁺	1,5-diphenylthiocarbazone (dithizone)	29.7	3.0×10 ⁻⁶	5.0×10 ⁻⁶ -1.0×10 ⁻²	20	14	(Hassan, 2013)
Hg ²⁺	Calix[2]thieno[2]pyrrole	27.8	1.0×10 ⁻⁶	1.0×10 ⁻⁶ -1.0×10 ⁻¹	20	-	(Abbas, 2012)
Hg ²⁺	1,2-bis-(N'-benzoylthioureido)cyclohexane	28.1	2.5×10 ⁻⁶	1.0×10 ⁻⁵ -1.0×10 ⁻¹	50-100	-	(Jumal et al., 2012)
Hg²⁺	L₁.Br	28.16	2.5×10⁻⁷	1.0×10⁻⁶-1.0×10⁻²	20	30	This work
Ag ⁺	p-tert-butylcalix[4]arene	59.8	1.0×10 ⁻⁷	5.0×10 ⁻⁷ -1.0×10 ⁻³	<10	<35	(Yan et al., 2013)
Ag ⁺	N,N'-bis(3-methyl-1-phenyl-4-benzylidene-5-pyrazole)propylenediamine	59.3	9.3×10 ⁻⁷	1.0×10 ⁻⁶ -1.0×10 ⁻¹	5-30	-	(Hassouna et al., 2010)
Ag ⁺	Isoquinoline-1,3-diones	58.4	5.8×10 ⁻⁶	5.0×10 ⁻⁶ -1.0×10 ⁻¹	12	<90	(Kamal et al., 2012)
Ag ⁺	Shift-base lariat ethers, A ₆	59.3	4.4×10 ⁻⁸	5.6×10 ⁻⁸ -1.0×10 ⁻¹	12	-	(Gupta et al., 2009)
Ag ⁺	L ₁ .Br	58.5	2.0×10 ⁻⁶	2.5×10 ⁻⁶ -1.0×10 ⁻¹	20	50	This work

4.4 Complexation of synthesized bis-benzimidazolium salts

In the synthesis of bis-NHC metal complexes, *in-situ* deprotonation of bis-benzimidazolium salts have been chosen as the preferred synthesis route. This method only produces desired complexes without having the free carbene which is unstable and difficult to handle (Weskamp et al., 2000). Mercury acetate and silver oxide have been used as metal precursors which play important roles in the formation of the desired metal complexes. Basic anions in metal precursor deprotonate -H carbene at -NCHN position, leading to the coordination of metal cations to the intermediate carbene of bis-benzimidazolium salts and the counter-ions (Br^- and PF_6^-) were attached to the ligand (Liu et al., 2015a). The schematic complexation reaction of bis-benzimidazolium salts with $\text{Hg}(\text{OAc})_2$ is expressed in Scheme 4.1.

The reactions of the synthesized bis-benzimidazolium salts with excess of $\text{Hg}(\text{OAc})_2$ in refluxed acetonitrile within 24 hours produces the complexes as solid powders. The complexes are insoluble in water. Thus to remove the residual of mercury acetate, plenty of water has been used to wash the crude product. In recrystallization process acetonitrile was used and pure complexes powders were obtained. The structure of bis-NHC mercury(II) complexes were illustrated in Figure 4.29.

In the complexation of bis-benzimidazolium salts with silver(I) oxide (Ag_2O), the reactions were conducted in dichloromethane (CH_2Cl_2) with a temperature maintained at 40 °C. After 24 hours of reaction black suspensions were observed. This unwanted side product was then removed by filtering through a celite to give a clear solution. The structures of bis-NHC silver(I) complexes were illustrated in Figure 4.30.



Scheme 4.1: The proposed mechanism of complex reaction between bis-benzimidazolium salts and mercury(II)

Table 4.17 shows the general characteristics of synthesized metal complexes. It should be noticed that the melting points of complexes were significantly higher than their respective ligands. According to the previous report, this effect demonstrate a preliminary confirmation of a successful synthesis of metal complexes (Iqbal et al., 2014).

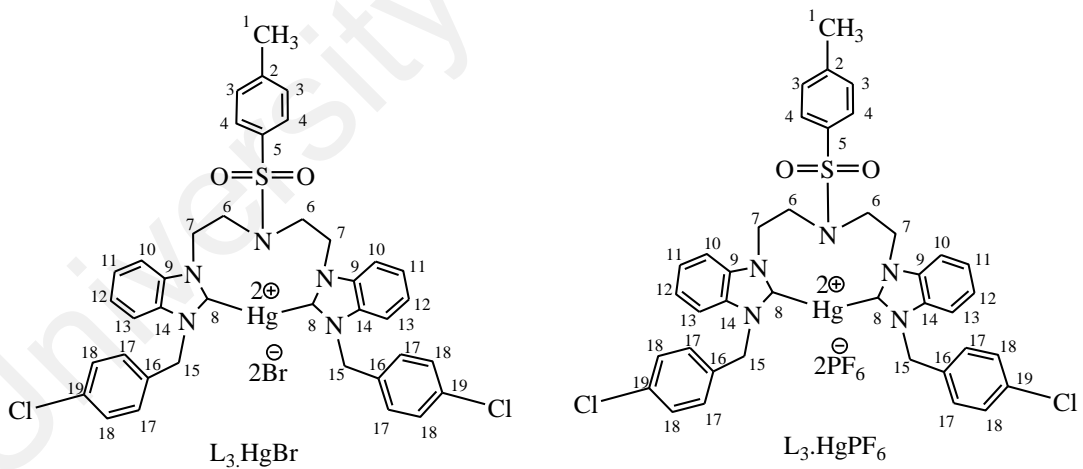
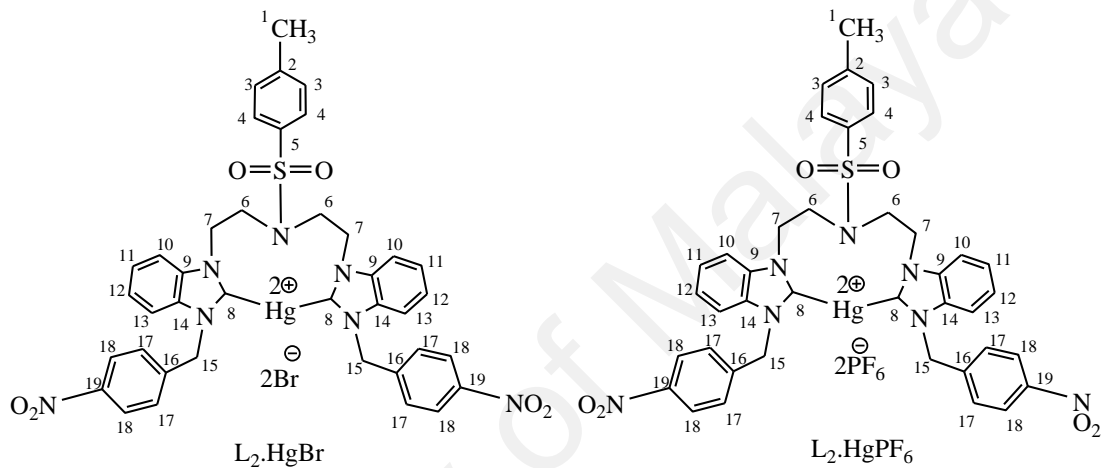
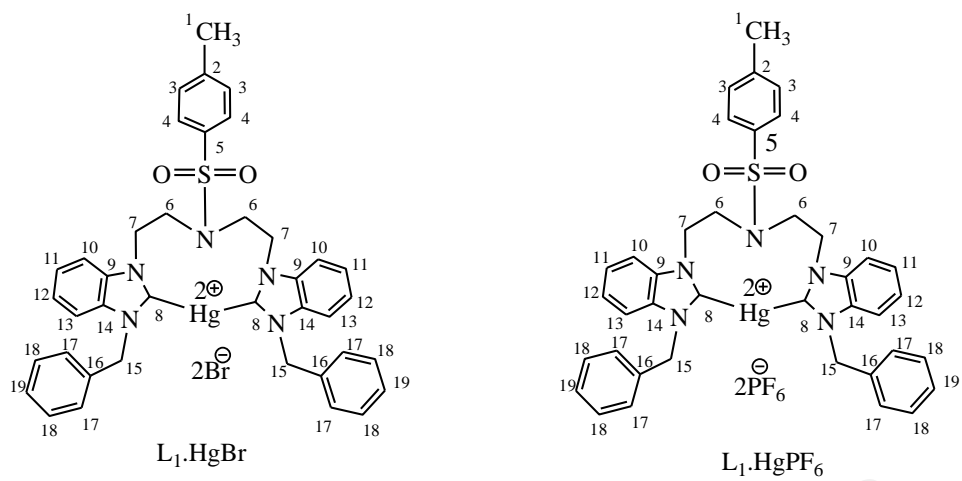


Figure 4.29: Structure of bis-NHC mercury(II) complexes

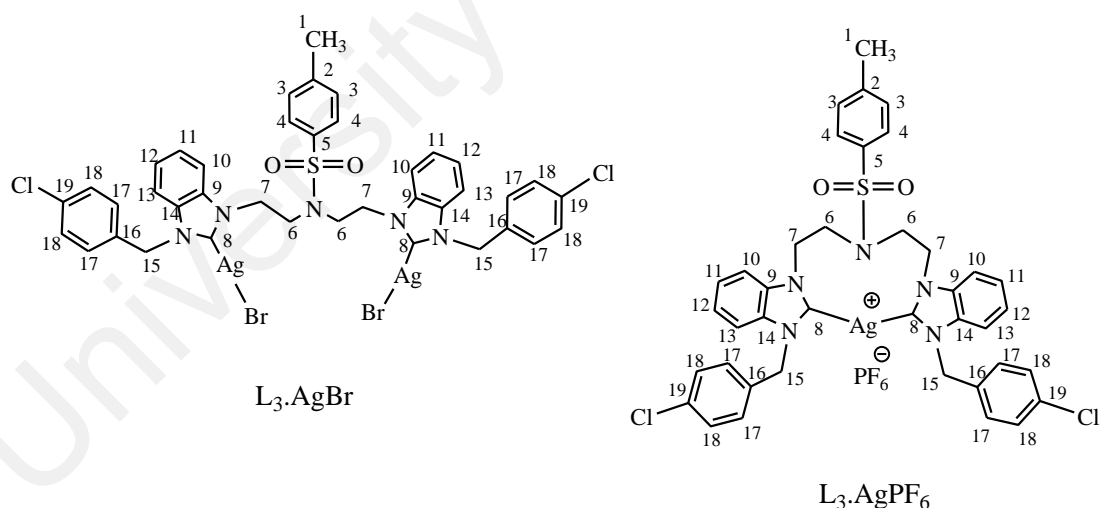
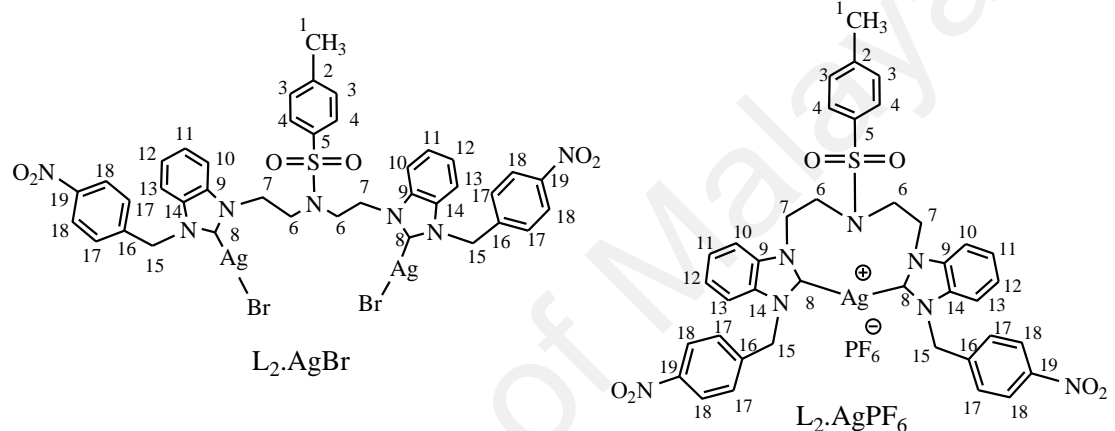
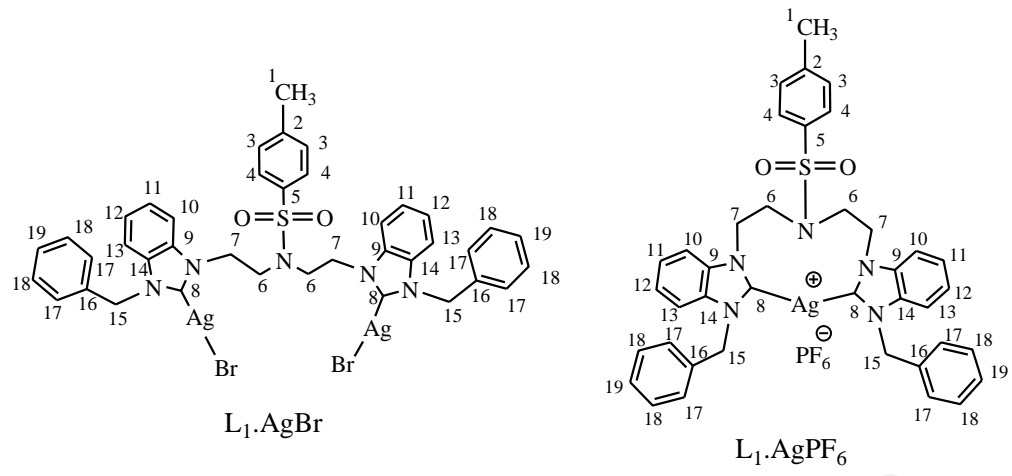


Figure 4.30: Structure of bis-NHC silver(I) complexes

Table 4.17: General characteristic of bis-NHC metal complexes

Bis-NHC complexes	Yield (%)	Color	Melting point (°C)	Molecular formula	Molecular weight (g/mol)
L ₁ .HgBr	79	white	215-218	C ₃₉ H ₃₇ N ₅ O ₂ S Br ₂ Hg	1000.2
L ₂ .HgBr	84	Off-white	205-207	C ₃₉ H ₃₅ N ₇ O ₆ S Br ₂ Hg	1090.2
L ₃ .HgBr	93	white	240-242	C ₃₉ H ₃₅ N ₅ O ₂ S Br ₂ Cl ₂ Hg	1069.1
L ₁ .HgPF ₆	89	white	260-262	C ₃₉ H ₃₇ N ₅ O ₂ S P ₂ F ₁₂ Hg	1132.3
L ₂ .HgPF ₆	98	Off-white	192-194	C ₃₉ H ₃₅ N ₇ O ₆ S P ₂ F ₁₂ Hg	1220.3
L ₃ .HgPF ₆	80	white	275-278	C ₃₉ H ₃₅ N ₅ O ₂ SCl ₂ P ₂ F ₁₂ Hg	1099.2
L ₁ .AgBr	78	white	140-143	C ₃₉ H ₃₇ N ₅ O ₂ S Br ₂ Ag ₂	1015.4
L ₂ .AgBr	90	white	152-155	C ₃₉ H ₃₅ N ₇ O ₆ S Br ₂ Ag ₂	1105.4
L ₃ .AgBr	60	brown	136-138	C ₃₉ H ₃₅ N ₅ O ₂ S Br ₂ Cl ₂ Ag ₂	1078.9
L ₁ .AgPF ₆	70	brown	178-180	C ₃₉ H ₃₇ N ₅ O ₂ S PF ₆ Ag	890.7
L ₂ .AgPF ₆	82	Pale brown	242-246	C ₃₉ H ₃₅ N ₇ O ₆ S PF ₆ Ag	980.7
L ₃ .AgPF ₆	63	white	192-194	C ₃₉ H ₃₅ N ₅ O ₂ S Cl ₂ PF ₆ Ag	959.6

In the FT-IR spectra for bis-NHC mercury(II) complexes and bis-NHC silver(I) complexes (APPENDIX I1-I12), disappearances of –N-C=N absorption peaks in range of 1566-1560 cm⁻¹ and appearance of N-C-N absorption peaks in range of 1421-1388 cm⁻¹ were noticed. This corresponds to the deprotonation of proton at carbene carbon in the formation of complex with respective metal cations. Although, the absorption peaks appear at unusual –C-N range (1350-1000 cm⁻¹). The absorption occurs at a higher frequency due to the resonance effect which increases the double-bond character between the ring and nitrogen atoms (Iqbal et al., 2014; Pavia et al., 2008). Table 4.18 and Table 4.19 summarized all significant FT-IR data for all metal complexes.

As expected, in all $^1\text{H-NMR}$ complexes spectra (APPENDIX J1-J12), the signals assigned for the all benzimidazolium salts carbene proton (H-8) in range δ 10.00-10.24 were disappeared upon deprotonation and coordination of carbene carbon with mercury(II) and silver(I). This is consistent with other studies reported for the formation of carbene complexes (Budagumpi et al., 2012b). Additionally, an obvious downfield movement of chemical shifts for H-7 and H-15 in all bis-NHC mercury(II) complexes spectra were observed. The H-7 and H-15 are the methylene groups (-CH₂-N) which are neighbors to nitrogen atoms in the benzimidazole ring. Thus, the changes in chemical shifts for both proton can also indicated that the complexation occurred at carbene position. However, in the spectra of bis-NHC silver(I) complexes only small changes can be observed.

Table 4.18: The significant of FT-IR absorption bands (cm^{-1}) for synthesized bis-NHC mercury(II) complexes, (types of absorption bands; w= weak, m= medium, s= strong)

Assignments	L ₁ .HgBr	L ₂ .HgBr	L ₃ .HgBr	L ₁ .HgPF ₆	L ₂ .HgPF ₆	L ₃ .HgPF ₆
CH _{Ar}	3033 (w)	3067 (w)	3034 (w)	3065 (w)	3031 (w)	3057 (w)
CH _{Aliph}	2950 (w)	2936 (w)	2947 (w)	2955 (w)	2936 (w)	2954 (w)
C=C	1599, 1451 (w, w)	1599, 1450 (w, w)	1597, 1451 (w, w)	1598, 1455 (w, w)	1607, 1449 (w, w)	1598, 1463 (m, w)
O=S=O	1336, 1157 (s, s)	1342, 1157 (s, s)	1337, 1157 (s, s)	1343, 1159 (m, m)	1345, 1158 (s, s)	1329, 1157 (s, s)
N-C-N	1416 (s)	1411 (m)	1410 (m)	1421 (m)	1416 (m)	1409 (m)
H ₂ C-N	1088 (w)	1089 (w)	1089 (w)	1088 (w)	1089 (w)	1089 (s)
O=N-O	-	1521 (m)	-	-	1523 (m)	-
PF ₆	-	-	-	832 (s)	834 (s)	838 (m)

Table 4.19: The significant of FT-IR absorption bands (cm^{-1}) for synthesized bis-NHC silver(I) complexes, (types of absorption bands; w= weak, m= medium, s= strong)

Assignments	L ₁ .AgBr	L ₂ .AgBr	L ₃ .AgBr	L ₁ .AgPF ₆	L ₂ .AgPF ₆	L ₃ .AgPF ₆
CH _{Ar}	3031 (w)	3029 (w)	3025 (w)	3045 (w)	3070 (w)	3065 (w)
CH _{Aliph}	2928 (w)	2911 (w)	2980 (w)	2961 (w)	2937 (w)	2932 (w)
C=C	1598, 1454 (w, m)	1599, 1449 (m, m)	1602, 1448 (w, w)	1599, 1452 (m, m)	1600, 1448 (w, w)	1599, 1449 (w, w)
N-C-N	1394 (s)	1399 (m)	1388 (s)	1394 (s)	1398 (m)	1397 (s)
O=S=O	1336, 1153 (s, s)	1340, 1153 (s, s)	1330, 1153 (s, s)	1336, 1157 (s, s)	1343, 1158 (s, s)	1335, 1558 (s, s)
H ₂ C-N	1088 (m)	1088 (w)	1091 (m)	1086 (w)	1089 (w)	1089 (w)
O=N-O	-	1517 (s)	-	-	1519 (m)	-
PF ₆	-	-	-	833 (s)	834 (s)	836 (s)

In ^{13}C -NMR spectra the formation of carbene complexes can be easily confirmed by the presence of new C-metal signal at δ 184.72-185.97 (APPENDIX K1-K6) which is attributed to the carbene carbon bound to mercury(II) metal cation. While, for silver(I) complexes, the corresponding signals were observed in the range of δ 153.90-168.02 (APPENDIX K7-K12). However, the signal of the carbene carbon for silver(I) complex L_1AgPF_6 , L_2AgPF_6 and L_3AgPF_6 were not observed. The absence of this peak is not usual and may result from the fluxional behavior of bis-NHC complex. Similar phenomenon has been reported in the literature for some silver(I) carbene complexes (Liu et al., 2015a).

The UV-visible absorbance spectra for all compounds were illustrated in Figure 4.31. In the bis-benzimidazolium salts absorption spectra Figure 4.31 (A), two characteristic bands were observed at 269 nm and 276 nm. These bands refer to intramolecular $\pi\rightarrow\pi^*$ and $n\rightarrow\pi^*$ transitions originated from the -CC, -CN and $\text{C}\equiv\text{N}$ modules. After the complexation with mercury(II) and silver(I), these bands show a red shift about 6-9 nm, indicating the formation of C-N modules in the benzimidazole ring. In addition, in complex spectra Figure 4.31 (B and C) usually d-d electronic transition absorption spectra at range 500-300 nm should be observed. However, in this study no bands less than 300 nm were observed, as expected. These conditions show similarity with previous studies reported in literature (Gümüş et al., 2014; Haque et al., 2012a; Montazerozohori et al., 2014).

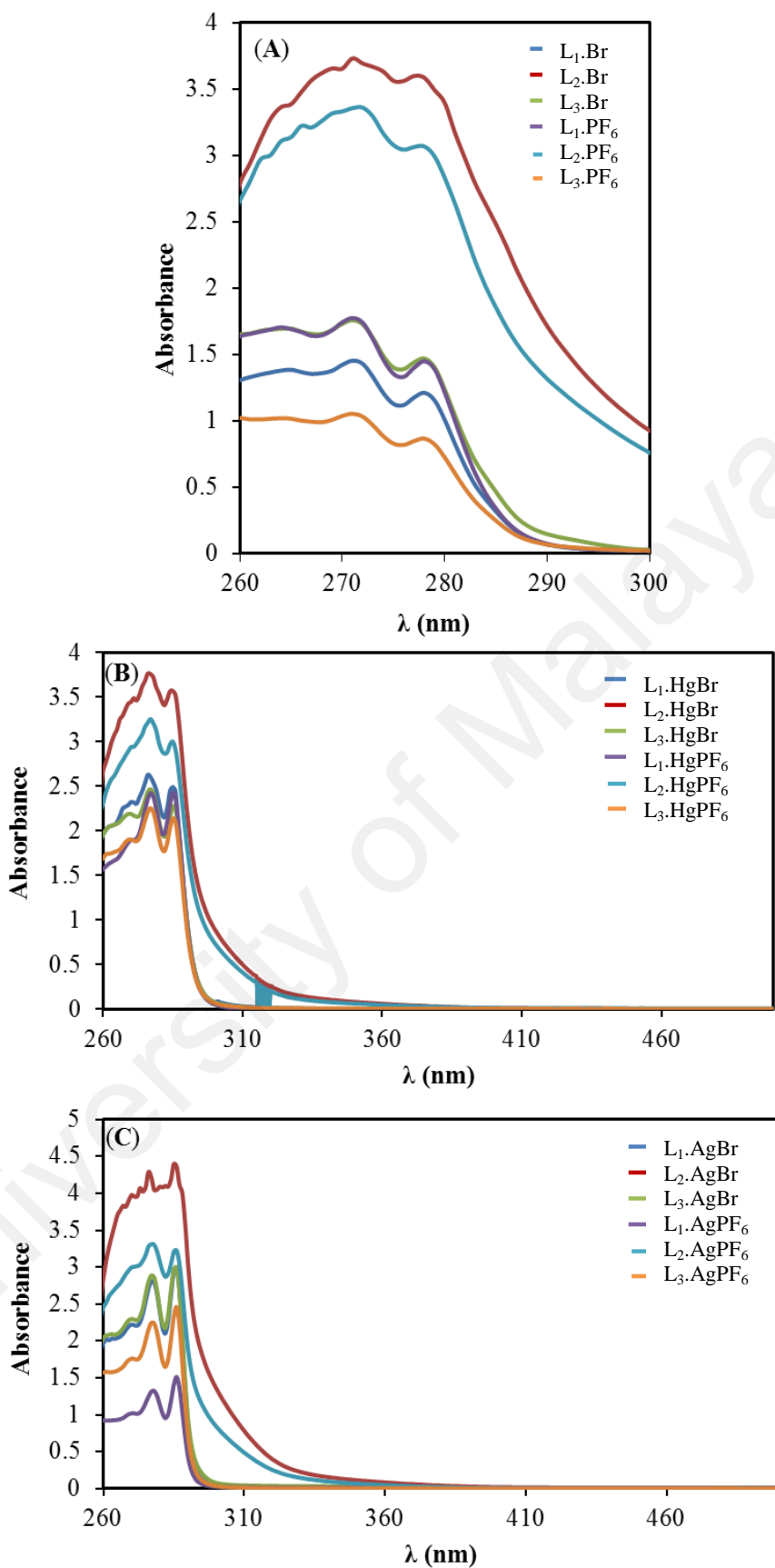


Figure 4.31: Absorbance spectra of (A) bis-benzimidazolium salts, (B) bis-NHC mercury(II) metal complexes and (C) bis-NHC silver(I) metal complexes

The combination results from all characterization methods show the successful synthesized of new bis-NHC mercury(II) complexes and bis-NHC silver(I) complexes based on synthesized ligand. The changes in FT-IR, ^1H -NMR and ^{13}C -NMR proved the coordination of metal cation at carbene carbon position. Hence, the molecular structure of the compound in Figure 4.29 and Figure 4.30 is confirmed by X-ray single structure crystallography study of compound L_1AgBr and L_3HgBr .

The crystal data and the structure refinement of L_1AgBr and L_3HgBr are tabulated in Table 4.20 (Appendix L1-L2). Single crystal L_1AgBr and L_3HgBr which are suitable for X-ray diffraction analysis were obtained from slow diffusion of diethyl ether into concentrated solution of L_1AgBr and L_3HgBr in DMSO at ambient temperature. The Ortep diagrams of these two complexes are presented in Figure 4.32 and Figure 4.33, respectively.

As can be seen in Figure 4.32, two silver atoms are in connection with one molecules of ligand. This complex was crystallized in a monoclinic system with space groups of $\text{I}2/\text{m}$. The L_1AgBr complex in solid sate is formed by the connection of two ligands via cage-like cation and anion unit Ag_6Br_6 (Liu et al., 2013). Its perfomed more complex dimeric structure in solid state which containg $(\text{AgBr})_2$ core come from residual AgBr or Ag_2Br_2 formed from minor decomposition of L_1AgBr (Baker et al., 2004). The internal ring angle (N-C-N) is $105.6 (7)^\circ$ and Ag-C bond length is $2.128 (12)$ \AA , which are comparable to those of the previously reported bis-NHC silver(I) complexes (Liu et al., 2013).

In case of Hg complex (L_3HgBr) (Figure 4.33), every ligand is only in connection with one Hg atom. The complex was crystallized in a triclinic system with

space groups of $P\bar{1}$. There are two water molecules in the asymmetric unit of the $L_3.HgBr$ crystal structure. This could be due to water absorbed from the atmosphere when growing the crystal or doing the reaction (Knapp et al., 2010). Mercury(II) is coordinated with one ligand at two carbene carbon and two bromide atoms, which one bromide was shared with another complex to form tetrahedral geometry. The internal ring angle (N-C-N) at the carbene center is 106.9 (8) $^{\circ}$. These results are in a good agreement with the previously reported bis-NHC metal complexes, indicating the variation (N-C-N) angles from 105.3 (4) $^{\circ}$ to 107.6 (6) $^{\circ}$ (Liu et al., 2015a). The Hg-C (carbene) bond length is 2.1 Å and the linear coordination geometry was observed with a C-Hg-C bond angle of 151.5 (4) $^{\circ}$ (Haque et al., 2011). However, both structures suffer from some disorders in the whole toluene rings.

Table 4.20: Crystal data and structures refinement for $L_1.AgBr$ and $L_3.HgBr$ complexes

Subject	$L_1.AgBr$	$L_3.HgBr$
Empirical formula	$C_{78}H_{74}N_{10}O_4S_2Br_6Ag_6$.($CH_3)_2SO$]	$C_{78}H_{70}N_{10}O_4S_2Br_4Cl_4Hg_2$.2 H_2O
Formula weight	2406.25	2138.19
Temperature (K)	100 (2)	100 (2)
Crystal system,	Monoclinic	Triclinic
Space group	I2/m	$P\bar{1}$
a(Å), $\alpha(^{\circ})$	18.1542(6), 90.000(4)	10.2023(3), 78.934(3)
b(Å), $\beta(^{\circ})$	19.6346(12), 101.50	11.6351(3), 83.730(3)
c(Å), $\gamma(^{\circ})$	26.272, 90.0(6)	17.8431(6), 80.391(3)
Volume (Å ³)	9176.4(6)	2080.3
Z, Calculate density(g/cm ³)	4, 1.855	1, 1.8614(1)
μ/mm^{-1}	4.014	6.4
F(000)	5008	1115.0
Crystal size (mm ³)	$3 \times 0.3 \times 0.25$	0.3 x 0.2 x 0.10
Goodness-of-fit on F ²	1.047	1.116
Final R indexes [I>=2σ (I)]	R ₁ = 0.0492, wR ₂ = 0.1204	R ₁ = 0.0684, wR ₂ = 0.1641
CCDC No.	1419793	1419761

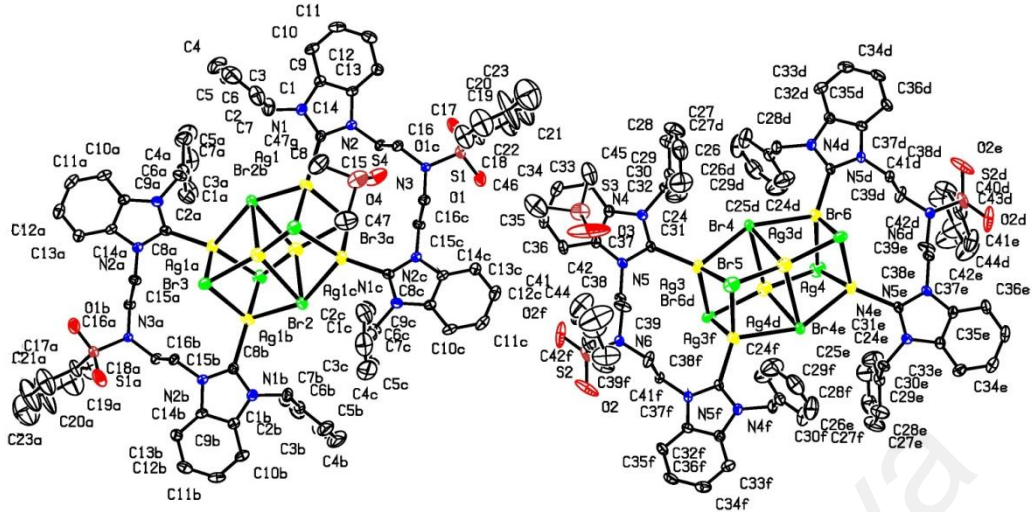


Figure 4.32: Ortep diagram of the molecule structure of $\text{L}_1\cdot\text{AgBr}$ complex

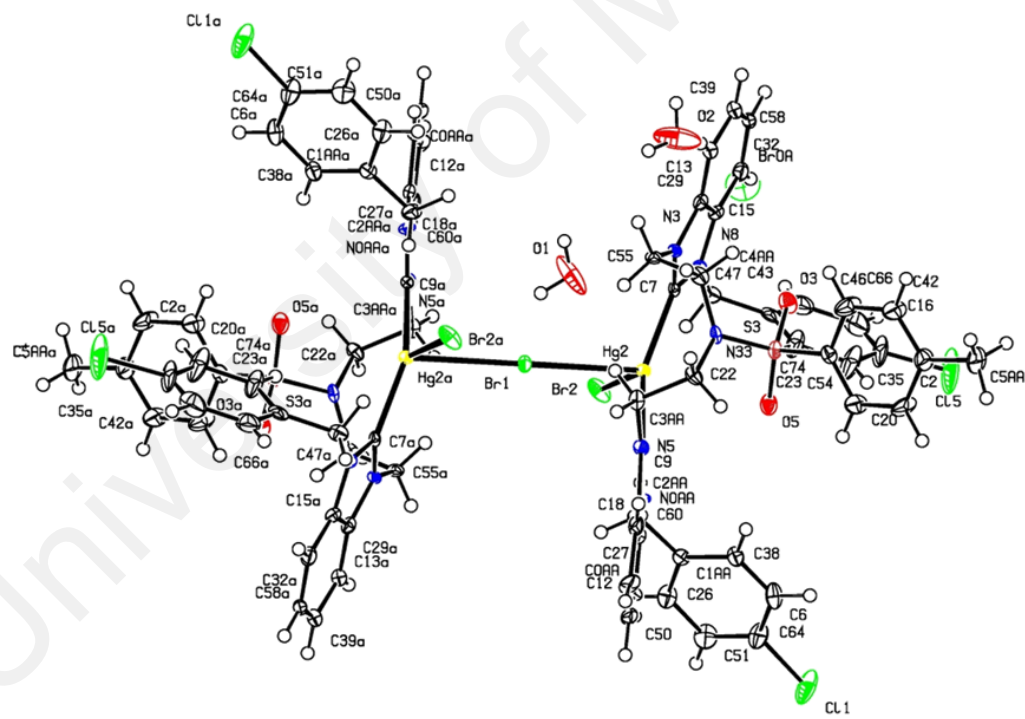


Figure 4.33: Ortep diagram of the molecule structure of $\text{L}_3\cdot\text{HgBr}$ complex

Above all, the new series of bis-benzimidazolium salts from benzimidazole moiety have been successfully synthesized and characterized. The results from conductometric study revealed that the complex formation of L₁.Br with Hg²⁺ and Ag⁺ cations are more stable as compared to other cations. Consequently, new potentiometric self-plasticizing polypyrrole sensors based on L₁.Br precursor as ionophore were fabricated for determination of Hg²⁺ and Ag⁺ cations. The study proved that the proposed Hg-ISE and Ag-ISE can be applied in determination of Hg²⁺ and Ag⁺ cations present in solution, respectively. The preparation and characterization of corresponding mercury(II) and silver(I) complexes for all synthesized bis-benzimidazolium salts are the evidence that the complexation has been occurred at carbene carbon position in imidazole ring.

CHAPTER 5

CONCLUSION AND RECOMMENDATIONS

5.1 Conclusion

In this research work, the diethanolamine has been successfully transformed to new types of bis-benzimidazolium salts through several steps of reactions. The reaction of diethanolamine with *p*-toluenesulfonyl chloride in the presence of triethylamine afforded the formation of tri-sulfonamide. Further reactions with benzimidazole by using KOH as catalyst gave the most important starting material, bis-benzimidazole. This compound was then converted to several bis-benzimidazolium bromide salts ($L_1\text{Br}$, $L_2\text{Br}$ and $L_3\text{Br}$) by alkylation reaction in order to introduce a new substituent at =N- position of the benzimidazole ring. By applying the metathesis reaction using KPF_6 in methanol, the bis-benzimidazolium bromide salts were converted to their corresponding PF_6^- counterpart ($L_1\text{PF}_6$, $L_2\text{PF}_6$ and $L_3\text{PF}_6$).

$L_1\text{Br}$ precursor has been chosen to study the complexation process with metal cations such as Ni^{2+} , Zn^{2+} , Pd^{2+} , Hg^{2+} and Ag^+ in $\text{MeOH:H}_2\text{O}$ binary phases at different temperatures using conductometric method. The plot of molar conductance, Λ_m versus mole ratio, $[L_1\text{Br}]_t/[M^{n+}]_t$ for all metal cations with $L_1\text{Br}$ in different solvent systems ($\text{MeOH-H}_2\text{O}$ binary mixture) at various temperatures gave the stoichiometry of the complexation reactions, respectively. The obtained results show that the stoichiometry of the complexes for Ni^{2+} , Zn^{2+} , and Pd^{2+} cations are 1:1 [M: $L_1\text{Br}$]. While, for Hg^{2+} and Ag^+ cations, they have two stoichiometries which are 2.1 [M: $L_1\text{Br}$] and 1:1 [M: $L_1\text{Br}$]. The stability constants ($\log K_f$) of complex formation have been determined by

fitting the molar conductivity curves using GENPLOT computer program. The output shows that the $\log K_f$ values for Hg^{2+} and Ag^+ cations are higher than the other metal cations studied indicating that the complexations of ligand are more stable and favorable with both metal cations. The obtained data also shows that in the pure MeOH solvent system, the stability constant varies as $\text{Ni}^{2+} < \text{Pd}^{2+} < \text{Zn}^{2+} < \text{Hg}^{2+} < \text{Ag}^+$ and the complexations process seems more stable in pure MeOH. The thermodynamic parameters ($\Delta G_C^o, \Delta H_C^o, \Delta S_C^o$) have been determined conductometrically. The thermodynamic results indicate that the complexations of L_1Br in most cases were found to be enthalpy destabilized but entropy stabilized. According to the obtained results from the effect of ionic radius study, the complexation of $\text{Ni}^{2+}, \text{Zn}^{2+}, \text{Pd}^{2+}, \text{Hg}^{2+}$ and Ag^+ cations with L_1Br can be explained in term of the size-fit concept. The L_1Br forms the most stable complex with a cation having a size which can fits best with its cavity size. The effects of mol% of H_2O and cationic radii of the studied cations on the complexation reactions were investigated and high correlation between experimental data and ANN kinetic model was obtained which further prove the high performance of conductometric method for the complex formation study. The theoretical study by using DFT method found that the binding energy increase monotonically with increasing the size of the studied metal cations in the sequence of $\text{Ni}^{2+}, \text{Pd}^{2+}, \text{Zn}^{2+}, \text{Hg}^{2+}$ and Ag^+ which shows similar agreement with other results. Due to the complexation ability of L_1Br ligand with Hg^{2+} and Ag^+ cations in this study, the fundamental finding of the potential of L_1Br as an ionophore in ISE application has been discovered.

Subsequently, new potentiometric self-plasticizing PPy potentiometric ISE sensors were constructed based on L_1Br precursor as ionophore for determination of Hg^{2+} and Ag^+ cation. The ISE fabrication revealed that the optimum membrane composition was obtained by using 89.4 wt.% monomer (pyrrole), 4.8 wt.%

photoinitiator (DMPP), 0.2 wt.% lipophilic salt (NaTFB), and 5.6 wt.% ionophore (L_1 .Br). This membrane demonstrated good Nernstian responses of 28.10 ± 0.29 mV/decade and 58.61 ± 1.12 mV/decade with the working ranges of 1.0×10^{-6} - 1.0×10^{-2} M and 2.5×10^{-6} - 1.0×10^{-1} M for Hg^{2+} and Ag^+ cations, respectively. The characterizations of optimized fabricated PPy membrane electrode before and after use in ISE study were conducted by using FT-IR, FESEM, EDX, and XRD. The findings confirmed that there is a complexation reaction occurred on the membranes surface between L_1 .Br ionophore and metal cations after being used in ISE study. While the characterization towards electrode performance based on effect of pH, response times, repeatability, reproducibility, stability and selectivity coefficient proved that the Hg-ISE and Ag-ISE proposed in this study can be applied in determination of Hg^{2+} and Ag^+ cations which are present in solution, respectively. This is due to the wide working range of pH, fast response time, repeatability and reproducibility, and also stability of more than 30 days without showing any significant drift in working concentration range, slope and response times. In addition, selective coefficients data shows no significant interference in the performance of the fabricated Hg-ISE and Ag-ISE for determining Hg^{2+} and Ag^+ cations in test solution, respectively. The electrode is also suitable as indicator electrode in the potentiometric titration of Hg^{2+} with EDTA and Ag^+ with NaCl. Finally, accuracy of the the proposed membrane sensor Hg-ISE and Ag-ISE was successfully by the determination of various concentrations of Hg^{2+} and Ag^+ in water and standard solution of sample, respectively through which satisfactory results were obtained.

The complexation reactions of desired metal complexes were formed by *in-situ* deprotonation of bis-benzimidazolium salts, which gave a series of mercury(II) and silver(I) complexes. The structure of synthesized compounds were confirmed by using FT-IR, 1H -NMR and ^{13}C -NMR, CHNS elemental analysis, UV-Vis spectroscopy and

single crystal X-ray diffraction. The results revealed that the ligands are coordinated with Hg^{2+} and Ag^+ metal cations through the carbene carbon and the X-ray single crystal diffraction data shows that the coordination geometry of both complexes are tetrahedral.

5.2 Recommendations

The selection of solvent should be critically studied to gain a suitable crystal structure for single crystal X-ray diffraction analysis. Thus, the real molecular structure of synthesized compound may be revealed clearly.

The fabrication of potentiometric ISE sensor should be done with other synthesized ligands to study the effect of additional different functionalities at benzyl substituent and different anions present in the structure toward the sensing ability.

REFERENCES

- Abbas, I. I. (2012). Mercury (II) selective membrane electrode based on calix [2] thieno [2] pyrrole. *International Journal of Chemistry*, 4(1), 23.
- Abdollahi, Y., Zakaria, A., Abbasiyannejad, M., Masoumi, H. R. F., Moghaddam, M. G., Matori, K. A., Keshavarzi, A. (2013) Artificial neural network modeling of p-cresol photodegradation. *Chemistry Central Journal*, 7(1), 1-7.
- Abraham, A. A., Rezayi, M., Manan, N. S., Narimani, L., Rosli, A. N. B., & Alias, Y. (2015). A novel potentiometric sensor based on 1, 2-bis(N'-benzoylthioureido) benzene and reduced graphene oxide for determination of lead (II) cation in raw milk. *Electrochimica Acta*, 165, 221-231.
- Abramova, N., & Bratov, A. (2015). Application of photocured polymer ion selective membranes for solid-state chemical sensors. *Chemosensors*, 3(2), 190-199.
- Ahamed, M., AlSalhi, M. S., & Siddiqui, M. (2010). Silver nanoparticle applications and human health. *Clinica Chimica Acta*, 411(23), 1841-1848.
- Ahmadzadeh, S., Kassim, A., Rezayi, M., & Rounaghi, G. H. (2011). Thermodynamic study of the complexation of p-isopropylcalix [6] arene with Cs⁺ cation in dimethylsulfoxide-acetonitrile binary media. *Molecules*, 16(9), 8130-8142.
- Ahmed, I. S., Moustafa, M. M., & El Aziz, M. M. A. (2011). Mono and binuclear Ag (I), Cu (II), Zn (II) and Hg (II) complexes of a new azo-azomethine as ligand: Synthesis, potentiometric, spectral and thermal studies. *Spectrochimica Acta Part A: Molecular and Biomolecular Spectroscopy*, 78(5), 1429-1436.
- Al-Mohammed, N. N., Alias, Y., Abdullah, Z., Shakir, R. M., Taha, E. M., & Hamid, A. A. (2013). Synthesis and antibacterial evaluation of some novel imidazole and benzimidazole sulfonamides. *Molecules*, 18(10), 11978-11995.
- Albrecht, M., Maji, P., Häusl, C., Monney, A., & Müller-Bunz, H. (2012). N-Heterocyclic carbene bonding to cobalt porphyrin complexes. *Inorganica Chimica Acta*, 380, 90-95.
- Alder, R. W., Blake, M. E., Bortolotti, C., Bufali, S., Butts, C. P., Linehan, E., & Quayle, M. J. (1999). Complexation of stable carbenes with alkali metals. *Chemical Communications*(3), 241-242.

- Amemiya, S., Buhlmann, P., & Umezawa, Y. (1998). A phase boundary potential model for apparently “twice-Nernstian” responses of liquid membrane ion-selective electrodes. *Analytical Chemistry*, 70, 445-454.
- Arduengo, A. J. (1992). 1,3-dialkylimidazole-2-thione catalysts and method of making same: US 5162482 A.
- Ashley, J. M., Farnaby, J. H., Hazari, N., Kim, K. E., Luzik, E. D., Meehan, R. E., & Tailor, A. N. (2012). Axially chiral dimeric Ir and Rh complexes bridged by flexible NHC ligands. *Inorganica Chimica Acta*, 380, 399-410.
- Baker, M. V., Brown, D. H., Haque, R. A., Skelton, B. W., & White, A. H. (2009a). Silver(I) and mercury(II) complexes of meta-and para-xylyl linked bis(imidazol-2-ylidenes). *Journal of Inclusion Phenomena and Macrocyclic Chemistry*, 65(1-2), 97-109.
- Baker, M. V., Brown, D. H., Haque, R. A., Simpson, P. V., Skelton, B. W., White, A. H., & Williams, C. C. (2009b). Mercury complexes of N-Heterocyclic carbenes derived from imidazolium-linked cyclophanes: synthesis, structure, and reactivity. *Organometallics*, 28, 3793-3803.
- Baker, M. V., Brown, D. H., Haque, R. A., Skelton, B. W., & White, A. H. (2004). Dinuclear N-heterocyclic carbene complexes of silver(I), derived from imidazolium-linked cyclophanes. *Dalton Transactions*, 21, 3756-3764.
- Budagumpi, S., Haque, R. A., & Salman, A. W. (2012a). Stereochemical and structural characteristics of single-and double-site Pd(II)-N-heterocyclic carbene complexes: Promising catalysts in organic syntheses ranging from C C coupling to olefin polymerizations. *Coordination Chemistry Reviews*, 256(17), 1787-1830.
- Budagumpi, S., Haque, R. A., Salman, A. W., & Ghdhayeb, M. Z. (2012b). Mercury(II)- and silver(I)-N-heterocyclic carbene complexes of CNC pincer-type ligands: Synthesis, crystal structures and Hofmann-type elimination studies. *Inorganica Chimica Acta*, 392, 61-72.
- Cao, C., Zhuang, Y., Zhao, J., Peng, Y., Li, X., Shi, Z., Shi, Y. (2010). Binuclear palladium complexes bridged by dicarbene with different lengths and their application in Mizoroki-Heck reaction. *Inorganica Chimica Acta*, 363(14), 3914-3918.
- Cazin, C. S. J. (2010). *N-Heterocyclic Carbenes in Transition Metal Catalysis and Organocatalysis* (Vol. 32): Springer Science & Business Media.

Cazin, C. S. J. (2011). *N-Heterocyclic Carbenes in Transition Metal Catalysis and Organocatalysis* (Vol. 32): Springer.

Chen, L. D., Mandal, D., Pozzi, G., Gladysz, J. A., & Bühlmann, P. (2011). Potentiometric sensors based on fluorous membranes doped with highly selective ionophores for carbonate. *Journal of the American Chemical Society*, 133(51), 20869-20877.

Christy, F. A., & Shrivastav, P. S. (2011). Conductometric studies on cation-crown ether complexes: a review. *Critical Reviews in Analytical Chemistry*, 41(3), 236-269.

Clavier, H., & Nolan, S. P. (2007). N-heterocyclic carbenes: advances in transition metal-mediated transformations and organocatalysis. *Annual Reports Section "B"(Organic Chemistry)*, 103, 193-222.

Crabtree, R. H. (2005). NHC ligands versus cyclopentadienyls and phosphines as spectator ligands in organometallic catalysis. *Journal of Organometallic Chemistry*, 690(24), 5451-5457.

Crudden, C. M., & Allen, D. P. (2004). Stability and reactivity of N-heterocyclic carbene complexes. *Coordination Chemistry Reviews*, 248(21), 2247-2273.

Dadkhah, A., Rofouei, M. K., & Mashhadizadeh, M. H. (2014). Synthesis and characterization of N, N'-bis (benzophenone imine) formamidine as ionophores for silver-selective electrodes. *Sensors and Actuators B: Chemical*, 202, 410-416.

De Castro, K. A., Ko, J., Park, D., Park, S., & Rhee, H. (2007). Reduction of ethyl benzoylacetate and selective protection of 2-(3-hydroxy-1-phenylpropyl)-4-methylphenol: A new and facile synthesis of tolterodine. *Organic Process Research & Development*, 11(5), 918-921.

Delaude, L. (2009). Betaine adducts of N-heterocyclic carbenes: synthesis, properties, and reactivity. *European Journal of Inorganic Chemistry*, 2009(13), 1681-1699.

Demir, E., Kemer, B., Bekircan, O., & Y Aboul-Enein, H. (2015). A novel iron(III)-selective membrane potentiometric sensor based on 5-chloro-3-[4-(trifluoromethoxy) phenylimino] indolin-2-one. *Current Analytical Chemistry*, 11(1), 29-35.

- Despagnet-Ayoub, E., & Grubbs, R. H. (2004). A stable four-membered N-heterocyclic carbene. *Journal of the American Chemical Society*, 126(33), 10198-10199.
- Dias, H. R., & Jin, W. (1994). A stable tridentate carbene ligand. *Tetrahedron Letters*, 35(9), 1365-1366.
- Díez-González, S., & Nolan, S. P. (2007). Stereoelectronic parameters associated with N-heterocyclic carbene (NHC) ligands: a quest for understanding. *Coordination Chemistry Reviews*, 251(5), 874-883.
- Dimeski, G., Badrick, T., & St John, A. (2010). Ion selective electrodes (ISEs) and interferences—a review. *Clinica Chimica Acta*, 411(5), 309-317.
- El-Dien, F. N., Mohamed, G. G., Frag, E. Y., & Mohamed, M. E.-B. (2012). Modified screen printed and carbon paste ion selective electrodes for potentiometric determination of naphazoline hydrochloride in pure and pharmaceutical preparations. *International Journal of Electrochemical Science*, 7, 10266-10281.
- El-Sonbati, A. Z., El-Binary, A. A.-A., Shoair, A.-G. F., & Younes, R. M. (2001). Stereochemistry of new nitrogen containing heterocyclic aldehyde. VII. Potentiometric, conductometric and thermodynamic studies of novel quinoline azodyes and their metal complexes with some transition metals. *Chemical and Pharmaceutical Bulletin*, 49(10), 1308-1313.
- Eseola, A. O., Adepitinan, O., Görts, H., & Plass, W. (2012). Electronic/substituents influence on imidazole ring donor–acceptor capacities using 1 H-imidazo [4, 5-f][1, 10] phenanthroline frameworks. *New Journal of Chemistry*, 36(4), 891-902.
- Faribod, F., Ganjali, M. R., Dinarvand, R., & Norouzi, P. (2007). The fabrication of potentiometric membrane sensors and their applications. *African Journal of Biotechnology*, 6(25).
- Faribod, F., Ganjali, M. R., Dinarvand, R., Norouzi, P., & Riahi, S. (2008a). Schiff's bases and crown ethers as supramolecular sensing materials in the construction of potentiometric membrane sensors. *Sensors*, 8(3), 1645-1703.
- Faribod, F., Norouzi, P., Dinarvand, R., & Ganjali, M. R. (2008b). Developments in the field of conducting and non-conducting polymer based potentiometric membrane sensors for ions over the past decade. *Sensors*, 8(4), 2331-2412.

- Frant, M., & Ross Jr, J. W. (1968). Use of a total ionic strength adjustment buffer for electrode determination of fluoride in water supplies. *Analytical Chemistry*, 40(7), 1169-1171.
- Ganjali, M., Rezapour, M., Pirali-Hamedani, M., & Rashedi, H. (2015). Cu(II)-all solid state sensor ion selective electrode (ASS-ISE) with a nano-molar detection limit and its use for the analysis of waste water samples. *International Journal of Electrochemical Science*, 10, 6924-6934.
- Garrison, J. C., & Youngs, W. J. (2005). Ag(I) N-heterocyclic carbene complexes: synthesis, structure, and application. *Chemical Reviews*, 105(11), 3978-4008.
- Genplot, A. (1989). Data Analysis and Graphical Plotting Program for Scientist and Engineers. *Computer Graphic Service, Ltd., Ithaca, NY*.
- Ghalami-Choobar, B., Mahmoodi, N., & Mossayyebzadeh-Shalkoohi, P. (2013). Thermodynamic properties determination of ternary mixture (NaCl+ Na₂HPO₄+ water) using potentiometric measurements. *The Journal of Chemical Thermodynamics*, 57, 108-113.
- Ghanei-Motlagh, M., Fayazi, M., & Taher, M. (2014). On the potentiometric response of mercury (ii) membrane sensors based on symmetrical thiourea derivatives—experimental and theoretical approaches. *Sensors and Actuators B: Chemical*, 199, 133-141.
- Gholami, M., Ghasemi, A.-M., Loghavi, M., Behkami, S., & Ahmadi-Dokht-Faraghe, A. (2013). Preparation of a miniaturised iodide ion selective sensor using polypyrrole and pencil lead: effect of double-coating, electropolymerisation time, and current density. *Chemical Papers*, 67(8), 1079-1086.
- Glorius, F., & Bellemin-Laponnaz, S. (2007). *N-heterocyclic carbenes in transition metal catalysis*. Heidelberg: Springer.
- Greene, T. W., & Wuts, P. G. (1999). *Protection for the carbonyl group*: Wiley Online Library.
- Gümüş, H. P., Tamer, Ö., Avcı, D., & Atalay, Y. (2014). Effects of donor–acceptor groups on the structural and electronic properties of 4-(methoxymethyl)-6-methyl-5-nitro-2-oxo-1, 2-dihydropyridine-3-carbonitrile. *Spectrochimica Acta Part A: Molecular and Biomolecular Spectroscopy*, 132, 183-190.

Gupta, K., & D'Arc, M. J. (2000). Performance evaluation of copper ion selective electrode based on cyanocopolymers. *Sensors and Actuators B: Chemical*, 62(3), 171-176.

Gupta, K., & D'Arc, M. J. (2001). Effect of concentration of ion exchanger, plasticizer and molecular weight of cyanocopolymers on selectivity and sensitivity of Cu(II) ion selective electrodes. *Analytica Chimica Acta*, 437(2), 199-216.

Gupta, V., Singh, A., Al Khayat, M., & Gupta, B. (2007). Neutral carriers based polymeric membrane electrodes for selective determination of mercury(II). *Analytica Chimica Acta*, 590(1), 81-90.

Gupta, V. K., Pal, M. K., & Singh, A. K. (2009). Comparative study of Ag (I) selective poly (vinyl chloride) membrane sensors based on newly developed Schiff-base lariat ethers derived from 4, 13-diaza-18-crown-6. *Analytica Chimica Acta*, 631(2), 161-169.

Gutmann, V. (1978). *The donor-acceptor approach to molecular interactions*. New York: Plenum Press.

Hahn, F. E., & Jahnke, M. C. (2008). Heterocyclic carbenes: synthesis and coordination chemistry. *Angewandte Chemie International Edition*, 47(17), 3122-3172.

Haque, R. A., Budagumpi, S., Choo, S. Y., Choong, M. K., Lokesh, B. E., & Sudesh, K. (2012a). Nitrile-functionalized Hg (II)-and Ag (I)-N-heterocyclic carbene complexes: synthesis, crystal structures, nuclease and DNA binding activities. *Applied Organometallic Chemistry*, 26(12), 689.

Haque, R. A., Ghdhayeb, M. Z., Budagumpi, S., Salman, A. W., Ahamed, M. B. K., & Majid, A. M. S. A. (2013). Non-symmetrically substituted N-heterocyclic carbene-Ag (I) complexes of benzimidazol-2-ylidenes: Synthesis, crystal structures, anticancer activity and transmetallation studies. *Inorganica Chimica Acta*, 394, 519-525.

Haque, R. A., Iqbal, M. A., Khadeer, M., Majeed, A., & Abdul Hameed, Z. (2012b). Design, synthesis and structural studies of meta-xylyl linked bis-benzimidazolium salts: Potential anticancer agents against 'human colon cancer'. *Chemistry Central Journal*, 6(1), 68.

Haque, R. A., Salman, A. W., Guan, T. S., & Abdallah, H. H. (2011). New N-heterocyclic carbene mercury(II) complexes: Close mercury–arene interaction. *Journal of Organometallic Chemistry*, 696(22), 3507-3512.

Hassan, A. K. (2013). Chemical Sensor for Determination of Mercury in Contaminated Water. *Modern Chemistry & Applications*, 1(4), 1-4.

Hassouna, M., Elsucary, S., & Graham, J. (2010). N, N'-Bis (3-methyl-1-phenyl-4-benzylidene-5-pyrazolone) propylenediamine Schiff base as a neutral carrier for silver (I) ion-selective electrodes. *Sensors and Actuators B: Chemical*, 146(1), 79-90.

Heng, L. Y., & Hall, E. A. (2000). Producing “self-plasticizing” ion-selective membranes. *Analytical Chemistry*, 72(1), 42-51.

Heng, L. Y., & Hall, E. A. (2001). Assessing a photocured self-plasticised acrylic membrane recipe for Na^+ and K^+ ion selective electrodes. *Analytica Chimica Acta*, 443(1), 25-40.

Heng, L. Y., & Hall, E. A. (2008). Characteristics of Solid-State Calcium Ion Sensors Based on Photocurableand Selfplasticising Polyacrylate Matrices. *ASEAN Journal on Science and Technology for Development*, 23(4), 261-273.

Herrmann, W. A. (2002). N-Heterocyclic carbenes: A new concept in organometallic catalysis. *Angewandte Chemie International Edition*, 41(8), 1290-1309.

Holmes, P., James, K., & Levy, L. (2009). Is low-level environmental mercury exposure of concern to human health? *Science of the Total Environment*, 408(2), 171-182.

Iglesias, M., Beetstra, D. J., Stasch, A., Horton, P. N., Hursthouse, M. B., Coles, S. J., Fallis, I. A. (2007). First examples of diazepanylidene carbenes and their late-transition-metal complexes. *Organometallics*, 26(19), 4800-4809.

Iqbal, M. A., Haque, R. A., Ahamed, M. B. K., & Majid, A. (2014). Synthesis and cytotoxicity of dinuclear silver(I)-N-heterocyclic carbene complexes. *Biochemistry and Analytical Biochemistry*, 3(1), 1.

Iqbal, M. A., Haque, R. A., Sulaiman, S., & Izzati, T. (2011). Synthesis, characterization, and theoretical studies of xylyl linked bis-imidazolium and bis-benzimidazolium salts. *Journal of Chemistry*, 2(1).

Ismail, A. A., Aroua, M. K., & Yusoff, R. (2012). Potentiometric determination of trace amounts of mercury (II) in water sample using a new modified palm shell activated carbon paste electrode based on kryptofix 5. *American Journal of Analytical Chemistry*, 3, 859-865.

- Jaubert, S., & Maurer, G. (2014). Quantitative NMR spectroscopy of binary liquid mixtures (aldehyde+alcohol) Part I: Acetaldehyde+(methanol or ethanol or 1-propanol). *The Journal of Chemical Thermodynamics*, 68, 332-342.
- Jazzar, R., Liang, H., Donnadieu, B., & Bertrand, G. (2006). A new synthetic method for the preparation of protonated-NHCs and related compounds. *Journal of Organometallic Chemistry*, 691(14), 3201-3205.
- Joshaghani, M., Gholivand, M. B., & Ahmadi, F. (2008). Spectrophotometric and conductometric study of complexation of salophen and some transition metal ions in nonaqueous polar solvents. *Spectrochimica Acta Part A: Molecular and Biomolecular Spectroscopy*, 70(5), 1073-1078.
- Jóźwiak, M., & Madej-Kiełbik, L. (2014). Effect of temperature on the process of complex formation crown ether 15C5 with Na⁺ in the mixture of water with methanol. *The Journal of Chemical Thermodynamics*, 68, 303-309.
- Jumal, J., Yamin, B. M., Ahmad, M., & Heng, L. Y. (2012). Mercury ion-selective electrode with self-plasticizing poly(n-buthylacrylate) membrane based on 1,2-bis-(n'-benzoylthioureido)cyclohexane as ionophore. *APCBEE Procedia*, 3, 116-123.
- Kamal, A., Puri, R. K., Raj, R., Kumar, V., & Mahajan, R. K. (2012). Silver ion recognition using potentiometric sensor based on recently synthesized isoquinoline-1, 3-dione derivatives. *Journal of Electrochemical Science and Engineering*, 2(3), 143-154.
- Kamel, A. H. (2015). New potentiometric transducer based on a Mn(II)[2-formylquinoline thiosemicarbazone] complex for static and hydrodynamic assessment of azides. *Talanta*, 144, 1085-1090.
- Kim, S., Noh, J. Y., Kim, K. Y., Kim, J. H., Kang, H. K., Nam, S.-W., Kim, J. (2012). Salicylimine-based fluorescent chemosensor for aluminum ions and application to bioimaging. *Inorganic chemistry*, 51(6), 3597-3602.
- Knapp, A. R., Panzner, M. J., Medvetz, D. A., Wright, B. D., Tessier, C. A., & Youngs, W. J. (2010). Synthesis and antimicrobial studies of silver N-heterocyclic carbene complexes bearing a methyl benzoate substituent. *Inorganica Chimica Acta*, 364(1), 125-131.
- Kore, R., Tumma, M., & Srivastava, R. (2012). Syntheses and catalytic activities of homogenous and hierarchical ZSM-5 grafted Pd (II) dicarbene complex of imidazole based ionic liquids. *Catalysis Today*, 198(1), 189-196.

Kuhn, K. M., & Grubbs, R. H. (2008). A facile preparation of imidazolinium chlorides. *Organic Letters*, 10(10), 2075-2077.

Kumar, Y., Prasad, M., Neela, P. K., & Misra, S. (2004). Process for the preparation of tolterodine: Patents US 2004024911 A1.

Lindner, E., & Pendley, B. D. (2013). A tutorial on the application of ion-selective electrode potentiometry: an analytical method with unique qualities, unexplored opportunities and potential pitfalls; Tutorial. *Analytica Chimica Acta*, 762, 1-13.

Liu, D., Liu, J., Tian, D., Hong, W., Zhou, X., & Jimmy, C. Y. (2000). Polymeric membrane silver-ion selective electrodes based on bis (dialkyldithiophosphates). *Analytica Chimica Acta*, 416(2), 139-144.

Liu, Q.-X., Chen, A.-H., Zhao, X.-J., Zang, Y., Wu, X.-M., Wang, X.-G., & Guo, J.-H. (2011a). N-Heterocyclic carbene copper (I), mercury (II) and silver (I) complexes containing durene linker: synthesis and structural studies. *CrystEngComm*, 13(1), 293-305.

Liu, Q.-X., Li, H.-L., Zhao, X.-J., Ge, S.-S., Shi, M.-C., Shen, G., Wang, X.-G. (2011b). Silver (I), mercury (II) and palladium (II) complexes of functionalized N-heterocyclic carbenes: Synthesis, structural studies and catalytic activity. *Inorganica Chimica Acta*, 376(1), 437-445.

Liu, Q.-X., Wang, H., Zhao, X.-J., Yao, Z.-Q., Wang, Z.-Q., Chen, A.-H., & Wang, X.-G. (2012). N-Heterocyclic carbene silver(I), palladium(II) and mercury(II) complexes: synthesis, structural studies and catalytic activity. *CrystEngComm*, 14(16), 5330-5348.

Liu, Q.-X., Wei, Q., Liu, R., Zhao, X.-J., & Zhao, Z.-X. (2015a). NHC macrometallocycles of mercury (ii) and silver (i): synthesis, structural studies and recognition of Hg (II) complex 4 for silver ion. *RSC Advances*, 5(36), 28435-28447.

Liu, Q.-X., Zhao, L.-X., Zhao, X.-J., Zhao, Z.-X., Wang, Z.-Q., Chen, A.-H., & Wang, X.-G. (2013). Silver (I), palladium (II) and mercury (II) NHC complexes based on bis-benzimidazole salts with mesitylene linker: Synthesis, structural studies and catalytic activity. *Journal of Organometallic Chemistry*, 731, 35-48.

Liu, Q.-X., Zhao, Z.-X., Zhao, X.-J., Wei, Q., Chen, A.-H., Li, H.-L., & Wang, X.-G. (2015b). Structures of NHC Hg (II) and Ag (I) complexes and selective recognition of nitrate anion. *CrystEngComm*, 17(6), 1358-1373.

Liu, Y., & Lynch, J. (2011). *The development of chloride ion selective polypyrrole thin film on a layer-by-layer carbon nanotube working electrode*. Paper presented at the SPIE Smart Structures and Materials+ Nondestructive Evaluation and Health Monitoring.

Logacheva, N. M., Baulin, V. E., Tsivadze, A. Y., Pyatova, E. N., Ivanova, I. S., Velikodny, Y. A., & Chernyshev, V. V. (2009). Ni (II), Co (II), Cu (II), Zn (II) and Na (I) complexes of a hybrid ligand 4'-(4 [triple prime]-benzo-15-crown-5)-methoxy-2, 2': 6', 2 "-terpyridine. *Dalton Transactions*(14), 2482-2489.

Mahajan, R., Kaur, I., & Lobana, T. (2003). A mercury(II) ion-selective electrode based on neutral salicylaldehyde thiosemicarbazone. *Talanta*, 59(1), 101-105.

Mahajan, R., Kaur, I., Sharma, V., & Kumar, M. (2002). Sensor for silver (I) ion based on Schiff-base-p-tertbutylcalix [4] arene. *Sensors*, 2(10), 417-423.

Malon, A., & Maj-Zurawska, M. (2005). The new methods of determination of Mg^{2+} , Ca^{2+} , Na^+ and K^+ ions in erythrocytes by ion selective electrodes. *Sensors and Actuators B: Chemical*, 108(1), 828-831.

Mandil, H., Alhaj Sakur, A., & Nasser, B. (2013). New ion selective electrode for potentiometric determination of gatifloxacin in pore form and pharmaceutical formulations. *International Journal of Pharmacy & Pharmaceutical Sciences*, 5.

Mashhadizadeh, M. H., Ramezani, S., & Rofouei, M. K. (2015). Development of a novel MWCNTs-triazene-modified carbon paste electrode for potentiometric assessment of $Hg(II)$ in the aquatic environments. *Materials Science and Engineering: C*, 47, 273-280.

Mehta, D. R., Chandra, R. S., Mehta, K. K., Maisuria, M., & Maisuria, M. M. (2014). Thermodynamic studies on metal complexes of Co^{2+} , Ni^{2+} , Cu^{2+} and Cd^{2+} with 8-hydroxy 5-quinolinesulfonic acid in water, methanol and water-methanol binary solvent systems at 303.15 K, 313.15 K and 323.15 K by conductometric method. *Journal of Physical and Chemical Science*, 1(2), 1.

Montazerozohori, M., Nasr-Esfahani, M., Hoseinpour, M., Naghiha, A., & Zahedi, S. (2014). Synthesis of some new antibacterial active cadmium and mercury complexes of 4-(3-(2-(4-(dimethyl aminophenyl allylidene aminopropyl-imino) prop-1-ethyl)-N, N-dimethyl benzene amine. *Chemical Speciation & Bioavailability*, 26(4), 240-248.

Mutter, J., Naumann, J., Sadaghiani, C., Walach, H., & Drasch, G. (2004). Amalgam studies: disregarding basic principles of mercury toxicity. *International Journal of Hygiene and Environmental Health*, 207(4), 391-397.

Nanda, D., Oak, M., & Kumar, M. P. (2007). Acrylic acid grafted PVC membrane based ion selective electrode for calcium and hardness measurement of water. *Indian Journal of Chemistry. Section A, Inorganic, Bio-inorganic, Physical, Theoretical & Analytical chemistry*, 46(2), 258.

Nezhadali, A., & Taslimi, G. (2013). Thermodynamic study of complex formation between 3,5-di iodo-hydroxy quinoline and Zn^{2+} , Ni^{2+} and Co^{2+} cations in some binary solvents using a conductometric method. *Alexandria Engineering Journal*, 52(4), 797-800.

Ngeontae, W., Janrungroatsakul, W., Morakot, N., Aeungmaitrepirom, W., & Tuntulani, T. (2008). New silver selective electrode fabricated from benzothiazole calix [4] arene: speciation analysis of silver nanoparticles. *Sensors and Actuators B: Chemical*, 134(2), 377-385.

Nia, P. M., Lorestani, F., Meng, W. P., & Alias, Y. (2015a). A novel non-enzymatic H_2O_2 sensor based on polypyrrole nanofibers–silver nanoparticles decorated reduced graphene oxide nano composites. *Applied Surface Science*, 332, 648-656.

Nia, P. M., Meng, W. P., Lorestani, F., Mahmoudian, M., & Alias, Y. (2015b). Electrodeposition of copper oxide/polypyrrole/reduced graphene oxide as a nonenzymatic glucose biosensor. *Sensors and Actuators B: Chemical*, 209, 100-108.

Özdemir, İ., Temelli, N., Günal, S., & Demir, S. (2010). Gold (I) complexes of N-heterocyclic carbene ligands containing benzimidazole: synthesis and antimicrobial activity. *Molecules*, 15(4), 2203-2210.

Pavia, D., Lampman, G., Kriz, G., & Vyvyan, J. (2008). *Introduction to Spectroscopy*: Cengage Learning.

Pearson, R. G. (1968). Hard and soft acids and bases, HSAB, part 1: Fundamental principles. *Journal of Chemical Education*, 45(9), 581.

Peris, E. (2007). Routes to N-heterocyclic carbene complexes *N-Heterocyclic Carbenes in Transition Metal Catalysis* (pp. 83-116): Springer.

Peris, E., & Crabtree, R. H. (2004). Recent homogeneous catalytic applications of chelate and pincer N-heterocyclic carbenes. *Coordination Chemistry Reviews*, 248(21), 2239-2246.

Peshkova, M. A., Sokalski, T., Mikhelson, K. N., & Lewenstam, A. (2008). Obtaining nernstian response of a Ca^{2+} -selective electrode in a broad concentration range by tuned galvanostatic polarization. *Analytical Chemistry*, 80(23), 9181-9187.

Petković, B. B., Milčić, M., Stanković, D., Stambolić, I., Manojlović, D., Jovanović, V. M., & Sovilj, S. P. (2013). Complexation ability of octaazamacrocyclic ligand toward Co^{2+} , Ni^{2+} , Cu^{2+} and Zn^{2+} metal cations: Experimental and theoretical study. *Electrochimica Acta*, 89, 680-687.

Piao, M.-H., Yoon, J.-H., Jeon, G., & Shim, Y.-B. (2003). Characterization of all solid state hydrogen ion selective electrode based on PVC-SR hybrid membranes. *Sensors*, 3(6), 192-201.

Radu, A., Radu, T., Mcgraw, C., Dillingham, P., Anastasova-Ivanova, S., & Diamond, D. (2013). Ion selective electrodes in environmental analysis. *Journal of the Serbian Chemical Society*, 78(11), 1729-1761.

Ragab, M. T., El-Rahman, M. K. A., Ramadan, N. K., El-Ragehy, N. A., & El-Zeany, B. A. (2015). Novel potentiometric application for the determination of pantoprazole sodium and itopride hydrochloride in their pure and combined dosage form. *Talanta*, 138, 28-35.

Rao, L., & Tian, G. (2008). Thermodynamic study of the complexation of uranium (VI) with nitrate at variable temperatures. *The Journal of Chemical Thermodynamics*, 40(6), 1001-1006.

Rezayi, M., Karazhian, R., Abdollahi, Y., Narimani, L., Sany, S. B. T., Ahmadzadeh, S., & Alias, Y. (2014). Titanium (III) cation selective electrode based on synthesized tris (2pyridyl) methylamine ionophore and its application in water samples. *Scientific reports*, 4, 4664.

Rezayi, M., Kassim, A., Ahmadzadeh, S., Naji, A., & Ahangar, H. (2011). Conductometric determination of formation constants of tris (2-pyridyl) methylamine and titanium (III) in water-acetonitrile mixture. *International Journal of Electrochemical Science*, 6, 4378-4387.

Rit, A., Pape, T., & Hahn, F. E. (2010). Self-assembly of molecular cylinders from polycarbene ligands and AgI or AuI . *Journal of the American Chemical Society*, 132(13), 4572-4573.

- Saito, S., Saika, M., Yamasaki, R., Azumaya, I., & Masu, H. (2011). Synthesis and structure of dinuclear silver (I) and palladium (II) complexes of 2, 7-Bis (methylene) naphthalene-bridged bis-N-heterocyclic carbene ligands. *Organometallics*, 30(6), 1366-1373.
- Sakajiri, T., Yajima, H., & Yamamura, T. (2012). Density functional theory study on metal-binding energies for Human serum transferrin-metal complexes. *ISRN Biophysics*, 2012, 1-5.
- Sany, S. B. T., Salleh, A., Rezayi, M., Saadati, N., Narimany, L., & Tehrani, G. M. (2013a). Distribution and contamination of heavy metal in the coastal sediments of Port Klang, Selangor, Malaysia. *Water, Air, & Soil Pollution*, 224(4), 1-18.
- Sany, S. B. T., Salleh, A., Sulaiman, A. H., Sasekumar, A., Rezayi, M., & Tehrani, G. M. (2013b). Heavy metal contamination in water and sediment of the Port Klang coastal area, Selangor, Malaysia. *Environmental Earth Sciences*, 69(6), 2013-2025.
- Sany, S. B. T., Salleh, A., Sulaiman, A. H., Sasekumar, A., Tehrani, G., & Rezayi, M. (2012). Distribution characteristics and ecological risk of heavy metals in surface sediments of West Port, Malaysia. *Environment Protection Engineering*, 38(4), 139-155.
- Sardohan-Koseoglu, T., Kir, E., & Dede, B. (2015). Preparation and analytical application of the novel Hg(II)-selective membrane electrodes based on oxime compounds. *Journal of Colloid and Interface Science*, 444, 17-23.
- Sato, K., Arai, S., & Yamagishi, T. (1999). A new tripodal anion receptor with C · H···X– hydrogen bonding. *Tetrahedron Letters*, 40(28), 5219-5222.
- Schaller, U., Bakker, E., & Pretsch, E. (1995). Carrier mechanism of acid ionophore in solvent polymeric membrane ion-selective electrodes. *Analytical Chemistry*, 67, 3123-3132.
- Schick, S., Pape, T., & Hahn, F. E. (2014). Coordination chemistry of bidentate bis (NHC) ligands with two different NHC donors. *Organometallics*, 33(15), 4035-4041.
- Sears, M. E., Kerr, K. J., & Bray, R. I. (2012). Arsenic, cadmium, lead, and mercury in sweat: a systematic review. *Journal of Environmental and Public Health*, 2012.

- Serra, D., Cao, P., Cabrera, J., Padilla, R., Rominger, F., & Limbach, M. (2011). Development of platinum(II) and-(IV) CNC pincer complexes and their application in a hydrovinylation reaction. *Organometallics*, 30(7), 1885-1895.
- Shah, B. A., Christy, F. A., Shrivastav, P. S., & Sanyal, M. (2014). Study on complex formation of dicyclohexyl-18-crown-6 with Mg^{2+} , Ca^{2+} and Sr^{2+} in acetonitrile-water binary mixtures by conductometry. *Journal of Physical and Chemical Sciences*, 1(2), 5.
- Singhal, D., Singh, A. K., & Upadhyay, A. (2014). Highly selective potentiometric and colorimetric determinations of cobalt(II) ion using thiazole based ligands. *Materials Science and Engineering: C*, 45, 216-224.
- Sivaram, H., Tan, J., & Huynh, H. V. (2012). Syntheses, characterizations, and a preliminary comparative cytotoxicity study of gold(I) and gold(III) complexes bearing benzimidazole-and pyrazole-derived N-heterocyclic carbenes. *Organometallics*, 31(16), 5875-5883.
- Sivaram, H., Tan, J., & Huynh, H. V. (2013). Cationic gold(I) heteroleptic complexes bearing a pyrazole-derived N-heterocyclic carbene: syntheses, characterizations, and cytotoxic activities. *Dalton Transactions*, 42(34), 12421-12428.
- Soleimani, M., & Afshar, M. G. (2013). Potentiometric sensor for trace level analysis of copper based on carbon paste electrode modified with multi-walled carbon nanotubes. *International Journal of Electrochemical Science*, 8, 8719-8729.
- Stringer, B. D., Quan, L. M., Barnard, P. J., Wilson, D. J., & Hogan, C. F. (2014). Iridium Complexes of N-Heterocyclic Carbene Ligands: Investigation into the Energetic Requirements for Efficient Electrogenerated Chemiluminescence. *Organometallics*, 33(18), 4860-4872.
- Tadayon, F., Katebi, A., Afkhami, A., Panahi, Y., & Bagheri, H. (2014). A new potentiometric sensor based on a high-performance composite for nanomolar determination of mercury (II) in environmental samples. *International Journal of Environmental Analytical Chemistry*, 94(9), 901-915.
- Umezawa, Y., Bühlmann, P., Umezawa, K., Tohda, K., & Amemiya, S. (2000). Potentiometric selectivity coefficients of ion-selective electrodes. Part I. Inorganic cations (technical report). *Pure and Applied Chemistry*, 72(10), 1851-2082.
- Valente, C., Çalimsiz, S., Hoi, K. H., Mallik, D., Sayah, M., & Organ, M. G. (2012). The development of bulky palladium NHC complexes for the most-challenging

cross-coupling reactions. *Angewandte Chemie International Edition*, 51(14), 3314-3332.

Wade Jr, L. (2006). Organic-chemistry 6th ed: Pearson Prentice Hall.

Wang, J., Feng, X., Anderson, C. W., Xing, Y., & Shang, L. (2012). Remediation of mercury contaminated sites—A review. *Journal of Hazardous Materials*, 221, 1-18.

Wang, M., Leung, K.-H., Lin, S., Chan, D. S.-H., Kwong, D. W., Leung, C.-H., & Ma, D.-L. (2014). A colorimetric chemosensor for Cu^{2+} ion detection based on an iridium (III) complex. *Scientific Reports*, 4, 6794.

Wanzlick, H. W., & Schönherr, H. J. (1968). Direct synthesis of a mercury salt-carbene complex. *Angewandte Chemie International Edition in English*, 7(2), 141-142.

Weskamp, T., Böhm, V. P., & Herrmann, W. A. (2000). N-Heterocyclic carbenes: state of the art in transition-metal-complex synthesis. *Journal of Organometallic Chemistry*, 600(1), 12-22.

Willans, C. E. (2010). Non-transition metal N-heterocyclic carbene complexes. *Organometallic Chemistry*, 36, 1-28.

Wright, F., & McDougal, W. (1972). Potassium-specific ion-exchanger microelectrodes to measure K^+ activity in the renal distal tubule. *The Yale Journal of Biology And Medicine*, 45(3-4), 373.

Xian-chen, G. H.-j. Z., Zheng-zhu, C. H.-m. Z., & Xiao-Chun, W. (2010). Comparison and optimization of total ionic strength adjustment buffer for the determination of fluoride in water [J]. *Environmental Chemistry*, 4, 042.

Yagyu, T., Tsubouchi, A., & Nishimura, Y. (2014). Syntheses and characterization of palladium (II) complexes with a bidentate bis-NHC ligand having methyl and aryl substituents on terminal nitrogen atoms. *Journal of Organometallic Chemistry*, 767, 1-5.

Yan, Z., Lu, Y., & Li, X. (2007). Silver ion-selective electrodes based on bis (dialkyldithiocarbamates) as neutral ionophores. *Sensors and Actuators B: Chemical*, 122(1), 174-181.

Yan, Z., Lu, Y., Wang, H., Wu, S., & Zhao, B. (2013). A heterocycle functionalized p-tert-butylcalix [4] arene as a neutral carrier for silver (I) ion-selective electrode. *Journal of Molecular Liquids*, 183, 72-78.

Yang, F., Zhang, C., Liu, Q., Xu, C., & Xiong, Y. L. (2015). Ca²⁺-selective electrode: A simple method to measure the phytase-aided release of bound calcium in soymilk. *Journal of Food Composition and Analysis*, 39, 43-47.

Zanganeh, A. R., & Amini, M. K. (2007). A potentiometric and voltammetric sensor based on polypyrrole film with electrochemically induced recognition sites for detection of silver ion. *Electrochimica Acta*, 52(11), 3822-3830.

Zareh, M. M. (2012). *Plasticizers and Their Role in Membrane Selective Electrodes*: INTECH Open Access Publisher.

Zhang, X.-B., Han, Z.-X., Fang, Z.-H., Shen, G.-L., & Yu, R.-Q. (2006). 5, 10, 15-Tris (pentafluorophenyl) corrole as highly selective neutral carrier for a silver ion-sensitive electrode. *Analytica Chimica Acta*, 562(2), 210-215.

SUPPLEMENTARY

LIST OF PUBLICATIONS

Nur Rahimah Said, Majid Rezayi, Leila Narimani, Nassir N. Al-Mohammed, Ninie Suhana Abdul Manan, Yatimah Alias. A New N-Heterocyclic Carbene Ionophore in Plasticizer-free Polypyrrole Membrane for Determining Ag^+ in Tap Water. Published in *Electrochimica Acta*. 2016, 197, 10-22. (DOI: 10.1016/j.electacta.2016.02.173).

Nur Rahimah Said, Majid Rezayi, Leila Narimani, Ninie Suhana Abdul Manan, Yatimah Alias. A Novel Potentiometric Self-plasticizing Polypyrrole Sensor Based on Bidentate bis-NHC Ligand for Determination of Hg(II) Cation. Published in *RSC Advances*. 2015, 5, 76263-76274. (DOI: 10.1039/C5RA10950G).

Nur Rahimah Said, Majid Rezayi, Ninie Suhana Abdul Manan, and Yatimah Alias. Thermodynamic measurements of complex formation between new bidentate bis-NHC ligand and some metal cations at different temperatures. Submitted to *Measurement*. 2014. (ID: MEAS-D-14-01491).

LIST OF PAPERS PRESENTED

Nur Rahimah Said, Ninie Suhana Abdul Manan, and Yatimah Alias. Synthesis of Characterization of New N-Heterocyclic Carbene (NHC) Complexes; The Potential of NHC Ligand as Ionophore in Potentiometric Sensor Application. The 2nd International Conference on Multidisciplinary Innovation for Sustainability and Growth (MISG). Kuala Lumpur. Malaysia. June 2015.

Nur Rahimah Said, Majid Rezayi, Ninie Suhana Abdul Manan, and Yatimah Alias. Complexation Reaction of NHCL with Ag⁺ And Pd²⁺ in Methanol-Water Media Based On Conductometric Method. The 7th HOPE Meeting with Nobel Laureates. Tokyo, Japan. March 2015.

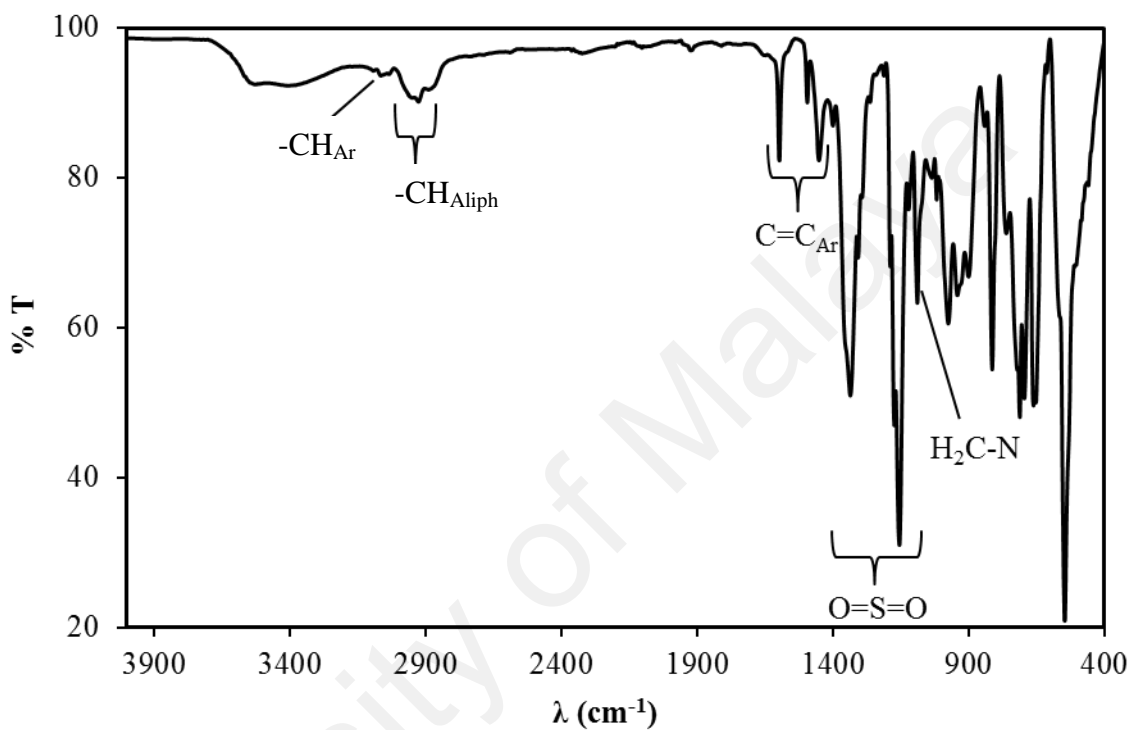
Nur Rahimah Said, Majid Rezayi, Ninie Suhana Abdul Manan, and Yatimah Alias. Synthesis and Conductometric Study of Bis[1-benzyl-benzimidazoliummethyl]-4-methylbenzenesufonamide bromide. The 6th International Conference on Postgraduate Education (ICPE-6 2014). Universiti Teknikal Malaysia Melaka, Malaysia. Dec 2014.

Nur Rahimah Said, Ninie Suhana Abdul Manan, Yatimah Alias. Synthesized and Characterization of New N-Heterocyclic Carbene Ligands based on Benzimidazole Compound. International Conference on Ionic Liquids 2013 (ICIL 2013), Langkawi Island, Malaysia, Dec 2013.

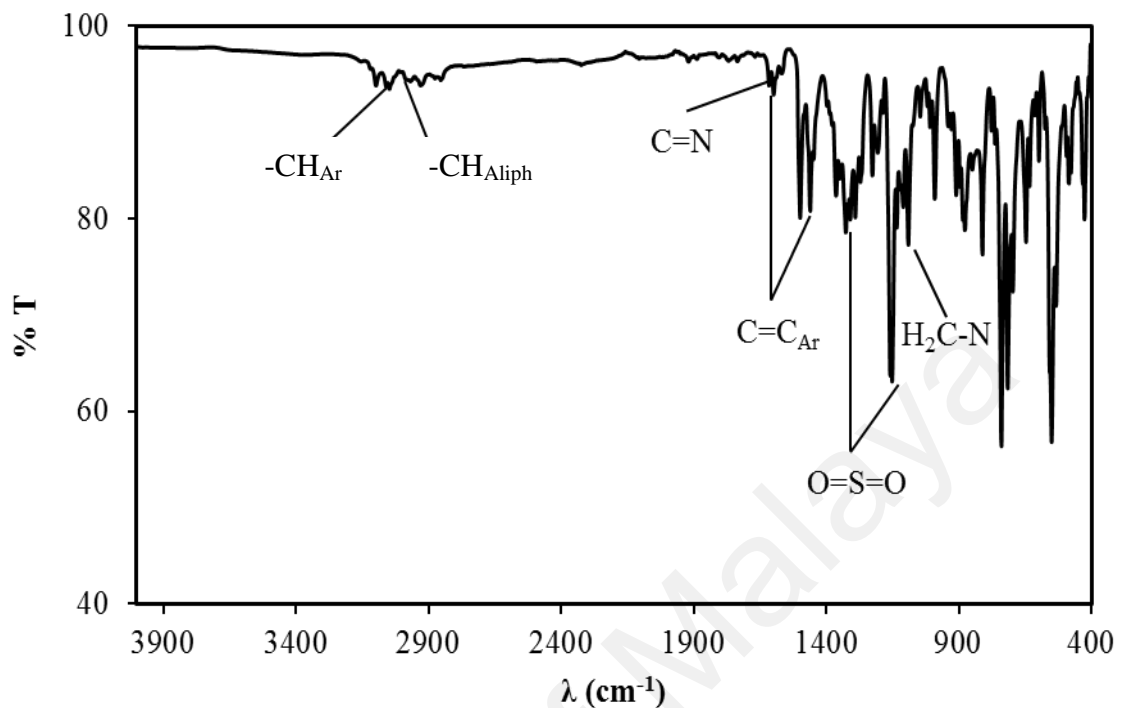
APPENDIX

APPENDIX A: FT-IR spectra of all synthesis compounds in section 4.1

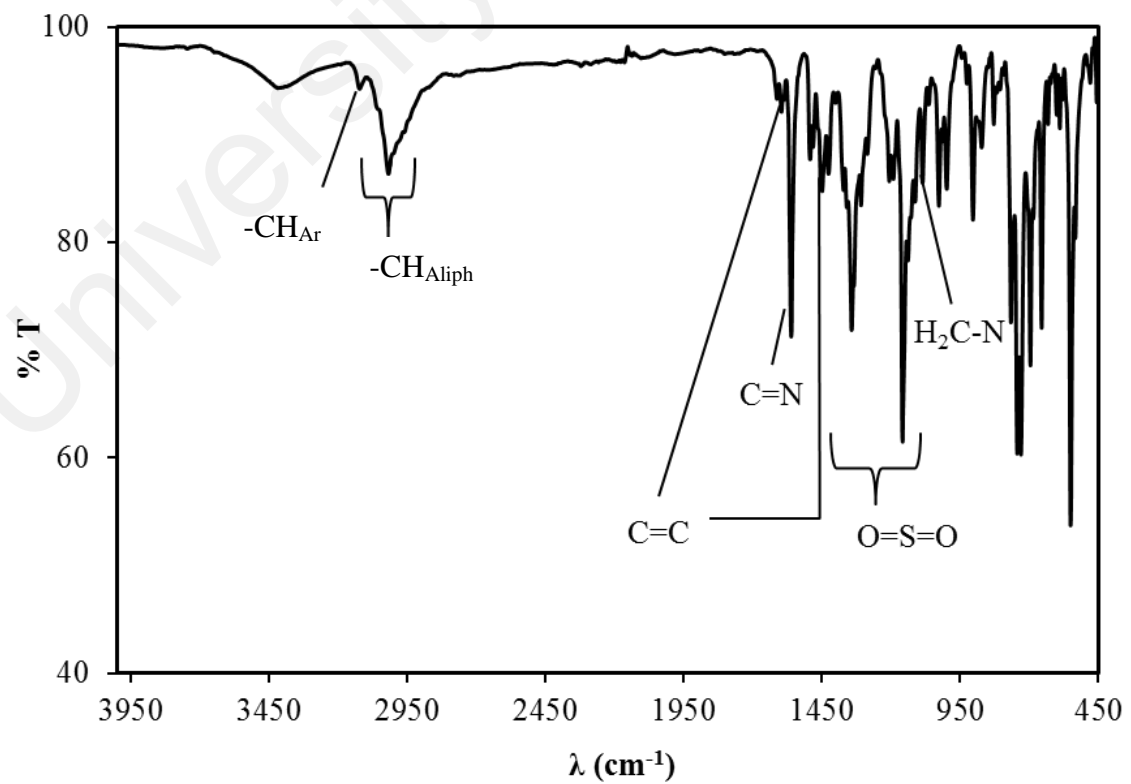
APPENDIX A1: FT-IR spectrum of *N*-[(4-methylbenzenesulfonyl)-bis-((4methylbenzenesulfonyl)-(oxy))ethyl]amine; (tri-sulfonamide)



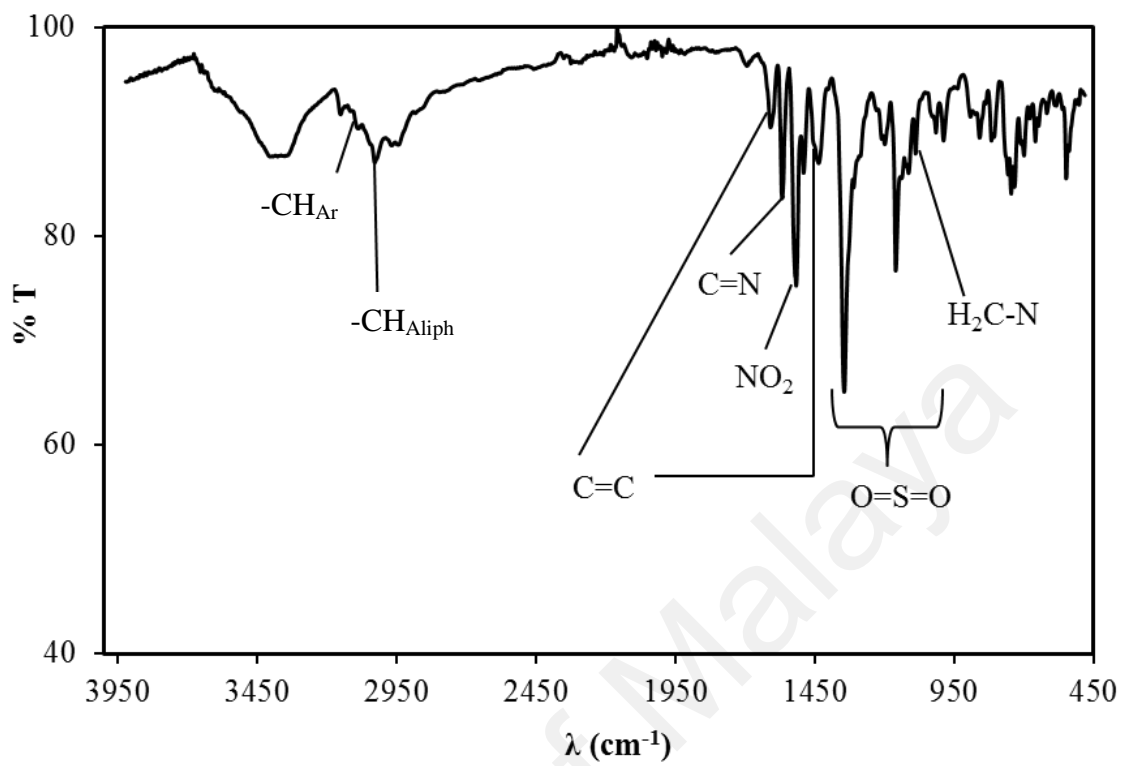
APPENDIX A2: FT-IR spectrum of *N,N'*-Bis[(benzimidazo-1-yl)ethyl]-4-methylbenzenesulfonamide; (bis-benzimidazole)



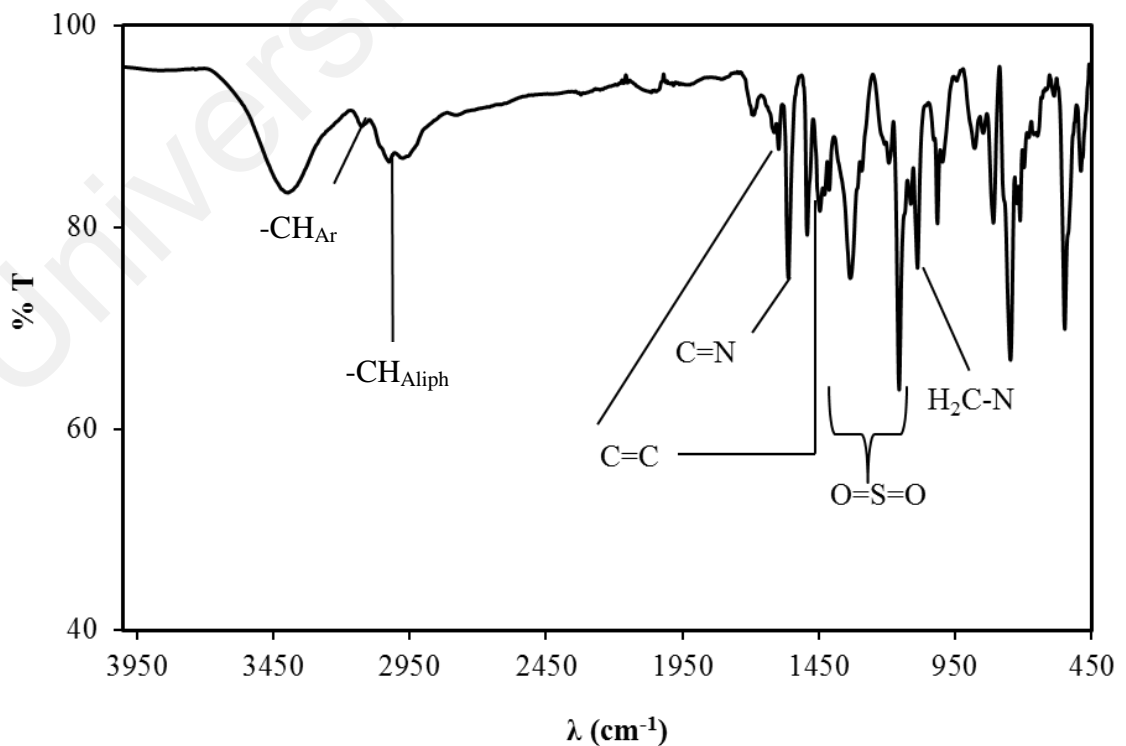
APPENDIX A3: FT-IR spectrum of *N,N'*-Bis[1-benzyl-benzimidazolium-ethyl]-4-methylbenzenesulfonamide dibromide (L₁.Br)



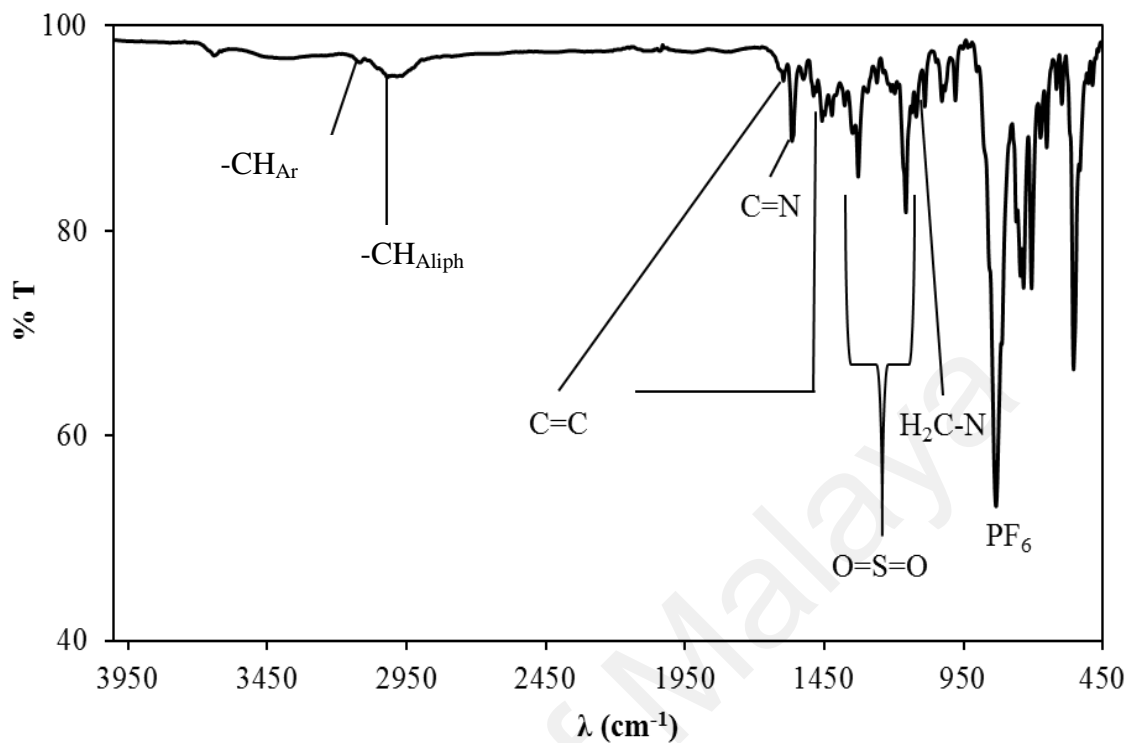
APPENDIX A4: FT-IR spectrum of *N,N'*-Bis[4-nitro-1-benzyl-benzimidazolium-ethyl]-4-methylbenzenesulfonamide dibromide ($L_2\text{Br}$)



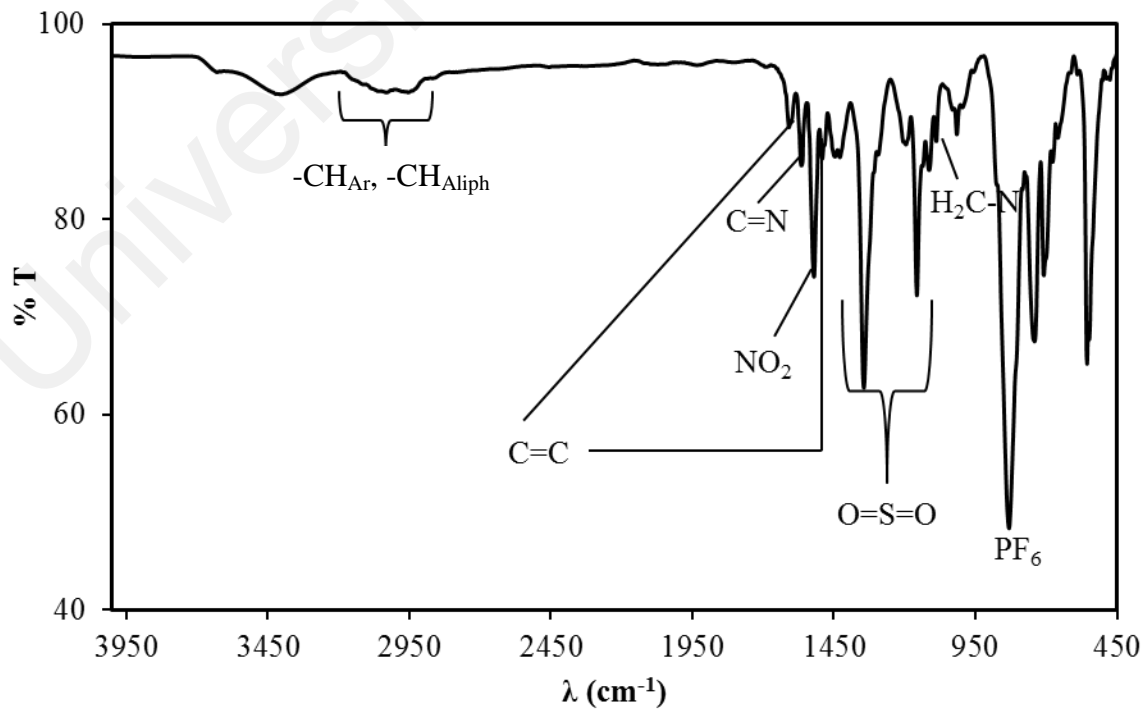
APPENDIX A5: FT-IR spectrum of *N,N'*-Bis[4-chloro-1-benzyl-benzimidazolium-ethyl]-4-methylbenzenesulfonamide dibromide ($L_3\text{Br}$)



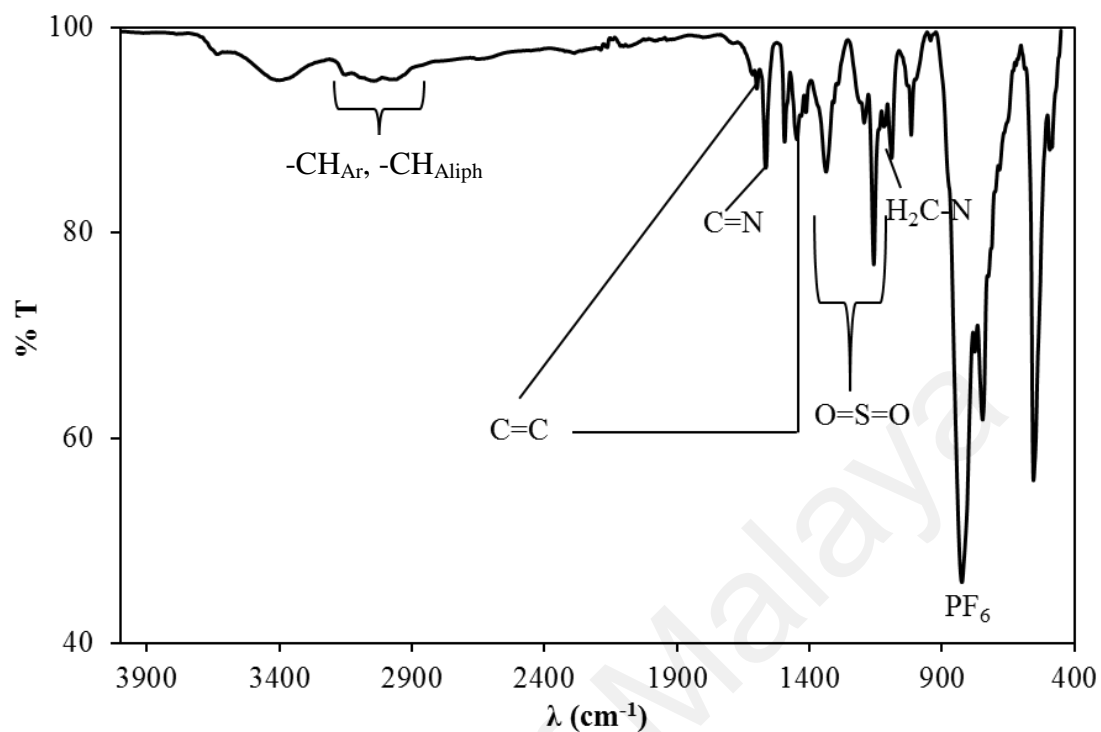
APPENDIX A6: FT-IR spectrum of *N,N'*-Bis[1-benzyl-benzimidazolium-ethyl]-4-methylbenzenesulfonamide dihexafluorophosphate ($L_1\text{.PF}_6$)



APPENDIX A7: FT-IR spectrum of *N,N'*-Bis[4-nitro-1-benzyl-benzimidazolium-ethyl]-4-methylbenzenesulfonamide dihexafluorophosphate ($L_2\text{.PF}_6$)

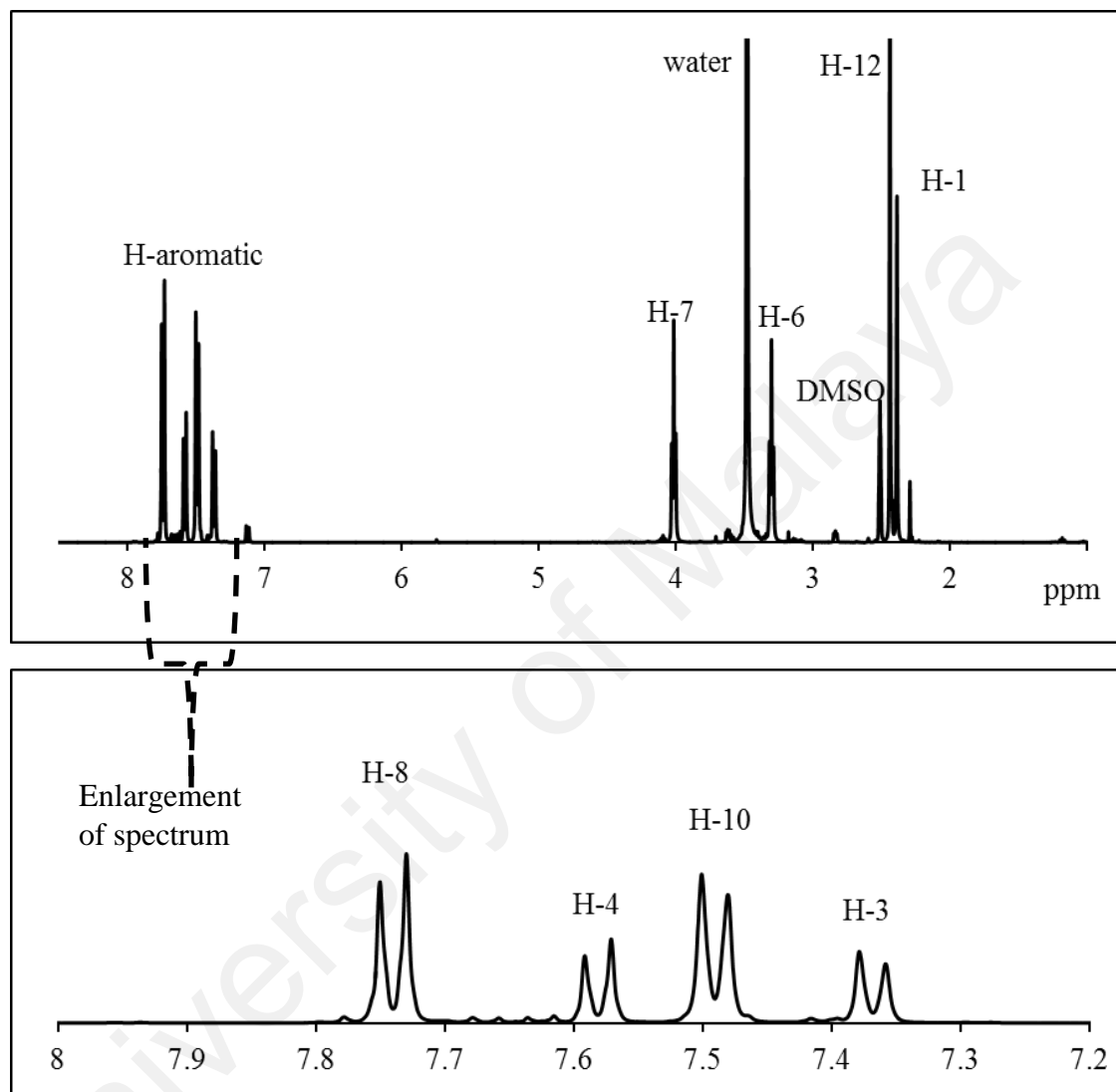


APPENDIX A8: FT-IR spectrum of *N,N'*-Bis[4-chloro-1-benzyl-benzimidazolium-ethyl]-4-methylbenzenesulfonamide dihexafluorophosphate ($L_3 \cdot PF_6$)



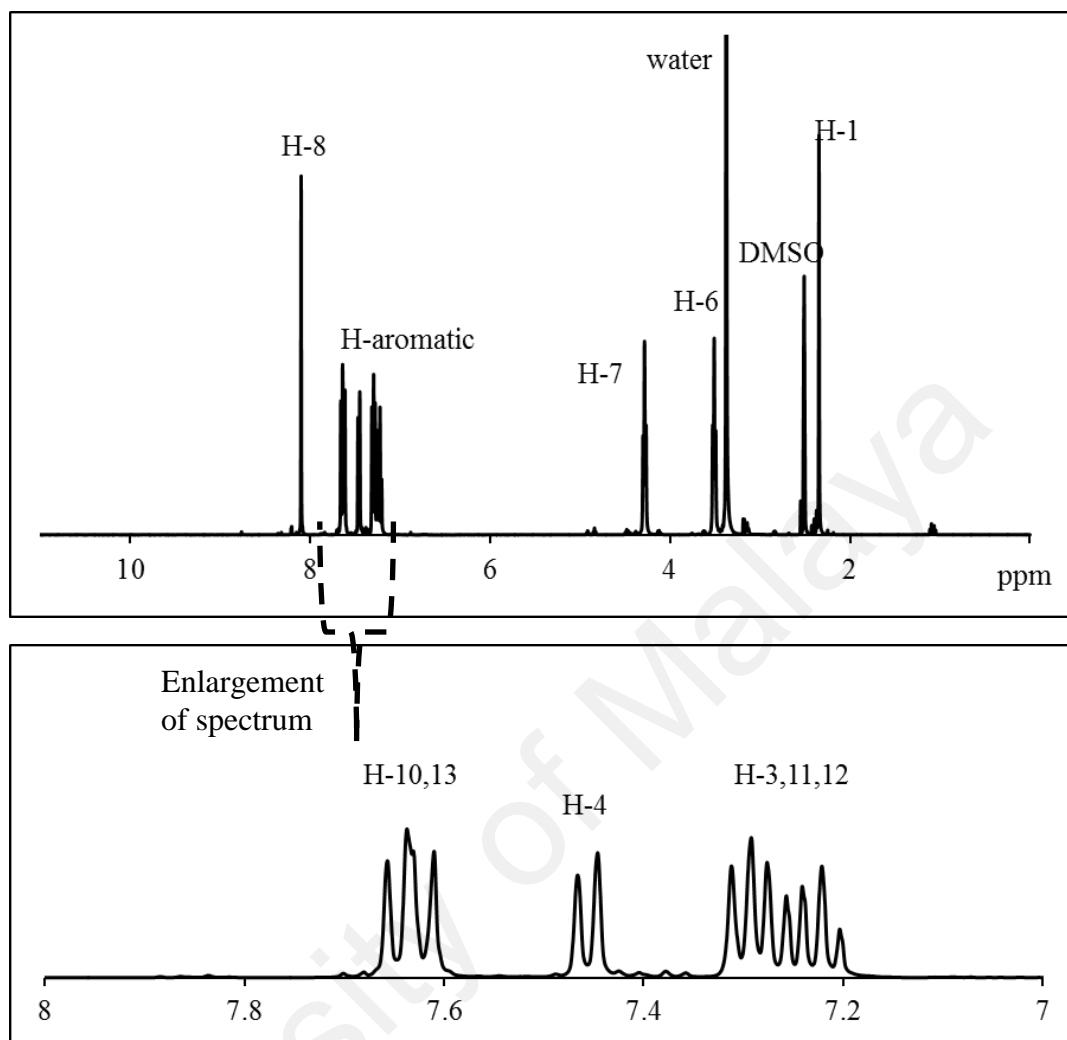
APPENDIX B: ^1H -NMR spectra of all synthesis compounds in section 4.1

APPENDIX B1: ^1H -NMR spectrum of *N*-[(4-methylbenzenesulfonyl)-bis-((4methylbenzenesulfonyl)-(oxy))ethyl]amine; (tri-sulfonamide)



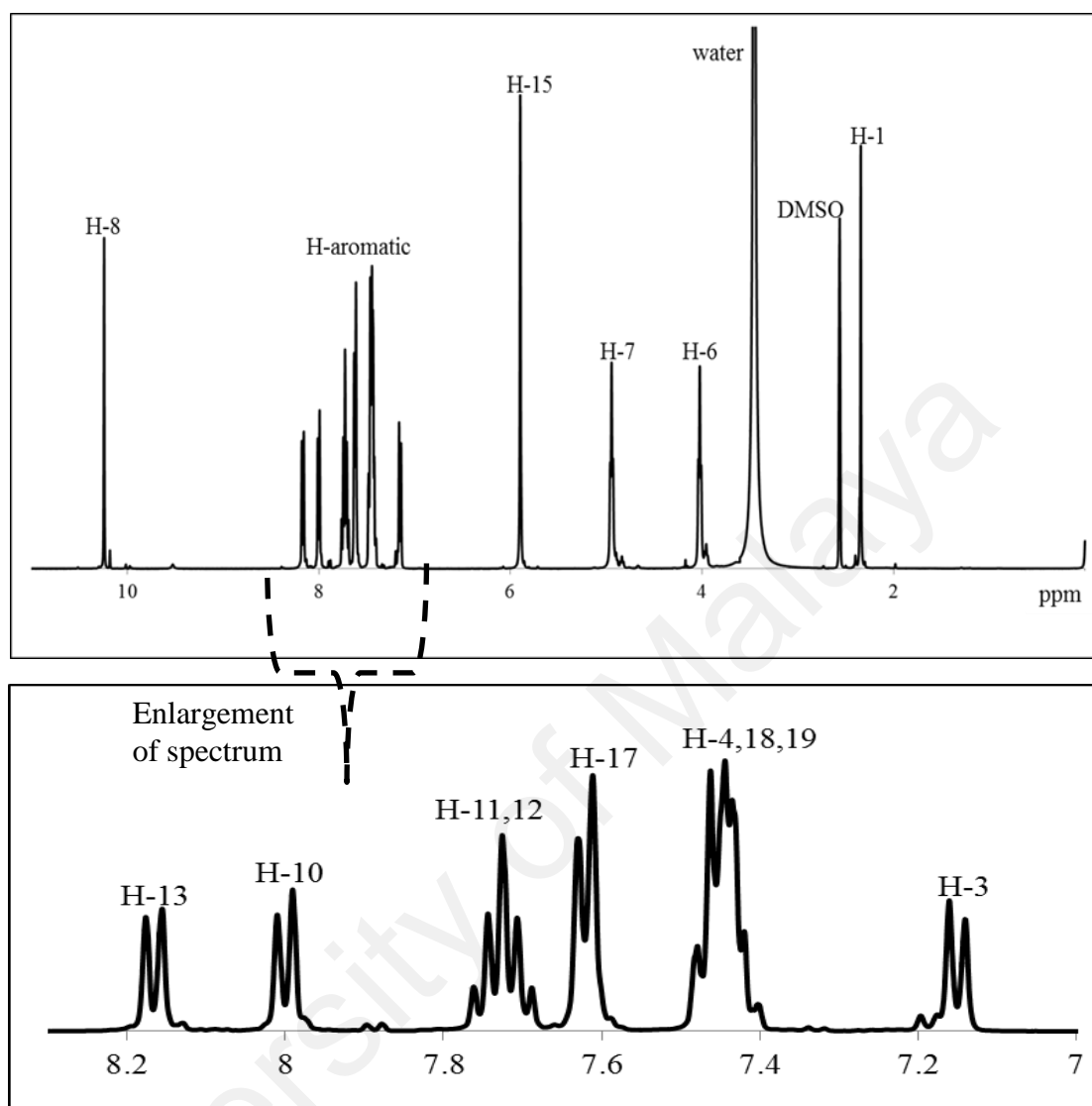
H-position	Integrations	Chemical shift, δ ppm	multiplicity	J_{HH} (Hz)
1	3H	2.39	s	-
12	6H	2.44	s	-
6	4H	3.30	t	8
7	4H	4.01	t	8
3	2H	7.37	d	8
10	4H	7.49	d	8
4	2H	7.58	d	8
8	4H	7.74	d	8

APPENDIX B2: ^1H -NMR spectrum of *N,N'*-Bis[(benzimidazo-1-yl)ethyl]-4-methylbenzenesulfonamide; (bis-benzimidazole)



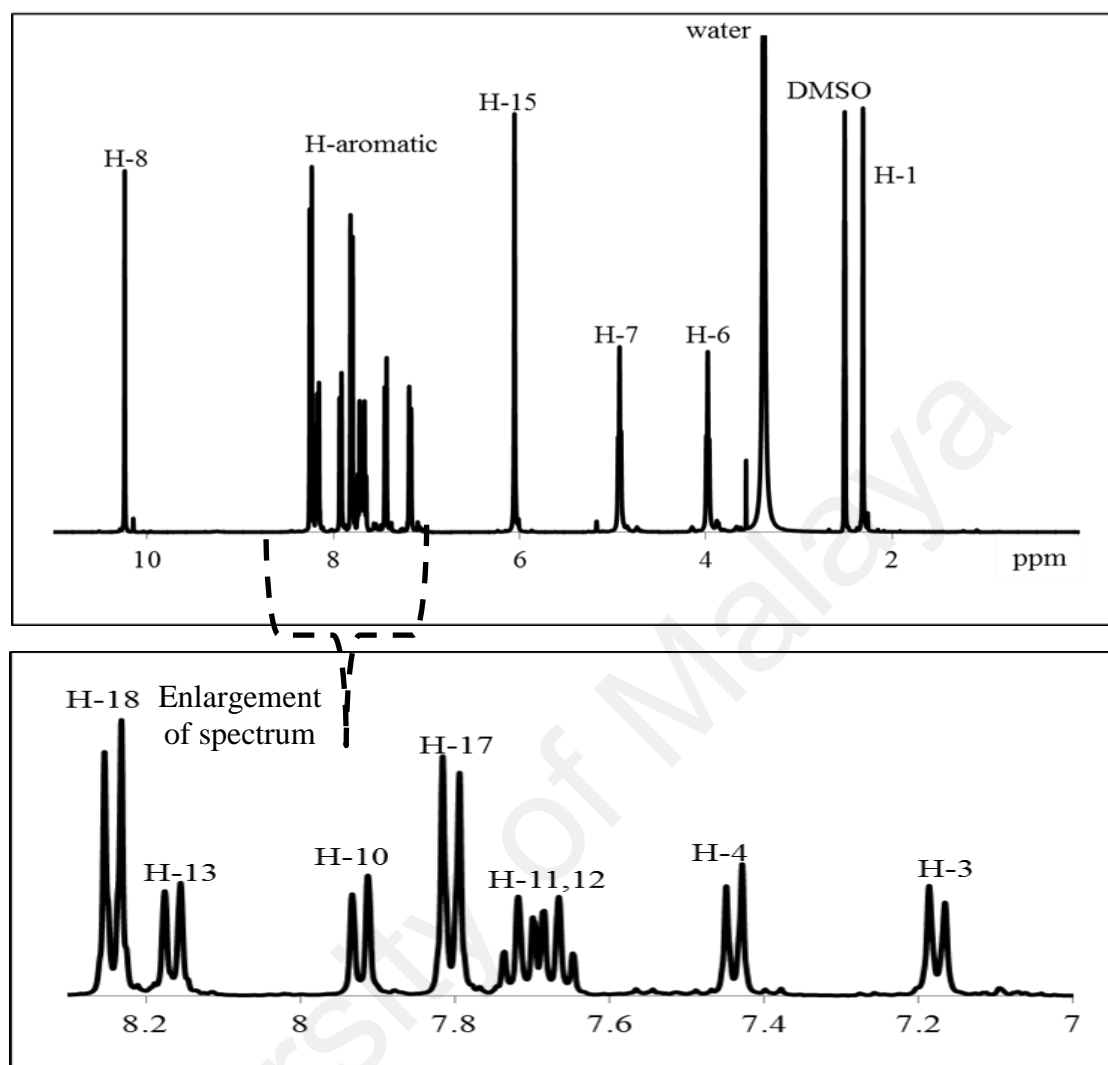
H-position	Integrations	Chemical shift, δ ppm	multiplicity	J_{HH} (Hz)
1	3H	2.34	s	-
6	4H	3.51	t	8
7	4H	4.28	t	8
3,11,12	6H	7.22, 7.31	m	-
4	2H	7.46	d	8
13,10	4H	7.61-7.66	m	-
8	2H	8.10	s	-

APPENDIX B3: ^1H -NMR spectrum of *N,N'*-Bis[1-benzyl-benzimidazolium-ethyl]-4-methylbenzenesulfonamide dibromide (L_1Br)



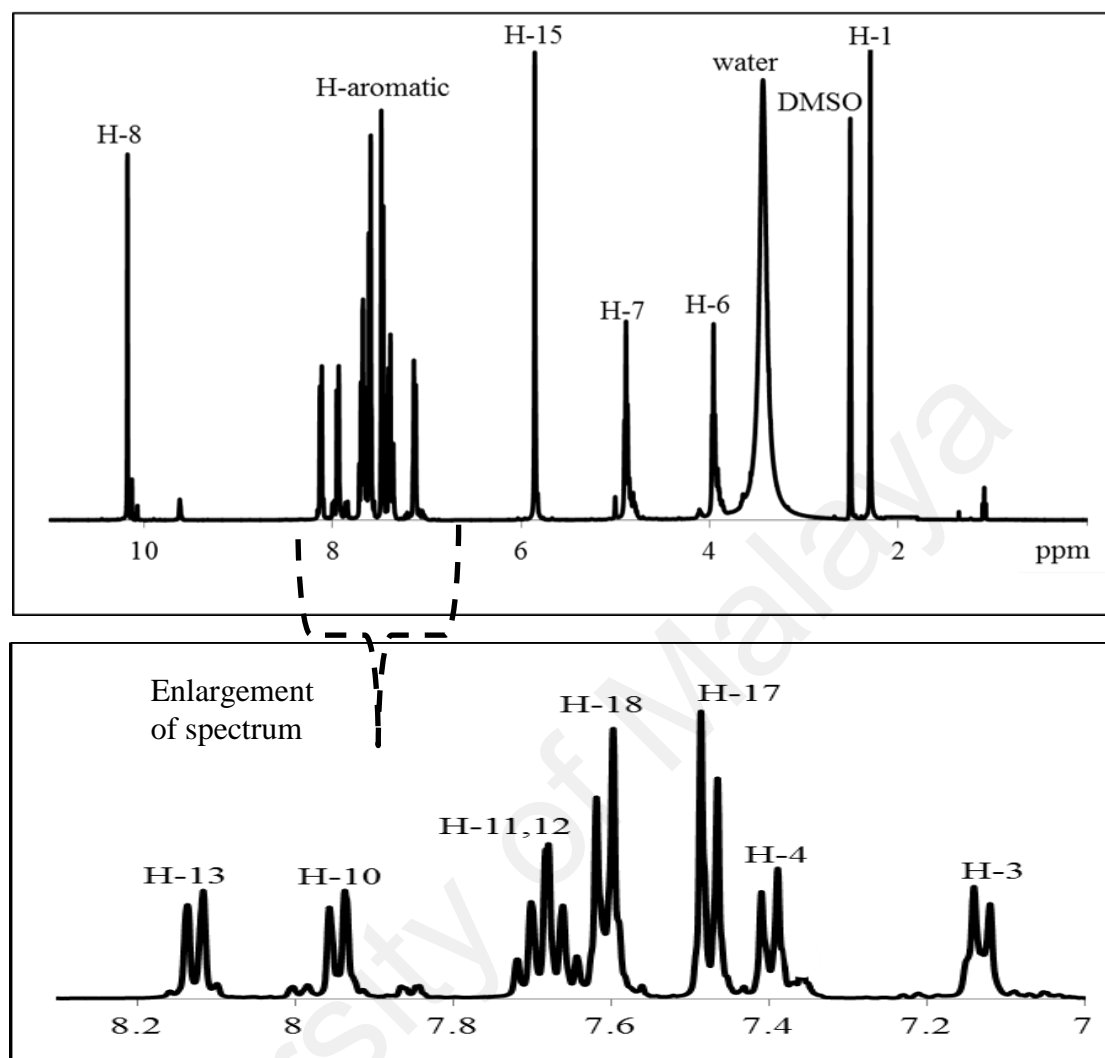
H-position	Integrations	Chemical shift, δ ppm	multiplicity	J_{HH} (Hz)
1	3H	2.34	s	-
6	4H	4.02	t	8
7	4H	4.94	t	8
15	4H	5.90	s	-
3	2H	7.15	d	8
4,18,19	8H	7.42-7.48	m	-
17	4H	7.62	d	8
11,12	4H	7.69-7.76	m	-
10	2H	8.00	d	8
13	2H	8.17	d	8
8	2H	10.24	s	-

APPENDIX B4: ^1H -NMR spectrum of *N,N'*-Bis[4-nitro-1-benzyl-benzimidazolium-ethyl]-4-methylbenzenesulfonamide dibromide (L_2Br)



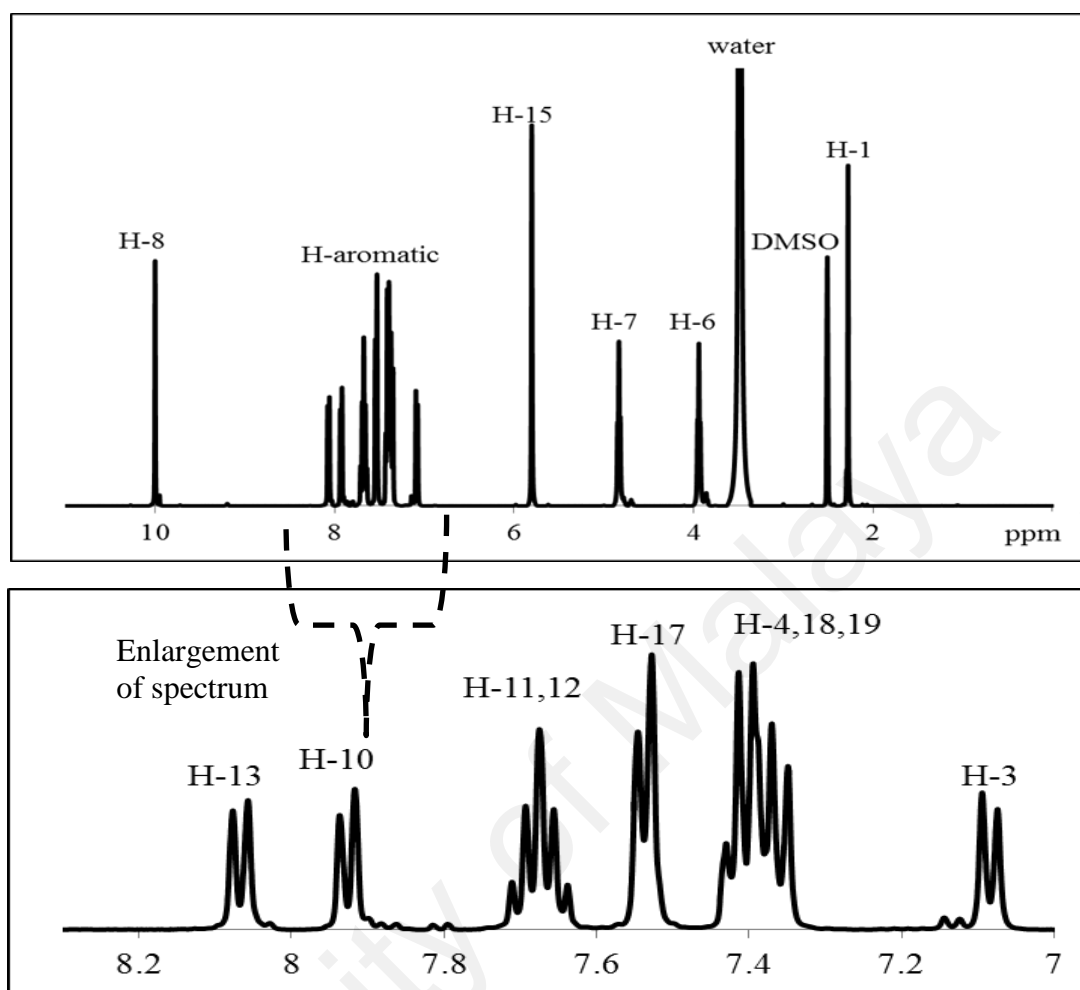
H-position	Integrations	Chemical shift, δ ppm	multiplicity	J_{HH} (Hz)
1	3H	2.31	s	-
6	4H	3.98	t	8
7	4H	4.93	t	8
15	4H	6.06	s	-
3	2H	7.17	d	8
4	2H	7.44	d	8
11,12	4H	7.65-7.74	m	-
17	4H	7.80	d	12
10	2H	7.92	d	8
13	2H	8.16	d	12
18	4H	8.24	d	8
8	2H	10.24	s	-

APPENDIX B5: ^1H -NMR spectrum of *N,N'*-Bis[4-chloro-1-benzyl-benzimidazolium-ethyl]-4-methylbenzenesulfonamide dibromide (L_3Br)



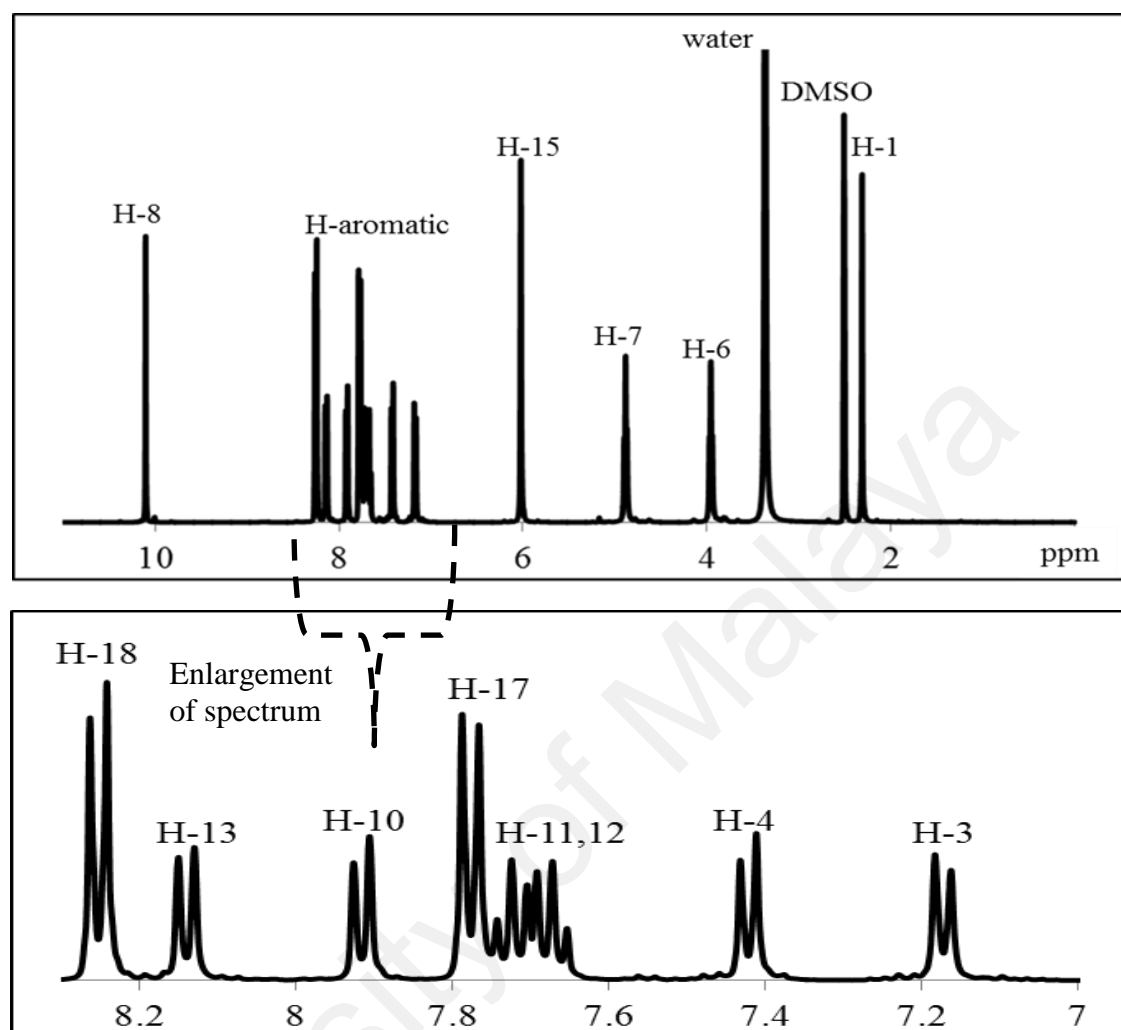
H-position	Integrations	Chemical shift, δ ppm	multiplicity	J_{HH} (Hz)
1	3H	2.30	s	-
6	4H	3.96	t	8
7	4H	4.89	t	4
15	4H	5.86	s	-
3	2H	7.13	d	8
4	2H	7.40	d	8
17	4H	7.48	d	8
18	4H	7.61	d	8
11,12	4H	7.64-7.72	m	-
10	2H	7.95	d	8
13	2H	8.13	d	8
8	2H	10.18	s	-

APPENDIX B6: ^1H -NMR spectrum of *N,N'*-Bis[1-benzyl-benzimidazolium-ethyl]-4-methylbenzenesulfonamide dihexafluorophosphate (L_1PF_6)



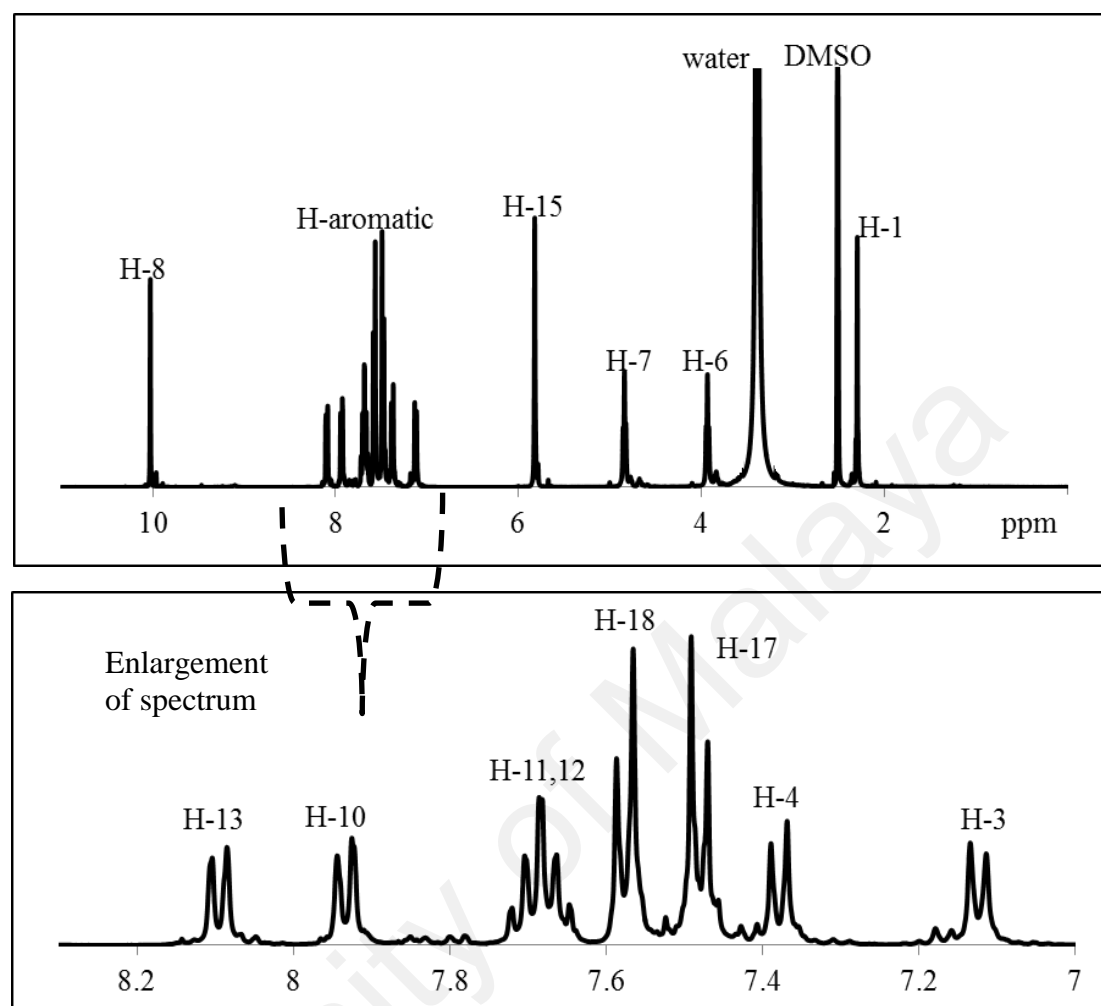
H-position	Integrations	Chemical shift, δ ppm	multiplicity	J_{HH} (Hz)
1	3H	2.28	s	-
6	4H	3.94	t	8
7	4H	4.83	t	8
15	4H	5.80	s	-
3	2H	7.08	d	8
4,18,19	8H	7.35-7.41	m	-
17	4H	7.54	d	8
11,12	4H	7.66-7.69	m	-
10	2H	7.93	d	8
13	2H	8.07	d	8
8	2H	10.00	s	-

APPENDIX B7: ^1H -NMR spectrum of *N,N'*-Bis[4-nitro-1-benzyl-benzimidazolium-ethyl]-4-methylbenzenesulfonamide dihexafluorophosphate (L_2PF_6)



H-position	Integrations	Chemical shift, δ ppm	multiplicity	J_{HH} (Hz)
1	3H	2.31	s	-
6	4H	3.96	t	4
7	4H	4.89	t	4
15	4H	6.02	s	-
3	2H	7.17	d	8
4	2H	7.42	d	8
11,12	4H	7.65-7.72	m	-
17	4H	7.76	d	8
10	2H	7.92	d	8
13	2H	8.14	d	8
18	4H	8.25	d	8
8	2H	10.10	s	-

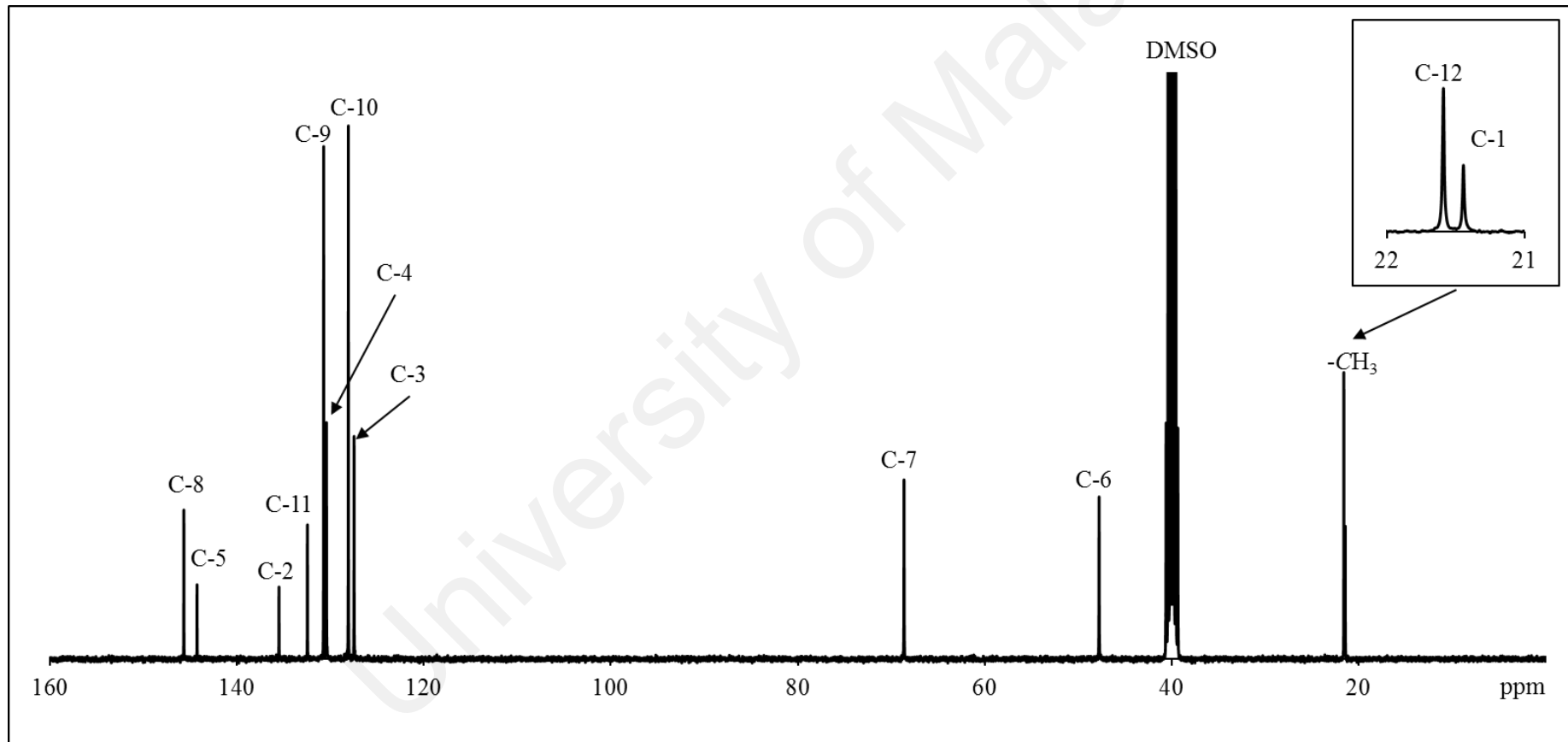
APPENDIX B8: ^1H -NMR spectrum of *N,N'*-Bis[4-chloro-1-benzyl-benzimidazolium-ethyl]-4-methylbenzenesulfonamide dihexafluorophosphate (L_3PF_6)



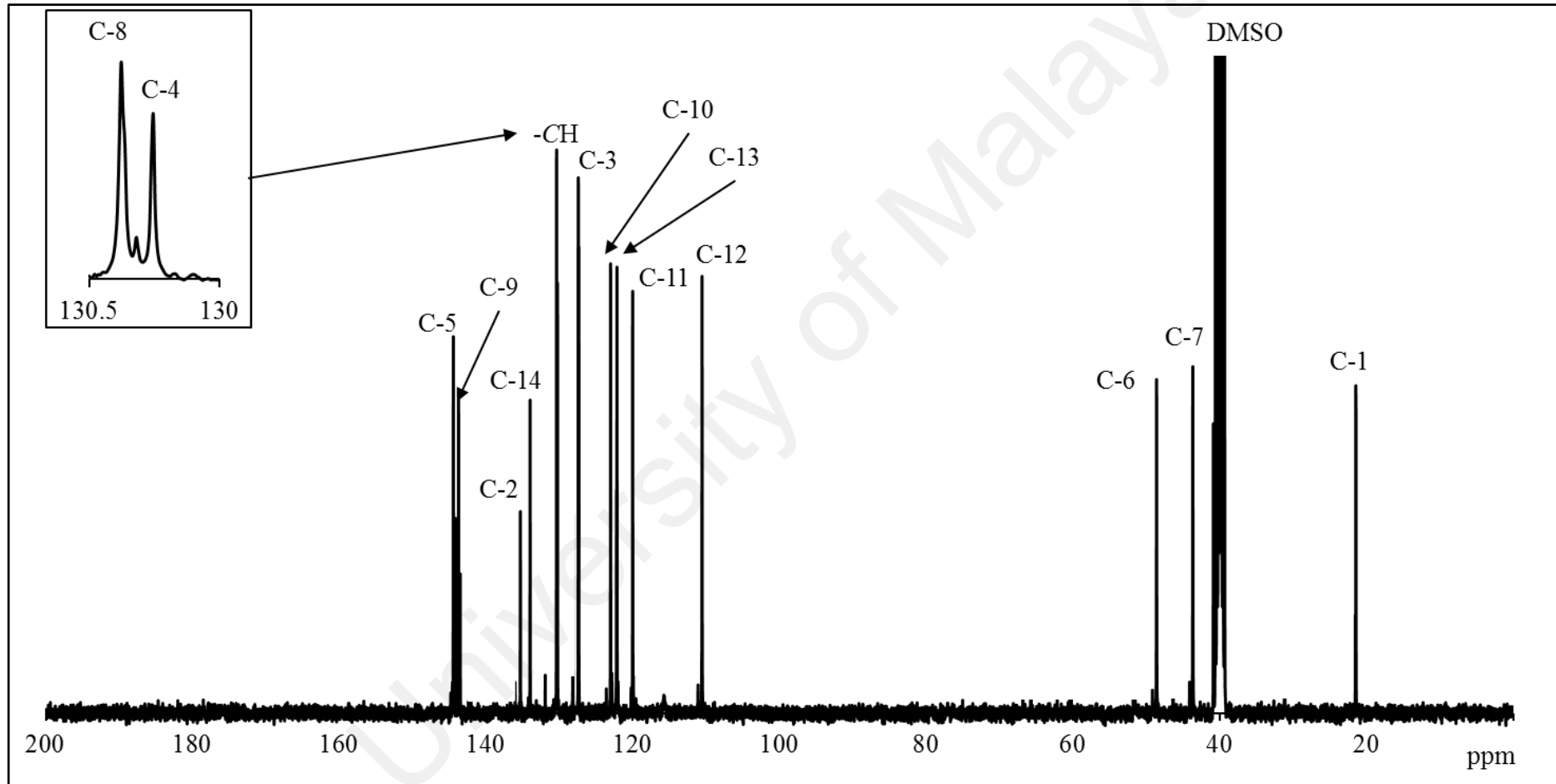
H-position	Integrations	Chemical shift, δ ppm	multiplicity	J_{HH} (Hz)
1	3H	2.30	s	-
6	4H	3.93	t	8
7	4H	4.84	t	8
15	4H	5.82	s	-
3	2H	7.12	d	8
4	2H	7.38	d	8
17	4H	7.48	d	8
18	4H	7.58	d	8
11,12	4H	7.69-7.72	m	-
10	2H	7.94	d	4
13	2H	8.09	d	4
8	2H	10.03	s	-

APPENDIX C: ^{13}C NMR spectra of all synthesis compounds in section 4.1

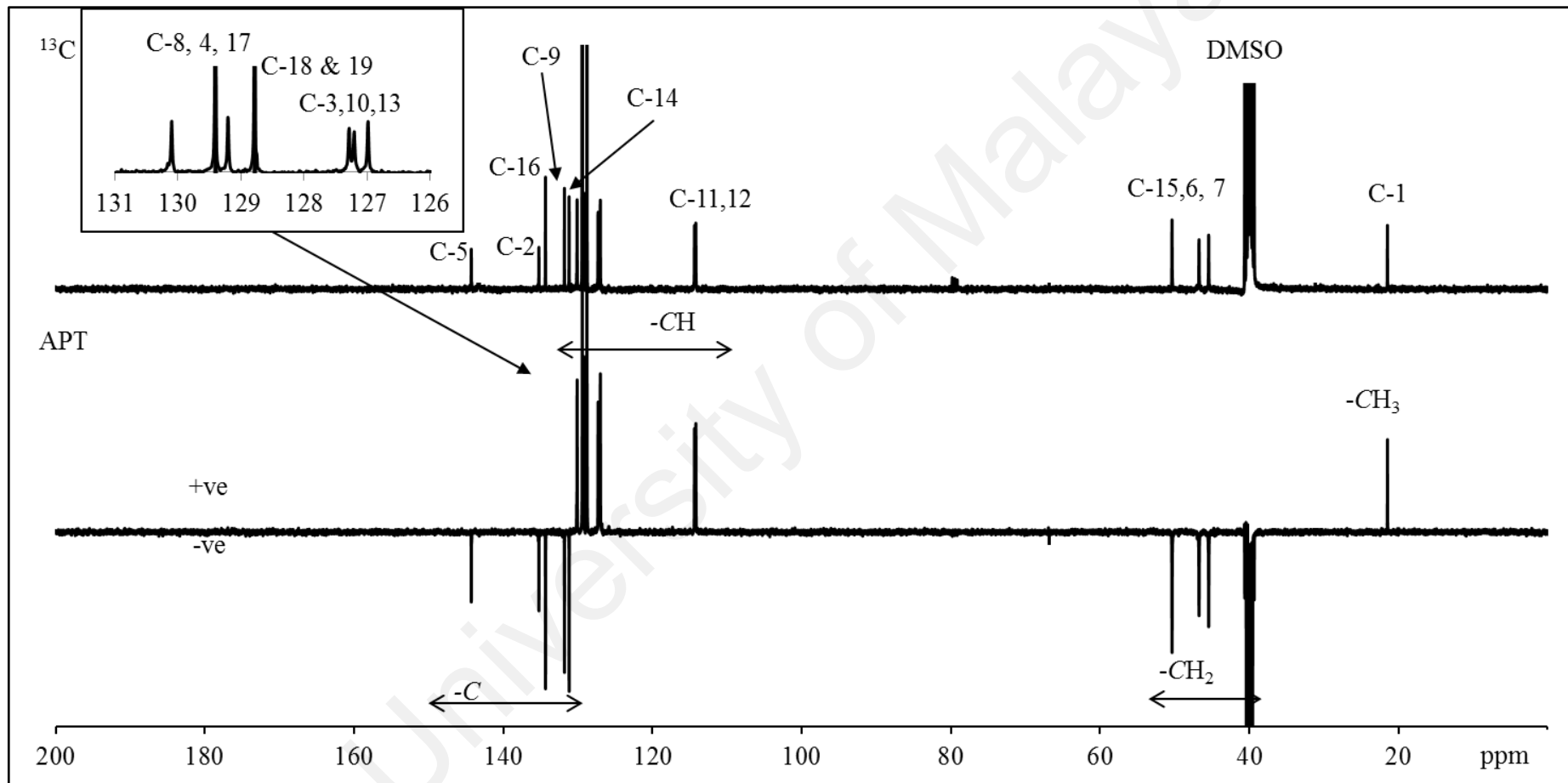
APPENDIX C1: ^{13}C -NMR spectrum of *N*-(4-methylbenzenesulfonyl)-bis-((4methylbenzenesulfonyl)-(oxy))ethyl]amine; (tri-sulfonamide)



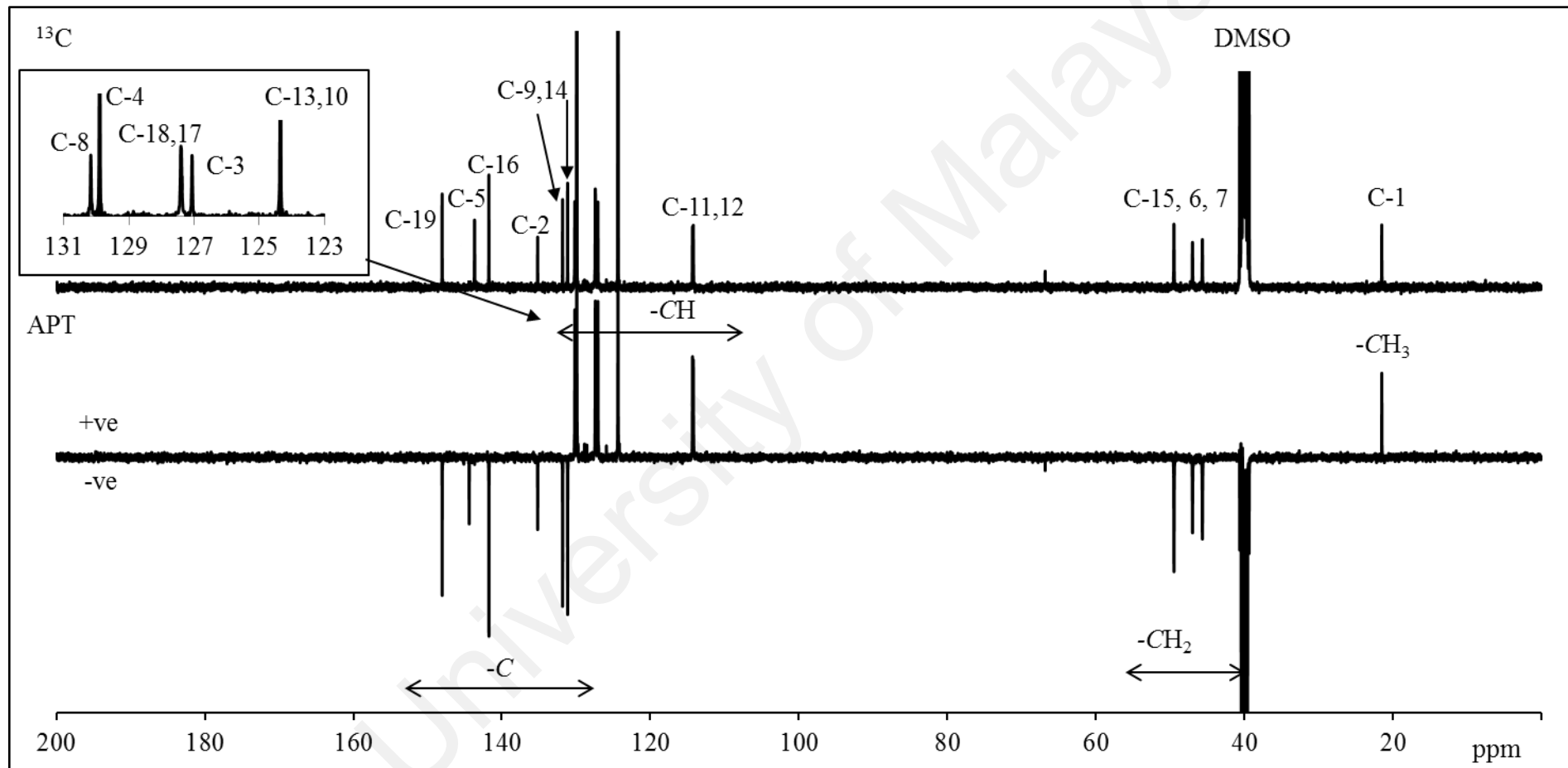
APPENDIX C2: ^{13}C -NMR spectrum of *N,N'*-Bis[(benzimidazo-1-yl)ethyl]-4-methylbenzenesulfonamide; (bis-benzimidazole)



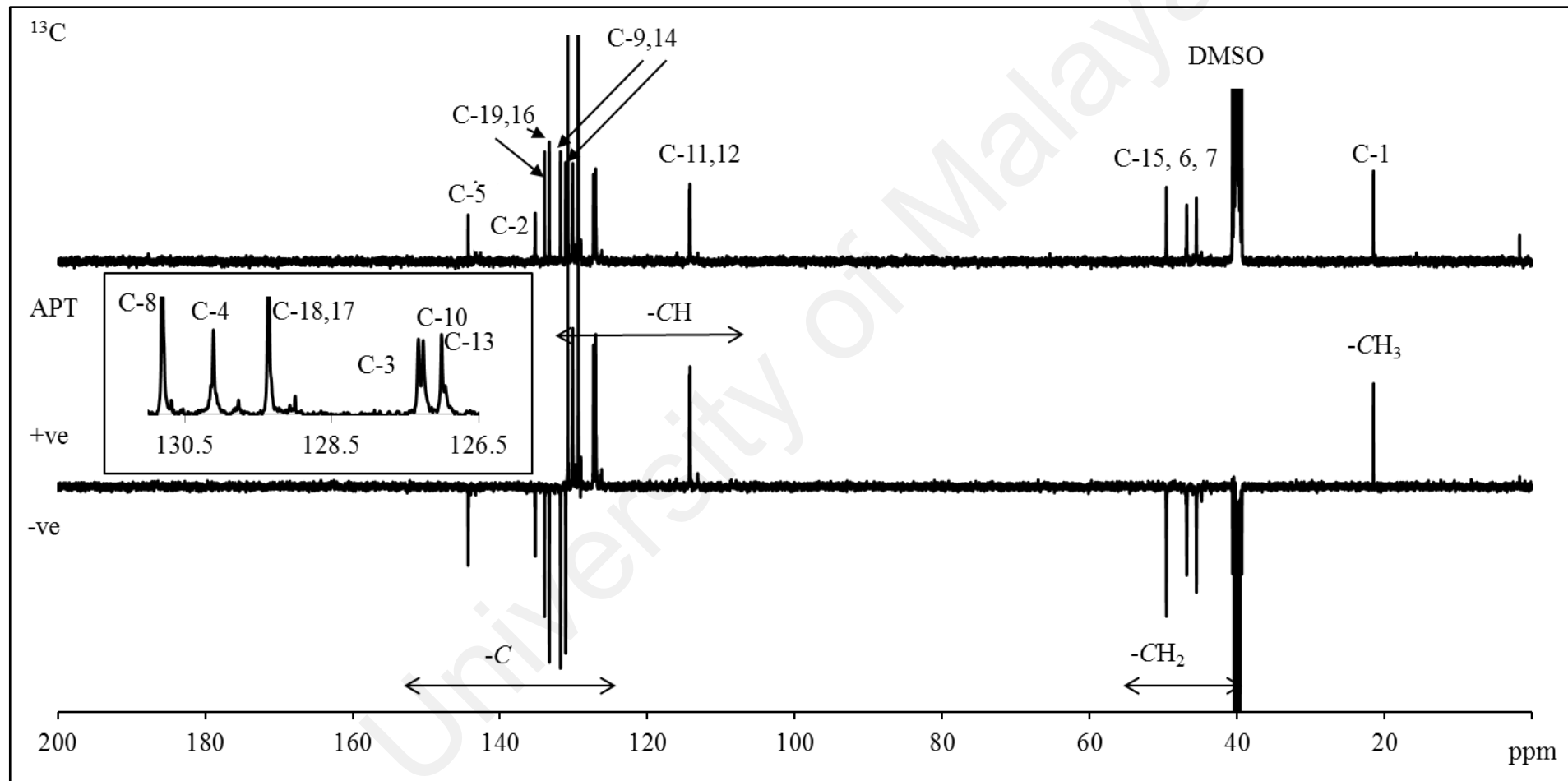
APPENDIX C3: ^{13}C -NMR spectrum of *N,N'*-Bis[1-benzyl-benzimidazolium-ethyl]-4-methylbenzenesulfonamide dibromide (L_1Br)



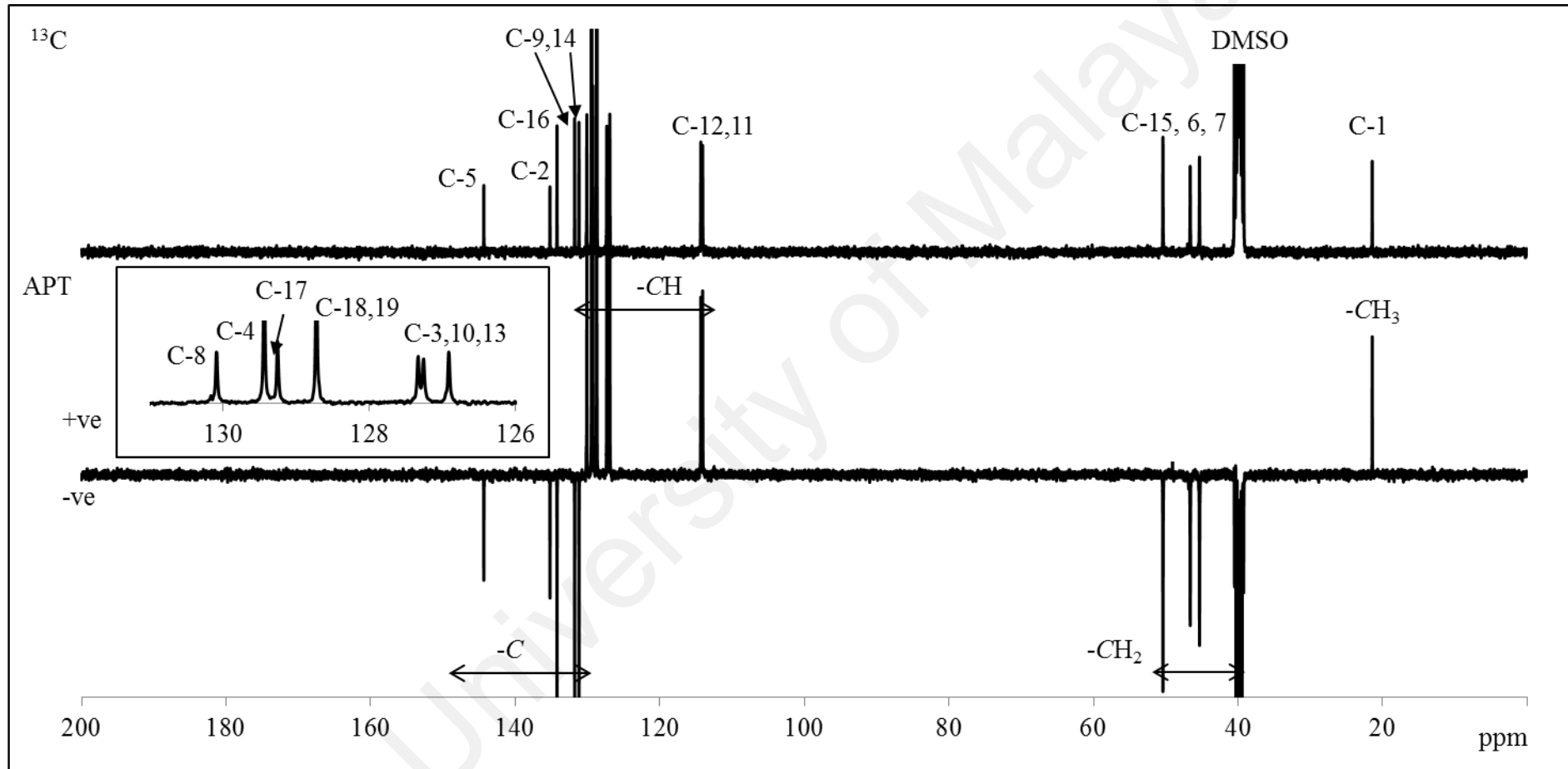
APPENDIX C4: ^{13}C -NMR spectrum of *N,N'*-Bis[4-nitro-1-benzyl-benzimidazolium-ethyl]-4-methylbenzenesulfonamide dibromide (L_2Br)



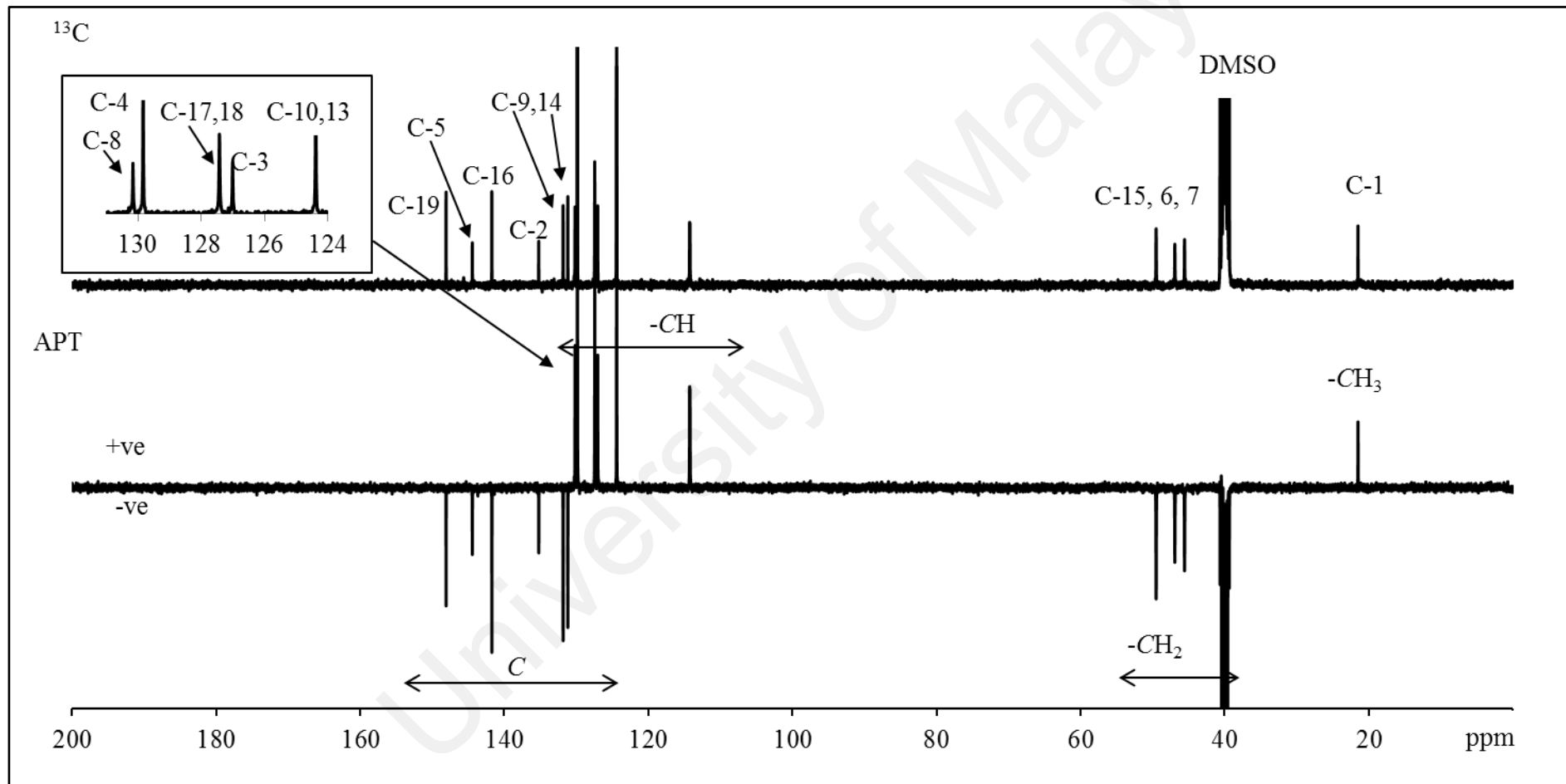
APPENDIX C5: ^{13}C -NMR spectrum of *N,N'*-Bis[4-chloro-1-benzyl-benzimidazolium-ethyl]-4-methylbenzenesulfonamide dibromide (L_3Br)



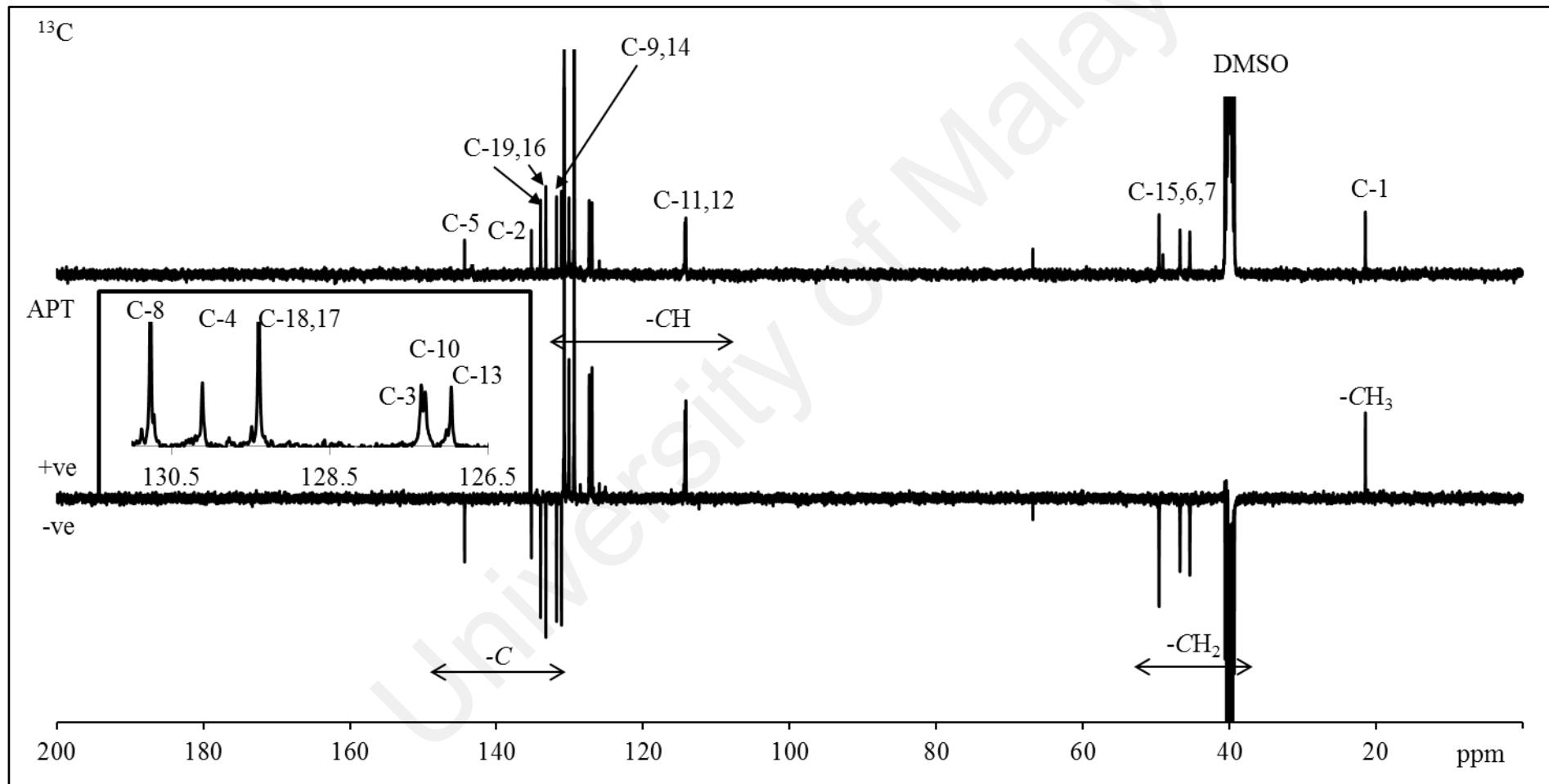
APPENDIX C6: ^{13}C -NMR spectrum of *N,N'*-Bis[1-benzyl-benzimidazolium-ethyl]-4-methylbenzenesulfonamide dihexafluorophosphate (L_1PF_6)



APPENDIX C7: ^{13}C -NMR spectrum of *N,N'*-Bis[4-nitro-1-benzyl-benzimidazolium-ethyl]-4-methylbenzenesulfonamide dihexafluorophosphate (L_2PF_6)



APPENDIX C8: ^{13}C -NMR spectrum of *N,N'*-Bis[4-chloro-1-benzyl-benzimidazolium-ethyl]-4-methylbenzenesulfonamide dihexafluorophosphate (L_3PF_6)



APPENDIX D: X-ray single crystallographic data

APPENDIX D1: Crystallographic data for *N,N'*-Bis[1-benzyl-benzimidazolium-ethyl]-4-methylbenzenesulfonamide dibromide ($L_1\cdot Br$)

Table D1.1: Crystal data and structure refinement for $L_1\cdot Br$

Empirical formula	$C_{39}H_{39}N_5O_2SBr_2$	
Formula weight	801.62	
Temperature	100.2(8) K	
Wavelength	0.71073 Å	
Crystal system, space group	Triclinic, P-1	
Unit cell dimensions	$a = 14.7495(9)$ Å	$\alpha = 108.720(5)$ deg.
	$b = 15.5216(8)$ Å	$\beta = 100.073(5)$ deg.
	$c = 19.1751(10)$ Å	$\gamma = 108.177(5)$ deg.
Volume	3761.1(3) Å ³	
Z, Calculated density	2, 1.416 Mg/m ³	
Absorption coefficient	2.251 mm ⁻¹	
F(000)	1640	
Crystal size	0.22×0.15×0.12 mm	
Theta range for data collection	2.93 to 26.50 deg.	
Limiting indices	$-18 \leq h \leq 18, -19 \leq k \leq 18, -24 \leq l \leq 24$	
Reflections collected / unique	38594 / 15583 [R(int) = 0.0786]	
Completeness to theta = 26.00	99.8 %	
Refinement method	Full-matrix least-squares on F ²	
Data / restraints / parameters	15583 / 0 / 885	
Goodness-of-fit on F ²	1.072	
Final R indices [I>2sigma(I)]	R1 = 0.0977, wR2 = 0.2737	
indices (all data)	R1 = 0.1599, wR2 = 0.3114	
Largest diff. peak and hole	2.21 and -2.81 e.Å ⁻³	

Table D1.2: Atomic coordinates ($x10^4$) and equivalent isotropic displacement parameters ($\text{\AA}^2 \times 10^3$) for $L_1.\text{Br}$. $U(\text{eq})$ is defined as one third of the trace of the orthogonalized U^{ij} tensor.

	x	y	z	U_{eq}
Br(4)	1652(1)	-3831(1)	6964(1)	40(1)
Br(3)	-42(1)	-1912(1)	5519(1)	41(1)
Br(2)	-630(1)	-3422(1)	8324(1)	50(1)
Br(1)	-838(1)	406(1)	9047(1)	53(1)
S(1)	3362(2)	1201(2)	8849(2)	15(1)
S(2)	2937(2)	-3707(2)	4140(2)	22(1)
O(1)	3715(6)	1865(6)	9654(5)	21(2)
O(4)	3231(7)	-4537(7)	3945(6)	34(2)
O(3)	3522(7)	-2853(7)	4881(5)	32(2)
O(2)	3601(6)	348(6)	8624(5)	21(2)
C(31)	3418(12)	-263(11)	5394(8)	34(1)
C(69)	-2821(12)	-4988(11)	-124(9)	33(3)
N(8)	1756(8)	-4143(7)	4103(6)	18(2)
N(1)	3372(8)	391(6)	10559(5)	13(2)
N(2)	2075(7)	-392(6)	9525(6)	12(2)
N(9)	383(7)	-3609(6)	3159(5)	11(2)
C(30)	3968(13)	387(11)	5194(8)	34(1)
N(4)	1156(7)	1497(7)	7456(6)	17(2)
N(3)	2148(8)	783(7)	8538(6)	18(2)
N(6)	3864(8)	-4243(7)	5995(6)	18(2)
C(45)	4454(9)	-3737(8)	7737(7)	16(3)
C(72)	2998(9)	-3231(8)	3426(7)	15(3)
N(5)	1288(9)	1140(7)	6292(6)	25(3)
N(10)	325(8)	-4046(7)	1926(6)	19(2)
C(21)	2142(10)	4089(9)	7616(7)	19(3)
N(7)	2335(8)	-5076(7)	5183(6)	16(2)
C(5)	3781(11)	774(8)	13010(7)	21(3)
C(4)	4736(11)	829(9)	13347(8)	26(3)
C(2)	5266(11)	1066(9)	12289(8)	24(3)
C(70)	-1971(11)	-4192(10)	-58(8)	27(3)
C(39)	4722(11)	3637(10)	7024(8)	27(3)
C(37)	4072(10)	2021(9)	7178(7)	19(3)
C(8)	3419(9)	-505(8)	10141(7)	12(2)
C(20)	1820(9)	3392(8)	7896(7)	16(3)
C(10)	3951(9)	-1807(9)	9733(7)	18(3)
C(42)	6366(10)	-3625(9)	8229(9)	29(3)
C(15)	1191(9)	-550(9)	8924(7)	19(3)
C(3)	5467(12)	971(9)	12992(8)	30(3)
C(1)	4346(10)	1026(8)	11966(6)	15(3)
C(36)	4398(9)	3012(9)	7496(7)	17(3)
C(61)	1400(11)	-1336(11)	2491(9)	32(4)
C(78)	3396(11)	-2158(11)	1653(8)	30(3)
C(51)	2592(9)	-6651(8)	4456(7)	16(3)
C(16)	1518(9)	-278(8)	8283(7)	18(3)

C(71)	-1067(11)	-4130(10)	317(7)	28(3)
C(57)	311(10)	-3688(9)	3894(7)	22(3)
C(68)	-2736(14)	-5629(10)	207(9)	40(4)
C(7)	4187(11)	1230(8)	11232(7)	21(3)
C(76)	3536(10)	-1886(9)	3039(8)	25(3)
C(9)	4135(10)	-886(9)	10295(7)	22(3)
C(67)	-1796(10)	-5546(9)	589(7)	21(3)
C(19)	1560(9)	2410(8)	7393(7)	15(3)
C(6)	3612(10)	872(9)	12331(7)	20(3)
C(56)	1317(9)	-3442(9)	4414(7)	20(3)
C(75)	3237(9)	-2537(8)	2270(7)	16(3)
C(77)	3415(10)	-2255(10)	3619(8)	26(3)
C(43)	5748(11)	-3761(8)	8667(7)	22(3)
C(22)	2206(10)	3847(9)	6870(8)	22(3)
C(40)	5077(10)	-3603(8)	7288(7)	19(3)
C(46)	4753(10)	-3404(9)	6587(7)	22(3)
C(47)	3832(10)	-5162(9)	5532(7)	18(3)
C(44)	4816(10)	-3809(8)	8437(8)	22(3)
C(48)	4562(10)	-5549(9)	5548(7)	17(3)
C(38)	3749(10)	1439(10)	7584(7)	20(3)
C(23)	1973(10)	2910(9)	6373(8)	23(3)
C(29)	3679(12)	1079(11)	5034(8)	34(1)
C(60)	1437(12)	-1039(11)	3286(9)	33(4)
C(50)	3314(10)	-7013(9)	4446(8)	23(3)
C(52)	2889(9)	-5696(9)	5023(7)	16(3)
C(11)	3146(10)	-2291(9)	9068(7)	19(3)
C(14)	2576(9)	427(9)	10172(7)	20(3)
C(41)	6059(9)	-3540(9)	7548(7)	22(3)
C(66)	-935(10)	-4768(10)	656(7)	23(3)
C(35)	4414(10)	3479(9)	8247(7)	19(3)
C(54)	1330(10)	-5315(9)	4758(8)	21(3)
C(17)	1719(10)	1529(10)	8788(8)	23(3)
C(34)	4127(9)	2935(8)	8676(7)	16(3)
C(58)	737(9)	-2741(8)	3046(7)	15(3)
C(12)	2436(9)	-1891(8)	8911(7)	15(3)
C(59)	1085(10)	-1753(9)	3565(8)	26(3)
C(63)	713(9)	-3001(9)	2285(8)	20(3)
C(74)	2808(10)	-3559(10)	2104(8)	24(3)
C(13)	2621(9)	-1001(8)	9486(7)	13(3)
C(24)	1630(9)	2168(8)	6651(8)	18(3)
C(53)	2986(10)	-4198(8)	5772(7)	17(3)
C(65)	120(11)	-4625(10)	1120(8)	27(3)
C(55)	1264(10)	-5177(9)	4002(7)	19(3)
C(25)	1016(10)	800(9)	6814(7)	19(3)
C(33)	3773(12)	1901(11)	8333(9)	34(1)
C(62)	1074(10)	-2280(10)	1986(8)	25(3)
C(49)	4263(10)	-6493(9)	4982(7)	19(3)
C(18)	842(10)	1373(10)	8106(8)	22(3)
C(73)	2680(9)	-3922(9)	2634(8)	22(3)
C(26)	1211(12)	536(11)	5485(8)	34(1)
C(27)	2194(12)	525(11)	5389(9)	34(1)
C(64)	117(10)	-4372(9)	2473(7)	19(3)

C(32)	2480(12)	-208(11)	5558(8)	34(1)
C(28)	2822(12)	1124(11)	5125(8)	34(1)

Table D1.3: Bond lengths [Å] and angles [deg] for L₁.Br.

S(1)-O(1)	1.443(9)
S(1)-O(2)	1.428(9)
S(1)-N(3)	1.624(11)
S(1)-C(33)	1.737(15)
S(2)-O(4)	1.444(10)
S(2)-O(3)	1.473(9)
S(2)-N(8)	1.639(11)
S(2)-C(72)	1.754(12)
C(31)-C(30)	1.29(2)
C(31)-C(32)	1.49(2)
C(31)-H(31)	0.9500
C(69)-C(70)	1.41(2)
C(69)-C(68)	1.37(2)
C(69)-H(69)	0.9500
N(8)-C(55)	1.472(15)
N(8)-C(56)	1.454(16)
N(1)-C(14)	1.301(17)
N(1)-C(8)	1.395(15)
N(1)-C(7)	1.487(15)
N(2)-C(14)	1.335(16)
N(2)-C(13)	1.415(15)
N(2)-C(15)	1.477(16)
N(9)-C(64)	1.348(15)
N(9)-C(58)	1.388(14)
N(9)-C(57)	1.473(15)
C(30)-C(29)	1.37(2)
C(30)-H(30)	0.9500
N(4)-C(25)	1.283(16)
N(4)-C(19)	1.409(14)
N(4)-C(18)	1.450(16)
N(3)-C(17)	1.476(16)
N(3)-C(16)	1.478(15)
N(6)-C(53)	1.322(17)
N(6)-C(47)	1.398(16)
N(6)-C(46)	1.473(15)
C(45)-C(40)	1.379(16)
C(45)-C(44)	1.407(19)
C(45)-H(45)	0.9500
C(72)-C(77)	1.337(17)
C(72)-C(73)	1.437(18)
N(5)-C(25)	1.339(16)
N(5)-C(24)	1.394(15)
N(5)-C(26)	1.493(17)
N(10)-C(64)	1.344(16)
N(10)-C(63)	1.414(16)
N(10)-C(65)	1.436(16)
C(21)-C(20)	1.351(17)
C(21)-C(22)	1.385(18)
C(21)-H(21)	0.9500

N(7)-C(53)	1.368(15)
N(7)-C(52)	1.441(16)
N(7)-C(54)	1.428(17)
C(5)-C(4)	1.41(2)
C(5)-C(6)	1.348(17)
C(5)-H(5)	0.9500
C(4)-C(3)	1.37(2)
C(4)-H(4)	0.9500
C(2)-C(1)	1.36(2)
C(2)-C(3)	1.39(2)
C(2)-H(2)	0.9500
C(70)-C(71)	1.36(2)
C(70)-H(70)	0.9500
C(39)-C(36)	1.556(16)
C(39)-H(39A)	0.9800
C(39)-H(39B)	0.9800
C(39)-H(39C)	0.9800
C(37)-C(36)	1.342(17)
C(37)-C(38)	1.401(17)
C(37)-H(37)	0.9500
C(8)-C(13)	1.360(17)
C(8)-C(9)	1.394(18)
C(20)-C(19)	1.401(16)
C(20)-H(20)	0.9500
C(10)-C(11)	1.377(18)
C(10)-C(9)	1.395(18)
C(10)-H(10)	0.9500
C(42)-C(43)	1.358(19)
C(42)-C(41)	1.37(2)
C(42)-H(42)	0.9500
C(15)-C(16)	1.527(16)
C(15)-H(15A)	0.9900
C(15)-H(15B)	0.9900
C(3)-H(3)	0.9500
C(1)-C(6)	1.388(17)
C(1)-C(7)	1.534(16)
C(36)-C(35)	1.379(17)
C(61)-C(62)	1.34(2)
C(61)-C(60)	1.43(2)
C(61)-H(61)	0.9500
C(78)-C(75)	1.503(17)
C(78)-H(78A)	0.9800
C(78)-H(78B)	0.9800
C(78)-H(78C)	0.9800
C(51)-C(50)	1.350(18)
C(51)-C(52)	1.402(17)
C(51)-H(51)	0.9500
C(16)-H(16A)	0.9900
C(16)-H(16B)	0.9900
C(71)-C(66)	1.388(19)
C(71)-H(71)	0.9500
C(57)-C(56)	1.492(18)

C(57)-H(57A)	0.9900
C(57)-H(57B)	0.9900
C(68)-C(67)	1.40(2)
C(68)-H(68)	0.9500
C(7)-H(7A)	0.9900
C(7)-H(7B)	0.9900
C(76)-C(75)	1.387(18)
C(76)-C(77)	1.419(19)
C(76)-H(76)	0.9500
C(9)-H(9)	0.9500
C(67)-C(66)	1.405(18)
C(67)-H(67)	0.9500
C(19)-C(24)	1.381(17)
C(6)-H(6)	0.9500
C(56)-H(56A)	0.9900
C(56)-H(56B)	0.9900
C(75)-C(74)	1.412(18)
C(77)-H(77)	0.9500
C(43)-C(44)	1.338(19)
C(43)-H(43)	0.9500
C(22)-C(23)	1.351(18)
C(22)-H(22)	0.9500
C(40)-C(41)	1.408(19)
C(40)-C(46)	1.505(18)
C(46)-H(46A)	0.9900
C(46)-H(46B)	0.9900
C(47)-C(52)	1.364(17)
C(47)-C(48)	1.389(18)
C(44)-H(44)	0.9500
C(48)-C(49)	1.387(17)
C(48)-H(48)	0.9500
C(38)-C(33)	1.373(18)
C(38)-H(38)	0.9500
C(23)-C(24)	1.413(16)
C(23)-H(23)	0.9500
C(29)-C(28)	1.33(2)
C(29)-H(29)	0.9500
C(60)-C(59)	1.38(2)
C(60)-H(60)	0.9500
C(50)-C(49)	1.387(19)
C(50)-H(50)	0.9500
C(11)-C(12)	1.410(18)
C(11)-H(11)	0.9500
C(14)-H(14)	0.9500
C(41)-H(41)	0.9500
C(66)-C(65)	1.56(2)
C(35)-C(34)	1.384(16)
C(35)-H(35)	0.9500
C(54)-C(55)	1.524(18)
C(54)-H(54A)	0.9900
C(54)-H(54B)	0.9900
C(17)-C(18)	1.566(19)

C(17)-H(17A)	0.9900
C(17)-H(17B)	0.9900
C(34)-C(33)	1.399(18)
C(34)-H(34)	0.9500
C(58)-C(63)	1.374(17)
C(58)-C(59)	1.399(17)
C(12)-C(13)	1.372(17)
C(12)-H(12)	0.9500
C(59)-H(59)	0.9500
C(63)-C(62)	1.418(18)
C(74)-C(73)	1.325(18)
C(74)-H(74)	0.9500
C(53)-H(53)	0.9500
C(65)-H(65A)	0.9900
C(65)-H(65B)	0.9900
C(55)-H(55A)	0.9900
C(55)-H(55B)	0.9900
C(25)-H(25)	0.9500
C(62)-H(62)	0.9500
C(49)-H(49)	0.9500
C(18)-H(18A)	0.9900
C(18)-H(18B)	0.9900
C(73)-H(73)	0.9500
C(26)-C(27)	1.50(2)
C(26)-H(26A)	0.9900
C(26)-H(26B)	0.9900
C(27)-C(32)	1.44(2)
C(27)-C(28)	1.38(2)
C(64)-H(64)	0.9500
C(32)-H(32)	0.9500
C(28)-H(28)	0.9500
O(1)-S(1)-O(2)	119.1(6)
O(1)-S(1)-N(3)	109.5(5)
O(2)-S(1)-N(3)	105.6(5)
O(1)-S(1)-C(33)	107.4(6)
O(2)-S(1)-C(33)	109.6(6)
N(3)-S(1)-C(33)	104.7(7)
O(4)-S(2)-O(3)	118.1(7)
O(4)-S(2)-N(8)	106.8(5)
O(3)-S(2)-N(8)	109.7(5)
O(4)-S(2)-C(72)	109.1(6)
O(3)-S(2)-C(72)	105.7(6)
N(8)-S(2)-C(72)	106.9(6)
C(30)-C(31)-C(32)	120.2(15)
C(30)-C(31)-H(31)	119.9
C(32)-C(31)-H(31)	119.9
C(70)-C(69)-C(68)	121.4(15)
C(70)-C(69)-H(69)	119.3
C(68)-C(69)-H(69)	119.3
C(55)-N(8)-C(56)	119.1(10)
C(55)-N(8)-S(2)	119.6(8)
C(56)-N(8)-S(2)	118.4(8)

C(14)-N(1)-C(8)	107.5(10)
C(14)-N(1)-C(7)	125.9(10)
C(8)-N(1)-C(7)	125.5(10)
C(14)-N(2)-C(13)	107.1(11)
C(14)-N(2)-C(15)	125.1(10)
C(13)-N(2)-C(15)	127.3(10)
C(64)-N(9)-C(58)	107.6(10)
C(64)-N(9)-C(57)	126.0(10)
C(58)-N(9)-C(57)	126.5(10)
C(31)-C(30)-C(29)	123.0(16)
C(31)-C(30)-H(30)	118.5
C(29)-C(30)-H(30)	118.5
C(25)-N(4)-C(19)	108.5(10)
C(25)-N(4)-C(18)	126.1(10)
C(19)-N(4)-C(18)	125.0(11)
C(17)-N(3)-C(16)	119.8(10)
C(17)-N(3)-S(1)	115.2(8)
C(16)-N(3)-S(1)	121.4(9)
C(53)-N(6)-C(47)	109.4(10)
C(53)-N(6)-C(46)	123.9(10)
C(47)-N(6)-C(46)	126.3(11)
C(40)-C(45)-C(44)	119.2(12)
C(40)-C(45)-H(45)	120.4
C(44)-C(45)-H(45)	120.4
C(77)-C(72)-C(73)	121.0(11)
C(77)-C(72)-S(2)	120.8(10)
C(73)-C(72)-S(2)	118.0(9)
C(25)-N(5)-C(24)	105.8(10)
C(25)-N(5)-C(26)	126.7(10)
C(24)-N(5)-C(26)	127.5(11)
C(64)-N(10)-C(63)	106.3(10)
C(64)-N(10)-C(65)	127.8(11)
C(63)-N(10)-C(65)	125.7(11)
C(20)-C(21)-C(22)	121.9(11)
C(20)-C(21)-H(21)	119.0
C(22)-C(21)-H(21)	119.1
C(53)-N(7)-C(52)	106.5(10)
C(53)-N(7)-C(54)	127.4(11)
C(52)-N(7)-C(54)	125.9(10)
C(4)-C(5)-C(6)	117.8(12)
C(4)-C(5)-H(5)	121.1
C(6)-C(5)-H(5)	121.1
C(5)-C(4)-C(3)	120.9(13)
C(5)-C(4)-H(4)	119.5
C(3)-C(4)-H(4)	119.6
C(1)-C(2)-C(3)	119.5(12)
C(1)-C(2)-H(2)	120.2
C(3)-C(2)-H(2)	120.2
C(71)-C(70)-C(69)	116.5(13)
C(71)-C(70)-H(70)	121.8
C(69)-C(70)-H(70)	121.7
C(36)-C(39)-H(39A)	109.5

C(36)-C(39)-H(39B)	109.5
H(39A)-C(39)-H(39B)	109.5
C(36)-C(39)-H(39C)	109.5
H(39A)-C(39)-H(39C)	109.5
H(39B)-C(39)-H(39C)	109.5
C(36)-C(37)-C(38)	122.2(11)
C(36)-C(37)-H(37)	118.9
C(38)-C(37)-H(37)	118.9
C(13)-C(8)-C(9)	121.6(11)
C(13)-C(8)-N(1)	108.2(10)
C(9)-C(8)-N(1)	130.1(11)
C(21)-C(20)-C(19)	116.4(11)
C(21)-C(20)-H(20)	121.8
C(19)-C(20)-H(20)	121.8
C(11)-C(10)-C(9)	123.0(12)
C(11)-C(10)-H(10)	118.5
C(9)-C(10)-H(10)	118.5
C(43)-C(42)-C(41)	121.6(13)
C(43)-C(42)-H(42)	119.2
C(41)-C(42)-H(42)	119.2
N(2)-C(15)-C(16)	109.9(10)
N(2)-C(15)-H(15A)	109.7
C(16)-C(15)-H(15A)	109.7
N(2)-C(15)-H(15B)	109.7
C(16)-C(15)-H(15B)	109.7
H(15A)-C(15)-H(15B)	108.2
C(2)-C(3)-C(4)	119.7(14)
C(2)-C(3)-H(3)	120.1
C(4)-C(3)-H(3)	120.1
C(6)-C(1)-C(2)	119.9(11)
C(6)-C(1)-C(7)	122.2(12)
C(2)-C(1)-C(7)	117.8(11)
C(37)-C(36)-C(35)	119.4(11)
C(37)-C(36)-C(39)	121.1(11)
C(35)-C(36)-C(39)	119.5(11)
C(62)-C(61)-C(60)	124.4(13)
C(62)-C(61)-H(61)	117.8
C(60)-C(61)-H(61)	117.8
C(75)-C(78)-H(78A)	109.5
C(75)-C(78)-H(78B)	109.5
H(78A)-C(78)-H(78B)	109.5
C(75)-C(78)-H(78C)	109.5
H(78A)-C(78)-H(78C)	109.5
H(78B)-C(78)-H(78C)	109.5
C(50)-C(51)-C(52)	115.0(12)
C(50)-C(51)-H(51)	122.5
C(52)-C(51)-H(51)	122.5
N(3)-C(16)-C(15)	113.9(10)
N(3)-C(16)-H(16A)	108.8
C(15)-C(16)-H(16A)	108.8
N(3)-C(16)-H(16B)	108.8
C(15)-C(16)-H(16B)	108.8

H(16A)-C(16)-H(16B)	107.7
C(70)-C(71)-C(66)	124.6(13)
C(70)-C(71)-H(71)	117.7
C(66)-C(71)-H(71)	117.7
N(9)-C(57)-C(56)	111.0(10)
N(9)-C(57)-H(57A)	109.4
C(56)-C(57)-H(57A)	109.4
N(9)-C(57)-H(57B)	109.4
C(56)-C(57)-H(57B)	109.4
H(57A)-C(57)-H(57B)	108.0
C(67)-C(68)-C(69)	120.8(14)
C(67)-C(68)-H(68)	119.6
C(69)-C(68)-H(68)	119.6
N(1)-C(7)-C(1)	113.4(9)
N(1)-C(7)-H(7A)	108.9
C(1)-C(7)-H(7A)	108.9
N(1)-C(7)-H(7B)	108.9
C(1)-C(7)-H(7B)	108.9
H(7A)-C(7)-H(7B)	107.7
C(75)-C(76)-C(77)	120.1(11)
C(75)-C(76)-H(76)	119.9
C(77)-C(76)-H(76)	119.9
C(8)-C(9)-C(10)	114.5(12)
C(8)-C(9)-H(9)	122.8
C(10)-C(9)-H(9)	122.8
C(68)-C(67)-C(66)	119.1(12)
C(68)-C(67)-H(67)	120.5
C(66)-C(67)-H(67)	120.5
C(24)-C(19)-N(4)	105.1(10)
C(24)-C(19)-C(20)	121.8(10)
N(4)-C(19)-C(20)	133.0(11)
C(1)-C(6)-C(5)	122.1(13)
C(1)-C(6)-H(6)	119.0
C(5)-C(6)-H(6)	118.9
N(8)-C(56)-C(57)	112.8(11)
N(8)-C(56)-H(56A)	109.0
C(57)-C(56)-H(56A)	109.0
N(8)-C(56)-H(56B)	109.0
C(57)-C(56)-H(56B)	109.0
H(56A)-C(56)-H(56B)	107.8
C(76)-C(75)-C(74)	117.1(11)
C(76)-C(75)-C(78)	120.7(11)
C(74)-C(75)-C(78)	122.2(11)
C(72)-C(77)-C(76)	120.1(12)
C(72)-C(77)-H(77)	120.0
C(76)-C(77)-H(77)	119.9
C(44)-C(43)-C(42)	119.9(12)
C(44)-C(43)-H(43)	120.0
C(42)-C(43)-H(43)	120.0
C(23)-C(22)-C(21)	123.3(12)
C(23)-C(22)-H(22)	118.3
C(21)-C(22)-H(22)	118.4

C(45)-C(40)-C(41)	118.7(12)
C(45)-C(40)-C(46)	120.2(12)
C(41)-C(40)-C(46)	120.7(11)
N(6)-C(46)-C(40)	112.0(10)
N(6)-C(46)-H(46A)	109.2
C(40)-C(46)-H(46A)	109.2
N(6)-C(46)-H(46B)	109.2
C(40)-C(46)-H(46B)	109.2
H(46A)-C(46)-H(46B)	107.9
C(52)-C(47)-C(48)	121.9(12)
C(52)-C(47)-N(6)	107.6(12)
C(48)-C(47)-N(6)	130.5(12)
C(43)-C(44)-C(45)	121.1(11)
C(43)-C(44)-H(44)	119.4
C(45)-C(44)-H(44)	119.4
C(49)-C(48)-C(47)	114.3(12)
C(49)-C(48)-H(48)	122.9
C(47)-C(48)-H(48)	122.9
C(37)-C(38)-C(33)	118.6(12)
C(37)-C(38)-H(38)	120.7
C(33)-C(38)-H(38)	120.7
C(22)-C(23)-C(24)	115.8(12)
C(22)-C(23)-H(23)	122.1
C(24)-C(23)-H(23)	122.1
C(28)-C(29)-C(30)	119.1(15)
C(28)-C(29)-H(29)	120.5
C(30)-C(29)-H(29)	120.4
C(61)-C(60)-C(59)	119.4(13)
C(61)-C(60)-H(60)	120.3
C(59)-C(60)-H(60)	120.3
C(51)-C(50)-C(49)	122.2(12)
C(51)-C(50)-H(50)	118.9
C(49)-C(50)-H(50)	118.9
C(47)-C(52)-C(51)	123.3(12)
C(47)-C(52)-N(7)	106.7(10)
C(51)-C(52)-N(7)	130.0(11)
C(10)-C(11)-C(12)	122.1(11)
C(10)-C(11)-H(11)	118.9
C(12)-C(11)-H(11)	118.9
N(1)-C(14)-N(2)	111.5(11)
N(1)-C(14)-H(14)	124.3
N(2)-C(14)-H(14)	124.3
C(40)-C(41)-C(42)	119.5(11)
C(40)-C(41)-H(41)	120.3
C(42)-C(41)-H(41)	120.3
C(71)-C(66)-C(67)	117.6(13)
C(71)-C(66)-C(65)	122.3(12)
C(67)-C(66)-C(65)	120.1(12)
C(36)-C(35)-C(34)	120.4(11)
C(36)-C(35)-H(35)	119.8
C(34)-C(35)-H(35)	119.8
N(7)-C(54)-C(55)	112.4(10)

N(7)-C(54)-H(54A)	109.1
C(55)-C(54)-H(54A)	109.1
N(7)-C(54)-H(54B)	109.1
C(55)-C(54)-H(54B)	109.1
H(54A)-C(54)-H(54B)	107.9
N(3)-C(17)-C(18)	110.7(11)
N(3)-C(17)-H(17A)	109.5
C(18)-C(17)-H(17A)	109.5
N(3)-C(17)-H(17B)	109.5
C(18)-C(17)-H(17B)	109.5
H(17A)-C(17)-H(17B)	108.1
C(33)-C(34)-C(35)	119.6(11)
C(33)-C(34)-H(34)	120.2
C(35)-C(34)-H(34)	120.2
C(63)-C(58)-N(9)	107.4(10)
C(63)-C(58)-C(59)	122.2(11)
N(9)-C(58)-C(59)	130.4(12)
C(11)-C(12)-C(13)	113.3(12)
C(11)-C(12)-H(12)	123.3
C(13)-C(12)-H(12)	123.3
C(60)-C(59)-C(58)	116.9(13)
C(60)-C(59)-H(59)	121.5
C(58)-C(59)-H(59)	121.6
C(58)-C(63)-C(62)	121.8(11)
C(58)-C(63)-N(10)	107.7(10)
C(62)-C(63)-N(10)	130.5(12)
C(73)-C(74)-C(75)	124.0(12)
C(73)-C(74)-H(74)	118.0
C(75)-C(74)-H(74)	118.0
C(8)-C(13)-C(12)	125.4(12)
C(8)-C(13)-N(2)	105.6(10)
C(12)-C(13)-N(2)	128.9(12)
C(23)-C(24)-N(5)	131.2(12)
C(23)-C(24)-C(19)	120.8(11)
N(5)-C(24)-C(19)	108.0(10)
N(6)-C(53)-N(7)	109.7(11)
N(6)-C(53)-H(53)	125.1
N(7)-C(53)-H(53)	125.1
N(10)-C(65)-C(66)	109.7(10)
N(10)-C(65)-H(65A)	109.7
C(66)-C(65)-H(65A)	109.7
N(10)-C(65)-H(65B)	109.7
C(66)-C(65)-H(65B)	109.7
H(65A)-C(65)-H(65B)	108.2
N(8)-C(55)-C(54)	114.0(10)
N(8)-C(55)-H(55A)	108.8
C(54)-C(55)-H(55A)	108.8
N(8)-C(55)-H(55B)	108.8
C(54)-C(55)-H(55B)	108.8
H(55A)-C(55)-H(55B)	107.6
N(4)-C(25)-N(5)	112.5(10)
N(4)-C(25)-H(25)	123.8

N(5)-C(25)-H(25)	123.7
C(34)-C(33)-C(38)	119.8(13)
C(34)-C(33)-S(1)	120.4(10)
C(38)-C(33)-S(1)	119.8(11)
C(61)-C(62)-C(63)	115.2(13)
C(61)-C(62)-H(62)	122.4
C(63)-C(62)-H(62)	122.4
C(50)-C(49)-C(48)	123.3(12)
C(50)-C(49)-H(49)	118.4
C(48)-C(49)-H(49)	118.3
N(4)-C(18)-C(17)	113.5(10)
N(4)-C(18)-H(18A)	108.9
C(17)-C(18)-H(18A)	108.9
N(4)-C(18)-H(18B)	108.9
C(17)-C(18)-H(18B)	108.8
H(18A)-C(18)-H(18B)	107.7
C(74)-C(73)-C(72)	117.7(12)
C(74)-C(73)-H(73)	121.1
C(72)-C(73)-H(73)	121.1
C(27)-C(26)-N(5)	113.4(13)
C(27)-C(26)-H(26A)	108.9
N(5)-C(26)-H(26A)	108.9
C(27)-C(26)-H(26B)	108.9
N(5)-C(26)-H(26B)	108.9
H(26A)-C(26)-H(26B)	107.7
C(32)-C(27)-C(28)	117.7(15)
C(32)-C(27)-C(26)	116.2(13)
C(28)-C(27)-C(26)	126.0(14)
N(10)-C(64)-N(9)	111.0(11)
N(10)-C(64)-H(64)	124.5
N(9)-C(64)-H(64)	124.5
C(27)-C(32)-C(31)	115.4(13)
C(27)-C(32)-H(32)	122.3
C(31)-C(32)-H(32)	122.3
C(29)-C(28)-C(27)	124.2(15)
C(29)-C(28)-H(28)	117.9
C(27)-C(28)-H(28)	117.9

Symmetry transformations used to generate equivalent atoms:

Table D1.4: Anisotropic displacement parameters ($A^2 \times 10^3$) for $L_1.Br$. The anisotropic displacement factor exponent takes the form: $-2 \pi i^2 [h^2 a^{*2} U^{11} + \dots + 2 h k a^{*} b^{*} U^{12}]$

	U ¹¹	U ²²	U ³³	U ²³	U ¹³	U ¹²
Br(4)	22(1)	35(1)	31(1)	-10(1)	9(1)	-2(1)
Br(3)	38(1)	26(1)	45(1)	4(1)	14(1)	6(1)
Br(2)	46(1)	32(1)	60(1)	8(1)	14(1)	14(1)
Br(1)	43(1)	69(1)	52(1)	29(1)	19(1)	21(1)
S(1)	8(2)	25(2)	13(2)	10(1)	1(1)	6(1)
S(2)	9(2)	37(2)	22(2)	17(2)	2(1)	8(1)
O(1)	16(5)	31(5)	11(4)	10(4)	-2(4)	5(4)
O(4)	23(6)	49(6)	50(7)	31(5)	22(5)	23(5)
O(3)	16(5)	48(6)	9(5)	4(4)	-7(4)	-4(4)
O(2)	9(4)	29(5)	30(5)	18(4)	6(4)	7(4)
C(31)	39(3)	38(3)	22(3)	8(2)	5(2)	17(2)
C(69)	26(8)	37(8)	28(8)	6(7)	1(7)	11(7)
N(8)	15(6)	21(5)	22(6)	9(4)	2(5)	11(4)
N(1)	17(6)	11(5)	2(5)	-2(4)	-2(4)	4(4)
N(2)	11(5)	12(5)	15(5)	3(4)	6(4)	6(4)
N(9)	8(5)	14(5)	8(5)	4(4)	-1(4)	6(4)
C(30)	39(3)	38(3)	22(3)	8(2)	5(2)	17(2)
N(4)	5(5)	20(5)	28(6)	16(5)	2(4)	4(4)
N(3)	9(5)	17(5)	21(6)	5(4)	-4(4)	3(4)
N(6)	25(6)	17(5)	8(5)	4(4)	2(5)	5(5)
C(45)	14(6)	7(5)	17(7)	1(5)	3(5)	-4(5)
C(72)	3(6)	17(6)	24(7)	8(5)	5(5)	4(5)
N(5)	38(7)	12(5)	18(6)	2(4)	2(5)	10(5)
N(10)	12(5)	22(5)	18(6)	2(4)	1(5)	8(4)
C(21)	18(7)	20(6)	21(7)	7(5)	3(6)	15(5)
N(7)	18(6)	19(5)	8(5)	2(4)	7(4)	5(4)
C(5)	32(8)	12(6)	8(6)	0(5)	5(6)	1(5)
C(4)	42(9)	20(7)	19(7)	9(6)	6(7)	14(6)
C(2)	30(8)	27(7)	18(7)	10(6)	13(6)	9(6)
C(70)	27(8)	34(7)	22(8)	16(6)	4(6)	10(6)
C(39)	37(9)	38(8)	21(7)	21(6)	18(7)	21(7)
C(37)	20(7)	33(7)	9(6)	14(5)	6(5)	11(6)
C(8)	9(6)	11(5)	16(6)	6(5)	1(5)	4(5)
C(20)	8(6)	22(6)	18(7)	7(5)	3(5)	8(5)
C(10)	10(6)	23(6)	24(7)	11(5)	9(5)	6(5)
C(42)	7(6)	24(7)	47(10)	11(7)	-4(6)	5(5)
C(15)	10(6)	30(7)	21(7)	17(6)	3(5)	7(5)
C(3)	34(9)	21(7)	26(8)	3(6)	-4(7)	14(6)
C(1)	25(7)	6(5)	4(6)	-1(4)	-4(5)	1(5)
C(36)	11(6)	24(6)	21(7)	13(5)	9(5)	6(5)
C(61)	16(7)	40(8)	45(10)	30(8)	-1(7)	10(6)
C(78)	20(8)	41(8)	30(8)	23(7)	7(6)	3(6)
C(51)	14(6)	15(6)	9(6)	2(5)	0(5)	0(5)

C(16)	12(6)	18(6)	21(7)	10(5)	3(5)	-1(5)
C(71)	24(8)	41(8)	10(7)	3(6)	3(6)	10(6)
C(57)	18(7)	26(7)	15(7)	0(5)	7(6)	8(6)
C(68)	58(11)	12(6)	24(8)	-9(6)	1(8)	4(7)
C(7)	37(8)	6(5)	4(6)	-1(4)	-8(6)	-1(5)
C(76)	21(7)	24(7)	27(8)	16(6)	2(6)	2(6)
C(9)	25(7)	25(7)	12(6)	8(5)	6(6)	6(6)
C(67)	29(8)	13(6)	15(7)	1(5)	3(6)	7(6)
C(19)	11(6)	12(6)	24(7)	8(5)	4(5)	6(5)
C(6)	20(7)	20(6)	10(6)	2(5)	-7(5)	6(5)
C(56)	9(6)	31(7)	18(7)	14(6)	-5(5)	5(5)
C(75)	9(6)	18(6)	20(7)	5(5)	6(5)	4(5)
C(77)	26(8)	26(7)	12(7)	-2(5)	1(6)	3(6)
C(43)	42(9)	13(6)	8(6)	4(5)	-4(6)	17(6)
C(22)	17(7)	29(7)	21(7)	15(6)	2(6)	9(6)
C(40)	30(8)	9(6)	12(6)	-1(5)	2(6)	7(5)
C(46)	21(7)	23(6)	4(6)	0(5)	-1(5)	-6(5)
C(47)	17(7)	23(6)	10(6)	7(5)	0(5)	3(5)
C(44)	21(7)	14(6)	21(7)	3(5)	9(6)	-1(5)
C(48)	19(7)	22(6)	16(7)	15(5)	8(5)	10(5)
C(38)	24(7)	33(7)	9(6)	7(5)	9(5)	18(6)
C(23)	25(7)	19(6)	32(8)	17(6)	8(6)	13(6)
C(29)	39(3)	38(3)	22(3)	8(2)	5(2)	17(2)
C(60)	35(9)	29(7)	28(8)	7(6)	-4(7)	14(7)
C(50)	26(8)	15(6)	32(8)	11(6)	13(6)	10(6)
C(52)	15(6)	21(6)	14(6)	14(5)	-1(5)	4(5)
C(11)	26(7)	25(6)	6(6)	0(5)	6(5)	15(6)
C(14)	16(7)	19(6)	22(7)	7(5)	11(6)	1(5)
C(41)	13(7)	23(6)	12(7)	-4(5)	2(5)	-2(5)
C(66)	27(8)	35(7)	12(7)	11(6)	10(6)	13(6)
C(35)	15(7)	20(6)	18(7)	7(5)	2(5)	4(5)
C(54)	18(7)	20(6)	24(7)	12(6)	3(6)	6(5)
C(17)	16(7)	30(7)	34(8)	19(6)	9(6)	13(6)
C(34)	14(6)	12(5)	6(6)	1(5)	-4(5)	-7(5)
C(58)	11(6)	15(6)	14(6)	2(5)	-5(5)	7(5)
C(12)	10(6)	18(6)	15(6)	9(5)	2(5)	2(5)
C(59)	25(8)	16(6)	26(8)	3(5)	-9(6)	11(6)
C(63)	10(6)	23(6)	25(7)	13(6)	3(5)	4(5)
C(74)	25(8)	39(8)	14(7)	9(6)	7(6)	19(6)
C(13)	17(7)	18(6)	15(6)	12(5)	15(5)	8(5)
C(24)	11(6)	17(6)	27(7)	12(5)	4(5)	4(5)
C(53)	23(7)	11(6)	13(6)	4(5)	5(5)	3(5)
C(65)	38(9)	37(8)	17(7)	13(6)	12(6)	25(7)
C(55)	16(7)	26(7)	18(7)	13(5)	-4(5)	14(6)
C(25)	18(7)	13(6)	22(7)	4(5)	3(6)	4(5)
C(33)	39(3)	38(3)	22(3)	8(2)	5(2)	17(2)
C(62)	20(7)	39(8)	23(8)	16(6)	5(6)	16(6)
C(49)	29(8)	18(6)	13(6)	9(5)	2(6)	14(6)
C(18)	12(7)	30(7)	33(8)	21(6)	6(6)	13(6)
C(73)	9(6)	23(6)	31(8)	9(6)	12(6)	1(5)
C(26)	39(3)	38(3)	22(3)	8(2)	5(2)	17(2)
C(27)	39(3)	38(3)	22(3)	8(2)	5(2)	17(2)

C(64)	19(7)	29(7)	12(6)	8(5)	6(5)	13(6)
C(32)	39(3)	38(3)	22(3)	8(2)	5(2)	17(2)
C(28)	39(3)	38(3)	22(3)	8(2)	5(2)	17(2)

Table D1.5: Hydrogen coordinates ($x \times 10^4$) and isotropic displacement parameters ($A^2 \times 10^3$) for L₁.Br.

	x	y	z	U _{eq}
H(31)	3611	-778	5437	41
H(69)	-3466	-5079	-405	40
H(30)	4601	386	5156	41
H(45)	3789	-3781	7576	19
H(21)	2330	4764	7940	23
H(5)	3272	673	13253	25
H(4)	4876	766	13827	32
H(2)	5767	1158	12037	29
H(70)	-2028	-3724	-264	33
H(39A)	5407	3726	7016	40
H(39B)	4696	4286	7264	40
H(39C)	4267	3294	6493	40
H(37)	4060	1705	6660	23
H(20)	1773	3559	8406	19
H(10)	4401	-2116	9812	22
H(42)	7027	-3587	8400	35
H(15A)	841	-136	9156	23
H(15B)	718	-1253	8704	23
H(3)	6109	1004	13224	36
H(61)	1620	-831	2307	38
H(78A)	3652	-1434	1879	45
H(78B)	2758	-2427	1245	45
H(78C)	3882	-2368	1433	45
H(51)	1933	-7017	4106	19
H(16A)	1895	-673	8074	22
H(16B)	913	-462	7858	22
H(71)	-484	-3615	350	34
H(57A)	-140	-4371	3788	26
H(57B)	18	-3231	4155	26
H(68)	-3323	-6137	177	48
H(7A)	4028	1825	11341	26
H(7B)	4820	1376	11097	26
H(76)	3822	-1193	3176	30
H(9)	4701	-545	10745	26
H(67)	-1740	-6009	801	25
H(6)	2970	833	12094	24
H(56A)	1772	-2771	4499	24
H(56B)	1253	-3432	4922	24
H(77)	3630	-1809	4146	31
H(43)	5976	-3824	9136	26
H(22)	2424	4365	6700	26
H(46A)	4599	-2806	6746	26
H(46B)	5310	-3272	6362	26
H(44)	4393	-3892	8752	26
H(48)	5212	-5198	5915	20

H(38)	3517	738	7345	24
H(23)	2037	2760	5867	27
H(29)	4087	1520	4860	41
H(60)	1702	-357	3619	40
H(50)	3168	-7645	4060	27
H(11)	3067	-2913	8705	23
H(14)	2377	967	10331	24
H(41)	6505	-3439	7252	26
H(35)	4623	4178	8470	23
H(54A)	1054	-4888	5080	25
H(54B)	915	-6011	4645	25
H(17A)	2247	2200	8972	28
H(17B)	1464	1475	9224	28
H(34)	4170	3261	9201	19
H(12)	1884	-2207	8451	18
H(59)	1080	-1582	4086	31
H(74)	2599	-4013	1580	29
H(53)	2830	-3639	5987	20
H(65A)	139	-5278	1051	33
H(65B)	638	-4284	924	33
H(55A)	1574	-5578	3694	23
H(55B)	549	-5434	3702	23
H(25)	750	117	6720	23
H(62)	1084	-2453	1466	30
H(49)	4730	-6798	4961	22
H(18A)	320	698	7924	26
H(18B)	537	1851	8300	26
H(73)	2388	-4616	2496	26
H(26A)	735	-153	5332	41
H(26B)	936	802	5132	41
H(64)	-177	-5051	2387	23
H(32)	2099	-628	5761	41
H(28)	2627	1598	5000	41

Table D1.6: Torsion angles [deg] for L_I.Br.

O(4)-S(2)-N(8)-C(55)	8.2(11)
O(3)-S(2)-N(8)-C(55)	-120.9(10)
C(72)-S(2)-N(8)-C(55)	124.9(9)
O(4)-S(2)-N(8)-C(56)	168.6(9)
O(3)-S(2)-N(8)-C(56)	39.5(11)
C(72)-S(2)-N(8)-C(56)	-74.6(10)
C(32)-C(31)-C(30)-C(29)	-8(2)
O(1)-S(1)-N(3)-C(17)	43.4(10)
O(2)-S(1)-N(3)-C(17)	172.8(9)
C(33)-S(1)-N(3)-C(17)	-71.5(10)
O(1)-S(1)-N(3)-C(16)	-115.0(9)
O(2)-S(1)-N(3)-C(16)	14.5(11)
C(33)-S(1)-N(3)-C(16)	130.1(10)
O(4)-S(2)-C(72)-C(77)	-135.1(11)
O(3)-S(2)-C(72)-C(77)	-7.2(12)
N(8)-S(2)-C(72)-C(77)	109.7(11)
O(4)-S(2)-C(72)-C(73)	38.8(11)
O(3)-S(2)-C(72)-C(73)	166.7(9)
N(8)-S(2)-C(72)-C(73)	-76.4(10)
C(6)-C(5)-C(4)-C(3)	-0.3(18)
C(68)-C(69)-C(70)-C(71)	3(2)
C(14)-N(1)-C(8)-C(13)	0.3(12)
C(7)-N(1)-C(8)-C(13)	-168.3(10)
C(14)-N(1)-C(8)-C(9)	178.2(12)
C(7)-N(1)-C(8)-C(9)	9.6(18)
C(22)-C(21)-C(20)-C(19)	0.4(19)
C(14)-N(2)-C(15)-C(16)	94.9(13)
C(13)-N(2)-C(15)-C(16)	-76.5(13)
C(1)-C(2)-C(3)-C(4)	0.6(19)
C(5)-C(4)-C(3)-C(2)	0.2(19)
C(3)-C(2)-C(1)-C(6)	-1.3(18)
C(3)-C(2)-C(1)-C(7)	174.5(11)
C(38)-C(37)-C(36)-C(35)	0(2)
C(38)-C(37)-C(36)-C(39)	-178.1(13)
C(17)-N(3)-C(16)-C(15)	-65.7(15)
S(1)-N(3)-C(16)-C(15)	91.7(12)
N(2)-C(15)-C(16)-N(3)	-65.0(14)
C(69)-C(70)-C(71)-C(66)	-2(2)
C(64)-N(9)-C(57)-C(56)	104.3(13)
C(58)-N(9)-C(57)-C(56)	-75.5(15)
C(70)-C(69)-C(68)-C(67)	-3(2)
C(14)-N(1)-C(7)-C(1)	121.4(13)
C(8)-N(1)-C(7)-C(1)	-72.1(15)
C(6)-C(1)-C(7)-N(1)	-63.6(15)
C(2)-C(1)-C(7)-N(1)	120.8(13)
C(13)-C(8)-C(9)-C(10)	-0.9(16)
N(1)-C(8)-C(9)-C(10)	-178.5(11)
C(11)-C(10)-C(9)-C(8)	1.9(17)
C(69)-C(68)-C(67)-C(66)	2(2)
C(25)-N(4)-C(19)-C(24)	0.4(14)

C(18)-N(4)-C(19)-C(24)	-172.7(11)
C(25)-N(4)-C(19)-C(20)	177.4(14)
C(18)-N(4)-C(19)-C(20)	4(2)
C(21)-C(20)-C(19)-C(24)	0.2(18)
C(21)-C(20)-C(19)-N(4)	-176.4(13)
C(2)-C(1)-C(6)-C(5)	1.2(18)
C(7)-C(1)-C(6)-C(5)	-174.4(11)
C(4)-C(5)-C(6)-C(1)	-0.4(17)
C(55)-N(8)-C(56)-C(57)	-64.8(14)
S(2)-N(8)-C(56)-C(57)	134.7(10)
N(9)-C(57)-C(56)-N(8)	-64.7(13)
C(77)-C(76)-C(75)-C(74)	1(2)
C(77)-C(76)-C(75)-C(78)	-177.7(13)
C(73)-C(72)-C(77)-C(76)	1(2)
S(2)-C(72)-C(77)-C(76)	174.7(11)
C(75)-C(76)-C(77)-C(72)	-1(2)
C(41)-C(42)-C(43)-C(44)	-0.5(19)
C(20)-C(21)-C(22)-C(23)	-1(2)
C(44)-C(45)-C(40)-C(41)	-0.2(16)
C(44)-C(45)-C(40)-C(46)	-172.7(10)
C(53)-N(6)-C(46)-C(40)	115.9(13)
C(47)-N(6)-C(46)-C(40)	-70.9(15)
C(45)-C(40)-C(46)-N(6)	-63.7(14)
C(41)-C(40)-C(46)-N(6)	123.9(12)
C(53)-N(6)-C(47)-C(52)	-1.4(13)
C(46)-N(6)-C(47)-C(52)	-175.5(10)
C(53)-N(6)-C(47)-C(48)	-179.7(12)
C(46)-N(6)-C(47)-C(48)	6(2)
C(42)-C(43)-C(44)-C(45)	1.2(18)
C(40)-C(45)-C(44)-C(43)	-0.9(17)
C(52)-C(47)-C(48)-C(49)	3.1(17)
N(6)-C(47)-C(48)-C(49)	-178.9(11)
C(36)-C(37)-C(38)-C(33)	0(2)
C(21)-C(22)-C(23)-C(24)	1(2)
C(31)-C(30)-C(29)-C(28)	4(2)
C(62)-C(61)-C(60)-C(59)	-3(2)
C(52)-C(51)-C(50)-C(49)	2.9(18)
C(48)-C(47)-C(52)-C(51)	-3.0(18)
N(6)-C(47)-C(52)-C(51)	178.5(10)
C(48)-C(47)-C(52)-N(7)	178.7(10)
N(6)-C(47)-C(52)-N(7)	0.2(12)
C(50)-C(51)-C(52)-C(47)	-0.1(17)
C(50)-C(51)-C(52)-N(7)	177.8(11)
C(53)-N(7)-C(52)-C(47)	1.0(12)
C(54)-N(7)-C(52)-C(47)	176.1(10)
C(53)-N(7)-C(52)-C(51)	-177.2(11)
C(54)-N(7)-C(52)-C(51)	-2.1(18)
C(9)-C(10)-C(11)-C(12)	-0.8(18)
C(8)-N(1)-C(14)-N(2)	0.8(13)
C(7)-N(1)-C(14)-N(2)	169.3(10)
C(13)-N(2)-C(14)-N(1)	-1.5(12)
C(15)-N(2)-C(14)-N(1)	-174.4(10)

C(45)-C(40)-C(41)-C(42)	0.8(17)
C(46)-C(40)-C(41)-C(42)	173.4(11)
C(43)-C(42)-C(41)-C(40)	-0.5(19)
C(70)-C(71)-C(66)-C(67)	1.7(19)
C(70)-C(71)-C(66)-C(65)	-176.4(12)
C(68)-C(67)-C(66)-C(71)	-1.6(18)
C(68)-C(67)-C(66)-C(65)	176.6(11)
C(37)-C(36)-C(35)-C(34)	2(2)
C(39)-C(36)-C(35)-C(34)	179.9(12)
C(53)-N(7)-C(54)-C(55)	96.0(14)
C(52)-N(7)-C(54)-C(55)	-78.0(14)
C(16)-N(3)-C(17)-C(18)	-62.9(14)
S(1)-N(3)-C(17)-C(18)	138.4(9)
C(36)-C(35)-C(34)-C(33)	-3(2)
C(64)-N(9)-C(58)-C(63)	-2.2(13)
C(57)-N(9)-C(58)-C(63)	177.6(11)
C(64)-N(9)-C(58)-C(59)	178.7(13)
C(57)-N(9)-C(58)-C(59)	-1(2)
C(10)-C(11)-C(12)-C(13)	-1.3(16)
C(61)-C(60)-C(59)-C(58)	2(2)
C(63)-C(58)-C(59)-C(60)	-2(2)
N(9)-C(58)-C(59)-C(60)	177.0(13)
N(9)-C(58)-C(63)-C(62)	-176.9(12)
C(59)-C(58)-C(63)-C(62)	2(2)
N(9)-C(58)-C(63)-N(10)	0.8(13)
C(59)-C(58)-C(63)-N(10)	179.9(12)
C(64)-N(10)-C(63)-C(58)	1.0(14)
C(65)-N(10)-C(63)-C(58)	176.1(12)
C(64)-N(10)-C(63)-C(62)	178.4(14)
C(65)-N(10)-C(63)-C(62)	-7(2)
C(76)-C(75)-C(74)-C(73)	0(2)
C(78)-C(75)-C(74)-C(73)	178.1(13)
C(9)-C(8)-C(13)-C(12)	-1.4(17)
N(1)-C(8)-C(13)-C(12)	176.7(10)
C(9)-C(8)-C(13)-N(2)	-179.2(10)
N(1)-C(8)-C(13)-N(2)	-1.2(11)
C(11)-C(12)-C(13)-C(8)	2.4(16)
C(11)-C(12)-C(13)-N(2)	179.8(10)
C(14)-N(2)-C(13)-C(8)	1.6(11)
C(15)-N(2)-C(13)-C(8)	174.3(10)
C(14)-N(2)-C(13)-C(12)	-176.2(11)
C(15)-N(2)-C(13)-C(12)	-3.5(17)
C(22)-C(23)-C(24)-N(5)	176.7(14)
C(22)-C(23)-C(24)-C(19)	-0.9(19)
C(25)-N(5)-C(24)-C(23)	-177.3(14)
C(26)-N(5)-C(24)-C(23)	1(2)
C(25)-N(5)-C(24)-C(19)	0.6(15)
C(26)-N(5)-C(24)-C(19)	179.1(13)
N(4)-C(19)-C(24)-C(23)	177.5(12)
C(20)-C(19)-C(24)-C(23)	0.1(19)
N(4)-C(19)-C(24)-N(5)	-0.6(14)
C(20)-C(19)-C(24)-N(5)	-178.0(11)

C(47)-N(6)-C(53)-N(7)	2.1(13)
C(46)-N(6)-C(53)-N(7)	176.3(9)
C(52)-N(7)-C(53)-N(6)	-2.0(12)
C(54)-N(7)-C(53)-N(6)	-176.9(10)
C(64)-N(10)-C(65)-C(66)	90.4(15)
C(63)-N(10)-C(65)-C(66)	-83.7(15)
C(71)-C(66)-C(65)-N(10)	92.6(14)
C(67)-C(66)-C(65)-N(10)	-85.5(14)
C(56)-N(8)-C(55)-C(54)	-69.5(15)
S(2)-N(8)-C(55)-C(54)	90.8(12)
N(7)-C(54)-C(55)-N(8)	-65.7(14)
C(19)-N(4)-C(25)-N(5)	0.0(16)
C(18)-N(4)-C(25)-N(5)	173.0(11)
C(24)-N(5)-C(25)-N(4)	-0.4(16)
C(26)-N(5)-C(25)-N(4)	-178.9(13)
C(35)-C(34)-C(33)-C(38)	2(2)
C(35)-C(34)-C(33)-S(1)	-177.4(11)
C(37)-C(38)-C(33)-C(34)	-1(2)
C(37)-C(38)-C(33)-S(1)	179.1(11)
O(1)-S(1)-C(33)-C(34)	-15.1(15)
O(2)-S(1)-C(33)-C(34)	-145.8(12)
N(3)-S(1)-C(33)-C(34)	101.3(13)
O(1)-S(1)-C(33)-C(38)	165.1(12)
O(2)-S(1)-C(33)-C(38)	34.3(15)
N(3)-S(1)-C(33)-C(38)	-78.6(14)
C(60)-C(61)-C(62)-C(63)	3(2)
C(58)-C(63)-C(62)-C(61)	-3(2)
N(10)-C(63)-C(62)-C(61)	-179.6(13)
C(51)-C(50)-C(49)-C(48)	-2.8(19)
C(47)-C(48)-C(49)-C(50)	-0.3(17)
C(25)-N(4)-C(18)-C(17)	103.2(15)
C(19)-N(4)-C(18)-C(17)	-84.9(14)
N(3)-C(17)-C(18)-N(4)	-62.7(13)
C(75)-C(74)-C(73)-C(72)	0(2)
C(77)-C(72)-C(73)-C(74)	-0.4(19)
S(2)-C(72)-C(73)-C(74)	-174.3(10)
C(25)-N(5)-C(26)-C(27)	-103.3(16)
C(24)-N(5)-C(26)-C(27)	78.5(18)
N(5)-C(26)-C(27)-C(32)	86.0(16)
N(5)-C(26)-C(27)-C(28)	-96.7(18)
C(63)-N(10)-C(64)-N(9)	-2.4(14)
C(65)-N(10)-C(64)-N(9)	-177.4(12)
C(58)-N(9)-C(64)-N(10)	3.0(14)
C(57)-N(9)-C(64)-N(10)	-176.9(11)
C(28)-C(27)-C(32)-C(31)	-2(2)
C(26)-C(27)-C(32)-C(31)	175.0(13)
C(30)-C(31)-C(32)-C(27)	7(2)
C(30)-C(29)-C(28)-C(27)	1(2)
C(32)-C(27)-C(28)-C(29)	-1(2)
C(26)-C(27)-C(28)-C(29)	-178.7(15)

Symmetry transformations used to generate equivalent atoms:

Table D1.7: Hydrogen bonds for $L_1\cdot Br$ [A and deg.]

D-H...A	d(D-H)	d(H...A)	d(D...A)	$\angle(DHA)$
---------	--------	----------	----------	---------------

APPENDIX D2: Crystallographic data for *N,N'*-Bis[1-benzyl-benzimidazolium-ethyl]-4-methylbenzenesulfonamide dihexafluorophosphate ($L_1\text{.PF}_6$)

Table D2.1: Crystal data and structure refinement for $L_1\text{.PF}_6$.

Empirical formula	$\text{C}_{39}\text{H}_{39}\text{N}_5\text{O}_2\text{S P}_2\text{F}_{12}$
Formula weight	931.75
Temperature	100(2) K
Wavelength	0.71073 Å
Crystal system, space group	Triclinic, P-1
Unit cell dimensions	$a = 9.0853(8)$ Å $\alpha = 100.8633(13)$ deg. $b = 12.1396(11)$ Å $\beta = 95.1932(13)$ deg. $c = 18.6260(17)$ Å $\gamma = 91.7243(13)$ deg.
Volume	2006.9(3) Å ³
Z, Calculated density	2, 1.542 Mg/m ³
Absorption coefficient	0.260 mm ⁻¹
F(000)	956
Crystal size	0.28 x 0.19 x 0.10 mm
Theta range for data collection	1.71 to 27.50 deg.
Limiting indices	-11≤h≤11, -15≤k≤15, -24≤l≤24
Reflections collected / unique	25567 / 9182 [R(int) = 0.0474]
Completeness to theta = 27.50	99.8 %
Absorption correction	Semi-empirical from equivalents
Max. and min. transmission	0.9745 and 0.9308
Refinement method	Full-matrix least-squares on F ²
Data / restraints / parameters	9182 / 0 / 550
Goodness-of-fit on F ²	1.116
Final R indices [I>2sigma(I)]	R1 = 0.0428, wR2 = 0.0920
R indices (all data)	R1 = 0.0744, wR2 = 0.1056
Largest diff. peak and hole	0.409 and -0.431 e.Å ⁻³

Table D2.2: Atomic coordinates ($x \times 10^4$) and equivalent isotropic displacement parameters ($\text{Å}^2 \times 10^3$) for Li_2PF_6 . $U(\text{eq})$ is defined as one third of the trace of the orthogonalized U_{ij} tensor.

	x	y	z	$U(\text{eq})$
S(1)	5964(1)	8386(1)	3456(1)	19(1)
P(1)	7863(1)	4940(1)	6101(1)	22(1)
P(3)	9886(1)	7131(1)	1545(1)	21(1)
F(1)	8277(2)	6247(1)	6197(1)	37(1)
F(2)	7411(2)	3637(1)	6012(1)	38(1)
F(3)	7199(2)	5177(1)	6879(1)	39(1)
F(4)	6279(2)	5115(1)	5703(1)	50(1)
F(5)	8533(2)	4708(1)	5338(1)	59(1)
F(6)	9421(2)	4768(1)	6515(1)	46(1)
F(7)	9745(2)	8044(1)	1034(1)	40(1)
F(8)	10043(2)	6194(1)	2041(1)	33(1)
F(9)	11552(2)	6960(1)	1359(1)	49(1)
F(10)	10438(2)	8086(1)	2227(1)	37(1)
F(11)	8236(2)	7300(1)	1728(1)	52(1)
F(12)	9339(2)	6162(1)	855(1)	52(1)
O(1)	4663(2)	8403(1)	3840(1)	25(1)
O(2)	7297(2)	8967(1)	3826(1)	27(1)
N(1)	2472(2)	4160(1)	1045(1)	21(1)
N(2)	4485(2)	5163(1)	1513(1)	18(1)
N(3)	7267(2)	6933(1)	4712(1)	17(1)
N(4)	5836(2)	7915(2)	5438(1)	21(1)
N(5)	6387(2)	7095(1)	3174(1)	18(1)
C(1)	61(3)	743(2)	1743(1)	31(1)
C(2)	680(3)	1688(2)	2219(1)	31(1)
C(3)	966(2)	2659(2)	1953(1)	28(1)
C(4)	640(2)	2688(2)	1216(1)	22(1)
C(5)	8(2)	1734(2)	743(1)	27(1)
C(6)	-284(3)	768(2)	1010(1)	32(1)
C(7)	901(2)	3757(2)	937(1)	26(1)
C(8)	3053(2)	4991(2)	1573(1)	21(1)
C(9)	3582(2)	3754(2)	616(1)	21(1)
C(10)	3566(3)	2898(2)	-2(1)	27(1)
C(11)	4886(3)	2733(2)	-300(1)	30(1)
C(12)	6183(3)	3383(2)	-10(1)	30(1)
C(13)	6202(3)	4240(2)	601(1)	25(1)
C(14)	4863(2)	4397(2)	907(1)	19(1)
C(15)	5495(2)	6060(2)	1956(1)	22(1)
C(16)	5241(2)	6285(2)	2767(1)	18(1)
C(17)	4096(3)	10560(2)	877(1)	38(1)
C(18)	4591(3)	9977(2)	1496(1)	25(1)
C(19)	6059(2)	10041(2)	1788(1)	26(1)
C(20)	6507(2)	9531(2)	2369(1)	24(1)
C(21)	5458(2)	8946(2)	2667(1)	18(1)
C(22)	3985(2)	8851(2)	2376(1)	21(1)

C(23)	3567(2)	9360(2)	1791(1)	24(1)
C(24)	7801(2)	6664(2)	3421(1)	20(1)
C(25)	7705(2)	6123(2)	4093(1)	21(1)
C(26)	5906(2)	7020(2)	4912(1)	21(1)
C(27)	8151(2)	7831(2)	5127(1)	19(1)
C(28)	9636(2)	8138(2)	5121(1)	23(1)
C(29)	10157(3)	9108(2)	5601(1)	30(1)
C(30)	9237(3)	9749(2)	6062(1)	32(1)
C(31)	7768(3)	9443(2)	6068(1)	29(1)
C(32)	7238(2)	8460(2)	5586(1)	20(1)
C(33)	4470(3)	8272(2)	5756(1)	30(1)
C(34)	4114(2)	7692(2)	6375(1)	22(1)
C(35)	5157(3)	7652(2)	6961(1)	28(1)
C(36)	4782(3)	7168(2)	7538(1)	30(1)
C(37)	3372(3)	6726(2)	7541(1)	31(1)
C(38)	2330(3)	6736(2)	6953(1)	33(1)
C(39)	2713(3)	7213(2)	6368(1)	31(1)

Table D2.3: Bond lengths [Å] and angles [deg] for L₁.PF₆.

S(1)-O(2)	1.4330(15)
S(1)-O(1)	1.4355(15)
S(1)-N(5)	1.6254(17)
S(1)-C(21)	1.763(2)
P(1)-F(5)	1.5760(15)
P(1)-F(6)	1.5893(14)
P(1)-F(1)	1.5924(14)
P(1)-F(4)	1.5961(14)
P(1)-F(2)	1.5964(14)
P(1)-F(3)	1.5997(14)
P(3)-F(11)	1.5780(15)
P(3)-F(10)	1.5825(13)
P(3)-F(7)	1.5935(14)
P(3)-F(9)	1.5940(15)
P(3)-F(8)	1.5954(13)
P(3)-F(12)	1.6001(14)
N(1)-C(8)	1.328(2)
N(1)-C(9)	1.388(3)
N(1)-C(7)	1.478(3)
N(2)-C(8)	1.329(3)
N(2)-C(14)	1.397(2)
N(2)-C(15)	1.473(2)
N(3)-C(26)	1.325(3)
N(3)-C(27)	1.396(2)
N(3)-C(25)	1.461(2)
N(4)-C(26)	1.327(3)
N(4)-C(32)	1.397(3)
N(4)-C(33)	1.466(3)
N(5)-C(16)	1.463(2)
N(5)-C(24)	1.469(3)
C(1)-C(2)	1.379(3)
C(1)-C(6)	1.380(3)
C(1)-H(1B)	0.9500
C(2)-C(3)	1.388(3)
C(2)-H(2B)	0.9500
C(3)-C(4)	1.385(3)
C(3)-H(3A)	0.9500
C(4)-C(5)	1.390(3)
C(4)-C(7)	1.507(3)
C(5)-C(6)	1.384(3)
C(5)-H(5A)	0.9500
C(6)-H(6A)	0.9500
C(7)-H(7A)	0.9900
C(7)-H(7B)	0.9900
C(8)-H(8A)	0.9500
C(9)-C(14)	1.389(3)
C(9)-C(10)	1.396(3)
C(10)-C(11)	1.371(3)
C(10)-H(10A)	0.9500

C(11)-C(12)	1.404(3)
C(11)-H(11A)	0.9500
C(12)-C(13)	1.387(3)
C(12)-H(12A)	0.9500
C(13)-C(14)	1.393(3)
C(13)-H(13A)	0.9500
C(15)-C(16)	1.524(3)
C(15)-H(15A)	0.9900
C(15)-H(15B)	0.9900
C(16)-H(16A)	0.9900
C(16)-H(16B)	0.9900
C(17)-C(18)	1.504(3)
C(17)-H(17A)	0.9800
C(17)-H(17B)	0.9800
C(17)-H(17C)	0.9800
C(18)-C(19)	1.389(3)
C(18)-C(23)	1.391(3)
C(19)-C(20)	1.382(3)
C(19)-H(19A)	0.9500
C(20)-C(21)	1.387(3)
C(20)-H(20A)	0.9500
C(21)-C(22)	1.391(3)
C(22)-C(23)	1.380(3)
C(22)-H(22A)	0.9500
C(23)-H(23A)	0.9500
C(24)-C(25)	1.527(3)
C(24)-H(24A)	0.9900
C(24)-H(24B)	0.9900
C(25)-H(25A)	0.9900
C(25)-H(25B)	0.9900
C(26)-H(26A)	0.9500
C(27)-C(32)	1.387(3)
C(27)-C(28)	1.391(3)
C(28)-C(29)	1.379(3)
C(28)-H(28A)	0.9500
C(29)-C(30)	1.400(3)
C(29)-H(29A)	0.9500
C(30)-C(31)	1.376(3)
C(30)-H(30A)	0.9500
C(31)-C(32)	1.395(3)
C(31)-H(31A)	0.9500
C(33)-C(34)	1.513(3)
C(33)-H(33A)	0.9900
C(33)-H(33B)	0.9900
C(34)-C(39)	1.381(3)
C(34)-C(35)	1.388(3)
C(35)-C(36)	1.381(3)
C(35)-H(35A)	0.9500
C(36)-C(37)	1.375(3)
C(36)-H(36A)	0.9500
C(37)-C(38)	1.383(3)
C(37)-H(37A)	0.9500

C(38)-C(39)	1.391(3)
C(38)-H(38A)	0.9500
C(39)-H(39A)	0.9500
O(2)-S(1)-O(1)	119.17(9)
O(2)-S(1)-N(5)	106.11(9)
O(1)-S(1)-N(5)	109.66(9)
O(2)-S(1)-C(21)	108.65(9)
O(1)-S(1)-C(21)	105.66(9)
N(5)-S(1)-C(21)	107.06(9)
F(5)-P(1)-F(6)	90.83(9)
F(5)-P(1)-F(1)	90.58(8)
F(6)-P(1)-F(1)	89.99(8)
F(5)-P(1)-F(4)	90.65(10)
F(6)-P(1)-F(4)	178.52(9)
F(1)-P(1)-F(4)	90.17(8)
F(5)-P(1)-F(2)	90.47(9)
F(6)-P(1)-F(2)	90.90(8)
F(1)-P(1)-F(2)	178.61(9)
F(4)-P(1)-F(2)	88.91(8)
F(5)-P(1)-F(3)	179.43(9)
F(6)-P(1)-F(3)	88.62(8)
F(1)-P(1)-F(3)	89.29(8)
F(4)-P(1)-F(3)	89.91(9)
F(2)-P(1)-F(3)	89.67(8)
F(11)-P(3)-F(10)	89.97(9)
F(11)-P(3)-F(7)	90.27(9)
F(10)-P(3)-F(7)	90.02(7)
F(11)-P(3)-F(9)	179.85(10)
F(10)-P(3)-F(9)	90.11(8)
F(7)-P(3)-F(9)	89.60(8)
F(11)-P(3)-F(8)	90.65(8)
F(10)-P(3)-F(8)	91.12(7)
F(7)-P(3)-F(8)	178.54(8)
F(9)-P(3)-F(8)	89.48(8)
F(11)-P(3)-F(12)	90.41(9)
F(10)-P(3)-F(12)	179.61(10)
F(7)-P(3)-F(12)	90.08(7)
F(9)-P(3)-F(12)	89.51(9)
F(8)-P(3)-F(12)	88.77(7)
C(8)-N(1)-C(9)	108.38(17)
C(8)-N(1)-C(7)	125.13(18)
C(9)-N(1)-C(7)	126.49(17)
C(8)-N(2)-C(14)	107.99(17)
C(8)-N(2)-C(15)	127.16(17)
C(14)-N(2)-C(15)	124.64(17)
C(26)-N(3)-C(27)	108.43(17)
C(26)-N(3)-C(25)	125.11(17)
C(27)-N(3)-C(25)	125.98(17)
C(26)-N(4)-C(32)	108.16(18)
C(26)-N(4)-C(33)	123.87(19)
C(32)-N(4)-C(33)	127.86(18)

C(16)-N(5)-C(24)	117.96(16)
C(16)-N(5)-S(1)	119.14(14)
C(24)-N(5)-S(1)	122.06(13)
C(2)-C(1)-C(6)	120.1(2)
C(2)-C(1)-H(1B)	119.9
C(6)-C(1)-H(1B)	119.9
C(1)-C(2)-C(3)	119.6(2)
C(1)-C(2)-H(2B)	120.2
C(3)-C(2)-H(2B)	120.2
C(4)-C(3)-C(2)	120.7(2)
C(4)-C(3)-H(3A)	119.7
C(2)-C(3)-H(3A)	119.7
C(3)-C(4)-C(5)	119.2(2)
C(3)-C(4)-C(7)	120.38(19)
C(5)-C(4)-C(7)	120.3(2)
C(6)-C(5)-C(4)	120.0(2)
C(6)-C(5)-H(5A)	120.0
C(4)-C(5)-H(5A)	120.0
C(1)-C(6)-C(5)	120.4(2)
C(1)-C(6)-H(6A)	119.8
C(5)-C(6)-H(6A)	119.8
N(1)-C(7)-C(4)	113.01(17)
N(1)-C(7)-H(7A)	109.0
C(4)-C(7)-H(7A)	109.0
N(1)-C(7)-H(7B)	109.0
C(4)-C(7)-H(7B)	109.0
H(7A)-C(7)-H(7B)	107.8
N(1)-C(8)-N(2)	110.50(19)
N(1)-C(8)-H(8A)	124.7
N(2)-C(8)-H(8A)	124.7
N(1)-C(9)-C(14)	106.63(17)
N(1)-C(9)-C(10)	131.7(2)
C(14)-C(9)-C(10)	121.7(2)
C(11)-C(10)-C(9)	116.0(2)
C(11)-C(10)-H(10A)	122.0
C(9)-C(10)-H(10A)	122.0
C(10)-C(11)-C(12)	122.6(2)
C(10)-C(11)-H(11A)	118.7
C(12)-C(11)-H(11A)	118.7
C(13)-C(12)-C(11)	121.6(2)
C(13)-C(12)-H(12A)	119.2
C(11)-C(12)-H(12A)	119.2
C(12)-C(13)-C(14)	115.7(2)
C(12)-C(13)-H(13A)	122.2
C(14)-C(13)-H(13A)	122.2
C(9)-C(14)-C(13)	122.48(19)
C(9)-C(14)-N(2)	106.50(18)
C(13)-C(14)-N(2)	131.0(2)
N(2)-C(15)-C(16)	112.82(16)
N(2)-C(15)-H(15A)	109.0
C(16)-C(15)-H(15A)	109.0
N(2)-C(15)-H(15B)	109.0

C(16)-C(15)-H(15B)	109.0
H(15A)-C(15)-H(15B)	107.8
N(5)-C(16)-C(15)	109.05(16)
N(5)-C(16)-H(16A)	109.9
C(15)-C(16)-H(16A)	109.9
N(5)-C(16)-H(16B)	109.9
C(15)-C(16)-H(16B)	109.9
H(16A)-C(16)-H(16B)	108.3
C(18)-C(17)-H(17A)	109.5
C(18)-C(17)-H(17B)	109.5
H(17A)-C(17)-H(17B)	109.5
C(18)-C(17)-H(17C)	109.5
H(17A)-C(17)-H(17C)	109.5
H(17B)-C(17)-H(17C)	109.5
C(19)-C(18)-C(23)	118.4(2)
C(19)-C(18)-C(17)	121.6(2)
C(23)-C(18)-C(17)	120.0(2)
C(20)-C(19)-C(18)	121.6(2)
C(20)-C(19)-H(19A)	119.2
C(18)-C(19)-H(19A)	119.2
C(19)-C(20)-C(21)	118.9(2)
C(19)-C(20)-H(20A)	120.6
C(21)-C(20)-H(20A)	120.6
C(20)-C(21)-C(22)	120.75(19)
C(20)-C(21)-S(1)	119.94(16)
C(22)-C(21)-S(1)	119.20(16)
C(23)-C(22)-C(21)	119.3(2)
C(23)-C(22)-H(22A)	120.4
C(21)-C(22)-H(22A)	120.4
C(22)-C(23)-C(18)	121.1(2)
C(22)-C(23)-H(23A)	119.4
C(18)-C(23)-H(23A)	119.4
N(5)-C(24)-C(25)	112.76(17)
N(5)-C(24)-H(24A)	109.0
C(25)-C(24)-H(24A)	109.0
N(5)-C(24)-H(24B)	109.0
C(25)-C(24)-H(24B)	109.0
H(24A)-C(24)-H(24B)	107.8
N(3)-C(25)-C(24)	110.75(16)
N(3)-C(25)-H(25A)	109.5
C(24)-C(25)-H(25A)	109.5
N(3)-C(25)-H(25B)	109.5
C(24)-C(25)-H(25B)	109.5
H(25A)-C(25)-H(25B)	108.1
N(3)-C(26)-N(4)	110.47(18)
N(3)-C(26)-H(26A)	124.8
N(4)-C(26)-H(26A)	124.8
C(32)-C(27)-C(28)	122.29(19)
C(32)-C(27)-N(3)	106.35(18)
C(28)-C(27)-N(3)	131.34(19)
C(29)-C(28)-C(27)	116.1(2)
C(29)-C(28)-H(28A)	121.9

C(27)-C(28)-H(28A)	121.9
C(28)-C(29)-C(30)	121.8(2)
C(28)-C(29)-H(29A)	119.1
C(30)-C(29)-H(29A)	119.1
C(31)-C(30)-C(29)	122.0(2)
C(31)-C(30)-H(30A)	119.0
C(29)-C(30)-H(30A)	119.0
C(30)-C(31)-C(32)	116.4(2)
C(30)-C(31)-H(31A)	121.8
C(32)-C(31)-H(31A)	121.8
C(27)-C(32)-C(31)	121.4(2)
C(27)-C(32)-N(4)	106.59(18)
C(31)-C(32)-N(4)	132.1(2)
N(4)-C(33)-C(34)	113.61(18)
N(4)-C(33)-H(33A)	108.8
C(34)-C(33)-H(33A)	108.8
N(4)-C(33)-H(33B)	108.8
C(34)-C(33)-H(33B)	108.8
H(33A)-C(33)-H(33B)	107.7
C(39)-C(34)-C(35)	119.0(2)
C(39)-C(34)-C(33)	119.5(2)
C(35)-C(34)-C(33)	121.4(2)
C(36)-C(35)-C(34)	120.3(2)
C(36)-C(35)-H(35A)	119.9
C(34)-C(35)-H(35A)	119.9
C(37)-C(36)-C(35)	120.5(2)
C(37)-C(36)-H(36A)	119.8
C(35)-C(36)-H(36A)	119.8
C(36)-C(37)-C(38)	119.9(2)
C(36)-C(37)-H(37A)	120.1
C(38)-C(37)-H(37A)	120.1
C(37)-C(38)-C(39)	119.6(2)
C(37)-C(38)-H(38A)	120.2
C(39)-C(38)-H(38A)	120.2
C(34)-C(39)-C(38)	120.7(2)
C(34)-C(39)-H(39A)	119.7
C(38)-C(39)-H(39A)	119.7

Symmetry transformations used to generate equivalent atoms:

Table D2.3: Anisotropic displacement parameters ($\text{Å}^2 \times 10^3$) for $L_1.\text{PF}_6$. The anisotropic displacement factor exponent takes the form: $-2 \pi^2 [h^2 a^{*2} U11 + \dots + 2 h k a^* b^* U12]$

	U^{11}	U^{22}	U^{33}	U^{23}	U^{13}	U^{12}
S(1)	24(1)	17(1)	16(1)	3(1)	-3(1)	1(1)
P(1)	22(1)	25(1)	20(1)	8(1)	0(1)	1(1)
P(3)	23(1)	20(1)	20(1)	6(1)	1(1)	2(1)
F(1)	44(1)	31(1)	36(1)	15(1)	-9(1)	-13(1)
F(2)	50(1)	23(1)	42(1)	7(1)	-1(1)	0(1)
F(3)	41(1)	42(1)	33(1)	1(1)	17(1)	-11(1)
F(4)	38(1)	36(1)	70(1)	14(1)	-30(1)	-4(1)
F(5)	83(1)	66(1)	28(1)	5(1)	25(1)	-4(1)
F(6)	25(1)	58(1)	57(1)	23(1)	-4(1)	7(1)
F(7)	67(1)	24(1)	31(1)	12(1)	-3(1)	5(1)
F(8)	49(1)	31(1)	26(1)	15(1)	12(1)	9(1)
F(9)	39(1)	51(1)	68(1)	25(1)	32(1)	17(1)
F(10)	45(1)	32(1)	28(1)	0(1)	-6(1)	-2(1)
F(11)	21(1)	38(1)	101(1)	18(1)	13(1)	2(1)
F(12)	97(1)	23(1)	31(1)	2(1)	-21(1)	2(1)
O(1)	32(1)	25(1)	20(1)	5(1)	8(1)	7(1)
O(2)	31(1)	19(1)	27(1)	2(1)	-13(1)	-5(1)
N(1)	24(1)	17(1)	20(1)	3(1)	-2(1)	0(1)
N(2)	22(1)	16(1)	15(1)	1(1)	0(1)	-2(1)
N(3)	19(1)	18(1)	15(1)	4(1)	-1(1)	0(1)
N(4)	22(1)	26(1)	16(1)	5(1)	2(1)	6(1)
N(5)	18(1)	15(1)	18(1)	1(1)	-3(1)	0(1)
C(1)	27(1)	26(1)	45(2)	14(1)	11(1)	3(1)
C(2)	27(1)	38(1)	30(1)	13(1)	1(1)	2(1)
C(3)	28(1)	25(1)	28(1)	1(1)	-4(1)	-2(1)
C(4)	19(1)	19(1)	26(1)	4(1)	-1(1)	1(1)
C(5)	27(1)	24(1)	27(1)	0(1)	0(1)	-1(1)
C(6)	31(1)	22(1)	42(2)	-2(1)	7(1)	-3(1)
C(7)	23(1)	23(1)	29(1)	5(1)	-6(1)	-2(1)
C(8)	26(1)	17(1)	19(1)	2(1)	-1(1)	2(1)
C(9)	29(1)	17(1)	17(1)	6(1)	-2(1)	2(1)
C(10)	43(2)	19(1)	18(1)	5(1)	-6(1)	3(1)
C(11)	55(2)	20(1)	16(1)	3(1)	3(1)	9(1)
C(12)	43(2)	32(1)	20(1)	9(1)	11(1)	15(1)
C(13)	32(1)	25(1)	21(1)	9(1)	3(1)	4(1)
C(14)	29(1)	18(1)	11(1)	5(1)	0(1)	4(1)
C(15)	23(1)	22(1)	18(1)	2(1)	0(1)	-7(1)
C(16)	19(1)	17(1)	18(1)	2(1)	-1(1)	-1(1)
C(17)	45(2)	42(2)	32(1)	20(1)	5(1)	15(1)
C(18)	32(1)	22(1)	21(1)	5(1)	5(1)	11(1)
C(19)	26(1)	25(1)	33(1)	13(1)	11(1)	5(1)
C(20)	21(1)	21(1)	33(1)	9(1)	3(1)	2(1)
C(21)	22(1)	16(1)	17(1)	4(1)	0(1)	3(1)

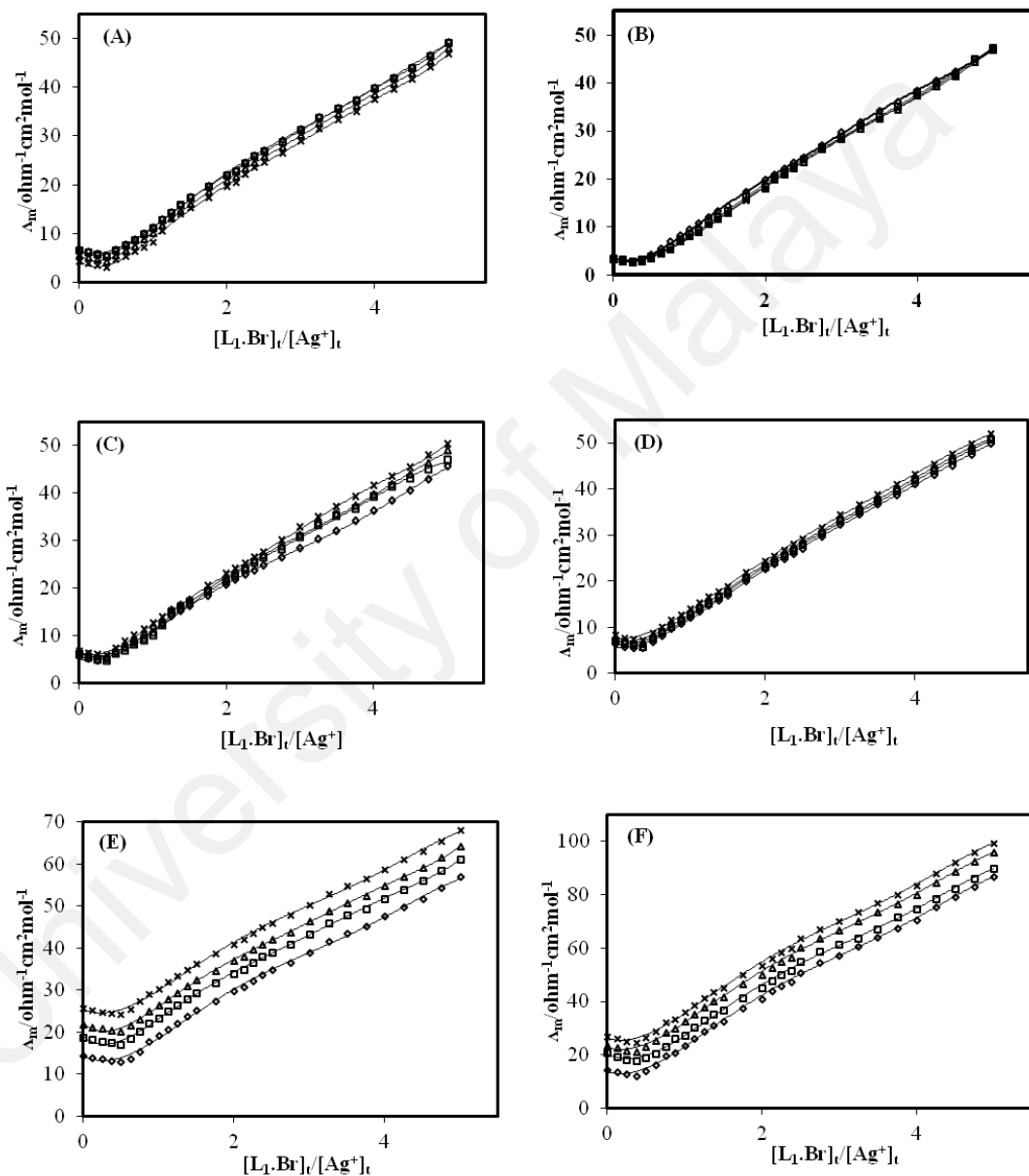
C(22)	20(1)	21(1)	20(1)	2(1)	1(1)	0(1)
C(23)	22(1)	26(1)	21(1)	2(1)	-1(1)	7(1)
C(24)	20(1)	20(1)	17(1)	2(1)	-1(1)	3(1)
C(25)	25(1)	20(1)	16(1)	2(1)	0(1)	4(1)
C(26)	19(1)	26(1)	18(1)	9(1)	-1(1)	0(1)
C(27)	24(1)	19(1)	14(1)	4(1)	-4(1)	0(1)
C(28)	22(1)	26(1)	21(1)	8(1)	-2(1)	2(1)
C(29)	28(1)	29(1)	31(1)	10(1)	-7(1)	-7(1)
C(30)	44(2)	22(1)	27(1)	4(1)	-11(1)	-6(1)
C(31)	45(2)	23(1)	17(1)	2(1)	-1(1)	6(1)
C(32)	26(1)	20(1)	16(1)	6(1)	-2(1)	3(1)
C(33)	26(1)	41(1)	26(1)	9(1)	5(1)	15(1)
C(34)	22(1)	26(1)	19(1)	4(1)	4(1)	9(1)
C(35)	24(1)	36(1)	24(1)	6(1)	1(1)	3(1)
C(36)	33(1)	38(1)	20(1)	9(1)	-2(1)	4(1)
C(37)	38(2)	29(1)	30(1)	12(1)	10(1)	8(1)
C(38)	26(1)	33(1)	42(2)	9(1)	6(1)	2(1)
C(39)	26(1)	37(1)	28(1)	5(1)	-3(1)	7(1)

Table D2.4: Hydrogen coordinates ($x \times 10^4$) and isotropic displacement parameters ($A^2 \times 10^3$) for $L_1.PF_6$.

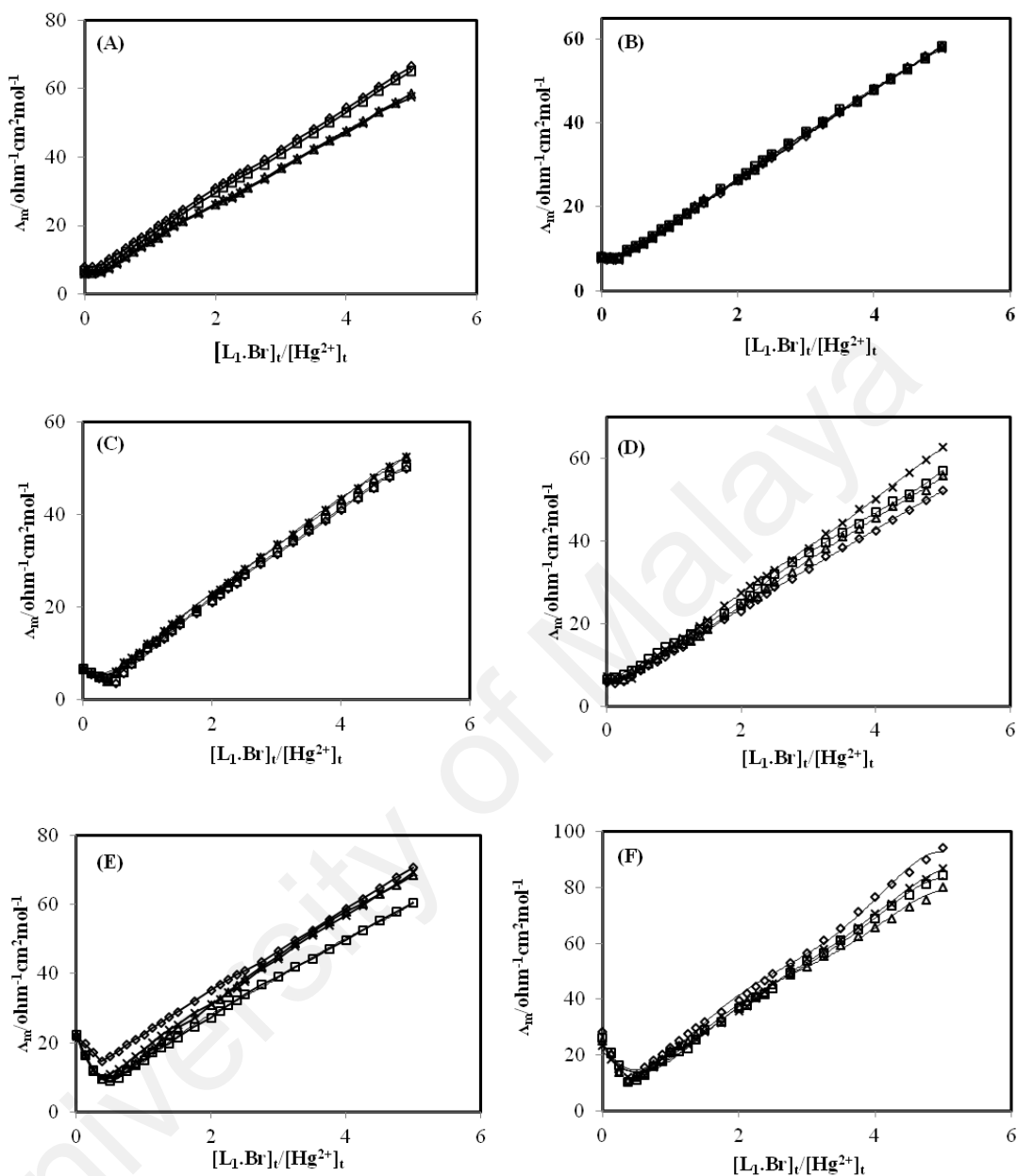
	x	y	z	U(eq)
H(1B)	-128	74	1921	37
H(2B)	909	1674	2725	37
H(3A)	1389	3311	2281	33
H(5A)	-224	1744	237	33
H(6A)	-724	119	687	39
H(7A)	560	3629	406	31
H(7B)	302	4347	1193	31
H(8A)	2521	5405	1941	25
H(10A)	2693	2456	-204	32
H(11A)	4925	2155	-719	36
H(12A)	7069	3233	-238	36
H(13A)	7071	4690	797	30
H(15A)	5359	6759	1762	26
H(15B)	6529	5846	1905	26
H(16A)	4252	6587	2832	22
H(16B)	5282	5576	2957	22
H(17A)	4950	10951	735	56
H(17B)	3361	11104	1038	56
H(17C)	3654	10004	456	56
H(19A)	6773	10446	1584	32
H(20A)	7517	9580	2562	29
H(22A)	3273	8439	2577	25
H(23A)	2564	9288	1587	28
H(24A)	8560	7290	3540	23
H(24B)	8121	6102	3014	23
H(25A)	6973	5478	3972	25
H(25B)	8679	5837	4231	25
H(26A)	5094	6511	4707	25
H(28A)	10256	7705	4804	27
H(29A)	11167	9348	5619	36
H(30A)	9640	10415	6381	38
H(31A)	7148	9879	6383	34
H(33A)	3637	8119	5364	36
H(33B)	4558	9093	5943	36
H(35A)	6132	7960	6966	33
H(36A)	5504	7141	7935	36
H(37A)	3114	6414	946	37
H(38A)	1359	6420	6948	40
H(39A)	2004	7209	5960	37

APPENDIX E: Plot of molar conductance, Λ_m versus mole ratio, $[L_1\cdot Br]_t/[M^{n+}]_t$ for Ag^+ , Hg^{2+} , Ni^{2+} , Pd^{2+} and Zn^{2+} in MeOH-H₂O binary solvent ((A) 100% MeOH, (B) 63.72% MeOH, (C) 39.73% MeOH, (D) 22.66% MeOH, (E) 9.90% MeOH, (F) 0% MeOH) at different temperature (\diamond 15 °C, \square 25 °C, Δ 35 °C, \times 45 °C).

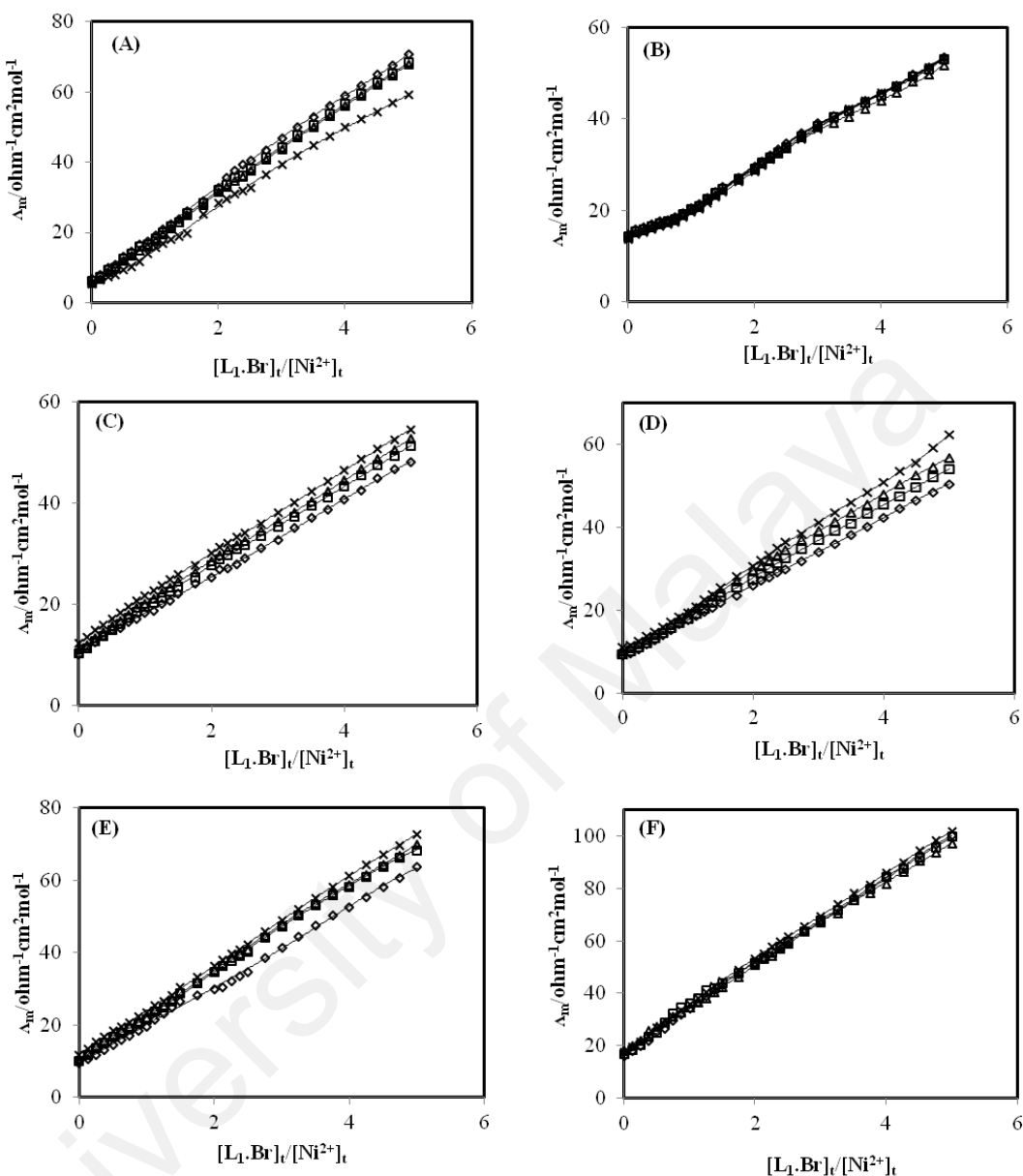
APPENDIX E1: Plot of molar conductance, Λ_m versus mole ratio, $[L_1\cdot Br]_t/[M^{n+}]_t$ for Ag^+



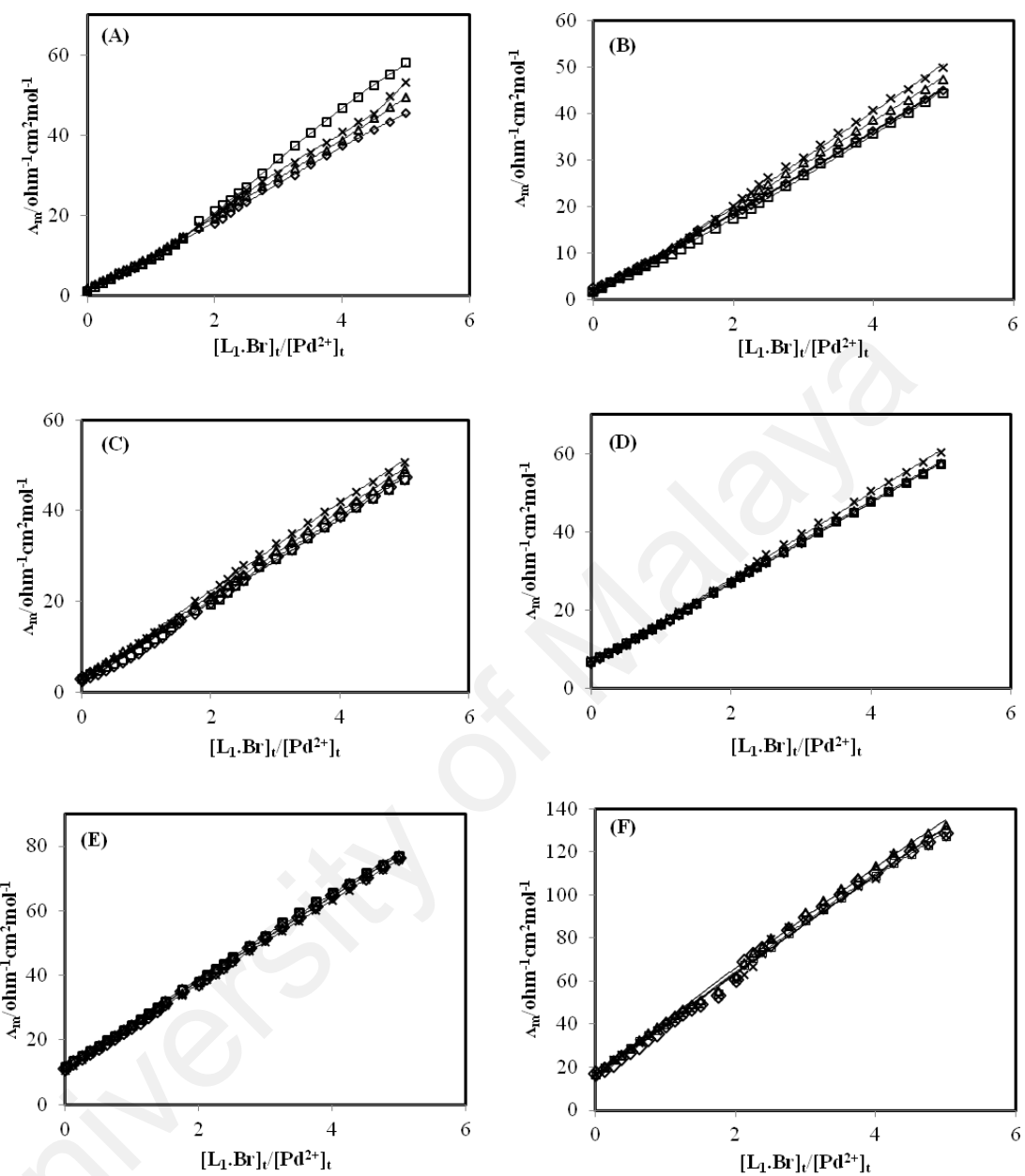
APPENDIX E2: Plot of molar conductance, Λ_m versus mole ratio, $[L_1\cdot Br]_t/[M^{n+}]_t$ for Hg^{2+}



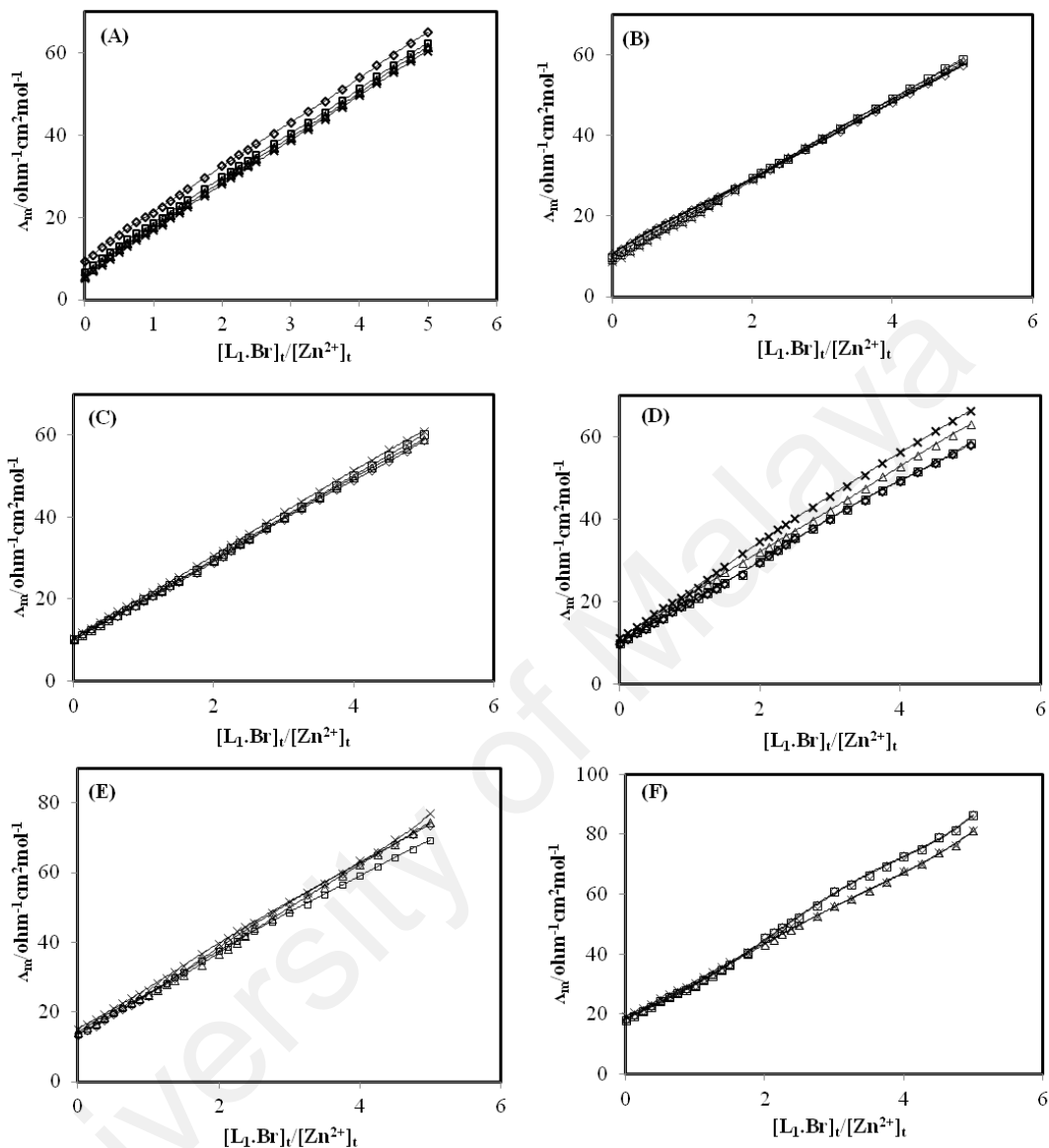
APPENDIX E3: Plot of molar conductance, Λ_m versus mole ratio, $[L_1.Br]_t/[M^{n+}]_t$ for Ni^{2+}



APPENDIX E4: Plot of molar conductance, Λ_m versus mole ratio, $[L_1.Br]_t/[M^{n+}]_t$ for Pd^{2+}



APPENDIX E5: Plot of molar conductance, Λ_m versus mole ratio, $[L_1\cdot Br]_t/[M^{n+}]_t$ for Zn^{2+}



APPENDIX F1: Matematical model applied for the curve fitting using GENPLOT software

The general reaction for 1:1 complex formation can be stated by equestion 1 and the corresponding equilibrium constant (K_f), is given by equation 2.



$$K_f = \frac{[L_1.Br - M^{n+}]f_{(L_1.Br-M^{n+})}}{[M^{n+}][L_1.Br]f_{(M^{n+})}f_{(L_1.Br)}} \quad (2)$$

The equation represents the equilibrium molar concentration of the complex $[L_1.Br - M^{n+}]$, the free cation $[M^{n+}]$, the free ligand $[L_1.Br]$, and the activity coefficients of the species, f . Since the dilute condition was used in this work, the activity coefficient of the uncharged ligand, $f_{(L_1.Br)}$ reasonably assumed to be unity.

Dilute condition is where the ionic strength is less than 0.001 M. Based on the Debye-Hückel limiting law of electrolytes, it can be concluded that $f_{(L_1.Br-M^{n+})} \approx f_{(M^{n+})}$. Thus, the above equation can be simplified as equation 3 (Christy and Shrivastav, 2011).

$$K_f = \frac{[L_1.Br - M^{n+}]}{[M^{n+}][L_1.Br]} \quad (3)$$

The specific conductivity (K) in each point of titration process is the value of the combination of conductivity of both metal salts, $K_{(M^{n+})}$ and $L_1.Br-M^{n+}$ complex, $K_{(L_1.Br-M^{n+})}$ can be seen in following equation 4.

$$K = K_{(M^{n+})} + K_{(L_1.Br-M^{n+})} \quad (4)$$

The equations 5, 6 and 7 show the molar conductance of metal salt before the addition of $L_1.Br$ ligand, $\Lambda_{(M^{n+})}$, molar conductance of $L_1.Br-M^{n+}$ complex, $\Lambda_{(L_1.BrM^{n+})}$ and observed molar conductance during titration, Λ_{Obs} .

$$\Lambda_{(M^{n+})} = \frac{K_{(M^{n+})}}{[M^{n+}]} \quad (5)$$

$$\Lambda_{(ML^{n+})} = \frac{K_{(L_1.Br - M^{n+})}}{[L_1.Br - M^{n+}]} \quad (6)$$

$$\Lambda_{Obs} = \frac{K}{[M^{n+}]_t} \quad (7)$$

Where the total analytical concentration of the metal cations $[M^{n+}]_t$ is the sum of the concentration of metal salts, $[M^{n+}]$ and $L_1.Br-M^{n+}$ complex, $[L_1.Br - M^{n+}]$ as shown in equation 8.

$$[M^{n+}]_t = [M^{n+}] + [L_1.Br - M^{n+}] \quad (8)$$

By combining and simplifying the equations 4, 5, 6 and 7, the following equation is obtained:

$$\Lambda_{Obs}[M^{n+}]_t = \Lambda_{(M^{n+})}[M^{n+}] + \Lambda_{(L_1.Br - M^{n+})}[L_1.Br - M^{n+}] \quad (9)$$

Then, the observed molar conductance of solution can be represented as equation 10 by substituting equation 3 to equation 9.

$$\Lambda_{Obs}[M^{n+}]_t = \Lambda_{(M^{n+})}[M^{n+}] + \Lambda_{(L_1.Br - M^{n+})} K_f [M^{n+}] [L_1.Br] \quad (10)$$

The equation 11 can be obtained by combining equations 3 and 8.

$$[M^{n+}]_t = [M^{n+}] + K_f [L_1.Br - M^{n+}] [L_1.Br] = [M^{n+}] (1 + K_f [L_1.Br]) \quad (11)$$

Thus, the observed molar conductance of solution can be simplified as equation 12 by substituting equation 11 into equation 10.

$$\Lambda_{Obs} = \frac{[M^{n+}] \Lambda_{(M^{n+})} + K_f \Lambda_{(L_1.Br - M^{n+})} [M^{n+}] [L_1.Br]}{[M^{n+}] (1 + K_f [L_1.Br])} = \frac{\Lambda_{(M^{n+})} + K_f \Lambda_{(L_1.Br - M^{n+})} [L_1.Br]}{1 + K_f [L_1.Br]} \quad (12)$$

In contrast, the total concentration of $L_1.Br$ ligand, $[L_1.Br]_t$, can be described as in equation 13.

$$[L_1.Br]_t = [L_1.Br] + [L_1.Br - M^{n+}] \quad (13)$$

The substitution equation 3 for equation 13 gave the following equation.

$$[L_1.Br]_t = [L_1.Br] + K_f [M^{n+}] [L_1.Br] = [L_1.Br] (1 + K_f [M^{n+}]) \quad (14)$$

Then, the combination of equations 11 and 14 resulted equation 15:

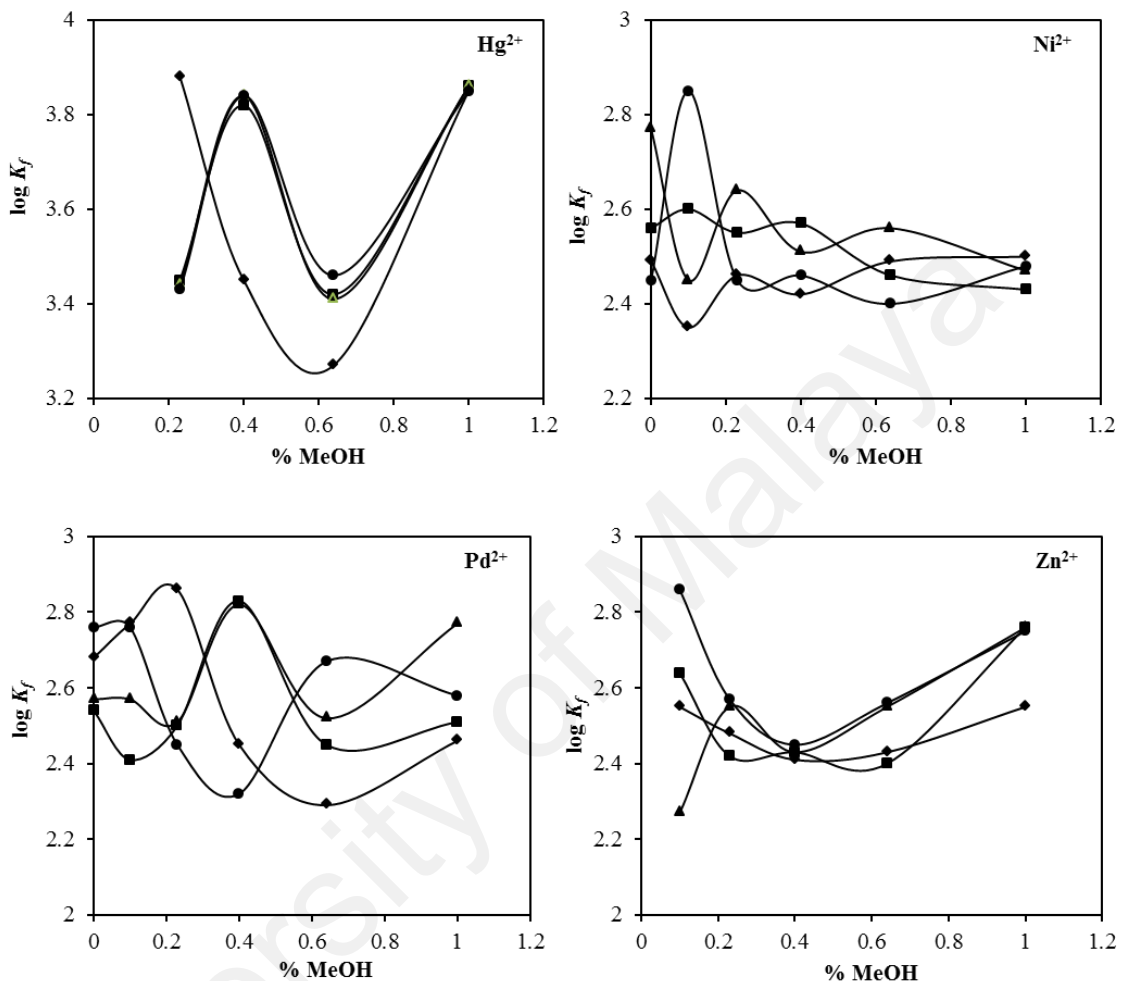
$$[L_1.Br]_t = [L_1.Br] + \frac{K_f [M^{n+}] [L_1.Br]}{1 + K_f [L_1.Br]} = \frac{[L_1.Br] + K_f [L_1.Br]^2 + K_f [L_1.Br] [M^{n+}]_t}{1 + K_f [L_1.Br]} \quad (15)$$

Rearranging the equation 15 gave the equation 16:

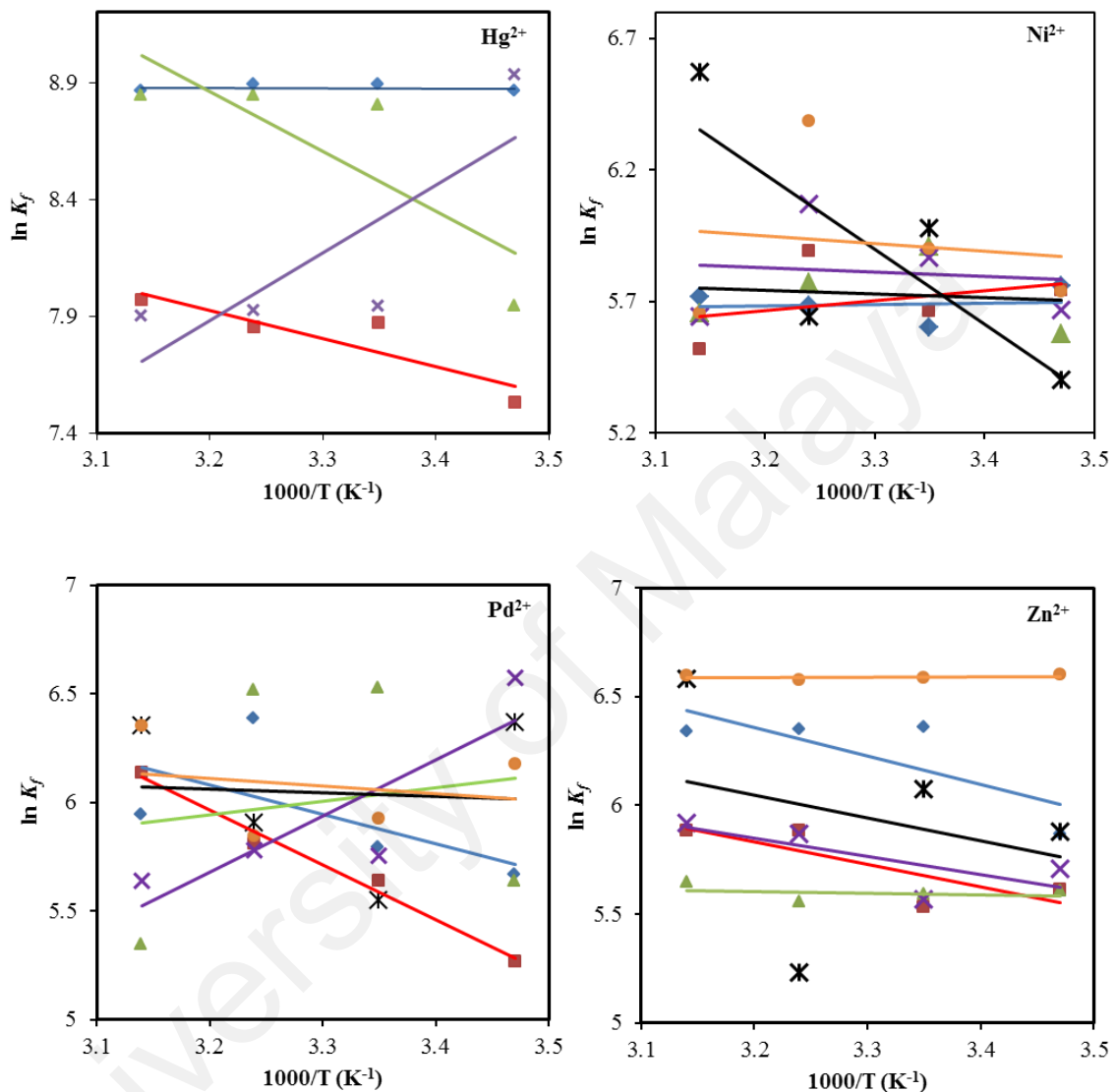
$$K_f [L_1.Br]^2 + (1 + K_f [M^{n+}]_t - K_f [L_1.Br]_t) [L_1.Br] - [L_1.Br]_t = 0 \quad (16)$$

With obtaining $[L_1.Br - M^{n+}]$ and $[L_1.Br]_t$, the values of other species have been involved by using the appraised amount of the formation constants at the current iteration step of the program. Refinement of the parameters is continued until the sum-of-squares of the residuals between calculated and observed values of the conductance for all experimental points is minimized. The output of the program GENPLOT comprises refined parameters, the sum-squares and the standard deviation of the data (Genplot, 1989)

APPENDIX G1: Stability constant ($\log K_f$) of complexes in MeOH-H₂O binary solvent system (mol% MeOH; 0.00, 9.99, 22.66, 39.73, 63.72 and 100.00%) at different temperatures ($\blacklozenge = 15^\circ\text{C}$, $\blacksquare = 25^\circ\text{C}$, $\blacktriangle = 35^\circ\text{C}$, $\bullet = 45^\circ\text{C}$) for Hg²⁺, Ni²⁺, Pd²⁺ and Zn²⁺

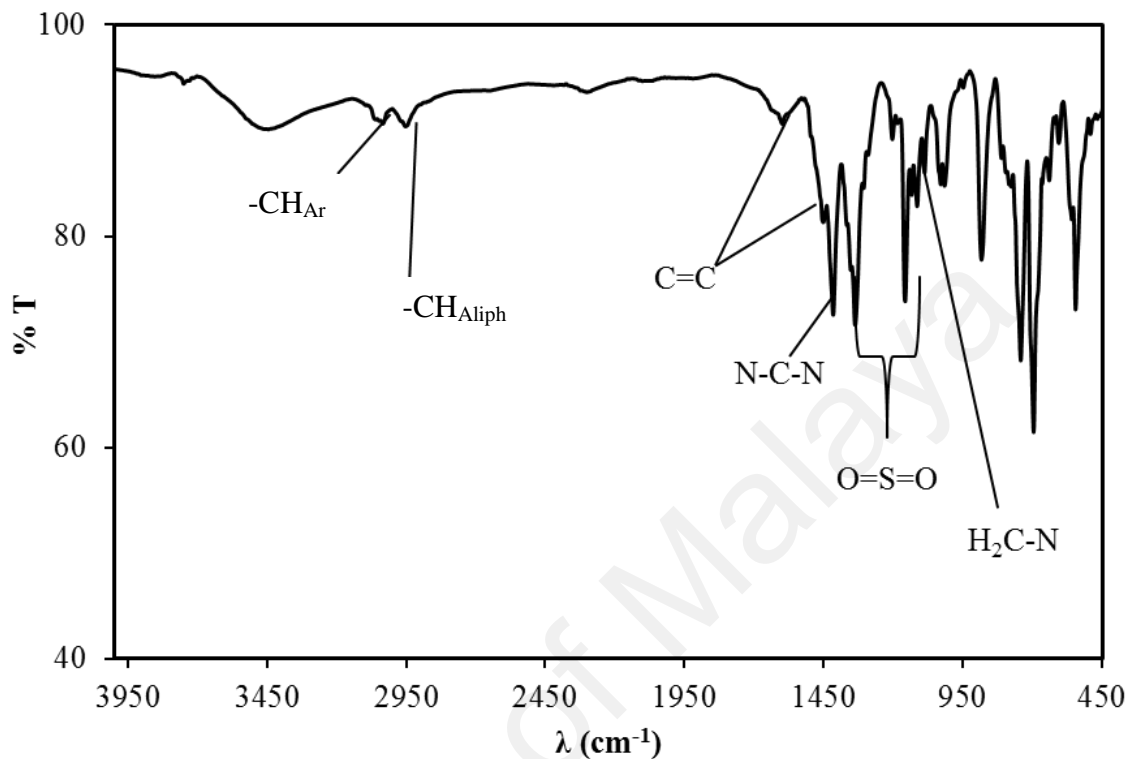


APPENDIX H1: Van't Hoff plot for L₁.Br-Mⁿ⁺ complex for Hg²⁺, Ni²⁺, Pd²⁺ and Zn²⁺ cations in MeOH-H₂O binary solvent system (mol% MeOH; \blacklozenge = 100, \blacksquare = 63.72, \blacktriangle = 39.73, \times = 22.66, \divideontimes = 9.90, \bullet = 0.00) at different temperatures.

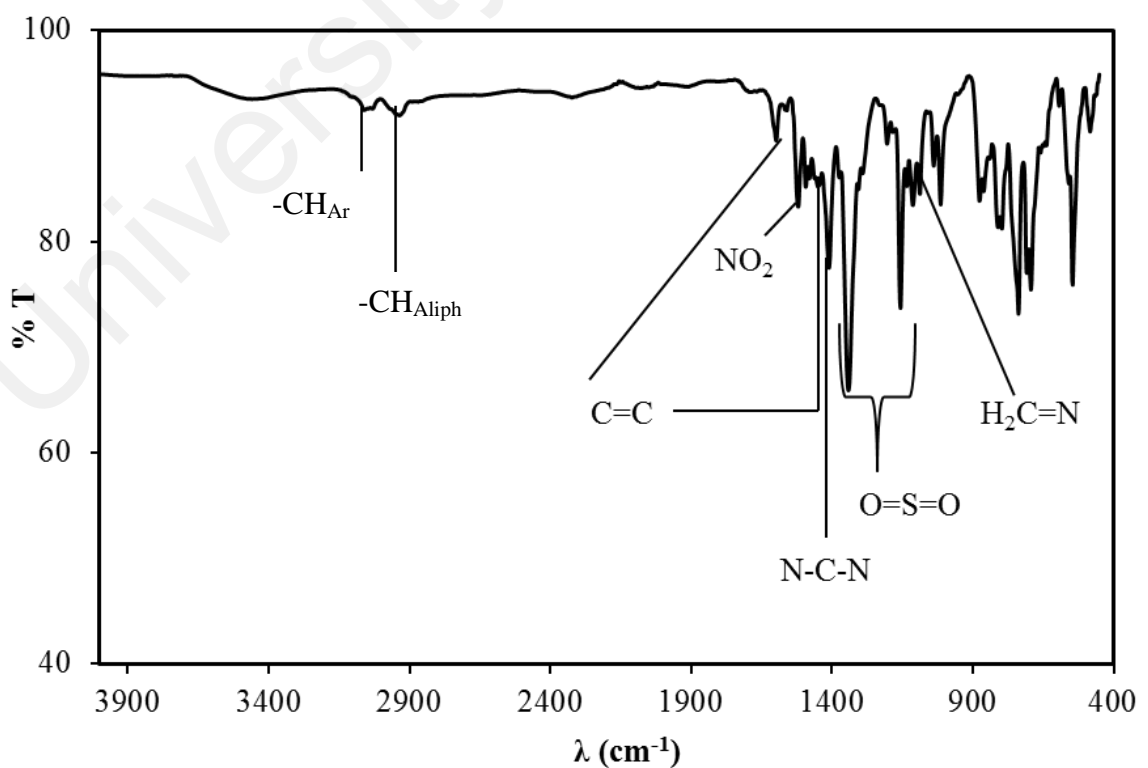


APPENDIX I: FT-IR spectra of bis-NHC metal complexes

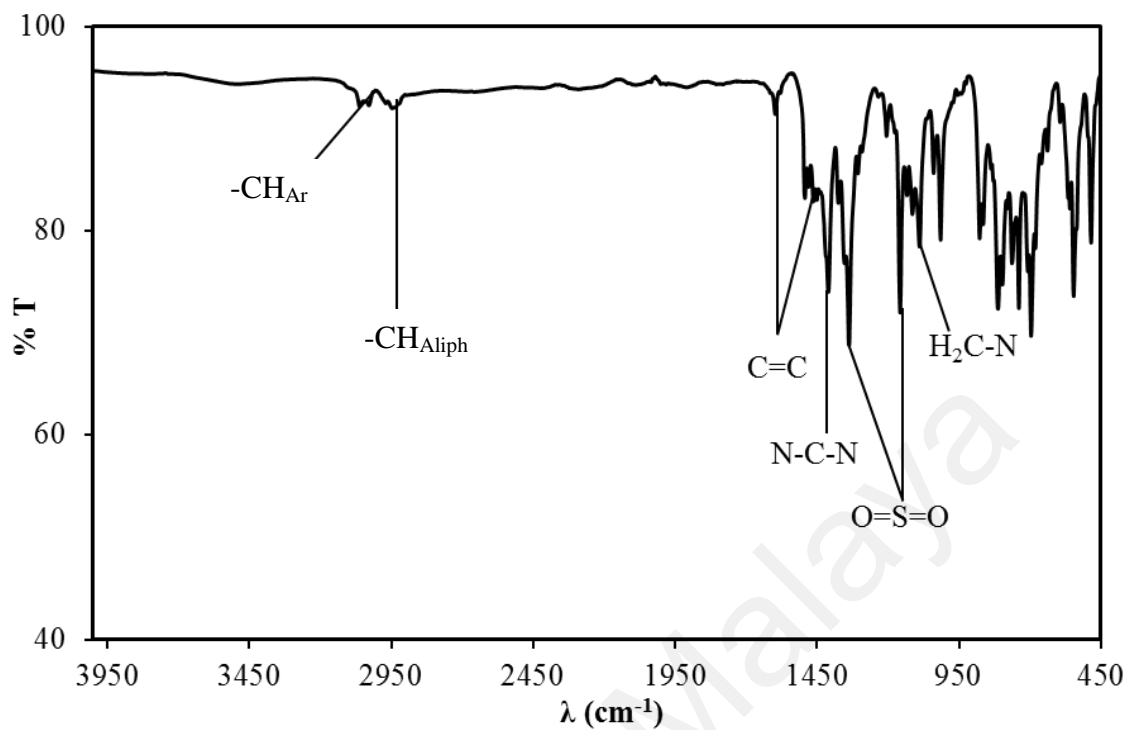
APPENDIX I1: FT-IR spectrum of L₁.HgBr



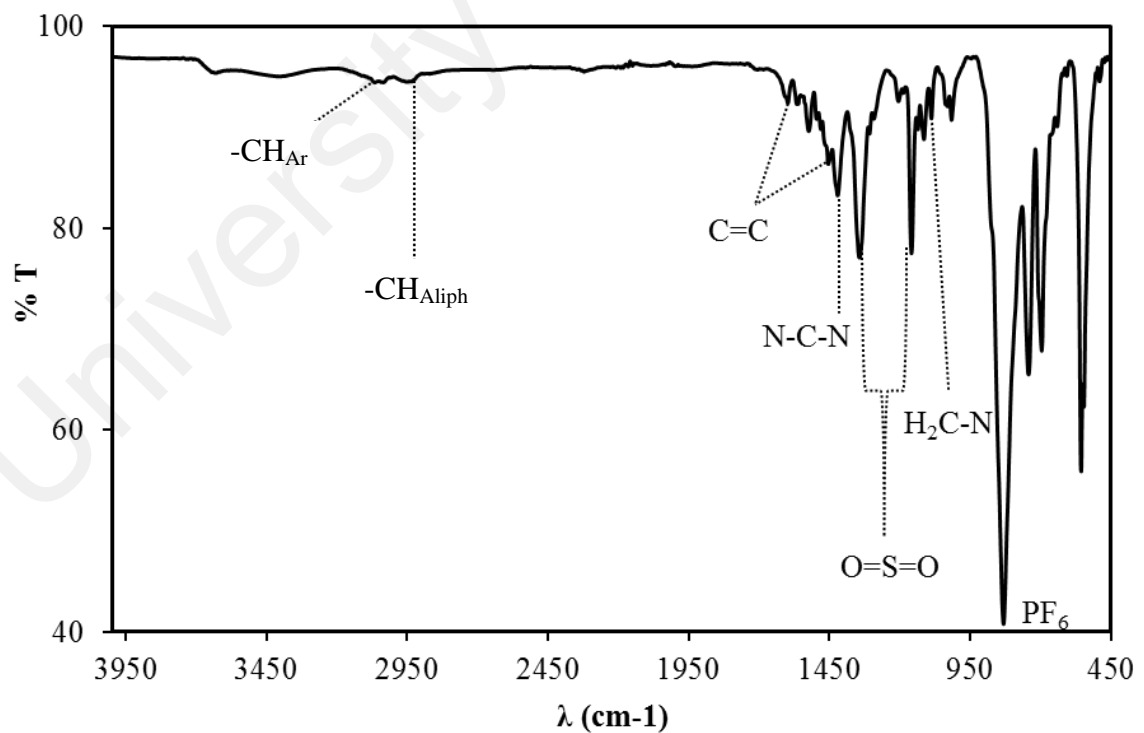
APPENDIX I2: FT-IR spectrum of L₂.HgBr



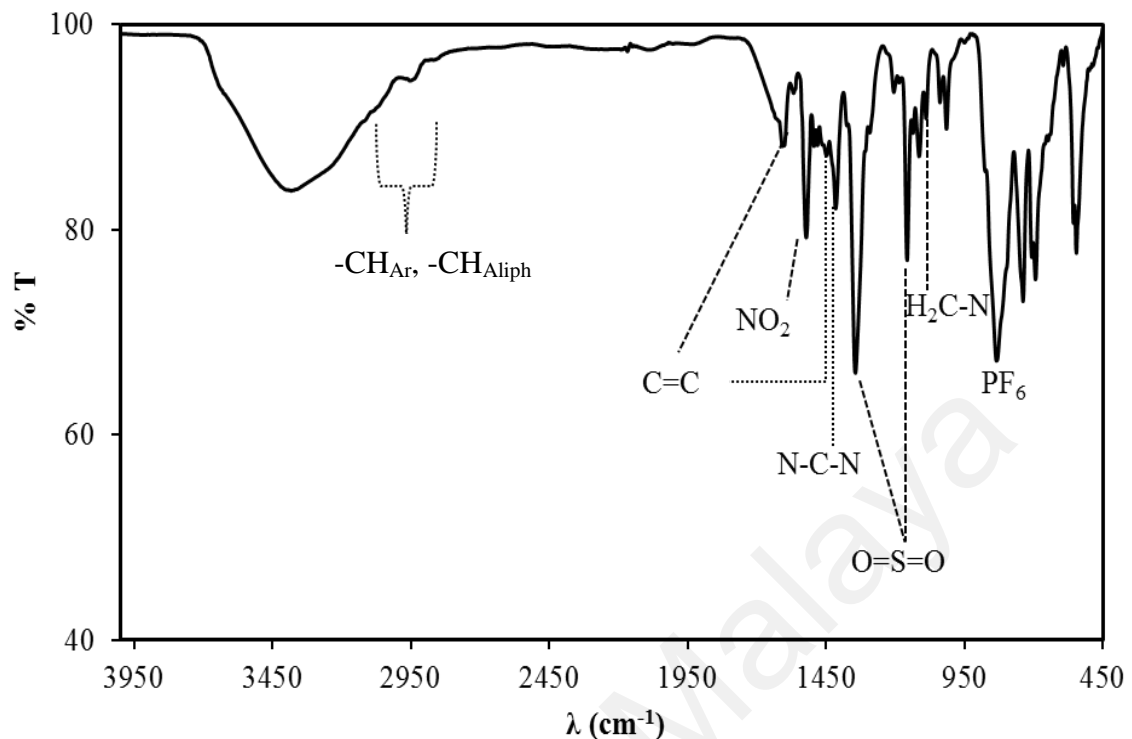
APPENDIX I3: FT-IR spectrum of L₃.HgBr



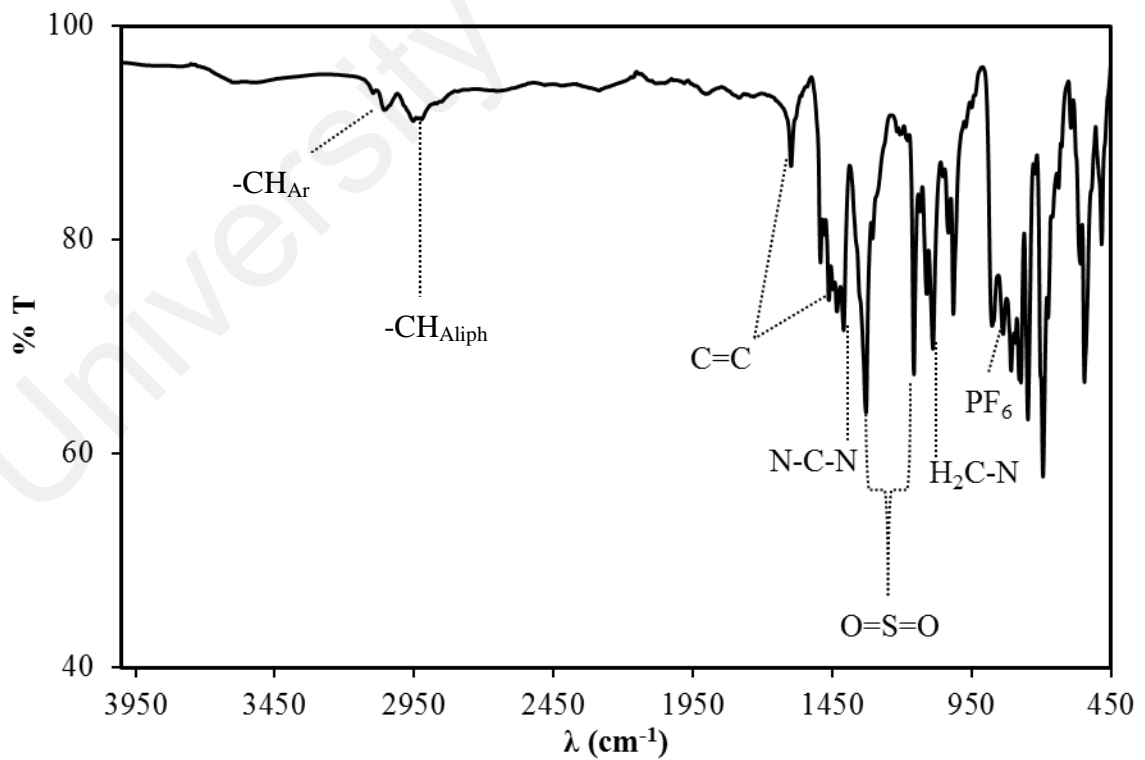
APPENDIX I4: FT-IR spectrum of L₁.HgPF₆



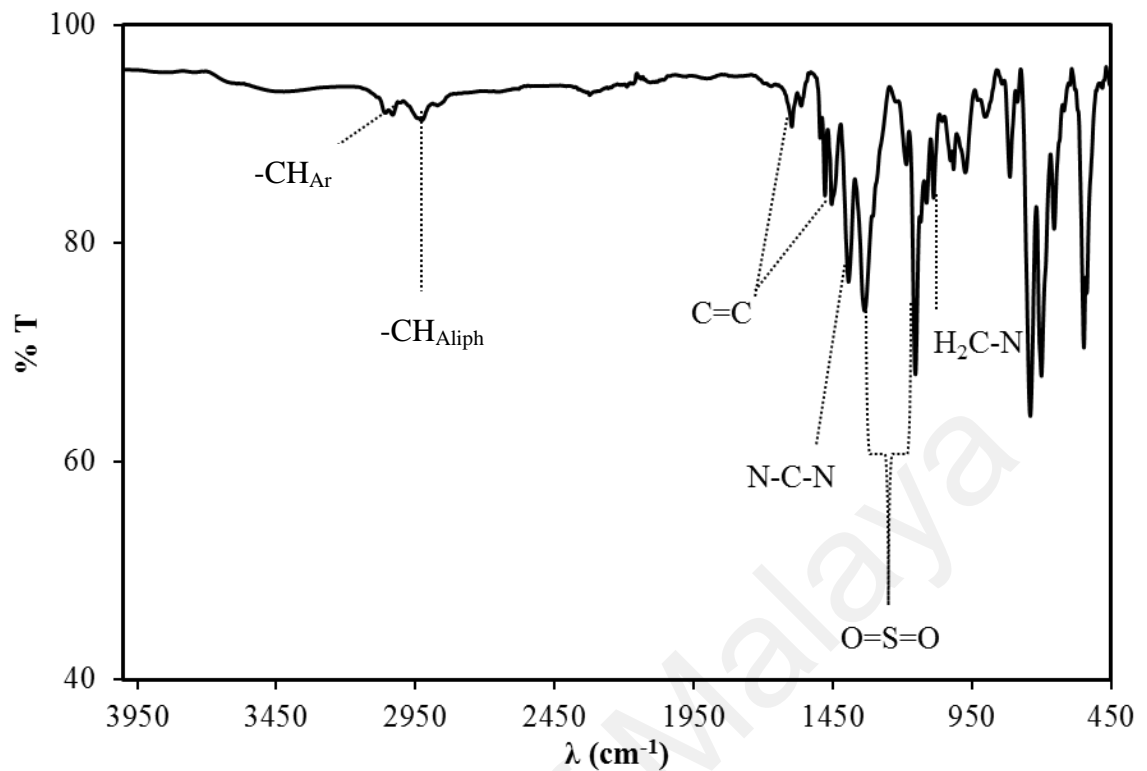
APPENDIX I5: FT-IR spectrum of L₂.HgPF₆



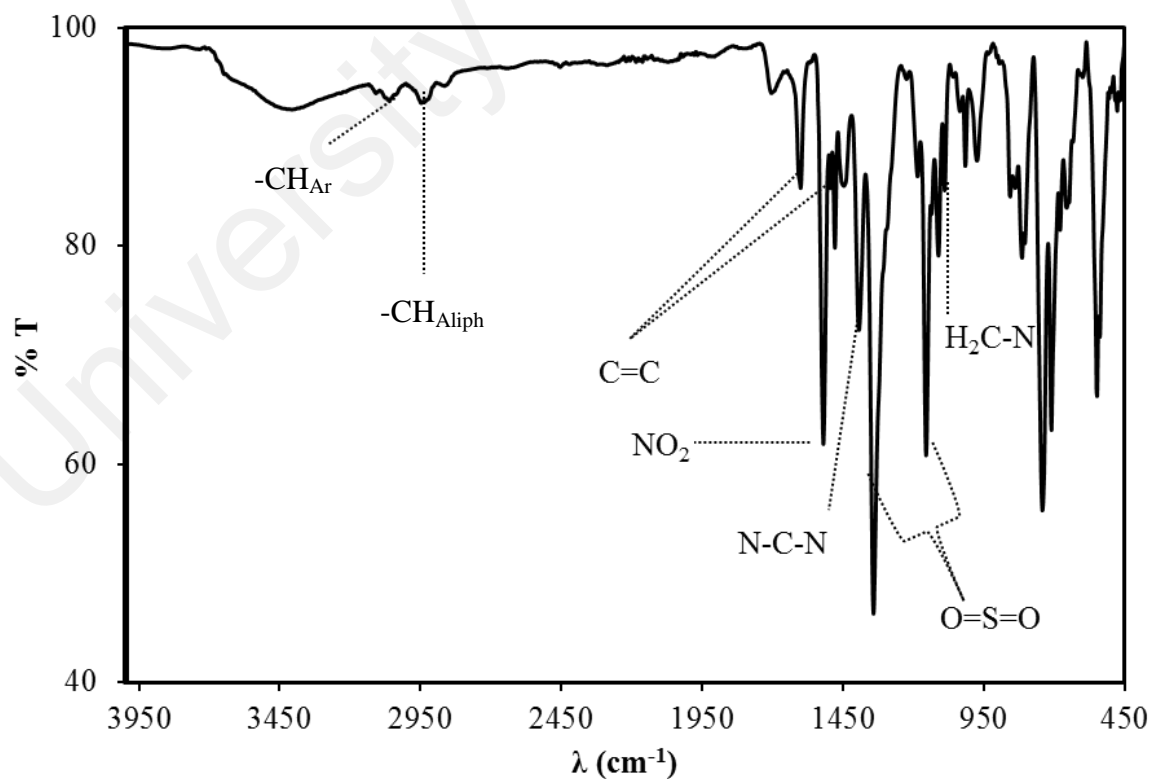
APPENDIX I6: FT-IR spectrum of L₃.HgPF₆



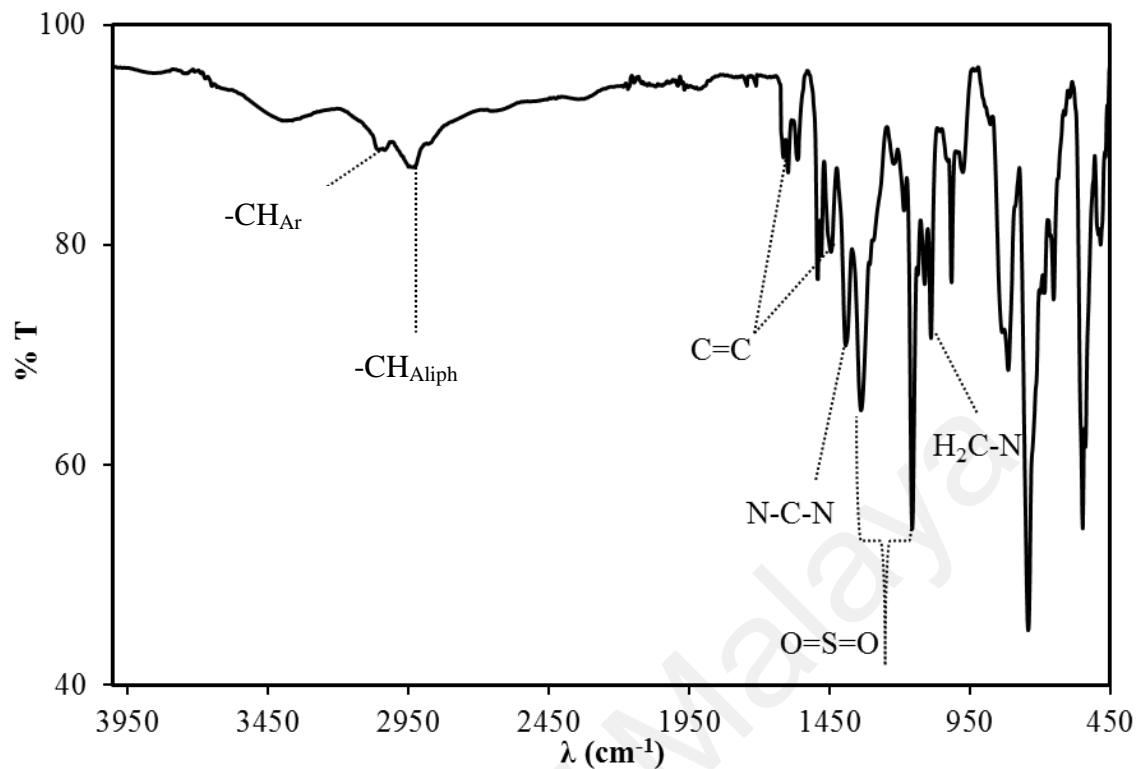
APPENDIX I7: FT-IR spectrum of L₁.AgBr



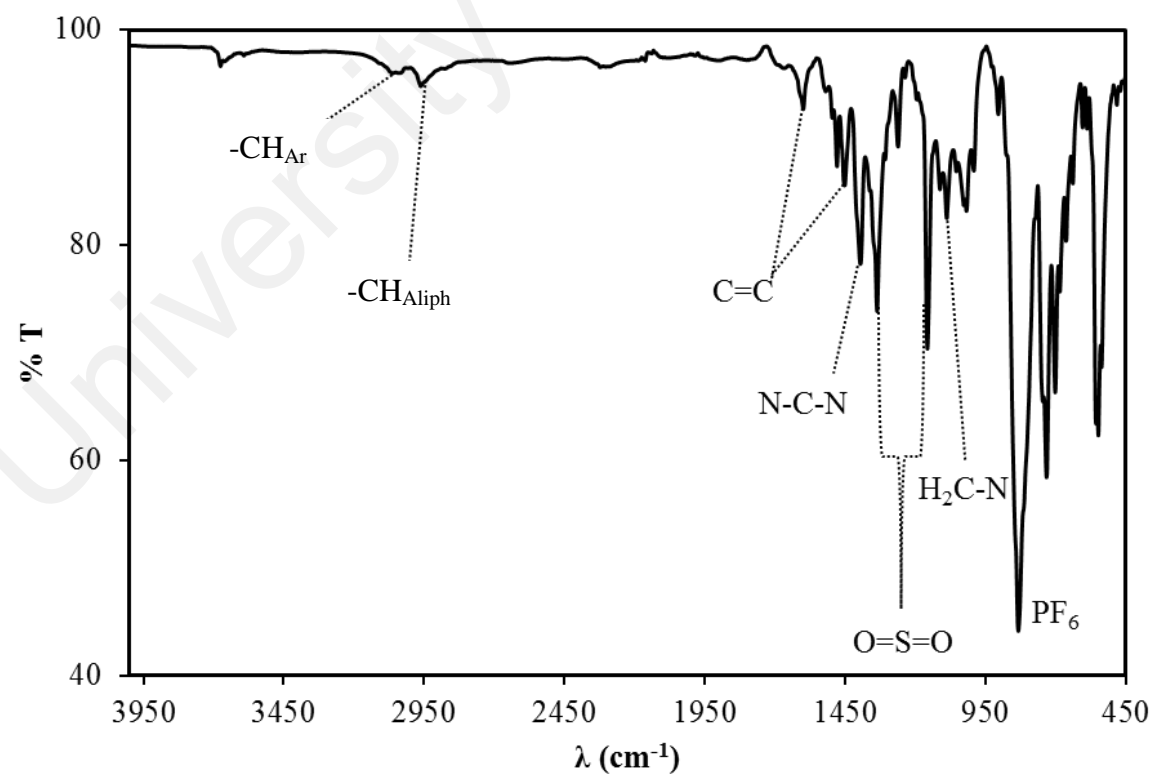
APPENDIX I8: FT-IR spectrum of L₂.AgBr



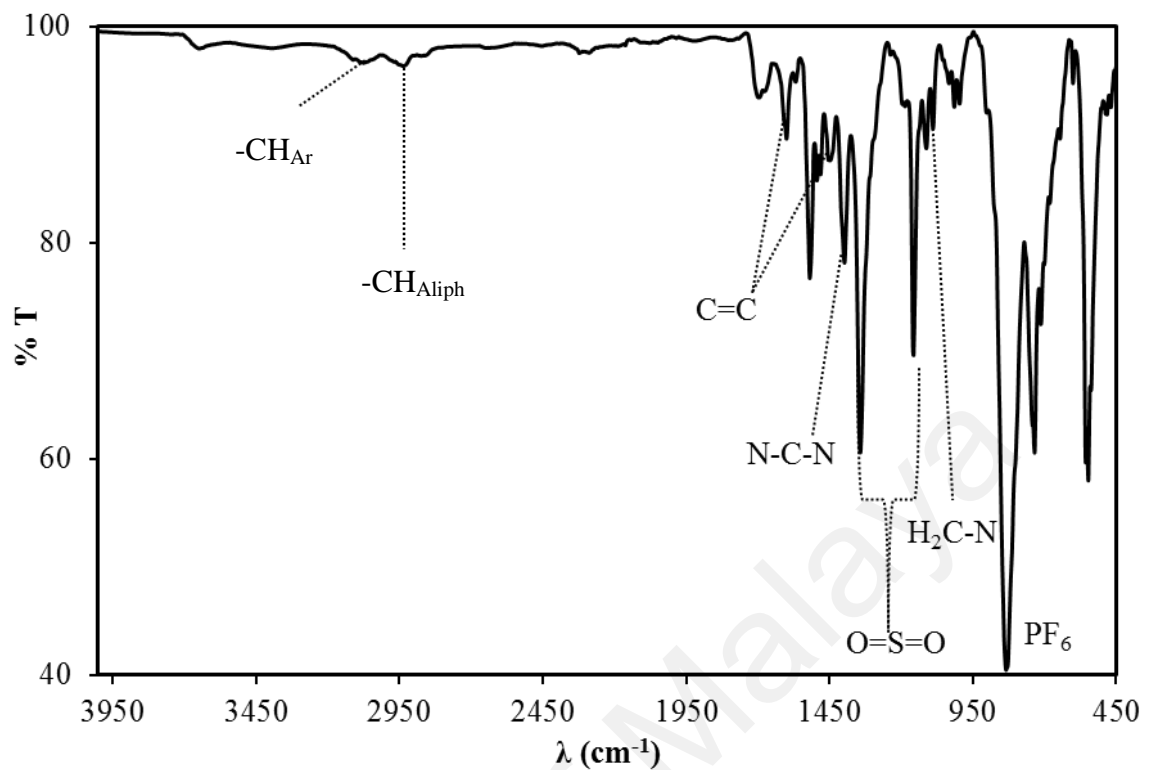
APPENDIX I9: FT-IR spectrum of L₃.AgBr



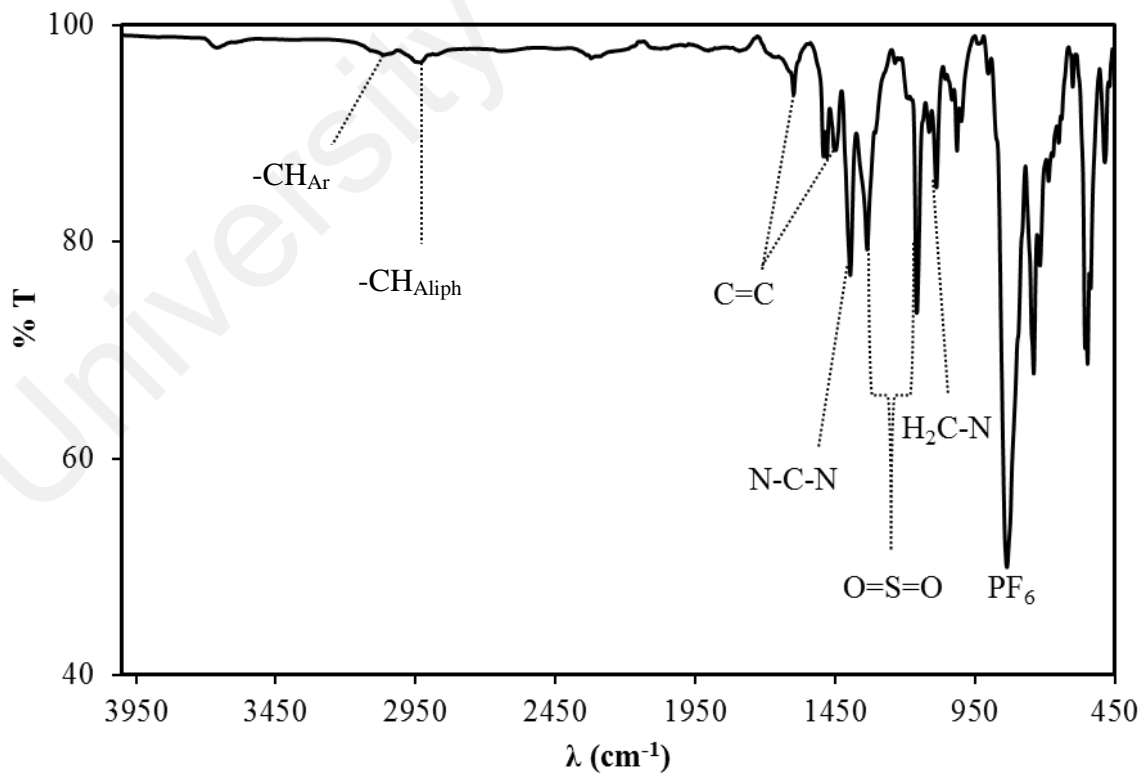
APPENDIX I10: FT-IR spectrum of L₁.AgPF₆



APPENDIX I11: FT-IR spectrum of L₂.AgPF₆

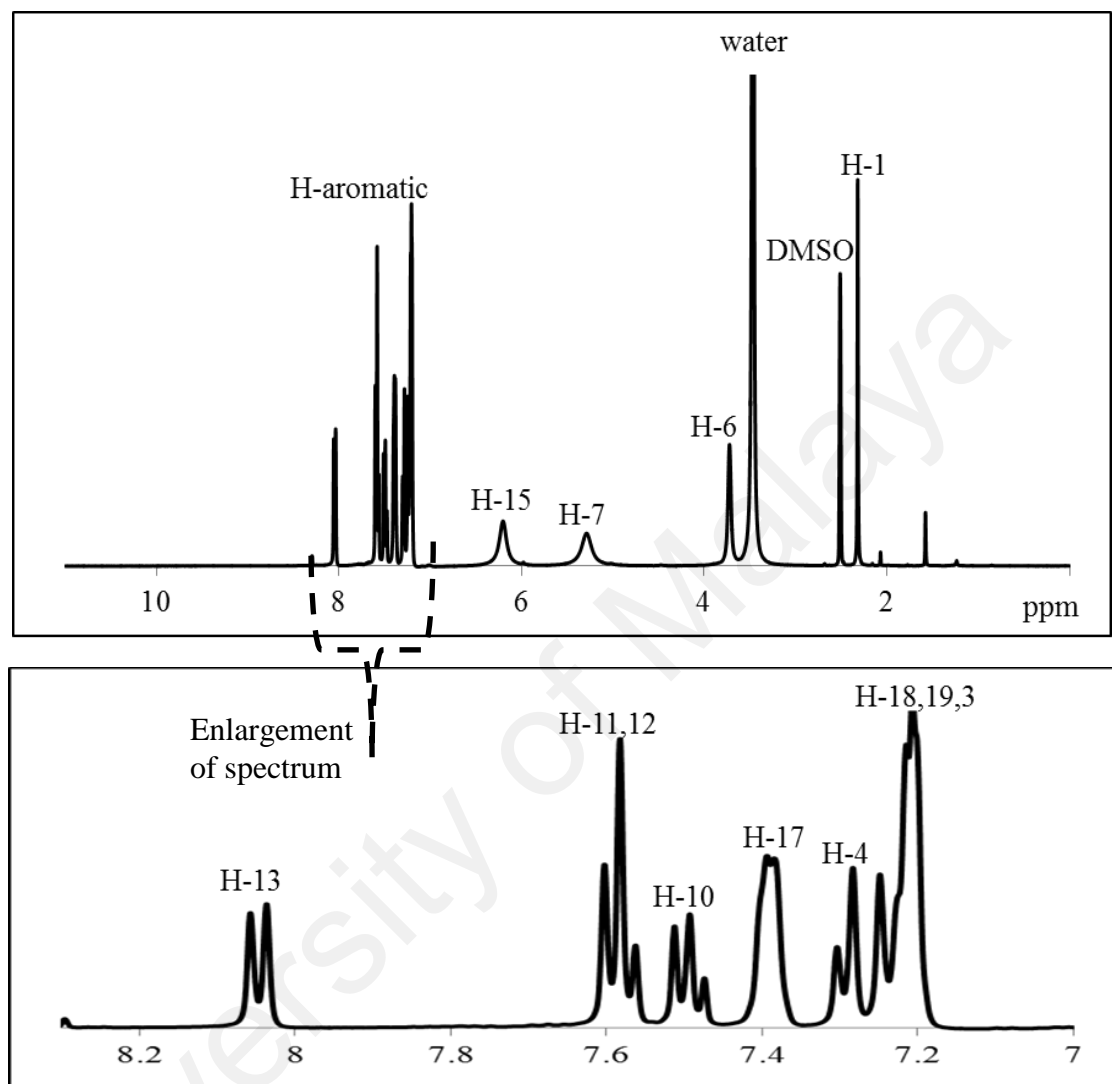


APPENDIX I12: FT-IR spectrum of L₃.AgPF₆



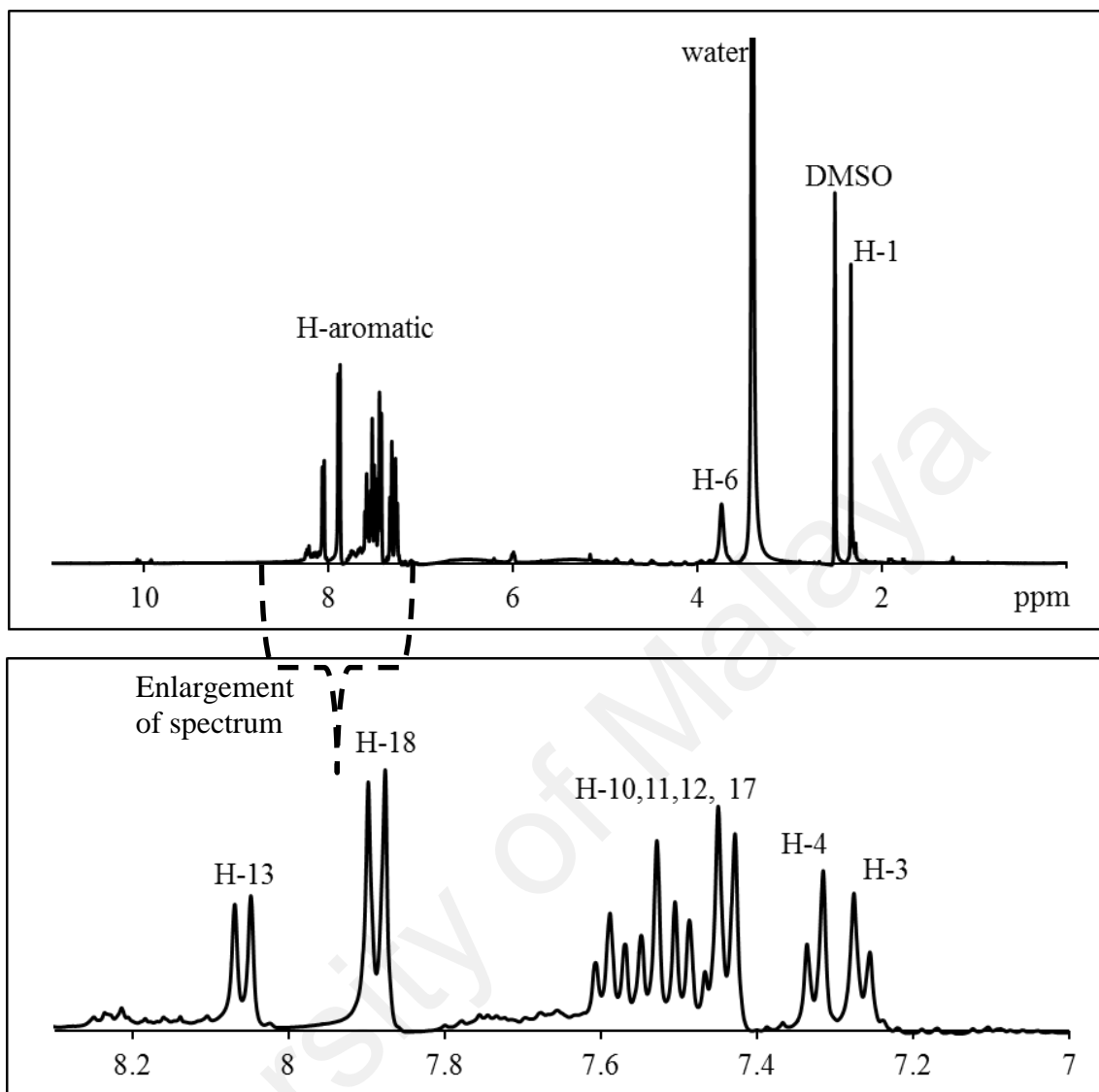
APPENDIX J: ^1H -NMR spectra of bis-NHC metal complexes

APPENDIX J1: ^1H -NMR spectrum of L₁.HgBr



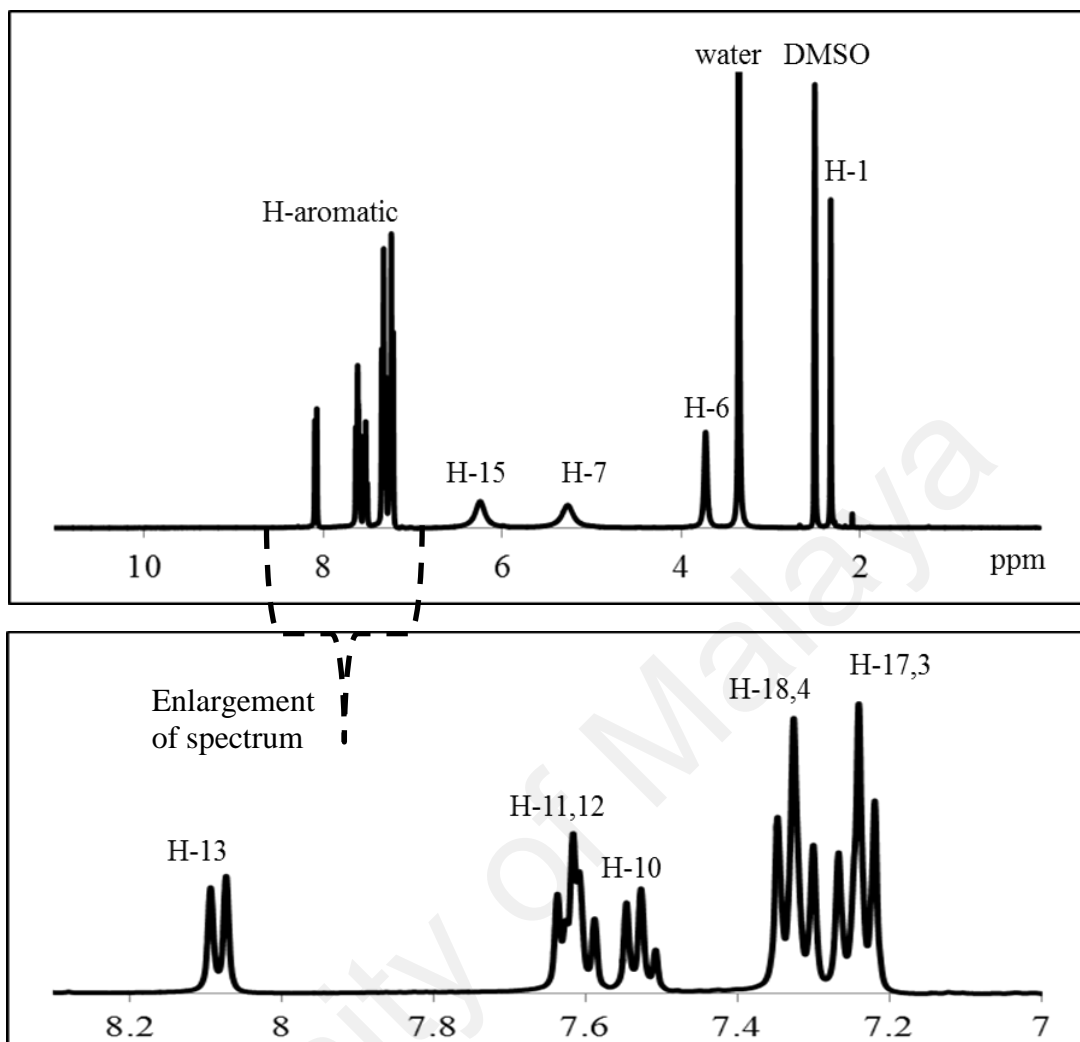
H-position	Integrations	Chemical shift, δ ppm	multiplicity	J_{HH} (Hz)
1	3H	2.32	s	-
6	4H	3.72	s	-
7	4H	5.29	s	-
15	4H	6.20	s	-
3,18,19, 4	10H	7.21-7.30	m	-
17	4H	7.39	d	4
10,11,12	6H	7.42-7.60	m	-
13	2H	8.05	d	8

APPENDIX J2: ^1H -NMR spectrum of L_2HgBr



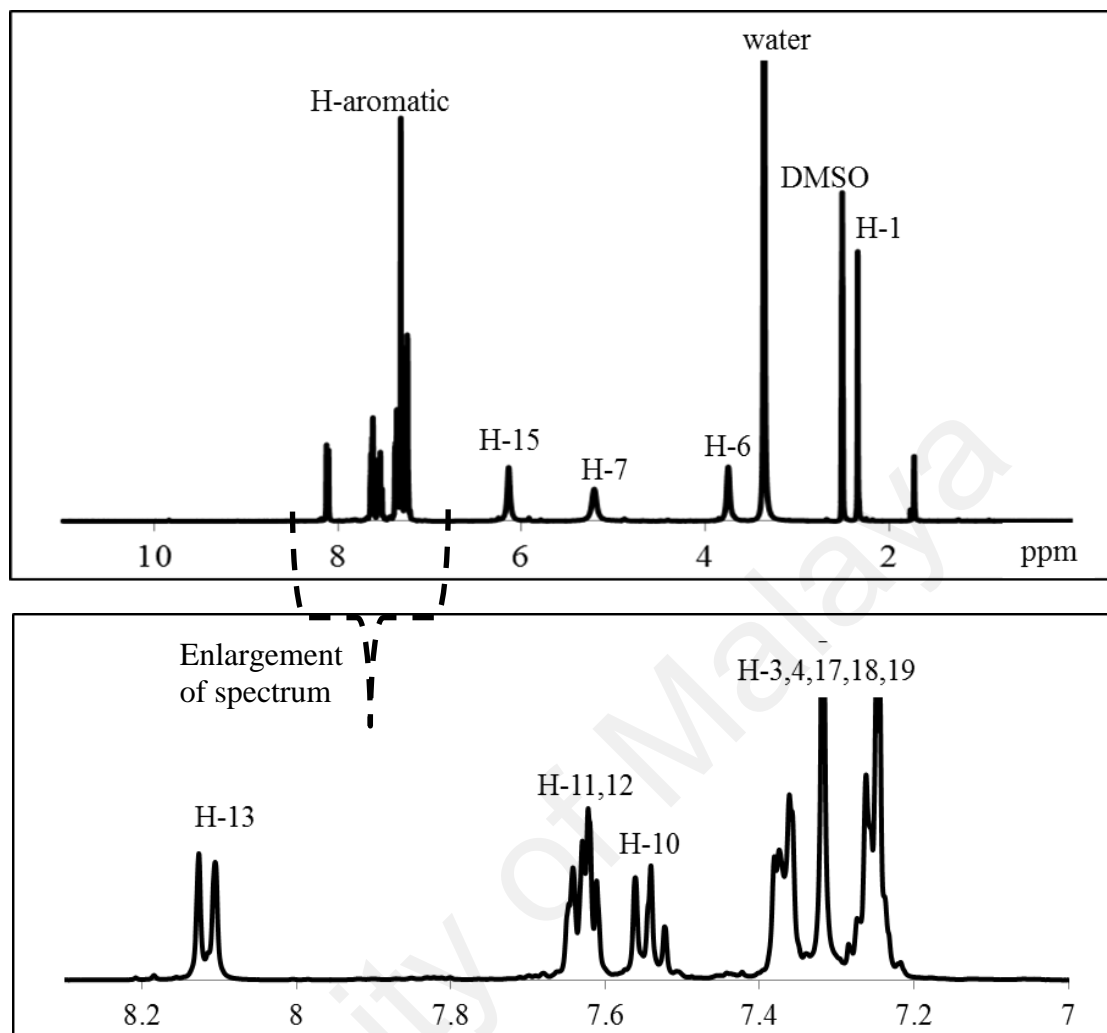
H-position	Integrations	Chemical shift, δ ppm	multiplicity	J_{HH} (Hz)
1	3H	2.34	s	-
6	4H	3.74	s	-
7	-	-	-	-
15	-	-	-	-
3	2H	7.27	d	8
4	2H	7.33	d	8
10,11,12, 17	10H	7.43-7.61	m	-
18	4H	7.89	d	8
13	2H	8.06	d	8

APPENDIX J3: ^1H -NMR spectrum of L_3HgBr



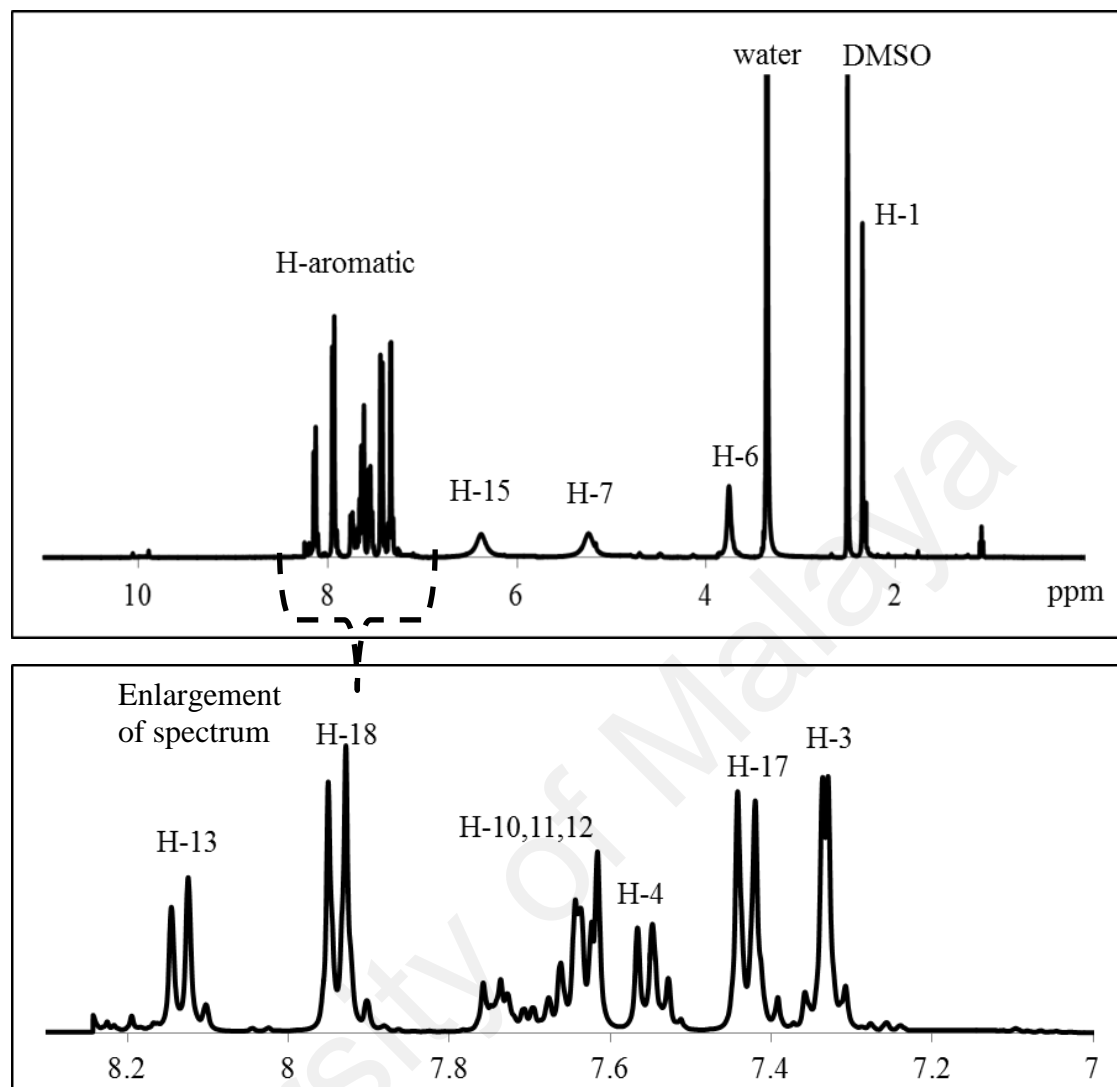
H-position	Integrations	Chemical shift, δ ppm	multiplicity	J_{HH} (Hz)
1	3H	2.33	s	-
6	4H	3.73	s	-
7	4H	5.27	s	-
15	4H	6.25	s	-
3,17,18,4	12H	7.22-7.35	m	-
10,11,12	6H	7.51-7.64	m	-
13	2H	8.08	d	8

APPENDIX J4: ^1H -NMR spectrum of $\text{L}_1\cdot\text{HgPF}_6$



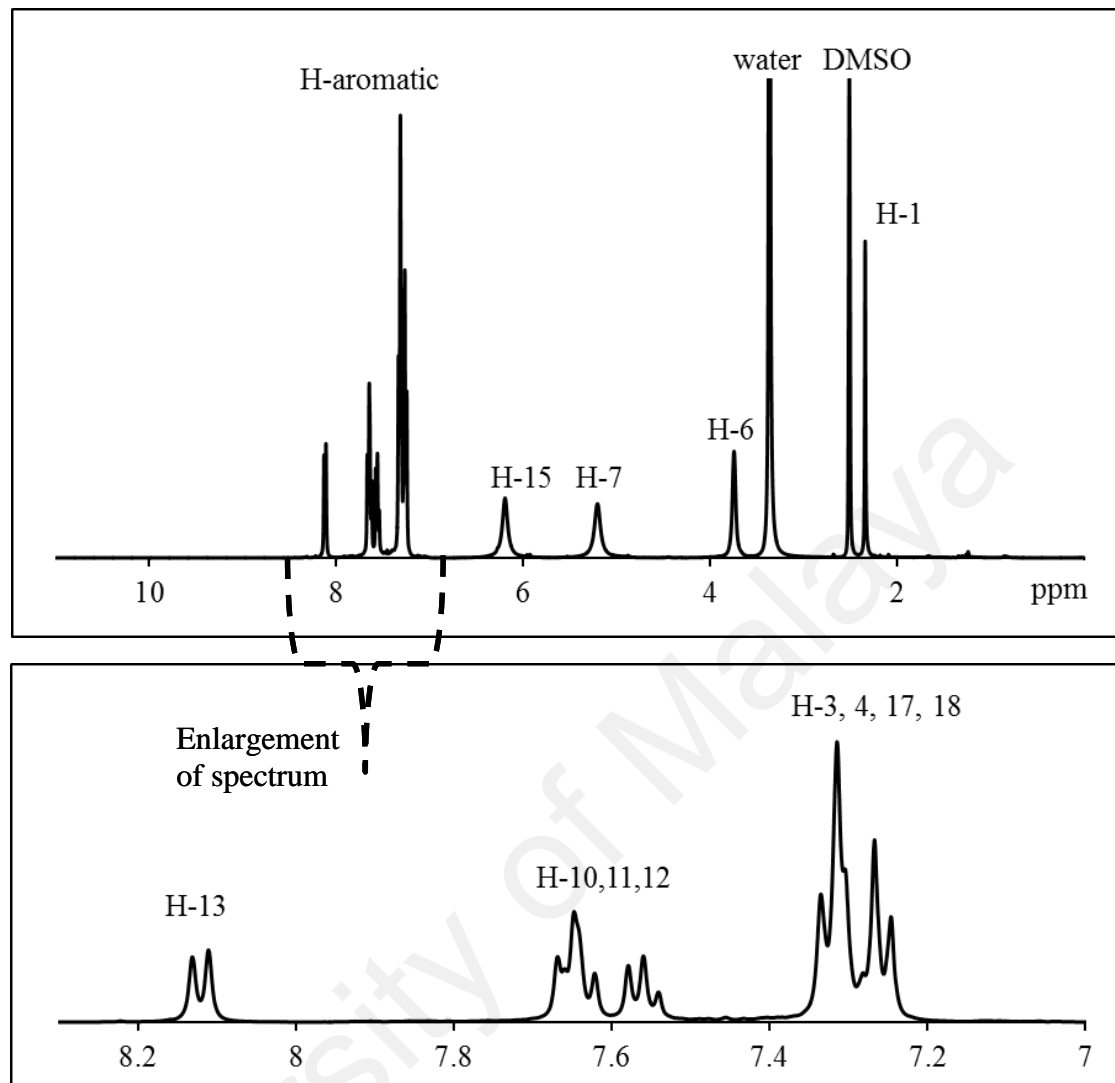
H-position	Integrations	Chemical shift, δ ppm	multiplicity	J_{HH} (Hz)
1	3H	2.34	s	-
6	4H	3.75	s	-
7	4H	5.21	s	-
15	4H	6.14	s	-
3,4, 17,18,19	14H	7.24-7.38	m	-
10, 11,12	6H	7.52-7.64	m	-
13	2H	8.12	d	8

APPENDIX J5: ^1H -NMR spectrum of L_2HgPF_6



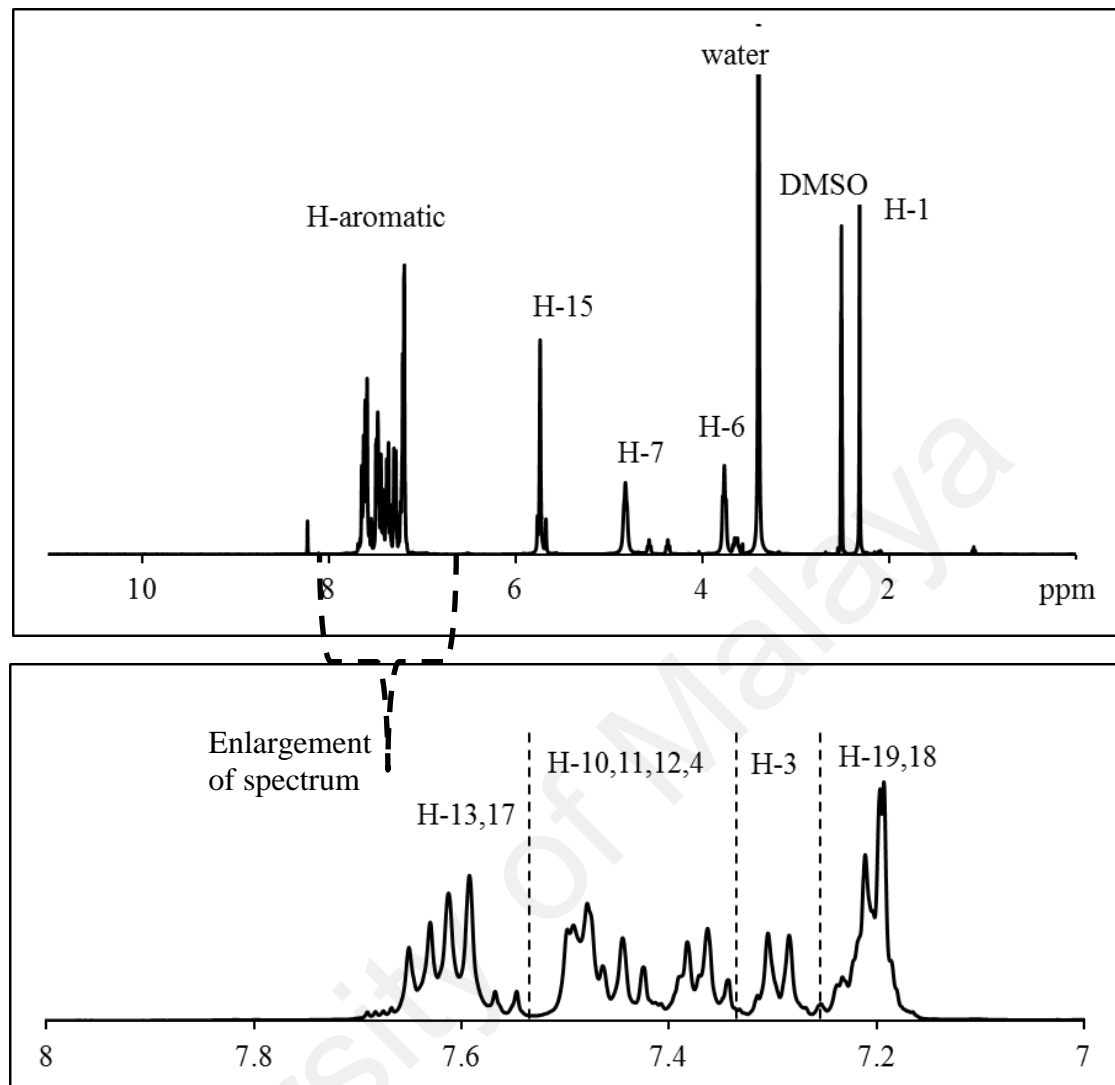
H-position	Integrations	Chemical shift, δ ppm	multiplicity	J_{HH} (Hz)
1	3H	2.35	s	-
6	4H	3.76	s	-
7	4H	5.24	s	-
15	4H	6.38	s	-
3	2H	7.33	d	4
17	4H	7.43	d	8
4	2H	7.56	d	8
10,11,12	6H	7.62-7.66	m	-
18	4H	7.94	d	8
13	2H	8.14	d	8

APPENDIX J6: ^1H -NMR spectrum of L_3HgPF_6



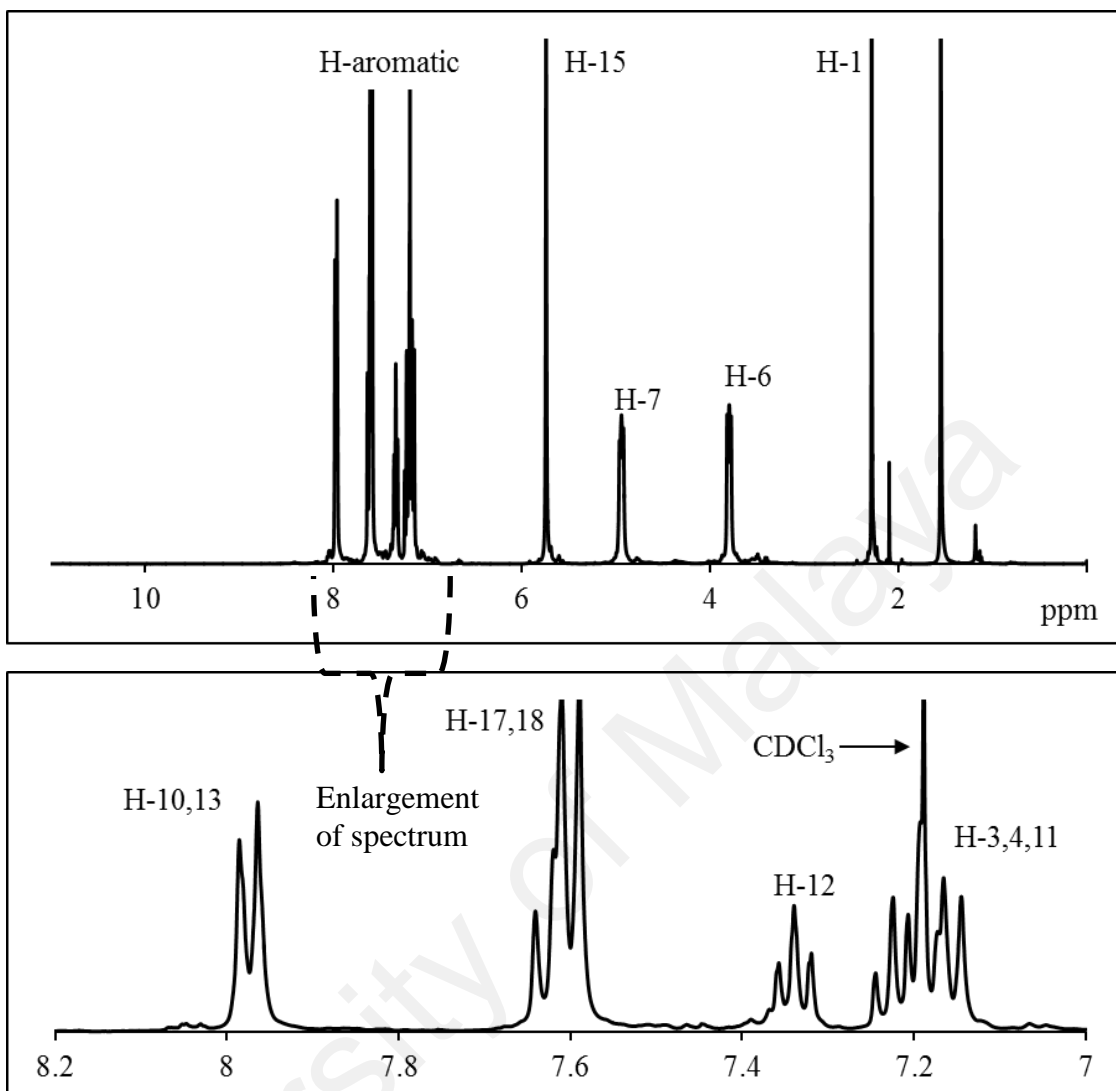
H-position	Integrations	Chemical shift, δ ppm	multiplicity	J_{HH} (Hz)
1	3H	2.34	s	-
6	4H	3.74	s	-
7	4H	5.20	s	-
15	4H	6.19	s	-
3,17,18,4	12H	7.25-7.33	m	-
10,11,12	6H	7.56-7.67	m	-
13	2H	8.12	d	8

APPENDIX J7: ^1H -NMR spectrum of L₁.AgBr



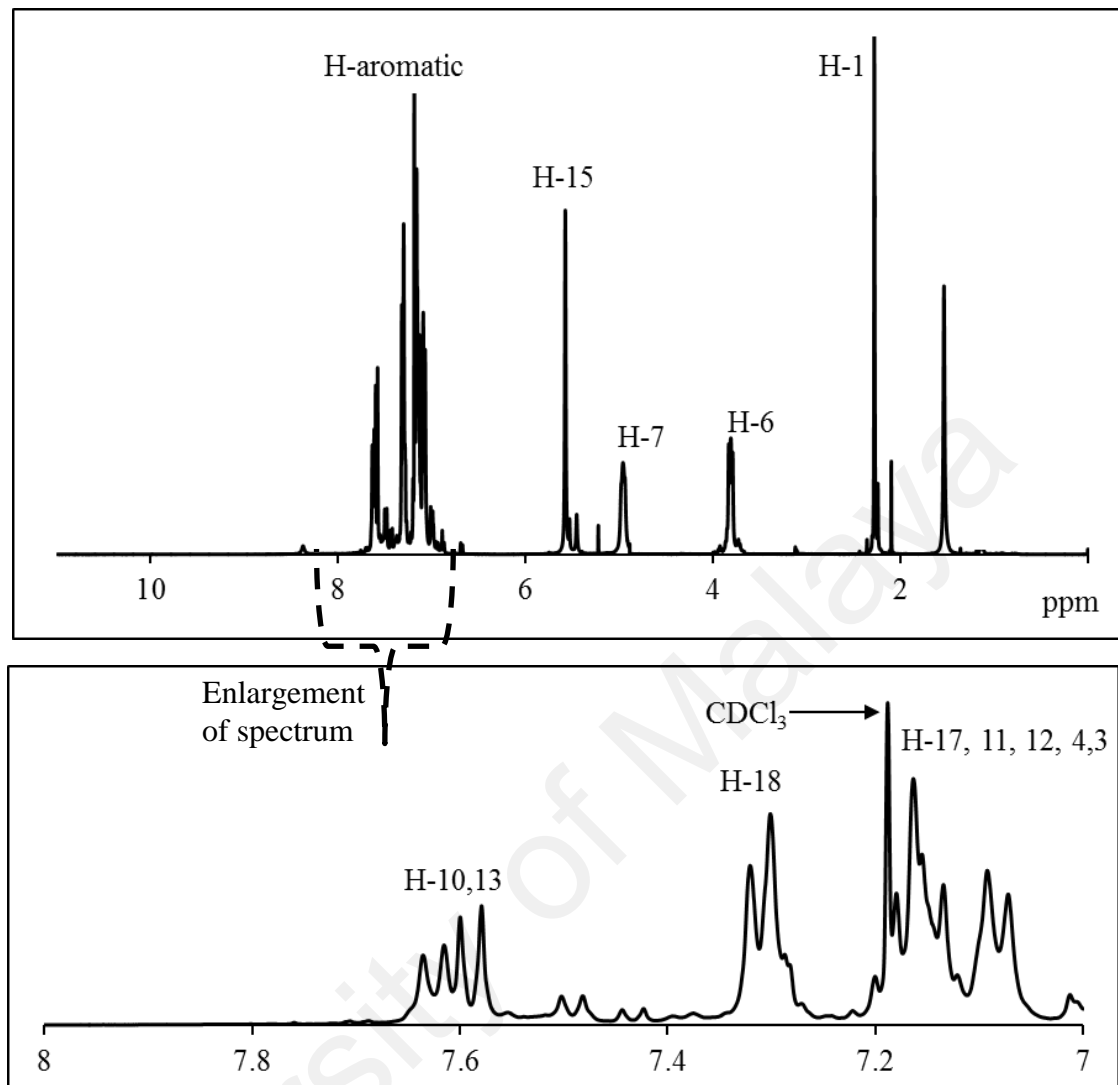
H-position	Integrations	Chemical shift, δ ppm	multiplicity	J_{HH} (Hz)
1	3H	2.31	s	-
6	4H	3.76	t	8
7	4H	4.82	s	-
15	4H	5.74	s	-
18,19	6H	7.19-7.21	m	-
H-3	2H	7.29	d	8
4, 10,11,12	8H	7.34-7.50	m	-
13, 17	6H	7.59-7.65	m	8,8

APPENDIX J8: ^1H -NMR spectrum of L₂.AgBr



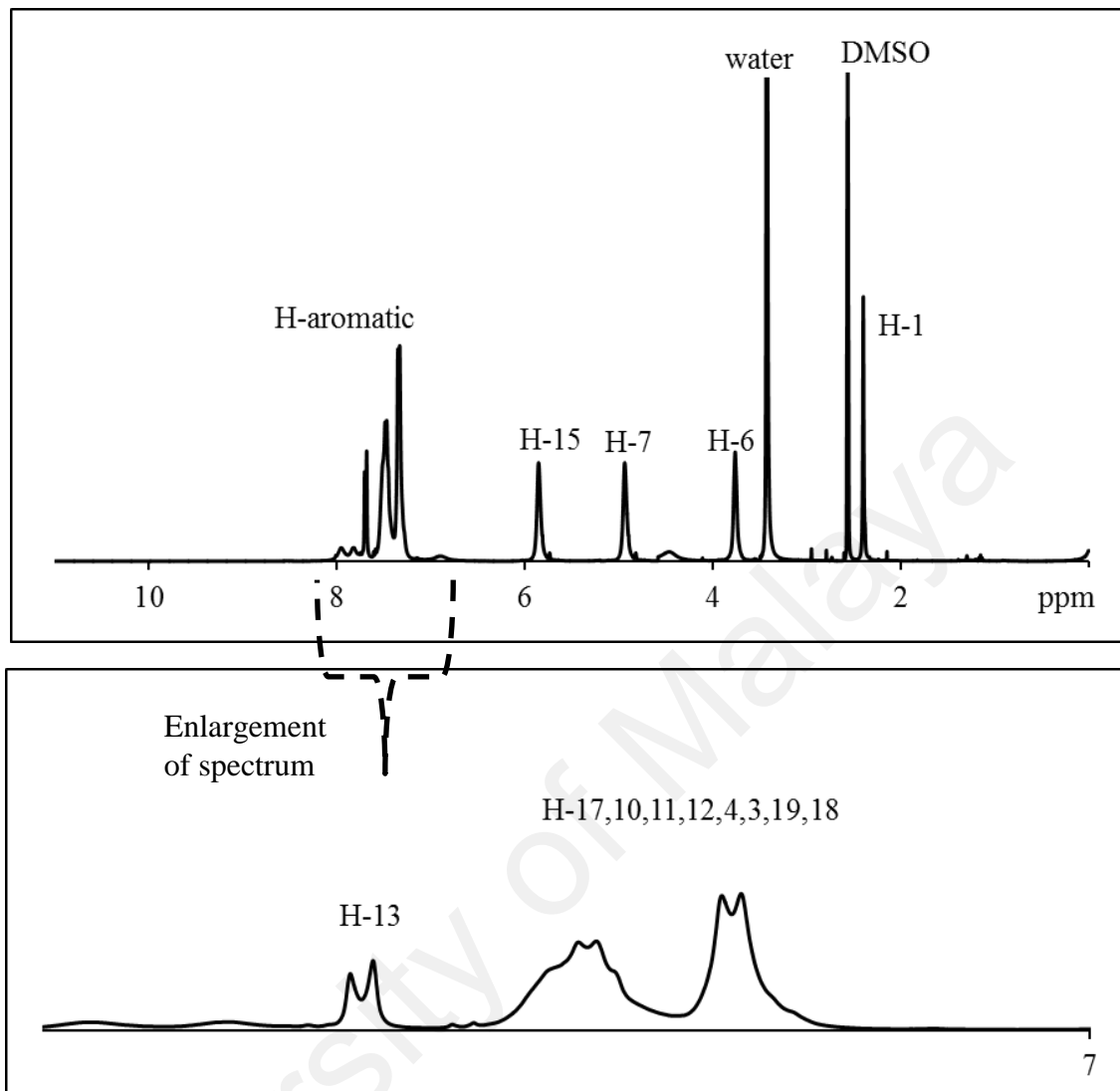
H-position	Integrations	Chemical shift, δ ppm	multiplicity	J_{HH} (Hz)
1	3H	2.28	s	-
6	4H	3.80	t	8
7	4H	4.94	t	8
15	4H	5.74	s	-
3, 4, 11	6H	7.14-7.24	m	-
12	2H	7.34	t	8
17, 18	8H	7.59-7.64	m	-
10, 13	4H	7.97	d	12

APPENDIX J9: ^1H -NMR spectrum of L_3AgBr



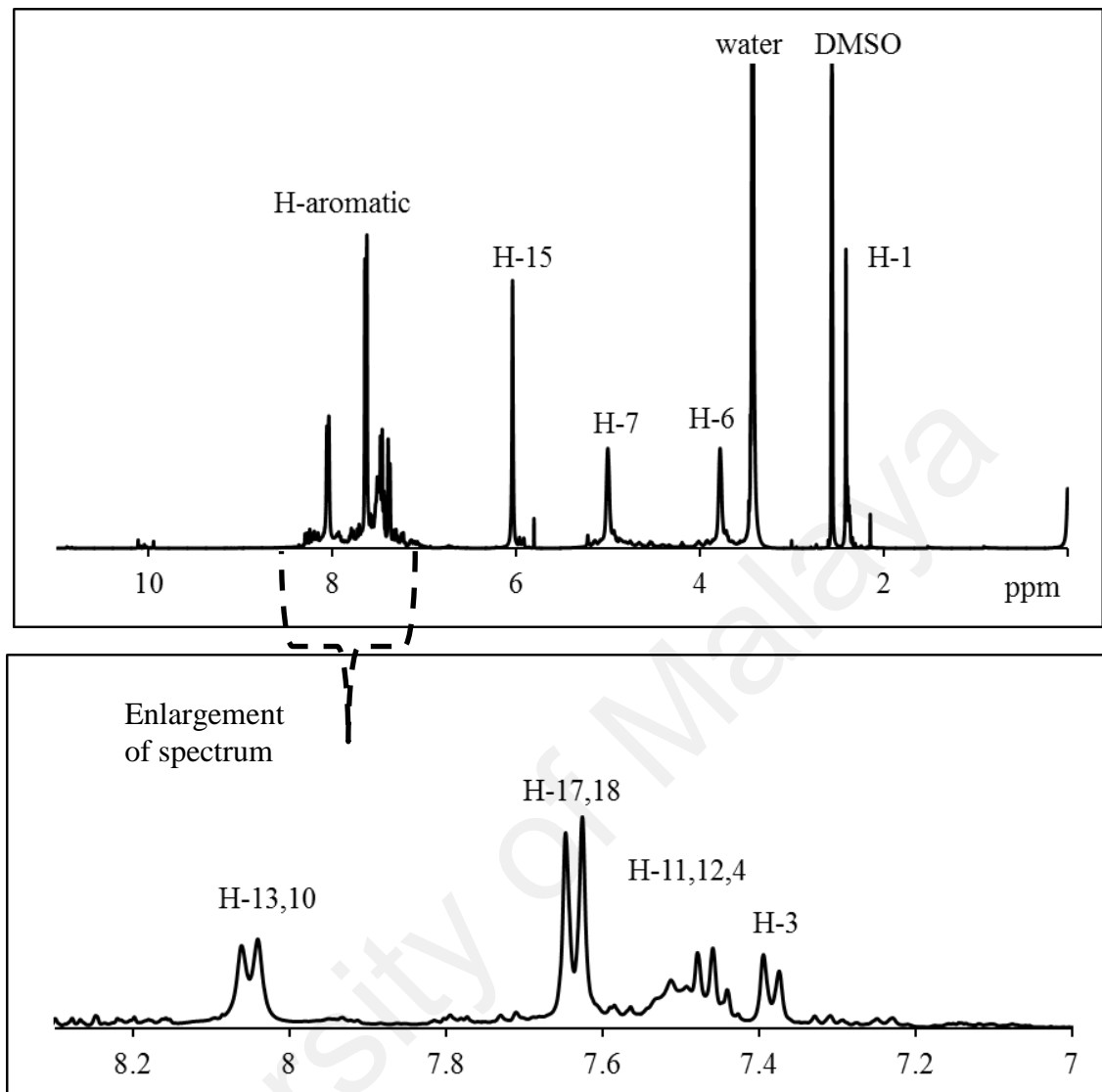
H-position	Integrations	Chemical shift, δ ppm	multiplicity	J_{HH} (Hz)
1	3H	2.28	s	-
6	4H	3.81	t	8
7	4H	4.96	s	-
15	4H	5.58	s	-
3, 4, 11, 12, 17	12H	7.07-7.20	m	-
18	4H	7.31	d	8
10, 13	4H	7.58-7.64	d, d	8,8

APPENDIX J10: ^1H -NMR spectrum of L_1AgPF_6



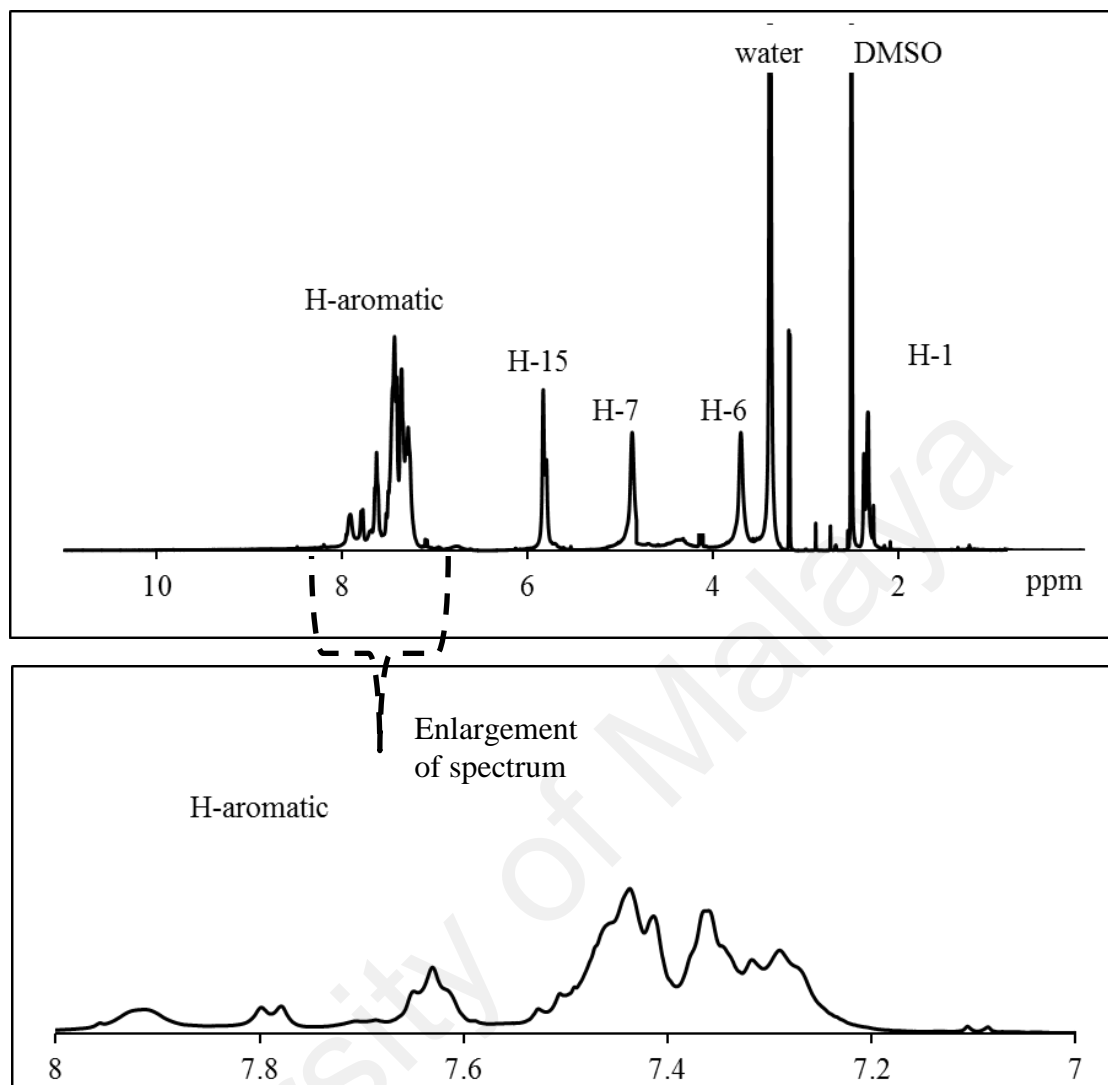
H-position	Integrations	Chemical shift, δ ppm	multiplicity	J_{HH} (Hz)
1	3H	2.40	s	-
6	4H	3.76	s	-
7	4H	5.02	s	-
15	4H	5.86	s	-
19,18,3,4,12,11,10,17	20H	7.33-7.49	m	-
13	2H	7.70	d	12

APPENDIX J11: ^1H -NMR spectrum of L_2AgPF_6



H-position	Integrations	Chemical shift, δ ppm	multiplicity	J_{HH} (Hz)
1	3H	2.41	s	-
6	4H	3.78	s	-
7	4H	5.03	s	-
15	4H	6.04	s	-
3	2H	7.38	d	8
4, 11, 12	6H	7.44-7.51	m	-
17, 18	8H	7.64	d	8
10, 13	4H	8.05	d	8

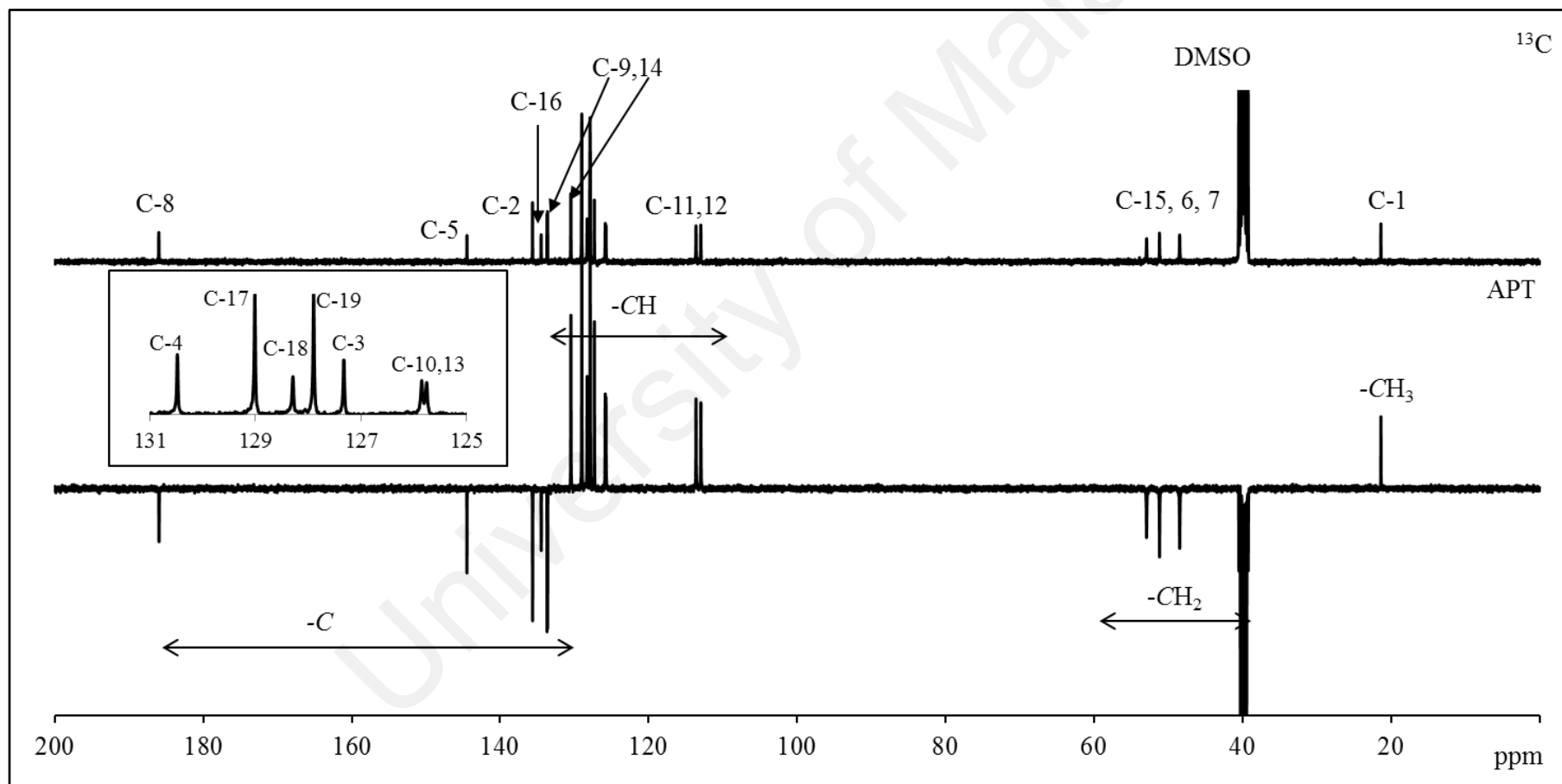
APPENDIX J12: ^1H -NMR spectrum of L_3AgPF_6



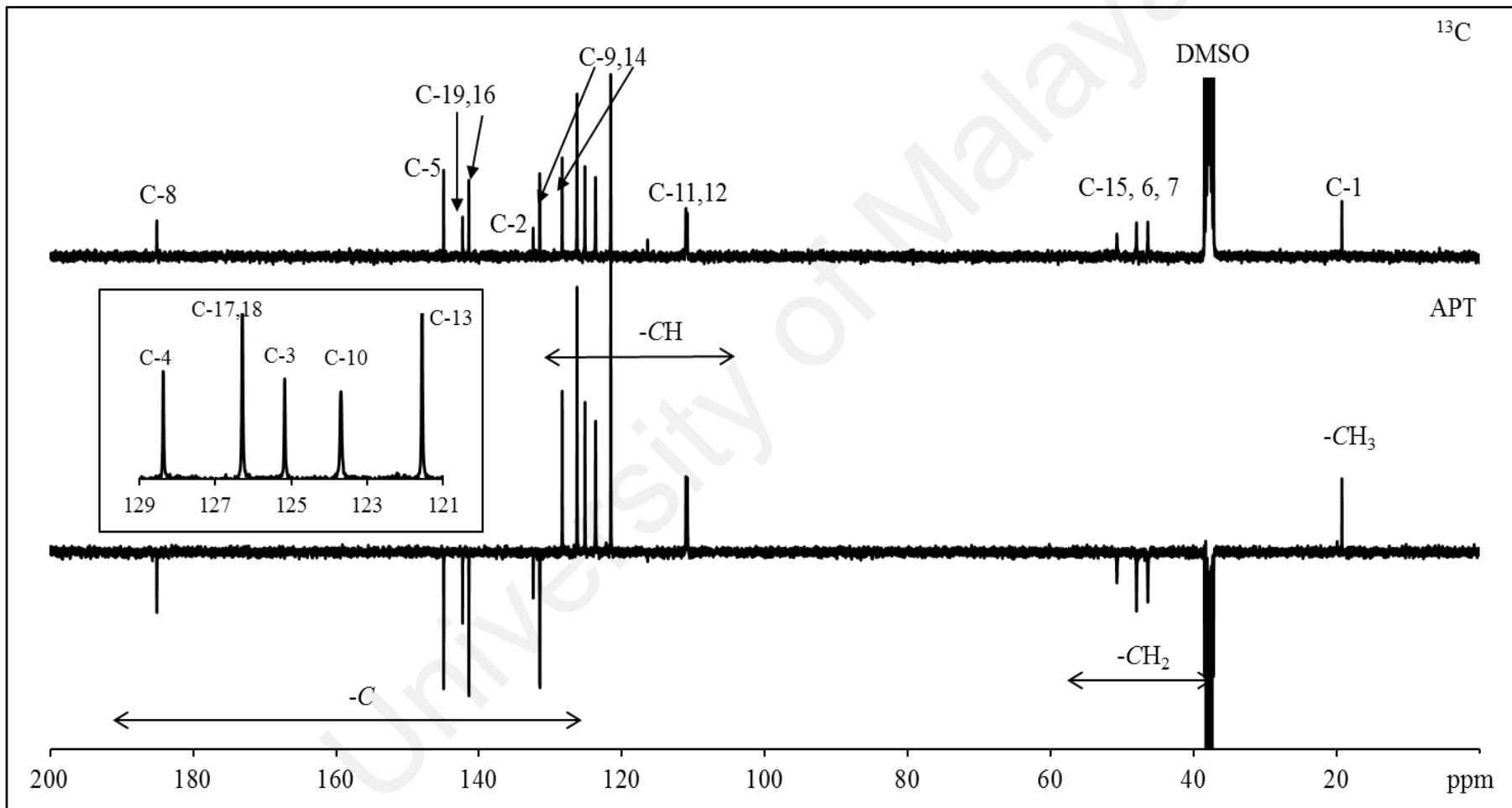
H-position	Integrations	Chemical shift, δ ppm	multiplicity	J_{HH} (Hz)
1	3H	2.33	s	-
6	4H	3.70	s	-
7	4H	4.98	s	-
15	4H	6.04	s	-
All aromatic	20H	7.29-7.91	m	-

APPENDIX K: ^{13}C -NMR spectra of bis-NHC metal complexes

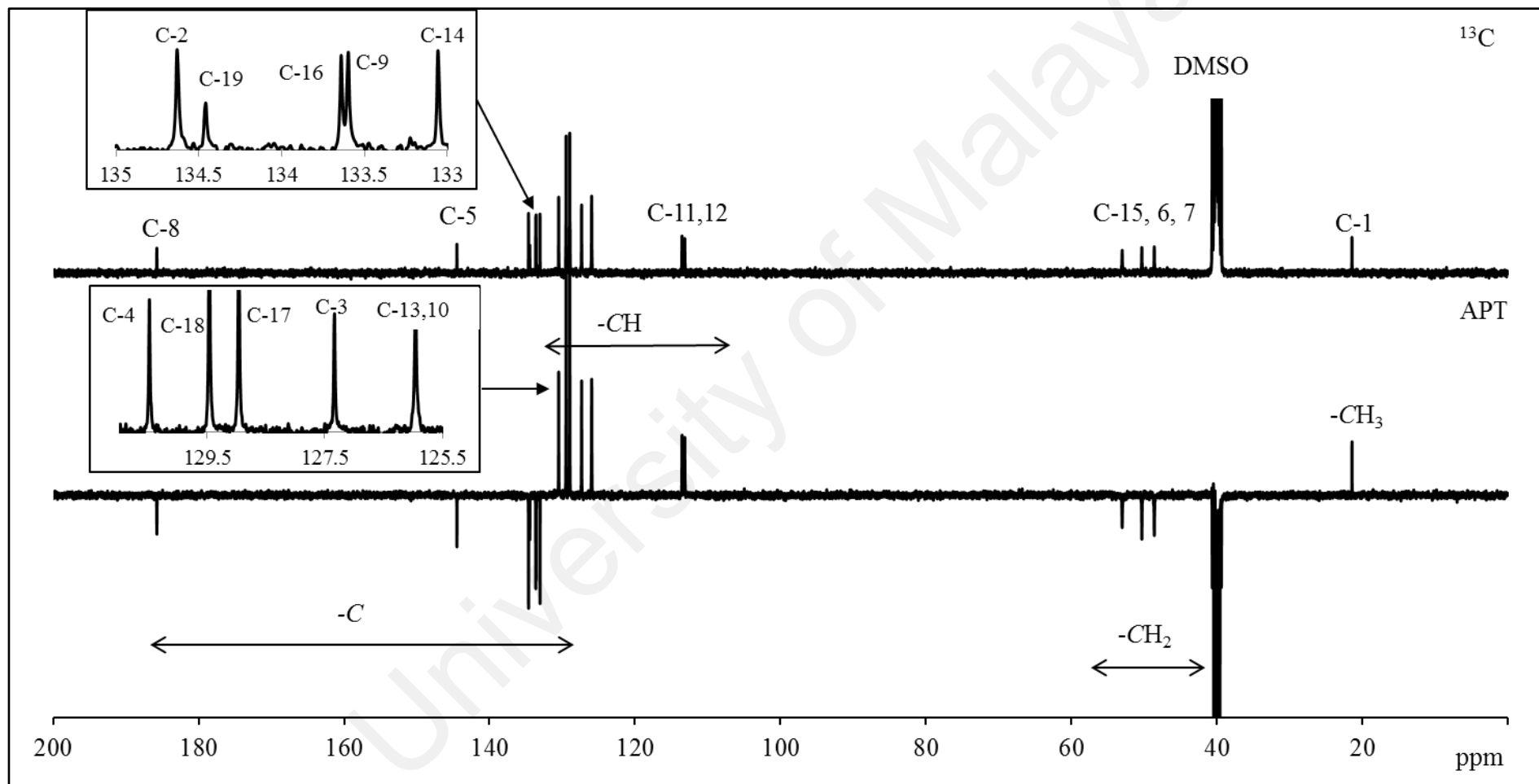
APPENDIX K1: ^{13}C -NMR spectrum of L₁.HgBr



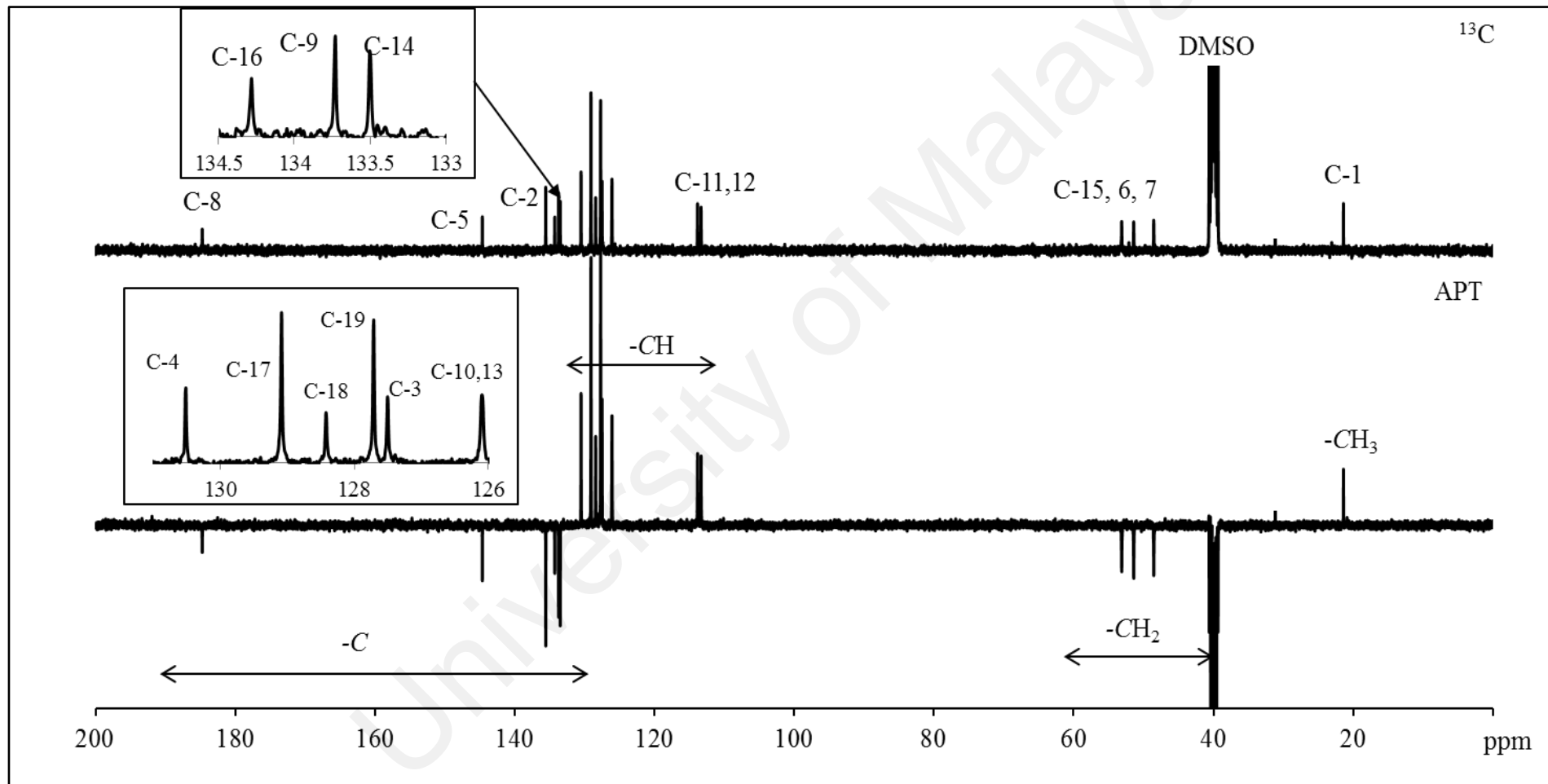
APPENDIX K2: ^{13}C -NMR spectrum of L_2HgBr



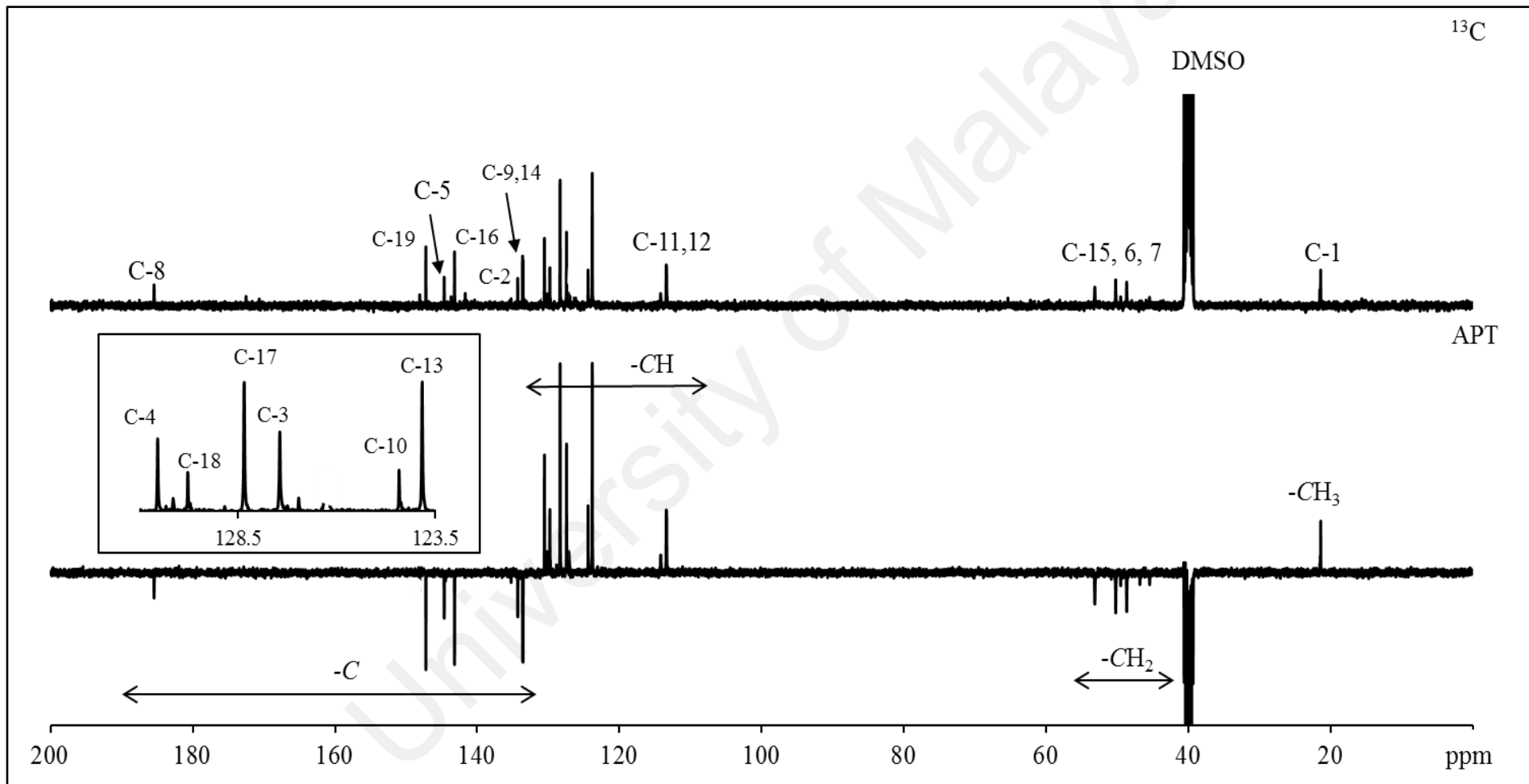
APPENDIX K3: ^{13}C -NMR spectrum of L_3HgBr



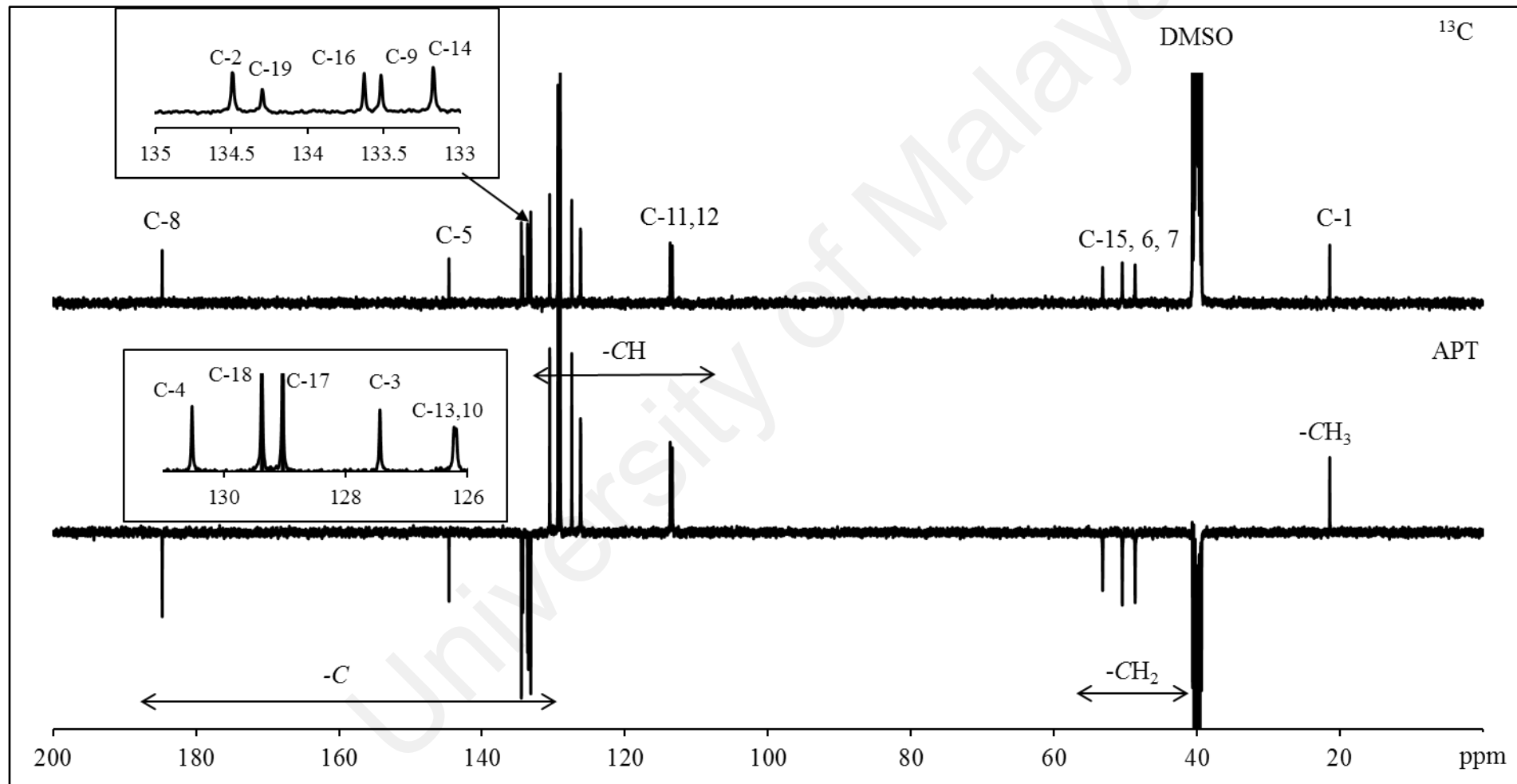
APPENDIX K4: ^{13}C -NMR spectrum of L_1HgPF_6



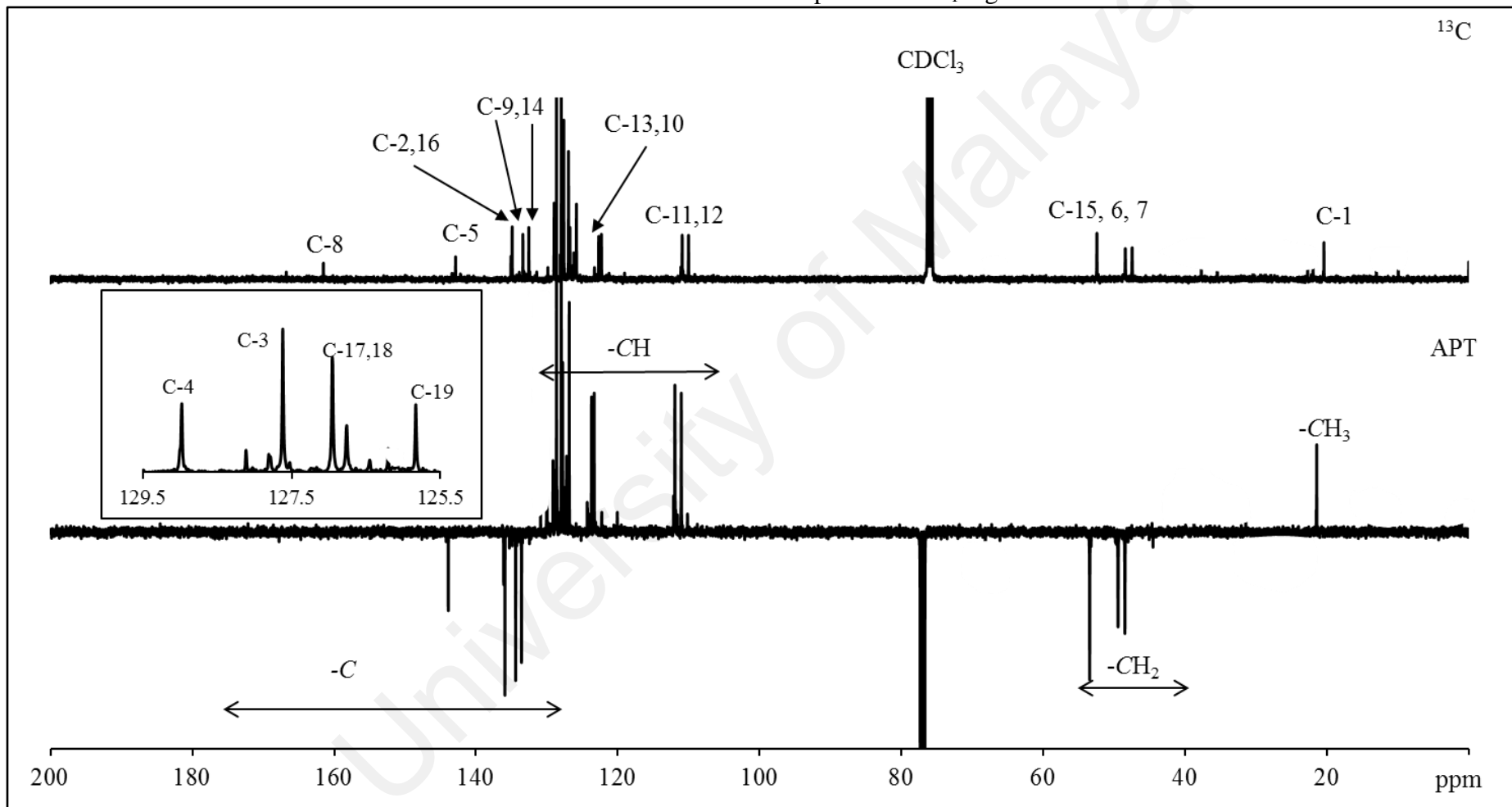
APPENDIX K5: ^{13}C -NMR spectrum of L_2HgPF_6



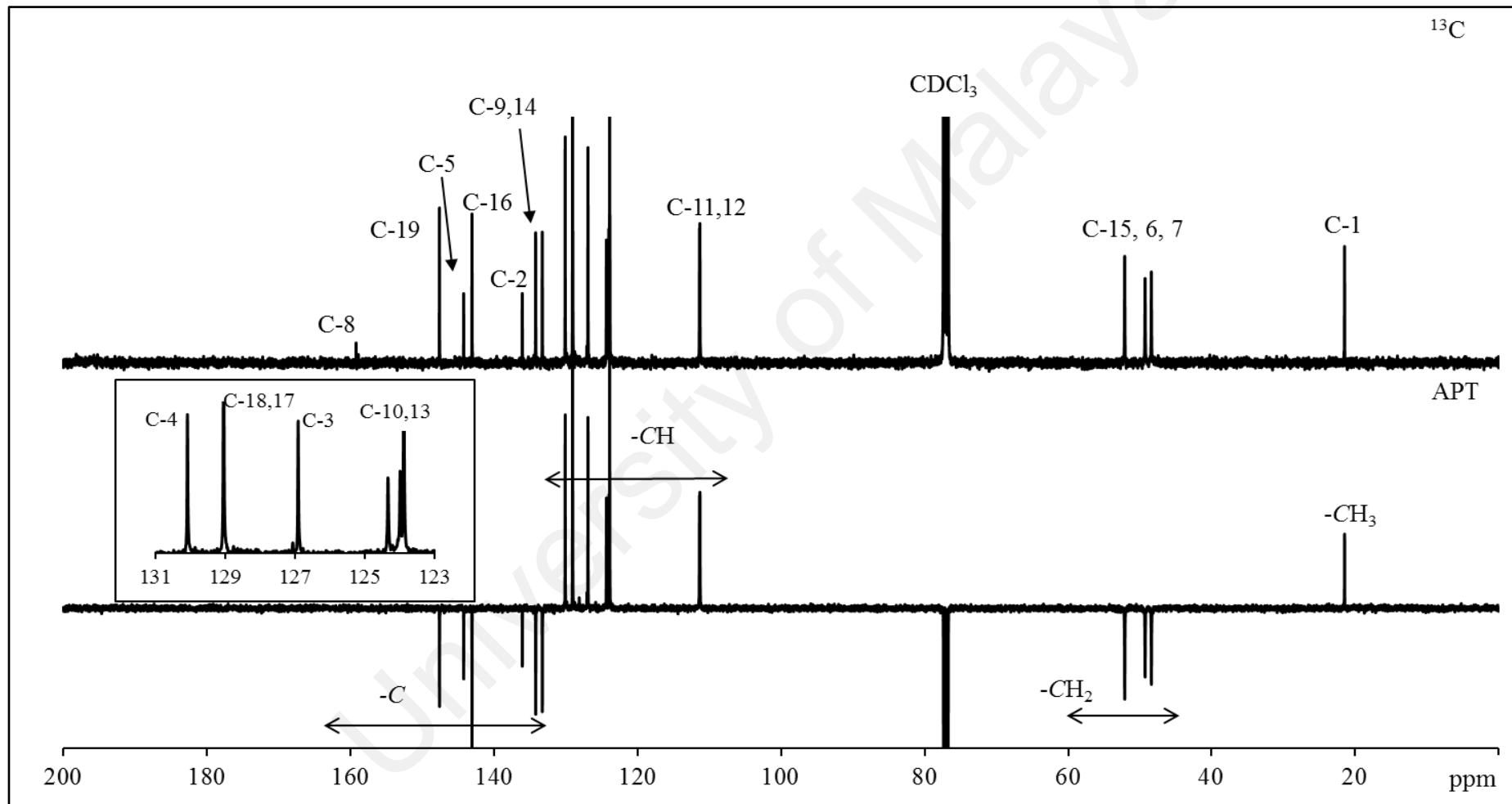
APPENDIX K6: ^{13}C -NMR spectrum of L_3HgPF_6



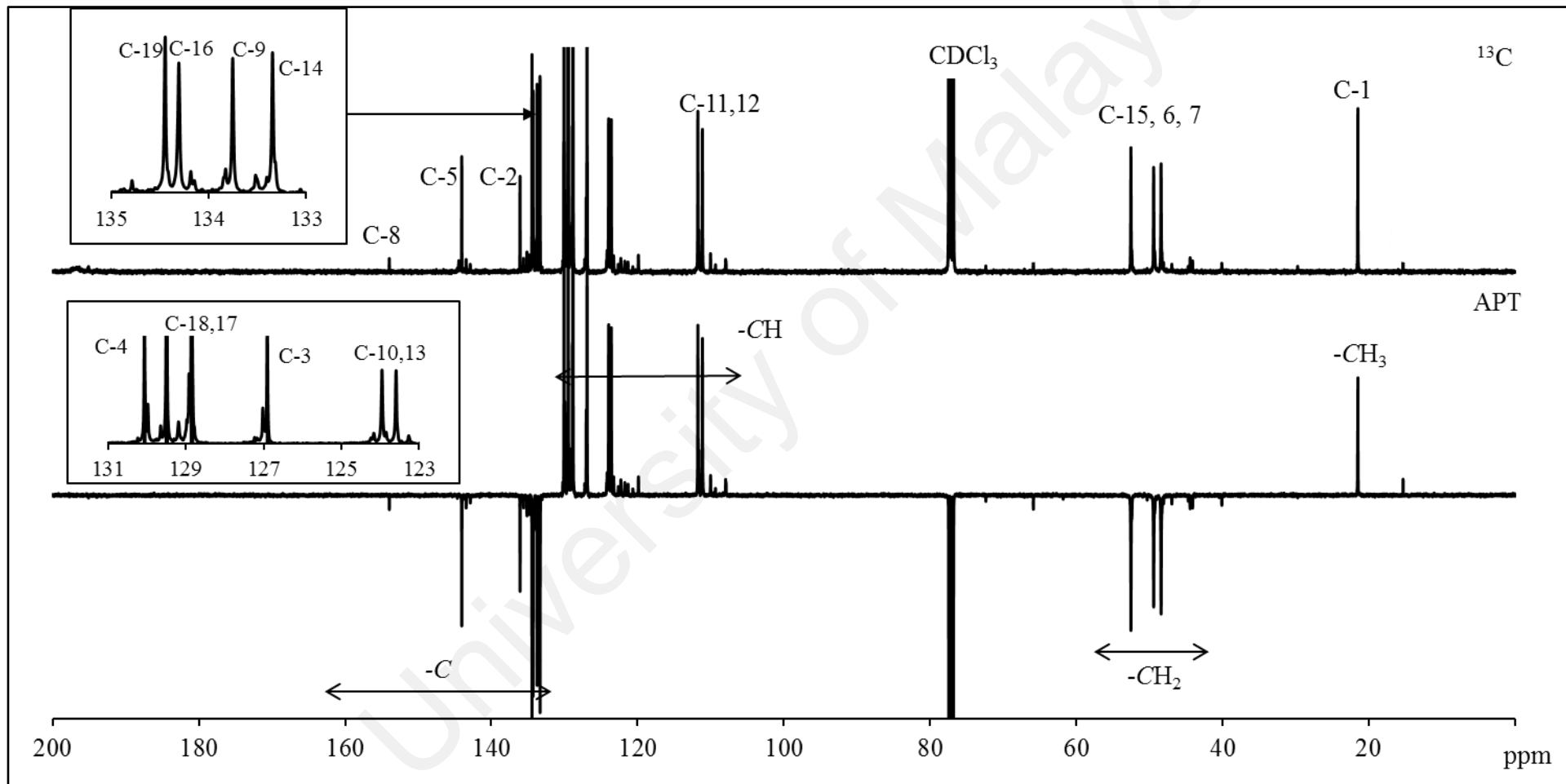
APPENDIX K7: ^{13}C -NMR spectrum of L₁.AgBr



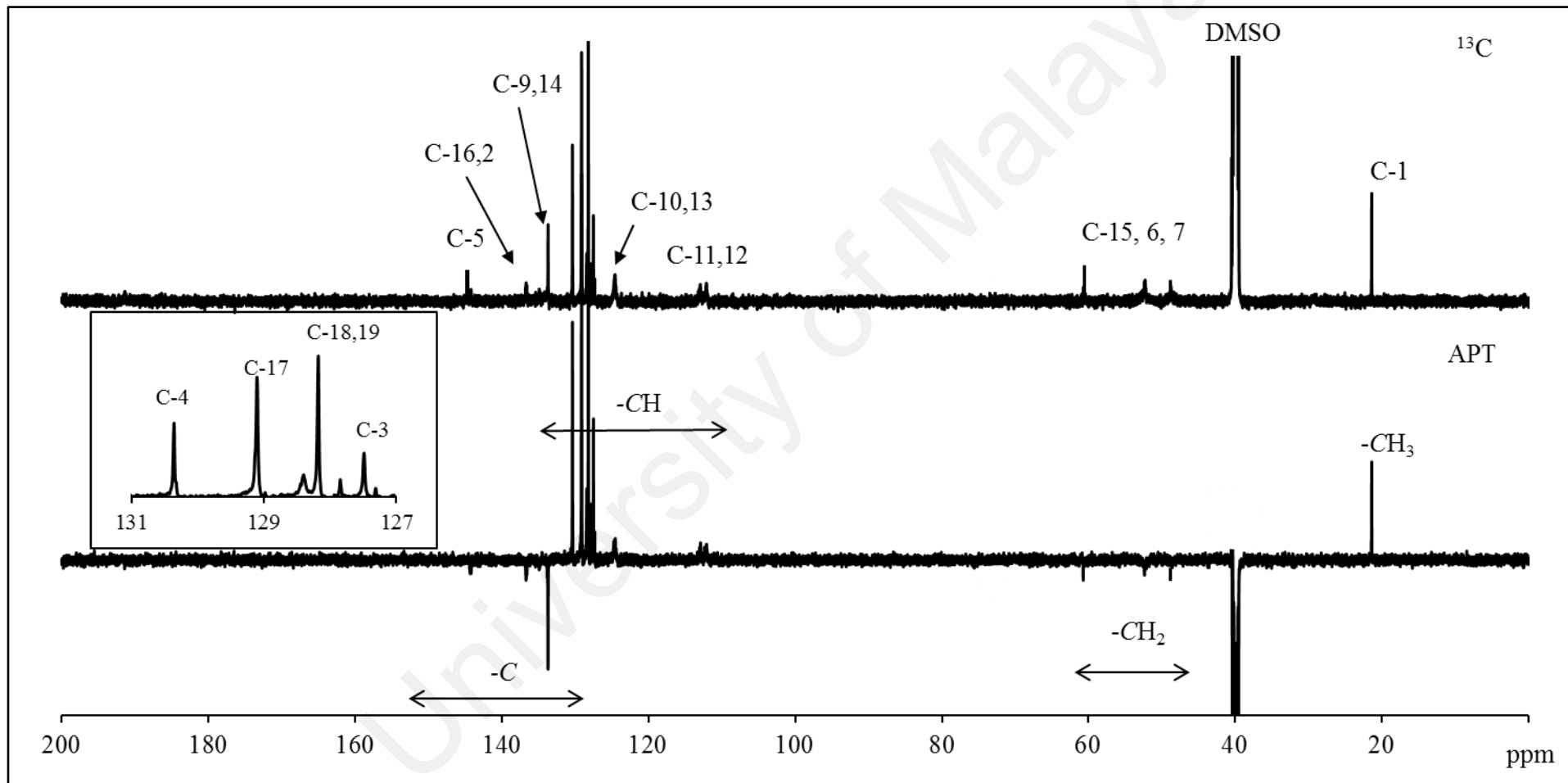
APPENDIX K8: ^{13}C -NMR spectrum of L₂.AgBr



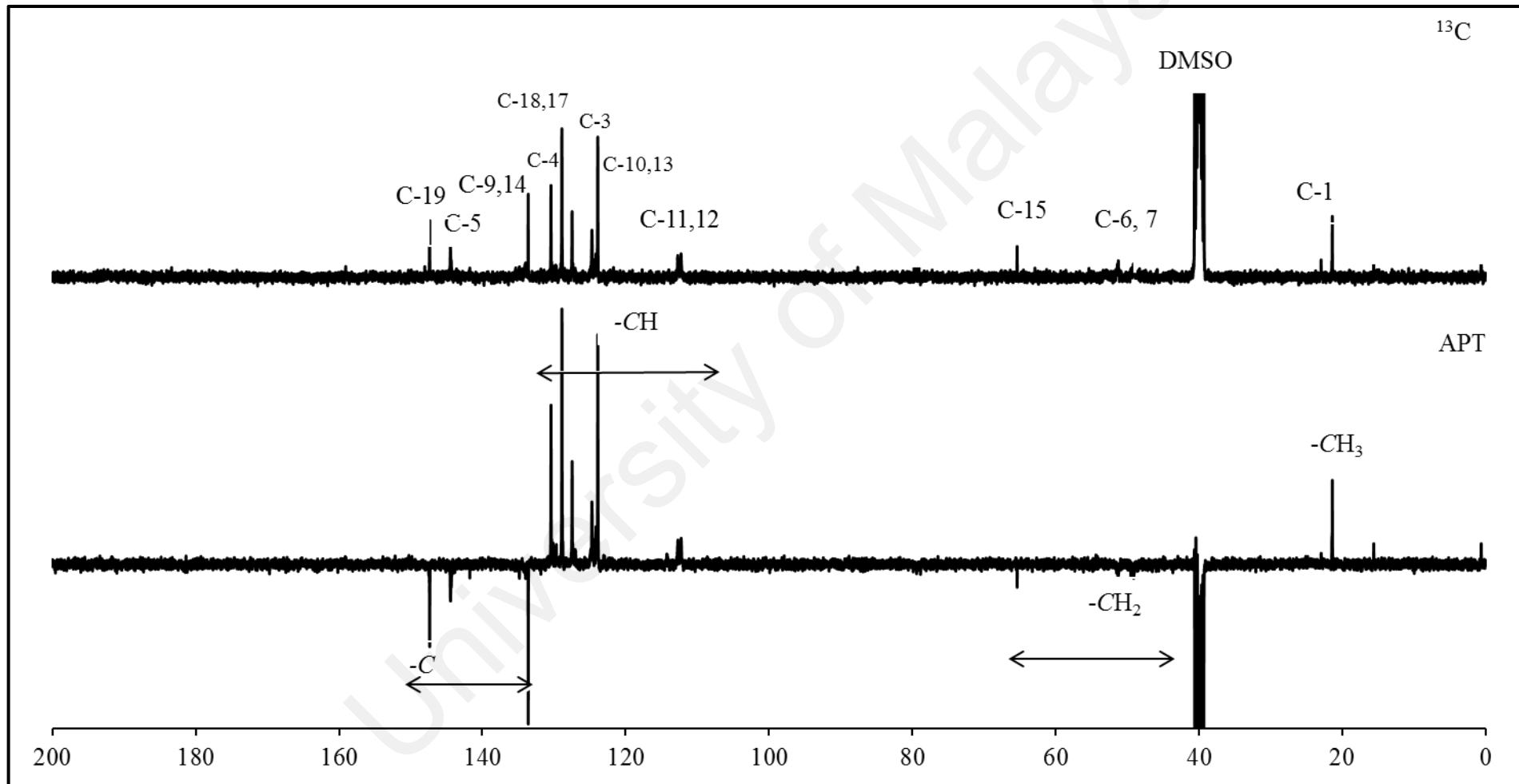
APPENDIX K9: ^{13}C -NMR spectrum of L_3AgBr



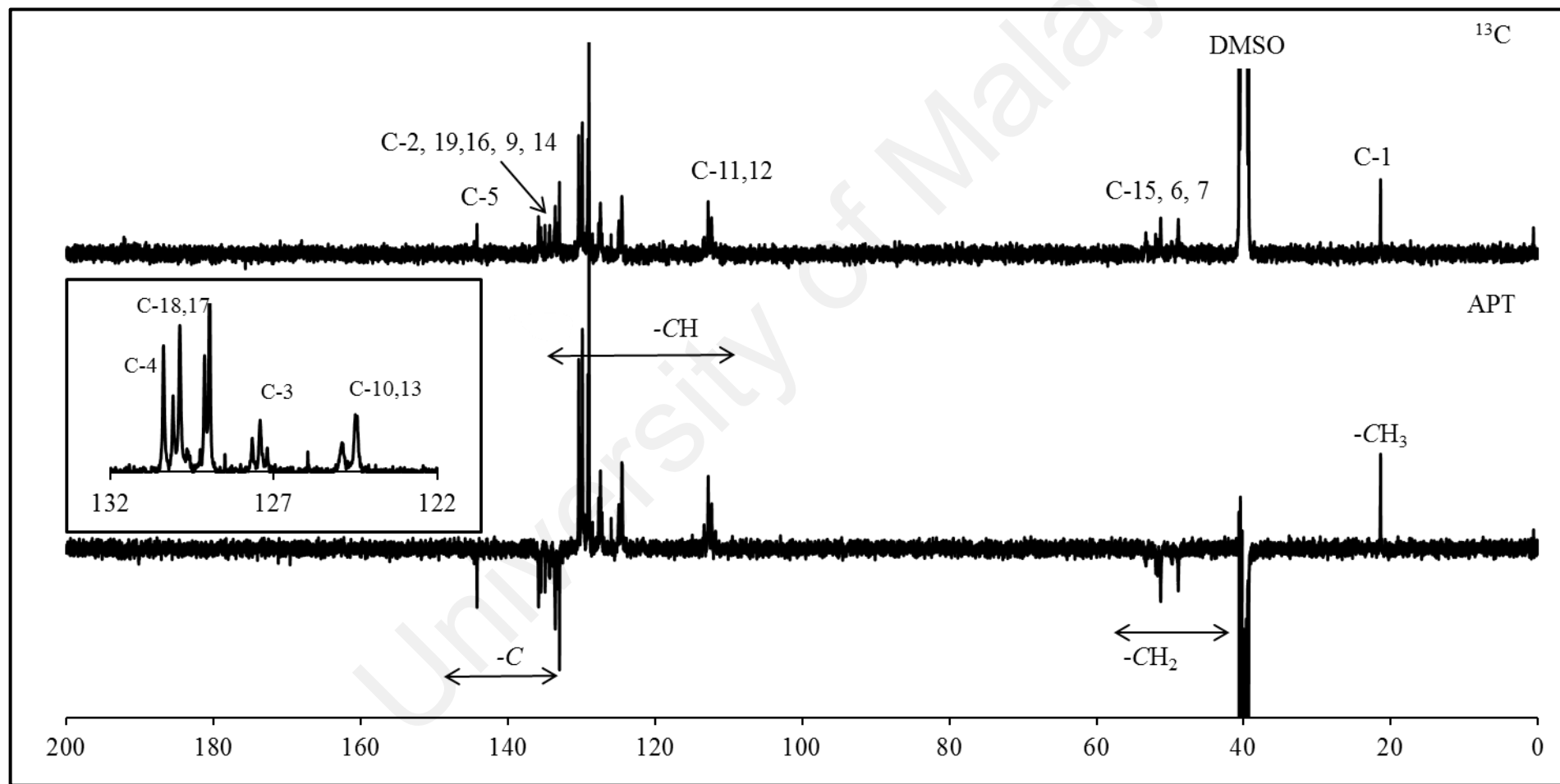
APPENDIX K10: ^{13}C -NMR spectrum of L₁.AgPF₆



APPENDIX K11: ^{13}C -NMR spectrum of L_2AgPF_6



APPENDIX K12: ^{13}C -NMR spectrum of L_3AgPF_6



APPENDIX L1: Crystallographic data for L₁.AgBr

Table L1.1: Crystal data and structure refinement for L₁.AgBr.

Empirical formula	C ₇₈ H ₇₄ Ag ₆ Br ₆ N ₁₀ O ₄ S ₂ ..(CH ₃) ₂ SO		
Formula weight	2406.25		
Temperature	100(2) K		
Wavelength	0.71073 Å		
Crystal system, space group	Monoclinic, I2/m		
Unit cell dimensions	a = 18.1542(6) Å	alpha = 90.000(4) deg.	
	b = 19.6346(12) Å	beta = 101.50 deg.	
	c = 26.272 Å	gamma = 90.0(6) deg.	
Volume	9176.4(6) Å ³		
Z, Calculated density	4, 1.855 Mg/m ³		
Absorption coefficient	4.014 mm ⁻¹		
F(000)	5008		
Crystal size	3.0 x 0.3 x 0.25 mm		
Theta range for data collection	3.03 to 30.39 deg.		
Limiting indices	-23<=h<=24, -27<=k<=27, -34<=l<=36		
Reflections collected / unique	60180 / 12989 [R(int) = 0.0563]		
Completeness to theta = 30.39	91.2 %		
Refinement method	Full-matrix least-squares on F ²		
Data / restraints / parameters	12989 / 18 / 575		
Goodness-of-fit on F ²	1.047		
Final R indices [I>2sigma(I)]	R1 = 0.0492, wR2 = 0.1204		
R indices (all data)	R1 = 0.0805, wR2 = 0.1383		
Largest diff. peak and hole	2.318 and -1.349 e.Å ⁻³		

Table L1.2: Atomic coordinates ($x \times 10^4$) and equivalent isotropic displacement parameters ($\text{Å}^2 \times 10^3$) for $L_1\text{AgBr}$. $U(\text{eq})$ is defined as one third of the trace of the orthogonalized U_{ij} tensor.

	x	y	z	$U(\text{eq})$
Ag(1)	1370(1)	5865(1)	5677(1)	36(1)
Ag(2)	-348(1)	5000	5476(1)	44(1)
Br(1)	778(1)	5000	6271(1)	32(1)
Br(2)	0	3781(1)	5000	26(1)
Br(3)	-1776(1)	5000	5162(1)	28(1)
S(1)	4934(1)	5000	6087(1)	21(1)
O(1)	5041(2)	4377(2)	5835(2)	44(1)
N(1)	2083(2)	7318(2)	5947(2)	21(1)
N(2)	2939(2)	6581(2)	5871(2)	19(1)
N(3)	4088(3)	5000	6196(2)	17(1)
C(1)	1559(3)	7413(3)	6939(2)	39(1)
C(2)	1502(3)	7613(4)	7430(2)	49(2)
C(3)	1203(4)	8221(4)	7509(3)	60(2)
C(4)	945(5)	8648(4)	7101(4)	68(2)
C(5)	1000(4)	8461(3)	6604(3)	48(2)
C(6)	1312(3)	7836(3)	6520(2)	27(1)
C(7)	1358(3)	7626(3)	5974(2)	26(1)
C(8)	2190(2)	6650(2)	5848(2)	19(1)
C(9)	2760(2)	7678(2)	6032(2)	20(1)
C(10)	2934(3)	8358(2)	6130(2)	27(1)
C(11)	3679(3)	8541(3)	6174(2)	32(1)
C(12)	4230(3)	8066(3)	6128(2)	32(1)
C(13)	4059(3)	7387(2)	6030(2)	26(1)
C(14)	3313(2)	7204(2)	5980(2)	20(1)
C(15)	3313(2)	5950(2)	5785(2)	21(1)
C(16)	3739(3)	5649(2)	6290(2)	21(1)
C(17)	5552(4)	5000	6687(3)	33(2)
C(18)	5324(6)	5000	7149(4)	67(3)
C(19)	5884(7)	5000	7602(4)	86(4)
C(20)	6570(6)	5000	7606(4)	128(8)
C(21)	6817(7)	5000	7144(5)	106(6)
C(22)	6299(6)	5000	6669(5)	83(4)
C(23)	7184(2)	5000	8108(6)	137(7)
Ag(3)	8552(1)	858(1)	5155(1)	35(1)
Ag(4)	10401(1)	0	5565(1)	43(1)
Br(4)	10000	1229(1)	5000	25(1)
Br(5)	9169(1)	0	5946(1)	38(1)
Br(6)	11855(1)	0	5711(1)	28(1)
S(2)	5466(1)	0	5864(1)	30(1)
O(2)	5105(2)	-637(3)	5705(2)	58(1)
N(4)	7947(2)	2325(2)	5324(2)	20(1)
N(5)	7036(2)	1601(2)	5207(2)	19(1)
N(6)	6240(3)	0	5650(2)	19(1)
C(24)	8992(4)	2152(4)	6334(3)	59(2)

C(25)	9287(5)	2213(4)	6862(3)	71(2)
C(26)	9617(4)	2811(4)	7059(3)	54(2)
C(27)	9665(4)	3328(4)	6737(3)	57(2)
C(28)	9358(3)	3277(3)	6212(2)	45(2)
C(29)	9013(3)	2684(3)	6009(2)	28(1)
C(30)	8709(3)	2614(2)	5438(2)	27(1)
C(31)	7788(2)	1658(2)	5230(2)	20(1)
C(32)	7309(2)	2692(2)	5372(2)	21(1)
C(33)	7198(3)	3379(2)	5467(2)	27(1)
C(34)	6475(3)	3567(3)	5494(2)	32(1)
C(35)	5886(3)	3095(3)	5429(2)	32(1)
C(36)	5993(3)	2416(3)	5334(2)	27(1)
C(37)	6723(2)	2228(2)	5303(2)	20(1)
C(38)	6632(2)	952(2)	5146(2)	19(1)
C(39)	6665(3)	635(3)	5678(2)	31(1)
C(40)	5716(4)	0	6542(3)	37(2)
C(41)	5830(4)	615(4)	6807(2)	51(2)
C(42)	6057(6)	601(5)	7340(3)	76(3)
C(43)	6140(8)	0	7608(3)	70(3)
C(44)	6348(12)	0	8205(4)	117(7)
S(3)	6881(2)	2610(2)	6664(1)	49(1)
O(3)	6917(9)	2076(5)	7001(5)	151(9)
C(45)	7480(7)	3224(6)	6840(5)	53(4)
C(46)	6050(8)	3094(8)	6789(6)	76(5)
S(4)	2771(2)	5000	7695(1)	50(1)
O(4)	3099(4)	5000	7236(2)	58(2)
C(47)	2105(5)	4327(4)	7601(3)	69(2)

Table L1.3: Bond lengths [Å] and angles [deg] for $L_1\text{AgBr}$.

Ag(1)-C(8)	2.128(12)
Ag(1)-Br(1)	2.672(7)
Ag(1)-Br(2)#1	2.840(6)
Ag(1)-Br(3)#1	2.988(4)
Ag(2)-Br(3)	2.5592(9)
Ag(2)-Br(1)	2.6140(10)
Ag(2)-Br(2)#1	2.829(5)
Ag(2)-Br(2)	2.829(5)
Ag(2)-Ag(2)#1	3.0198(15)
Br(1)-Ag(1)#2	2.672(7)
Br(2)-Ag(2)#1	2.829(5)
Br(2)-Ag(1)#1	2.840(6)
Br(2)-Ag(1)#2	2.840(6)
Br(3)-Ag(1)#1	2.987(4)
Br(3)-Ag(1)#3	2.987(4)
S(1)-O(1)	1.423(4)
S(1)-O(1)#2	1.423(4)
S(1)-N(3)	1.618(5)
S(1)-C(17)	1.743(7)
N(1)-C(8)	1.357(6)
N(1)-C(9)	1.398(8)
N(1)-C(7)	1.463(8)
N(2)-C(8)	1.357(6)
N(2)-C(14)	1.400(8)
N(2)-C(15)	1.453(8)
N(3)-C(16)#2	1.465(7)
N(3)-C(16)	1.465(7)
C(1)-C(2)	1.372(8)
C(1)-C(6)	1.380(8)
C(1)-H(1)	0.9500
C(2)-C(3)	1.346(12)
C(2)-H(2)	0.9500
C(3)-C(4)	1.367(12)
C(3)-H(3)	0.9500
C(4)-C(5)	1.381(10)
C(4)-H(4)	0.9500
C(5)-C(6)	1.386(9)
C(5)-H(5)	0.9500
C(6)-C(7)	1.512(7)
C(7)-H(7A)	0.9900
C(7)-H(7B)	0.9900
C(9)-C(10)	1.385(7)
C(9)-C(14)	1.395(9)
C(10)-C(11)	1.381(8)
C(10)-H(10)	0.9500
C(11)-C(12)	1.392(10)
C(11)-H(11)	0.9500
C(12)-C(13)	1.380(8)
C(12)-H(12)	0.9500

C(13)-C(14)	1.384(7)
C(13)-H(13)	0.9500
C(15)-C(16)	1.514(7)
C(15)-H(15A)	0.9900
C(15)-H(15B)	0.9900
C(16)-H(16A)	0.9900
C(16)-H(16B)	0.9900
C(17)-C(18)	1.358(13)
C(17)-C(22)	1.366(13)
C(18)-C(19)	1.404(15)
C(18)-H(18)	0.9500
C(19)-C(20)	1.242(16)
C(19)-H(19)	0.9500
C(20)-C(21)	1.376(16)
C(20)-C(23)	1.549(12)
C(21)-C(22)	1.405(17)
C(21)-H(21)	0.9500
C(22)-H(22)	0.9500
C(23)-H(23A)	0.980(2)
C(23)-H(23B)	0.9800(6)
Ag(3)-C(31)	2.129(11)
Ag(3)-Br(5)	2.735(7)
Ag(3)-Br(6)#4	2.810(4)
Ag(3)-Br(4)	2.835(7)
Ag(3)-Ag(3)#5	3.3698(8)
Ag(4)-Br(6)	2.5905(10)
Ag(4)-Br(5)	2.6255(10)
Ag(4)-Br(4)#4	2.850(6)
Ag(4)-Br(4)	2.850(6)
Ag(4)-Ag(4)#4	3.0336(15)
Br(4)-Ag(3)#6	2.835(7)
Br(4)-Ag(4)#4	2.850(6)
Br(5)-Ag(3)#5	2.735(7)
Br(6)-Ag(3)#4	2.810(4)
Br(6)-Ag(3)#6	2.810(4)
S(2)-O(2)	1.434(7)
S(2)-O(2)#5	1.434(7)
S(2)-N(6)	1.615(5)
S(2)-C(40)	1.746(8)
N(4)-C(31)	1.354(6)
N(4)-C(32)	1.392(8)
N(4)-C(30)	1.468(8)
N(5)-C(31)	1.360(5)
N(5)-C(37)	1.400(8)
N(5)-C(38)	1.462(8)
N(6)-C(39)	1.460(8)
N(6)-C(39)#5	1.460(8)
C(24)-C(29)	1.355(9)
C(24)-C(25)	1.388(10)
C(24)-H(24)	0.9500
C(25)-C(26)	1.371(12)
C(25)-H(25)	0.9500

C(26)-C(27)	1.337(11)
C(26)-H(26)	0.9500
C(27)-C(28)	1.384(9)
C(27)-H(27)	0.9500
C(28)-C(29)	1.377(9)
C(28)-H(28)	0.9500
C(29)-C(30)	1.498(7)
C(30)-H(30A)	0.9900
C(30)-H(30B)	0.9900
C(32)-C(37)	1.384(9)
C(32)-C(33)	1.394(7)
C(33)-C(34)	1.378(8)
C(33)-H(33)	0.9500
C(34)-C(35)	1.401(10)
C(34)-H(34)	0.9500
C(35)-C(36)	1.377(7)
C(35)-H(35)	0.9500
C(36)-C(37)	1.394(7)
C(36)-H(36)	0.9500
C(38)-C(39)	1.520(6)
C(38)-H(38A)	0.9900
C(38)-H(38B)	0.9900
C(39)-H(39A)	0.9900
C(39)-H(39B)	0.9900
C(40)-C(41)	1.389(8)
C(40)-C(41)#5	1.389(8)
C(41)-C(42)	1.378(9)
C(41)-H(41)	0.9500
C(42)-C(43)	1.368(10)
C(42)-H(42)	0.9500
C(43)-C(42)#5	1.368(10)
C(43)-C(44)	1.539(12)
C(44)-H(44A)	0.9800
C(44)-H(44B)	0.9800
C(44)-H(44C)	0.9800
S(3)-O(3)	1.367(9)
S(3)-C(45)	1.628(14)
S(3)-C(46)	1.865(16)
C(45)-H(45A)	0.9800
C(45)-H(45B)	0.9800
C(45)-H(45C)	0.9800
C(46)-H(46A)	0.9800
C(46)-H(46B)	0.9800
C(46)-H(46C)	0.9800
S(4)-O(4)	1.448(6)
S(4)-C(47)#2	1.775(12)
S(4)-C(47)	1.775(12)
C(47)-H(47A)	0.9800
C(47)-H(47B)	0.9800
C(47)-H(47C)	0.9800

C(8)-Ag(1)-Br(1)	133.1(2)
C(8)-Ag(1)-Br(2)#1	116.3(2)
Br(1)-Ag(1)-Br(2)#1	96.7(3)
C(8)-Ag(1)-Br(3)#1	107.63(14)
Br(1)-Ag(1)-Br(3)#1	104.87(6)
Br(2)#1-Ag(1)-Br(3)#1	89.5(3)
Br(3)-Ag(2)-Br(1)	146.97(4)
Br(3)-Ag(2)-Br(2)#1	99.1(5)
Br(1)-Ag(2)-Br(2)#1	98.4(4)
Br(3)-Ag(2)-Br(2)	99.1(5)
Br(1)-Ag(2)-Br(2)	98.4(4)
Br(2)#1-Ag(2)-Br(2)	115.49(3)
Br(3)-Ag(2)-Ag(2)#1	107.23(4)
Br(1)-Ag(2)-Ag(2)#1	105.81(3)
Br(2)#1-Ag(2)-Ag(2)#1	57.75(17)
Br(2)-Ag(2)-Ag(2)#1	57.75(17)
Ag(2)-Br(1)-Ag(1)#2	82.8(3)
Ag(2)-Br(1)-Ag(1)	82.8(3)
Ag(1)#2-Br(1)-Ag(1)	78.89(3)
Ag(2)#1-Br(2)-Ag(2)	64.51(3)
Ag(2)#1-Br(2)-Ag(1)#1	76.2(4)
Ag(2)-Br(2)-Ag(1)#1	79.9(4)
Ag(2)#1-Br(2)-Ag(1)#2	79.9(4)
Ag(2)-Br(2)-Ag(1)#2	76.2(4)
Ag(1)#1-Br(2)-Ag(1)#2	151.67(3)
Ag(2)-Br(3)-Ag(1)#1	81.7(3)
Ag(2)-Br(3)-Ag(1)#3	81.7(3)
Ag(1)#1-Br(3)-Ag(1)#3	69.26(2)
O(1)-S(1)-O(1)#2	118.6(4)
O(1)-S(1)-N(3)	107.7(5)
O(1)#2-S(1)-N(3)	107.7(5)
O(1)-S(1)-C(17)	107.4(4)
O(1)#2-S(1)-C(17)	107.4(4)
N(3)-S(1)-C(17)	107.6(3)
C(8)-N(1)-C(9)	111.4(5)
C(8)-N(1)-C(7)	125.0(6)
C(9)-N(1)-C(7)	123.7(4)
C(8)-N(2)-C(14)	111.3(6)
C(8)-N(2)-C(15)	125.0(6)
C(14)-N(2)-C(15)	123.7(4)
C(16)#2-N(3)-C(16)	120.7(5)
C(16)#2-N(3)-S(1)	119.2(5)
C(16)-N(3)-S(1)	119.2(5)
C(2)-C(1)-C(6)	120.3(6)
C(2)-C(1)-H(1)	119.9
C(6)-C(1)-H(1)	119.9
C(3)-C(2)-C(1)	120.5(7)
C(3)-C(2)-H(2)	119.8
C(1)-C(2)-H(2)	119.8
C(2)-C(3)-C(4)	120.6(7)
C(2)-C(3)-H(3)	119.7
C(4)-C(3)-H(3)	119.7

C(3)-C(4)-C(5)	120.0(7)
C(3)-C(4)-H(4)	120.0
C(5)-C(4)-H(4)	120.0
C(4)-C(5)-C(6)	119.7(7)
C(4)-C(5)-H(5)	120.2
C(6)-C(5)-H(5)	120.2
C(1)-C(6)-C(5)	118.9(6)
C(1)-C(6)-C(7)	121.4(5)
C(5)-C(6)-C(7)	119.6(5)
N(1)-C(7)-C(6)	112.3(4)
N(1)-C(7)-H(7A)	109.1
C(6)-C(7)-H(7A)	109.1
N(1)-C(7)-H(7B)	109.1
C(6)-C(7)-H(7B)	109.1
H(7A)-C(7)-H(7B)	107.9
N(2)-C(8)-N(1)	105.6(7)
N(2)-C(8)-Ag(1)	126.1(4)
N(1)-C(8)-Ag(1)	128.3(4)
C(10)-C(9)-C(14)	121.4(5)
C(10)-C(9)-N(1)	132.7(6)
C(14)-C(9)-N(1)	105.9(4)
C(11)-C(10)-C(9)	116.7(7)
C(11)-C(10)-H(10)	121.7
C(9)-C(10)-H(10)	121.7
C(10)-C(11)-C(12)	121.8(5)
C(10)-C(11)-H(11)	119.1
C(12)-C(11)-H(11)	119.1
C(13)-C(12)-C(11)	121.6(5)
C(13)-C(12)-H(12)	119.2
C(11)-C(12)-H(12)	119.2
C(12)-C(13)-C(14)	116.7(7)
C(12)-C(13)-H(13)	121.7
C(14)-C(13)-H(13)	121.7
C(13)-C(14)-C(9)	121.8(5)
C(13)-C(14)-N(2)	132.3(6)
C(9)-C(14)-N(2)	105.9(4)
N(2)-C(15)-C(16)	111.8(4)
N(2)-C(15)-H(15A)	109.3
C(16)-C(15)-H(15A)	109.3
N(2)-C(15)-H(15B)	109.3
C(16)-C(15)-H(15B)	109.3
H(15A)-C(15)-H(15B)	107.9
N(3)-C(16)-C(15)	110.8(5)
N(3)-C(16)-H(16A)	109.5
C(15)-C(16)-H(16A)	109.5
N(3)-C(16)-H(16B)	109.5
C(15)-C(16)-H(16B)	109.5
H(16A)-C(16)-H(16B)	108.1
C(18)-C(17)-C(22)	120.8(9)
C(18)-C(17)-S(1)	123.5(6)
C(22)-C(17)-S(1)	115.7(7)
C(17)-C(18)-C(19)	117.4(10)

C(17)-C(18)-H(18)	121.3
C(19)-C(18)-H(18)	121.3
C(20)-C(19)-C(18)	124.2(11)
C(20)-C(19)-H(19)	117.9
C(18)-C(19)-H(19)	117.9
C(19)-C(20)-C(21)	119.7(10)
C(19)-C(20)-C(23)	123.9(10)
C(21)-C(20)-C(23)	116.4(10)
C(20)-C(21)-C(22)	120.4(11)
C(20)-C(21)-H(21)	119.8
C(22)-C(21)-H(21)	119.8
C(17)-C(22)-C(21)	117.5(11)
C(17)-C(22)-H(22)	121.2
C(21)-C(22)-H(22)	121.2
C(20)-C(23)-H(23A)	91(3)
C(20)-C(23)-H(23B)	111(10)
H(23A)-C(23)-H(23B)	109.4(5)
C(31)-Ag(3)-Br(5)	124.0(2)
C(31)-Ag(3)-Br(6)#4	116.54(13)
Br(5)-Ag(3)-Br(6)#4	104.32(7)
C(31)-Ag(3)-Br(4)	117.6(3)
Br(5)-Ag(3)-Br(4)	90.9(3)
Br(6)#4-Ag(3)-Br(4)	98.0(3)
C(31)-Ag(3)-Ag(3)#5	137.5(3)
Br(5)-Ag(3)-Ag(3)#5	51.97(19)
Br(6)#4-Ag(3)-Ag(3)#5	53.15(12)
Br(4)-Ag(3)-Ag(3)#5	104.9(5)
Br(6)-Ag(4)-Br(5)	149.71(4)
Br(6)-Ag(4)-Br(4)#4	102.9(5)
Br(5)-Ag(4)-Br(4)#4	92.9(4)
Br(6)-Ag(4)-Br(4)	102.9(5)
Br(5)-Ag(4)-Br(4)	92.9(4)
Br(4)#4-Ag(4)-Br(4)	115.68(3)
Br(6)-Ag(4)-Ag(4)#4	114.90(4)
Br(5)-Ag(4)-Ag(4)#4	95.40(3)
Br(4)#4-Ag(4)-Ag(4)#4	57.8(2)
Br(4)-Ag(4)-Ag(4)#4	57.8(2)
Ag(3)#6-Br(4)-Ag(3)	150.25(3)
Ag(3)#6-Br(4)-Ag(4)	73.1(4)
Ag(3)-Br(4)-Ag(4)	81.7(4)
Ag(3)#6-Br(4)-Ag(4)#4	81.7(4)
Ag(3)-Br(4)-Ag(4)#4	73.1(4)
Ag(4)-Br(4)-Ag(4)#4	64.31(3)
Ag(4)-Br(5)-Ag(3)#5	87.8(3)
Ag(4)-Br(5)-Ag(3)	87.8(3)
Ag(3)#5-Br(5)-Ag(3)	76.06(3)
Ag(4)-Br(6)-Ag(3)#4	77.6(3)
Ag(4)-Br(6)-Ag(3)#6	77.6(3)
Ag(3)#4-Br(6)-Ag(3)#6	73.69(3)
O(2)-S(2)-O(2)#5	121.3(4)
O(2)-S(2)-N(6)	106.0(4)
O(2)#5-S(2)-N(6)	106.0(4)

O(2)-S(2)-C(40)	108.0(2)
O(2) ^{#5} -S(2)-C(40)	108.0(2)
N(6)-S(2)-C(40)	106.7(3)
C(31)-N(4)-C(32)	111.5(5)
C(31)-N(4)-C(30)	124.6(6)
C(32)-N(4)-C(30)	123.3(4)
C(31)-N(5)-C(37)	111.0(6)
C(31)-N(5)-C(38)	123.6(6)
C(37)-N(5)-C(38)	125.0(3)
C(39)-N(6)-C(39) ^{#5}	117.2(6)
C(39)-N(6)-S(2)	118.1(5)
C(39) ^{#5} -N(6)-S(2)	118.1(5)
C(29)-C(24)-C(25)	120.6(7)
C(29)-C(24)-H(24)	119.7
C(25)-C(24)-H(24)	119.7
C(26)-C(25)-C(24)	120.3(7)
C(26)-C(25)-H(25)	119.8
C(24)-C(25)-H(25)	119.8
C(27)-C(26)-C(25)	119.3(7)
C(27)-C(26)-H(26)	120.4
C(25)-C(26)-H(26)	120.4
C(26)-C(27)-C(28)	120.8(7)
C(26)-C(27)-H(27)	119.6
C(28)-C(27)-H(27)	119.6
C(29)-C(28)-C(27)	120.7(6)
C(29)-C(28)-H(28)	119.7
C(27)-C(28)-H(28)	119.7
C(24)-C(29)-C(28)	118.3(6)
C(24)-C(29)-C(30)	120.6(5)
C(28)-C(29)-C(30)	121.0(5)
N(4)-C(30)-C(29)	112.5(4)
N(4)-C(30)-H(30A)	109.1
C(29)-C(30)-H(30A)	109.1
N(4)-C(30)-H(30B)	109.1
C(29)-C(30)-H(30B)	109.1
H(30A)-C(30)-H(30B)	107.8
N(4)-C(31)-N(5)	105.3(7)
N(4)-C(31)-Ag(3)	127.7(4)
N(5)-C(31)-Ag(3)	127.0(5)
C(37)-C(32)-N(4)	106.2(4)
C(37)-C(32)-C(33)	121.8(5)
N(4)-C(32)-C(33)	132.0(6)
C(34)-C(33)-C(32)	116.1(7)
C(34)-C(33)-H(33)	121.9
C(32)-C(33)-H(33)	121.9
C(33)-C(34)-C(35)	122.0(5)
C(33)-C(34)-H(34)	119.0
C(35)-C(34)-H(34)	119.0
C(36)-C(35)-C(34)	122.1(5)
C(36)-C(35)-H(35)	119.0
C(34)-C(35)-H(35)	119.0
C(35)-C(36)-C(37)	115.9(7)

C(35)-C(36)-H(36)	122.0
C(37)-C(36)-H(36)	122.0
C(32)-C(37)-C(36)	122.1(5)
C(32)-C(37)-N(5)	106.0(4)
C(36)-C(37)-N(5)	131.9(6)
N(5)-C(38)-C(39)	109.1(4)
N(5)-C(38)-H(38A)	109.9
C(39)-C(38)-H(38A)	109.9
N(5)-C(38)-H(38B)	109.9
C(39)-C(38)-H(38B)	109.9
H(38A)-C(38)-H(38B)	108.3
N(6)-C(39)-C(38)	112.4(4)
N(6)-C(39)-H(39A)	109.1
C(38)-C(39)-H(39A)	109.1
N(6)-C(39)-H(39B)	109.1
C(38)-C(39)-H(39B)	109.1
H(39A)-C(39)-H(39B)	107.9
C(41)-C(40)-C(41)#5	120.7(8)
C(41)-C(40)-S(2)	119.6(4)
C(41)#5-C(40)-S(2)	119.6(4)
C(42)-C(41)-C(40)	118.5(7)
C(42)-C(41)-H(41)	120.7
C(40)-C(41)-H(41)	120.7
C(43)-C(42)-C(41)	121.3(8)
C(43)-C(42)-H(42)	119.4
C(41)-C(42)-H(42)	119.4
C(42)#5-C(43)-C(42)	119.4(9)
C(42)#5-C(43)-C(44)	120.3(5)
C(42)-C(43)-C(44)	120.3(5)
C(43)-C(44)-H(44A)	109.5
C(43)-C(44)-H(44B)	109.5
H(44A)-C(44)-H(44B)	109.5
C(43)-C(44)-H(44C)	109.5
H(44A)-C(44)-H(44C)	109.5
H(44B)-C(44)-H(44C)	109.5
O(3)-S(3)-C(45)	116.1(7)
O(3)-S(3)-C(46)	102.3(7)
C(45)-S(3)-C(46)	95.2(8)
S(3)-C(45)-H(45A)	109.5
S(3)-C(45)-H(45B)	109.5
H(45A)-C(45)-H(45B)	109.5
S(3)-C(45)-H(45C)	109.5
H(45A)-C(45)-H(45C)	109.5
H(45B)-C(45)-H(45C)	109.5
S(3)-C(46)-H(46A)	109.5
S(3)-C(46)-H(46B)	109.5
H(46A)-C(46)-H(46B)	109.5
S(3)-C(46)-H(46C)	109.5
H(46A)-C(46)-H(46C)	109.5
H(46B)-C(46)-H(46C)	109.5
O(4)-S(4)-C(47)#2	105.4(4)
O(4)-S(4)-C(47)	105.4(4)

C(47)#2-S(4)-C(47)	96.3(6)
S(4)-C(47)-H(47A)	109.5
S(4)-C(47)-H(47B)	109.5
H(47A)-C(47)-H(47B)	109.5
S(4)-C(47)-H(47C)	109.5
H(47A)-C(47)-H(47C)	109.5
H(47B)-C(47)-H(47C)	109.5

Symmetry transformations used to generate equivalent atoms:

#1 -x,-y+1,-z+1 #2 x,-y+1,z #3 -x,y,-z+1
#4 -x+2,-y,-z+1 #5 x,-y,z #6 -x+2,y,-z+1

Table L1.4: Anisotropic displacement parameters ($\text{Å}^2 \times 10^3$) for $L_1\text{AgBr}$. The anisotropic displacement factor exponent takes the form: $-2 \pi i^2 [h^2 a^{*2} U11 + \dots + 2 h k a^* b^* U12]$

	U^{11}	U^{22}	U^{33}	U^{23}	U^{13}	U^{12}
Ag(1)	22(1)	26(1)	58(1)	-3(1)	2(1)	-6(1)
Ag(2)	34(1)	32(1)	62(1)	0	3(1)	0
Br(1)	34(1)	31(1)	31(1)	0	10(1)	0
Br(2)	18(1)	26(1)	35(1)	0	4(1)	0
Br(3)	29(1)	21(1)	32(1)	0	0(1)	0
S(1)	15(1)	24(1)	25(1)	0	5(1)	0
O(1)	24(2)	50(2)	58(3)	-29(2)	11(2)	2(2)
N(1)	20(2)	19(2)	23(2)	1(2)	2(2)	3(1)
N(2)	19(2)	13(2)	25(2)	-1(2)	5(2)	0(1)
N(3)	14(2)	11(2)	25(3)	0	4(2)	0
C(1)	34(3)	51(4)	30(3)	-2(3)	3(2)	11(3)
C(2)	35(3)	79(5)	31(3)	-8(3)	3(2)	0(3)
C(3)	58(4)	78(5)	47(4)	-33(4)	17(3)	-18(4)
C(4)	82(5)	44(4)	90(6)	-32(4)	45(5)	-2(4)
C(5)	58(4)	30(3)	60(4)	-10(3)	27(3)	2(3)
C(6)	20(2)	29(3)	33(3)	-6(2)	3(2)	2(2)
C(7)	23(2)	27(2)	27(3)	-1(2)	-1(2)	9(2)
C(8)	19(2)	19(2)	19(2)	1(2)	1(2)	3(2)
C(9)	24(2)	18(2)	17(2)	3(2)	3(2)	1(2)
C(10)	39(3)	15(2)	25(2)	3(2)	4(2)	1(2)
C(11)	46(3)	20(2)	30(3)	1(2)	7(2)	-12(2)
C(12)	32(3)	33(3)	32(3)	4(2)	7(2)	-11(2)
C(13)	23(2)	24(2)	30(3)	3(2)	8(2)	-1(2)
C(14)	25(2)	13(2)	20(2)	2(2)	5(2)	-1(2)
C(15)	21(2)	18(2)	22(2)	-5(2)	1(2)	4(2)
C(16)	23(2)	17(2)	23(2)	-2(2)	5(2)	2(2)
C(17)	17(3)	56(5)	26(4)	0	4(3)	0
C(18)	50(6)	107(10)	43(6)	0	9(5)	0
C(19)	76(8)	148(13)	29(5)	0	1(5)	0
C(20)	28(5)	330(30)	25(5)	0	7(4)	0
C(21)	42(6)	220(20)	50(7)	0	-3(5)	0
C(22)	46(6)	142(13)	62(7)	0	16(5)	0
C(23)	111(9)	187(11)	110(9)	0	17(8)	0
Ag(3)	22(1)	25(1)	61(1)	-6(1)	18(1)	3(1)
Ag(4)	36(1)	33(1)	59(1)	0	5(1)	0
Br(4)	15(1)	22(1)	39(1)	0	9(1)	0
Br(5)	50(1)	36(1)	31(1)	0	16(1)	0
Br(6)	32(1)	18(1)	32(1)	0	-2(1)	0
S(2)	15(1)	49(1)	27(1)	0	8(1)	0
O(2)	43(2)	91(4)	38(2)	3(2)	3(2)	-48(2)
N(4)	17(2)	18(2)	26(2)	-1(2)	7(2)	-3(1)
N(5)	14(2)	18(2)	26(2)	2(2)	5(1)	-3(1)
N(6)	16(2)	18(2)	24(3)	0	9(2)	0

C(24)	76(5)	39(4)	52(4)	4(3)	-12(4)	-3(3)
C(25)	88(6)	60(5)	53(5)	17(4)	-13(4)	3(4)
C(26)	38(3)	81(5)	39(4)	-11(4)	0(3)	6(3)
C(27)	55(4)	69(5)	49(4)	-24(4)	16(3)	-29(4)
C(28)	47(3)	49(4)	44(4)	-13(3)	18(3)	-21(3)
C(29)	18(2)	30(3)	35(3)	-2(2)	4(2)	0(2)
C(30)	20(2)	25(2)	39(3)	-7(2)	11(2)	-6(2)
C(31)	14(2)	21(2)	25(2)	1(2)	8(2)	0(2)
C(32)	19(2)	23(2)	20(2)	1(2)	7(2)	2(2)
C(33)	36(3)	20(2)	29(3)	2(2)	11(2)	1(2)
C(34)	39(3)	27(3)	33(3)	2(2)	13(2)	12(2)
C(35)	25(2)	36(3)	38(3)	8(2)	13(2)	15(2)
C(36)	16(2)	33(3)	34(3)	4(2)	7(2)	5(2)
C(37)	19(2)	21(2)	21(2)	4(2)	6(2)	5(2)
C(38)	17(2)	19(2)	23(2)	0(2)	4(2)	-4(2)
C(39)	33(3)	33(3)	23(2)	5(2)	0(2)	-18(2)
C(40)	30(4)	60(5)	26(4)	0	18(3)	0
C(41)	61(4)	67(4)	28(3)	-4(3)	16(3)	30(3)
C(42)	128(8)	74(5)	28(4)	-4(4)	19(4)	27(5)
C(43)	110(10)	80(8)	18(5)	0	11(5)	0
C(44)	230(20)	87(10)	29(6)	0	19(9)	0
S(3)	60(2)	50(2)	35(2)	5(1)	7(1)	-5(2)
O(3)	300(20)	83(9)	110(11)	-35(8)	139(14)	-128(13)
C(45)	35(6)	91(11)	28(6)	14(7)	0(5)	10(7)
C(46)	71(10)	117(15)	48(9)	1(9)	30(8)	-22(10)
S(4)	80(2)	45(1)	30(1)	0	23(1)	0
O(4)	110(6)	33(3)	41(4)	0	40(4)	0
C(47)	91(6)	57(5)	63(5)	20(4)	25(4)	-11(4)

Table L1.5: Hydrogen coordinates ($\times 10^4$) and isotropic displacement parameters ($A^2 \times 10^3$) for $L_1\text{AgBr}$.

	x	y	z	U(eq)
H(1)	1769	6982	6886	47
H(2)	1675	7319	7716	59
H(3)	1170	8355	7851	72
H(4)	729	9075	7160	82
H(5)	825	8758	6320	57
H(7A)	952	7296	5843	32
H(7B)	1278	8031	5745	32
H(10)	2559	8683	6164	32
H(11)	3818	9005	6237	39
H(12)	4737	8212	6164	39
H(13)	4436	7063	5999	31
H(15A)	3667	6037	5551	25
H(15B)	2934	5617	5613	25
H(16A)	4132	5972	6456	25
H(16B)	3389	5575	6529	25
H(18)	4806	5000	7164	80
H(19)	5730	5000	7927	103
H(21)	7341	5000	7146	127
H(22)	6462	5000	6347	99
H(23A)	7048(3)	4535(9)	8190(20)	205
H(23B)	7690(40)	5000	8030(70)	205
H(24)	8774	1733	6200	71
H(25)	9260	1840	7087	85
H(26)	9809	2857	7421	65
H(27)	9912	3736	6869	69
H(28)	9386	3653	5990	55
H(30A)	8701	3067	5272	32
H(30B)	9048	2317	5285	32
H(33)	7598	3700	5511	33
H(34)	6374	4030	5558	39
H(35)	5396	3247	5451	38
H(36)	5593	2095	5292	33
H(38A)	6864	641	4926	23
H(38B)	6102	1028	4973	23
H(39A)	7197	544	5841	37
H(39B)	6462	962	5901	37
H(41)	5754	1035	6625	61
H(42)	6157	1018	7524	91
H(44A)	5960	-242	8345	175
H(44B)	6384	471	8332	175
H(44C)	6833	-228	8318	175
H(45A)	7505	3329	7208	79
H(45B)	7318	630	6630	79
H(45C)	7977	3083	6788	79
H(46A)	5636	2777	6799	114

H(46B)	5892	3427	6510	114
H(46C)	6184	3331	7122	114
H(47A)	1773	4375	7260	104
H(47B)	1806	4344	7873	104
H(47C)	2369	3889	7619	104

APPENDIX L2: Crystallographic data for L₃.HgBr

Table L2.1: Crystal data and structure refinement for L₃.HgBr.

Empirical formula	C ₇₈ H ₇₀ Hg ₂ Br ₄ Cl ₄ N ₁₀ O ₄ S ₂ .2H ₂ O
Formula weight	2138.19
Temperature	100(2) K
Wavelength	0.71073 Å
Crystal system, space group	Triclinic, P1
Unit cell dimensions	a = 10.2023(3) Å alpha = 78.934(3) deg. b = 11.6351(3) Å beta = 83.730(3) deg. c = 17.8431(6) Å gamma = 80.391(3) deg.
Volume	2042.99(11) Å ³
Z, Calculated density	17, 1.861 Mg/m ³
Absorption coefficient	6.440 mm ⁻¹
F(000)	1115
Crystal size	0.3 x 0.2 x 0.1 mm
Theta range for data collection	2.91 to 26.50 deg.
Limiting indices	- 12<=h<=12, -14<=k<=14, -22<=l<=20
Reflections collected / unique	20592 / 8465 [R(int) = 0.0457]
Completeness to theta = 26.00	99.9%
Absorption correction	None
Refinement method	Full-matrix least-squares on F ²
Data / restraints / parameters	8465 / 0 / 500
Goodness-of-fit on F ²	1.152
Final R indices [I>2sigma(I)]	R1 = 0.0684, wR2 = 0.1620
R indices (all data)	R1 = 0.0724, wR2 = 0.1641
Largest diff. peak and hole	1.655 and -4.929 e.Å ⁻³

Table L2.2: Atomic coordinates ($x \times 10^4$) and equivalent isotropic displacement parameters ($\text{Å}^2 \times 10^3$) for L_3HgBr . $U(\text{eq})$ is defined as one third of the trace of the orthogonalized U_{ij} tensor.

	x	y	z	$U(\text{eq})$
Hg(2)	4773(1)	1833(1)	3555(1)	11(1)
Br(1)	5000	0	5000	16(1)
Br(2)	1944(1)	2039(1)	3846(1)	25(1)
Cl(1)	2071(4)	538(4)	-735(2)	48(1)
S(3)	7648(3)	2981(2)	2243(1)	14(1)
Cl(5)	3783(6)	7007(6)	-74(3)	95(2)
O(3)	7141(8)	4138(7)	2420(5)	21(2)
O(5)	6837(8)	2372(7)	1897(5)	21(2)
C(5AA)	12292(14)	3972(14)	-60(8)	36(3)
C(2)	10271(13)	2970(13)	397(7)	32(3)
N(0AA)	4822(9)	-234(8)	2631(5)	15(2)
N(5)	6736(9)	-242(7)	3078(5)	15(2)
N(8)	4223(9)	4562(7)	3631(5)	13(2)
C(9)	5471(10)	339(8)	3044(6)	11(2)
C(12)	7709(16)	-2983(10)	2249(7)	33(3)
C(13)	6860(11)	5448(10)	4431(6)	18(2)
C(15)	4821(11)	5424(9)	3849(6)	16(2)
C(18)	7960(14)	-2070(9)	2603(6)	24(3)
C(20)	9223(12)	2714(11)	944(7)	25(3)
C(1AA)	3076(10)	209(9)	1706(6)	15(2)
N(3)	6069(8)	3660(7)	4093(5)	10(2)
C(6)	3593(11)	819(10)	353(7)	24(2)
C(7)	4987(10)	3509(9)	3790(6)	11(2)
C(0AA)	5455(13)	-2097(10)	2054(6)	23(2)
C(3AA)	7776(10)	-5(9)	3503(6)	16(2)
C(14)	3157(12)	5372(10)	2416(7)	23(2)
C(74)	4142(13)	4874(14)	1952(7)	33(3)
C(54)	4363(15)	5348(18)	1166(8)	49(5)
C(16)	3525(19)	6340(18)	881(8)	54(5)
C(46)	2480(20)	6855(14)	1335(10)	58(6)
C(43)	2280(16)	6373(12)	2106(8)	37(3)
C(4AA)	2953(11)	4849(10)	3259(6)	19(2)
C(2AA)	6870(12)	-1213(9)	2701(6)	18(2)
C(22)	8632(10)	897(9)	3032(6)	16(2)
C(23)	9101(11)	3131(9)	1620(6)	18(2)
C(26)	1919(11)	-138(11)	1552(7)	23(2)
C(27)	5645(11)	-1189(9)	2415(6)	16(2)
C(29)	6007(11)	4844(9)	4139(6)	16(2)
C(32)	4391(12)	6632(10)	3848(6)	20(2)
N(33)	8032(9)	2142(7)	3057(5)	14(2)
C(35)	11186(12)	3636(12)	528(7)	26(3)
C(38)	3900(11)	710(10)	1096(6)	19(2)
C(39)	6436(12)	6641(10)	4425(6)	23(2)
C(42)	11072(13)	4001(13)	1231(8)	35(3)

C(47)	8334(10)	2682(10)	3683(6)	16(2)
C(50)	6497(15)	-2983(10)	1983(7)	29(3)
C(51)	1593(12)	-31(12)	799(8)	30(3)
C(55)	7201(10)	2745(9)	4322(6)	14(2)
C(58)	5216(12)	7218(9)	4143(6)	21(2)
C(60)	3383(11)	48(11)	2526(7)	22(2)
C(64)	2448(12)	436(12)	212(7)	27(3)
C(66)	10027(13)	3782(14)	1774(8)	34(3)
Br(0A)	919(2)	7943(2)	3628(1)	62(1)
O(1)	8751(12)	528(10)	5206(8)	61(4)
O(2)	9954(12)	3810(11)	4992(9)	64(4)

Table L2.3: Bond lengths [Å] and angles [deg] for $L_3\text{HgBr}$

Hg(2)-C(9)	2.100(10)
Hg(2)-C(7)	2.121(10)
Hg(2)-Br(2)	2.8544(11)
Hg(2)-Br(1)	3.0167(4)
Br(1)-Hg(2)#1	3.0167(4)
Cl(1)-C(64)	1.752(12)
S(3)-O(5)	1.430(8)
S(3)-O(3)	1.440(8)
S(3)-N(33)	1.634(9)
S(3)-C(23)	1.764(11)
Cl(5)-C(16)	1.744(14)
C(5AA)-C(35)	1.503(16)
C(5AA)-H(5AA)	0.9600
C(5AA)-H(5AB)	0.9600
C(5AA)-H(5AC)	0.9600
C(2)-C(35)	1.373(17)
C(2)-C(20)	1.397(16)
C(2)-H(2)	0.9300
N(0AA)-C(9)	1.367(12)
N(0AA)-C(27)	1.368(14)
N(0AA)-C(60)	1.474(14)
N(5)-C(9)	1.356(13)
N(5)-C(2AA)	1.402(13)
N(5)-C(3AA)	1.460(14)
N(8)-C(7)	1.336(13)
N(8)-C(15)	1.391(13)
N(8)-C(4AA)	1.480(13)
C(12)-C(50)	1.37(2)
C(12)-C(18)	1.404(17)
C(12)-H(12)	0.9300
C(13)-C(39)	1.381(16)
C(13)-C(29)	1.403(15)
C(13)-H(13)	0.9300
C(15)-C(29)	1.385(15)
C(15)-C(32)	1.400(15)
C(18)-C(2AA)	1.385(16)
C(18)-H(18)	0.9300
C(20)-C(23)	1.371(16)
C(20)-H(20)	0.9300
C(1AA)-C(26)	1.381(15)
C(1AA)-C(38)	1.397(15)
C(1AA)-C(60)	1.499(15)
N(3)-C(7)	1.332(13)
N(3)-C(29)	1.387(13)
N(3)-C(55)	1.469(13)
C(6)-C(38)	1.373(17)
C(6)-C(64)	1.381(17)
C(6)-H(6)	0.9300
C(0AA)-C(50)	1.365(18)

C(0AA)-C(27)	1.388(15)
C(0AA)-H(0AA)	0.9300
C(3AA)-C(22)	1.542(14)
C(3AA)-H(3AA)	0.9700
C(3AA)-H(3AB)	0.9700
C(14)-C(74)	1.356(19)
C(14)-C(43)	1.406(18)
C(14)-C(4AA)	1.515(16)
C(74)-C(54)	1.414(18)
C(74)-H(74)	0.9300
C(54)-C(16)	1.36(3)
C(54)-H(54)	0.9300
C(16)-C(46)	1.39(3)
C(46)-C(43)	1.39(2)
C(46)-H(46)	0.9300
C(43)-H(43)	0.9300
C(4AA)-H(4AA)	0.9700
C(4AA)-H(4AB)	0.9700
C(2AA)-C(27)	1.394(16)
C(22)-N(33)	1.482(13)
C(22)-H(22A)	0.9700
C(22)-H(22B)	0.9700
C(23)-C(66)	1.385(16)
C(26)-C(51)	1.397(17)
C(26)-H(26)	0.9300
C(32)-C(58)	1.370(16)
C(32)-H(32)	0.9300
N(33)-C(47)	1.465(14)
C(35)-C(42)	1.387(17)
C(38)-H(38)	0.9300
C(39)-C(58)	1.408(18)
C(39)-H(39)	0.9300
C(42)-C(66)	1.382(17)
C(42)-H(42)	0.9300
C(47)-C(55)	1.537(15)
C(47)-H(47A)	0.9700
C(47)-H(47B)	0.9700
C(50)-H(50)	0.9300
C(51)-C(64)	1.376(18)
C(51)-H(51)	0.9300
C(55)-H(55A)	0.9700
C(55)-H(55B)	0.9700
C(58)-H(58)	0.9300
C(60)-H(60A)	0.9700
C(60)-H(60B)	0.9700
C(66)-H(66)	0.9300
O(1)-H(1A)	0.8501
O(1)-H(1B)	0.8501
O(2)-H(2A)	0.8500
O(2)-H(2B)	0.8500

C(9)-Hg(2)-C(7)	151.5(4)
C(9)-Hg(2)-Br(2)	109.2(3)
C(7)-Hg(2)-Br(2)	97.4(3)
C(9)-Hg(2)-Br(1)	81.9(3)
C(7)-Hg(2)-Br(1)	109.8(3)
Br(2)-Hg(2)-Br(1)	88.00(3)
Hg(2)-Br(1)-Hg(2)#1	179.999(14)
O(5)-S(3)-O(3)	120.4(5)
O(5)-S(3)-N(33)	106.9(5)
O(3)-S(3)-N(33)	105.7(5)
O(5)-S(3)-C(23)	106.9(5)
O(3)-S(3)-C(23)	106.6(5)
N(33)-S(3)-C(23)	110.1(5)
C(35)-C(2)-C(20)	120.7(11)
C(35)-C(2)-H(2)	119.6
C(20)-C(2)-H(2)	119.6
C(9)-N(0AA)-C(27)	110.8(9)
C(9)-N(0AA)-C(60)	124.0(9)
C(27)-N(0AA)-C(60)	124.7(9)
C(9)-N(5)-C(2AA)	109.1(9)
C(9)-N(5)-C(3AA)	126.8(8)
C(2AA)-N(5)-C(3AA)	123.8(9)
C(7)-N(8)-C(15)	109.6(9)
C(7)-N(8)-C(4AA)	128.1(9)
C(15)-N(8)-C(4AA)	122.3(8)
N(5)-C(9)-N(0AA)	106.9(8)
N(5)-C(9)-Hg(2)	123.2(7)
N(0AA)-C(9)-Hg(2)	129.9(7)
C(50)-C(12)-C(18)	122.3(12)
C(50)-C(12)-H(12)	118.8
C(18)-C(12)-H(12)	118.8
C(39)-C(13)-C(29)	116.3(11)
C(39)-C(13)-H(13)	121.9
C(29)-C(13)-H(13)	121.9
C(29)-C(15)-N(8)	106.0(9)
C(29)-C(15)-C(32)	122.2(10)
N(8)-C(15)-C(32)	131.8(10)
C(2AA)-C(18)-C(12)	114.8(12)
C(2AA)-C(18)-H(18)	122.6
C(12)-C(18)-H(18)	122.6
C(23)-C(20)-C(2)	119.9(11)
C(23)-C(20)-H(20)	120.0
C(2)-C(20)-H(20)	120.0
C(26)-C(1AA)-C(38)	118.9(10)
C(26)-C(1AA)-C(60)	118.3(10)
C(38)-C(1AA)-C(60)	122.8(10)
C(7)-N(3)-C(29)	109.6(8)
C(7)-N(3)-C(55)	126.6(8)
C(29)-N(3)-C(55)	123.7(8)
C(38)-C(6)-C(64)	119.3(11)
C(38)-C(6)-H(6)	120.4
C(64)-C(6)-H(6)	120.4

N(3)-C(7)-N(8)	108.3(8)
N(3)-C(7)-Hg(2)	121.0(7)
N(8)-C(7)-Hg(2)	130.5(7)
C(50)-C(0AA)-C(27)	118.1(12)
C(50)-C(0AA)-H(0AA)	120.9
C(27)-C(0AA)-H(0AA)	120.9
N(5)-C(3AA)-C(22)	113.2(9)
N(5)-C(3AA)-H(3AA)	108.9
C(22)-C(3AA)-H(3AA)	108.9
N(5)-C(3AA)-H(3AB)	108.9
C(22)-C(3AA)-H(3AB)	108.9
H(3AA)-C(3AA)-H(3AB)	107.8
C(74)-C(14)-C(43)	119.4(12)
C(74)-C(14)-C(4AA)	121.4(11)
C(43)-C(14)-C(4AA)	119.2(12)
C(14)-C(74)-C(54)	122.6(15)
C(14)-C(74)-H(74)	118.7
C(54)-C(74)-H(74)	118.7
C(16)-C(54)-C(74)	117.0(16)
C(16)-C(54)-H(54)	121.5
C(74)-C(54)-H(54)	121.5
C(54)-C(16)-C(46)	122.0(13)
C(54)-C(16)-Cl(5)	119.4(16)
C(46)-C(16)-Cl(5)	118.6(14)
C(43)-C(46)-C(16)	120.0(15)
C(43)-C(46)-H(46)	120.0
C(16)-C(46)-H(46)	120.0
C(46)-C(43)-C(14)	118.9(16)
C(46)-C(43)-H(43)	120.5
C(14)-C(43)-H(43)	120.5
N(8)-C(4AA)-C(14)	111.9(9)
N(8)-C(4AA)-H(4AA)	109.2
C(14)-C(4AA)-H(4AA)	109.2
N(8)-C(4AA)-H(4AB)	109.2
C(14)-C(4AA)-H(4AB)	109.2
H(4AA)-C(4AA)-H(4AB)	107.9
C(18)-C(2AA)-C(27)	123.2(11)
C(18)-C(2AA)-N(5)	129.9(11)
C(27)-C(2AA)-N(5)	106.9(9)
N(33)-C(22)-C(3AA)	112.8(9)
N(33)-C(22)-H(22A)	109.0
C(3AA)-C(22)-H(22A)	109.0
N(33)-C(22)-H(22B)	109.0
C(3AA)-C(22)-H(22B)	109.0
H(22A)-C(22)-H(22B)	107.8
C(20)-C(23)-C(66)	120.5(11)
C(20)-C(23)-S(3)	119.1(8)
C(66)-C(23)-S(3)	120.0(9)
C(1AA)-C(26)-C(51)	120.9(11)
C(1AA)-C(26)-H(26)	119.5
C(51)-C(26)-H(26)	119.5
N(0AA)-C(27)-C(0AA)	133.7(11)

N(0AA)-C(27)-C(2AA)	106.4(9)
C(0AA)-C(27)-C(2AA)	119.7(11)
C(15)-C(29)-N(3)	106.5(9)
C(15)-C(29)-C(13)	121.4(10)
N(3)-C(29)-C(13)	132.0(10)
C(58)-C(32)-C(15)	116.4(11)
C(58)-C(32)-H(32)	121.8
C(15)-C(32)-H(32)	121.8
C(47)-N(33)-C(22)	118.2(8)
C(47)-N(33)-S(3)	119.6(7)
C(22)-N(33)-S(3)	116.9(7)
C(2)-C(35)-C(42)	118.1(11)
C(2)-C(35)-C(5AA)	122.2(12)
C(42)-C(35)-C(5AA)	119.7(11)
C(6)-C(38)-C(1AA)	120.8(10)
C(6)-C(38)-H(38)	119.6
C(1AA)-C(38)-H(38)	119.6
C(13)-C(39)-C(58)	121.9(10)
C(13)-C(39)-H(39)	119.1
C(58)-C(39)-H(39)	119.1
C(66)-C(42)-C(35)	122.2(11)
C(66)-C(42)-H(42)	118.9
C(35)-C(42)-H(42)	118.9
N(33)-C(47)-C(55)	113.5(8)
N(33)-C(47)-H(47A)	108.9
C(55)-C(47)-H(47A)	108.9
N(33)-C(47)-H(47B)	108.9
C(55)-C(47)-H(47B)	108.9
H(47A)-C(47)-H(47B)	107.7
C(0AA)-C(50)-C(12)	121.7(11)
C(0AA)-C(50)-H(50)	119.2
C(12)-C(50)-H(50)	119.2
C(64)-C(51)-C(26)	118.5(11)
C(64)-C(51)-H(51)	120.7
C(26)-C(51)-H(51)	120.7
N(3)-C(55)-C(47)	112.4(8)
N(3)-C(55)-H(55A)	109.1
C(47)-C(55)-H(55A)	109.1
N(3)-C(55)-H(55B)	109.1
C(47)-C(55)-H(55B)	109.1
H(55A)-C(55)-H(55B)	107.9
C(32)-C(58)-C(39)	121.9(10)
C(32)-C(58)-H(58)	119.0
C(39)-C(58)-H(58)	119.0
N(0AA)-C(60)-C(1AA)	113.3(9)
N(0AA)-C(60)-H(60A)	108.9
C(1AA)-C(60)-H(60A)	108.9
N(0AA)-C(60)-H(60B)	108.9
C(1AA)-C(60)-H(60B)	108.9
H(60A)-C(60)-H(60B)	107.7
C(51)-C(64)-C(6)	121.6(11)
C(51)-C(64)-Cl(1)	118.9(10)

C(6)-C(64)-Cl(1)	119.5(10)
C(42)-C(66)-C(23)	118.5(11)
C(42)-C(66)-H(66)	120.7
C(23)-C(66)-H(66)	120.7
H(1A)-O(1)-H(1B)	109.5
H(2A)-O(2)-H(2B)	109.5

Symmetry transformations used to generate equivalent atoms:
#1 -x+1,-y,-z+1

Table L2.4: Anisotropic displacement parameters ($\text{\AA}^2 \times 10^3$) for $L_3\text{HgBr}$. The anisotropic displacement factor exponent takes the form: $-2 \pi i^2 [h^2 a^{*2} U11 + \dots + 2 h k a^* b^* U12]$

	U11	U22	U33	U23	U13	U12
Hg(2)	10(1)	10(1)	12(1)	-3(1)	-1(1)	-1(1)
Br(1)	22(1)	13(1)	12(1)	0(1)	2(1)	-4(1)
Br(2)	11(1)	17(1)	46(1)	-3(1)	3(1)	-3(1)
Cl(1)	35(2)	88(3)	18(2)	9(2)	-10(1)	-20(2)
S(3)	13(1)	17(1)	12(1)	1(1)	1(1)	-2(1)
Cl(5)	102(4)	153(6)	34(2)	53(3)	-41(2)	-91(4)
O(3)	20(4)	13(4)	26(4)	-1(3)	2(3)	2(3)
O(5)	18(4)	27(4)	19(4)	2(3)	-3(3)	-8(3)
C(5AA)	34(7)	50(9)	25(7)	-6(6)	16(6)	-20(7)
C(2)	26(7)	53(8)	23(6)	-24(6)	13(5)	-14(6)
N(0AA)	20(5)	17(4)	12(4)	-8(3)	0(3)	-6(4)
N(5)	18(5)	9(4)	15(4)	-2(3)	0(3)	1(3)
N(8)	17(4)	9(4)	12(4)	-3(3)	1(3)	0(3)
C(9)	12(5)	10(4)	10(5)	-2(4)	0(4)	-4(4)
C(12)	65(10)	13(5)	18(6)	-10(5)	4(6)	6(6)
C(13)	22(6)	17(5)	15(5)	-2(4)	1(4)	-7(4)
C(15)	23(6)	15(5)	11(5)	-4(4)	-1(4)	-3(4)
C(18)	44(7)	10(5)	14(5)	2(4)	0(5)	2(5)
C(20)	17(6)	33(7)	28(6)	-12(5)	3(5)	-9(5)
C(1AA)	13(5)	15(5)	18(5)	-6(4)	4(4)	-2(4)
N(3)	13(4)	7(4)	12(4)	-3(3)	1(3)	-1(3)
C(6)	15(5)	24(6)	26(6)	5(5)	5(5)	1(4)
C(7)	11(5)	10(4)	10(5)	0(4)	3(4)	-1(4)
C(0AA)	40(7)	17(5)	15(5)	-5(4)	4(5)	-17(5)
C(3AA)	12(5)	15(5)	17(5)	0(4)	2(4)	3(4)
C(14)	28(6)	19(5)	26(6)	-2(5)	-12(5)	-15(5)
C(74)	26(7)	58(9)	16(6)	5(6)	-6(5)	-16(6)
C(54)	28(7)	104(14)	17(6)	7(8)	-8(6)	-32(8)
C(16)	66(11)	86(13)	16(7)	22(8)	-22(7)	-55(10)
C(46)	99(15)	32(8)	47(10)	17(7)	-49(11)	-25(9)
C(43)	58(9)	24(6)	35(8)	-1(6)	-24(7)	-12(6)
C(4AA)	18(5)	16(5)	23(6)	-3(4)	-9(4)	-1(4)
C(2AA)	27(6)	13(5)	12(5)	-2(4)	3(4)	-2(4)
C(22)	13(5)	13(5)	23(6)	0(4)	-4(4)	-3(4)
C(23)	17(5)	16(5)	19(5)	-1(4)	1(4)	-5(4)
C(26)	14(5)	30(6)	23(6)	-1(5)	0(4)	-2(5)
C(27)	26(6)	16(5)	8(5)	-1(4)	2(4)	-9(4)
C(29)	20(5)	17(5)	11(5)	-3(4)	3(4)	-3(4)
C(32)	25(6)	18(5)	14(5)	0(4)	-1(4)	-2(4)
N(33)	14(4)	10(4)	13(4)	3(3)	2(3)	-2(3)
C(35)	23(6)	35(7)	23(6)	-4(5)	4(5)	-13(5)
C(38)	19(6)	19(5)	20(6)	1(4)	-2(4)	-6(4)
C(39)	33(7)	21(6)	17(6)	-2(4)	3(5)	-15(5)

C(42)	29(7)	55(9)	29(7)	-19(6)	10(5)	-30(6)
C(47)	8(5)	19(5)	23(6)	-2(4)	-4(4)	-4(4)
C(50)	61(9)	14(5)	13(5)	-5(4)	3(5)	-8(6)
C(51)	19(6)	42(8)	31(7)	-1(6)	-10(5)	-9(5)
C(55)	15(5)	14(5)	15(5)	-4(4)	-6(4)	-4(4)
C(58)	38(7)	11(5)	14(5)	-6(4)	11(5)	-8(5)
C(60)	20(6)	33(6)	20(6)	-12(5)	5(4)	-16(5)
C(64)	20(6)	35(7)	20(6)	5(5)	-9(5)	2(5)
C(66)	25(7)	58(9)	27(7)	-24(6)	9(5)	-19(6)
Br(0A)	56(1)	64(1)	67(1)	-16(1)	-6(1)	-3(1)
O(1)	42(6)	28(6)	105(11)	30(6)	-30(7)	-18(5)
O(2)	39(6)	51(7)	118(12)	-57(8)	-20(7)	9(6)

Table L2.5: Hydrogen coordinates ($x \times 10^4$) and isotropic displacement parameters ($A^2 \times 10^3$) for $L_3.HgBr$.

	x	y	z	U(eq)
H(5AA)	12386	3490	-449	54
H(5AB)	13111	3851	182	54
H(5AC)	12085	4791	-290	54
H(2)	10349	2687	-62	38
H(12)	8389	-3608	2194	40
H(13)	7666	5068	4617	22
H(18)	8793	-2044	2759	29
H(20)	8610	2261	850	30
H(6)	4149	1148	-50	29
H(0AA)	4641	-2102	1867	27
H(3AA)	8352	-742	3669	19
H(3AB)	7363	294	3958	19
H(74)	4694	4193	2159	40
H(54)	5049	5000	857	59
H(46)	1913	7522	1122	69
H(43)	1578	6707	2411	45
H(4AA)	2341	5409	3515	22
H(4AB)	2554	4134	3312	22
H(22A)	9507	750	3227	20
H(22B)	8750	780	2504	20
H(26)	1349	-449	1955	28
H(32)	3589	7016	3657	24
H(38)	4666	973	1195	23
H(39)	6972	7076	4614	27
H(42)	11720	4406	1340	41
H(47A)	8520	3478	3475	20
H(47B)	9133	2230	3901	20
H(50)	6382	-3603	1747	35
H(51)	815	-270	697	36
H(55A)	6894	1981	4462	17
H(55B)	7542	2912	4771	17
H(58)	4962	8019	4158	25
H(60A)	3025	769	2722	27
H(60B)	2938	-585	2825	27
H(66)	9948	4066	2233	41
H(1A)	9016	842	5543	91
H(1B)	8411	-84	5422	91
H(2A)	10099	3109	5244	96
H(2B)	10073	4299	5266	96

Table L2.6: Torsion angles [deg] for L₃.HgBr.

C(9)-Hg(2)-Br(1)-Hg(2)#1	-31(14)
C(7)-Hg(2)-Br(1)-Hg(2)#1	176(14)
Br(2)-Hg(2)-Br(1)-Hg(2)#1	79(14)
C(2AA)-N(5)-C(9)-N(0AA)	-1.8(11)
C(3AA)-N(5)-C(9)-N(0AA)	-175.4(9)
C(2AA)-N(5)-C(9)-Hg(2)	178.3(7)
C(3AA)-N(5)-C(9)-Hg(2)	4.7(14)
C(27)-N(0AA)-C(9)-N(5)	1.4(11)
C(60)-N(0AA)-C(9)-N(5)	173.7(9)
C(27)-N(0AA)-C(9)-Hg(2)	-178.7(7)
C(60)-N(0AA)-C(9)-Hg(2)	-6.4(15)
C(7)-Hg(2)-C(9)-N(5)	46.1(13)
Br(2)-Hg(2)-C(9)-N(5)	-156.0(7)
Br(1)-Hg(2)-C(9)-N(5)	-71.0(8)
C(7)-Hg(2)-C(9)-N(0AA)	-133.8(9)
Br(2)-Hg(2)-C(9)-N(0AA)	24.1(10)
Br(1)-Hg(2)-C(9)-N(0AA)	109.1(9)
C(7)-N(8)-C(15)-C(29)	1.0(11)
C(4AA)-N(8)-C(15)-C(29)	-177.1(9)
C(7)-N(8)-C(15)-C(32)	-175.6(11)
C(4AA)-N(8)-C(15)-C(32)	6.3(17)
C(50)-C(12)-C(18)-C(2AA)	3.6(17)
C(35)-C(2)-C(20)-C(23)	0(2)
C(29)-N(3)-C(7)-N(8)	0.4(11)
C(55)-N(3)-C(7)-N(8)	-177.4(9)
C(29)-N(3)-C(7)-Hg(2)	175.9(7)
C(55)-N(3)-C(7)-Hg(2)	-1.9(13)
C(15)-N(8)-C(7)-N(3)	-0.9(11)
C(4AA)-N(8)-C(7)-N(3)	177.1(9)
C(15)-N(8)-C(7)-Hg(2)	-175.7(7)
C(4AA)-N(8)-C(7)-Hg(2)	2.2(16)
C(9)-Hg(2)-C(7)-N(3)	-53.8(12)
Br(2)-Hg(2)-C(7)-N(3)	147.2(7)
Br(1)-Hg(2)-C(7)-N(3)	56.7(8)
C(9)-Hg(2)-C(7)-N(8)	120.5(10)
Br(2)-Hg(2)-C(7)-N(8)	-38.5(9)
Br(1)-Hg(2)-C(7)-N(8)	-129.0(9)
C(9)-N(5)-C(3AA)-C(22)	-90.4(12)
C(2AA)-N(5)-C(3AA)-C(22)	96.9(11)
C(43)-C(14)-C(74)-C(54)	2.5(19)
C(4AA)-C(14)-C(74)-C(54)	-179.4(12)
C(14)-C(74)-C(54)-C(16)	-1(2)
C(74)-C(54)-C(16)-C(46)	-1(2)
C(74)-C(54)-C(16)-Cl(5)	177.3(11)
C(54)-C(16)-C(46)-C(43)	1(2)
Cl(5)-C(16)-C(46)-C(43)	-177.4(11)
C(16)-C(46)-C(43)-C(14)	1(2)
C(74)-C(14)-C(43)-C(46)	-2.5(18)
C(4AA)-C(14)-C(43)-C(46)	179.4(11)

C(7)-N(8)-C(4AA)-C(14)	-99.4(12)
C(15)-N(8)-C(4AA)-C(14)	78.3(12)
C(74)-C(14)-C(4AA)-N(8)	46.8(14)
C(43)-C(14)-C(4AA)-N(8)	-135.1(10)
C(12)-C(18)-C(2AA)-C(27)	-5.3(16)
C(12)-C(18)-C(2AA)-N(5)	174.7(11)
C(9)-N(5)-C(2AA)-C(18)	-178.4(11)
C(3AA)-N(5)-C(2AA)-C(18)	-4.6(17)
C(9)-N(5)-C(2AA)-C(27)	1.6(11)
C(3AA)-N(5)-C(2AA)-C(27)	175.4(9)
N(5)-C(3AA)-C(22)-N(33)	85.3(11)
C(2)-C(20)-C(23)-C(66)	-2(2)
C(2)-C(20)-C(23)-S(3)	171.0(10)
O(5)-S(3)-C(23)-C(20)	1.7(11)
O(3)-S(3)-C(23)-C(20)	-128.2(10)
N(33)-S(3)-C(23)-C(20)	117.5(10)
O(5)-S(3)-C(23)-C(66)	174.4(10)
O(3)-S(3)-C(23)-C(66)	44.4(12)
N(33)-S(3)-C(23)-C(66)	-69.8(12)
C(38)-C(1AA)-C(26)-C(51)	2.1(18)
C(60)-C(1AA)-C(26)-C(51)	-178.8(11)
C(9)-N(0AA)-C(27)-C(0AA)	173.7(11)
C(60)-N(0AA)-C(27)-C(0AA)	1.5(18)
C(9)-N(0AA)-C(27)-C(2AA)	-0.4(12)
C(60)-N(0AA)-C(27)-C(2AA)	-172.7(10)
C(50)-C(0AA)-C(27)-N(0AA)	-174.5(11)
C(50)-C(0AA)-C(27)-C(2AA)	-0.9(16)
C(18)-C(2AA)-C(27)-N(0AA)	179.3(10)
N(5)-C(2AA)-C(27)-N(0AA)	-0.7(11)
C(18)-C(2AA)-C(27)-C(0AA)	4.2(16)
N(5)-C(2AA)-C(27)-C(0AA)	-175.8(9)
N(8)-C(15)-C(29)-N(3)	-0.7(11)
C(32)-C(15)-C(29)-N(3)	176.3(10)
N(8)-C(15)-C(29)-C(13)	-178.6(9)
C(32)-C(15)-C(29)-C(13)	-1.6(16)
C(7)-N(3)-C(29)-C(15)	0.2(11)
C(55)-N(3)-C(29)-C(15)	178.0(9)
C(7)-N(3)-C(29)-C(13)	177.8(11)
C(55)-N(3)-C(29)-C(13)	-4.4(17)
C(39)-C(13)-C(29)-C(15)	1.2(16)
C(39)-C(13)-C(29)-N(3)	-176.0(11)
C(29)-C(15)-C(32)-C(58)	0.6(16)
N(8)-C(15)-C(32)-C(58)	176.7(11)
C(3AA)-C(22)-N(33)-C(47)	87.6(11)
C(3AA)-C(22)-N(33)-S(3)	-118.3(8)
O(5)-S(3)-N(33)-C(47)	-153.6(8)
O(3)-S(3)-N(33)-C(47)	-24.2(9)
C(23)-S(3)-N(33)-C(47)	90.6(8)
O(5)-S(3)-N(33)-C(22)	52.8(8)
O(3)-S(3)-N(33)-C(22)	-177.8(7)
C(23)-S(3)-N(33)-C(22)	-63.0(8)
C(20)-C(2)-C(35)-C(42)	3(2)

C(20)-C(2)-C(35)-C(5AA)	-177.4(13)
C(64)-C(6)-C(38)-C(1AA)	0.5(18)
C(26)-C(1AA)-C(38)-C(6)	-2.2(17)
C(60)-C(1AA)-C(38)-C(6)	178.7(11)
C(29)-C(13)-C(39)-C(58)	0.0(16)
C(2)-C(35)-C(42)-C(66)	-4(2)
C(5AA)-C(35)-C(42)-C(66)	175.8(15)
C(22)-N(33)-C(47)-C(55)	-102.1(10)
S(3)-N(33)-C(47)-C(55)	104.6(9)
C(27)-C(0AA)-C(50)-C(12)	-0.7(17)
C(18)-C(12)-C(50)-C(0AA)	-0.7(19)
C(1AA)-C(26)-C(51)-C(64)	0(2)
C(7)-N(3)-C(55)-C(47)	93.2(11)
C(29)-N(3)-C(55)-C(47)	-84.2(11)
N(33)-C(47)-C(55)-N(3)	-73.7(11)
C(15)-C(32)-C(58)-C(39)	0.7(16)
C(13)-C(39)-C(58)-C(32)	-1.0(17)
C(9)-N(0AA)-C(60)-C(1AA)	130.5(10)
C(27)-N(0AA)-C(60)-C(1AA)	-58.3(14)
C(26)-C(1AA)-C(60)-N(0AA)	146.3(10)
C(38)-C(1AA)-C(60)-N(0AA)	-34.6(15)
C(26)-C(51)-C(64)-C(6)	-1(2)
C(26)-C(51)-C(64)-Cl(1)	178.3(10)
C(38)-C(6)-C(64)-C(51)	1.3(19)
C(38)-C(6)-C(64)-Cl(1)	-178.4(9)
C(35)-C(42)-C(66)-C(23)	3(2)
C(20)-C(23)-C(66)-C(42)	0(2)
S(3)-C(23)-C(66)-C(42)	-172.5(12)

Symmetry transformations used to generate equivalent atoms: #1 -x+1,-y,-z+1